Nuclear Science
NEA/NSC/DOC(2005)22

ISBN 92-64-01084-X

# VENUS-2 MOX-fuelled Reactor Dosimetry Calculations

## Final Report


NEA No. 6192

NUCLEAR ENERGY AGENCY
ORGANISATION FOR ECONOMIC CO-OPERATION AND DEVELOPMENT

**ORGANISATION FOR ECONOMIC CO-OPERATION AND DEVELOPMENT**

The OECD is a unique forum where the governments of 30 democracies work together to address the economic, social and environmental challenges of globalisation. The OECD is also at the forefront of efforts to understand and to help governments respond to new developments and concerns, such as corporate governance, the information economy and the challenges of an ageing population. The Organisation provides a setting where governments can compare policy experiences, seek answers to common problems, identify good practice and work to co-ordinate domestic and international policies.

The OECD member countries are: Australia, Austria, Belgium, Canada, the Czech Republic, Denmark, Finland, France, Germany, Greece, Hungary, Iceland, Ireland, Italy, Japan, Korea, Luxembourg, Mexico, the Netherlands, New Zealand, Norway, Poland, Portugal, the Slovak Republic, Spain, Sweden, Switzerland, Turkey, the United Kingdom and the United States. The Commission of the European Communities takes part in the work of the OECD.

OECD Publishing disseminates widely the results of the Organisation's statistics gathering and research on economic, social and environmental issues, as well as the conventions, guidelines and standards agreed by its members.

* * *

*This work is published on the responsibility of the Secretary-General of the OECD. The opinions expressed and arguments employed herein do not necessarily reflect the official views of the Organisation or of the governments of its member countries.*

**NUCLEAR ENERGY AGENCY**

The OECD Nuclear Energy Agency (NEA) was established on 1st February 1958 under the name of the OEEC European Nuclear Energy Agency. It received its present designation on 20th April 1972, when Japan became its first non-European full member. NEA membership today consists of 28 OECD member countries: Australia, Austria, Belgium, Canada, the Czech Republic, Denmark, Finland, France, Germany, Greece, Hungary, Iceland, Ireland, Italy, Japan, Luxembourg, Mexico, the Netherlands, Norway, Portugal, Republic of Korea, the Slovak Republic, Spain, Sweden, Switzerland, Turkey, the United Kingdom and the United States. The Commission of the European Communities also takes part in the work of the Agency.

The mission of the NEA is:

- to assist its member countries in maintaining and further developing, through international co-operation, the scientific, technological and legal bases required for a safe, environmentally friendly and economical use of nuclear energy for peaceful purposes, as well as
- to provide authoritative assessments and to forge common understandings on key issues, as input to government decisions on nuclear energy policy and to broader OECD policy analyses in areas such as energy and sustainable development.

Specific areas of competence of the NEA include safety and regulation of nuclear activities, radioactive waste management, radiological protection, nuclear science, economic and technical analyses of the nuclear fuel cycle, nuclear law and liability, and public information. The NEA Data Bank provides nuclear data and computer program services for participating countries.

In these and related tasks, the NEA works in close collaboration with the International Atomic Energy Agency in Vienna, with which it has a Co-operation Agreement, as well as with other international organisations in the nuclear field.

## FOREWORD

The OECD/NEA Nuclear Science Committee organised the two-dimensional VENUS-1 and the three-dimensional VENUS-3 international intercomparison exercises to examine state-of-the-art computation methods for calculating the neutron flux on reactor components. Both benchmarks dealt with $UO_2$-fuelled systems and were completed in 2000. The analysis of the results revealed that 3-D neutron fluence calculations provide results that are significantly more accurate than those obtained from 2-D calculations. They further demonstrated that performing 3-D calculations is technically feasible given the power of today's computers.

As a follow-up to these benchmarks, and given that the use of MOX fuel in LWRs presents different neutron characteristics, a three-dimensional VENUS-2 MOX-fuelled reactor dosimetry benchmark was launched in 2004 based on experimental data released by SCK•CEN, Mol, Belgium. Twelve participants contributed to this benchmark, providing 15 solutions. This report provides details of the comparative analysis of calculated results against experimental data.

*Acknowledgements*

The Secretariat expresses its sincere gratitude to the participants who willingly devoted their time and effort to this benchmark exercise and to SCK•CEN (Mol, Belgium) for the release of valuable experimental data. Special thanks go to Prof. Jong-Kyung Kim, Dr. Chi-Young Han, Mr. Chang-Ho Shin and Mr. Hong-Chul Kim of Hanyang University (Korea) for their valuable help and useful comments.

## TABLE OF CONTENTS

*List of tables*

*List of figures*

## EXECUTIVE SUMMARY

It is essential to calculate the structural integrity of reactor components with a high degree of accuracy to make correct decisions on design plant lifetime, safety margins and potential plant lifetime extension.

The Nuclear Science Committee of the OECD Nuclear Energy Agency (NEA) is thus organising a series of benchmarks on this subject to verify the current international level of accuracy in pressure vessel fluence calculations and to clarify the relative merits of various methodologies and hence the areas of possible improvements in various calculation schemes.

The main finding from the previous $UO_2$-fuelled VENUS-1 two-dimensional (2-D) and VENUS-3 three-dimensional (3-D) benchmarks was that the calculated results of the 3-D benchmark are in general much closer to the experimental values than those for the 2-D benchmark.

Knowing that many of commercial power plants in Europe and in Japan use MOX fuel and that the use of MOX fuel in LWRs presents different neutron characteristics, the present benchmark was launched in 2004 to test the current state-of-the-art computation methods of calculating neutron flux to reactor components against the measured data of the VENUS-2 MOX-fuelled critical experiments.

The latest versions of nuclear data sets and of three-dimensional calculation methods (both deterministic and stochastic methods) were applied by the participants. The 3-D results of most of the calculations are within the desired accuracy of ±10% for dosimetry calculations. It is demonstrated that some precise calculations can achieve, for most of the detector positions, an accuracy of ±5% when compared with the experimental values.

*Chapter 1*

# INTRODUCTION

It is of importance to be able to calculate the structural integrity of reactor components with a high degree of accuracy to make correct decisions on design plant lifetime, safety margins and potential plant lifetime extension. Ensuring the reactor pressure vessel integrity is essential for both safe operation of the power plant and economic reasons due to the possibility of plant lifetime extension.

Therefore, the Nuclear Science Committee of the OECD Nuclear Energy Agency (NEA) is organising a series of benchmarks on this subject to verify the current international level of accuracy in pressure vessel fluence calculations and to clarify the relative merits of various methodologies and hence the areas of possible improvements in various calculation schemes.

As a first step, the $UO_2$-fuelled VENUS-1 two-dimensional and VENUS-3 three-dimensional exercises were launched and completed in 2000 [1]. All calculated results were compared with measured data. The comparative analysis of these two exercises revealed that three-dimensional neutron fluence calculations provide results that are significantly more accurate than those obtained from two-dimensional calculations. Moreover, performing three-dimensional calculations is technically feasible given the power of today's computers.

In addition to the standard $UO_2$ fuel, many commercial power plants in Europe and in Japan use MOX fuel, even though the quantity allowed in the core is limited. The use of MOX fuel in LWRs presents different neutron characteristics. Therefore, the present benchmark was launched in 2004 to test the current state-of-the-art computation methods of calculating neutron flux to reactor components against the measured data of the VENUS-2 MOX-fuelled critical experiments, released by SCK•CEN (Mol, Belgium) to the OECD/NEA.

The measured data used for this benchmark are the equivalent fission fluxes measured using $^{58}$Ni(n,p), $^{115}$In(n,n′), $^{103}$Rh(n,n′), $^{64}$Zn(n,p), $^{237}$Np(n,f) and $^{27}$Al(n,$\alpha$) detectors at several important positions on the core mid-plane of the reactor [2]. It was requested to calculate reaction rates and corresponding equivalent fission fluxes measured on the core mid-plane at specific positions outside the core of the VENUS-2 MOX-fuelled reactor. Contrary to the previous VENUS-1 and VENUS-3 benchmarks, the source term was not provided to the participants in the present VENUS-2 MOX benchmark, since the results of the other benchmarks confirmed that 3-D pin power distributions can be accurately calculated by the modern 3-D calculation codes and nuclear data [3.4].

Twelve participating groups provided 15 solutions. The latest nuclear data libraries and computer codes were applied and tested. In deterministic calculations, the 3-D $S_N$ codes TORT, ATTILA, LUCKY and DANTSYS are used and a 3-D code being developed, MultiTrans, was also applied. Two participants used 2-D codes such as DORT and HELIOS. In Monte Carlo calculations, MCNP-4C, MCU and MCNPX codes were applied.

This report provides an analysis of all the participant results compared to the measured data.

*Chapter 2*

# BENCHMARK MODEL

The VENUS facility is a zero power critical reactor located at SCK•CEN in Belgium. As shown in Figure 2.1, the core comprises twelve (12) "15 × 15" subassemblies, instead of those of "17 × 17" (the pin-to-pin pitch remains typical of the "17 × 17" subassembly). The central part of the core (four 15 × 15 assemblies) consists of fuel pins 3.3 wt.% enriched in $^{235}U$ (called 3/0 $UO_2$ pins). There are five Pyrex pins in 1/8 of the core. Of the eight assemblies on the periphery of the core, all of which contain fuel pins 4.0 wt.% enriched in $^{235}U$ (called 4/0 $UO_2$ pins), eight rows of the most external fuel pins have been replaced by mixed oxide fuel pins ($UO_2$-$PuO_2$) enriched 2.0 wt.% in $^{235}U$ and 2.7 wt.% in high-grade plutonium (called 2/2.7 MOX pins).

The measured data used for this benchmark are the equivalent fission fluxes measured using $^{58}Ni(n,p)$, $^{115}In(n,n')$, $^{103}Rh(n,n')$, $^{64}Zn(n,p)$, $^{237}Np(n,f)$ and $^{27}Al(n,\alpha)$ detectors at several important positions in the reactor. The measurement positions are shown in Figure 2.2, and corresponding co-ordinates are given in Table 2.1. The six detectors were placed on the core mid-plane of the reactor at 34 locations in the central hole, the core inner baffle, the core outer baffle, the water reflector, the core barrel, the water gap and the neutron pad. The horizontal and vertical reactor descriptions are shown in Figures 2.3 and 2.4.

For the source term preparation, in addition to the average fission rate in the core corresponding to absolute reference irradiation, the fission rate distribution of 121 fuel pins measured on the core mid-plane and the axial fission rate distribution of six fuel pins were provided to the participants [3,4].

The objective of the benchmark is to verify the current level of accuracy in pressure vessel fluence calculations for MOX-fuelled systems. It will also validate the latest nuclear data sets and production codes used in the OECD member countries. The comparison with experimental data would allow to identify the origins of discrepancies between calculations and measurements and to quantify the relative merits of the different calculation methods.

The present benchmark is therefore defined to calculate reaction rates and corresponding equivalent fission fluxes measured on the core mid-plane at specific positions outside the core of the VENUS-2 MOX-fuelled reactor.

As for the calculation results, the reaction rates and corresponding equivalent fission fluxes, neutron fluxes at threshold energies $E_{th}$ > 1.0 MeV and $E_{th}$ > 0.1 MeV, and DPA rates (optional) were requested for the measurement points described above. All calculated reaction rates and corresponding equivalent fission fluxes and neutron fluxes were to be normalised to 100% VENUS-2 power by using the given fission rates in the core corresponding to absolute reference irradiation (1.87E+08 fissions/cm/sec at the core mid-plane and 4.596E+12 fissions/sec/core quadrant).

In the calculations, the participants were also requested to use **IRDF-90** ***Version*** **2** dosimeter cross-section data in order to ensure the comparability of results. Finally, the calculated $^{235}U$ fission spectrum averaged dosimeter cross-sections used for converting calculated reaction rates into equivalent fission fluxes were to be reported.

It is worthwhile to reiterate the definition of the equivalent fission fluxes. The equivalent fission fluxes are the reaction rates divided by the $^{235}U$ fission spectrum averaged cross-sections of the corresponding dosimeter. That is, the equivalent fission flux can be calculated as follows:

$$\phi_{eqfiss.} = \frac{\int_0^\infty \sigma_i(E)\phi(E)dE}{\langle \sigma_i \rangle_{fiss.}}$$

where $\sigma_i(E)$ is the energy-dependent cross-section of reaction i, $\phi(E)$ is the energy-dependent calculated flux at the measured position and $<\sigma_i>_{fiss.}$ is the $^{235}U$ fission spectrum averaged cross-section of reaction i.

The $^{235}U$ fission spectrum averaged cross-section of reaction i is defined as follows:

$$\langle \sigma_i \rangle_{fiss.} = \frac{\int_0^\infty \chi_5(E)\sigma_i(E)dE}{\int_0^\infty \chi_5(E)dE}$$

where $\chi_5(E)$ is the $^{235}U$ fission spectrum.

A complete description of the benchmark specification, including details of the VENUS-2 reactor, is given in Appendix A. Included in this specification are all geometry and material data required to develop the detailed three-dimensional computational model of the 1/4 fraction of the VENUS-2 reactor. Apart from the geometry and material data, the isotopic concentrations of each medium were also provided to minimise the discrepancies from the atomic density calculations, as in the previous benchmark exercises.

*Chapter 3*

## PARTICIPANTS, CODES AND DATA

Twelve participants contributed to the benchmark, providing 15 solutions. The complete list of participants, basic libraries and codes used are presented below and summarised in Table 3.1. Calculation details provided by the participants can be found in Appendix B. Eight solutions were obtained using 3-D deterministic codes such as TORT, ATTILA, LUCKY, DANTSYS, MultiTrans, and two solutions applied 2-D calculation codes DORT and HELIOS. As for Monte Carlo methods, four solutions were obtained using MCNP-4C and MCU. Two solutions applied the MCNPX code.

1. ***Hanyang University (HYU), Korea***
   Participants: Chang-Ho Shin and Jong Kyung Kim
   Code: TORT
   Cross-section library: ENDF/B-VI.8
   Response functions: IRDF 90 V.2
   Remarks: 35 groups, $S_8P_3$, $119 \times 126 \times 111$ meshes in Cartesian co-ordinate, separate source term calculation

2. ***Hanyang University (HYU), Korea***
   Participants: Hong-Chul Kim, Chang-Hi Shin, Chi Young Han and Jong Kyung Kim
   Code: MCNP-4C and MCNPX (version 2.5.d)
   Cross-section library: ENDF/B-VI.8
   Response functions: IRDF 90 V.2
   Remarks: 2 sets of contributions, separate source term calculation (KCODE)

3. ***Transpire, Inc., USA***
   Participants: Todd Wareing, Allen Barnett, John McGhee and Greg Failla
   Code: ATTILA
   Cross-section library: ENDF/B-VI
   Response functions: IRDF 90 V.2
   Remarks: 30 groups, $S_8P_3$, 117 752 tetrahedral elements, use the given axial fission source

4. ***Kurchatov Institute (KI), Russia***
   Participant: Mikhail A. Kalugin
   Code: MCU
   Cross-section library: MCUDAT-2.2 (based on ENDF/B-VI, JENDL-3.2, BROND)
   Response functions: IRDF 90 V.2 (ENDF/B-VI.5 for Np)
   Remarks: Continuous energy group, Monte Carlo method, separate source term calculation

5. ***Kurchatov Institute (KI), Russia***
   Participants: Alexey V. Moriakov and Sergei M. Zaritsky
   Code: LUCKY
   Cross-section library: BUGLE 96
   Response functions: IRDF 90 V.2
   Remarks: 26 groups, $S_8P_3$, Cartesian co-ordinate, use the given axial fission source

6. ***Korea Power Engineering Co. (KOPEC), Korea***
   Participants: Bok Ja Moon and Joon Ghi Ahn
   Code: DORT (version 2.8.14)
   Cross-section library: BUGLE 96
   Response functions: IRDF 90 V.2 (BUGLE 96 for Np)
   Remarks: 47 groups, $S_8P_3$, 2-D/1-D synthesis method, use the given axial fission source

7. ***Vuje Trnava Inc. (VTI)/ Slovak University of Technology (SUT), Slovak***
   Participants: Petr Darilek, Vladimir Sebian and Vladimir Necas
   Code: HELIOS-1.7
   Cross-section library: ENDF/B-VI
   Response functions: ENDF/B-VI
   Remarks: 190 groups, 2-D current-coupling collision-probability (CCCP) method, Only Np reaction results provided

8. ***WTI GmbH, Germany***
   Participants: Maik Hennebach and Helmut Kühl
   Code: MCNP-4C2
   Cross-section library: ENDF/B-VI
   Response functions: IRDF 90 V.2
   Remarks: Continuous energy group, use the given axial fission source

9. ***VTT, Finland***
   Participant: Petri Kotiluoto
   Code: TORT, MultiTrans (in-house code**)**
   Cross-section library: BUGLE96
   Response functions: IRDF 90 V.2
   Remarks: 2 sets of contributions, 47 groups, $S_8P_3$ and $147 \times 98 \times 45$ meshes (TORT), $SP_3$ and 2 530 817 octree cells (MultiTrans), a direct $k_{eff}$ search

10. ***Korea Atomic Energy Research Institute (KAERI), Korea***
    Participants: Do Heon Kim, Choong-Sub Gil, Jonghwa Chang and Jung-Do Kim
    Code: DANTSYS 3.0
    Cross-section library: ENDF/B-VI.8
    Response functions: IRDF 90 V.2
    Remarks: 47 groups, $S_8P_3$, mesh size = about 0.63cm (a half pitch)

11. ***VTT, Finland***
    Participant: Frej Wasastjerna
    Code: MCNP-4C
    Cross-section library: ENDF/B-VI
    Response functions: IRDF 90 V.2
    Remarks: 2 sets of contributions, continuous energy group, KCODE calculation and use the given axial fission source

12. ***SCK•CEN, Belgium***
    Participants: Nadia Messaoudi and Wim Haeck
    Code: MCNPX
    Cross-section library: ENDF/B-VI.8
    Response functions: IRDF 90 V.2
    Remarks: Continuous energy group, KCODE calculation

## *Chapter 4*
## RESULTS OF THE BENCHMARK

In the experiments, the equivalent fission fluxes at several important positions on the core mid-plane of the reactor were measured using $^{58}$Ni(n,p), $^{115}$In(n,n′), $^{103}$Rh(n,n′), $^{64}$Zn(n,p), $^{237}$Np(n,f), and $^{27}$Al(n,$\alpha$) detectors. The measured values of equivalent fission fluxes for each detector are given in Tables 4.1 and 4.2 for the detector positions in stainless steel zones and in water zones, respectively. The reported uncertainty of experimental equivalent fission flux values is not known.

The $^{58}$Ni(n,p) detector covers the flux above 2.8 MeV. The $^{64}$Zn(n,p) detector has the same activation threshold as the $^{58}$Ni(n,p) detector. The $^{115}$In(n,n′) detector covers the flux above 1 MeV and corresponds to the local variation of the DPA rate, and the $^{27}$Al(n,$\alpha$) detector indicates the extreme hard end of the neutron spectrum above 7.6 MeV.

The "experimental" dosimeter cross-sections, i.e. the $^{235}$U fission spectrum averaged cross-sections of each dosimeter, used to convert measured reaction rates to experimental equivalent fission fluxes, were not given in the original VENUS-2 documents [2]. However, the values used in VENUS-3 experiments were reported in Ref. [5]: 108.50 mbarn for $^{58}$Ni(n,p), 190.30 mbarn for $^{115}$In(n,n′) and 0.706 mbarn for $^{27}$Al(n,$\alpha$) detectors. It is therefore assumed that these values might also have been used for obtaining equivalent fission fluxes from the VENUS-2 experiments, and thus are designated "Mol values" of the dosimeter cross-sections and are used for our analysis below.

As mentioned earlier, a full set of the 3-D source term was not provided to the participants in the present benchmark, since the results of the previous benchmarks on the VENUS-2 MOX core calculations confirmed that 3-D pin power distributions can be adequately calculated by the modern 3-D calculation codes and nuclear data [3,4].

In the previous 3-D VENUS-2 MOX core calculation results, averaged pin powers from both deterministic and Monte Carlo calculations showed a scatter band less than ±2% for most of the axial positions in the MOX pins. For a few axial positions, both calculations reported more than ±3% of scatter band. For 4/0 $UO_2$ pins, both deterministic and Monte Carlo calculations gave an excellent agreement within ±1% of discrepancy for almost all positions. As for 3/0 $UO_2$ pins, the agreement within ±1% was observed for almost all positions in both deterministic and Monte Carlo calculation results. The discrepancies in the calculated pin power results were within the reported uncertainties of the measured data (1$\sigma$) that are ±2.2% for $UO_2$ pins and ±3.4% for MOX pins.

Nevertheless, one should keep in mind that the source terms calculated and used by the different participants could contain about a difference of ±1% to ±3% among them and hence the use of these different source terms can result in corresponding differences in the calculated reaction rates and equivalent fission fluxes.

## 4.1. Comparison of dosimeter cross-sections

The calculated dosimeter cross-sections reported by the participants are summarised in Table 4.3.

The dosimeter cross-sections averaged over the $^{235}$U fission spectrum are an important parameter since they could directly affect equivalent fission flux values converted from reaction rates. If there is 1% of discrepancy in the dosimeter cross-section values, this automatically implies 1% of discrepancy in the calculated equivalent fission fluxes.

Table 4.4 shows a relative comparison of the calculated dosimeter cross-sections based on an average value of all calculated results. The results show that the participants calculated the dosimeter cross-sections close to the values of the others. For most of the cases, the difference is less than 1%. The maximum differences are about 2.5% for the Ni and the In detectors, about 2% for the Rh and the Np detectors, and about 5% for the Zn and the Al detectors. The VTI/SUT HELIOS calculation reported a value with high difference of 8.8% in the Np detector cross-section. The VTI/SUT value was obtained based on ENDF/B-VI. The KI MCU calculation used the same library for the Np detector, but gives a value with a 1.7% difference. This shows that the large difference observed for the VTI/SUT value does not seem to come from the library used. KOPEC applied BUGLE96 for obtaining the Np dosimeter cross-section, which shows a difference of 0.2% from the average value.

Table 4.5 presents a relative comparison of the calculated dosimeter cross-sections compared to the Mol values used to convert reaction rates to experimental equivalent fission fluxes. The Mol values differ from the calculated detector cross-sections in average about 1.5%, 2% and 6% for $^{58}$Ni(n,p), $^{115}$In(n,n′), and $^{27}$Al(n,$\alpha$) detectors, respectively. Even with the same basic and dosimetry data libraries, the calculated dosimeter cross-sections show differences depending on the computer codes used. It is interesting to note that two MCNP-4C results (HYU and VTT) give quite similar values for all three detectors, while in HYU calculations the values from TORT and MCNP-4C are very different even though the same set of libraries was used for both calculations.

In the following analysis, one should keep in mind that the calculated equivalent fission fluxes would contain an intrinsic difference compared to the experimental values due to the differences between the calculated and the experimental dosimeter cross-sections: 0.6-3.5% for Ni, 0-5% for In, and 2-10% for Al detectors.

## 4.2. Comparison of equivalent fission fluxes

The participants reported the calculated equivalent fission fluxes for $^{58}$Ni(n,p), $^{115}$In(n,n′), $^{103}$Rh(n,n′), $^{64}$Zn(n,p), $^{237}$Np(n,f) and $^{27}$Al(n,$\alpha$) detectors. The calculated results are compared with the experimental values as C/E values. The provided results and C/E comparisons are given in Tables 4.6 to 4.11, and C/E values are plotted in Figures 4.1 to 4.12. In addition, underneath the tables, the statistics of calculation results (i.e. numbers of C/E values within ±5%, ±10% and ±20%) is also given.

### *$^{58}$Ni(n,p) detector*

The calculated results for stainless steel zones show in general a good agreement with the experimental values. For most of the detection positions, the scatter band is less than ±10%. Some solutions obtained from both deterministic and Monte Carlo methods report a scatter band within ±5%.

The 2-D result also gives a reasonably good agreement for the positions near the core centre (±5%) and the scatter band becomes larger for the positions outside the core (about ±10%). A systematic trend of slight overestimation in the 2-D calculation results might be due to the buckling correction used in 2-D calculations. As noted already in the previous VENUS-1 benchmark, the buckling correction applied in 2-D calculations seems to be able to reproduce reasonable results near the core, but fails to do so when the distance from the core centre increases.

The results obtained by using $SP_3$ approximation give larger discrepancies. It was reported that $SP_3$ approximation produces less accurate results when the solution starts to behave more transport-like and that the approximation shows some limitations in deep penetration problems.

As observed in the previous VENUS-1 and VENUS-3 benchmarks, the accuracy of calculations is lower and deteriorates as the distance from the core increases, and is mainly attributable to the lack of material symmetry which is assumed with reflective boundary condition.

Compared to the results in stainless steel zones, the discrepancies in C/E values in water zones are larger. For most of the solutions, the scatter band is about ±10% in the reflector zone (i.e. near the core) whereas it becomes larger in the water gap zone up to ±20% (i.e. when the distance from the core increases).

Some solutions report a scatter band less than ±10% in all positions. Nevertheless, a trend of slight overestimation is observed in all reported results.

### $^{115}$*In(n,n') detector*

In detector solutions are in general slightly better than those of the Ni detector. The solutions show a scatter band less than ±5% in stainless steel zones and less than ±10% in water zones for most of the positions. Slightly larger discrepancies (still within ±5-10%), are observed when the distance from the core increases.

The 2-D solution gives about ±10% of discrepancies. The results from the $SP_3$ approximation show about ±20% of scatter band in stainless steel zones and about ±30% in water zones.

### $^{103}$*Rh(n,n') detector*

For this detector, a problem with the BUGLE 96 cross-section was observed in the previous VENUS-1 benchmark. For the current benchmark, all participants employed IRDF 90 Version 2 cross-sections, reporting consistent results.

An excellent agreement between calculated and experimental equivalent fission fluxes is observed in most of the solutions in both stainless steel and water gap zones: the scatter band is less than ±5% for most of the detector positions.

Some Monte Carlo solutions give C/E values almost 1 for most of the detector positions in both stainless steel and water gap zones, whereas deterministic solutions show a slightly larger scatter band. This might be due to the coarse space approximation used. The trend of a slight underestimation of the equivalent fission fluxes is observed in calculation results.

***$^{64}$Zn(n,p) detector***

For most of the solutions, a general scatter band of about ±10% is observed in both stainless steel and water gap zones. In many calculation results, a scatter band of about ±5% is observed in stainless zones, and about ±10% in water zones.

In the stainless steel zones, for the detector position at 42°, the two MCNPX results show a large discrepancy (more than ±20%). In water zones, for the detector position (-51.53, -19.78), i.e. at 21.14°, all results from both deterministic and Monte Carlo calculations report a discrepancy more than +10% up to +40%. This could raise a question about the accuracy of the experimental value at that position.

***$^{237}$Np(n,f) detector***

Before analysing the results, it is worth noting that the experimental results for the $^{237}$Np(n,f) reaction include the photo-fission effect approximately 3%, which is not included in the calculation results (except that from DORT calculations). The C/E results must therefore be adjusted by +3%.

As in the $^{64}$Zn(n,p) case, for most of the solutions, some calculation results report a scatter band of less than ±5%. However, a general scatter band of about ±10% is observed in both stainless steel and water gap zones.

Two-dimensional HELIOS calculation results show a large scatter band, systematically more than ±20%. Besides the possible buckling correction-induced errors, this might be due to a large discrepancy (-8.8%) in the calculated Np dosimeter cross-section used to convert reaction rates to equivalent fission fluxes.

***$^{27}$Al(n,$\alpha$) detector***

$^{27}$Al(n,$\alpha$) detector calculations show the most discrepant results compared to the results for the other detectors. A general scatter band of about ±20% is observed while some calculations give a scatter band of ±10% in both deterministic and Monte Carlo methods.

A trend of slight underestimation of equivalent fission fluxes in stainless steel zones is observed in all results. All Monte Carlo solutions reported higher statistical perturbation in their calculation results for the Al detector. SCK MCNPX calculations could not obtain the statistically valid results for the positions 21°, 42° in stainless steel zones and for all positions in water zones for which the code reported too-high statistical uncertainty. In fact, in water gap zones, HYU MCNP and MCNPX results show a high statistical perturbation.

*A complementary comparison*

VTT made a comparative analysis by using two different sources: a KOCDE source calculated by MCNP-4C itself and the fixed source given in the benchmark specification. The results are summarised in Table 4.12. For most of the detector positions, the differences are about ±5% to ±10% and for the Al detector, the discrepancies are higher up to ±30%. In addition, for most of the positions except in the inner baffle and in the central hole and water reflector, the KCODE results show systematically larger values than those from the fixed source calculation. However, when compared to the experimental values, the results from the KOCDE show a slightly better agreement than those from the fixed source calculation.

### 4.3. Comparison of reaction rates

As an attempt to remove the impact of dosimeter cross-sections used to convert reaction rates to equivalent fission fluxes, the experimental equivalent fission fluxes for Ni, In and Al detectors are converted back to "quasi-experimental" reaction rates by using the corresponding Mol values of dosimeter cross-sections.

The "quasi-experimental" reaction rates for Ni, In and Al detectors are then compared to calculated reaction values provided by the participants as C/E values. The calculated reaction rate results and C/E comparisons are given in Tables 4.13 to 4.15, and C/E values are plotted in Figures 4.13 to 4.18.

However, it should be noted that the following analysis is based on the "assumption" that the Mol values of the dosimeter cross-sections were used for converting the measured reactor rates into experimental equivalent fission fluxes.

#### $^{58}$*Ni(n,p) detector*

With regard to C/E values, very similar comments can be made as in the comparison of the equivalent fission fluxes. For most of the calculation results, a scatter band of ±10% is observed in both the stainless steel and water zones. Some solutions report a scatter band of less than ±5% in stainless steel zones, which becomes larger, between ±5% and ±10%, in water zones.

A difference between the experimental and calculated dosimeter cross-sections (for the Ni case, about 1.3%) does not seem to affect the reaction rate comparison and the calculated reaction rates show a good agreement with the experimental reaction rates.

#### $^{115}$*In(n,n') detector*

As observed in the comparison of equivalent fission fluxes, In detector solutions are slightly better than those of the Ni detector. However, the general observation is a scatter band of about ±10% in both stainless steel and water zones. As with the Ni detector, some solutions report a scatter band less than ±5% in stainless steel zones, which becomes larger (between ±5% and ±10%) in water zones.

#### $^{27}$*Al(n,α) detector*

Since the difference between the experimental dosimeter cross-section and calculated dosimeter cross-section is high (about 6%), it was expected to some extent that the comparison of reaction rates would show much more discrepant results. However, a general scatter band of about ±20% is observed while some calculations give a scatter band of ±10% for most of the detector positions, as in the equivalent fission flux comparison.

In summary, the observed differences between the experimental dosimeter cross-sections and calculated dosimeter cross-sections do not really affect the final results in both equivalent fission flux and reaction rate comparisons. There could be some type of mutual compensation effect among the parameters considered.

## 4.4. Comparison of theoretical parameters

Important theoretical parameters such as fast neutron fluxes above 0.1 MeV and 1.0 MeV and DPA rates were also calculated and compared. As they cannot be directly compared against the measured values, relative intercomparisons of calculated results are made with an arbitrary reference solution. KI MCU results were taken as arbitrary reference solutions for the intercomparisons. The results provided by the participants and relative intercomparisons are given in Tables 4.16 to 4.18, and are also plotted in Figures 4.19 to 4.24.

### *Fast neutron fluxes above 0.1 MeV and 1.0 MeV*

For most of the calculations, an excellent agreement is observed in both stainless steel and water zones: the scatter band is less than ±5%. This confirms the important fast neutron fluxes can be calculated by the modern computer codes and nuclear data with a sufficient level of accuracy.

Two-dimensional DORT calculations show a scatter band of about ±10% in stainless steel zones and about ±20% in water zones. This might be due to the applied axial buckling correction. Two-dimensional HELIOS calculations show a scatter band of more than ±20%.

### *DPA rates*

Only five solutions from HYU, KI and KOPEC were provided for DPA rates, as it was an optional request in the benchmark calculations. The scatter band observed among the calculations is about ±30%. HYU used the DPA cross-section of $^{56}$Fe from ENDF/B-VI.8 while KI used the EUR standard damage cross-section in steel. As the very high accuracy of calculated fast fluxes above 1.0 MeV is observed, the main differences observed in the DPA rates would be due to the differences in DPA cross-sections.

## *Chapter 5*

## CONCLUSIONS

Subsequent to the previous $UO_2$-fuelled VENUS-1 two-dimensional (2-D) and the VENUS-3 three-dimensional (3-D) fluence calculation benchmarks, the present benchmark was launched in 2004 to test the current state-of-the-art computation methods of calculating neutron flux to reactor components against the measured data of the VENUS-2 MOX-fuelled critical experiments.

The measured data used for this benchmark were the equivalent fission fluxes measured using $^{58}$Ni(n,p), $^{115}$In(n,n′), $^{103}$Rh(n,n′), $^{64}$Zn(n,p), $^{237}$Np(n,f) and $^{27}$Al(n,$\alpha$) detectors at several important positions on the core mid-plane of the reactor. The calculated reaction rates and corresponding equivalent fission fluxes were compared directly to the experimental values. In addition, some important theoretical parameters such as fast neutron fluxes (E > 0.1 MeV and E > 1.0 MeV) and DPA rates were also analysed. Contrary to the previous VENUS-1 and VENUS-3 benchmarks, the source term was calculated by the participants in the present VENUS-2 MOX benchmark.

Twelve participating groups provided 15 solutions. The latest nuclear data libraries and computer codes were applied and tested. As for the transport cross-section libraries, different versions of ENDF/B-VI, BUGLE 96, and MUCDAT 2.2 (based on ENDF/B-VI, JENDL-3.2 and BROND) were used. IRDF90 Version 2 was mainly used for dosimeter cross-sections. In deterministic calculations, the 3-D $S_N$ codes TORT, ATTILA, LUCKY and DANTSYS were used and a 3-D code being developed (MultiTrans) was applied. Two participants used 2-D codes such as DORT and HELIOS. In Monte Carlo calculations, MCNP-4C, MCU and MCNPX codes were applied.

In all combinations of the latest versions of nuclear data sets and of three-dimensional calculation methods (both deterministic and stochastic methods), the analysis of calculated results confirmed that the 3-D results of most of the calculations are within the accuracy of ±10% desired for dosimetry calculations. It was also demonstrated that some precise calculations can achieve, for most of the detector positions, an accuracy of ±5% when compared against the experimental values.

As an attempt to remove the uncertainties possibly emerging from the dosimeter cross-sections, calculated reaction rates were directly compared to “quasi-experimental” reaction rates converted back from experimental equivalent fission fluxes. The comparison confirmed that C/E values from 3-D precise calculations are within an accuracy of ±10% for most of the detector positions. The rather large differences observed between the experimental and calculated dosimeter cross-sections do not greatly affect the final comparison and conclusion.

As for the theoretical parameters such as fast neutron fluxes, the agreement among calculation results was surprisingly good. It was demonstrated that these quantities can be calculated by the modern 3-D computer codes and latest nuclear data sets with a sufficient level of accuracy. However, with regard to DPA rates, there remains a need to improve DPA cross-section data.

In summary, the results with a very high accuracy can be obtained from precise 3-D calculations (about ±5% for almost all detector positions). Though the uncertainty of experimental data is unknown and, in consequence, a final conclusion can not be drawn, the computer codes and nuclear data currently used in the OECD member countries seem to able to produce results with a sufficiently high level of accuracy in dosimetry calculations for MOX-fuelled systems.

## REFERENCES


[1] Hehn, G. and B.C. Na, *Prediction of Neutron Embrittlement in the Reactor Pressure Vessel: VENUS-1 and VENUS-3 Benchmarks*, OECD/NEA Report, NEA/NSC/DOC(2000)5, ISBN 92-64-17637-3 (2000).

[2] *LWR-PV Surveillance Dosimetry Improvement Program: VENUS-2 PWR Core Source and Azimuthal Lead Factor Experiments*, SCK•CEN report (1983).

[3] Na, B.C., *Benchmark on the VENUS-2 MOX Core Measurements*, OECD/NEA Report, NEA/NSC/DOC(2000)7, ISBN 92-64-18276-4 (2000).

[4] Messaoudi, N. and B.C. Na, *Benchmark on the Three-dimensional VENUS-2 MOX Core Measurements – Final Report*, OECD/NEA, NEA/NSC/DOC(2003)5, ISBN 92-64-02160-4 (2003).

[5] Maerker, R.E., *Analysis of the VENUS-3 Experiments*, NUREG/CR-5338, ORNL/TM-11106, Oak Ridge National Laboratory, August 1989.

# TABLES

**Table 2.1. Co-ordinates of VENUS-2 measurement positions**

| No. | Measurement point zone | (x,y) co-ordinates with respect to reactor grid | (r,θ) in [cm,°] co-ordinates with respect to core centre | (x,y) in [cm,cm] co-ordinates with respect to core centre |
|---|---|---|---|---|
| 1 | Central hole | (+2.5,+2.5) | | (0.00,0.00) |
| 2 | Inner baffle | (-1,+2) | (–,8.1°) | (-4.41,-0.63) |
| 3 | | (-1,-1) | (–,45.0°) | (-4.41,-4.41) |
| 4 | Outer baffle | (-29,+2) | (–,0.9°) | (-39.69,-0.69) |
| 5 | | (-29,-2) | (–,8.1°) | (-39.69,-5.67) |
| 6 | | (-29,-7) | (–,16.8°) | (-39.69,-11.97) |
| 7 | | (-29,-12) | (–,24.7°) | (-39.69,-18.27) |
| 8 | | (-27,-14) | (–,29.2°) | (-37.17,-20.79) |
| 9 | | (-22,-14) | (–,34.0°) | (-30.87,-20.79) |
| 10 | | (-17,-14) | (–,40.2°) | (-24.57,-20.79) |
| 11 | Barrel | (-37,+2) | (–,0.7°) | (-49.77,-0.63) |
| 12 | | (-37,-5) | (–,10.8°) | (-49.77,-9.45) |
| 13 | | (-35,-12) | (–,21.1°) | (-47.25,-18.27) |
| 14 | | (-34,-15) | (–,25.6°) | (-45.99,-22.05) |
| 15 | | (-33,-17) | (–,28.8°) | (-44.73,-24.57) |
| 16 | | (-31,-20) | (–,33.9°) | (-42.21,-28.35) |
| 17 | | (-28,-24) | (–,41.0°) | (-38.43,-33.39) |
| 18 | | (-26,-26) | (–,45.0°) | (-35.91,-35.91) |
| 19 | Water gap | (–,–) | (55.2,10.8°) | (-54.36,-9.59) |
| 20 | | (–,–) | (55.2,16.6°) | (-52.89,-15.80) |
| 21 | | (–,–) | (55.2,21.1°) | (-51.53,-19.78) |
| 22 | | (–,–) | (55.2,25.6°) | (-50.03,-23.33) |
| 23 | | (–,–) | (55.2,28.8°) | (-48.74,-25.91) |
| 24 | | (–,–) | (55.2,33.9°) | (-46.29,-30.06) |
| 25 | | (–,–) | (55.2,37.4°) | (-44.08,-33.22) |
| 26 | | (–,–) | (55.2,41.0°) | (-42.29,-35.48) |
| 27 | | (–,–) | (55.2,45.0°) | (-39.03,-39.03) |
| 28 | Neutron pad | (–,–) | (62.7,21.1°) | (-58.54,-22.47) |
| 29 | | (–,–) | (62.7,42.0°) | (-46.60,-41.95) |
| 30 | Reflector | (-16,-16) | (–,45°) | (-23.31,-23.31) |
| 31 | | (-18,-18) | (–,45°) | (-25.83,-25.83) |
| 32 | | (-20,-20) | (–,45°) | (-28.35,-28.35) |
| 33 | | (-22,-22) | (–,45°) | (-30.87,-30.87) |
| 34 | | (-24,-24) | (–,45°) | (-33.39,-33.39) |

**Table 3.1. Participants, data libraries and computer codes used**

| Institute (country) | Participants | Codes | Data | Comments |
|---|---|---|---|---|
| ***Deterministic methods*** | | | | |
| Hanyang University (Korea) | C.H. Shin<br>J.K. Kim | TORT | ENDF/B-VI.8<br>IRDF90 V.2 | $S_8P_3$, 35 groups<br>$119 \times 126 \times 111$ meshes |
| Transpire Inc. (USA) | T. Wareing<br>A. Barnett<br>J. McGhee<br>G. Failla | ATTILA | ENDF/B-VI<br>IRDF90 V.2 | $S_8P_3$, 30 groups<br>117 752 tetrahedra elements |
| Kurchatov Institute (Russia) | A.V. Moriakov<br>S.M. Zaritsky | LUCKY | BUGLE 96<br>IRDF90 V.2 | $S_8P_3$, 26 groups |
| KOPEC (Korea) | B.J. Moon<br>H.R. Hwang<br>J. G. Ahn | DORT | BUGLE 96<br>IRDF90 V.2 | 2-D/1-D Synthesis method<br>47 groups |
| VTI/SUT (Slovak) | V. Sebian<br>P. Darilek<br>V. Necas | HELIOS-1.7 | ENDF/B-VI<br>ENDF/B-VI | 2-D CCCP calculation<br>190 groups<br>Only Np reaction results submitted |
| VTT (Finland) | P. Kotiluoto | TORT<br>MultiTrans | BUGLE 96<br>IRDF90 V.2 | $S_8P_3$ (TORT), 47 groups<br>$147 \times 98 \times 45$ meshes<br>$SP_3$ (MultiTrans)<br>2 sets of contributions |
| KAERI (Korea) | D.H. Kim<br>J.D. Kim<br>C.S. Gil<br>J.H. Chang | DANTSYS | ENDF/B-VI.8<br>IRDF90 V.2 | $S_8P_3$, 47 groups |
| ***Monte Carlo methods*** | | | | |
| Hanyang University (Korea) | H.C. Kim<br>C.H. Shin<br>C.Y. Han<br>J.K. Kim | MCNP-4C<br>MCNPX | ENDF/B-VI.8<br>IRDF90 V.2 | 2 sets of contributions |
| KI (Russia) | M. Kalugin | MCU | MCUDAT 2.2<br>IRDF90 V.2 | |
| WTI GmbH (Germany) | M. Hennebach<br>H. Kühl | MCNP-4C | ENDF/B-VI<br>IRDF90 V.2 | |
| VTT (Finland) | F. Wasastjerna | MCNP-4C | ENDF/B-VI<br>IRDF90 V.2 | 2 sets of contributions (KCODE and fixed source calculations) |
| SCK•CEN (Belgium) | N. Messaoudi<br>W. Haeck | MCNPX | ENDF/B-VI.8<br>IRDF90 V.2 | |

**Table 4.1. Equivalent fission fluxes in stainless steel zones VENUS-2**

| Measurement position | $^{58}$Ni(n,p) | $^{115}$In(n,n′) | $^{103}$Rh(n,n′) | $^{64}$Zn(n,p) | $^{237}$Np(n,f) | $^{27}$Al(n,α) |
|---|---|---|---|---|---|---|
| Inner baffle | | | | | | |
| (-1,+2) | 1.51E+09 | 1.94E+09 | 2.40E+09 | 1.52E+09 | 2.49E+09 | 1.43E+09 |
| (-1,-1) | 1.83E+09 | 2.36E+09 | 2.82E+09 | 1.83E+09 | 2.95E+09 | 1.70E+09 |
| Outer baffle | | | | | | |
| (-29,+2) | 5.80E+08 | 7.14E+08 | – | 5.76E+08 | – | 5.92E+08 |
| (-29,-2) | 5.52E+08 | – | 8.06E+08 | – | – | – |
| (-29,-7) | 4.47E+08 | 5.48E+08 | 6.54E+08 | 4.36E+08 | 6.88E+08 | 4.52E+08 |
| (-29,-12) | 2.62E+08 | 3.33E+08 | 3.97E+08 | 2.54E+08 | 4.34E+08 | 2.69E+08 |
| (-27,-14) | 2.75E+08 | 3.53E+08 | 4.20E+08 | – | – | 2.76E+08 |
| (-22,-14) | 5.44E+08 | – | – | – | – | – |
| (-17,-14) | 8.69E+08 | 1.12E+09 | 1.37E+09 | 8.55E+08 | 1.46E+09 | 8.30E+08 |
| Barrel | | | | | | |
| (-37,+2) | 7.36E+07 | 8.97E+07 | 1.04E+08 | 7.42E+07 | – | 9.62E+07 |
| (-37,-5) | 6.13E+07 | 7.90E+07 | 9.49E+07 | 6.24E+07 | 1.03E+08 | 8.50E+07 |
| (-35,-12) | 6.02E+07 | 7.91E+07 | 9.60E+07 | 6.10E+07 | 1.04E+08 | 7.33E+07 |
| (-34,-15) | 5.06E+07 | 6.90E+07 | 8.50E+07 | 5.00E+07 | 9.04E+07 | 6.01E+07 |
| (-33,-17) | 4.50E+07 | 6.05E+07 | 7.63E+07 | 4.55E+07 | – | 5.48E+07 |
| (-31,-20) | 4.16E+07 | 5.37E+07 | 6.55E+07 | 4.15E+07 | 7.02E+07 | 5.71E+07 |
| (-28,-24) | 3.67E+07 | 4.36E+07 | 5.29E+07 | 3.66E+07 | 5.49E+07 | 5.19E+07 |
| (-26,-26) | 3.59E+07 | 4.38E+07 | 5.11E+07 | 3.59E+07 | 5.35E+07 | 5.12E+07 |
| Neutron pad | | | | | | |
| 21° | 5.89E+06 | 8.19E+06 | – | 5.78E+06 | 1.12E+07 | 1.05E+07 |
| 42° | – | 5.90E+06 | – | 3.99E+06 | 7.70E+06 | 8.39E+06 |

**Table 4.2. Equivalent fission fluxes in water zones VENUS-2**

| Measurement position | $^{58}$Ni(n,p) | $^{115}$In(n,n′) | $^{103}$Rh(n,n′) | $^{64}$Zn(n,p) | $^{237}$Np(n,f) | $^{27}$Al(n,α) |
|---|---|---|---|---|---|---|
| Center hole | | | | | | |
| (+2.5,+2.5) | – | – | – | – | – | – |
| Water I | | | | | | |
| (-16,-16) | 6.32E+08 | 7.91E+08 | 8.46E+08 | – | 9.77E+08 | 6.66E+08 |
| (-18,-18) | 3.41E+08 | 4.00E+08 | 4.35E+08 | 3.46E+08 | 4.62E+08 | 4.06E+08 |
| (-20,-20) | 1.88E+08 | 2.07E+08 | 2.21E+08 | 1.99E+08 | 2.31E+08 | 2.53E+08 |
| (-22,-22) | 1.05E+08 | 1.11E+08 | 1.13E+08 | 1.12E+08 | 1.24E+08 | 1.52E+08 |
| (-24,-24) | 5.91E+07 | 6.66E+07 | 7.27E+07 | – | – | 9.71E+07 |
| Water II | | | | | | |
| (R = 55.26) | | | | | | |
| 10.75° | 2.09E+07 | – | 2.98E+07 | – | | – |
| 16.63° | 2.06E+07 | 2.59E+07 | 3.13E+07 | 2.17E+07 | – | 3.15E+07 |
| 21.14° | 1.96E+07 | 2.53E+07 | 2.99E+07 | 1.68E+07 | – | 2.52E+07 |
| 25.62° | 1.77E+07 | 2.30E+07 | 2.80E+07 | 1.89E+07 | – | 2.67E+07 |
| 28.78° | 1.62E+07 | 2.13E+07 | 2.60E+07 | 1.71E+07 | – | 2.54E+07 |
| 33.89° | 1.48E+07 | 1.87E+07 | 2.19E+07 | 1.60E+07 | – | 2.50E+07 |
| 37.44° | 1.39E+07 | – | – | – | – | – |
| 40.99° | 1.32E+07 | – | 1.87E+07 | 1.45E+07 | – | 2.30E+07 |
| 45.00° | 1.31E+07 | 1.57E+07 | 1.83E+07 | 1.51E+07 | 1.95E+07 | 2.30E+07 |

**Table 4.3. Calculated dosimeter cross-sections by the participants**

| Institute | Country | Basic data | Dosimetry data | Code | $^{58}$Ni(n,p) | $^{115}$In(n,n′) | $^{103}$Rh(n,n′) | $^{64}$Zn(n,p) | $^{237}$Np(n,f) | $^{27}$Al(n,α) |
|---|---|---|---|---|---|---|---|---|---|---|
| **Mol values** | **Belgium** | | | | **108.50** | **190.30** | | | | **0.706** |
| HYU | Korea | ENDF/B-VI.8 | IRDF 90 V.2 | TORT | 104.754 | 181.203 | 695.670 | 38.121 | 1318.832 | 0.780 |
| HYU | Korea | ENDF/B-VI.8 | IRDF 90 V.2 | MCNP-4C MCNPX | 107.200 | 185.779 | 703.982 | 39.020 | 1326.027 | 0.721 |
| Transpire Inc. | USA | ENDF/B-VI | IRDF 90 V.2 | ATTILA | 107.252 | 186.690 | 705.660 | 39.015 | 1349.940 | 0.753 |
| KI | Russia | MCUDAT 2.2 (based on ENDF/B-VI, JENDL-3.2, BROND) | IRDF 90 V.2 (ENDF/B-VI for Np) | MCU | 106.2 | 184.2 | 690.6 | 41.13 | 1313.0 | 0.7512 |
| KI | Russia | BUGLE 96 | IRDF 90 V.2 | LUCKY | 109.19 | 190.37 | 713.73 | 39.7 | 1363.000 | 0.766 |
| KOPEC | Korea | BUGLE 96 | IRDF 90 V.2 (BUGLE 96 for Np) | DORT | 106.580 | 186.030 | 705.700 | 38.693 | 1330.500 | 0.775 |
| VTI/SUT | Slovak | ENDF/B-VI | ENDF/B-VI | HELIOS-1.7 | | | | | 1215.725 | |
| WTI | Germany | ENDF/B-VI | IRDF 90 V.2 | MCNP-4C2 | 109.506 | 188.815 | 711.281 | 39.883 | 1356.606 | 0.747 |
| VTT | Finland | BUGLE 96 | IRDF 90 V.2 | TORT MultiTrans | 107.339 | 187.544 | 708.720 | 39.024 | 1357.720 | 0.747 |
| KAERI | Korea | ENDF/B-VI.8 | IRDF 90 V.2 | DANTSYS 3.0 | 105.686 | 186.263 | 705.472 | 38.397 | 1363.510 | 0.728 |
| VTT | Finland | ENDF/B-VI | IRDF 90 V.2 | MCNP 4C | 106.651 | 185.356 | 703.077 | 38.814 | 1347.054 | 0.721 |
| SCK•CEN | Belgium | ENDF/B-VI.8 | IRDF 90 V.2 | MCNPX | 105.73 | 186.35 | 706.03 | 38.40 | 1355.11 | 0.73 |
| **Average** | | | | | **106.69** | **185.82** | **703.62** | **39.05** | **1335.09** | **0.75** |

**Table 4.4. Relative errors (%) of calculated dosimeter cross-sections compared to the average values**

| Institute | Country | Basic data | Dosimetry data | Code | $^{58}$Ni(n,p) | $^{115}$In(n,n′) | $^{103}$Rh(n,n′) | $^{64}$Zn(n,p) | $^{237}$Np(n,f) | $^{27}$Al(n,α) |
|---|---|---|---|---|---|---|---|---|---|---|
| HYU | Korea | ENDF/B-VI.8 | IRDF 90 V.2 | TORT | -1.8 | -2.5 | -1.1 | -2.4 | -1.1 | 4.7 |
| HYU | Korea | ENDF/B-VI.8 | IRDF 90 V.2 | MCNP-4C MCNPX | 0.5 | 0.0 | 0.1 | -0.1 | -0.5 | -3.2 |
| Transpire Inc. | USA | ENDF/B-VI | IRDF 90 V.2 | ATTILA | 0.5 | 0.5 | 0.3 | -0.1 | 1.3 | 1.1 |
| KI | Russia | MCUDAT 2.2 (based on ENDF/B-VI, JENDL-3.2, BROND) | IRDF 90 V.2 (ENDF/B-VI for Np) | MCU | -0.5 | -0.9 | -1.9 | 5.3 | -1.5 | 0.8 |
| KI | Russia | BUGLE 9 | IRDF 90 V.2 | LUCKY | 2.3 | 2.4 | 1.4 | 1.7 | 2.2 | 2.8 |
| KOPEC | Korea | BUGLE 96 | IRDF 90 V.2 (BUGLE 96 for Np) | DORT | -0.1 | 0.1 | 0.3 | -0.9 | -0.2 | 4.1 |
| VTI/SUT | Slovak | ENDF/B-VI | ENDF/B-VI | HELIOS-1.7 | – | – | – | – | -8.8 | – |
| WTI | Germany | ENDF/B-VI | IRDF 90 V.2 | MCNP-4C2 | 2.6 | 1.6 | 1.1 | 2.1 | 1.8 | 0.2 |
| VTT | Finland | BUGLE 96 | IRDF 90 V.2 | TORT MultiTrans | 0.6 | 0.9 | 0.7 | -0.1 | 1.8 | 0.3 |
| KAERI | Korea | ENDF/B-VI.8 | IRDF 90 V.2 | DANTSYS 3.0 | -0.9 | 0.2 | 0.3 | -1.7 | 2.3 | -2.3 |
| VTT | Finland | ENDF/B-VI | IRDF 90 V.2 | MCNP 4C | 0.0 | -0.3 | -0.1 | -0.6 | 1.0 | -3.3 |
| SCK•CEN | Belgium | ENDF/B-VI.8 | IRDF 90 V.2 | MCNPX | -0.9 | 0.3 | 0.3 | -1.7 | 1.7 | -2.4 |

**Table 4.5. Relative errors (%) of calculated dosimeter cross-sections compared to the Mol values**

| Institute | Country | Basic data | Dosimetry data | Code | $^{58}$Ni(n,p) | $^{115}$In(n,n′) | $^{27}$Al(n,α) |
|---|---|---|---|---|---|---|---|
| **Mol values** | | | | | **108.5** | **190.3** | **0.706** |
| HYU | Korea | ENDF/B-VI.8 | IRDF 90 V.2 | TORT | -3.5 | -4.8 | 10.4 |
| HYU | Korea | ENDF/B-VI.8 | IRDF 90 V.2 | MCNP-4C MCNPX | -1.2 | -2.4 | 2.1 |
| Transpire Inc. | USA | ENDF/B-VI | IRDF 90 V.2 | ATTILA | -1.2 | -1.9 | 6.7 |
| KI | Russia | MCUDAT 2.2 (based on ENDF/B-VI, JENDL-3.2, BROND) | IRDF 90 V.2 (ENDF/B-VI for Np) | MCU | -2.1 | -3.2 | 6.4 |
| KI | Russia | BUGLE 9 | IRDF 90 V.2 | LUCKY | 0.6 | 0.0 | 8.5 |
| KOPEC | Korea | BUGLE 96 | IRDF 90 V.2 (BUGLE 96 for Np) | DORT | -1.8 | -2.2 | 9.8 |
| VTI/SUT | Slovak | ENDF/B-VI | ENDF/B-VI | HELIOS-1.7 | – | – | – |
| WTI | Germany | ENDF/B-VI | IRDF 90 V.2 | MCNP-4C2 | 0.9 | -0.8 | 5.8 |
| VTT | Finland | BUGLE 96 | IRDF 90 V.2 | TORT MultiTrans | -1.1 | -1.4 | 5.8 |
| KAERI | Korea | ENDF/B-VI.8 | IRDF 90 V.2 | DANTSYS 3.0 | -2.6 | -2.1 | 3.1 |
| VTT | Finland | ENDF/B-VI | IRDF 90 V.2 | MCNP 4C | -1.7 | -2.6 | 2.1 |
| SCK•CEN | Belgium | ENDF/B-VI.8 | IRDF 90 V.2 | MCNPX | -2.6 | -2.1 | 3.0 |
| **Average** | | | | | **-1.3** | **-2.1** | **5.8** |

# Table 4.6(a). Equivalent fission fluxes: $^{58}$Ni(n,p) detector results and C/E comparison in stainless steel zones

Calculated results

| $^{58}$Ni (n,p) | Position in cm | Grid Position | Experimental Value | HYU-TORT Korea | HYU-MCNP Korea | HYU-MCNPX Korea | Transpire Inc.-ATTILA USA | KI-MCU Russia | KOPEC-DORT Korea | WTI-MCNP Germany | VTT-TORT Finland | VTT-MT Finland | KI-LUCKY Russia | KAERI-DANTSYS Korea | VTT-MCNP-K Finland | VTT-MCNP-F Finland | SCK-MCNPX Belgium |
|---|---|---|---|---|---|---|---|---|---|---|---|---|---|---|---|---|---|
| Inner Baffle | ( -4.41, -0.63) | (-1,+2) | 1.51E+09 | 1.53E+09 | 1.42E+09 | 1.42E+09 | 1.57E+09 | 1.48E+09 | 1.55E+09 | 1.47E+09 | 1.56E+09 | 1.50E+09 | 0.151E+10 | 1.40E+09 | 1.28E+09 | 1.40E+09 | 1.48E+09 |
| | ( -4.41, -4.41) | (-1,-1) | 1.83E+09 | 1.84E+09 | 1.73E+09 | 1.72E+09 | 1.87E+09 | 1.80E+09 | 1.89E+09 | 1.78E+09 | 1.79E+09 | 2.02E+09 | 0.179E+10 | 1.68E+09 | 1.70E+09 | 1.87E+09 | 1.72E+09 |
| Outer Baffle | (-39.69, -0.63) | (-29,+2) | 5.80E+08 | 5.02E+08 | 5.89E+08 | 5.67E+08 | 5.75E+08 | 5.76E+08 | 6.01E+08 | 5.77E+08 | 5.15E+08 | 5.25E+08 | 0.523E+09 | 5.68E+08 | 5.23E+08 | 4.94E+08 | 5.69E+08 |
| | (-39.69, -5.67) | (-29,-2) | 5.52E+08 | 4.78E+08 | 5.84E+08 | 5.70E+08 | 5.58E+08 | 5.46E+08 | 5.71E+08 | 5.46E+08 | 4.79E+08 | 5.12E+08 | 0.497E+09 | 5.40E+08 | 5.20E+08 | 4.92E+08 | 5.51E+08 |
| | (-39.69, -11.97) | (-29,-7) | 4.47E+08 | 3.92E+08 | 4.42E+08 | 4.43E+08 | 4.52E+08 | 4.37E+08 | 4.65E+08 | 4.51E+08 | 3.82E+08 | 4.19E+08 | 0.404E+09 | 4.40E+08 | 4.35E+08 | 4.06E+08 | 4.39E+08 |
| | (-39.69, -18.27) | (-29,-12) | 2.62E+08 | 2.34E+08 | 2.50E+08 | 2.65E+08 | 2.63E+08 | 2.54E+08 | 2.76E+08 | 2.65E+08 | 2.15E+08 | 2.43E+08 | 0.239E+09 | 2.56E+08 | 2.50E+08 | 2.43E+08 | 2.50E+08 |
| | (-37.17, -20.79) | (-27,-14) | 2.75E+08 | 2.57E+08 | 2.83E+08 | 2.72E+08 | 2.75E+08 | 2.69E+08 | 2.88E+08 | 2.72E+08 | 2.38E+08 | 2.62E+08 | 0.243E+09 | 2.65E+08 | 2.64E+08 | 2.50E+08 | 2.64E+08 |
| | (-30.87, -20.79) | (-22,-14) | 5.44E+08 | 5.23E+08 | 5.41E+08 | 5.35E+08 | 5.60E+08 | 5.35E+08 | 5.67E+08 | 5.36E+08 | 5.35E+08 | 5.44E+08 | 0.493E+09 | 5.25E+08 | 5.23E+08 | 5.11E+08 | 5.47E+08 |
| | (-24.57, -20.79) | (-17,-14) | 8.69E+08 | 8.80E+08 | 8.75E+08 | 8.79E+08 | 9.07E+08 | 8.60E+08 | 9.28E+08 | 8.55E+08 | 8.08E+08 | 9.47E+08 | 0.845E+09 | 8.34E+08 | 8.29E+08 | 8.73E+08 | 8.46E+08 |
| Barrel | (-49.77, -0.63) | (-37,+2) | 7.36E+07 | 6.80E+07 | 7.87E+07 | 7.47E+07 | 7.53E+07 | 7.45E+07 | 8.02E+07 | 7.41E+07 | 6.34E+07 | 5.95E+07 | 0.701E+08 | 7.55E+07 | 6.55E+07 | 6.31E+07 | 7.33E+07 |
| | (-49.77, -9.45) | (-37,-5) | 6.13E+07 | 5.79E+07 | 6.35E+07 | 6.42E+07 | 6.35E+07 | 6.41E+07 | 6.81E+07 | 6.26E+07 | 5.18E+07 | 5.11E+07 | 0.598E+08 | 6.54E+07 | 6.01E+07 | 5.69E+07 | 5.98E+07 |
| | (-47.25, -18.27) | (-35,-12) | 6.02E+07 | 5.49E+07 | 5.97E+07 | 6.10E+07 | 6.15E+07 | 6.00E+07 | 6.49E+07 | 5.96E+07 | 5.09E+07 | 5.07E+07 | 0.559E+08 | 5.97E+07 | 5.86E+07 | 5.53E+07 | 6.44E+07 |
| | (-45.99, -22.05) | (-34,-15) | 5.06E+07 | 4.75E+07 | 5.31E+07 | 4.86E+07 | 5.19E+07 | 5.17E+07 | 5.38E+07 | 4.98E+07 | 4.59E+07 | 4.40E+07 | 0.483E+08 | 4.92E+07 | 4.99E+07 | 4.62E+07 | 5.51E+07 |
| | (-44.73, -24.57) | (-33,-17) | 4.50E+07 | 4.16E+07 | 4.52E+07 | 4.52E+07 | 4.53E+07 | 4.57E+07 | 4.92E+07 | 4.51E+07 | 4.17E+07 | 4.09E+07 | 0.437E+08 | 4.31E+07 | 4.36E+07 | 4.23E+07 | 4.97E+07 |
| | (-42.21, -28.35) | (-31,-20) | 4.16E+07 | 4.10E+07 | 4.16E+07 | 4.50E+07 | 4.38E+07 | 4.27E+07 | 4.61E+07 | 4.17E+07 | 3.79E+07 | 3.69E+07 | 0.415E+08 | 4.02E+07 | 3.96E+07 | 3.90E+07 | 4.14E+07 |
| | (-38.43, -33.39) | (-28,-24) | 3.67E+07 | 3.73E+07 | 3.73E+07 | 3.70E+07 | 3.69E+07 | 3.72E+07 | 4.12E+07 | 3.57E+07 | 3.40E+07 | 3.10E+07 | 0.364E+08 | 3.56E+07 | 3.41E+07 | 3.48E+07 | 3.67E+07 |
| | (-35.91, -35.91) | (-26,-26) | 3.59E+07 | 3.70E+07 | 3.72E+07 | 3.83E+07 | 3.70E+07 | 3.71E+07 | 4.14E+07 | 3.63E+07 | 3.34E+07 | 3.08E+07 | 0.352E+08 | 3.57E+07 | 3.50E+07 | 3.49E+07 | 3.67E+07 |
| Neutron Pad | (-58.54, -22.47) | 21 degree | 5.89E+06 | 5.93E+06 | 6.00E+06 | 5.78E+06 | 6.24E+06 | 5.99E+06 | 6.50E+06 | 5.82E+06 | 5.05E+06 | 4.72E+06 | 0.595E+07 | 6.09E+06 | 5.89E+06 | 5.58E+06 | 4.36E+06 |
| | (-46.60, -41.95) | 42 degree | N/A | 4.36E+06 | 4.45E+06 | 4.98E+06 | 4.56E+06 | 4.48E+06 | 5.07E+06 | 4.29E+06 | 3.95E+06 | 3.46E+06 | 0.438E+07 | 4.29E+06 | 4.16E+06 | 4.15E+06 | 3.14E+06 |

C/E comparison

| $^{58}$Ni (n,p) | Position in cm | Grid Position | Experimental Value | HYU-TORT Korea | HYU-MCNP Korea | HYU-MCNPX Korea | Transpire Inc.-ATTILA USA | KI-MCU Russia | KOPEC-DORT Korea | WTI-MCNP Germany | VTT-TORT Finland | VTT-MT Finland | KI-LUCKY Russia | KAERI-DANTSYS Korea | VTT-MCNP-K Finland | VTT-MCNP-F Finland | SCK-MCNPX Belgium |
|---|---|---|---|---|---|---|---|---|---|---|---|---|---|---|---|---|---|
| Inner Baffle | ( -4.41, -0.63) | (-1,+2) | 1.51E+09 | 1.01 | 0.94 | 0.94 | 1.04 | 0.98 | 1.03 | 0.97 | 1.04 | 0.99 | 1.00 | 0.93 | 0.85 | 0.93 | 0.98 |
| | ( -4.41, -4.41) | (-1,-1) | 1.83E+09 | 1.01 | 0.94 | 0.94 | 1.02 | 0.98 | 1.03 | 0.97 | 0.98 | 1.10 | 0.98 | 0.92 | 0.93 | 1.02 | 0.94 |
| Outer Baffle | (-39.69, -0.63) | (-29,+2) | 5.80E+08 | 0.87 | 1.02 | 0.98 | 0.99 | 0.99 | 1.04 | 0.99 | 0.89 | 0.90 | 0.90 | 0.98 | 0.90 | 0.85 | 0.98 |
| | (-39.69, -5.67) | (-29,-2) | 5.52E+08 | 0.87 | 1.06 | 1.03 | 1.01 | 0.99 | 1.03 | 0.99 | 0.87 | 0.93 | 0.90 | 0.98 | 0.94 | 0.89 | 1.00 |
| | (-39.69, -11.97) | (-29,-7) | 4.47E+08 | 0.88 | 0.99 | 0.99 | 1.01 | 0.98 | 1.04 | 1.01 | 0.85 | 0.94 | 0.90 | 0.99 | 0.97 | 0.91 | 0.98 |
| | (-39.69, -18.27) | (-29,-12) | 2.62E+08 | 0.89 | 0.96 | 1.01 | 1.00 | 0.97 | 1.05 | 1.01 | 0.82 | 0.93 | 0.91 | 0.98 | 0.95 | 0.93 | 0.95 |
| | (-37.17, -20.79) | (-27,-14) | 2.75E+08 | 0.94 | 1.03 | 0.99 | 1.00 | 0.98 | 1.05 | 0.99 | 0.87 | 0.95 | 0.88 | 0.96 | 0.96 | 0.91 | 0.96 |
| | (-30.87, -20.79) | (-22,-14) | 5.44E+08 | 0.96 | 0.99 | 0.98 | 1.03 | 0.98 | 1.04 | 0.99 | 0.98 | 1.00 | 0.91 | 0.96 | 0.96 | 0.94 | 1.01 |
| | (-24.57, -20.79) | (-17,-14) | 8.69E+08 | 1.01 | 1.01 | 1.01 | 1.04 | 0.99 | 1.07 | 0.98 | 0.93 | 1.09 | 0.97 | 0.96 | 0.95 | 1.00 | 0.97 |
| Barrel | (-49.77, -0.63) | (-37,+2) | 7.36E+07 | 0.92 | 1.07 | 1.02 | 1.02 | 1.01 | 1.09 | 1.01 | 0.86 | 0.81 | 0.95 | 1.03 | 0.89 | 0.86 | 1.00 |
| | (-49.77, -9.45) | (-37,-5) | 6.13E+07 | 0.94 | 1.04 | 1.05 | 1.04 | 1.05 | 1.11 | 1.02 | 0.84 | 0.83 | 0.98 | 1.07 | 0.98 | 0.93 | 0.97 |
| | (-47.25, -18.27) | (-35,-12) | 6.02E+07 | 0.91 | 0.99 | 1.01 | 1.02 | 1.00 | 1.08 | 0.99 | 0.85 | 0.84 | 0.93 | 0.99 | 0.97 | 0.92 | 1.07 |
| | (-45.99, -22.05) | (-34,-15) | 5.06E+07 | 0.94 | 1.05 | 0.96 | 1.03 | 1.02 | 1.06 | 0.98 | 0.91 | 0.87 | 0.95 | 0.97 | 0.99 | 0.91 | 1.09 |
| | (-44.73, -24.57) | (-33,-17) | 4.50E+07 | 0.92 | 1.00 | 1.00 | 1.01 | 1.02 | 1.09 | 1.00 | 0.93 | 0.91 | 0.97 | 0.96 | 0.97 | 0.94 | 1.10 |
| | (-42.21, -28.35) | (-31,-20) | 4.16E+07 | 0.99 | 1.00 | 1.08 | 1.05 | 1.03 | 1.11 | 1.00 | 0.91 | 0.89 | 1.00 | 0.97 | 0.95 | 0.94 | 1.00 |
| | (-38.43, -33.39) | (-28,-24) | 3.67E+07 | 1.02 | 1.02 | 1.01 | 1.01 | 1.01 | 1.12 | 0.97 | 0.93 | 0.84 | 0.99 | 0.97 | 0.93 | 0.95 | 1.00 |
| | (-35.91, -35.91) | (-26,-26) | 3.59E+07 | 1.03 | 1.04 | 1.07 | 1.03 | 1.03 | 1.15 | 1.01 | 0.93 | 0.86 | 0.98 | 1.00 | 0.97 | 0.97 | 1.02 |
| Neutron Pad | (-58.54, -22.47) | 21 degree | 5.89E+06 | 1.01 | 1.02 | 0.98 | 1.06 | 1.02 | 1.10 | 0.99 | 0.86 | 0.80 | 1.01 | 1.03 | 1.00 | 0.95 | 0.74 |
| | (-46.60, -41.95) | 42 degree | N/A | N/A | N/A | N/A | N/A | N/A | N/A | N/A | N/A | N/A | N/A | N/A | N/A | N/A | N/A |
| | Number of positions within +-5% = | | | 8 | 13 | 14 | 16 | 18 | 7 | 18 | 3 | 3 | 11 | 15 | 12 | 3 | 13 |
| | Number of positions within +-10% = | | | 14 | 18 | 18 | 18 | 18 | 13 | 18 | 9 | 9 | 17 | 18 | 16 | 15 | 16 |
| | Number of positions within +-20% = | | | 18 | 18 | 18 | 18 | 18 | 18 | 18 | 18 | 18 | 18 | 18 | 18 | 18 | 17 |

# Table 4.6(b). Equivalent fission fluxes: $^{58}$Ni(n,p) detector results and C/E comparison in water zones

Calculated results

| $^{58}$Ni (n,p) | Position in cm | Grid Position | Experimental Value | HYU-TORT | HYU-MCNP | HYU-MCNPX | Transpire Inc.-ATTILA | KI-MCU | KOPEC-DORT | WTI-MCNP | VTT-TORT | VTT-MT | KI-LUCKY | KAERI-DANTSYS | VTT-MCNP-K | VTT-MCNP-F | SCK-MCNPX |
|---|---|---|---|---|---|---|---|---|---|---|---|---|---|---|---|---|---|
| | | | | Korea | Korea | Korea | USA | Russia | Korea | Germany | Finland | Finland | Russia | Korea | Finland | Finland | Belgium |
| Central Hole | ( 0.0, 0.0) | (+2.5,+2.5) | N/A | 1.14E+09 | 2.74E+08 | 2.84E+08 | 1.13E+09 | 6.74E+07 | 1.16E+09 | 1.08E+09 | 1.11E+09 | 1.02E+09 | 0.115E+10 | 1.05E+09 | 1.05E+09 | 1.14E+09 | 2.62E+08 |
| Water Gap | (-54.36, -9.59) | 10.75 degree | 2.09E+07 | 2.18E+07 | 2.27E+07 | 2.43E+07 | 2.34E+07 | 2.32E+07 | 2.46E+07 | 2.23E+07 | 2.02E+07 | 1.99E+07 | 0.222E+08 | 2.14E+07 | 2.14E+07 | 2.05E+07 | 2.20E+07 |
| | (-52.89, -15.80) | 16.63 degree | 2.06E+07 | 2.14E+07 | 2.19E+07 | 2.31E+07 | 2.26E+07 | 2.20E+07 | 2.41E+07 | 2.23E+07 | 2.01E+07 | 1.94E+07 | 0.214E+08 | 2.56E+07 | 2.09E+07 | 2.02E+07 | 2.19E+07 |
| | (-51.53, -19.78) | 21.14 degree | 1.96E+07 | 2.08E+07 | 2.20E+07 | 2.18E+07 | 2.22E+07 | 2.12E+07 | 2.32E+07 | 2.12E+07 | 1.95E+07 | 1.89E+07 | 0.208E+08 | 2.40E+07 | 2.09E+07 | 1.95E+07 | 2.16E+07 |
| | (-50.03, -23.33) | 25.62 degree | 1.77E+07 | 1.91E+07 | 2.07E+07 | 2.09E+07 | 2.02E+07 | 1.99E+07 | 2.07E+07 | 1.93E+07 | 1.75E+07 | 1.76E+07 | 0.190E+08 | 1.97E+07 | 2.03E+07 | 1.81E+07 | 1.99E+07 |
| | (-48.74, -25.91) | 28.78 degree | 1.62E+07 | 1.74E+07 | 1.78E+07 | 1.86E+07 | 1.87E+07 | 1.84E+07 | 1.95E+07 | 1.78E+07 | 1.67E+07 | 1.72E+07 | 0.178E+08 | 1.82E+07 | 1.77E+07 | 1.70E+07 | 2.04E+07 |
| | (-46.29, -30.06) | 33.89 degree | 1.48E+07 | 1.63E+07 | 1.78E+07 | 1.66E+07 | 1.72E+07 | 1.67E+07 | 1.79E+07 | 1.60E+07 | 1.52E+07 | 1.60E+07 | 0.160E+08 | 1.76E+07 | 1.57E+07 | 1.55E+07 | 1.89E+07 |
| | (-44.08, -33.22) | 37.44 degree | 1.39E+07 | 1.53E+07 | 1.50E+07 | 1.84E+07 | 1.55E+07 | 1.57E+07 | 1.72E+07 | 1.52E+07 | 1.45E+07 | 1.41E+07 | 0.155E+08 | 1.54E+07 | 1.50E+07 | 1.48E+07 | 1.79E+07 |
| | (-42.29, -35.48) | 40.99 degree | 1.32E+07 | 1.45E+07 | 1.59E+07 | 1.61E+07 | 1.54E+07 | 1.52E+07 | 1.67E+07 | 1.43E+07 | 1.41E+07 | 1.35E+07 | 0.150E+08 | 1.38E+07 | 1.44E+07 | 1.40E+07 | 1.25E+07 |
| | (-39.03, -39.03) | 45 degree | 1.31E+07 | 1.46E+07 | 1.42E+07 | 1.44E+07 | 1.51E+07 | 1.49E+07 | 1.65E+07 | 1.42E+07 | 1.39E+07 | 1.29E+07 | 0.146E+08 | 1.66E+07 | 1.40E+07 | 1.36E+07 | 1.41E+07 |
| Reflector | (-23.31, -23.31) | (-16,-16) | 6.32E+08 | 6.44E+08 | 6.29E+08 | 6.19E+08 | 6.62E+08 | 6.39E+08 | 6.83E+08 | 6.29E+08 | 6.35E+08 | 6.94E+08 | 0.628E+09 | 6.18E+08 | 6.12E+08 | 6.36E+08 | 6.44E+08 |
| | (-25.83, -25.83) | (-18,-18) | 3.41E+08 | 3.48E+08 | 3.45E+08 | 3.47E+08 | 3.56E+08 | 3.49E+08 | 3.77E+08 | 3.41E+08 | 3.35E+08 | 3.78E+08 | 0.343E+09 | 3.42E+08 | 3.33E+08 | 3.40E+08 | 3.50E+08 |
| | (-28.35, -28.35) | (-20,-20) | 1.88E+08 | 1.92E+08 | 1.90E+08 | 1.85E+08 | 1.97E+08 | 1.94E+08 | 2.13E+08 | 1.90E+08 | 1.85E+08 | 2.01E+08 | 0.191E+09 | 1.90E+08 | 1.83E+08 | 1.85E+08 | 1.93E+08 |
| | (-30.87, -30.87) | (-22,-22) | 1.05E+08 | 1.07E+08 | 1.09E+08 | 1.10E+08 | 1.11E+08 | 1.09E+08 | 1.23E+08 | 1.05E+08 | 9.64E+07 | 1.02E+08 | 0.109E+09 | 1.08E+08 | 1.06E+08 | 1.05E+08 | 1.17E+08 |
| | (-33.39, -33.39) | (-24,-24) | 5.91E+07 | 6.27E+07 | 6.58E+07 | 6.39E+07 | 6.47E+07 | 6.37E+07 | 7.28E+07 | 6.23E+07 | 5.59E+07 | 5.38E+07 | 0.632E+08 | 6.34E+07 | 6.15E+07 | 5.98E+07 | 6.05E+07 |

C/E comparison

| $^{58}$Ni (n,p) | Position in cm | Grid Position | Experimental Value | HYU-TORT | HYU-MCNP | HYU-MCNPX | Transpire Inc.-ATTILA | KI-MCU | KOPEC-DORT | WTI-MCNP | VTT-TORT | VTT-MT | KI-LUCKY | KAERI-DANTSYS | VTT-MCNP-K | VTT-MCNP-F | SCK-MCNPX |
|---|---|---|---|---|---|---|---|---|---|---|---|---|---|---|---|---|---|
| | | | | Korea | Korea | Korea | USA | Russia | Korea | Germany | Finland | Finland | Russia | Korea | Finland | Finland | Belgium |
| Central Hole | ( 0.0, 0.0) | (+2.5,+2.5) | N/A | N/A | N/A | N/A | N/A | N/A | N/A | N/A | N/A | N/A | N/A | N/A | N/A | N/A | N/A |
| Water Gap | (-54.36, -9.59) | 10.75 degree | 2.09E+07 | 1.04 | 1.09 | 1.16 | 1.12 | 1.11 | 1.18 | 1.07 | 0.97 | 0.95 | 1.06 | 1.02 | 1.02 | 0.98 | 1.05 |
| | (-52.89, -15.80) | 16.63 degree | 2.06E+07 | 1.04 | 1.06 | 1.12 | 1.10 | 1.07 | 1.17 | 1.08 | 0.98 | 0.94 | 1.04 | 1.24 | 1.01 | 0.98 | 1.06 |
| | (-51.53, -19.78) | 21.14 degree | 1.96E+07 | 1.06 | 1.12 | 1.11 | 1.13 | 1.08 | 1.18 | 1.08 | 0.99 | 0.96 | 1.06 | 1.22 | 1.07 | 1.00 | 1.10 |
| | (-50.03, -23.33) | 25.62 degree | 1.77E+07 | 1.08 | 1.17 | 1.18 | 1.14 | 1.12 | 1.17 | 1.09 | 0.99 | 0.99 | 1.07 | 1.11 | 1.15 | 1.02 | 1.12 |
| | (-48.74, -25.91) | 28.78 degree | 1.62E+07 | 1.07 | 1.10 | 1.15 | 1.15 | 1.14 | 1.20 | 1.10 | 1.03 | 1.06 | 1.10 | 1.12 | 1.10 | 1.05 | 1.26 |
| | (-46.29, -30.06) | 33.89 degree | 1.48E+07 | 1.10 | 1.20 | 1.12 | 1.16 | 1.13 | 1.21 | 1.08 | 1.03 | 1.08 | 1.08 | 1.19 | 1.06 | 1.05 | 1.28 |
| | (-44.08, -33.22) | 37.44 degree | 1.39E+07 | 1.10 | 1.08 | 1.32 | 1.12 | 1.13 | 1.24 | 1.10 | 1.05 | 1.01 | 1.12 | 1.11 | 1.08 | 1.06 | 1.29 |
| | (-42.29, -35.48) | 40.99 degree | 1.32E+07 | 1.10 | 1.21 | 1.22 | 1.17 | 1.15 | 1.26 | 1.08 | 1.07 | 1.02 | 1.14 | 1.04 | 1.09 | 1.06 | 0.95 |
| | (-39.03, -39.03) | 45 degree | 1.31E+07 | 1.11 | 1.08 | 1.10 | 1.15 | 1.14 | 1.26 | 1.09 | 1.06 | 0.99 | 1.11 | 1.27 | 1.07 | 1.04 | 1.08 |
| Reflector | (-23.31, -23.31) | (-16,-16) | 6.32E+08 | 1.02 | 1.00 | 0.98 | 1.05 | 1.01 | 1.08 | 0.99 | 1.01 | 1.10 | 0.99 | 0.98 | 0.97 | 1.01 | 1.02 |
| | (-25.83, -25.83) | (-18,-18) | 3.41E+08 | 1.02 | 1.01 | 1.02 | 1.04 | 1.02 | 1.11 | 1.00 | 0.98 | 1.11 | 1.01 | 1.00 | 0.98 | 1.00 | 1.03 |
| | (-28.35, -28.35) | (-20,-20) | 1.88E+08 | 1.02 | 1.01 | 0.98 | 1.05 | 1.03 | 1.13 | 1.01 | 0.98 | 1.07 | 1.02 | 1.01 | 0.97 | 0.99 | 1.03 |
| | (-30.87, -30.87) | (-22,-22) | 1.05E+08 | 1.02 | 1.04 | 1.05 | 1.06 | 1.04 | 1.17 | 1.00 | 0.92 | 0.98 | 1.04 | 1.03 | 1.01 | 1.00 | 1.12 |
| | (-33.39, -33.39) | (-24,-24) | 5.91E+07 | 1.06 | 1.11 | 1.08 | 1.09 | 1.08 | 1.23 | 1.05 | 0.95 | 0.91 | 1.07 | 1.07 | 1.04 | 1.01 | 1.02 |
| | Number of positions within +-5% = | | | 6 | 4 | 4 | 3 | 4 | 0 | 4 | 10 | 7 | 5 | 6 | 7 | 12 | 4 |
| | Number of positions within +-10% = | | | 11 | 8 | 5 | 6 | 7 | 1 | 14 | 14 | 13 | 11 | 7 | 13 | 14 | 8 |
| | Number of positions within +-20% = | | | 14 | 12 | 12 | 14 | 14 | 8 | 14 | 14 | 14 | 14 | 11 | 14 | 14 | 11 |

# Table 4.7(a). Equivalent fission fluxes: $^{115}$In(n,n′) detector results and C/E comparison in stainless steel zones

Calculated results

| $^{115}$In (n,n') | Position in cm | Grid Position | Experimental Value | HYU-TORT | HYU-MCNP | HYU-MCNPX | Transpire Inc.-ATTILA | KI-MCU | KOPEC-DORT | WTI-MCNP | VTT-TORT | VTT-MT | KI-LUCKY | KAERI-DANTSYS | VTT-MCNP-K | VTT-MCNP-F | SCK-MCNPX |
|---|---|---|---|---|---|---|---|---|---|---|---|---|---|---|---|---|---|
| | | | | Korea | Korea | Korea | USA | Russia | Korea | Germany | Finland | Finland | Russia | Korea | Finland | Finland | Belgium |
| Inner Baffle | ( -4.41, -0.63) | (-1,+2) | 1.94E+09 | 1.93E+09 | 1.84E+09 | 1.82E+09 | 1.97E+09 | 1.87E+09 | 1.95E+09 | 1.90E+09 | 1.98E+09 | 1.83E+09 | 0.190E+10 | 1.77E+09 | 1.63E+09 | 1.75E+09 | 1.84E+09 |
| | ( -4.41, -4.41) | (-1,-1) | 2.36E+09 | 2.30E+09 | 2.21E+09 | 2.22E+09 | 2.33E+09 | 2.24E+09 | 2.35E+09 | 2.27E+09 | 2.26E+09 | 2.38E+09 | 0.224E+10 | 2.11E+09 | 2.14E+09 | 2.34E+09 | 2.19E+09 |
| Outer Baffle | (-39.69, -0.63) | (-29,+2) | 7.14E+08 | 6.22E+08 | 7.18E+08 | 6.96E+08 | 6.98E+08 | 7.08E+08 | 7.29E+08 | 7.18E+08 | 6.36E+08 | 6.32E+08 | 0.640E+09 | 6.93E+08 | 6.44E+08 | 6.00E+08 | 6.96E+08 |
| | (-39.69, -5.67) | (-29,-2) | N/A | 5.92E+08 | 6.89E+08 | 6.94E+08 | 6.70E+08 | 6.70E+08 | 6.94E+08 | 6.80E+08 | 5.92E+08 | 6.12E+08 | 0.609E+09 | 6.59E+08 | 6.51E+08 | 6.02E+08 | 6.68E+08 |
| | (-39.69, -11.97) | (-29,-7) | 5.48E+08 | 4.86E+08 | 5.46E+08 | 5.52E+08 | 5.45E+08 | 5.42E+08 | 5.65E+08 | 5.59E+08 | 4.74E+08 | 5.01E+08 | 0.497E+09 | 5.38E+08 | 5.34E+08 | 4.95E+08 | 5.39E+08 |
| | (-39.69, -18.27) | (-29,-12) | 3.33E+08 | 2.96E+08 | 3.23E+08 | 3.29E+08 | 3.25E+08 | 3.24E+08 | 3.43E+08 | 3.35E+08 | 2.71E+08 | 2.98E+08 | 0.299E+09 | 3.21E+08 | 3.15E+08 | 3.00E+08 | 3.21E+08 |
| | (-37.17, -20.79) | (-27,-14) | 3.53E+08 | 3.24E+08 | 3.48E+08 | 3.40E+08 | 3.41E+08 | 3.35E+08 | 3.58E+08 | 3.46E+08 | 3.01E+08 | 3.15E+08 | 0.305E+09 | 3.32E+08 | 3.32E+08 | 3.14E+08 | 3.34E+08 |
| | (-30.87, -20.79) | (-22,-14) | N/A | 6.53E+08 | 6.71E+08 | 6.61E+08 | 6.82E+08 | 6.63E+08 | 6.98E+08 | 6.78E+08 | 6.69E+08 | 6.49E+08 | 0.612E+09 | 6.50E+08 | 6.48E+08 | 6.35E+08 | 6.60E+08 |
| | (-24.57, -20.79) | (-17,-14) | 1.12E+09 | 1.11E+09 | 1.09E+09 | 1.09E+09 | 1.13E+09 | 1.08E+09 | 1.16E+09 | 1.10E+09 | 1.02E+09 | 1.14E+09 | 0.106E+10 | 1.05E+09 | 1.05E+09 | 1.10E+09 | 1.06E+09 |
| Barrel | (-49.77, -0.63) | (-37,+2) | 8.97E+07 | 7.97E+07 | 9.03E+07 | 8.87E+07 | 8.80E+07 | 8.84E+07 | 9.32E+07 | 8.93E+07 | 7.50E+07 | 6.60E+07 | 0.833E+08 | 9.05E+07 | 7.81E+07 | 7.30E+07 | 8.55E+07 |
| | (-49.77, -9.45) | (-37,-5) | 7.90E+07 | 7.01E+07 | 7.83E+07 | 7.89E+07 | 7.76E+07 | 7.82E+07 | 8.22E+07 | 7.84E+07 | 6.41E+07 | 5.89E+07 | 0.730E+08 | 7.92E+07 | 7.43E+07 | 6.93E+07 | 7.56E+07 |
| | (-47.25, -18.27) | (-35,-12) | 7.91E+07 | 6.98E+07 | 7.67E+07 | 7.73E+07 | 7.76E+07 | 7.76E+07 | 8.11E+07 | 7.75E+07 | 6.50E+07 | 6.12E+07 | 0.709E+08 | 7.57E+07 | 7.51E+07 | 6.95E+07 | 7.74E+07 |
| | (-45.99, -22.05) | (-34,-15) | 6.90E+07 | 6.24E+07 | 6.72E+07 | 6.56E+07 | 6.75E+07 | 6.66E+07 | 6.97E+07 | 6.70E+07 | 6.04E+07 | 5.38E+07 | 0.628E+08 | 6.39E+07 | 6.48E+07 | 5.98E+07 | 6.76E+07 |
| | (-44.73, -24.57) | (-33,-17) | 6.05E+07 | 5.52E+07 | 5.94E+07 | 6.11E+07 | 5.98E+07 | 5.98E+07 | 6.35E+07 | 6.07E+07 | 5.48E+07 | 4.98E+07 | 0.570E+08 | 5.62E+07 | 5.75E+07 | 5.44E+07 | 6.09E+07 |
| | (-42.21, -28.35) | (-31,-20) | 5.37E+07 | 5.04E+07 | 5.29E+07 | 5.38E+07 | 5.39E+07 | 5.27E+07 | 5.65E+07 | 5.29E+07 | 4.73E+07 | 4.25E+07 | 0.509E+08 | 5.01E+07 | 5.02E+07 | 4.84E+07 | 5.09E+07 |
| | (-38.43, -33.39) | (-28,-24) | 4.36E+07 | 4.24E+07 | 4.35E+07 | 4.19E+07 | 4.32E+07 | 4.31E+07 | 4.73E+07 | 4.29E+07 | 3.94E+07 | 3.33E+07 | 0.420E+08 | 4.18E+07 | 4.04E+07 | 4.02E+07 | 4.13E+07 |
| | (-35.91, -35.91) | (-26,-26) | 4.38E+07 | 4.16E+07 | 4.26E+07 | 4.35E+07 | 4.27E+07 | 4.24E+07 | 4.69E+07 | 4.25E+07 | 3.84E+07 | 3.26E+07 | 0.404E+08 | 4.12E+07 | 3.99E+07 | 4.01E+07 | 4.08E+07 |
| Neutron Pad | (-58.54, -22.47) | 21 degree | 8.19E+06 | 7.35E+06 | 7.63E+06 | 7.87E+06 | 7.80E+06 | 7.40E+06 | 8.25E+06 | 7.66E+06 | 6.42E+06 | 5.35E+06 | 0.736E+07 | 7.47E+06 | 7.42E+06 | 6.84E+06 | 6.98E+06 |
| | (-46.60, -41.95) | 42 degree | 5.90E+06 | 5.21E+06 | 5.03E+06 | 5.58E+06 | 5.53E+06 | 5.29E+06 | 6.14E+06 | 5.47E+06 | 4.80E+06 | 3.72E+06 | 0.517E+07 | 5.12E+06 | 5.07E+06 | 4.92E+06 | 3.92E+06 |

C/E comparison

| $^{115}$In (n,n') | Position in cm | Grid Position | Experimental Value | HYU-TORT | HYU-MCNP | HYU-MCNPX | Transpire Inc.-ATTILA | KI-MCU | KOPEC-DORT | WTI-MCNP | VTT-TORT | VTT-MT | KI-LUCKY | KAERI-DANTSYS | VTT-MCNP-K | VTT-MCNP-F | SCK-MCNPX |
|---|---|---|---|---|---|---|---|---|---|---|---|---|---|---|---|---|---|
| | | | | Korea | Korea | Korea | USA | Russia | Korea | Germany | Finland | Finland | Russia | Korea | Finland | Finland | Belgium |
| Inner Baffle | ( -4.41, -0.63) | (-1,+2) | 1.94E+09 | 0.99 | 0.95 | 0.94 | 1.02 | 0.96 | 1.01 | 0.98 | 1.02 | 0.94 | 0.98 | 0.91 | 0.84 | 0.90 | 0.95 |
| | ( -4.41, -4.41) | (-1,-1) | 2.36E+09 | 0.98 | 0.94 | 0.94 | 0.99 | 0.95 | 1.00 | 0.96 | 0.96 | 1.01 | 0.95 | 0.90 | 0.91 | 0.99 | 0.93 |
| Outer Baffle | (-39.69, -0.63) | (-29,+2) | 7.14E+08 | 0.87 | 1.01 | 0.98 | 0.98 | 0.99 | 1.02 | 1.01 | 0.89 | 0.89 | 0.90 | 0.97 | 0.90 | 0.84 | 0.98 |
| | (-39.69, -5.67) | (-29,-2) | N/A | | | | | | | | | | | | | | |
| | (-39.69, -11.97) | (-29,-7) | 5.48E+08 | 0.89 | 1.00 | 1.01 | 0.99 | 0.99 | 1.03 | 1.02 | 0.86 | 0.91 | 0.91 | 0.98 | 0.98 | 0.90 | 0.98 |
| | (-39.69, -18.27) | (-29,-12) | 3.33E+08 | 0.89 | 0.97 | 0.99 | 0.98 | 0.97 | 1.03 | 1.01 | 0.81 | 0.89 | 0.90 | 0.96 | 0.95 | 0.90 | 0.96 |
| | (-37.17, -20.79) | (-27,-14) | 3.53E+08 | 0.92 | 0.99 | 0.96 | 0.97 | 0.95 | 1.01 | 0.98 | 0.85 | 0.89 | 0.86 | 0.94 | 0.94 | 0.89 | 0.95 |
| | (-30.87, -20.79) | (-22,-14) | N/A | | | | | | | | | | | | | | |
| | (-24.57, -20.79) | (-17,-14) | 1.12E+09 | 0.99 | 0.98 | 0.97 | 1.01 | 0.97 | 1.04 | 0.98 | 0.91 | 1.02 | 0.95 | 0.94 | 0.93 | 0.98 | 0.94 |
| Barrel | (-49.77, -0.63) | (-37,+2) | 8.97E+07 | 0.89 | 1.01 | 0.99 | 0.98 | 0.99 | 1.04 | 1.00 | 0.84 | 0.74 | 0.93 | 1.01 | 0.87 | 0.81 | 0.95 |
| | (-49.77, -9.45) | (-37,-5) | 7.90E+07 | 0.89 | 0.99 | 1.00 | 0.98 | 0.99 | 1.04 | 0.99 | 0.81 | 0.75 | 0.92 | 1.00 | 0.94 | 0.88 | 0.96 |
| | (-47.25, -18.27) | (-35,-12) | 7.91E+07 | 0.88 | 0.97 | 0.98 | 0.98 | 0.98 | 1.03 | 0.98 | 0.82 | 0.77 | 0.90 | 0.96 | 0.95 | 0.88 | 0.98 |
| | (-45.99, -22.05) | (-34,-15) | 6.90E+07 | 0.90 | 0.97 | 0.95 | 0.98 | 0.96 | 1.01 | 0.97 | 0.88 | 0.78 | 0.91 | 0.93 | 0.94 | 0.87 | 0.98 |
| | (-44.73, -24.57) | (-33,-17) | 6.05E+07 | 0.91 | 0.98 | 1.01 | 0.99 | 0.99 | 1.05 | 1.00 | 0.91 | 0.82 | 0.94 | 0.93 | 0.95 | 0.90 | 1.01 |
| | (-42.21, -28.35) | (-31,-20) | 5.37E+07 | 0.94 | 0.98 | 1.00 | 1.00 | 0.98 | 1.05 | 0.99 | 0.88 | 0.79 | 0.95 | 0.93 | 0.93 | 0.90 | 0.95 |
| | (-38.43, -33.39) | (-28,-24) | 4.36E+07 | 0.97 | 1.00 | 0.96 | 0.99 | 0.99 | 1.08 | 0.98 | 0.90 | 0.76 | 0.96 | 0.96 | 0.93 | 0.92 | 0.95 |
| | (-35.91, -35.91) | (-26,-26) | 4.38E+07 | 0.95 | 0.97 | 0.99 | 0.98 | 0.97 | 1.07 | 0.97 | 0.88 | 0.74 | 0.92 | 0.94 | 0.91 | 0.92 | 0.93 |
| Neutron Pad | (-58.54, -22.47) | 21 degree | 8.19E+06 | 0.90 | 0.93 | 0.96 | 0.95 | 0.90 | 1.01 | 0.93 | 0.78 | 0.65 | 0.90 | 0.91 | 0.91 | 0.84 | 0.85 |
| | (-46.60, -41.95) | 42 degree | 5.90E+06 | 0.88 | 0.85 | 0.95 | 0.94 | 0.90 | 1.04 | 0.93 | 0.81 | 0.63 | 0.88 | 0.87 | 0.86 | 0.83 | 0.66 |
| Number of positions within +-5% = | | | | 4 | 13 | 14 | 16 | 15 | 14 | 15 | 2 | 2 | 2 | 7 | 1 | 2 | 8 |
| Number of positions within +-10% = | | | | 9 | 16 | 17 | 17 | 16 | 17 | 17 | 5 | 4 | 11 | 15 | 14 | 8 | 15 |
| Number of positions within +-20% = | | | | 17 | 17 | 17 | 17 | 17 | 17 | 17 | 16 | 8 | 17 | 17 | 17 | 17 | 16 |

# Table 4.7(b). Equivalent fission fluxes: $^{115}$In(n,n′) detector results and C/E comparison in water zones

Calculated results

| $^{115}$In (n,n') | Position in cm | Grid Position | Experimental Value | HYU-TORT | HYU-MCNP | HYU-MCNPX | Transpire Inc.-ATTILA | KI-MCU | KOPEC-DORT | WTI-MCNP | VTT-TORT | VTT-MT | KI-LUCKY | KAERI-DANTSYS | VTT-MCNP-K | VTT-MCNP-F | SCK-MCNPX |
|---|---|---|---|---|---|---|---|---|---|---|---|---|---|---|---|---|---|
| | | | | Korea | Korea | Korea | USA | Russia | Korea | Germany | Finland | Finland | Russia | Korea | Finland | Finland | Belgium |
| Central Hole | ( 0.0, 0.0) | (+2.5,+2.5) | N/A | 1.28E+09 | 3.05E+08 | 3.11E+08 | 1.25E+09 | 7.57E+07 | 1.31E+09 | 1.24E+09 | 1.25E+09 | 1.12E+09 | 0.127E+10 | 1.17E+09 | 1.19E+09 | 1.30E+09 | 2.93E+08 |
| Water Gap | (-54.36, -9.59) | 10.75 degree | N/A | 2.37E+07 | 2.51E+07 | 2.52E+07 | 2.56E+07 | 2.54E+07 | 2.68E+07 | 2.51E+07 | 2.24E+07 | 2.18E+07 | 0.241E+08 | 2.31E+07 | 2.34E+07 | 2.24E+07 | 2.51E+07 |
| | (-52.89, -15.80) | 16.63 degree | 2.59E+07 | 2.42E+07 | 2.50E+07 | 2.57E+07 | 2.55E+07 | 2.51E+07 | 2.68E+07 | 2.56E+07 | 2.27E+07 | 2.14E+07 | 0.238E+08 | 2.92E+07 | 2.43E+07 | 2.28E+07 | 2.55E+07 |
| | (-51.53, -19.78) | 21.14 degree | 2.53E+07 | 2.35E+07 | 2.45E+07 | 2.55E+07 | 2.50E+07 | 2.45E+07 | 2.60E+07 | 2.46E+07 | 2.23E+07 | 2.14E+07 | 0.230E+08 | 2.76E+07 | 2.38E+07 | 2.22E+07 | 2.33E+07 |
| | (-50.03, -23.33) | 25.62 degree | 2.30E+07 | 2.22E+07 | 2.32E+07 | 2.28E+07 | 2.35E+07 | 2.30E+07 | 2.37E+07 | 2.28E+07 | 2.05E+07 | 1.95E+07 | 0.215E+08 | 2.30E+07 | 2.26E+07 | 2.09E+07 | 2.23E+07 |
| | (-48.74, -25.91) | 28.78 degree | 2.13E+07 | 2.00E+07 | 2.04E+07 | 2.09E+07 | 2.16E+07 | 2.12E+07 | 2.21E+07 | 2.12E+07 | 1.94E+07 | 1.93E+07 | 0.202E+08 | 2.13E+07 | 2.05E+07 | 1.96E+07 | 2.27E+07 |
| | (-46.29, -30.06) | 33.89 degree | 1.87E+07 | 1.82E+07 | 1.93E+07 | 1.88E+07 | 1.94E+07 | 1.87E+07 | 1.97E+07 | 1.85E+07 | 1.70E+07 | 1.77E+07 | 0.175E+08 | 2.01E+07 | 1.77E+07 | 1.75E+07 | 1.83E+07 |
| | (-44.08, -33.22) | 37.44 degree | N/A | 1.66E+07 | 1.64E+07 | 1.78E+07 | 1.69E+07 | 1.69E+07 | 1.83E+07 | 1.69E+07 | 1.58E+07 | 1.48E+07 | 0.165E+08 | 1.73E+07 | 1.62E+07 | 1.59E+07 | 1.68E+07 |
| | (-42.29, -35.48) | 40.99 degree | N/A | 1.51E+07 | 1.62E+07 | 1.67E+07 | 1.64E+07 | 1.61E+07 | 1.74E+07 | 1.58E+07 | 1.49E+07 | 1.39E+07 | 0.156E+08 | 1.46E+07 | 1.54E+07 | 1.50E+07 | 1.43E+07 |
| | (-39.03, -39.03) | 45 degree | 1.57E+07 | 1.48E+07 | 1.49E+07 | 1.51E+07 | 1.57E+07 | 1.55E+07 | 1.70E+07 | 1.51E+07 | 1.45E+07 | 1.29E+07 | 0.149E+08 | 1.78E+07 | 1.47E+07 | 1.44E+07 | 1.36E+07 |
| Reflector | (-23.31, -23.31) | (-16,-16) | 7.91E+08 | 7.56E+08 | 7.45E+08 | 7.24E+08 | 7.78E+08 | 7.40E+08 | 7.89E+08 | 7.46E+08 | 7.48E+08 | 8.20E+08 | 0.722E+09 | 7.17E+08 | 7.21E+08 | 7.45E+08 | 7.33E+08 |
| | (-25.83, -25.83) | (-18,-18) | 4.00E+08 | 3.77E+08 | 3.75E+08 | 3.72E+08 | 3.84E+08 | 3.74E+08 | 4.04E+08 | 3.74E+08 | 3.65E+08 | 4.22E+08 | 0.368E+09 | 3.69E+08 | 3.64E+08 | 3.71E+08 | 3.68E+08 |
| | (-28.35, -28.35) | (-20,-20) | 2.07E+08 | 1.96E+08 | 1.97E+08 | 1.90E+08 | 2.02E+08 | 1.98E+08 | 2.15E+08 | 1.97E+08 | 1.91E+08 | 2.10E+08 | 0.194E+09 | 1.95E+08 | 1.90E+08 | 1.92E+08 | 1.94E+08 |
| | (-30.87, -30.87) | (-22,-22) | 1.11E+08 | 1.04E+08 | 1.07E+08 | 1.07E+08 | 1.09E+08 | 1.06E+08 | 1.19E+08 | 1.06E+08 | 9.49E+07 | 9.86E+07 | 0.106E+09 | 1.07E+08 | 1.04E+08 | 1.04E+08 | 1.14E+08 |
| | (-33.39, -33.39) | (-24,-24) | 6.66E+07 | 6.10E+07 | 6.43E+07 | 6.29E+07 | 6.42E+07 | 6.29E+07 | 7.09E+07 | 6.25E+07 | 5.59E+07 | 5.01E+07 | 0.622E+08 | 6.28E+07 | 6.07E+07 | 6.02E+07 | 6.07E+07 |

C/E comparison

| $^{115}$In (n,n') | Position in cm | Grid Position | Experimental Value | HYU-TORT | HYU-MCNP | HYU-MCNPX | Transpire Inc.-ATTILA | KI-MCU | KOPEC-DORT | WTI-MCNP | VTT-TORT | VTT-MT | KI-LUCKY | KAERI-DANTSYS | VTT-MCNP-K | VTT-MCNP-F | SCK-MCNPX |
|---|---|---|---|---|---|---|---|---|---|---|---|---|---|---|---|---|---|
| | | | | Korea | Korea | Korea | USA | Russia | Korea | Germany | Finland | Finland | Russia | Korea | Finland | Finland | Belgium |
| Central Hole | ( 0.0, 0.0) | (+2.5,+2.5) | N/A | | | | | | | | | | | | | | |
| Water Gap | (-54.36, -9.59) | 10.75 degree | N/A | | | | | | | | | | | | | | |
| | (-52.89, -15.80) | 16.63 degree | 2.59E+07 | 0.93 | 0.97 | 0.99 | 0.99 | 0.97 | 1.03 | 0.99 | 0.88 | 0.83 | 0.92 | 1.13 | 0.94 | 0.88 | 0.99 |
| | (-51.53, -19.78) | 21.14 degree | 2.53E+07 | 0.93 | 0.97 | 1.01 | 0.99 | 0.97 | 1.03 | 0.97 | 0.88 | 0.84 | 0.91 | 1.09 | 0.94 | 0.88 | 0.92 |
| | (-50.03, -23.33) | 25.62 degree | 2.30E+07 | 0.97 | 1.01 | 0.99 | 1.02 | 1.00 | 1.03 | 0.99 | 0.89 | 0.85 | 0.93 | 1.00 | 0.98 | 0.91 | 0.97 |
| | (-48.74, -25.91) | 28.78 degree | 2.13E+07 | 0.94 | 0.96 | 0.98 | 1.01 | 0.99 | 1.04 | 0.99 | 0.91 | 0.91 | 0.95 | 1.00 | 0.96 | 0.92 | 1.06 |
| | (-46.29, -30.06) | 33.89 degree | 1.87E+07 | 0.97 | 1.03 | 1.01 | 1.04 | 1.00 | 1.05 | 0.99 | 0.91 | 0.95 | 0.94 | 1.07 | 0.95 | 0.93 | 0.98 |
| | (-44.08, -33.22) | 37.44 degree | N/A | | | | | | | | | | | | | | |
| | (-42.29, -35.48) | 40.99 degree | N/A | | | | | | | | | | | | | | |
| | (-39.03, -39.03) | 45 degree | 1.57E+07 | 0.94 | 0.95 | 0.96 | 1.00 | 0.99 | 1.08 | 0.96 | 0.93 | 0.82 | 0.95 | 1.13 | 0.93 | 0.92 | 0.87 |
| Reflector | (-23.31, -23.31) | (-16,-16) | 7.91E+08 | 0.96 | 0.94 | 0.92 | 0.98 | 0.94 | 1.00 | 0.94 | 0.95 | 1.04 | 0.91 | 0.91 | 0.91 | 0.94 | 0.93 |
| | (-25.83, -25.83) | (-18,-18) | 4.00E+08 | 0.94 | 0.94 | 0.93 | 0.96 | 0.94 | 1.01 | 0.94 | 0.91 | 1.06 | 0.92 | 0.92 | 0.91 | 0.93 | 0.92 |
| | (-28.35, -28.35) | (-20,-20) | 2.07E+08 | 0.95 | 0.95 | 0.92 | 0.97 | 0.96 | 1.04 | 0.95 | 0.92 | 1.02 | 0.94 | 0.94 | 0.92 | 0.93 | 0.94 |
| | (-30.87, -30.87) | (-22,-22) | 1.11E+08 | 0.93 | 0.96 | 0.96 | 0.98 | 0.96 | 1.07 | 0.95 | 0.85 | 0.89 | 0.95 | 0.96 | 0.94 | 0.94 | 1.02 |
| | (-33.39, -33.39) | (-24,-24) | 6.66E+07 | 0.92 | 0.97 | 0.94 | 0.96 | 0.94 | 1.06 | 0.94 | 0.84 | 0.75 | 0.93 | 0.94 | 0.91 | 0.90 | 0.91 |
| Number of positions within +-5% = | | | | 3 | 8 | 7 | 11 | 8 | 7 | 8 | 0 | 2 | 1 | 3 | 2 | 0 | 4 |
| Number of positions within +-10% = | | | | 11 | 11 | 11 | 11 | 11 | 11 | 11 | 6 | 5 | 11 | 9 | 11 | 9 | 10 |
| Number of positions within +-20% = | | | | 11 | 11 | 11 | 11 | 11 | 11 | 11 | 11 | 10 | 11 | 11 | 11 | 11 | 11 |

# Table 4.8(a). Equivalent fission fluxes: $^{103}$Rh(n,n′) detector results and C/E comparison in stainless steel zones

Calculated results

| $^{103}$Rh (n,n') | Position in cm | Grid Position | Experimental Value | HYU-TORT | HYU-MCNP | HYU-MCNPX | Transpire Inc.-ATTILA | KI-MCU | KOPEC-DORT | WTI-MCNP | VTT-TORT | VTT-MT | KI-LUCKY | KAERI-DANTSYS | VTT-MCNP-K | VTT-MCNP-F | SCK-MCNPX |
|---|---|---|---|---|---|---|---|---|---|---|---|---|---|---|---|---|---|
| | | | | Korea | Korea | Korea | USA | Russia | Korea | Germany | Finland | Finland | Russia | Korea | Finland | Finland | Belgium |
| Inner Baffle | ( -4.41, -0.63) | (-1,+2) | 2.40E+09 | 2.30E+09 | 2.23E+09 | 2.22E+09 | 2.36E+09 | 2.28E+09 | 2.37E+09 | 2.28E+09 | 2.40E+09 | 2.18E+09 | 0.230E+10 | 2.16E+09 | 1.97E+09 | 2.12E+09 | 2.22E+09 |
| | ( -4.41, -4.41) | (-1,-1) | 2.82E+09 | 2.73E+09 | 2.67E+09 | 2.67E+09 | 2.78E+09 | 2.72E+09 | 2.83E+09 | 2.72E+09 | 2.73E+09 | 2.77E+09 | 0.272E+10 | 2.55E+09 | 2.53E+09 | 2.80E+09 | 2.65E+09 |
| Outer Baffle | (-39.69, -0.63) | (-29,+2) | N/A | 7.32E+08 | 8.48E+08 | 8.36E+08 | 8.22E+08 | 8.49E+08 | 8.65E+08 | 8.47E+08 | 7.54E+08 | 7.43E+08 | 0.763E+09 | 8.24E+08 | 7.72E+08 | 7.04E+08 | 8.24E+08 |
| | (-39.69, -5.67) | (-29,-2) | 8.06E+08 | 6.97E+08 | 8.13E+08 | 8.23E+08 | 7.84E+08 | 8.07E+08 | 8.24E+08 | 8.02E+08 | 7.05E+08 | 7.16E+08 | 0.726E+09 | 7.83E+08 | 7.73E+08 | 7.20E+08 | 7.98E+08 |
| | (-39.69, -11.97) | (-29,-7) | 6.54E+08 | 5.72E+08 | 6.54E+08 | 6.55E+08 | 6.39E+08 | 6.54E+08 | 6.72E+08 | 6.60E+08 | 5.65E+08 | 5.87E+08 | 0.593E+09 | 6.40E+08 | 6.38E+08 | 5.86E+08 | 6.42E+08 |
| | (-39.69, -18.27) | (-29,-12) | 3.97E+08 | 3.54E+08 | 3.93E+08 | 3.97E+08 | 3.88E+08 | 3.99E+08 | 4.15E+08 | 4.02E+08 | 3.29E+08 | 3.56E+08 | 0.363E+09 | 3.89E+08 | 3.94E+08 | 3.59E+08 | 3.89E+08 |
| | (-37.17, -20.79) | (-27,-14) | 4.20E+08 | 3.88E+08 | 4.21E+08 | 4.12E+08 | 4.07E+08 | 4.13E+08 | 4.34E+08 | 4.16E+08 | 3.66E+08 | 3.74E+08 | 0.372E+09 | 4.03E+08 | 4.04E+08 | 3.76E+08 | 4.06E+08 |
| | (-30.87, -20.79) | (-22,-14) | N/A | 7.74E+08 | 8.09E+08 | 8.01E+08 | 8.06E+08 | 8.06E+08 | 8.39E+08 | 8.07E+08 | 8.03E+08 | 7.62E+08 | 0.738E+09 | 7.82E+08 | 7.81E+08 | 7.50E+08 | 7.92E+08 |
| | (-24.57, -20.79) | (-17,-14) | 1.37E+09 | 1.33E+09 | 1.32E+09 | 1.32E+09 | 1.34E+09 | 1.32E+09 | 1.40E+09 | 1.32E+09 | 1.24E+09 | 1.35E+09 | 0.128E+10 | 1.27E+09 | 1.25E+09 | 1.32E+09 | 1.28E+09 |
| Barrel | (-49.77, -0.63) | (-37,+2) | 1.04E+08 | 9.25E+07 | 1.05E+08 | 1.04E+08 | 1.01E+08 | 1.05E+08 | 1.09E+08 | 1.04E+08 | 8.79E+07 | 7.52E+07 | 0.988E+08 | 1.07E+08 | 9.10E+07 | 8.74E+07 | 1.01E+08 |
| | (-49.77, -9.45) | (-37,-5) | 9.49E+07 | 8.33E+07 | 9.37E+07 | 9.45E+07 | 9.20E+07 | 9.43E+07 | 9.88E+07 | 9.35E+07 | 7.74E+07 | 6.88E+07 | 0.886E+08 | 9.44E+07 | 9.02E+07 | 8.45E+07 | 9.00E+07 |
| | (-47.25, -18.27) | (-35,-12) | 9.60E+07 | 8.53E+07 | 9.42E+07 | 9.55E+07 | 9.41E+07 | 9.57E+07 | 9.98E+07 | 9.47E+07 | 8.03E+07 | 7.37E+07 | 0.883E+08 | 9.31E+07 | 9.31E+07 | 8.50E+07 | 9.65E+07 |
| | (-45.99, -22.05) | (-34,-15) | 8.50E+07 | 7.78E+07 | 8.43E+07 | 8.27E+07 | 8.38E+07 | 8.43E+07 | 8.80E+07 | 8.35E+07 | 7.62E+07 | 6.57E+07 | 0.796E+08 | 8.03E+07 | 8.03E+07 | 7.62E+07 | 8.46E+07 |
| | (-44.73, -24.57) | (-33,-17) | 7.63E+07 | 6.93E+07 | 7.58E+07 | 7.66E+07 | 7.47E+07 | 7.59E+07 | 8.00E+07 | 7.59E+07 | 6.90E+07 | 6.08E+07 | 0.724E+08 | 7.07E+07 | 7.25E+07 | 6.94E+07 | 7.60E+07 |
| | (-42.21, -28.35) | (-31,-20) | 6.55E+07 | 6.11E+07 | 6.48E+07 | 6.51E+07 | 6.49E+07 | 6.49E+07 | 6.92E+07 | 6.43E+07 | 5.81E+07 | 5.06E+07 | 0.625E+08 | 6.15E+07 | 5.94E+07 | 5.78E+07 | 6.25E+07 |
| | (-38.43, -33.39) | (-28,-24) | 5.29E+07 | 4.94E+07 | 5.15E+07 | 5.00E+07 | 5.08E+07 | 5.14E+07 | 5.60E+07 | 5.05E+07 | 4.64E+07 | 3.83E+07 | 0.499E+08 | 4.97E+07 | 4.81E+07 | 4.61E+07 | 4.91E+07 |
| | (-35.91, -35.91) | (-26,-26) | 5.11E+07 | 4.81E+07 | 4.99E+07 | 5.09E+07 | 4.98E+07 | 5.00E+07 | 5.51E+07 | 4.96E+07 | 4.51E+07 | 3.72E+07 | 0.478E+08 | 4.84E+07 | 4.80E+07 | 4.67E+07 | 4.71E+07 |
| Neutron Pad | (-58.54, -22.47) | 21 degree | N/A | 9.19E+06 | 9.74E+06 | 9.99E+06 | 9.68E+06 | 9.23E+06 | 1.06E+07 | 9.66E+06 | 8.13E+06 | 6.43E+06 | 0.932E+07 | 9.27E+06 | 9.39E+06 | 8.09E+06 | 8.52E+06 |
| | (-46.60, -41.95) | 42 degree | N/A | 6.48E+06 | 6.50E+06 | 6.90E+06 | 6.83E+06 | 6.50E+06 | 7.80E+06 | 6.86E+06 | 6.01E+06 | 4.43E+06 | 0.643E+07 | 6.29E+06 | 6.84E+06 | 5.48E+06 | 5.06E+06 |

C/E comparison

| $^{103}$Rh (n,n') | Position in cm | Grid Position | Experimental Value | HYU-TORT | HYU-MCNP | HYU-MCNPX | Transpire Inc.-ATTILA | KI-MCU | KOPEC-DORT | WTI-MCNP | VTT-TORT | VTT-MT | KI-LUCKY | KAERI-DANTSYS | VTT-MCNP-K | VTT-MCNP-F | SCK-MCNPX |
|---|---|---|---|---|---|---|---|---|---|---|---|---|---|---|---|---|---|
| | | | | Korea | Korea | Korea | USA | Russia | Korea | Germany | Finland | Finland | Russia | Korea | Finland | Finland | Belgium |
| Inner Baffle | ( -4.41, -0.63) | (-1,+2) | 2.40E+09 | 0.96 | 0.93 | 0.92 | 0.98 | 0.95 | 0.99 | 0.95 | 1.00 | 0.91 | 0.96 | 0.90 | 0.82 | 0.88 | 0.92 |
| | ( -4.41, -4.41) | (-1,-1) | 2.82E+09 | 0.97 | 0.95 | 0.95 | 0.99 | 0.96 | 1.00 | 0.96 | 0.97 | 0.98 | 0.96 | 0.90 | 0.90 | 0.99 | 0.94 |
| Outer Baffle | (-39.69, -0.63) | (-29,+2) | N/A | | | | | | | | | | | | | | |
| | (-39.69, -5.67) | (-29,-2) | 8.06E+08 | 0.86 | 1.01 | 1.02 | 0.97 | 1.00 | 1.02 | 0.99 | 0.87 | 0.89 | 0.90 | 0.97 | 0.96 | 0.89 | 0.99 |
| | (-39.69, -11.97) | (-29,-7) | 6.54E+08 | 0.88 | 1.00 | 1.00 | 0.98 | 1.00 | 1.03 | 1.01 | 0.86 | 0.90 | 0.91 | 0.98 | 0.98 | 0.90 | 0.98 |
| | (-39.69, -18.27) | (-29,-12) | 3.97E+08 | 0.89 | 0.99 | 1.00 | 0.98 | 1.00 | 1.05 | 1.01 | 0.83 | 0.90 | 0.91 | 0.98 | 0.99 | 0.91 | 0.98 |
| | (-37.17, -20.79) | (-27,-14) | 4.20E+08 | 0.92 | 1.00 | 0.98 | 0.97 | 0.98 | 1.03 | 0.99 | 0.87 | 0.89 | 0.89 | 0.96 | 0.96 | 0.90 | 0.97 |
| | (-30.87, -20.79) | (-22,-14) | N/A | | | | | | | | | | | | | | |
| | (-24.57, -20.79) | (-17,-14) | 1.37E+09 | 0.97 | 0.96 | 0.96 | 0.98 | 0.96 | 1.02 | 0.96 | 0.91 | 0.98 | 0.93 | 0.93 | 0.91 | 0.96 | 0.94 |
| Barrel | (-49.77, -0.63) | (-37,+2) | 1.04E+08 | 0.89 | 1.01 | 1.00 | 0.98 | 1.00 | 1.05 | 1.00 | 0.85 | 0.72 | 0.95 | 1.03 | 0.87 | 0.84 | 0.97 |
| | (-49.77, -9.45) | (-37,-5) | 9.49E+07 | 0.88 | 0.99 | 1.00 | 0.97 | 0.99 | 1.04 | 0.99 | 0.82 | 0.73 | 0.93 | 0.99 | 0.95 | 0.89 | 0.95 |
| | (-47.25, -18.27) | (-35,-12) | 9.60E+07 | 0.89 | 0.98 | 0.99 | 0.98 | 1.00 | 1.04 | 0.99 | 0.84 | 0.77 | 0.92 | 0.97 | 0.97 | 0.89 | 1.01 |
| | (-45.99, -22.05) | (-34,-15) | 8.50E+07 | 0.92 | 0.99 | 0.97 | 0.99 | 0.99 | 1.04 | 0.98 | 0.90 | 0.77 | 0.94 | 0.94 | 0.95 | 0.90 | 1.00 |
| | (-44.73, -24.57) | (-33,-17) | 7.63E+07 | 0.91 | 0.99 | 1.00 | 0.98 | 0.99 | 1.05 | 0.99 | 0.90 | 0.80 | 0.95 | 0.93 | 0.95 | 0.91 | 1.00 |
| | (-42.21, -28.35) | (-31,-20) | 6.55E+07 | 0.93 | 0.99 | 0.99 | 0.99 | 0.99 | 1.06 | 0.98 | 0.89 | 0.77 | 0.95 | 0.94 | 0.91 | 0.88 | 0.95 |
| | (-38.43, -33.39) | (-28,-24) | 5.29E+07 | 0.93 | 0.97 | 0.94 | 0.96 | 0.97 | 1.06 | 0.96 | 0.88 | 0.72 | 0.94 | 0.94 | 0.91 | 0.87 | 0.93 |
| | (-35.91, -35.91) | (-26,-26) | 5.11E+07 | 0.94 | 0.98 | 1.00 | 0.97 | 0.98 | 1.08 | 0.97 | 0.88 | 0.73 | 0.94 | 0.95 | 0.94 | 0.91 | 0.92 |
| Neutron Pad | (-58.54, -22.47) | 21 degree | N/A | | | | | | | | | | | | | | |
| | (-46.60, -41.95) | 42 degree | N/A | | | | | | | | | | | | | | |
| Number of positions within +-5% = | | | | 3 | 13 | 12 | 15 | 15 | 12 | 15 | 2 | 2 | 3 | 7 | 5 | 2 | 9 |
| Number of positions within +-10% = | | | | 9 | 15 | 15 | 15 | 15 | 15 | 15 | 4 | 3 | 14 | 14 | 12 | 5 | 15 |
| Number of positions within +-20% = | | | | 15 | 15 | 15 | 15 | 15 | 15 | 15 | 15 | 7 | 15 | 15 | 15 | 15 | 15 |

# Table 4.8(b). Equivalent fission fluxes: $^{103}$Rh(n,n′) detector results and C/E comparison in water zones

Calculated results

| $^{103}$Rh (n,n') | Position in cm | Grid Position | Experimental Value | HYU-TORT | HYU-MCNP | HYU-MCNPX | Transpire Inc.-ATTILA | KI-MCU | KOPEC-DORT | WTI-MCNP | VTT-TORT | VTT-MT | KI-LUCKY | KAERI-DANTSYS | VTT-MCNP-K | VTT-MCNP-F | SCK-MCNPX |
|---|---|---|---|---|---|---|---|---|---|---|---|---|---|---|---|---|---|
| | | | | Korea | Korea | Korea | USA | Russia | Korea | Germany | Finland | Finland | Russia | Korea | Finland | Finland | Belgium |
| Central Hole | ( 0.0, 0.0) | (+2.5,+2.5) | N/A | 1.44E+09 | 3.47E+08 | 3.52E+08 | 1.40E+09 | 8.73E+07 | 1.50E+09 | 1.41E+09 | 1.42E+09 | 1.24E+09 | 0.144E+10 | 1.33E+09 | 1.37E+09 | 1.51E+09 | 3.30E+08 |
| Water Gap | (-54.36, -9.59) | 10.75 degree | 2.98E+07 | 2.70E+07 | 2.92E+07 | 2.93E+07 | 2.93E+07 | 2.95E+07 | 3.10E+07 | 2.90E+07 | 2.61E+07 | 2.51E+07 | 0.277E+08 | 2.64E+07 | 2.94E+07 | 2.57E+07 | 2.94E+07 |
| | (-52.89, -15.80) | 16.63 degree | 3.13E+07 | 2.82E+07 | 2.92E+07 | 2.98E+07 | 2.97E+07 | 2.96E+07 | 3.14E+07 | 2.97E+07 | 2.67E+07 | 2.50E+07 | 0.277E+08 | 3.45E+07 | 2.88E+07 | 2.73E+07 | 2.94E+07 |
| | (-51.53, -19.78) | 21.14 degree | 2.99E+07 | 2.75E+07 | 2.89E+07 | 3.01E+07 | 2.92E+07 | 2.91E+07 | 3.07E+07 | 2.90E+07 | 2.64E+07 | 2.52E+07 | 0.269E+08 | 3.30E+07 | 2.96E+07 | 2.65E+07 | 2.80E+07 |
| | (-50.03, -23.33) | 25.62 degree | 2.80E+07 | 2.63E+07 | 2.74E+07 | 2.71E+07 | 2.80E+07 | 2.76E+07 | 2.84E+07 | 2.72E+07 | 2.47E+07 | 2.27E+07 | 0.255E+08 | 2.76E+07 | 2.61E+07 | 2.48E+07 | 2.60E+07 |
| | (-48.74, -25.91) | 28.78 degree | 2.60E+07 | 2.37E+07 | 2.46E+07 | 2.52E+07 | 2.55E+07 | 2.55E+07 | 2.64E+07 | 2.53E+07 | 2.33E+07 | 2.29E+07 | 0.239E+08 | 2.58E+07 | 2.48E+07 | 2.34E+07 | 2.64E+07 |
| | (-46.29, -30.06) | 33.89 degree | 2.19E+07 | 2.13E+07 | 2.24E+07 | 2.24E+07 | 2.27E+07 | 2.21E+07 | 2.31E+07 | 2.18E+07 | 2.00E+07 | 2.09E+07 | 0.203E+08 | 2.40E+07 | 2.09E+07 | 2.06E+07 | 2.17E+07 |
| | (-44.08, -33.22) | 37.44 degree | N/A | 1.91E+07 | 1.92E+07 | 2.04E+07 | 1.93E+07 | 1.97E+07 | 2.12E+07 | 1.96E+07 | 1.85E+07 | 1.70E+07 | 0.190E+08 | 2.04E+07 | 1.78E+07 | 1.90E+07 | 1.89E+07 |
| | (-42.29, -35.48) | 40.99 degree | 1.87E+07 | 1.70E+07 | 1.84E+07 | 1.88E+07 | 1.87E+07 | 1.86E+07 | 1.99E+07 | 1.81E+07 | 1.72E+07 | 1.59E+07 | 0.177E+08 | 1.68E+07 | 1.82E+07 | 1.61E+07 | 1.66E+07 |
| | (-39.03, -39.03) | 45 degree | 1.83E+07 | 1.66E+07 | 1.68E+07 | 1.73E+07 | 1.77E+07 | 1.77E+07 | 1.94E+07 | 1.72E+07 | 1.65E+07 | 1.45E+07 | 0.168E+08 | 2.05E+07 | 1.57E+07 | 1.56E+07 | 1.55E+07 |
| Reflector | (-23.31, -23.31) | (-16,-16) | 8.46E+08 | 8.71E+08 | 8.66E+08 | 8.51E+08 | 9.05E+08 | 8.71E+08 | 9.20E+08 | 8.67E+08 | 8.77E+08 | 9.59E+08 | 0.836E+09 | 8.35E+08 | 8.26E+08 | 8.56E+08 | 8.57E+08 |
| | (-25.83, -25.83) | (-18,-18) | 4.35E+08 | 4.16E+08 | 4.19E+08 | 4.16E+08 | 4.25E+08 | 4.22E+08 | 4.50E+08 | 4.16E+08 | 4.08E+08 | 4.80E+08 | 0.408E+09 | 4.11E+08 | 4.09E+08 | 4.10E+08 | 4.11E+08 |
| | (-28.35, -28.35) | (-20,-20) | 2.21E+08 | 2.10E+08 | 2.14E+08 | 2.08E+08 | 2.16E+08 | 2.16E+08 | 2.32E+08 | 2.13E+08 | 2.07E+08 | 2.30E+08 | 0.210E+09 | 2.10E+08 | 2.04E+08 | 2.09E+08 | 2.10E+08 |
| | (-30.87, -30.87) | (-22,-22) | 1.13E+08 | 1.08E+08 | 1.13E+08 | 1.13E+08 | 1.15E+08 | 1.14E+08 | 1.25E+08 | 1.12E+08 | 1.00E+08 | 1.03E+08 | 0.112E+09 | 1.13E+08 | 1.06E+08 | 1.11E+08 | 1.18E+08 |
| | (-33.39, -33.39) | (-24,-24) | 7.27E+07 | 6.43E+07 | 6.85E+07 | 6.73E+07 | 6.83E+07 | 6.80E+07 | 7.57E+07 | 6.68E+07 | 6.01E+07 | 5.24E+07 | 0.665E+08 | 6.71E+07 | 6.62E+07 | 6.39E+07 | 6.52E+07 |

C/E comparison

| $^{103}$Rh (n,n') | Position in cm | Grid Position | Experimental Value | HYU-TORT | HYU-MCNP | HYU-MCNPX | Transpire Inc.-ATTILA | KI-MCU | KOPEC-DORT | WTI-MCNP | VTT-TORT | VTT-MT | KI-LUCKY | KAERI-DANTSYS | VTT-MCNP-K | VTT-MCNP-F | SCK-MCNPX |
|---|---|---|---|---|---|---|---|---|---|---|---|---|---|---|---|---|---|
| | | | | Korea | Korea | Korea | USA | Russia | Korea | Germany | Finland | Finland | Russia | Korea | Finland | Finland | Belgium |
| Central Hole | ( 0.0, 0.0) | (+2.5,+2.5) | N/A | | | | | | | | | | | | | | |
| Water Gap | (-54.36, -9.59) | 10.75 degree | 2.98E+07 | 0.91 | 0.98 | 0.98 | 0.98 | 0.99 | 1.04 | 0.97 | 0.87 | 0.84 | 0.93 | 0.89 | 0.99 | 0.86 | 0.99 |
| | (-52.89, -15.80) | 16.63 degree | 3.13E+07 | 0.90 | 0.93 | 0.95 | 0.95 | 0.95 | 1.00 | 0.95 | 0.85 | 0.80 | 0.88 | 1.10 | 0.92 | 0.87 | 0.94 |
| | (-51.53, -19.78) | 21.14 degree | 2.99E+07 | 0.92 | 0.97 | 1.01 | 0.98 | 0.97 | 1.03 | 0.97 | 0.88 | 0.84 | 0.90 | 1.10 | 0.99 | 0.89 | 0.94 |
| | (-50.03, -23.33) | 25.62 degree | 2.80E+07 | 0.94 | 0.98 | 0.97 | 1.00 | 0.98 | 1.01 | 0.97 | 0.88 | 0.81 | 0.91 | 0.98 | 0.93 | 0.88 | 0.93 |
| | (-48.74, -25.91) | 28.78 degree | 2.60E+07 | 0.91 | 0.94 | 0.97 | 0.98 | 0.98 | 1.02 | 0.97 | 0.90 | 0.88 | 0.92 | 0.99 | 0.96 | 0.90 | 1.02 |
| | (-46.29, -30.06) | 33.89 degree | 2.19E+07 | 0.97 | 1.02 | 1.02 | 1.03 | 1.01 | 1.06 | 1.00 | 0.91 | 0.95 | 0.93 | 1.09 | 0.95 | 0.94 | 0.99 |
| | (-44.08, -33.22) | 37.44 degree | N/A | | | | | | | | | | | | | | |
| | (-42.29, -35.48) | 40.99 degree | 1.87E+07 | 0.91 | 0.99 | 1.01 | 1.00 | 0.99 | 1.06 | 0.97 | 0.92 | 0.85 | 0.95 | 0.90 | 0.97 | 0.86 | 0.89 |
| | (-39.03, -39.03) | 45 degree | 1.83E+07 | 0.90 | 0.92 | 0.94 | 0.97 | 0.97 | 1.06 | 0.94 | 0.90 | 0.79 | 0.92 | 1.12 | 0.86 | 0.85 | 0.85 |
| Reflector | (-23.31, -23.31) | (-16,-16) | 8.46E+08 | 1.03 | 1.02 | 1.01 | 1.07 | 1.03 | 1.09 | 1.02 | 1.04 | 1.13 | 0.99 | 0.99 | 0.98 | 1.01 | 1.01 |
| | (-25.83, -25.83) | (-18,-18) | 4.35E+08 | 0.96 | 0.96 | 0.96 | 0.98 | 0.97 | 1.03 | 0.96 | 0.94 | 1.10 | 0.94 | 0.95 | 0.94 | 0.94 | 0.95 |
| | (-28.35, -28.35) | (-20,-20) | 2.21E+08 | 0.95 | 0.97 | 0.94 | 0.98 | 0.98 | 1.05 | 0.96 | 0.94 | 1.04 | 0.95 | 0.95 | 0.92 | 0.95 | 0.95 |
| | (-30.87, -30.87) | (-22,-22) | 1.13E+08 | 0.96 | 1.00 | 1.00 | 1.01 | 1.01 | 1.11 | 0.99 | 0.89 | 0.91 | 0.99 | 1.00 | 0.94 | 0.98 | 1.04 |
| | (-33.39, -33.39) | (-24,-24) | 7.27E+07 | 0.88 | 0.94 | 0.93 | 0.94 | 0.94 | 1.04 | 0.92 | 0.83 | 0.72 | 0.91 | 0.92 | 0.91 | 0.88 | 0.90 |
| Number of positions within +-5% = | | | | 4 | 9 | 10 | 10 | 11 | 7 | 11 | 1 | 2 | 3 | 5 | 6 | 2 | 5 |
| Number of positions within +-10% = | | | | 12 | 13 | 13 | 13 | 13 | 12 | 13 | 6 | 3 | 11 | 8 | 12 | 6 | 10 |
| Number of positions within +-20% = | | | | 13 | 13 | 13 | 13 | 13 | 13 | 13 | 13 | 10 | 13 | 13 | 13 | 13 | 13 |

# Table 4.9(a). Equivalent fission fluxes: $^{64}$Zn(n,p) detector results and C/E comparison in stainless steel zones

Calculated results

| $^{64}$Zn (n,p) | Position in cm | Grid Position | Experimental Value | HYU-TORT | HYU-MCNP | HYU-MCNPX | Transpire Inc.-ATTILA | KI-MCU | KOPEC-DORT | WTI-MCNP | VTT-TORT | VTT-MT | KI-LUCKY | KAERI-DANTSYS | VTT-MCNP-K | VTT-MCNP-F | SCK-MCNPX |
|---|---|---|---|---|---|---|---|---|---|---|---|---|---|---|---|---|---|
| | | | | Korea | Korea | Korea | USA | Russia | Korea | Germany | Finland | Finland | Russia | Korea | Finland | Finland | Belgium |
| Inner Baffle | ( -4.41, -0.63) | (-1,+2) | 1.52E+09 | 1.47E+09 | 1.36E+09 | 1.36E+09 | 1.52E+09 | 1.34E+09 | 1.49E+09 | 1.41E+09 | 1.51E+09 | 1.46E+09 | 0.146E+10 | 1.35E+09 | 1.24E+09 | 1.35E+09 | 1.43E+09 |
| | ( -4.41, -4.41) | (-1,-1) | 1.83E+09 | 1.77E+09 | 1.67E+09 | 1.66E+09 | 1.81E+09 | 1.64E+09 | 1.83E+09 | 1.71E+09 | 1.73E+09 | 1.97E+09 | 0.173E+10 | 1.62E+09 | 1.64E+09 | 1.80E+09 | 1.67E+09 |
| Outer Baffle | (-39.69, -0.63) | (-29,+2) | 5.76E+08 | 4.85E+08 | 5.69E+08 | 5.49E+08 | 5.59E+08 | 5.23E+08 | 5.83E+08 | 5.58E+08 | 4.99E+08 | 5.09E+08 | 0.506E+09 | 5.50E+08 | 5.06E+08 | 4.78E+08 | 5.52E+08 |
| | (-39.69, -5.67) | (-29,-2) | N/A | 4.61E+08 | 5.65E+08 | 5.53E+08 | 5.43E+08 | 4.98E+08 | 5.54E+08 | 5.29E+08 | 4.63E+08 | 4.98E+08 | 0.481E+09 | 5.23E+08 | 5.03E+08 | 4.77E+08 | 5.35E+08 |
| | (-39.69, -11.97) | (-29,-7) | 4.36E+08 | 3.78E+08 | 4.28E+08 | 4.30E+08 | 4.40E+08 | 3.96E+08 | 4.51E+08 | 4.36E+08 | 3.69E+08 | 4.07E+08 | 0.391E+09 | 4.26E+08 | 4.20E+08 | 3.93E+08 | 4.22E+08 |
| | (-39.69, -18.27) | (-29,-12) | 2.54E+08 | 2.25E+08 | 2.41E+08 | 2.56E+08 | 2.55E+08 | 2.29E+08 | 2.66E+08 | 2.55E+08 | 2.07E+08 | 2.35E+08 | 0.230E+09 | 2.47E+08 | 2.40E+08 | 2.35E+08 | 2.40E+08 |
| | (-37.17, -20.79) | (-27,-14) | N/A | 2.47E+08 | 2.73E+08 | 2.60E+08 | 2.66E+08 | 2.43E+08 | 2.78E+08 | 2.62E+08 | 2.29E+08 | 2.54E+08 | 0.234E+09 | 2.55E+08 | 2.54E+08 | 2.41E+08 | 2.57E+08 |
| | (-30.87, -20.79) | (-22,-14) | N/A | 5.04E+08 | 5.24E+08 | 5.16E+08 | 5.44E+08 | 4.85E+08 | 5.48E+08 | 5.17E+08 | 5.16E+08 | 5.29E+08 | 0.476E+09 | 5.07E+08 | 5.06E+08 | 4.94E+08 | 5.29E+08 |
| | (-24.57, -20.79) | (-17,-14) | 8.55E+08 | 8.48E+08 | 8.43E+08 | 8.49E+08 | 8.79E+08 | 7.80E+08 | 8.96E+08 | 8.23E+08 | 7.79E+08 | 9.19E+08 | 0.815E+09 | 8.05E+08 | 8.00E+08 | 8.43E+08 | 8.19E+08 |
| Barrel | (-49.77, -0.63) | (-37,+2) | 7.42E+07 | 6.55E+07 | 7.56E+07 | 7.25E+07 | 7.29E+07 | 6.73E+07 | 7.76E+07 | 7.13E+07 | 6.11E+07 | 5.80E+07 | 0.677E+08 | 7.27E+07 | 6.32E+07 | 6.10E+07 | 7.13E+07 |
| | (-49.77, -9.45) | (-37,-5) | 6.24E+07 | 5.55E+07 | 6.07E+07 | 6.22E+07 | 6.11E+07 | 5.77E+07 | 6.55E+07 | 6.00E+07 | 4.96E+07 | 4.95E+07 | 0.574E+08 | 6.29E+07 | 5.76E+07 | 5.46E+07 | 5.71E+07 |
| | (-47.25, -18.27) | (-35,-12) | 6.10E+07 | 5.23E+07 | 5.69E+07 | 5.79E+07 | 5.90E+07 | 5.37E+07 | 6.21E+07 | 5.67E+07 | 4.86E+07 | 4.89E+07 | 0.535E+08 | 5.71E+07 | 5.59E+07 | 5.28E+07 | 6.20E+07 |
| | (-45.99, -22.05) | (-34,-15) | 5.00E+07 | 4.51E+07 | 5.05E+07 | 4.59E+07 | 4.96E+07 | 4.62E+07 | 5.13E+07 | 4.72E+07 | 4.36E+07 | 4.23E+07 | 0.460E+08 | 4.68E+07 | 4.73E+07 | 4.39E+07 | 5.23E+07 |
| | (-44.73, -24.57) | (-33,-17) | 4.55E+07 | 3.94E+07 | 4.27E+07 | 4.27E+07 | 4.32E+07 | 4.07E+07 | 4.68E+07 | 4.27E+07 | 3.97E+07 | 3.94E+07 | 0.416E+08 | 4.11E+07 | 4.15E+07 | 4.02E+07 | 4.78E+07 |
| | (-42.21, -28.35) | (-31,-20) | 4.15E+07 | 3.91E+07 | 3.96E+07 | 4.33E+07 | 4.21E+07 | 3.85E+07 | 4.42E+07 | 3.98E+07 | 3.63E+07 | 3.57E+07 | 0.398E+08 | 3.84E+07 | 3.77E+07 | 3.73E+07 | 3.98E+07 |
| | (-38.43, -33.39) | (-28,-24) | 3.66E+07 | 3.60E+07 | 3.56E+07 | 3.57E+07 | 3.57E+07 | 3.36E+07 | 3.98E+07 | 3.43E+07 | 3.28E+07 | 3.02E+07 | 0.351E+08 | 3.42E+07 | 3.28E+07 | 3.36E+07 | 3.61E+07 |
| | (-35.91, -35.91) | (-26,-26) | 3.59E+07 | 3.57E+07 | 3.56E+07 | 3.70E+07 | 3.58E+07 | 3.35E+07 | 4.00E+07 | 3.49E+07 | 3.22E+07 | 3.01E+07 | 0.341E+08 | 3.45E+07 | 3.37E+07 | 3.37E+07 | 3.58E+07 |
| Neutron Pad | (-58.54, -22.47) | 21 degree | 5.78E+06 | 5.63E+06 | 5.66E+06 | 5.35E+06 | 5.95E+06 | 5.35E+06 | 6.16E+06 | 5.49E+06 | 4.79E+06 | 4.54E+06 | 0.567E+07 | 5.80E+06 | 5.60E+06 | 5.33E+06 | 3.88E+06 |
| | (-46.60, -41.95) | 42 degree | 3.99E+06 | 4.15E+06 | 4.29E+06 | 4.81E+06 | 4.36E+06 | 4.02E+06 | 4.83E+06 | 4.05E+06 | 3.76E+06 | 3.35E+06 | 0.419E+07 | 4.10E+06 | 3.95E+06 | 3.95E+06 | 2.98E+06 |

C/E comparison

| $^{64}$Zn (n,p) | Position in cm | Grid Position | Experimental Value | HYU-TORT | HYU-MCNP | HYU-MCNPX | Transpire Inc.-ATTILA | KI-MCU | KOPEC-DORT | WTI-MCNP | VTT-TORT | VTT-MT | KI-LUCKY | KAERI-DANTSYS | VTT-MCNP-K | VTT-MCNP-F | SCK-MCNPX |
|---|---|---|---|---|---|---|---|---|---|---|---|---|---|---|---|---|---|
| | | | | Korea | Korea | Korea | USA | Russia | Korea | Germany | Finland | Finland | Russia | Korea | Finland | Finland | Belgium |
| Inner Baffle | ( -4.41, -0.63) | (-1,+2) | 1.52E+09 | 0.97 | 0.90 | 0.90 | 1.00 | 0.88 | 0.98 | 0.93 | 0.99 | 0.96 | 0.96 | 0.89 | 0.81 | 0.89 | 0.94 |
| | ( -4.41, -4.41) | (-1,-1) | 1.83E+09 | 0.97 | 0.91 | 0.91 | 0.99 | 0.89 | 1.00 | 0.94 | 0.95 | 1.07 | 0.95 | 0.89 | 0.89 | 0.99 | 0.91 |
| Outer Baffle | (-39.69, -0.63) | (-29,+2) | 5.76E+08 | 0.84 | 0.99 | 0.95 | 0.97 | 0.91 | 1.01 | 0.97 | 0.87 | 0.88 | 0.88 | 0.96 | 0.88 | 0.83 | 0.96 |
| | (-39.69, -5.67) | (-29,-2) | N/A | | | | | | | | | | | | | | |
| | (-39.69, -11.97) | (-29,-7) | 4.36E+08 | 0.87 | 0.98 | 0.99 | 1.01 | 0.91 | 1.03 | 1.00 | 0.85 | 0.93 | 0.90 | 0.98 | 0.96 | 0.90 | 0.97 |
| | (-39.69, -18.27) | (-29,-12) | 2.54E+08 | 0.88 | 0.95 | 1.01 | 1.00 | 0.90 | 1.05 | 1.00 | 0.81 | 0.93 | 0.91 | 0.97 | 0.95 | 0.92 | 0.94 |
| | (-37.17, -20.79) | (-27,-14) | N/A | | | | | | | | | | | | | | |
| | (-30.87, -20.79) | (-22,-14) | N/A | | | | | | | | | | | | | | |
| | (-24.57, -20.79) | (-17,-14) | 8.55E+08 | 0.99 | 0.99 | 0.99 | 1.03 | 0.91 | 1.05 | 0.96 | 0.91 | 1.07 | 0.95 | 0.94 | 0.94 | 0.99 | 0.96 |
| Barrel | (-49.77, -0.63) | (-37,+2) | 7.42E+07 | 0.88 | 1.02 | 0.98 | 0.98 | 0.91 | 1.05 | 0.96 | 0.82 | 0.78 | 0.91 | 0.98 | 0.85 | 0.82 | 0.96 |
| | (-49.77, -9.45) | (-37,-5) | 6.24E+07 | 0.89 | 0.97 | 1.00 | 0.98 | 0.92 | 1.05 | 0.96 | 0.80 | 0.79 | 0.92 | 1.01 | 0.92 | 0.88 | 0.91 |
| | (-47.25, -18.27) | (-35,-12) | 6.10E+07 | 0.86 | 0.93 | 0.95 | 0.97 | 0.88 | 1.02 | 0.93 | 0.80 | 0.80 | 0.88 | 0.94 | 0.92 | 0.87 | 1.02 |
| | (-45.99, -22.05) | (-34,-15) | 5.00E+07 | 0.90 | 1.01 | 0.92 | 0.99 | 0.92 | 1.03 | 0.94 | 0.87 | 0.85 | 0.92 | 0.94 | 0.95 | 0.88 | 1.05 |
| | (-44.73, -24.57) | (-33,-17) | 4.55E+07 | 0.87 | 0.94 | 0.94 | 0.95 | 0.90 | 1.03 | 0.94 | 0.87 | 0.87 | 0.91 | 0.90 | 0.91 | 0.88 | 1.05 |
| | (-42.21, -28.35) | (-31,-20) | 4.15E+07 | 0.94 | 0.95 | 1.04 | 1.02 | 0.93 | 1.06 | 0.96 | 0.87 | 0.86 | 0.96 | 0.93 | 0.91 | 0.90 | 0.96 |
| | (-38.43, -33.39) | (-28,-24) | 3.66E+07 | 0.98 | 0.97 | 0.97 | 0.97 | 0.92 | 1.09 | 0.94 | 0.90 | 0.83 | 0.96 | 0.94 | 0.89 | 0.92 | 0.99 |
| | (-35.91, -35.91) | (-26,-26) | 3.59E+07 | 0.99 | 0.99 | 1.03 | 1.00 | 0.93 | 1.11 | 0.97 | 0.90 | 0.84 | 0.95 | 0.96 | 0.94 | 0.94 | 1.00 |
| Neutron Pad | (-58.54, -22.47) | 21 degree | 5.78E+06 | 0.97 | 0.98 | 0.93 | 1.03 | 0.93 | 1.07 | 0.95 | 0.83 | 0.79 | 0.98 | 1.00 | 0.97 | 0.92 | 0.67 |
| | (-46.60, -41.95) | 42 degree | 3.99E+06 | 1.04 | 1.08 | 1.21 | 1.09 | 1.01 | 1.21 | 1.02 | 0.94 | 0.84 | 1.05 | 1.03 | 0.99 | 0.99 | 0.75 |
| Number of positions within +-5% = | | | | 7 | 10 | 9 | 14 | 1 | 11 | 9 | 1 | 1 | 5 | 8 | 3 | 3 | 10 |
| Number of positions within +-10% = | | | | 9 | 15 | 14 | 16 | 12 | 14 | 16 | 4 | 5 | 13 | 14 | 11 | 8 | 14 |
| Number of positions within +-20% = | | | | 16 | 16 | 15 | 16 | 16 | 15 | 16 | 14 | 13 | 16 | 16 | 16 | 16 | 14 |

# Table 4.9(b). Equivalent fission fluxes: $^{64}$Zn(n,p) detector results and C/E comparison in water zones

Calculated results

| $^{64}$Zn (n,p) | Position in cm | Grid Position | Experimental Value | HYU-TORT Korea | HYU-MCNP Korea | HYU-MCNPX Korea | Transpire Inc.-ATTILA USA | KI-MCU Russia | KOPEC-DORT Korea | WTI-MCNP Germany | VTT-TORT Finland | VTT-MT Finland | KI-LUCKY Russia | KAERI-DANTSYS Korea | VTT-MCNP-K Finland | VTT-MCNP-F Finland | SCK-MCNPX Belgium |
|---|---|---|---|---|---|---|---|---|---|---|---|---|---|---|---|---|---|
| Central Hole | ( 0.0, 0.0) | (+2.5,+2.5) | N/A | 1.11E+09 | 2.68E+08 | 2.76E+08 | 1.11E+09 | 6.20E+07 | 1.13E+09 | 1.06E+09 | 1.08E+09 | 1.01E+09 | 0.112E+10 | 1.03E+09 | 1.02E+09 | 1.11E+09 | 2.56E+08 |
| Water Gap | (-54.36, -9.59) | 10.75 degree | N/A | 2.12E+07 | 2.21E+07 | 2.37E+07 | 2.28E+07 | 2.11E+07 | 2.40E+07 | 2.16E+07 | 1.96E+07 | 1.94E+07 | 0.217E+08 | 2.08E+07 | 2.08E+07 | 2.00E+07 | 2.12E+07 |
| | (-52.89, -15.80) | 16.63 degree | 2.17E+07 | 2.07E+07 | 2.11E+07 | 2.25E+07 | 2.19E+07 | 2.01E+07 | 2.35E+07 | 2.16E+07 | 1.95E+07 | 1.88E+07 | 0.208E+08 | 2.48E+07 | 2.02E+07 | 1.96E+07 | 2.10E+07 |
| | (-51.53, -19.78) | 21.14 degree | 1.68E+07 | 2.02E+07 | 2.13E+07 | 2.09E+07 | 2.16E+07 | 1.93E+07 | 2.25E+07 | 2.05E+07 | 1.89E+07 | 1.83E+07 | 0.202E+08 | 2.32E+07 | 2.02E+07 | 1.89E+07 | 2.12E+07 |
| | (-50.03, -23.33) | 25.62 degree | 1.89E+07 | 1.85E+07 | 2.00E+07 | 2.02E+07 | 1.95E+07 | 1.80E+07 | 2.00E+07 | 1.86E+07 | 1.69E+07 | 1.71E+07 | 0.184E+08 | 1.90E+07 | 1.96E+07 | 1.75E+07 | 1.91E+07 |
| | (-48.74, -25.91) | 28.78 degree | 1.71E+07 | 1.68E+07 | 1.73E+07 | 1.82E+07 | 1.81E+07 | 1.67E+07 | 1.89E+07 | 1.71E+07 | 1.61E+07 | 1.67E+07 | 0.173E+08 | 1.76E+07 | 1.72E+07 | 1.63E+07 | 2.00E+07 |
| | (-46.29, -30.06) | 33.89 degree | 1.60E+07 | 1.58E+07 | 1.71E+07 | 1.59E+07 | 1.68E+07 | 1.53E+07 | 1.74E+07 | 1.55E+07 | 1.47E+07 | 1.55E+07 | 0.156E+08 | 1.71E+07 | 1.53E+07 | 1.50E+07 | 1.86E+07 |
| | (-44.08, -33.22) | 37.44 degree | N/A | 1.49E+07 | 1.45E+07 | 1.78E+07 | 1.51E+07 | 1.44E+07 | 1.67E+07 | 1.48E+07 | 1.41E+07 | 1.37E+07 | 0.151E+08 | 1.49E+07 | 1.46E+07 | 1.43E+07 | 1.72E+07 |
| | (-42.29, -35.48) | 40.99 degree | 1.45E+07 | 1.41E+07 | 1.56E+07 | 1.56E+07 | 1.50E+07 | 1.39E+07 | 1.63E+07 | 1.39E+07 | 1.37E+07 | 1.32E+07 | 0.146E+08 | 1.34E+07 | 1.40E+07 | 1.37E+07 | 1.22E+07 |
| | (-39.03, -39.03) | 45 degree | 1.51E+07 | 1.42E+07 | 1.39E+07 | 1.40E+07 | 1.48E+07 | 1.37E+07 | 1.61E+07 | 1.38E+07 | 1.35E+07 | 1.27E+07 | 0.143E+08 | 1.61E+07 | 1.37E+07 | 1.32E+07 | 1.42E+07 |
| Reflector | (-23.31, -23.31) | (-16,-16) | N/A | 6.26E+08 | 6.12E+08 | 6.01E+08 | 6.46E+08 | 5.85E+08 | 6.67E+08 | 6.12E+08 | 6.19E+08 | 6.75E+08 | 0.613E+09 | 6.03E+08 | 5.95E+08 | 6.20E+08 | 6.31E+08 |
| | (-25.83, -25.83) | (-18,-18) | 3.46E+08 | 3.41E+08 | 3.38E+08 | 3.39E+08 | 3.51E+08 | 3.22E+08 | 3.71E+08 | 3.34E+08 | 3.29E+08 | 3.70E+08 | 0.337E+09 | 3.36E+08 | 3.27E+08 | 3.33E+08 | 3.44E+08 |
| | (-28.35, -28.35) | (-20,-20) | 1.99E+08 | 1.89E+08 | 1.86E+08 | 1.82E+08 | 1.94E+08 | 1.80E+08 | 2.10E+08 | 1.87E+08 | 1.82E+08 | 1.98E+08 | 0.189E+09 | 1.87E+08 | 1.80E+08 | 1.82E+08 | 1.90E+08 |
| | (-30.87, -30.87) | (-22,-22) | 1.12E+08 | 1.05E+08 | 1.08E+08 | 1.08E+08 | 1.10E+08 | 1.02E+08 | 1.22E+08 | 1.04E+08 | 9.53E+07 | 1.02E+08 | 0.107E+09 | 1.07E+08 | 1.04E+08 | 1.04E+08 | 1.16E+08 |
| | (-33.39, -33.39) | (-24,-24) | N/A | 6.18E+07 | 6.45E+07 | 6.25E+07 | 6.38E+07 | 5.89E+07 | 7.18E+07 | 6.13E+07 | 5.50E+07 | 5.35E+07 | 0.624E+08 | 6.24E+07 | 6.03E+07 | 5.90E+07 | 5.94E+07 |

C/E comparison

| $^{64}$Zn (n,p) | Position in cm | Grid Position | Experimental Value | HYU-TORT Korea | HYU-MCNP Korea | HYU-MCNPX Korea | Transpire Inc.-ATTILA USA | KI-MCU Russia | KOPEC-DORT Korea | WTI-MCNP Germany | VTT-TORT Finland | VTT-MT Finland | KI-LUCKY Russia | KAERI-DANTSYS Korea | VTT-MCNP-K Finland | VTT-MCNP-F Finland | SCK-MCNPX Belgium |
|---|---|---|---|---|---|---|---|---|---|---|---|---|---|---|---|---|---|
| Central Hole | ( 0.0, 0.0) | (+2.5,+2.5) | N/A | | | | | | | | | | | | | | |
| Water Gap | (-54.36, -9.59) | 10.75 degree | N/A | | | | | | | | | | | | | | |
| | (-52.89, -15.80) | 16.63 degree | 2.17E+07 | 0.95 | 0.97 | 1.04 | 1.01 | 0.92 | 1.08 | 0.99 | 0.90 | 0.87 | 0.96 | 1.14 | 0.93 | 0.91 | 0.97 |
| | (-51.53, -19.78) | 21.14 degree | 1.68E+07 | 1.20 | 1.27 | 1.24 | 1.29 | 1.15 | 1.34 | 1.22 | 1.12 | 1.09 | 1.20 | 1.38 | 1.20 | 1.12 | 1.26 |
| | (-50.03, -23.33) | 25.62 degree | 1.89E+07 | 0.98 | 1.06 | 1.07 | 1.03 | 0.95 | 1.06 | 0.98 | 0.89 | 0.91 | 0.97 | 1.01 | 1.04 | 0.93 | 1.01 |
| | (-48.74, -25.91) | 28.78 degree | 1.71E+07 | 0.98 | 1.01 | 1.06 | 1.06 | 0.98 | 1.10 | 1.00 | 0.94 | 0.97 | 1.01 | 1.03 | 1.01 | 0.96 | 1.17 |
| | (-46.29, -30.06) | 33.89 degree | 1.60E+07 | 0.99 | 1.07 | 0.99 | 1.05 | 0.95 | 1.09 | 0.97 | 0.92 | 0.97 | 0.98 | 1.07 | 0.96 | 0.94 | 1.16 |
| | (-44.08, -33.22) | 37.44 degree | N/A | | | | | | | | | | | | | | |
| | (-42.29, -35.48) | 40.99 degree | 1.45E+07 | 0.97 | 1.07 | 1.08 | 1.04 | 0.96 | 1.12 | 0.96 | 0.95 | 0.91 | 1.01 | 0.93 | 0.97 | 0.94 | 0.84 |
| | (-39.03, -39.03) | 45 degree | 1.51E+07 | 0.94 | 0.92 | 0.92 | 0.98 | 0.91 | 1.06 | 0.92 | 0.90 | 0.84 | 0.95 | 1.07 | 0.91 | 0.87 | 0.94 |
| Reflector | (-23.31, -23.31) | (-16,-16) | N/A | | | | | | | | | | | | | | |
| | (-25.83, -25.83) | (-18,-18) | 3.46E+08 | 0.98 | 0.98 | 0.98 | 1.01 | 0.93 | 1.07 | 0.97 | 0.95 | 1.07 | 0.97 | 0.97 | 0.94 | 0.96 | 0.99 |
| | (-28.35, -28.35) | (-20,-20) | 1.99E+08 | 0.95 | 0.94 | 0.91 | 0.98 | 0.90 | 1.06 | 0.94 | 0.92 | 1.00 | 0.95 | 0.94 | 0.90 | 0.92 | 0.96 |
| | (-30.87, -30.87) | (-22,-22) | 1.12E+08 | 0.94 | 0.96 | 0.97 | 0.98 | 0.91 | 1.09 | 0.93 | 0.85 | 0.91 | 0.96 | 0.95 | 0.93 | 0.93 | 1.04 |
| | (-33.39, -33.39) | (-24,-24) | N/A | | | | | | | | | | | | | | |
| Number of positions within +-5% = | | | | 6 | 4 | 4 | 8 | 4 | 0 | 6 | 1 | 3 | 7 | 4 | 4 | 2 | 5 |
| Number of positions within +-10% = | | | | 9 | 9 | 9 | 9 | 9 | 7 | 9 | 5 | 8 | 9 | 8 | 9 | 8 | 6 |
| Number of positions within +-20% = | | | | 10 | 9 | 9 | 9 | 10 | 9 | 9 | 10 | 10 | 9 | 9 | 9 | 10 | 9 |

# Table 4.10(a). Equivalent fission fluxes: $^{237}$Np(n,f) detector results and C/E comparison in stainless steel zones

Calculated results

| $^{237}$Np (n,f) | Position in cm | Grid Position | Experimental Value | HYU-TORT | HYU-MCNP | HYU-MCNPX | Transpire Inc.-ATTILA | KI-MCU | KOPEC-DORT | VTI/SUT-HELIOS | WTI-MCNP | VTT-TORT | VTT-MT | KI-LUCKY | KAERI-DANTSYS | VTT-MCNP-K | VTT-MCNP-F | SCK-MCNPX |
|---|---|---|---|---|---|---|---|---|---|---|---|---|---|---|---|---|---|---|
| | | | | Korea | Korea | Korea | USA | Russia | Korea | Slovak | Germany | Finland | Finland | Russia | Korea | Finland | Finland | Belgium |
| Inner Baffle | ( -4.41, -0.63) | (-1,+2) | 2.49E+09 | 2.64E+09 | 2.59E+09 | 2.57E+09 | 2.60E+09 | 2.46E+09 | 2.59E+09 | 1.73E+09 | 2.53E+09 | 2.65E+09 | 2.40E+09 | 0.248E+10 | 2.39E+09 | 2.17E+09 | 2.34E+09 | 2.56E+09 |
| | ( -4.41, -4.41) | (-1,-1) | 2.95E+09 | 3.10E+09 | 3.06E+09 | 3.06E+09 | 3.04E+09 | 2.91E+09 | 3.07E+09 | 2.00E+09 | 2.99E+09 | 3.01E+09 | 3.01E+09 | 0.292E+10 | 2.81E+09 | 2.78E+09 | 3.07E+09 | 3.01E+09 |
| Outer Baffle | (-39.69, -0.63) | (-29,+2) | N/A | 8.32E+08 | 9.63E+08 | 9.57E+08 | 8.96E+08 | 9.06E+08 | 9.34E+08 | 6.44E+08 | 9.30E+08 | 8.26E+08 | 8.11E+08 | 0.815E+09 | 9.02E+08 | 8.45E+08 | 7.71E+08 | 9.36E+08 |
| | (-39.69, -5.67) | (-29,-2) | N/A | 7.91E+08 | 9.23E+08 | 9.35E+08 | 8.54E+08 | 8.62E+08 | 8.89E+08 | 6.15E+08 | 8.80E+08 | 7.73E+08 | 7.79E+08 | 0.776E+09 | 8.57E+08 | 8.46E+08 | 7.89E+08 | 9.04E+08 |
| | (-39.69, -11.97) | (-29,-7) | 6.88E+08 | 6.51E+08 | 7.49E+08 | 7.47E+08 | 6.97E+08 | 6.99E+08 | 7.26E+08 | 5.01E+08 | 7.24E+08 | 6.20E+08 | 6.39E+08 | 0.634E+09 | 7.01E+08 | 7.01E+08 | 6.42E+08 | 7.33E+08 |
| | (-39.69, -18.27) | (-29,-12) | 4.34E+08 | 4.06E+08 | 4.55E+08 | 4.57E+08 | 4.26E+08 | 4.31E+08 | 4.52E+08 | 3.20E+08 | 4.44E+08 | 3.64E+08 | 3.91E+08 | 0.390E+09 | 4.29E+08 | 4.34E+08 | 3.97E+08 | 4.49E+08 |
| | (-37.17, -20.79) | (-27,-14) | N/A | 4.45E+08 | 4.85E+08 | 4.75E+08 | 4.48E+08 | 4.45E+08 | 4.73E+08 | 3.35E+08 | 4.61E+08 | 4.05E+08 | 4.11E+08 | 0.400E+09 | 4.46E+08 | 4.46E+08 | 4.16E+08 | 4.68E+08 |
| | (-30.87, -20.79) | (-22,-14) | N/A | 8.81E+08 | 9.28E+08 | 9.21E+08 | 8.82E+08 | 8.64E+08 | 9.10E+08 | 6.03E+08 | 8.90E+08 | 8.83E+08 | 8.34E+08 | 0.791E+09 | 8.60E+08 | 8.59E+08 | 8.27E+08 | 9.02E+08 |
| | (-24.57, -20.79) | (-17,-14) | 1.46E+09 | 1.52E+09 | 1.52E+09 | 1.51E+09 | 1.48E+09 | 1.42E+09 | 1.52E+09 | 9.76E+08 | 1.46E+09 | 1.37E+09 | 1.48E+09 | 0.138E+10 | 1.41E+09 | 1.38E+09 | 1.45E+09 | 1.47E+09 |
| Barrel | (-49.77, -0.63) | (-37,+2) | N/A | 1.06E+08 | 1.21E+08 | 1.20E+08 | 1.11E+08 | 1.10E+08 | 1.20E+08 | 9.55E+07 | 1.14E+08 | 9.70E+07 | 8.15E+07 | 0.105E+09 | 1.17E+08 | 1.00E+08 | 9.66E+07 | 1.17E+08 |
| | (-49.77, -9.45) | (-37,-5) | 1.03E+08 | 9.59E+07 | 1.09E+08 | 1.10E+08 | 1.01E+08 | 9.97E+07 | 1.09E+08 | 9.19E+07 | 1.04E+08 | 8.60E+07 | 7.54E+07 | 0.951E+08 | 1.04E+08 | 1.00E+08 | 9.30E+07 | 1.06E+08 |
| | (-47.25, -18.27) | (-35,-12) | 1.04E+08 | 9.97E+07 | 1.11E+08 | 1.13E+08 | 1.04E+08 | 1.04E+08 | 1.11E+08 | 9.01E+07 | 1.06E+08 | 8.99E+07 | 8.16E+07 | 0.955E+08 | 1.04E+08 | 1.04E+08 | 9.49E+07 | 1.15E+08 |
| | (-45.99, -22.05) | (-34,-15) | 9.04E+07 | 9.15E+07 | 1.00E+08 | 9.87E+07 | 9.35E+07 | 9.21E+07 | 9.83E+07 | 8.05E+07 | 9.43E+07 | 8.59E+07 | 7.31E+07 | 0.866E+08 | 9.02E+07 | 9.06E+07 | 8.62E+07 | 1.02E+08 |
| | (-44.73, -24.57) | (-33,-17) | N/A | 8.17E+07 | 9.05E+07 | 9.01E+07 | 8.35E+07 | 8.34E+07 | 8.95E+07 | 7.93E+07 | 8.57E+07 | 7.77E+07 | 6.76E+07 | 0.787E+08 | 7.94E+07 | 8.20E+07 | 7.84E+07 | 9.18E+07 |
| | (-42.21, -28.35) | (-31,-20) | 7.02E+07 | 7.09E+07 | 7.61E+07 | 7.56E+07 | 7.16E+07 | 6.99E+07 | 7.69E+07 | 7.23E+07 | 7.19E+07 | 6.48E+07 | 5.56E+07 | 0.673E+08 | 6.85E+07 | 6.64E+07 | 6.45E+07 | 7.27E+07 |
| | (-38.43, -33.39) | (-28,-24) | 5.49E+07 | 5.59E+07 | 5.90E+07 | 5.72E+07 | 5.52E+07 | 5.57E+07 | 6.15E+07 | 6.37E+07 | 5.56E+07 | 5.09E+07 | 4.14E+07 | 0.531E+08 | 5.45E+07 | 5.29E+07 | 5.11E+07 | 5.53E+07 |
| | (-35.91, -35.91) | (-26,-26) | 5.35E+07 | 5.41E+07 | 5.68E+07 | 5.78E+07 | 5.39E+07 | 5.41E+07 | 6.03E+07 | 6.47E+07 | 5.44E+07 | 4.93E+07 | 4.00E+07 | 0.508E+08 | 5.29E+07 | 5.30E+07 | 5.13E+07 | 5.28E+07 |
| Neutron Pad | (-58.54, -22.47) | 21 degree | 1.12E+07 | 1.08E+07 | 1.14E+07 | 1.17E+07 | 1.08E+07 | 9.93E+06 | 1.19E+07 | 1.31E+07 | 1.09E+07 | 9.12E+06 | 7.04E+06 | 0.101E+08 | 1.03E+07 | 1.06E+07 | 9.11E+06 | 1.04E+07 |
| | (-46.60, -41.95) | 42 degree | 7.70E+06 | 7.53E+06 | 7.63E+06 | 7.94E+06 | 7.57E+06 | 7.02E+06 | 8.74E+06 | 1.08E+07 | 7.70E+06 | 6.70E+06 | 4.83E+06 | 0.694E+07 | 6.99E+06 | 7.60E+06 | 6.05E+06 | 5.98E+06 |

C/E comparison

| $^{237}$Np (n,f) | Position in cm | Grid Position | Experimental Value | HYU-TORT | HYU-MCNP | HYU-MCNPX | Transpire Inc.-ATTILA | KI-MCU | KOPEC-DORT | VTI/SUT-HELIOS | WTI-MCNP | VTT-TORT | VTT-MT | KI-LUCKY | KAERI-DANTSYS | VTT-MCNP-K | VTT-MCNP-F | SCK-MCNPX |
|---|---|---|---|---|---|---|---|---|---|---|---|---|---|---|---|---|---|---|
| | | | | Korea | Korea | Korea | USA | Russia | Korea | Slovak | Germany | Finland | Finland | Russia | Korea | Finland | Finland | Belgium |
| Inner Baffle | ( -4.41, -0.63) | (-1,+2) | 2.49E+09 | 1.06 | 1.04 | 1.03 | 1.05 | 0.99 | 1.04 | 0.69 | 1.02 | 1.06 | 0.96 | 1.00 | 0.96 | 0.87 | 0.94 | 1.03 |
| | ( -4.41, -4.41) | (-1,-1) | 2.95E+09 | 1.05 | 1.04 | 1.04 | 1.03 | 0.99 | 1.04 | 0.68 | 1.01 | 1.02 | 1.02 | 0.99 | 0.95 | 0.94 | 1.04 | 1.02 |
| Outer Baffle | (-39.69, -0.63) | (-29,+2) | N/A | | | | | | | | | | | | | | | |
| | (-39.69, -5.67) | (-29,-2) | N/A | | | | | | | | | | | | | | | |
| | (-39.69, -11.97) | (-29,-7) | 6.88E+08 | 0.95 | 1.09 | 1.09 | 1.01 | 1.02 | 1.05 | 0.73 | 1.05 | 0.90 | 0.93 | 0.92 | 1.02 | 1.02 | 0.93 | 1.07 |
| | (-39.69, -18.27) | (-29,-12) | 4.34E+08 | 0.94 | 1.05 | 1.05 | 0.98 | 0.99 | 1.04 | 0.74 | 1.02 | 0.84 | 0.90 | 0.90 | 0.99 | 1.00 | 0.91 | 1.04 |
| | (-37.17, -20.79) | (-27,-14) | N/A | | | | | | | | | | | | | | | |
| | (-30.87, -20.79) | (-22,-14) | N/A | | | | | | | | | | | | | | | |
| | (-24.57, -20.79) | (-17,-14) | 1.46E+09 | 1.04 | 1.04 | 1.04 | 1.01 | 0.97 | 1.04 | 0.67 | 1.00 | 0.94 | 1.01 | 0.95 | 0.96 | 0.95 | 0.99 | 1.01 |
| Barrel | (-49.77, -0.63) | (-37,+2) | N/A | | | | | | | | | | | | | | | |
| | (-49.77, -9.45) | (-37,-5) | 1.03E+08 | 0.93 | 1.06 | 1.06 | 0.98 | 0.97 | 1.06 | 0.89 | 1.01 | 0.83 | 0.73 | 0.92 | 1.01 | 0.98 | 0.90 | 1.03 |
| | (-47.25, -18.27) | (-35,-12) | 1.04E+08 | 0.96 | 1.07 | 1.08 | 1.00 | 1.00 | 1.06 | 0.87 | 1.02 | 0.86 | 0.78 | 0.92 | 1.00 | 1.00 | 0.91 | 1.10 |
| | (-45.99, -22.05) | (-34,-15) | 9.04E+07 | 1.01 | 1.11 | 1.09 | 1.03 | 1.02 | 1.09 | 0.89 | 1.04 | 0.95 | 0.81 | 0.96 | 1.00 | 1.00 | 0.95 | 1.12 |
| | (-44.73, -24.57) | (-33,-17) | N/A | | | | | | | | | | | | | | | |
| | (-42.21, -28.35) | (-31,-20) | 7.02E+07 | 1.01 | 1.08 | 1.08 | 1.02 | 1.00 | 1.10 | 1.03 | 1.02 | 0.92 | 0.79 | 0.96 | 0.98 | 0.95 | 0.92 | 1.04 |
| | (-38.43, -33.39) | (-28,-24) | 5.49E+07 | 1.02 | 1.07 | 1.04 | 1.01 | 1.01 | 1.12 | 1.16 | 1.01 | 0.93 | 0.75 | 0.97 | 0.99 | 0.96 | 0.93 | 1.01 |
| | (-35.91, -35.91) | (-26,-26) | 5.35E+07 | 1.01 | 1.06 | 1.08 | 1.01 | 1.01 | 1.13 | 1.21 | 1.02 | 0.92 | 0.75 | 0.95 | 0.99 | 0.99 | 0.96 | 0.99 |
| Neutron Pad | (-58.54, -22.47) | 21 degree | 1.12E+07 | 0.96 | 1.02 | 1.04 | 0.96 | 0.89 | 1.07 | 1.17 | 0.97 | 0.81 | 0.63 | 0.90 | 0.92 | 0.94 | 0.81 | 0.93 |
| | (-46.60, -41.95) | 42 degree | 7.70E+06 | 0.98 | 0.99 | 1.03 | 0.98 | 0.91 | 1.14 | 1.41 | 1.00 | 0.87 | 0.63 | 0.90 | 0.91 | 0.99 | 0.79 | 0.78 |
| Number of positions within +-5% = | | | | 8 | 6 | 6 | 13 | 11 | 4 | 1 | 12 | 2 | 3 | 5 | 11 | 8 | 4 | 8 |
| Number of positions within +-10% = | | | | 13 | 12 | 13 | 13 | 12 | 10 | 1 | 13 | 8 | 5 | 12 | 13 | 12 | 11 | 10 |
| Number of positions within +-20% = | | | | 13 | 13 | 13 | 13 | 13 | 13 | 6 | 13 | 13 | 6 | 13 | 13 | 13 | 12 | 12 |

# Table 4.10(b). Equivalent fission fluxes: $^{237}$Np(n,f) detector results and C/E comparison in water zones

Calculated results

| $^{237}$Np (n,f) | Position in cm | Grid Position | Experimental Value | HYU-TORT Korea | HYU-MCNP Korea | HYU-MCNPX Korea | Transpire Inc.-ATTILA USA | KI-MCU Russia | KOPEC-DORT Korea | VTI/SUT-HELIOS Slovak | WTI-MCNP Germany | VTT-TORT Finland | VTT-MT Finland | KI-LUCKY Russia | KAERI-DANTSYS Korea | VTT-MCNP-K Finland | VTT-MCNP-F Finland | SCK-MCNPX Belgium |
|---|---|---|---|---|---|---|---|---|---|---|---|---|---|---|---|---|---|---|
| Central Hole | ( 0.0, 0.0) | (+2.5,+2.5) | N/A | 1.68E+09 | 4.25E+08 | 4.31E+08 | 1.64E+09 | 9.69E+07 | 1.61E+09 | 1.16E+09 | 1.61E+09 | 1.58E+09 | 1.42E+09 | 0.151E+10 | 1.47E+09 | 1.54E+09 | 1.69E+09 | 4.05E+08 |
| Water Gap | (-54.36, -9.59) | 10.75 degree | N/A | 3.13E+07 | 3.60E+07 | 3.60E+07 | 3.39E+07 | 3.27E+07 | 3.39E+07 | 2.99E+07 | 3.32E+07 | 2.97E+07 | 2.81E+07 | 0.290E+08 | 2.92E+07 | 3.34E+07 | 2.89E+07 | 3.60E+07 |
| | (-52.89, -15.80) | 16.63 degree | N/A | 3.32E+07 | 3.65E+07 | 3.65E+07 | 3.45E+07 | 3.33E+07 | 3.44E+07 | 3.14E+07 | 3.42E+07 | 3.08E+07 | 2.82E+07 | 0.292E+08 | 3.84E+07 | 3.28E+07 | 3.09E+07 | 3.68E+07 |
| | (-51.53, -19.78) | 21.14 degree | N/A | 3.24E+07 | 3.55E+07 | 3.72E+07 | 3.41E+07 | 3.27E+07 | 3.39E+07 | 3.00E+07 | 3.35E+07 | 3.05E+07 | 2.86E+07 | 0.283E+08 | 3.70E+07 | 3.37E+07 | 3.01E+07 | 3.48E+07 |
| | (-50.03, -23.33) | 25.62 degree | N/A | 3.13E+07 | 3.44E+07 | 3.38E+07 | 3.29E+07 | 3.09E+07 | 3.15E+07 | 2.84E+07 | 3.17E+07 | 2.88E+07 | 2.59E+07 | 0.270E+08 | 3.11E+07 | 3.00E+07 | 2.87E+07 | 3.29E+07 |
| | (-48.74, -25.91) | 28.78 degree | N/A | 2.82E+07 | 3.10E+07 | 3.19E+07 | 3.01E+07 | 2.89E+07 | 2.93E+07 | 2.86E+07 | 2.94E+07 | 2.71E+07 | 2.60E+07 | 0.254E+08 | 2.91E+07 | 2.88E+07 | 2.69E+07 | 3.17E+07 |
| | (-46.29, -30.06) | 33.89 degree | N/A | 2.52E+07 | 2.76E+07 | 2.78E+07 | 2.64E+07 | 2.48E+07 | 2.55E+07 | 2.62E+07 | 2.53E+07 | 2.30E+07 | 2.34E+07 | 0.214E+08 | 2.68E+07 | 2.39E+07 | 2.31E+07 | 2.71E+07 |
| | (-44.08, -33.22) | 37.44 degree | N/A | 2.22E+07 | 2.37E+07 | 2.49E+07 | 2.24E+07 | 2.22E+07 | 2.33E+07 | 2.45E+07 | 2.24E+07 | 2.11E+07 | 1.90E+07 | 0.199E+08 | 2.27E+07 | 2.04E+07 | 2.14E+07 | 2.25E+07 |
| | (-42.29, -35.48) | 40.99 degree | N/A | 1.96E+07 | 2.24E+07 | 2.26E+07 | 2.14E+07 | 2.03E+07 | 2.17E+07 | 2.42E+07 | 2.06E+07 | 1.94E+07 | 1.75E+07 | 0.185E+08 | 1.85E+07 | 2.04E+07 | 1.80E+07 | 1.99E+07 |
| | (-39.03, -39.03) | 45 degree | 1.95E+07 | 1.89E+07 | 2.03E+07 | 2.09E+07 | 2.02E+07 | 1.97E+07 | 2.11E+07 | 2.38E+07 | 1.95E+07 | 1.86E+07 | 1.59E+07 | 0.175E+08 | 2.26E+07 | 1.77E+07 | 1.77E+07 | 1.89E+07 |
| Reflector | (-23.31, -23.31) | (-16,-16) | 9.77E+08 | 1.01E+09 | 1.03E+09 | 1.02E+09 | 1.02E+09 | 9.46E+08 | 9.90E+08 | 6.73E+08 | 9.71E+08 | 9.80E+08 | 1.07E+09 | 0.880E+09 | 9.19E+08 | 9.19E+08 | 9.56E+08 | 1.02E+09 |
| | (-25.83, -25.83) | (-18,-18) | 4.62E+08 | 4.81E+08 | 5.23E+08 | 5.18E+08 | 5.05E+08 | 4.73E+08 | 4.78E+08 | 3.48E+08 | 4.81E+08 | 4.72E+08 | 5.43E+08 | 0.422E+09 | 4.55E+08 | 4.63E+08 | 4.65E+08 | 5.08E+08 |
| | (-28.35, -28.35) | (-20,-20) | 2.31E+08 | 2.37E+08 | 2.72E+08 | 2.66E+08 | 2.64E+08 | 2.46E+08 | 2.44E+08 | 1.99E+08 | 2.50E+08 | 2.44E+08 | 2.63E+08 | 0.214E+09 | 2.34E+08 | 2.36E+08 | 2.41E+08 | 2.58E+08 |
| | (-30.87, -30.87) | (-22,-22) | 1.24E+08 | 1.20E+08 | 1.42E+08 | 1.42E+08 | 1.39E+08 | 1.31E+08 | 1.31E+08 | 1.18E+08 | 1.31E+08 | 1.17E+08 | 1.17E+08 | 0.113E+09 | 1.25E+08 | 1.24E+08 | 1.28E+08 | 1.41E+08 |
| | (-33.39, -33.39) | (-24,-24) | N/A | 7.11E+07 | 8.13E+07 | 8.00E+07 | 7.81E+07 | 7.49E+07 | 8.05E+07 | 7.86E+07 | 7.50E+07 | 6.70E+07 | 5.66E+07 | 0.677E+08 | 7.29E+07 | 7.50E+07 | 7.19E+07 | 7.64E+07 |

C/E comparison

| $^{237}$Np (n,f) | Position in cm | Grid Position | Experimental Value | HYU-TORT Korea | HYU-MCNP Korea | HYU-MCNPX Korea | Transpire Inc.-ATTILA USA | KI-MCU Russia | KOPEC-DORT Korea | VTI/SUT-HELIOS Slovak | WTI-MCNP Germany | VTT-TORT Finland | VTT-MT Finland | KI-LUCKY Russia | KAERI-DANTSYS Korea | VTT-MCNP-K Finland | VTT-MCNP-F Finland | SCK-MCNPX Belgium |
|---|---|---|---|---|---|---|---|---|---|---|---|---|---|---|---|---|---|---|
| Central Hole | ( 0.0, 0.0) | (+2.5,+2.5) | N/A | | | | | | | | | | | | | | | |
| Water Gap | (-54.36, -9.59) | 10.75 degree | N/A | | | | | | | | | | | | | | | |
| | (-52.89, -15.80) | 16.63 degree | N/A | | | | | | | | | | | | | | | |
| | (-51.53, -19.78) | 21.14 degree | N/A | | | | | | | | | | | | | | | |
| | (-50.03, -23.33) | 25.62 degree | N/A | | | | | | | | | | | | | | | |
| | (-48.74, -25.91) | 28.78 degree | N/A | | | | | | | | | | | | | | | |
| | (-46.29, -30.06) | 33.89 degree | N/A | | | | | | | | | | | | | | | |
| | (-44.08, -33.22) | 37.44 degree | N/A | | | | | | | | | | | | | | | |
| | (-42.29, -35.48) | 40.99 degree | N/A | | | | | | | | | | | | | | | |
| | (-39.03, -39.03) | 45 degree | 1.95E+07 | 0.97 | 1.04 | 1.07 | 1.03 | 1.01 | 1.08 | 1.22 | 1.00 | 0.95 | 0.82 | 0.90 | 1.16 | 0.91 | 0.91 | 0.97 |
| Reflector | (-23.31, -23.31) | (-16,-16) | 9.77E+08 | 1.03 | 1.05 | 1.04 | 1.04 | 0.97 | 1.01 | 0.69 | 0.99 | 1.00 | 1.09 | 0.90 | 0.94 | 0.94 | 0.98 | 1.04 |
| | (-25.83, -25.83) | (-18,-18) | 4.62E+08 | 1.04 | 1.13 | 1.12 | 1.09 | 1.02 | 1.04 | 0.75 | 1.04 | 1.02 | 1.18 | 0.91 | 0.98 | 1.00 | 1.01 | 1.10 |
| | (-28.35, -28.35) | (-20,-20) | 2.31E+08 | 1.03 | 1.18 | 1.15 | 1.14 | 1.07 | 1.06 | 0.86 | 1.08 | 1.06 | 1.14 | 0.93 | 1.01 | 1.02 | 1.04 | 1.12 |
| | (-30.87, -30.87) | (-22,-22) | 1.24E+08 | 0.97 | 1.14 | 1.15 | 1.12 | 1.06 | 1.06 | 0.95 | 1.06 | 0.95 | 0.94 | 0.91 | 1.01 | 1.00 | 1.03 | 1.14 |
| | (-33.39, -33.39) | (-24,-24) | N/A | | | | | | | | | | | | | | | |
| Number of positions within +-5% = | | | | 5 | 1 | 1 | 2 | 3 | 2 | 0 | 3 | 3 | 0 | 0 | 3 | 3 | 4 | 2 |
| Number of positions within +-10% = | | | | 5 | 2 | 2 | 3 | 5 | 5 | 1 | 5 | 5 | 2 | 4 | 4 | 5 | 5 | 2 |
| Number of positions within +-20% = | | | | 5 | 5 | 5 | 5 | 5 | 5 | 2 | 5 | 5 | 5 | 5 | 5 | 5 | 5 | 5 |

# Table 4.11(a). Equivalent fission fluxes: $^{27}$Al(n,α) detector results and C/E comparison in stainless steel zones

Calculated results

| $^{27}$Al (n,a) | Position in cm | Grid Position | Experimental Value | HYU-TORT | HYU-MCNP | HYU-MCNPX | Transpire Inc.-ATTILA | KI-MCU | KOPEC-DORT | WTI-MCNP | VTT-TORT | VTT-MT | KI-LUCKY | KAERI-DANTSYS | VTT-MCNP-K | VTT-MCNP-F | SCK-MCNPX |
|---|---|---|---|---|---|---|---|---|---|---|---|---|---|---|---|---|---|
| | | | | Korea | Korea | Korea | USA | Russia | Korea | Germany | Finland | Finland | Russia | Korea | Finland | Finland | Belgium |
| Inner Baffle | ( -4.41, -0.63) | (-1,+2) | 1.43E+09 | 1.43E+09 | 1.08E+09 | 1.11E+09 | 1.43E+09 | 1.38E+09 | 1.43E+09 | 1.32E+09 | 1.40E+09 | 1.43E+09 | 1.37E+09 | 1.27E+09 | 1.19E+09 | 1.29E+09 | 1.48E+09 |
| | ( -4.41, -4.41) | (-1,-1) | 1.70E+09 | 1.69E+09 | 1.35E+09 | 1.59E+09 | 1.67E+09 | 1.72E+09 | 1.73E+09 | 1.60E+09 | 1.60E+09 | 1.92E+09 | 0.161E+10 | 1.51E+09 | 1.48E+09 | 1.68E+09 | 1.51E+09 |
| Outer Baffle | (-39.69, -0.63) | (-29,+2) | 5.92E+08 | 4.70E+08 | 4.74E+08 | 6.38E+08 | 5.34E+08 | 5.25E+08 | 5.70E+08 | 5.58E+08 | 4.69E+08 | 4.93E+08 | 0.478E+09 | 5.31E+08 | 4.95E+08 | 4.78E+08 | 5.32E+08 |
| | (-39.69, -5.67) | (-29,-2) | N/A | 4.47E+08 | 6.72E+08 | 4.44E+08 | 5.22E+08 | 5.09E+08 | 5.41E+08 | 5.34E+08 | 4.35E+08 | 4.84E+08 | 0.454E+09 | 5.04E+08 | 5.03E+08 | 4.73E+08 | 5.39E+08 |
| | (-39.69, -11.97) | (-29,-7) | 4.52E+08 | 3.70E+08 | 4.22E+08 | 2.98E+08 | 4.24E+08 | 3.83E+08 | 4.42E+08 | 4.34E+08 | 3.49E+08 | 3.97E+08 | 0.372E+09 | 4.13E+08 | 4.30E+08 | 3.83E+08 | 4.42E+08 |
| | (-39.69, -18.27) | (-29,-12) | 2.69E+08 | 2.25E+08 | 2.22E+08 | 2.58E+08 | 2.49E+08 | 2.53E+08 | 2.66E+08 | 2.60E+08 | 2.00E+08 | 2.33E+08 | 0.223E+09 | 2.43E+08 | 2.61E+08 | 2.40E+08 | 2.70E+08 |
| | (-37.17, -20.79) | (-27,-14) | 2.76E+08 | 2.49E+08 | 4.85E+08 | 2.60E+08 | 2.60E+08 | 2.74E+08 | 2.80E+08 | 2.69E+08 | 2.22E+08 | 2.55E+08 | 0.228E+09 | 2.52E+08 | 2.92E+08 | 2.52E+08 | 2.35E+08 |
| | (-30.87, -20.79) | (-22,-14) | N/A | 4.90E+08 | 5.84E+08 | 6.23E+08 | 5.20E+08 | 4.85E+08 | 5.34E+08 | 5.06E+08 | 4.83E+08 | 5.18E+08 | 0.451E+09 | 4.87E+08 | 5.57E+08 | 4.57E+08 | 4.92E+08 |
| | (-24.57, -20.79) | (-17,-14) | 8.30E+08 | 8.00E+08 | 1.00E+09 | 8.49E+08 | 8.16E+08 | 7.93E+08 | 8.46E+08 | 8.18E+08 | 7.16E+08 | 8.85E+08 | 0.754E+09 | 7.47E+08 | 7.76E+08 | 7.65E+08 | 6.75E+08 |
| Barrel | (-49.77, -0.63) | (-37,+2) | 9.62E+07 | 8.40E+07 | 1.09E+08 | 8.63E+07 | 8.64E+07 | 8.50E+07 | 9.51E+07 | 8.73E+07 | 7.15E+07 | 7.09E+07 | 0.783E+08 | 8.66E+07 | 8.07E+07 | 7.58E+07 | 8.53E+07 |
| | (-49.77, -9.45) | (-37,-5) | 8.50E+07 | 7.08E+07 | 6.54E+07 | 6.60E+07 | 7.10E+07 | 7.08E+07 | 7.90E+07 | 7.54E+07 | 5.69E+07 | 5.95E+07 | 0.659E+08 | 7.57E+07 | 6.53E+07 | 5.91E+07 | 5.76E+07 |
| | (-47.25, -18.27) | (-35,-12) | 7.33E+07 | 6.33E+07 | 6.03E+07 | 7.56E+07 | 6.60E+07 | 6.56E+07 | 7.27E+07 | 6.25E+07 | 5.41E+07 | 5.67E+07 | 0.592E+08 | 6.54E+07 | 5.76E+07 | 6.26E+07 | 5.76E+07 |
| | (-45.99, -22.05) | (-34,-15) | 6.01E+07 | 5.45E+07 | 6.00E+07 | 4.82E+07 | 5.52E+07 | 5.54E+07 | 5.93E+07 | 5.55E+07 | 4.78E+07 | 4.96E+07 | 0.507E+08 | 5.41E+07 | 6.35E+07 | 4.83E+07 | 7.17E+07 |
| | (-44.73, -24.57) | (-33,-17) | 5.48E+07 | 4.72E+07 | 5.08E+07 | 4.05E+07 | 4.75E+07 | 5.08E+07 | 5.49E+07 | 5.24E+07 | 4.40E+07 | 4.70E+07 | 0.455E+08 | 4.67E+07 | 4.85E+07 | 5.02E+07 | 3.98E+07 |
| | (-42.21, -28.35) | (-31,-20) | 5.71E+07 | 5.29E+07 | 5.22E+07 | 6.11E+07 | 5.15E+07 | 4.78E+07 | 5.55E+07 | 5.07E+07 | 4.34E+07 | 4.54E+07 | 0.480E+08 | 4.78E+07 | 5.20E+07 | 4.35E+07 | 4.52E+07 |
| | (-38.43, -33.39) | (-28,-24) | 5.19E+07 | 5.30E+07 | 5.29E+07 | 4.33E+07 | 4.70E+07 | 4.73E+07 | 5.45E+07 | 4.55E+07 | 4.32E+07 | 4.16E+07 | 0.457E+08 | 4.58E+07 | 4.38E+07 | 4.24E+07 | 6.33E+07 |
| | (-35.91, -35.91) | (-26,-26) | 5.12E+07 | 5.31E+07 | 5.21E+07 | 5.27E+07 | 4.77E+07 | 5.09E+07 | 5.55E+07 | 4.94E+07 | 4.29E+07 | 4.20E+07 | 0.447E+08 | 4.72E+07 | 4.25E+07 | 4.43E+07 | 5.16E+07 |
| Neutron Pad | (-58.54, -22.47) | 21 degree | 1.05E+07 | 9.40E+06 | 7.28E+06 | 6.72E+06 | 8.81E+06 | 7.81E+06 | 9.11E+06 | 8.07E+06 | 6.81E+06 | 7.17E+06 | 0.815E+07 | 8.94E+06 | 7.38E+06 | 8.80E+06 | N/A |
| | (-46.60, -41.95) | 42 degree | 8.39E+06 | 7.64E+06 | 6.86E+06 | 8.65E+06 | 6.89E+06 | 6.50E+06 | 7.87E+06 | 6.56E+06 | 5.90E+06 | 5.95E+06 | 0.655E+07 | 6.58E+06 | 6.44E+06 | 7.20E+06 | N/A |

C/E comparison

| $^{27}$Al (n,a) | Position in cm | Grid Position | Experimental Value | HYU-TORT | HYU-MCNP | HYU-MCNPX | Transpire Inc.-ATTILA | KI-MCU | KOPEC-DORT | WTI-MCNP | VTT-TORT | VTT-MT | KI-LUCKY | KAERI-DANTSYS | VTT-MCNP-K | VTT-MCNP-F | SCK-MCNPX |
|---|---|---|---|---|---|---|---|---|---|---|---|---|---|---|---|---|---|
| | | | | Korea | Korea | Korea | USA | Russia | Korea | Germany | Finland | Finland | Russia | Korea | Finland | Finland | Belgium |
| Inner Baffle | ( -4.41, -0.63) | (-1,+2) | 1.43E+09 | 1.00 | 0.75 | 0.78 | 1.00 | 0.96 | 1.00 | 0.92 | 0.98 | 1.00 | 0.96 | 0.89 | 0.83 | 0.90 | 1.03 |
| | ( -4.41, -4.41) | (-1,-1) | 1.70E+09 | 1.00 | 0.79 | 0.93 | 0.98 | 1.01 | 1.02 | 0.94 | 0.94 | 1.13 | 0.95 | 0.89 | 0.87 | 0.99 | 0.89 |
| Outer Baffle | (-39.69, -0.63) | (-29,+2) | 5.92E+08 | 0.79 | 0.80 | 1.08 | 0.90 | 0.89 | 0.96 | 0.94 | 0.79 | 0.83 | 0.81 | 0.90 | 0.84 | 0.81 | 0.90 |
| | (-39.69, -5.67) | (-29,-2) | N/A | | | | | | | | | | | | | | |
| | (-39.69, -11.97) | (-29,-7) | 4.52E+08 | 0.82 | 0.93 | 0.66 | 0.94 | 0.85 | 0.98 | 0.96 | 0.77 | 0.88 | 0.82 | 0.91 | 0.95 | 0.85 | 0.98 |
| | (-39.69, -18.27) | (-29,-12) | 2.69E+08 | 0.84 | 0.83 | 0.96 | 0.92 | 0.94 | 0.99 | 0.97 | 0.74 | 0.86 | 0.83 | 0.90 | 0.97 | 0.89 | 1.00 |
| | (-37.17, -20.79) | (-27,-14) | 2.76E+08 | 0.90 | 1.76 | 0.94 | 0.94 | 0.99 | 1.01 | 0.98 | 0.80 | 0.92 | 0.83 | 0.91 | 1.06 | 0.91 | 0.85 |
| | (-30.87, -20.79) | (-22,-14) | N/A | | | | | | | | | | | | | | |
| | (-24.57, -20.79) | (-17,-14) | 8.30E+08 | 0.96 | 1.21 | 1.02 | 0.98 | 0.95 | 1.02 | 0.99 | 0.86 | 1.07 | 0.91 | 0.90 | 0.94 | 0.92 | 0.81 |
| Barrel | (-49.77, -0.63) | (-37,+2) | 9.62E+07 | 0.87 | 1.13 | 0.90 | 0.90 | 0.88 | 0.99 | 0.91 | 0.74 | 0.74 | 0.81 | 0.90 | 0.84 | 0.79 | 0.89 |
| | (-49.77, -9.45) | (-37,-5) | 8.50E+07 | 0.83 | 0.77 | 0.78 | 0.84 | 0.83 | 0.93 | 0.89 | 0.67 | 0.70 | 0.78 | 0.89 | 0.77 | 0.69 | 0.68 |
| | (-47.25, -18.27) | (-35,-12) | 7.33E+07 | 0.86 | 0.82 | 1.03 | 0.90 | 0.90 | 0.99 | 0.85 | 0.74 | 0.77 | 0.81 | 0.89 | 0.79 | 0.85 | 0.79 |
| | (-45.99, -22.05) | (-34,-15) | 6.01E+07 | 0.91 | 1.00 | 0.80 | 0.92 | 0.92 | 0.99 | 0.92 | 0.79 | 0.83 | 0.84 | 0.90 | 1.06 | 0.80 | 1.19 |
| | (-44.73, -24.57) | (-33,-17) | 5.48E+07 | 0.86 | 0.93 | 0.74 | 0.87 | 0.93 | 1.00 | 0.96 | 0.80 | 0.86 | 0.83 | 0.85 | 0.88 | 0.92 | 0.73 |
| | (-42.21, -28.35) | (-31,-20) | 5.71E+07 | 0.93 | 0.91 | 1.07 | 0.90 | 0.84 | 0.97 | 0.89 | 0.76 | 0.80 | 0.84 | 0.84 | 0.91 | 0.76 | 0.79 |
| | (-38.43, -33.39) | (-28,-24) | 5.19E+07 | 1.02 | 1.02 | 0.83 | 0.91 | 0.91 | 1.05 | 0.88 | 0.83 | 0.80 | 0.88 | 0.88 | 0.84 | 0.82 | 1.22 |
| | (-35.91, -35.91) | (-26,-26) | 5.12E+07 | 1.04 | 1.02 | 1.03 | 0.93 | 0.99 | 1.08 | 0.96 | 0.84 | 0.82 | 0.87 | 0.92 | 0.83 | 0.86 | 1.01 |
| Neutron Pad | (-58.54, -22.47) | 21 degree | 1.05E+07 | 0.90 | 0.69 | 0.64 | 0.84 | 0.74 | 0.87 | 0.77 | 0.65 | 0.68 | 0.78 | 0.85 | 0.70 | 0.84 | |
| | (-46.60, -41.95) | 42 degree | 8.39E+06 | 0.91 | 0.82 | 1.03 | 0.82 | 0.77 | 0.94 | 0.78 | 0.70 | 0.71 | 0.78 | 0.78 | 0.77 | 0.86 | |
| Number of positions within +-5% = | | | | 5 | 3 | 5 | 3 | 5 | 12 | 6 | 1 | 1 | 1 | 0 | 2 | 1 | 4 |
| Number of positions within +-10% = | | | | 9 | 6 | 9 | 12 | 9 | 16 | 11 | 2 | 3 | 3 | 5 | 6 | 4 | 4 |
| Number of positions within +-20% = | | | | 16 | 11 | 12 | 17 | 15 | 17 | 15 | 7 | 11 | 14 | 16 | 13 | 14 | 10 |

# Table 4.11(b). Equivalent fission fluxes: $^{27}$Al(n,α) detector results and C/E comparison in water zones

Calculated results

| $^{27}$Al (n,a) | Position in cm | Grid Position | Experimental Value | HYU-TORT | HYU-MCNP | HYU-MCNPX | Transpire Inc.-ATTILA | KI-MCU | KOPEC-DORT | WTI-MCNP | VTT-TORT | VTT-MT | KI-LUCKY | KAERI-DANTSYS | VTT-MCNP-K | VTT-MCNP-F |
|---|---|---|---|---|---|---|---|---|---|---|---|---|---|---|---|---|
| | | | | Korea | Korea | Korea | USA | Russia | Korea | Germany | Finland | Finland | Russia | Korea | Finland | Finland |
| Central Hole | ( 0.0, 0.0) | (+2.5,+2.5) | N/A | 1.24E+09 | 3.21E+08 | 3.04E+08 | 1.19E+09 | 7.30E+07 | 1.22E+09 | 1.18E+09 | 1.14E+09 | 1.10E+09 | 0.119E+10 | 1.10E+09 | 1.10E+09 | 1.16E+09 |
| Water Gap | (-54.36, -9.59) | 10.75 degree | N/A | 3.22E+07 | 3.10E+07 | 4.15E+07 | 3.12E+07 | 2.88E+07 | 3.36E+07 | 3.01E+07 | 2.63E+07 | 2.59E+07 | 0.292E+08 | 2.96E+07 | 2.72E+07 | 2.55E+07 |
| | (-52.89, -15.80) | 16.63 degree | 3.15E+07 | 2.97E+07 | 2.57E+07 | 2.31E+07 | 2.87E+07 | 2.70E+07 | 3.23E+07 | 2.98E+07 | 2.57E+07 | 2.49E+07 | 0.272E+08 | 3.28E+07 | 2.46E+07 | 2.49E+07 |
| | (-51.53, -19.78) | 21.14 degree | 2.52E+07 | 2.99E+07 | 2.72E+07 | 2.74E+07 | 2.92E+07 | 2.72E+07 | 3.09E+07 | 2.87E+07 | 2.48E+07 | 2.41E+07 | 0.271E+08 | 3.14E+07 | 2.66E+07 | 2.58E+07 |
| | (-50.03, -23.33) | 25.62 degree | 2.67E+07 | 2.68E+07 | 2.82E+07 | 4.28E+07 | 2.54E+07 | 2.46E+07 | 2.71E+07 | 2.61E+07 | 2.18E+07 | 2.30E+07 | 0.241E+08 | 2.54E+07 | 2.93E+07 | 2.12E+07 |
| | (-48.74, -25.91) | 28.78 degree | 2.54E+07 | 2.44E+07 | 2.05E+07 | 2.59E+07 | 2.38E+07 | 2.27E+07 | 2.60E+07 | 2.41E+07 | 2.10E+07 | 2.25E+07 | 0.226E+08 | 2.35E+07 | 2.34E+07 | 2.38E+07 |
| | (-46.29, -30.06) | 33.89 degree | 2.50E+07 | 2.45E+07 | 2.49E+07 | 2.25E+07 | 2.33E+07 | 2.14E+07 | 2.52E+07 | 2.32E+07 | 2.03E+07 | 2.17E+07 | 0.218E+08 | 2.40E+07 | 2.19E+07 | 2.00E+07 |
| | (-44.08, -33.22) | 37.44 degree | N/A | 2.43E+07 | 2.69E+07 | 3.61E+07 | 2.17E+07 | 2.18E+07 | 2.52E+07 | 2.13E+07 | 2.03E+07 | 2.03E+07 | 0.217E+08 | 2.14E+07 | 2.23E+07 | 2.15E+07 |
| | (-42.29, -35.48) | 40.99 degree | 2.30E+07 | 2.41E+07 | 2.76E+07 | 2.40E+07 | 2.24E+07 | 2.19E+07 | 2.52E+07 | 2.14E+07 | 2.05E+07 | 1.99E+07 | 0.217E+08 | 2.07E+07 | 1.97E+07 | 2.08E+07 |
| | (-39.03, -39.03) | 45 degree | 2.30E+07 | 2.49E+07 | 1.77E+07 | 2.26E+07 | 2.28E+07 | 2.21E+07 | 2.52E+07 | 2.12E+07 | 2.05E+07 | 1.96E+07 | 0.217E+08 | 2.47E+07 | 2.27E+07 | 2.35E+07 |
| Reflector | (-23.31, -23.31) | (-16,-16) | 6.66E+08 | 6.48E+08 | 5.87E+08 | 6.87E+08 | 6.42E+08 | 6.28E+08 | 6.88E+08 | 6.16E+08 | 6.15E+08 | 6.77E+08 | 0.619E+09 | 6.11E+08 | 6.55E+08 | 6.14E+08 |
| | (-25.83, -25.83) | (-18,-18) | 4.06E+08 | 3.98E+08 | 3.99E+08 | 4.77E+08 | 3.91E+08 | 3.70E+08 | 4.24E+08 | 3.90E+08 | 3.63E+08 | 3.98E+08 | 0.375E+09 | 3.81E+08 | 3.66E+08 | 3.68E+08 |
| | (-28.35, -28.35) | (-20,-20) | 2.53E+08 | 2.46E+08 | 2.18E+08 | 2.51E+08 | 2.35E+08 | 2.12E+08 | 2.63E+08 | 2.32E+08 | 2.18E+08 | 2.33E+08 | 0.228E+09 | 2.30E+08 | 2.16E+08 | 2.16E+08 |
| | (-30.87, -30.87) | (-22,-22) | 1.52E+08 | 1.52E+08 | 1.50E+08 | 1.51E+08 | 1.44E+08 | 1.39E+08 | 1.65E+08 | 1.41E+08 | 1.25E+08 | 1.32E+08 | 0.140E+09 | 1.43E+08 | 1.46E+08 | 1.40E+08 |
| | (-33.39, -33.39) | (-24,-24) | 9.71E+07 | 9.44E+07 | 9.38E+07 | 8.40E+07 | 8.80E+07 | 8.29E+07 | 1.03E+08 | 8.44E+07 | 7.55E+07 | 7.60E+07 | 0.851E+08 | 8.81E+07 | 8.89E+07 | 7.67E+07 |

C/E comparison

| $^{27}$Al (n,a) | Position in cm | Grid Position | Experimental Value | HYU-TORT | HYU-MCNP | HYU-MCNPX | Transpire Inc.-ATTILA | KI-MCU | KOPEC-DORT | WTI-MCNP | VTT-TORT | VTT-MT | KI-LUCKY | KAERI-DANTSYS | VTT-MCNP-K | VTT-MCNP-F |
|---|---|---|---|---|---|---|---|---|---|---|---|---|---|---|---|---|
| | | | | Korea | Korea | Korea | USA | Russia | Korea | Germany | Finland | Finland | Russia | Korea | Finland | Finland |
| Central Hole | ( 0.0, 0.0) | (+2.5,+2.5) | N/A | | | | | | | | | | | | | |
| Water Gap | (-54.36, -9.59) | 10.75 degree | N/A | | | | | | | | | | | | | |
| | (-52.89, -15.80) | 16.63 degree | 3.15E+07 | 0.94 | 0.81 | 0.73 | 0.91 | 0.86 | 1.03 | 0.95 | 0.81 | 0.79 | 0.86 | 1.04 | 0.78 | 0.79 |
| | (-51.53, -19.78) | 21.14 degree | 2.52E+07 | 1.19 | 1.08 | 1.09 | 1.16 | 1.08 | 1.23 | 1.14 | 0.98 | 0.96 | 1.08 | 1.25 | 1.05 | 1.02 |
| | (-50.03, -23.33) | 25.62 degree | 2.67E+07 | 1.00 | 1.06 | 1.60 | 0.95 | 0.92 | 1.01 | 0.98 | 0.82 | 0.86 | 0.90 | 0.95 | 1.10 | 0.79 |
| | (-48.74, -25.91) | 28.78 degree | 2.54E+07 | 0.96 | 0.81 | 1.02 | 0.94 | 0.89 | 1.02 | 0.95 | 0.83 | 0.88 | 0.89 | 0.93 | 0.92 | 0.94 |
| | (-46.29, -30.06) | 33.89 degree | 2.50E+07 | 0.98 | 1.00 | 0.90 | 0.93 | 0.86 | 1.01 | 0.93 | 0.81 | 0.87 | 0.87 | 0.96 | 0.88 | 0.80 |
| | (-44.08, -33.22) | 37.44 degree | N/A | | | | | | | | | | | | | |
| | (-42.29, -35.48) | 40.99 degree | 2.30E+07 | 1.05 | 1.20 | 1.05 | 0.97 | 0.95 | 1.10 | 0.93 | 0.89 | 0.87 | 0.94 | 0.90 | 0.86 | 0.90 |
| | (-39.03, -39.03) | 45 degree | 2.30E+07 | 1.08 | 0.77 | 0.98 | 0.99 | 0.96 | 1.09 | 0.92 | 0.89 | 0.85 | 0.94 | 1.08 | 0.99 | 1.02 |
| Reflector | (-23.31, -23.31) | (-16,-16) | 6.66E+08 | 0.97 | 0.88 | 1.03 | 0.96 | 0.94 | 1.03 | 0.93 | 0.92 | 1.02 | 0.93 | 0.92 | 0.98 | 0.92 |
| | (-25.83, -25.83) | (-18,-18) | 4.06E+08 | 0.98 | 0.98 | 1.17 | 0.96 | 0.91 | 1.04 | 0.96 | 0.89 | 0.98 | 0.92 | 0.94 | 0.90 | 0.91 |
| | (-28.35, -28.35) | (-20,-20) | 2.53E+08 | 0.97 | 0.86 | 0.99 | 0.93 | 0.84 | 1.04 | 0.92 | 0.86 | 0.92 | 0.90 | 0.91 | 0.85 | 0.85 |
| | (-30.87, -30.87) | (-22,-22) | 1.52E+08 | 1.00 | 0.99 | 0.99 | 0.95 | 0.92 | 1.09 | 0.93 | 0.82 | 0.87 | 0.92 | 0.94 | 0.96 | 0.92 |
| | (-33.39, -33.39) | (-24,-24) | 9.71E+07 | 0.97 | 0.97 | 0.86 | 0.91 | 0.85 | 1.06 | 0.87 | 0.78 | 0.78 | 0.88 | 0.91 | 0.92 | 0.79 |
| Number of positions within +-5% = | | | | 9 | 4 | 6 | 5 | 2 | 7 | 2 | 1 | 3 | 0 | 3 | 3 | 2 |
| Number of positions within +-10% = | | | | 11 | 6 | 7 | 11 | 7 | 11 | 10 | 2 | 4 | 8 | 11 | 8 | 7 |
| Number of positions within +-20% = | | | | 12 | 10 | 10 | 12 | 12 | 11 | 12 | 11 | 10 | 12 | 11 | 11 | 9 |

**Table 4.12(a). Ratios of equivalent fission fluxes from KCODE calculation to those from fixed source calculation of VTT in stainless steel zones**

[Unit: neutrons/cm$^2$/sec]

| Measurement Position [1] | $^{58}$Ni (n,p) | $^{115}$In (n,n') | $^{103}$Rh (n,n') | $^{64}$Zn (n,p) | $^{237}$Np (n,f) | $^{27}$Al (n,α) | Flux at E>0.1MeV | Flux at E>1.0MeV | Optional DPA [2] |
|---|---|---|---|---|---|---|---|---|---|
| Inner Baffle | | | | | | | | | |
| ( -4.41, -0.63) | 0.92 | 0.93 | 0.93 | 0.92 | 0.93 | 0.93 | 0.93 | 0.93 | |
| ( -4.41, -4.41) | 0.91 | 0.92 | 0.90 | 0.91 | 0.90 | 0.88 | 0.91 | 0.89 | |
| Outer Baffle | | | | | | | | | |
| (-39.69, -0.69) | 1.06 | 1.07 | 1.10 | 1.06 | 1.10 | 1.04 | 1.09 | 1.11 | |
| (-39.69, -5.67) | 1.06 | 1.08 | 1.07 | 1.05 | 1.07 | 1.06 | 1.07 | 1.08 | |
| (-39.69, -11.97) | 1.07 | 1.08 | 1.09 | 1.07 | 1.09 | 1.12 | 1.10 | 1.08 | |
| (-39.69, -18.27) | 1.03 | 1.05 | 1.10 | 1.02 | 1.09 | 1.09 | 1.10 | 1.11 | |
| (-37.17, -20.79) | 1.05 | 1.06 | 1.07 | 1.05 | 1.07 | 1.16 | 1.06 | 1.07 | |
| (-30.87, -20.79) | 1.02 | 1.02 | 1.04 | 1.02 | 1.04 | 1.22 | 1.02 | 1.06 | |
| (-24.57, -20.79) | 0.95 | 0.95 | 0.95 | 0.95 | 0.95 | 1.01 | 0.95 | 0.95 | |
| Barrel | | | | | | | | | |
| (-49.77, -0.63) | 1.04 | 1.07 | 1.04 | 1.04 | 1.04 | 1.06 | 1.06 | 1.03 | |
| (-49.77, -9.45) | 1.06 | 1.07 | 1.07 | 1.05 | 1.08 | 1.11 | 1.10 | 1.06 | |
| (-47.25, -18.27) | 1.06 | 1.08 | 1.09 | 1.06 | 1.09 | 0.92 | 1.08 | 1.09 | |
| (-45.99, -22.05) | 1.08 | 1.08 | 1.05 | 1.08 | 1.05 | 1.31 | 1.06 | 1.04 | |
| (-44.73, -24.57) | 1.03 | 1.06 | 1.04 | 1.03 | 1.05 | 0.97 | 1.03 | 1.05 | |
| (-42.21, -28.35) | 1.01 | 1.04 | 1.03 | 1.01 | 1.03 | 1.19 | 1.04 | 1.02 | |
| (-38.43, -33.39) | 0.98 | 1.00 | 1.04 | 0.97 | 1.03 | 1.03 | 1.04 | 1.07 | |
| (-35.91, -35.91) | 1.00 | 0.99 | 1.03 | 1.00 | 1.03 | 0.96 | 1.04 | 1.05 | |
| Neutron Pad | | | | | | | | | |
| (-58.54, -22.47) | 1.06 | 1.08 | 1.16 | 1.05 | 1.16 | 0.84 | 1.10 | 1.16 | |
| (-46.60, -41.95) | 1.00 | 1.03 | 1.25 | 1.00 | 1.26 | 0.89 | 1.28 | 1.24 | |

1) (x,y) in [cm,cm] co-ordinates with respect to core center

2) Unit: DPAs/sec

**Table 4.12(b). Ratios of equivalent fission fluxes from KCODE calculation to those from fixed source calculation of VTT in water zones**

[Unit: neutrons/cm$^2$/sec]

| Measurement Position [1] | $^{58}$Ni (n,p) | $^{115}$In (n,n') | $^{103}$Rh (n,n') | $^{64}$Zn (n,p) | $^{237}$Np (n,f) | $^{27}$Al (n,α) | Flux at E>0.1MeV | Flux at E>1.0MeV | Optional DPA [2] |
|---|---|---|---|---|---|---|---|---|---|
| Central Hole | | | | | | | | | |
| ( 00.00, 00.00) | 0.92 | 0.92 | 0.91 | 0.92 | 0.91 | 0.95 | 0.91 | 0.92 | |
| Water Gap | | | | | | | | | |
| (-54.36, -9.59) | 1.04 | 1.04 | 1.14 | 1.04 | 1.15 | 1.07 | 1.16 | 1.10 | |
| (-52.89, -15.80) | 1.03 | 1.07 | 1.06 | 1.03 | 1.06 | 0.99 | 1.06 | 1.06 | |
| (-51.53, -19.78) | 1.07 | 1.07 | 1.12 | 1.07 | 1.12 | 1.03 | 1.10 | 1.13 | |
| (-50.03, -23.33) | 1.12 | 1.08 | 1.06 | 1.12 | 1.04 | 1.38 | 1.04 | 1.05 | |
| (-48.74, -25.91) | 1.05 | 1.05 | 1.06 | 1.05 | 1.07 | 0.99 | 1.06 | 1.05 | |
| (-46.29, -30.06) | 1.01 | 1.01 | 1.01 | 1.02 | 1.03 | 1.09 | 1.07 | 1.03 | |
| (-44.08, -33.22) | 1.02 | 1.02 | 0.94 | 1.02 | 0.96 | 1.04 | 0.99 | 0.95 | |
| (-42.29, -35.48) | 1.03 | 1.02 | 1.13 | 1.03 | 1.13 | 0.95 | 1.06 | 1.15 | |
| (-39.03, -39.03) | 1.03 | 1.01 | 1.01 | 1.04 | 1.00 | 0.96 | 1.02 | 1.02 | |
| Reflector | | | | | | | | | |
| (-23.31, -23.31) | 0.96 | 0.97 | 0.96 | 0.96 | 0.96 | 1.07 | 0.95 | 0.97 | |
| (-25.83, -25.83) | 0.98 | 0.98 | 1.00 | 0.98 | 1.00 | 0.99 | 1.00 | 0.98 | |
| (-28.35, -28.35) | 0.99 | 0.99 | 0.98 | 0.99 | 0.98 | 1.00 | 1.00 | 0.96 | |
| (-30.87, -30.87) | 1.01 | 1.00 | 0.96 | 1.00 | 0.97 | 1.04 | 0.99 | 0.95 | |
| (-33.39, -33.39) | 1.03 | 1.01 | 1.04 | 1.02 | 1.04 | 1.16 | 1.05 | 1.03 | |

1) (x,y) in [cm,cm] co-ordinates with respect to core center

2) Unit: DPAs/sec

# Table 4.13(a). Reaction rates: $^{58}$Ni(n,p) detector results and C/E comparison in stainless steel zones

Calculated results (**Reaction Rates**)

| $^{58}$Ni (n,p) | Position in cm | Grid Position | Experimental Value **Equiv. Fiss. Flux** | Experimental Value **Reaction Rates** | HYU-TORT Korea | HYU-MCNP Korea | HYU-MCNPX Korea | Transpire Inc.-ATTILA USA | KI-MCU Russia | KOPEC-DORT Korea | WTI-MCNP Germany | VTT-TORT Finland | VTT-MT Finland | KI-LUCKY Russia | KAERI-DANTSYS Korea | VTT-MCNP-K Finland | VTT-MCNP-F Finland | SCK-MCNPX Belgium |
|---|---|---|---|---|---|---|---|---|---|---|---|---|---|---|---|---|---|---|
| Inner Baffle | ( -4.41, -0.63) | (-1,+2) | 1.51E+09 | 1.64E-16 | 1.60E-16 | 1.52E-16 | 1.52E-16 | 1.69E-16 | 1.57E-16 | 1.65E-16 | 1.60E-16 | 1.68E-16 | 1.67E-16 | 0.165E-15 | 1.48E-16 | 1.37E-16 | 1.49E-16 | 1.57E-16 |
| | ( -4.41, -4.41) | (-1,-1) | 1.83E+09 | 1.99E-16 | 1.93E-16 | 1.85E-16 | 1.85E-16 | 2.00E-16 | 1.91E-16 | 2.01E-16 | 1.95E-16 | 1.92E-16 | 2.20E-16 | 0.196E-15 | 1.78E-16 | 1.81E-16 | 1.99E-16 | 1.82E-16 |
| Outer Baffle | (-39.69, -0.63) | (-29,+2) | 5.80E+08 | 6.29E-17 | 5.26E-17 | 6.31E-17 | 6.08E-17 | 6.17E-17 | 6.12E-17 | 6.41E-17 | 6.32E-17 | 5.53E-17 | 4.98E-17 | 0.571E-16 | 6.00E-17 | 5.58E-17 | 5.27E-17 | 6.01E-17 |
| | (-39.69, -5.67) | (-29,-2) | 5.52E+08 | 5.99E-17 | 5.00E-17 | 6.26E-17 | 6.11E-17 | 5.98E-17 | 5.80E-17 | 6.09E-17 | 5.98E-17 | 5.14E-17 | 4.72E-17 | 0.542E-16 | 5.71E-17 | 5.54E-17 | 5.25E-17 | 5.82E-17 |
| | (-39.69, -11.97) | (-29,-7) | 4.47E+08 | 4.85E-17 | 4.11E-17 | 4.74E-17 | 4.75E-17 | 4.85E-17 | 4.64E-17 | 4.96E-17 | 4.94E-17 | 4.10E-17 | 3.82E-17 | 0.442E-16 | 4.65E-17 | 4.64E-17 | 4.33E-17 | 4.64E-17 |
| | (-39.69, -18.27) | (-29,-12) | 2.62E+08 | 2.84E-17 | 2.45E-17 | 2.68E-17 | 2.84E-17 | 2.82E-17 | 2.70E-17 | 2.94E-17 | 2.90E-17 | 2.31E-17 | 2.28E-17 | 0.261E-16 | 2.71E-17 | 2.66E-17 | 2.59E-17 | 2.64E-17 |
| | (-37.17, -20.79) | (-27,-14) | 2.75E+08 | 2.98E-17 | 2.70E-17 | 3.04E-17 | 2.91E-17 | 2.95E-17 | 2.85E-17 | 3.07E-17 | 2.98E-17 | 2.56E-17 | 2.42E-17 | 0.266E-16 | 2.80E-17 | 2.81E-17 | 2.67E-17 | 2.79E-17 |
| | (-30.87, -20.79) | (-22,-14) | 5.44E+08 | 5.90E-17 | 5.48E-17 | 5.80E-17 | 5.74E-17 | 6.01E-17 | 5.68E-17 | 6.04E-17 | 5.87E-17 | 5.74E-17 | 5.25E-17 | 0.538E-16 | 5.55E-17 | 5.58E-17 | 5.45E-17 | 5.79E-17 |
| | (-24.57, -20.79) | (-17,-14) | 8.69E+08 | 9.43E-17 | 9.22E-17 | 9.37E-17 | 9.42E-17 | 9.73E-17 | 9.13E-17 | 9.89E-17 | 9.37E-17 | 8.67E-17 | 9.32E-17 | 0.922E-16 | 8.82E-17 | 8.84E-17 | 9.31E-17 | 8.94E-17 |
| Barrel | (-49.77, -0.63) | (-37,+2) | 7.36E+07 | 7.99E-18 | 7.13E-18 | 8.43E-18 | 8.01E-18 | 8.07E-18 | 7.91E-18 | 8.55E-18 | 8.12E-18 | 6.80E-18 | 5.97E-18 | 0.766E-17 | 7.98E-18 | 6.98E-18 | 6.73E-18 | 7.75E-18 |
| | (-49.77, -9.45) | (-37,-5) | 6.13E+07 | 6.65E-18 | 6.06E-18 | 6.81E-18 | 6.88E-18 | 6.81E-18 | 6.81E-18 | 7.26E-18 | 6.86E-18 | 5.56E-18 | 5.05E-18 | 0.653E-17 | 6.92E-18 | 6.41E-18 | 6.06E-18 | 6.32E-18 |
| | (-47.25, -18.27) | (-35,-12) | 6.02E+07 | 6.53E-18 | 5.75E-18 | 6.40E-18 | 6.53E-18 | 6.59E-18 | 6.38E-18 | 6.91E-18 | 6.52E-18 | 5.46E-18 | 5.06E-18 | 0.611E-17 | 6.31E-18 | 6.25E-18 | 5.90E-18 | 6.81E-18 |
| | (-45.99, -22.05) | (-34,-15) | 5.06E+07 | 5.49E-18 | 4.98E-18 | 5.70E-18 | 5.21E-18 | 5.57E-18 | 5.49E-18 | 5.74E-18 | 5.46E-18 | 4.92E-18 | 4.50E-18 | 0.528E-17 | 5.20E-18 | 5.32E-18 | 4.92E-18 | 5.82E-18 |
| | (-44.73, -24.57) | (-33,-17) | 4.50E+07 | 4.88E-18 | 4.36E-18 | 4.84E-18 | 4.84E-18 | 4.86E-18 | 4.85E-18 | 5.24E-18 | 4.94E-18 | 4.48E-18 | 4.14E-18 | 0.477E-17 | 4.56E-18 | 4.65E-18 | 4.51E-18 | 5.25E-18 |
| | (-42.21, -28.35) | (-31,-20) | 4.16E+07 | 4.51E-18 | 4.29E-18 | 4.46E-18 | 4.82E-18 | 4.70E-18 | 4.54E-18 | 4.91E-18 | 4.57E-18 | 4.07E-18 | 3.73E-18 | 0.453E-17 | 4.25E-18 | 4.22E-18 | 4.16E-18 | 4.38E-18 |
| | (-38.43, -33.39) | (-28,-24) | 3.67E+07 | 3.98E-18 | 3.91E-18 | 4.00E-18 | 3.97E-18 | 3.96E-18 | 3.95E-18 | 4.39E-18 | 3.91E-18 | 3.65E-18 | 3.18E-18 | 0.397E-17 | 3.76E-18 | 3.63E-18 | 3.71E-18 | 3.88E-18 |
| | (-35.91, -35.91) | (-26,-26) | 3.59E+07 | 3.90E-18 | 3.87E-18 | 3.99E-18 | 4.11E-18 | 3.97E-18 | 3.94E-18 | 4.41E-18 | 3.98E-18 | 3.58E-18 | 3.15E-18 | 0.385E-17 | 3.78E-18 | 3.73E-18 | 3.72E-18 | 3.88E-18 |
| Neutron Pad | (-58.54, -22.47) | 21 degree | 5.89E+06 | 6.39E-19 | 6.21E-19 | 6.43E-19 | 6.20E-19 | 6.70E-19 | 6.37E-19 | 6.92E-19 | 6.38E-19 | 5.42E-19 | 3.79E-19 | 0.650E-18 | 6.43E-19 | 6.29E-19 | 5.95E-19 | 4.61E-19 |
| | (-46.60, -41.95) | 42 degree | N/A | N/A | 4.56E-19 | 4.77E-19 | 5.34E-19 | 4.89E-19 | 4.76E-19 | 5.40E-19 | 4.70E-19 | 4.24E-19 | 2.71E-19 | 0.478E-18 | 4.53E-19 | 4.43E-19 | 4.42E-19 | 3.32E-19 |

C/E comparison

| $^{58}$Ni (n,p) | Position in cm | Grid Position | Experimental Value **Equiv. Fiss. Flux** | Experimental Value **Reaction Rates** | HYU-TORT Korea | HYU-MCNP Korea | HYU-MCNPX Korea | Transpire Inc.-ATTILA USA | KI-MCU Russia | KOPEC-DORT Korea | WTI-MCNP Germany | VTT-TORT Finland | VTT-MT Finland | KI-LUCKY Russia | KAERI-DANTSYS Korea | VTT-MCNP-K Finland | VTT-MCNP-F Finland | SCK-MCNPX Belgium |
|---|---|---|---|---|---|---|---|---|---|---|---|---|---|---|---|---|---|---|
| Inner Baffle | ( -4.41, -0.63) | (-1,+2) | 1.51E+09 | 1.64E-16 | 0.98 | 0.93 | 0.93 | 1.03 | 0.96 | 1.01 | 0.98 | 1.02 | 1.02 | 1.01 | 0.90 | 0.84 | 0.91 | 0.96 |
| | ( -4.41, -4.41) | (-1,-1) | 1.83E+09 | 1.99E-16 | 0.97 | 0.93 | 0.93 | 1.01 | 0.96 | 1.01 | 0.98 | 0.97 | 1.11 | 0.99 | 0.90 | 0.91 | 1.00 | 0.92 |
| Outer Baffle | (-39.69, -0.63) | (-29,+2) | 5.80E+08 | 6.29E-17 | 0.84 | 1.00 | 0.97 | 0.98 | 0.97 | 1.02 | 1.00 | 0.88 | 0.79 | 0.91 | 0.95 | 0.89 | 0.84 | 0.96 |
| | (-39.69, -5.67) | (-29,-2) | 5.52E+08 | 5.99E-17 | 0.84 | 1.05 | 1.02 | 1.00 | 0.97 | 1.02 | 1.00 | 0.86 | 0.79 | 0.90 | 0.95 | 0.93 | 0.88 | 0.97 |
| | (-39.69, -11.97) | (-29,-7) | 4.47E+08 | 4.85E-17 | 0.85 | 0.98 | 0.98 | 1.00 | 0.96 | 1.02 | 1.02 | 0.85 | 0.79 | 0.91 | 0.96 | 0.96 | 0.89 | 0.96 |
| | (-39.69, -18.27) | (-29,-12) | 2.62E+08 | 2.84E-17 | 0.86 | 0.94 | 1.00 | 0.99 | 0.95 | 1.03 | 1.02 | 0.81 | 0.80 | 0.92 | 0.95 | 0.94 | 0.91 | 0.93 |
| | (-37.17, -20.79) | (-27,-14) | 2.75E+08 | 2.98E-17 | 0.90 | 1.02 | 0.98 | 0.99 | 0.96 | 1.03 | 1.00 | 0.86 | 0.81 | 0.89 | 0.94 | 0.94 | 0.89 | 0.93 |
| | (-30.87, -20.79) | (-22,-14) | 5.44E+08 | 5.90E-17 | 0.93 | 0.98 | 0.97 | 1.02 | 0.96 | 1.02 | 0.99 | 0.97 | 0.89 | 0.91 | 0.94 | 0.95 | 0.92 | 0.98 |
| | (-24.57, -20.79) | (-17,-14) | 8.69E+08 | 9.43E-17 | 0.98 | 0.99 | 1.00 | 1.03 | 0.97 | 1.05 | 0.99 | 0.92 | 0.99 | 0.98 | 0.93 | 0.94 | 0.99 | 0.95 |
| Barrel | (-49.77, -0.63) | (-37,+2) | 7.36E+07 | 7.99E-18 | 0.89 | 1.06 | 1.00 | 1.01 | 0.99 | 1.07 | 1.02 | 0.85 | 0.75 | 0.96 | 1.00 | 0.87 | 0.84 | 0.97 |
| | (-49.77, -9.45) | (-37,-5) | 6.13E+07 | 6.65E-18 | 0.91 | 1.02 | 1.04 | 1.02 | 1.02 | 1.09 | 1.03 | 0.84 | 0.76 | 0.98 | 1.04 | 0.96 | 0.91 | 0.95 |
| | (-47.25, -18.27) | (-35,-12) | 6.02E+07 | 6.53E-18 | 0.88 | 0.98 | 1.00 | 1.01 | 0.98 | 1.06 | 1.00 | 0.84 | 0.77 | 0.94 | 0.97 | 0.96 | 0.90 | 1.04 |
| | (-45.99, -22.05) | (-34,-15) | 5.06E+07 | 5.49E-18 | 0.91 | 1.04 | 0.95 | 1.01 | 1.00 | 1.04 | 0.99 | 0.90 | 0.82 | 0.96 | 0.95 | 0.97 | 0.90 | 1.06 |
| | (-44.73, -24.57) | (-33,-17) | 4.50E+07 | 4.88E-18 | 0.89 | 0.99 | 0.99 | 1.00 | 0.99 | 1.07 | 1.01 | 0.92 | 0.85 | 0.98 | 0.93 | 0.95 | 0.92 | 1.08 |
| | (-42.21, -28.35) | (-31,-20) | 4.16E+07 | 4.51E-18 | 0.95 | 0.99 | 1.07 | 1.04 | 1.00 | 1.09 | 1.01 | 0.90 | 0.83 | 1.00 | 0.94 | 0.93 | 0.92 | 0.97 |
| | (-38.43, -33.39) | (-28,-24) | 3.67E+07 | 3.98E-18 | 0.98 | 1.00 | 1.00 | 1.00 | 0.99 | 1.10 | 0.98 | 0.92 | 0.80 | 1.00 | 0.94 | 0.91 | 0.93 | 0.97 |
| | (-35.91, -35.91) | (-26,-26) | 3.59E+07 | 3.90E-18 | 0.99 | 1.02 | 1.05 | 1.02 | 1.01 | 1.13 | 1.02 | 0.92 | 0.81 | 0.99 | 0.97 | 0.96 | 0.96 | 1.00 |
| Neutron Pad | (-58.54, -22.47) | 21 degree | 5.89E+06 | 6.39E-19 | 0.97 | 1.01 | 0.97 | 1.05 | 1.00 | 1.08 | 1.00 | 0.85 | 0.59 | 1.02 | 1.01 | 0.98 | 0.93 | 0.72 |
| | (-46.60, -41.95) | 42 degree | N/A | N/A | | | | | | | | | | | | | | |
| Number of positions within +-5% = | | | | | 7 | 14 | 13 | 18 | 17 | 10 | 18 | 3 | 2 | 11 | 9 | 7 | 3 | 10 |
| Number of positions within +-10% = | | | | | 11 | 18 | 18 | 18 | 18 | 16 | 18 | 8 | 2 | 17 | 17 | 15 | 12 | 17 |
| Number of positions within +-20% = | | | | | 18 | 18 | 18 | 18 | 18 | 18 | 18 | 18 | 10 | 18 | 18 | 18 | 18 | 17 |

# Table 4.13(b). Reaction rates: $^{58}$Ni(n,p) detector results and C/E comparison in water zones

Calculated results (**Reaction Rates**)

| $^{58}$Ni (n,p) | Position in cm | Grid Position | Experimental Value **Equiv. Fiss. Flux** | Experimental Value **Reaction Rates** | HYU-TORT Korea | HYU-MCNP Korea | HYU-MCNPX Korea | Transpire Inc.-ATTILA USA | KI-MCU Russia | KOPEC-DORT Korea | WTI-MCNP Germany | VTT-TORT Finland | VTT-MT Finland | KI-LUCKY Russia | KAERI-DANTSYS Korea | VTT-MCNP-K Finland | VTT-MCNP-F Finland | SCK-MCNPX Belgium |
|---|---|---|---|---|---|---|---|---|---|---|---|---|---|---|---|---|---|---|
| Central Hole | ( 0.0, 0.0) | (+2.5,+2.5) | N/A | N/A | 1.19E-16 | 2.94E-17 | 3.04E-17 | 1.21E-16 | 7.16E-18 | 1.24E-16 | 1.19E-16 | 1.19E-16 | 1.13E-16 | 0.125E-15 | 1.11E-16 | 1.12E-16 | 1.22E-16 | 2.77E-17 |
| Water Gap | (-54.36, -9.59) | 10.75 degree | 2.09E+07 | 2.26765E-18 | 2.28E-18 | 2.44E-18 | 2.61E-18 | 2.51E-18 | 2.46E-18 | 2.63E-18 | 2.44E-18 | 2.17E-18 | 2.18E-18 | 0.242E-17 | 2.26E-18 | 2.28E-18 | 2.19E-18 | 2.32E-18 |
| | (-52.89, -15.80) | 16.63 degree | 2.06E+07 | 2.2351E-18 | 2.24E-18 | 2.35E-18 | 2.48E-18 | 2.42E-18 | 2.34E-18 | 2.57E-18 | 2.44E-18 | 2.16E-18 | 2.09E-18 | 0.234E-17 | 2.70E-18 | 2.23E-18 | 2.16E-18 | 2.31E-18 |
| | (-51.53, -19.78) | 21.14 degree | 1.96E+07 | 2.1266E-18 | 2.18E-18 | 2.36E-18 | 2.34E-18 | 2.38E-18 | 2.25E-18 | 2.47E-18 | 2.32E-18 | 2.09E-18 | 2.33E-18 | 0.227E-17 | 2.54E-18 | 2.23E-18 | 2.08E-18 | 2.29E-18 |
| | (-50.03, -23.33) | 25.62 degree | 1.77E+07 | 1.92045E-18 | 2.01E-18 | 2.22E-18 | 2.24E-18 | 2.16E-18 | 2.11E-18 | 2.20E-18 | 2.11E-18 | 1.88E-18 | 2.64E-18 | 0.207E-17 | 2.08E-18 | 2.16E-18 | 1.93E-18 | 2.10E-18 |
| | (-48.74, -25.91) | 28.78 degree | 1.62E+07 | 1.7577E-18 | 1.82E-18 | 1.91E-18 | 2.00E-18 | 2.01E-18 | 1.95E-18 | 2.08E-18 | 1.95E-18 | 1.79E-18 | 1.95E-18 | 0.194E-17 | 1.93E-18 | 1.89E-18 | 1.81E-18 | 2.15E-18 |
| | (-46.29, -30.06) | 33.89 degree | 1.48E+07 | 1.6058E-18 | 1.71E-18 | 1.91E-18 | 1.78E-18 | 1.85E-18 | 1.78E-18 | 1.91E-18 | 1.76E-18 | 1.63E-18 | 2.03E-18 | 0.175E-17 | 1.86E-18 | 1.68E-18 | 1.66E-18 | 2.00E-18 |
| | (-44.08, -33.22) | 37.44 degree | 1.39E+07 | 1.50815E-18 | 1.60E-18 | 1.61E-18 | 1.97E-18 | 1.66E-18 | 1.67E-18 | 1.83E-18 | 1.67E-18 | 1.56E-18 | 1.60E-18 | 0.169E-17 | 1.63E-18 | 1.60E-18 | 1.57E-18 | 1.89E-18 |
| | (-42.29, -35.48) | 40.99 degree | 1.32E+07 | 1.4322E-18 | 1.52E-18 | 1.71E-18 | 1.73E-18 | 1.65E-18 | 1.61E-18 | 1.78E-18 | 1.57E-18 | 1.51E-18 | 1.56E-18 | 0.163E-17 | 1.46E-18 | 1.54E-18 | 1.49E-18 | 1.32E-18 |
| | (-39.03, -39.03) | 45 degree | 1.31E+07 | 1.42135E-18 | 1.53E-18 | 1.52E-18 | 1.55E-18 | 1.62E-18 | 1.59E-18 | 1.75E-18 | 1.56E-18 | 1.49E-18 | 1.55E-18 | 0.159E-17 | 1.75E-18 | 1.50E-18 | 1.45E-18 | 1.49E-18 |
| Reflector | (-23.31, -23.31) | (-16,-16) | 6.32E+08 | 6.8572E-17 | 6.75E-17 | 6.75E-17 | 6.63E-17 | 7.10E-17 | 6.79E-17 | 7.28E-17 | 6.88E-17 | 6.82E-17 | 6.74E-17 | 0.685E-16 | 6.53E-17 | 6.53E-17 | 6.78E-17 | 6.81E-17 |
| | (-25.83, -25.83) | (-18,-18) | 3.41E+08 | 3.69985E-17 | 3.64E-17 | 3.70E-17 | 3.71E-17 | 3.82E-17 | 3.71E-17 | 4.02E-17 | 3.73E-17 | 3.60E-17 | 3.76E-17 | 0.375E-16 | 3.61E-17 | 3.56E-17 | 3.62E-17 | 3.70E-17 |
| | (-28.35, -28.35) | (-20,-20) | 1.88E+08 | 2.0398E-17 | 2.01E-17 | 2.03E-17 | 1.98E-17 | 2.11E-17 | 2.06E-17 | 2.27E-17 | 2.08E-17 | 1.99E-17 | 1.98E-17 | 0.209E-16 | 2.00E-17 | 1.95E-17 | 1.98E-17 | 2.04E-17 |
| | (-30.87, -30.87) | (-22,-22) | 1.05E+08 | 1.13925E-17 | 1.12E-17 | 1.17E-17 | 1.18E-17 | 1.19E-17 | 1.16E-17 | 1.31E-17 | 1.15E-17 | 1.04E-17 | 1.01E-17 | 0.119E-16 | 1.14E-17 | 1.13E-17 | 1.12E-17 | 1.24E-17 |
| | (-33.39, -33.39) | (-24,-24) | 5.91E+07 | 6.41235E-18 | 6.57E-18 | 7.05E-18 | 6.84E-18 | 6.94E-18 | 6.76E-18 | 7.76E-18 | 6.82E-18 | 6.00E-18 | 5.32E-18 | 0.690E-17 | 6.70E-18 | 6.56E-18 | 6.38E-18 | 6.39E-18 |

C/E comparison

| $^{58}$Ni (n,p) | Position in cm | Grid Position | Experimental Value **Equiv. Fiss. Flux** | Experimental Value **Reaction Rates** | HYU-TORT Korea | HYU-MCNP Korea | HYU-MCNPX Korea | Transpire Inc.-ATTILA USA | KI-MCU Russia | KOPEC-DORT Korea | WTI-MCNP Germany | VTT-TORT Finland | VTT-MT Finland | KI-LUCKY Russia | KAERI-DANTSYS Korea | VTT-MCNP-K Finland | VTT-MCNP-F Finland | SCK-MCNPX Belgium |
|---|---|---|---|---|---|---|---|---|---|---|---|---|---|---|---|---|---|---|
| Central Hole | ( 0.0, 0.0) | (+2.5,+2.5) | N/A | N/A | | | | | | | | | | | | | | |
| Water Gap | (-54.36, -9.59) | 10.75 degree | 2.09E+07 | 2.26765E-18 | 1.01 | 1.07 | 1.15 | 1.11 | 1.08 | 1.16 | 1.08 | 0.96 | 0.96 | 1.07 | 1.00 | 1.01 | 0.97 | 1.02 |
| | (-52.89, -15.80) | 16.63 degree | 2.06E+07 | 2.2351E-18 | 1.00 | 1.05 | 1.11 | 1.08 | 1.05 | 1.15 | 1.09 | 0.97 | 0.93 | 1.05 | 1.21 | 1.00 | 0.96 | 1.04 |
| | (-51.53, -19.78) | 21.14 degree | 1.96E+07 | 2.1266E-18 | 1.03 | 1.11 | 1.10 | 1.12 | 1.06 | 1.16 | 1.09 | 0.98 | 1.10 | 1.07 | 1.19 | 1.05 | 0.98 | 1.08 |
| | (-50.03, -23.33) | 25.62 degree | 1.77E+07 | 1.92045E-18 | 1.04 | 1.15 | 1.17 | 1.13 | 1.10 | 1.15 | 1.10 | 0.98 | 1.38 | 1.08 | 1.08 | 1.13 | 1.01 | 1.09 |
| | (-48.74, -25.91) | 28.78 degree | 1.62E+07 | 1.7577E-18 | 1.04 | 1.09 | 1.14 | 1.14 | 1.11 | 1.18 | 1.11 | 1.02 | 1.11 | 1.10 | 1.10 | 1.08 | 1.03 | 1.23 |
| | (-46.29, -30.06) | 33.89 degree | 1.48E+07 | 1.6058E-18 | 1.06 | 1.19 | 1.11 | 1.15 | 1.11 | 1.19 | 1.09 | 1.02 | 1.26 | 1.09 | 1.16 | 1.05 | 1.03 | 1.24 |
| | (-44.08, -33.22) | 37.44 degree | 1.39E+07 | 1.50815E-18 | 1.06 | 1.07 | 1.31 | 1.10 | 1.11 | 1.21 | 1.11 | 1.03 | 1.06 | 1.12 | 1.08 | 1.06 | 1.04 | 1.25 |
| | (-42.29, -35.48) | 40.99 degree | 1.32E+07 | 1.4322E-18 | 1.06 | 1.19 | 1.21 | 1.15 | 1.13 | 1.24 | 1.09 | 1.06 | 1.09 | 1.14 | 1.02 | 1.08 | 1.04 | 0.92 |
| | (-39.03, -39.03) | 45 degree | 1.31E+07 | 1.42135E-18 | 1.07 | 1.07 | 1.09 | 1.14 | 1.12 | 1.23 | 1.10 | 1.05 | 1.09 | 1.12 | 1.23 | 1.05 | 1.02 | 1.05 |
| Reflector | (-23.31, -23.31) | (-16,-16) | 6.32E+08 | 6.8572E-17 | 0.98 | 0.98 | 0.97 | 1.04 | 0.99 | 1.06 | 1.00 | 0.99 | 0.98 | 1.00 | 0.95 | 0.95 | 0.99 | 0.99 |
| | (-25.83, -25.83) | (-18,-18) | 3.41E+08 | 3.69985E-17 | 0.98 | 1.00 | 1.00 | 1.03 | 1.00 | 1.09 | 1.01 | 0.97 | 1.02 | 1.01 | 0.98 | 0.96 | 0.98 | 1.00 |
| | (-28.35, -28.35) | (-20,-20) | 1.88E+08 | 2.0398E-17 | 0.99 | 1.00 | 0.97 | 1.03 | 1.01 | 1.11 | 1.02 | 0.97 | 0.97 | 1.02 | 0.98 | 0.96 | 0.97 | 1.00 |
| | (-30.87, -30.87) | (-22,-22) | 1.05E+08 | 1.13925E-17 | 0.98 | 1.03 | 1.03 | 1.04 | 1.02 | 1.15 | 1.01 | 0.91 | 0.88 | 1.04 | 1.00 | 0.99 | 0.98 | 1.09 |
| | (-33.39, -33.39) | (-24,-24) | 5.91E+07 | 6.41235E-18 | 1.02 | 1.10 | 1.07 | 1.08 | 1.05 | 1.21 | 1.06 | 0.94 | 0.83 | 1.08 | 1.04 | 1.02 | 0.99 | 1.00 |
| | | Number of positions within +-5% = | | | 10 | 4 | 4 | 4 | 5 | 0 | 4 | 11 | 4 | 5 | 7 | 9 | 14 | 7 |
| | | Number of positions within +-10% = | | | 14 | 10 | 7 | 6 | 9 | 2 | 12 | 14 | 9 | 10 | 10 | 13 | 14 | 11 |
| | | Number of positions within +-20% = | | | 14 | 14 | 12 | 14 | 14 | 10 | 14 | 14 | 12 | 14 | 12 | 14 | 14 | 11 |

# Table 4.14(a). Reaction rates: $^{115}$In(n,n′) detector results and C/E comparison in stainless steel zones

Calculated results (**Reaction Rates**)

| $^{115}$In (n,n') | Position in cm | Grid Position | Experimental Value **Equiv. Fiss. Flux** | Experimental Value **Reaction Rates** | HYU-TORT Korea | HYU-MCNP Korea | HYU-MCNPX Korea | Transpire Inc.-ATTILA USA | KI-MCU Russia | KOPEC-DORT Korea | WTI-MCNP Germany | VTT-TORT Finland | VTT-MT Finland | KI-LUCKY Russia | KAERI-DANTSYS Korea | VTT-MCNP-K Finland | VTT-MCNP-F Finland | SCK-MCNPX Belgium |
|---|---|---|---|---|---|---|---|---|---|---|---|---|---|---|---|---|---|---|
| Inner Baffle | ( -4.41, -0.63) | (-1,+2) | 1.94E+09 | 3.69E-16 | 3.49E-16 | 3.41E-16 | 3.38E-16 | 3.68E-16 | 3.44E-16 | 3.64E-16 | 3.58E-16 | 3.71E-16 | 3.60E-16 | 0.361E-15 | 3.30E-16 | 3.02E-16 | 3.25E-16 | 3.43E-16 |
| | ( -4.41, -4.41) | (-1,-1) | 2.36E+09 | 4.49E-16 | 4.17E-16 | 4.11E-16 | 4.13E-16 | 4.35E-16 | 4.13E-16 | 4.38E-16 | 4.29E-16 | 4.24E-16 | 4.57E-16 | 0.427E-15 | 3.94E-16 | 3.97E-16 | 4.33E-16 | 4.07E-16 |
| Outer Baffle | (-39.69, -0.63) | (-29,+2) | 7.14E+08 | 1.36E-16 | 1.13E-16 | 1.33E-16 | 1.29E-16 | 1.30E-16 | 1.30E-16 | 1.36E-16 | 1.36E-16 | 1.19E-16 | 1.06E-16 | 0.122E-15 | 1.29E-16 | 1.19E-16 | 1.11E-16 | 1.30E-16 |
| | (-39.69, -5.67) | (-29,-2) | N/A | N/A | 1.07E-16 | 1.28E-16 | 1.29E-16 | 1.25E-16 | 1.23E-16 | 1.29E-16 | 1.28E-16 | 1.11E-16 | 1.00E-16 | 0.116E-15 | 1.23E-16 | 1.21E-16 | 1.12E-16 | 1.24E-16 |
| | (-39.69, -11.97) | (-29,-7) | 5.48E+08 | 1.04E-16 | 8.80E-17 | 1.01E-16 | 1.03E-16 | 1.02E-16 | 9.99E-17 | 1.05E-16 | 1.06E-16 | 8.88E-17 | 8.13E-17 | 0.946E-16 | 1.00E-16 | 9.91E-17 | 9.17E-17 | 1.00E-16 |
| | (-39.69, -18.27) | (-29,-12) | 3.33E+08 | 6.34E-17 | 5.35E-17 | 6.00E-17 | 6.11E-17 | 6.07E-17 | 5.96E-17 | 6.38E-17 | 6.33E-17 | 5.08E-17 | 4.94E-17 | 0.568E-16 | 5.97E-17 | 5.84E-17 | 5.57E-17 | 5.98E-17 |
| | (-37.17, -20.79) | (-27,-14) | 3.53E+08 | 6.72E-17 | 5.88E-17 | 6.47E-17 | 6.32E-17 | 6.36E-17 | 6.18E-17 | 6.66E-17 | 6.54E-17 | 5.64E-17 | 5.25E-17 | 0.581E-16 | 6.18E-17 | 6.16E-17 | 5.82E-17 | 6.22E-17 |
| | (-30.87, -20.79) | (-22,-14) | N/A | N/A | 1.18E-16 | 1.25E-16 | 1.23E-16 | 1.27E-16 | 1.22E-16 | 1.30E-16 | 1.28E-16 | 1.25E-16 | 1.12E-16 | 0.116E-15 | 1.21E-16 | 1.20E-16 | 1.18E-16 | 1.23E-16 |
| | (-24.57, -20.79) | (-17,-14) | 1.12E+09 | 2.13E-16 | 2.02E-16 | 2.03E-16 | 2.03E-16 | 2.10E-16 | 2.00E-16 | 2.16E-16 | 2.08E-16 | 1.92E-16 | 2.01E-16 | 0.201E-15 | 1.96E-16 | 1.94E-16 | 2.03E-16 | 1.97E-16 |
| Barrel | (-49.77, -0.63) | (-37,+2) | 8.97E+07 | 1.71E-17 | 1.44E-17 | 1.68E-17 | 1.65E-17 | 1.64E-17 | 1.63E-17 | 1.73E-17 | 1.69E-17 | 1.41E-17 | 1.17E-17 | 0.159E-16 | 1.68E-17 | 1.45E-17 | 1.35E-17 | 1.59E-17 |
| | (-49.77, -9.45) | (-37,-5) | 7.90E+07 | 1.50E-17 | 1.27E-17 | 1.46E-17 | 1.47E-17 | 1.45E-17 | 1.44E-17 | 1.53E-17 | 1.48E-17 | 1.20E-17 | 1.03E-17 | 0.139E-16 | 1.47E-17 | 1.38E-17 | 1.28E-17 | 1.41E-17 |
| | (-47.25, -18.27) | (-35,-12) | 7.91E+07 | 1.51E-17 | 1.26E-17 | 1.42E-17 | 1.44E-17 | 1.45E-17 | 1.43E-17 | 1.51E-17 | 1.46E-17 | 1.22E-17 | 1.08E-17 | 0.135E-16 | 1.41E-17 | 1.39E-17 | 1.29E-17 | 1.44E-17 |
| | (-45.99, -22.05) | (-34,-15) | 6.90E+07 | 1.31E-17 | 1.13E-17 | 1.25E-17 | 1.22E-17 | 1.26E-17 | 1.23E-17 | 1.30E-17 | 1.26E-17 | 1.13E-17 | 9.76E-18 | 0.120E-16 | 1.19E-17 | 1.20E-17 | 1.11E-17 | 1.26E-17 |
| | (-44.73, -24.57) | (-33,-17) | 6.05E+07 | 1.15E-17 | 1.00E-17 | 1.10E-17 | 1.14E-17 | 1.12E-17 | 1.10E-17 | 1.18E-17 | 1.15E-17 | 1.03E-17 | 8.94E-18 | 0.109E-16 | 1.05E-17 | 1.07E-17 | 1.01E-17 | 1.13E-17 |
| | (-42.21, -28.35) | (-31,-20) | 5.37E+07 | 1.02E-17 | 9.14E-18 | 9.82E-18 | 9.99E-18 | 1.01E-17 | 9.70E-18 | 1.05E-17 | 9.99E-18 | 8.87E-18 | 7.63E-18 | 0.968E-17 | 9.33E-18 | 9.30E-18 | 8.97E-18 | 9.48E-18 |
| | (-38.43, -33.39) | (-28,-24) | 4.36E+07 | 8.30E-18 | 7.69E-18 | 8.09E-18 | 7.78E-18 | 8.07E-18 | 7.94E-18 | 8.79E-18 | 8.10E-18 | 7.40E-18 | 6.05E-18 | 0.800E-17 | 7.79E-18 | 7.48E-18 | 7.45E-18 | 7.69E-18 |
| | (-35.91, -35.91) | (-26,-26) | 4.38E+07 | 8.34E-18 | 7.53E-18 | 7.91E-18 | 8.07E-18 | 7.98E-18 | 7.82E-18 | 8.72E-18 | 8.03E-18 | 7.20E-18 | 5.90E-18 | 0.770E-17 | 7.67E-18 | 7.40E-18 | 7.44E-18 | 7.61E-18 |
| Neutron Pad | (-58.54, -22.47) | 21 degree | 8.19E+06 | 1.56E-18 | 1.33E-18 | 1.42E-18 | 1.46E-18 | 1.46E-18 | 1.36E-18 | 1.54E-18 | 1.45E-18 | 1.20E-18 | 7.66E-19 | 0.140E-17 | 1.39E-18 | 1.38E-18 | 1.27E-18 | 1.30E-18 |
| | (-46.60, -41.95) | 42 degree | 5.90E+06 | 1.12E-18 | 9.43E-19 | 9.35E-19 | 1.04E-18 | 1.03E-18 | 9.74E-19 | 1.14E-18 | 1.03E-18 | 9.00E-19 | 5.19E-19 | 0.984E-18 | 9.53E-19 | 9.40E-19 | 9.11E-19 | 7.31E-19 |

C/E comparison

| $^{115}$In (n,n') | Position in cm | Grid Position | Experimental Value **Equiv. Fiss. Flux** | Experimental Value **Reaction Rates** | HYU-TORT Korea | HYU-MCNP Korea | HYU-MCNPX Korea | Transpire Inc.-ATTILA USA | KI-MCU Russia | KOPEC-DORT Korea | WTI-MCNP Germany | VTT-TORT Finland | VTT-MT Finland | KI-LUCKY Russia | KAERI-DANTSYS Korea | VTT-MCNP-K Finland | VTT-MCNP-F Finland | SCK-MCNPX Belgium |
|---|---|---|---|---|---|---|---|---|---|---|---|---|---|---|---|---|---|---|
| Inner Baffle | ( -4.41, -0.63) | (-1,+2) | 1.94E+09 | 3.69E-16 | 0.95 | 0.92 | 0.91 | 1.00 | 0.93 | 0.98 | 0.97 | 1.01 | 0.97 | 0.98 | 0.89 | 0.82 | 0.88 | 0.93 |
| | ( -4.41, -4.41) | (-1,-1) | 2.36E+09 | 4.49E-16 | 0.93 | 0.92 | 0.92 | 0.97 | 0.92 | 0.97 | 0.96 | 0.94 | 1.02 | 0.95 | 0.88 | 0.88 | 0.96 | 0.91 |
| Outer Baffle | (-39.69, -0.63) | (-29,+2) | 7.14E+08 | 1.36E-16 | 0.83 | 0.98 | 0.95 | 0.96 | 0.96 | 1.00 | 1.00 | 0.88 | 0.78 | 0.90 | 0.95 | 0.88 | 0.82 | 0.95 |
| | (-39.69, -5.67) | (-29,-2) | N/A | N/A | | | | | | | | | | | | | | |
| | (-39.69, -11.97) | (-29,-7) | 5.48E+08 | 1.04E-16 | 0.84 | 0.97 | 0.98 | 0.98 | 0.96 | 1.01 | 1.01 | 0.85 | 0.78 | 0.91 | 0.96 | 0.95 | 0.88 | 0.96 |
| | (-39.69, -18.27) | (-29,-12) | 3.33E+08 | 6.34E-17 | 0.85 | 0.95 | 0.96 | 0.96 | 0.94 | 1.01 | 1.00 | 0.80 | 0.78 | 0.90 | 0.94 | 0.92 | 0.88 | 0.94 |
| | (-37.17, -20.79) | (-27,-14) | 3.53E+08 | 6.72E-17 | 0.88 | 0.96 | 0.94 | 0.95 | 0.92 | 0.99 | 0.97 | 0.84 | 0.78 | 0.86 | 0.92 | 0.92 | 0.87 | 0.93 |
| | (-30.87, -20.79) | (-22,-14) | N/A | N/A | | | | | | | | | | | | | | |
| | (-24.57, -20.79) | (-17,-14) | 1.12E+09 | 2.13E-16 | 0.95 | 0.95 | 0.95 | 0.99 | 0.94 | 1.01 | 0.98 | 0.90 | 0.94 | 0.94 | 0.92 | 0.91 | 0.95 | 0.93 |
| Barrel | (-49.77, -0.63) | (-37,+2) | 8.97E+07 | 1.71E-17 | 0.85 | 0.98 | 0.97 | 0.96 | 0.95 | 1.02 | 0.99 | 0.82 | 0.69 | 0.93 | 0.99 | 0.85 | 0.79 | 0.93 |
| | (-49.77, -9.45) | (-37,-5) | 7.90E+07 | 1.50E-17 | 0.84 | 0.97 | 0.98 | 0.96 | 0.96 | 1.02 | 0.99 | 0.80 | 0.68 | 0.92 | 0.98 | 0.92 | 0.85 | 0.94 |
| | (-47.25, -18.27) | (-35,-12) | 7.91E+07 | 1.51E-17 | 0.84 | 0.95 | 0.95 | 0.96 | 0.95 | 1.00 | 0.97 | 0.81 | 0.72 | 0.90 | 0.94 | 0.92 | 0.86 | 0.96 |
| | (-45.99, -22.05) | (-34,-15) | 6.90E+07 | 1.31E-17 | 0.86 | 0.95 | 0.93 | 0.96 | 0.93 | 0.99 | 0.96 | 0.86 | 0.74 | 0.91 | 0.91 | 0.92 | 0.84 | 0.96 |
| | (-44.73, -24.57) | (-33,-17) | 6.05E+07 | 1.15E-17 | 0.87 | 0.96 | 0.99 | 0.97 | 0.96 | 1.03 | 1.00 | 0.89 | 0.78 | 0.95 | 0.91 | 0.93 | 0.88 | 0.99 |
| | (-42.21, -28.35) | (-31,-20) | 5.37E+07 | 1.02E-17 | 0.89 | 0.96 | 0.98 | 0.98 | 0.95 | 1.03 | 0.98 | 0.87 | 0.75 | 0.95 | 0.91 | 0.91 | 0.88 | 0.93 |
| | (-38.43, -33.39) | (-28,-24) | 4.36E+07 | 8.30E-18 | 0.93 | 0.97 | 0.94 | 0.97 | 0.96 | 1.06 | 0.98 | 0.89 | 0.73 | 0.96 | 0.94 | 0.90 | 0.90 | 0.93 |
| | (-35.91, -35.91) | (-26,-26) | 4.38E+07 | 8.34E-18 | 0.90 | 0.95 | 0.97 | 0.96 | 0.94 | 1.05 | 0.96 | 0.86 | 0.71 | 0.92 | 0.92 | 0.89 | 0.89 | 0.91 |
| Neutron Pad | (-58.54, -22.47) | 21 degree | 8.19E+06 | 1.56E-18 | 0.85 | 0.91 | 0.94 | 0.93 | 0.87 | 0.98 | 0.93 | 0.77 | 0.49 | 0.90 | 0.89 | 0.88 | 0.81 | 0.84 |
| | (-46.60, -41.95) | 42 degree | 5.90E+06 | 1.12E-18 | 0.84 | 0.83 | 0.92 | 0.92 | 0.87 | 1.02 | 0.92 | 0.80 | 0.46 | 0.88 | 0.85 | 0.84 | 0.81 | 0.65 |
| Number of positions within +-5% = | | | | | 0 | 10 | 10 | 14 | 6 | 16 | 15 | 1 | 2 | 3 | 3 | 0 | 2 | 5 |
| Number of positions within +-10% = | | | | | 5 | 16 | 17 | 17 | 15 | 17 | 17 | 3 | 3 | 11 | 13 | 10 | 2 | 15 |
| Number of positions within +-20% = | | | | | 17 | 17 | 17 | 17 | 17 | 17 | 17 | 15 | 3 | 17 | 17 | 17 | 16 | 16 |

# Table 4.14(b). Reaction rates: $^{115}$In(n,n′) detector results and C/E comparison in water zones

Calculated results (**Reaction Rates**)

| $^{115}$In (n,n') | Position in cm | Grid Position | Experimental Value **Equiv. Fiss. Flux** | Experimental Value **Reaction Rates** | HYU-TORT Korea | HYU-MCNP Korea | HYU-MCNPX Korea | Transpire Inc.-ATTILA USA | KI-MCU Russia | KOPEC-DORT Korea | WTI-MCNP Germany | VTT-TORT Finland | VTT-MT Finland | KI-LUCKY Russia | KAERI-DANTSYS Korea | VTT-MCNP-K Finland | VTT-MCNP-F Finland | SCK-MCNPX Belgium |
|---|---|---|---|---|---|---|---|---|---|---|---|---|---|---|---|---|---|---|
| Central Hole | ( 0.0, 0.0) | (+2.5,+2.5) | N/A | N/A | 2.32E-16 | 5.66E-17 | 5.77E-17 | 2.33E-16 | 1.39E-17 | 2.43E-16 | 2.35E-16 | 2.34E-16 | 2.20E-16 | 0.242E-15 | 2.18E-16 | 2.21E-16 | 2.41E-16 | 5.46E-17 |
| Water Gap | (-54.36, -9.59) | 10.75 degree | N/A | N/A | 4.29E-18 | 4.67E-18 | 4.69E-18 | 4.78E-18 | 4.68E-18 | 4.98E-18 | 4.74E-18 | 4.20E-18 | 4.19E-18 | 0.459E-17 | 4.30E-18 | 4.34E-18 | 4.16E-18 | 4.68E-18 |
| | (-52.89, -15.80) | 16.63 degree | 2.59E+07 | 4.93E-18 | 4.39E-18 | 4.65E-18 | 4.77E-18 | 4.77E-18 | 4.63E-18 | 4.98E-18 | 4.83E-18 | 4.26E-18 | 4.08E-18 | 0.453E-17 | 5.44E-18 | 4.50E-18 | 4.22E-18 | 4.76E-18 |
| | (-51.53, -19.78) | 21.14 degree | 2.53E+07 | 4.81E-18 | 4.26E-18 | 4.55E-18 | 4.75E-18 | 4.66E-18 | 4.52E-18 | 4.83E-18 | 4.64E-18 | 4.18E-18 | 4.72E-18 | 0.438E-17 | 5.15E-18 | 4.41E-18 | 4.12E-18 | 4.34E-18 |
| | (-50.03, -23.33) | 25.62 degree | 2.30E+07 | 4.38E-18 | 4.02E-18 | 4.30E-18 | 4.24E-18 | 4.40E-18 | 4.23E-18 | 4.41E-18 | 4.31E-18 | 3.85E-18 | 5.43E-18 | 0.410E-17 | 4.28E-18 | 4.19E-18 | 3.88E-18 | 4.15E-18 |
| | (-48.74, -25.91) | 28.78 degree | 2.13E+07 | 4.05E-18 | 3.63E-18 | 3.79E-18 | 3.88E-18 | 4.03E-18 | 3.90E-18 | 4.11E-18 | 3.99E-18 | 3.64E-18 | 3.94E-18 | 0.385E-17 | 3.97E-18 | 3.80E-18 | 3.63E-18 | 4.22E-18 |
| | (-46.29, -30.06) | 33.89 degree | 1.87E+07 | 3.56E-18 | 3.30E-18 | 3.59E-18 | 3.49E-18 | 3.61E-18 | 3.44E-18 | 3.66E-18 | 3.50E-18 | 3.19E-18 | 3.96E-18 | 0.333E-17 | 3.74E-18 | 3.28E-18 | 3.24E-18 | 3.41E-18 |
| | (-44.08, -33.22) | 37.44 degree | N/A | N/A | 3.00E-18 | 3.04E-18 | 3.30E-18 | 3.15E-18 | 3.11E-18 | 3.41E-18 | 3.20E-18 | 2.97E-18 | 3.02E-18 | 0.315E-17 | 3.23E-18 | 3.00E-18 | 2.94E-18 | 3.14E-18 |
| | (-42.29, -35.48) | 40.99 degree | N/A | N/A | 2.74E-18 | 3.01E-18 | 3.10E-18 | 3.07E-18 | 2.96E-18 | 3.23E-18 | 2.98E-18 | 2.80E-18 | 2.87E-18 | 0.297E-17 | 2.73E-18 | 2.85E-18 | 2.78E-18 | 2.66E-18 |
| | (-39.03, -39.03) | 45 degree | 1.57E+07 | 2.99E-18 | 2.69E-18 | 2.77E-18 | 2.80E-18 | 2.93E-18 | 2.86E-18 | 3.16E-18 | 2.86E-18 | 2.72E-18 | 2.78E-18 | 0.284E-17 | 3.31E-18 | 2.72E-18 | 2.68E-18 | 2.54E-18 |
| Reflector | (-23.31, -23.31) | (-16,-16) | 7.91E+08 | 1.51E-16 | 1.37E-16 | 1.38E-16 | 1.35E-16 | 1.45E-16 | 1.36E-16 | 1.47E-16 | 1.41E-16 | 1.40E-16 | 1.43E-16 | 0.137E-15 | 1.34E-16 | 1.34E-16 | 1.38E-16 | 1.37E-16 |
| | (-25.83, -25.83) | (-18,-18) | 4.00E+08 | 7.61E-17 | 6.84E-17 | 6.96E-17 | 6.92E-17 | 7.17E-17 | 6.89E-17 | 7.51E-17 | 7.06E-17 | 6.84E-17 | 7.56E-17 | 0.700E-16 | 6.87E-17 | 6.75E-17 | 6.87E-17 | 6.85E-17 |
| | (-28.35, -28.35) | (-20,-20) | 2.07E+08 | 3.94E-17 | 3.55E-17 | 3.66E-17 | 3.54E-17 | 3.76E-17 | 3.65E-17 | 4.01E-17 | 3.73E-17 | 3.58E-17 | 3.68E-17 | 0.370E-16 | 3.63E-17 | 3.53E-17 | 3.56E-17 | 3.61E-17 |
| | (-30.87, -30.87) | (-22,-22) | 1.11E+08 | 2.11E-17 | 1.88E-17 | 1.99E-17 | 1.99E-17 | 2.03E-17 | 1.96E-17 | 2.21E-17 | 1.99E-17 | 1.78E-17 | 1.71E-17 | 0.202E-16 | 1.99E-17 | 1.93E-17 | 1.93E-17 | 2.12E-17 |
| | (-33.39, -33.39) | (-24,-24) | 6.66E+07 | 1.27E-17 | 1.11E-17 | 1.20E-17 | 1.17E-17 | 1.20E-17 | 1.16E-17 | 1.32E-17 | 1.18E-17 | 1.05E-17 | 8.73E-18 | 0.118E-16 | 1.17E-17 | 1.13E-17 | 1.12E-17 | 1.13E-17 |

C/E comparison

| $^{115}$In (n,n') | Position in cm | Grid Position | Experimental Value **Equiv. Fiss. Flux** | Experimental Value **Reaction Rates** | HYU-TORT Korea | HYU-MCNP Korea | HYU-MCNPX Korea | Transpire Inc.-ATTILA USA | KI-MCU Russia | KOPEC-DORT Korea | WTI-MCNP Germany | VTT-TORT Finland | VTT-MT Finland | KI-LUCKY Russia | KAERI-DANTSYS Korea | VTT-MCNP-K Finland | VTT-MCNP-F Finland | SCK-MCNPX Belgium |
|---|---|---|---|---|---|---|---|---|---|---|---|---|---|---|---|---|---|---|
| Central Hole | ( 0.0, 0.0) | (+2.5,+2.5) | N/A | N/A | | | | | | | | | | | | | | |
| Water Gap | (-54.36, -9.59) | 10.75 degree | N/A | N/A | | | | | | | | | | | | | | |
| | (-52.89, -15.80) | 16.63 degree | 2.59E+07 | 4.93E-18 | 0.89 | 0.94 | 0.97 | 0.97 | 0.94 | 1.01 | 0.98 | 0.86 | 0.83 | 0.92 | 1.10 | 0.91 | 0.86 | 0.97 |
| | (-51.53, -19.78) | 21.14 degree | 2.53E+07 | 4.81E-18 | 0.88 | 0.95 | 0.99 | 0.97 | 0.94 | 1.00 | 0.96 | 0.87 | 0.98 | 0.91 | 1.07 | 0.92 | 0.86 | 0.90 |
| | (-50.03, -23.33) | 25.62 degree | 2.30E+07 | 4.38E-18 | 0.92 | 0.98 | 0.97 | 1.00 | 0.97 | 1.01 | 0.99 | 0.88 | 1.24 | 0.94 | 0.98 | 0.96 | 0.89 | 0.95 |
| | (-48.74, -25.91) | 28.78 degree | 2.13E+07 | 4.05E-18 | 0.90 | 0.93 | 0.96 | 0.99 | 0.96 | 1.02 | 0.99 | 0.90 | 0.97 | 0.95 | 0.98 | 0.94 | 0.90 | 1.04 |
| | (-46.29, -30.06) | 33.89 degree | 1.87E+07 | 3.56E-18 | 0.93 | 1.01 | 0.98 | 1.02 | 0.97 | 1.03 | 0.98 | 0.90 | 1.11 | 0.94 | 1.05 | 0.92 | 0.91 | 0.96 |
| | (-44.08, -33.22) | 37.44 degree | N/A | N/A | | | | | | | | | | | | | | |
| | (-42.29, -35.48) | 40.99 degree | N/A | N/A | | | | | | | | | | | | | | |
| | (-39.03, -39.03) | 45 degree | 1.57E+07 | 2.99E-18 | 0.90 | 0.93 | 0.94 | 0.98 | 0.96 | 1.06 | 0.96 | 0.91 | 0.93 | 0.95 | 1.11 | 0.91 | 0.90 | 0.85 |
| Reflector | (-23.31, -23.31) | (-16,-16) | 7.91E+08 | 1.51E-16 | 0.91 | 0.92 | 0.89 | 0.96 | 0.91 | 0.98 | 0.94 | 0.93 | 0.95 | 0.91 | 0.89 | 0.89 | 0.92 | 0.91 |
| | (-25.83, -25.83) | (-18,-18) | 4.00E+08 | 7.61E-17 | 0.90 | 0.91 | 0.91 | 0.94 | 0.91 | 0.99 | 0.93 | 0.90 | 0.99 | 0.92 | 0.90 | 0.89 | 0.90 | 0.90 |
| | (-28.35, -28.35) | (-20,-20) | 2.07E+08 | 3.94E-17 | 0.90 | 0.93 | 0.90 | 0.96 | 0.93 | 1.02 | 0.95 | 0.91 | 0.94 | 0.94 | 0.92 | 0.90 | 0.90 | 0.92 |
| | (-30.87, -30.87) | (-22,-22) | 1.11E+08 | 2.11E-17 | 0.89 | 0.94 | 0.94 | 0.96 | 0.93 | 1.05 | 0.94 | 0.84 | 0.81 | 0.96 | 0.94 | 0.91 | 0.91 | 1.00 |
| | (-33.39, -33.39) | (-24,-24) | 6.66E+07 | 1.27E-17 | 0.87 | 0.94 | 0.92 | 0.95 | 0.91 | 1.04 | 0.93 | 0.83 | 0.69 | 0.93 | 0.92 | 0.89 | 0.88 | 0.89 |
| Number of positions within +-5% = | | | | | 0 | 2 | 5 | 9 | 4 | 10 | 6 | 0 | 4 | 2 | 2 | 1 | 0 | 4 |
| Number of positions within +-10% = | | | | | 4 | 11 | 9 | 11 | 11 | 11 | 11 | 3 | 6 | 11 | 8 | 7 | 5 | 9 |
| Number of positions within +-20% = | | | | | 11 | 11 | 11 | 11 | 11 | 11 | 11 | 11 | 9 | 11 | 11 | 11 | 11 | 11 |

# Table 4.15(a). Reaction rates: $^{27}$Al(n,α) detector results and C/E comparison in stainless steel zones

Calculated results (**Reaction Rates**)

| $^{27}$Al (n,a) | Position in cm | Grid Position | Experimental Value **Equiv. Fiss. Flux** | Experimental Value **Reaction Rates** | HYU-TORT Korea | HYU-MCNP Korea | HYU-MCNPX Korea | Transpire Inc.-ATTILA USA | KI-MCU Russia | KOPEC-DORT Korea | WTI-MCNP Germany | VTT-TORT Finland | VTT-MT Finland | KI-LUCKY Russia | KAERI-DANTSYS Korea | VTT-MCNP-K Finland | VTT-MCNP-F Finland | SCK-MCNPX Belgium |
|---|---|---|---|---|---|---|---|---|---|---|---|---|---|---|---|---|---|---|
| Inner Baffle | ( -4.41, -0.63) | (-1,+2) | 1.43E+09 | 1.01E-18 | 1.12E-18 | 7.77E-19 | 7.99E-19 | 1.08E-18 | 1.04E-18 | 1.11E-18 | 9.86E-19 | 1.05E-18 | 1.09E-18 | 0.105E-17 | 9.28E-19 | 8.59E-19 | 9.27E-19 | 1.08E-18 |
| | ( -4.41, -4.41) | (-1,-1) | 1.70E+09 | 1.20E-18 | 1.32E-18 | 9.73E-19 | 1.14E-18 | 1.26E-18 | 1.29E-18 | 1.34E-18 | 1.19E-18 | 1.19E-18 | 1.45E-18 | 0.123E-17 | 1.10E-18 | 1.06E-18 | 1.21E-18 | 1.10E-18 |
| Outer Baffle | (-39.69, -0.63) | (-29,+2) | 5.92E+08 | 4.18E-19 | 3.67E-19 | 3.42E-19 | 4.60E-19 | 4.02E-19 | 3.94E-19 | 4.42E-19 | 4.17E-19 | 3.50E-19 | 3.25E-19 | 0.366E-18 | 3.87E-19 | 3.57E-19 | 3.44E-19 | 3.87E-19 |
| | (-39.69, -5.67) | (-29,-2) | N/A | N/A | 3.48E-19 | 4.84E-19 | 3.20E-19 | 3.93E-19 | 3.82E-19 | 4.19E-19 | 3.99E-19 | 3.25E-19 | 3.09E-19 | 0.348E-18 | 3.67E-19 | 3.63E-19 | 3.41E-19 | 3.92E-19 |
| | (-39.69, -11.97) | (-29,-7) | 4.52E+08 | 3.19E-19 | 2.89E-19 | 3.05E-19 | 2.15E-19 | 3.20E-19 | 2.88E-19 | 3.43E-19 | 3.24E-19 | 2.60E-19 | 2.51E-19 | 0.285E-18 | 3.01E-19 | 3.10E-19 | 2.76E-19 | 3.22E-19 |
| | (-39.69, -18.27) | (-29,-12) | 2.69E+08 | 1.90E-19 | 1.75E-19 | 1.60E-19 | 1.86E-19 | 1.87E-19 | 1.90E-19 | 2.06E-19 | 1.94E-19 | 1.50E-19 | 1.52E-19 | 0.171E-18 | 1.77E-19 | 1.88E-19 | 1.73E-19 | 1.96E-19 |
| | (-37.17, -20.79) | (-27,-14) | 2.76E+08 | 1.95E-19 | 1.94E-19 | 3.50E-19 | 1.87E-19 | 1.96E-19 | 2.06E-19 | 2.17E-19 | 2.01E-19 | 1.66E-19 | 1.62E-19 | 0.174E-18 | 1.84E-19 | 2.10E-19 | 1.82E-19 | 1.71E-19 |
| | (-30.87, -20.79) | (-22,-14) | N/A | N/A | 3.82E-19 | 4.21E-19 | 4.49E-19 | 3.92E-19 | 3.64E-19 | 4.14E-19 | 3.78E-19 | 3.61E-19 | 3.44E-19 | 0.345E-18 | 3.55E-19 | 4.01E-19 | 3.29E-19 | 3.58E-19 |
| | (-24.57, -20.79) | (-17,-14) | 8.30E+08 | 5.86E-19 | 6.24E-19 | 7.22E-19 | 6.12E-19 | 6.14E-19 | 5.95E-19 | 6.56E-19 | 6.10E-19 | 5.35E-19 | 5.97E-19 | 0.578E-18 | 5.44E-19 | 5.59E-19 | 5.51E-19 | 4.91E-19 |
| Barrel | (-49.77, -0.63) | (-37,+2) | 9.62E+07 | 6.79E-20 | 6.55E-20 | 7.86E-20 | 6.22E-20 | 6.51E-20 | 6.38E-20 | 7.38E-20 | 6.51E-20 | 5.34E-20 | 4.99E-20 | 0.600E-19 | 6.30E-20 | 5.82E-20 | 5.46E-20 | 6.20E-20 |
| | (-49.77, -9.45) | (-37,-5) | 8.50E+07 | 6.00E-20 | 5.52E-20 | 4.71E-20 | 4.76E-20 | 5.35E-20 | 5.32E-20 | 6.12E-20 | 5.63E-20 | 4.25E-20 | 4.13E-20 | 0.505E-19 | 5.51E-20 | 4.71E-20 | 4.26E-20 | 4.19E-20 |
| | (-47.25, -18.27) | (-35,-12) | 7.33E+07 | 5.17E-20 | 4.93E-20 | 4.35E-20 | 5.45E-20 | 4.97E-20 | 4.93E-20 | 5.63E-20 | 4.66E-20 | 4.04E-20 | 3.98E-20 | 0.454E-19 | 4.76E-20 | 4.15E-20 | 4.51E-20 | 4.19E-20 |
| | (-45.99, -22.05) | (-34,-15) | 6.01E+07 | 4.24E-20 | 4.25E-20 | 4.33E-20 | 3.47E-20 | 4.16E-20 | 4.16E-20 | 4.60E-20 | 4.14E-20 | 3.57E-20 | 3.56E-20 | 0.389E-19 | 3.94E-20 | 4.57E-20 | 3.48E-20 | 5.21E-20 |
| | (-44.73, -24.57) | (-33,-17) | 5.48E+07 | 3.87E-20 | 3.68E-20 | 3.66E-20 | 2.92E-20 | 3.58E-20 | 3.81E-20 | 4.26E-20 | 3.92E-20 | 3.28E-20 | 3.33E-20 | 0.348E-19 | 3.40E-20 | 3.49E-20 | 3.62E-20 | 2.89E-20 |
| | (-42.21, -28.35) | (-31,-20) | 5.71E+07 | 4.03E-20 | 4.13E-20 | 3.76E-20 | 4.41E-20 | 3.88E-20 | 3.59E-20 | 4.30E-20 | 3.79E-20 | 3.24E-20 | 3.21E-20 | 0.368E-19 | 3.48E-20 | 3.75E-20 | 3.14E-20 | 3.28E-20 |
| | (-38.43, -33.39) | (-28,-24) | 5.19E+07 | 3.66E-20 | 4.13E-20 | 3.81E-20 | 3.12E-20 | 3.54E-20 | 3.55E-20 | 4.23E-20 | 3.40E-20 | 3.23E-20 | 2.98E-20 | 0.350E-19 | 3.34E-20 | 3.16E-20 | 3.06E-20 | 4.61E-20 |
| | (-35.91, -35.91) | (-26,-26) | 5.12E+07 | 3.61E-20 | 4.14E-20 | 3.76E-20 | 3.80E-20 | 3.59E-20 | 3.82E-20 | 4.30E-20 | 3.68E-20 | 3.20E-20 | 3.00E-20 | 0.342E-19 | 3.44E-20 | 3.07E-20 | 3.19E-20 | 3.75E-20 |
| Neutron Pad | (-58.54, -22.47) | 21 degree | 1.05E+07 | 7.41E-21 | 7.33E-21 | 5.25E-21 | 4.85E-21 | 6.63E-21 | 5.87E-21 | 7.06E-21 | 6.03E-21 | 5.09E-21 | 4.11E-21 | 0.625E-20 | 6.51E-21 | 5.32E-21 | 6.34E-21 | N/A |
| | (-46.60, -41.95) | 42 degree | 8.39E+06 | 5.92E-21 | 5.96E-21 | 4.95E-21 | 6.23E-21 | 5.19E-21 | 4.88E-21 | 6.10E-21 | 4.89E-21 | 4.41E-21 | 3.30E-21 | 0.501E-20 | 4.79E-21 | 4.64E-21 | 5.19E-21 | N/A |

C/E comparison

| $^{27}$Al (n,a) | Position in cm | Grid Position | Experimental Value **Equiv. Fiss. Flux** | Experimental Value **Reaction Rates** | HYU-TORT Korea | HYU-MCNP Korea | HYU-MCNPX Korea | Transpire Inc.-ATTILA USA | KI-MCU Russia | KOPEC-DORT Korea | WTI-MCNP Germany | VTT-TORT Finland | VTT-MT Finland | KI-LUCKY Russia | KAERI-DANTSYS Korea | VTT-MCNP-K Finland | VTT-MCNP-F Finland | SCK-MCNPX Belgium |
|---|---|---|---|---|---|---|---|---|---|---|---|---|---|---|---|---|---|---|
| Inner Baffle | ( -4.41, -0.63) | (-1,+2) | 1.43E+09 | 1.01E-18 | 1.11 | 0.77 | 0.79 | 1.07 | 1.03 | 1.10 | 0.98 | 1.04 | 1.08 | 1.04 | 0.92 | 0.85 | 0.92 | 1.06 |
| | ( -4.41, -4.41) | (-1,-1) | 1.70E+09 | 1.20E-18 | 1.10 | 0.81 | 0.95 | 1.05 | 1.07 | 1.12 | 0.99 | 0.99 | 1.21 | 1.02 | 0.91 | 0.89 | 1.01 | 0.92 |
| Outer Baffle | (-39.69, -0.63) | (-29,+2) | 5.92E+08 | 4.18E-19 | 0.88 | 0.82 | 1.10 | 0.96 | 0.94 | 1.06 | 1.00 | 0.84 | 0.78 | 0.88 | 0.93 | 0.85 | 0.82 | 0.93 |
| | (-39.69, -5.67) | (-29,-2) | N/A | N/A | | | | | | | | | | | | | | |
| | (-39.69, -11.97) | (-29,-7) | 4.52E+08 | 3.19E-19 | 0.90 | 0.95 | 0.67 | 1.00 | 0.90 | 1.07 | 1.02 | 0.82 | 0.79 | 0.89 | 0.94 | 0.97 | 0.86 | 1.01 |
| | (-39.69, -18.27) | (-29,-12) | 2.69E+08 | 1.90E-19 | 0.92 | 0.84 | 0.98 | 0.99 | 1.00 | 1.09 | 1.02 | 0.79 | 0.80 | 0.90 | 0.93 | 0.99 | 0.91 | 1.03 |
| | (-37.17, -20.79) | (-27,-14) | 2.76E+08 | 1.95E-19 | 0.99 | 1.80 | 0.96 | 1.01 | 1.05 | 1.11 | 1.03 | 0.85 | 0.83 | 0.89 | 0.94 | 1.08 | 0.93 | 0.88 |
| | (-30.87, -20.79) | (-22,-14) | N/A | N/A | | | | | | | | | | | | | | |
| | (-24.57, -20.79) | (-17,-14) | 8.30E+08 | 5.86E-19 | 1.06 | 1.23 | 1.04 | 1.05 | 1.02 | 1.12 | 1.04 | 0.91 | 1.02 | 0.99 | 0.93 | 0.95 | 0.94 | 0.84 |
| Barrel | (-49.77, -0.63) | (-37,+2) | 9.62E+07 | 6.79E-20 | 0.96 | 1.16 | 0.92 | 0.96 | 0.94 | 1.09 | 0.96 | 0.79 | 0.73 | 0.88 | 0.93 | 0.86 | 0.80 | 0.91 |
| | (-49.77, -9.45) | (-37,-5) | 8.50E+07 | 6.00E-20 | 0.92 | 0.79 | 0.79 | 0.89 | 0.89 | 1.02 | 0.94 | 0.71 | 0.69 | 0.84 | 0.92 | 0.78 | 0.71 | 0.70 |
| | (-47.25, -18.27) | (-35,-12) | 7.33E+07 | 5.17E-20 | 0.95 | 0.84 | 1.05 | 0.96 | 0.95 | 1.09 | 0.90 | 0.78 | 0.77 | 0.88 | 0.92 | 0.80 | 0.87 | 0.81 |
| | (-45.99, -22.05) | (-34,-15) | 6.01E+07 | 4.24E-20 | 1.00 | 1.02 | 0.82 | 0.98 | 0.98 | 1.08 | 0.98 | 0.84 | 0.84 | 0.92 | 0.93 | 1.08 | 0.82 | 1.23 |
| | (-44.73, -24.57) | (-33,-17) | 5.48E+07 | 3.87E-20 | 0.95 | 0.95 | 0.75 | 0.93 | 0.99 | 1.10 | 1.01 | 0.85 | 0.86 | 0.90 | 0.88 | 0.90 | 0.93 | 0.75 |
| | (-42.21, -28.35) | (-31,-20) | 5.71E+07 | 4.03E-20 | 1.02 | 0.93 | 1.09 | 0.96 | 0.89 | 1.07 | 0.94 | 0.80 | 0.80 | 0.91 | 0.86 | 0.93 | 0.78 | 0.81 |
| | (-38.43, -33.39) | (-28,-24) | 5.19E+07 | 3.66E-20 | 1.13 | 1.04 | 0.85 | 0.97 | 0.97 | 1.15 | 0.93 | 0.88 | 0.81 | 0.96 | 0.91 | 0.86 | 0.83 | 1.26 |
| | (-35.91, -35.91) | (-26,-26) | 5.12E+07 | 3.61E-20 | 1.15 | 1.04 | 1.05 | 0.99 | 1.06 | 1.19 | 1.02 | 0.89 | 0.83 | 0.95 | 0.95 | 0.85 | 0.88 | 1.04 |
| Neutron Pad | (-58.54, -22.47) | 21 degree | 1.05E+07 | 7.41E-21 | 0.99 | 0.71 | 0.65 | 0.89 | 0.79 | 0.95 | 0.81 | 0.69 | 0.56 | 0.84 | 0.88 | 0.72 | 0.86 | |
| | (-46.60, -41.95) | 42 degree | 8.39E+06 | 5.92E-21 | 1.01 | 0.84 | 1.05 | 0.88 | 0.82 | 1.03 | 0.83 | 0.74 | 0.56 | 0.85 | 0.81 | 0.78 | 0.88 | |
| Number of positions within +-5% = | | | | | 8 | 4 | 4 | 12 | 7 | 3 | 11 | 2 | 1 | 4 | 1 | 3 | 1 | 3 |
| Number of positions within +-10% = | | | | | 13 | 6 | 9 | 14 | 13 | 11 | 15 | 3 | 2 | 8 | 13 | 7 | 6 | 7 |
| Number of positions within +-20% = | | | | | 17 | 12 | 12 | 17 | 16 | 17 | 17 | 11 | 7 | 17 | 17 | 14 | 15 | 11 |

# Table 4.15(b). Reaction rates: $^{27}$Al(n,α) detector results and C/E comparison in water zones

Calculated results (**Reaction Rates**)

| $^{27}$Al (n,a) | Position in cm | Grid Position | Experimental Value **Equiv. Fiss. Flux** | Experimental Value **Reaction Rates** | HYU-TORT Korea | HYU-MCNP Korea | HYU-MCNPX Korea | Transpire Inc.-ATTILA USA | KI-MCU Russia | KOPEC-DORT Korea | WTI-MCNP Germany | VTT-TORT Finland | VTT-MT Finland | KI-LUCKY Russia | KAERI-DANTSYS Korea | VTT-MCNP-K Finland | VTT-MCNP-F Finland |
|---|---|---|---|---|---|---|---|---|---|---|---|---|---|---|---|---|---|
| Central Hole | ( 0.0, 0.0) | (+2.5,+2.5) | N/A | N/A | 9.64E-19 | 2.32E-19 | 2.19E-19 | 8.94E-19 | 5.48E-20 | 9.47E-19 | 8.77E-19 | 8.54E-19 | 8.35E-19 | 0.915E-18 | 8.03E-19 | 7.96E-19 | 8.36E-19 |
| Water Gap | (-54.36, -9.59) | 10.75 degree | N/A | N/A | 2.51E-20 | 2.23E-20 | 2.99E-20 | 2.35E-20 | 2.16E-20 | 2.60E-20 | 2.25E-20 | 1.97E-20 | 1.99E-20 | 0.223E-19 | 2.16E-20 | 1.96E-20 | 1.84E-20 |
| | (-52.89, -15.80) | 16.63 degree | 3.15E+07 | 2.2239E-20 | 2.32E-20 | 1.85E-20 | 1.67E-20 | 2.16E-20 | 2.03E-20 | 2.50E-20 | 2.22E-20 | 1.92E-20 | 1.88E-20 | 0.208E-19 | 2.39E-20 | 1.77E-20 | 1.79E-20 |
| | (-51.53, -19.78) | 21.14 degree | 2.52E+07 | 1.77912E-20 | 2.33E-20 | 1.96E-20 | 1.98E-20 | 2.20E-20 | 2.04E-20 | 2.40E-20 | 2.14E-20 | 1.85E-20 | 2.04E-20 | 0.208E-19 | 2.29E-20 | 1.91E-20 | 1.86E-20 |
| | (-50.03, -23.33) | 25.62 degree | 2.67E+07 | 1.88502E-20 | 2.09E-20 | 2.03E-20 | 3.08E-20 | 1.91E-20 | 1.85E-20 | 2.10E-20 | 1.95E-20 | 1.63E-20 | 2.27E-20 | 0.185E-19 | 1.85E-20 | 2.11E-20 | 1.53E-20 |
| | (-48.74, -25.91) | 28.78 degree | 2.54E+07 | 1.79324E-20 | 1.90E-20 | 1.48E-20 | 1.87E-20 | 1.80E-20 | 1.70E-20 | 2.02E-20 | 1.80E-20 | 1.57E-20 | 1.76E-20 | 0.173E-19 | 1.71E-20 | 1.69E-20 | 1.71E-20 |
| | (-46.29, -30.06) | 33.89 degree | 2.50E+07 | 1.765E-20 | 1.91E-20 | 1.79E-20 | 1.62E-20 | 1.75E-20 | 1.61E-20 | 1.96E-20 | 1.73E-20 | 1.52E-20 | 1.94E-20 | 0.167E-19 | 1.75E-20 | 1.58E-20 | 1.44E-20 |
| | (-44.08, -33.22) | 37.44 degree | N/A | N/A | 1.90E-20 | 1.94E-20 | 2.61E-20 | 1.63E-20 | 1.64E-20 | 1.96E-20 | 1.59E-20 | 1.52E-20 | 1.58E-20 | 0.167E-19 | 1.56E-20 | 1.60E-20 | 1.55E-20 |
| | (-42.29, -35.48) | 40.99 degree | 2.30E+07 | 1.6238E-20 | 1.88E-20 | 1.99E-20 | 1.73E-20 | 1.69E-20 | 1.65E-20 | 1.95E-20 | 1.60E-20 | 1.53E-20 | 1.57E-20 | 0.166E-19 | 1.51E-20 | 1.42E-20 | 1.50E-20 |
| | (-39.03, -39.03) | 45 degree | 2.30E+07 | 1.6238E-20 | 1.94E-20 | 1.28E-20 | 1.63E-20 | 1.72E-20 | 1.66E-20 | 1.95E-20 | 1.58E-20 | 1.53E-20 | 1.61E-20 | 0.166E-19 | 1.80E-20 | 1.64E-20 | 1.69E-20 |
| Reflector | (-23.31, -23.31) | (-16,-16) | 6.66E+08 | 4.70196E-19 | 5.06E-19 | 4.23E-19 | 4.95E-19 | 4.84E-19 | 4.72E-19 | 5.34E-19 | 4.60E-19 | 4.59E-19 | 4.46E-19 | 0.474E-18 | 4.45E-19 | 4.72E-19 | 4.43E-19 |
| | (-25.83, -25.83) | (-18,-18) | 4.06E+08 | 2.86636E-19 | 3.10E-19 | 2.88E-19 | 3.44E-19 | 2.94E-19 | 2.78E-19 | 3.29E-19 | 2.91E-19 | 2.71E-19 | 2.69E-19 | 0.287E-18 | 2.78E-19 | 2.64E-19 | 2.65E-19 |
| | (-28.35, -28.35) | (-20,-20) | 2.53E+08 | 1.78618E-19 | 1.92E-19 | 1.57E-19 | 1.81E-19 | 1.77E-19 | 1.59E-19 | 2.04E-19 | 1.73E-19 | 1.63E-19 | 1.57E-19 | 0.175E-18 | 1.68E-19 | 1.55E-19 | 1.55E-19 |
| | (-30.87, -30.87) | (-22,-22) | 1.52E+08 | 1.07312E-19 | 1.18E-19 | 1.08E-19 | 1.09E-19 | 1.08E-19 | 1.05E-19 | 1.28E-19 | 1.06E-19 | 9.33E-20 | 8.99E-20 | 0.108E-18 | 1.04E-19 | 1.05E-19 | 1.01E-19 |
| | (-33.39, -33.39) | (-24,-24) | 9.71E+07 | 6.85526E-20 | 7.36E-20 | 6.76E-20 | 6.05E-20 | 6.63E-20 | 6.23E-20 | 7.95E-20 | 6.30E-20 | 5.64E-20 | 5.22E-20 | 0.652E-19 | 6.41E-20 | 6.40E-20 | 5.52E-20 |

C/E comparison

| $^{27}$Al (n,a) | Position in cm | Grid Position | Experimental Value **Equiv. Fiss. Flux** | Experimental Value **Reaction Rates** | HYU-TORT Korea | HYU-MCNP Korea | HYU-MCNPX Korea | Transpire Inc.-ATTILA USA | KI-MCU Russia | KOPEC-DORT Korea | WTI-MCNP Germany | VTT-TORT Finland | VTT-MT Finland | KI-LUCKY Russia | KAERI-DANTSYS Korea | VTT-MCNP-K Finland | VTT-MCNP-F Finland |
|---|---|---|---|---|---|---|---|---|---|---|---|---|---|---|---|---|---|
| Central Hole | ( 0.0, 0.0) | (+2.5,+2.5) | N/A | N/A | | | | | | | | | | | | | |
| Water Gap | (-54.36, -9.59) | 10.75 degree | N/A | N/A | | | | | | | | | | | | | |
| | (-52.89, -15.80) | 16.63 degree | 3.15E+07 | 2.2239E-20 | 1.04 | 0.83 | 0.75 | 0.97 | 0.91 | 1.13 | 1.00 | 0.86 | 0.85 | 0.94 | 1.07 | 0.80 | 0.81 |
| | (-51.53, -19.78) | 21.14 degree | 2.52E+07 | 1.77912E-20 | 1.31 | 1.10 | 1.11 | 1.23 | 1.15 | 1.35 | 1.20 | 1.04 | 1.15 | 1.17 | 1.29 | 1.08 | 1.05 |
| | (-50.03, -23.33) | 25.62 degree | 2.67E+07 | 1.88502E-20 | 1.11 | 1.08 | 1.64 | 1.01 | 0.98 | 1.11 | 1.04 | 0.87 | 1.20 | 0.98 | 0.98 | 1.12 | 0.81 |
| | (-48.74, -25.91) | 28.78 degree | 2.54E+07 | 1.79324E-20 | 1.06 | 0.83 | 1.04 | 1.00 | 0.95 | 1.13 | 1.00 | 0.87 | 0.98 | 0.96 | 0.96 | 0.94 | 0.96 |
| | (-46.29, -30.06) | 33.89 degree | 2.50E+07 | 1.765E-20 | 1.08 | 1.02 | 0.92 | 0.99 | 0.91 | 1.11 | 0.98 | 0.86 | 1.10 | 0.95 | 0.99 | 0.90 | 0.82 |
| | (-44.08, -33.22) | 37.44 degree | N/A | N/A | | | | | | | | | | | | | |
| | (-42.29, -35.48) | 40.99 degree | 2.30E+07 | 1.6238E-20 | 1.16 | 1.23 | 1.07 | 1.04 | 1.02 | 1.20 | 0.98 | 0.94 | 0.97 | 1.02 | 0.93 | 0.87 | 0.92 |
| | (-39.03, -39.03) | 45 degree | 2.30E+07 | 1.6238E-20 | 1.20 | 0.79 | 1.00 | 1.06 | 1.02 | 1.20 | 0.97 | 0.94 | 0.99 | 1.02 | 1.11 | 1.01 | 1.04 |
| Reflector | (-23.31, -23.31) | (-16,-16) | 6.66E+08 | 4.70196E-19 | 1.08 | 0.90 | 1.05 | 1.03 | 1.00 | 1.14 | 0.98 | 0.98 | 0.95 | 1.01 | 0.95 | 1.00 | 0.94 |
| | (-25.83, -25.83) | (-18,-18) | 4.06E+08 | 2.86636E-19 | 1.08 | 1.00 | 1.20 | 1.03 | 0.97 | 1.15 | 1.02 | 0.94 | 0.94 | 1.00 | 0.97 | 0.92 | 0.93 |
| | (-28.35, -28.35) | (-20,-20) | 2.53E+08 | 1.78618E-19 | 1.07 | 0.88 | 1.01 | 0.99 | 0.89 | 1.14 | 0.97 | 0.91 | 0.88 | 0.98 | 0.94 | 0.87 | 0.87 |
| | (-30.87, -30.87) | (-22,-22) | 1.52E+08 | 1.07312E-19 | 1.10 | 1.01 | 1.01 | 1.01 | 0.98 | 1.20 | 0.98 | 0.87 | 0.84 | 1.01 | 0.97 | 0.98 | 0.94 |
| | (-33.39, -33.39) | (-24,-24) | 9.71E+07 | 6.85526E-20 | 1.07 | 0.99 | 0.88 | 0.97 | 0.91 | 1.16 | 0.92 | 0.82 | 0.76 | 0.95 | 0.94 | 0.93 | 0.81 |
| Number of positions within +-5% = | | | | | 1 | 4 | 4 | 10 | 7 | 0 | 10 | 2 | 3 | 9 | 5 | 3 | 3 |
| Number of positions within +-10% = | | | | | 7 | 5 | 7 | 11 | 10 | 0 | 11 | 6 | 6 | 11 | 10 | 7 | 7 |
| Number of positions within +-20% = | | | | | 11 | 10 | 10 | 11 | 12 | 9 | 11 | 12 | 10 | 12 | 11 | 11 | 12 |

# Table 4.16(a). Fast neutron fluxes E > 0.1 MeV: Comparison relative to KI MCU calculations in stainless steel zones

Calculated results

| Flux E>0.1 MeV | Position in cm | Grid Position | KI-MCU Russia | HYU-TORT Korea | HYU-MCNP Korea | HYU-MCNPX Korea | Transpire Inc.-ATTILA USA | KOPEC-DORT Korea | VTI/SUT-HELIOS Slovak | WTI-MCNP Germany | VTT-TORT Finland | VTT-MT Finland | KI-LUCKY Russia | KAERI-DANTSYS Korea | VTT-MCNP-K Finland | VTT-MCNP-F Finland | SCK-MCNPX Belgium |
|---|---|---|---|---|---|---|---|---|---|---|---|---|---|---|---|---|---|
| Inner Baffle | ( -4.41, -0.63) | (-1,+2) | **3.32E+09** | 3.32E+09 | 3.34E+09 | 3.33E+09 | 3.51E+09 | 3.57E+09 | 2.13E+09 | 3.36E+09 | 3.60E+09 | 3.22E+09 | 0.355E+10 | 3.20E+09 | 2.92E+09 | 3.14E+09 | 3.30E+09 |
| | ( -4.41, -4.41) | (-1,-1) | **3.90E+09** | 3.88E+09 | 3.94E+09 | 3.93E+09 | 4.10E+09 | 4.19E+09 | 2.46E+09 | 3.96E+09 | 4.06E+09 | 3.94E+09 | 0.416E+10 | 3.74E+09 | 3.72E+09 | 4.07E+09 | 3.91E+09 |
| Outer Baffle | (-39.69, -0.63) | (-29,+2) | **1.20E+09** | 1.03E+09 | 1.22E+09 | 1.22E+09 | 1.19E+09 | 1.26E+09 | 7.86E+08 | 1.21E+09 | 1.10E+09 | 1.08E+09 | 0.114E+10 | 1.18E+09 | 1.11E+09 | 1.03E+09 | 1.21E+09 |
| | (-39.69, -5.67) | (-29,-2) | **1.14E+09** | 9.83E+08 | 1.16E+09 | 1.18E+09 | 1.13E+09 | 1.20E+09 | 7.49E+08 | 1.15E+09 | 1.03E+09 | 1.03E+09 | 0.109E+10 | 1.12E+09 | 1.12E+09 | 1.04E+09 | 1.16E+09 |
| | (-39.69, -11.97) | (-29,-7) | **9.27E+08** | 8.09E+08 | 9.52E+08 | 9.47E+08 | 9.19E+08 | 9.80E+08 | 6.13E+08 | 9.46E+08 | 8.27E+08 | 8.47E+08 | 0.891E+09 | 9.20E+08 | 9.29E+08 | 8.43E+08 | 9.29E+08 |
| | (-39.69, -18.27) | (-29,-12) | **5.76E+08** | 5.12E+08 | 5.87E+08 | 5.86E+08 | 5.72E+08 | 6.21E+08 | 3.93E+08 | 5.89E+08 | 4.94E+08 | 5.30E+08 | 0.562E+09 | 5.72E+08 | 5.87E+08 | 5.32E+08 | 5.86E+08 |
| | (-37.17, -20.79) | (-27,-14) | **6.06E+08** | 5.61E+08 | 6.24E+08 | 6.17E+08 | 6.03E+08 | 6.50E+08 | 4.10E+08 | 6.12E+08 | 5.51E+08 | 5.50E+08 | 0.578E+09 | 5.96E+08 | 6.02E+08 | 5.67E+08 | 6.14E+08 |
| | (-30.87, -20.79) | (-22,-14) | **1.16E+09** | 1.10E+09 | 1.19E+09 | 1.18E+09 | 1.17E+09 | 1.24E+09 | 7.43E+08 | 1.17E+09 | 1.19E+09 | 1.10E+09 | 0.112E+10 | 1.14E+09 | 1.14E+09 | 1.12E+09 | 1.17E+09 |
| | (-24.57, -20.79) | (-17,-14) | **1.92E+09** | 1.91E+09 | 1.95E+09 | 1.95E+09 | 1.99E+09 | 2.09E+09 | 1.21E+09 | 1.94E+09 | 1.87E+09 | 1.97E+09 | 0.197E+10 | 1.88E+09 | 1.85E+09 | 1.95E+09 | 1.92E+09 |
| Barrel | (-49.77, -0.63) | (-37,+2) | **1.45E+08** | 1.29E+08 | 1.49E+08 | 1.47E+08 | 1.42E+08 | 1.57E+08 | 1.09E+08 | 1.46E+08 | 1.26E+08 | 1.03E+08 | 0.150E+09 | 1.51E+08 | 1.28E+08 | 1.21E+08 | 1.38E+08 |
| | (-49.77, -9.45) | (-37,-5) | **1.34E+08** | 1.20E+08 | 1.36E+08 | 1.37E+08 | 1.34E+08 | 1.47E+08 | 1.08E+08 | 1.36E+08 | 1.16E+08 | 9.83E+07 | 0.139E+09 | 1.35E+08 | 1.32E+08 | 1.20E+08 | 1.33E+08 |
| | (-47.25, -18.27) | (-35,-12) | **1.42E+08** | 1.28E+08 | 1.43E+08 | 1.46E+08 | 1.42E+08 | 1.54E+08 | 1.09E+08 | 1.43E+08 | 1.24E+08 | 1.10E+08 | 0.145E+09 | 1.40E+08 | 1.39E+08 | 1.28E+08 | 1.45E+08 |
| | (-45.99, -22.05) | (-34,-15) | **1.29E+08** | 1.19E+08 | 1.31E+08 | 1.31E+08 | 1.30E+08 | 1.40E+08 | 9.94E+07 | 1.29E+08 | 1.21E+08 | 1.01E+08 | 0.134E+09 | 1.24E+08 | 1.26E+08 | 1.19E+08 | 1.31E+08 |
| | (-44.73, -24.57) | (-33,-17) | **1.16E+08** | 1.07E+08 | 1.20E+08 | 1.20E+08 | 1.17E+08 | 1.27E+08 | 9.68E+07 | 1.17E+08 | 1.10E+08 | 9.30E+07 | 0.122E+09 | 1.10E+08 | 1.11E+08 | 1.08E+08 | 1.17E+08 |
| | (-42.21, -28.35) | (-31,-20) | **9.53E+07** | 9.02E+07 | 9.83E+07 | 9.73E+07 | 9.62E+07 | 1.06E+08 | 8.57E+07 | 9.57E+07 | 8.89E+07 | 7.44E+07 | 0.100E+09 | 9.21E+07 | 9.01E+07 | 8.66E+07 | 9.50E+07 |
| | (-38.43, -33.39) | (-28,-24) | **7.15E+07** | 6.88E+07 | 7.37E+07 | 7.15E+07 | 7.21E+07 | 8.09E+07 | 7.25E+07 | 7.13E+07 | 6.66E+07 | 5.35E+07 | 0.756E+08 | 7.08E+07 | 6.90E+07 | 6.65E+07 | 7.14E+07 |
| | (-35.91, -35.91) | (-26,-26) | **6.87E+07** | 6.62E+07 | 6.98E+07 | 7.14E+07 | 6.98E+07 | 7.86E+07 | 7.28E+07 | 6.91E+07 | 6.42E+07 | 5.11E+07 | 0.718E+08 | 6.79E+07 | 6.79E+07 | 6.54E+07 | 6.61E+07 |
| Neutron Pad | (-58.54, -22.47) | 21 degree | **1.36E+07** | 1.40E+07 | 1.53E+07 | 1.53E+07 | 1.48E+07 | 1.72E+07 | 1.70E+07 | 1.50E+07 | 1.29E+07 | 9.32E+06 | 0.157E+08 | 1.39E+07 | 1.47E+07 | 1.34E+07 | 1.34E+07 |
| | (-46.60, -41.95) | 42 degree | **9.27E+06** | 9.84E+06 | 1.02E+07 | 1.05E+07 | 1.04E+07 | 1.24E+07 | 1.39E+07 | 1.05E+07 | 9.37E+06 | 6.37E+06 | 0.105E+08 | 9.36E+06 | 1.06E+07 | 8.26E+06 | 7.47E+06 |

Comparison relative to KI MCU calculation

| Flux E>0.1 MeV | Position in cm | Grid Position | KI-MCU Russia | HYU-TORT Korea | HYU-MCNP Korea | HYU-MCNPX Korea | Transpire Inc.-ATTILA USA | KOPEC-DORT Korea | VTI/SUT-HELIOS Slovak | WTI-MCNP Germany | VTT-TORT Finland | VTT-MT Finland | KI-LUCKY Russia | KAERI-DANTSYS Korea | VTT-MCNP-K Finland | VTT-MCNP-F Finland | SCK-MCNPX Belgium |
|---|---|---|---|---|---|---|---|---|---|---|---|---|---|---|---|---|---|
| Inner Baffle | ( -4.41, -0.63) | (-1,+2) | **3.32E+09** | 1.00 | 1.01 | 1.00 | 1.06 | 1.08 | 0.64 | 1.01 | 1.09 | 0.97 | 1.07 | 0.96 | 0.88 | 0.95 | 1.00 |
| | ( -4.41, -4.41) | (-1,-1) | **3.90E+09** | 0.99 | 1.01 | 1.01 | 1.05 | 1.07 | 0.63 | 1.01 | 1.04 | 1.01 | 1.07 | 0.96 | 0.95 | 1.04 | 1.00 |
| Outer Baffle | (-39.69, -0.63) | (-29,+2) | **1.20E+09** | 0.86 | 1.01 | 1.01 | 0.99 | 1.05 | 0.65 | 1.01 | 0.91 | 0.90 | 0.95 | 0.98 | 0.93 | 0.85 | 1.00 |
| | (-39.69, -5.67) | (-29,-2) | **1.14E+09** | 0.86 | 1.02 | 1.03 | 0.98 | 1.05 | 0.65 | 1.00 | 0.90 | 0.90 | 0.95 | 0.98 | 0.98 | 0.91 | 1.01 |
| | (-39.69, -11.97) | (-29,-7) | **9.27E+08** | 0.87 | 1.03 | 1.02 | 0.99 | 1.06 | 0.66 | 1.02 | 0.89 | 0.91 | 0.96 | 0.99 | 1.00 | 0.91 | 1.00 |
| | (-39.69, -18.27) | (-29,-12) | **5.76E+08** | 0.89 | 1.02 | 1.02 | 0.99 | 1.08 | 0.68 | 1.02 | 0.86 | 0.92 | 0.98 | 0.99 | 1.02 | 0.92 | 1.02 |
| | (-37.17, -20.79) | (-27,-14) | **6.06E+08** | 0.93 | 1.03 | 1.02 | 1.00 | 1.07 | 0.68 | 1.01 | 0.91 | 0.91 | 0.95 | 0.98 | 0.99 | 0.94 | 1.01 |
| | (-30.87, -20.79) | (-22,-14) | **1.16E+09** | 0.95 | 1.02 | 1.02 | 1.01 | 1.07 | 0.64 | 1.01 | 1.02 | 0.95 | 0.96 | 0.98 | 0.98 | 0.96 | 1.01 |
| | (-24.57, -20.79) | (-17,-14) | **1.92E+09** | 0.99 | 1.02 | 1.02 | 1.03 | 1.09 | 0.63 | 1.01 | 0.97 | 1.02 | 1.02 | 0.98 | 0.96 | 1.01 | 1.00 |
| Barrel | (-49.77, -0.63) | (-37,+2) | **1.45E+08** | 0.89 | 1.02 | 1.01 | 0.98 | 1.08 | 0.75 | 1.01 | 0.87 | 0.71 | 1.03 | 1.04 | 0.88 | 0.83 | 0.95 |
| | (-49.77, -9.45) | (-37,-5) | **1.34E+08** | 0.89 | 1.01 | 1.02 | 0.99 | 1.09 | 0.80 | 1.01 | 0.86 | 0.73 | 1.03 | 1.01 | 0.98 | 0.89 | 0.99 |
| | (-47.25, -18.27) | (-35,-12) | **1.42E+08** | 0.90 | 1.01 | 1.03 | 1.00 | 1.09 | 0.77 | 1.01 | 0.88 | 0.78 | 1.02 | 0.99 | 0.98 | 0.90 | 1.02 |
| | (-45.99, -22.05) | (-34,-15) | **1.29E+08** | 0.93 | 1.02 | 1.02 | 1.01 | 1.09 | 0.77 | 1.01 | 0.94 | 0.78 | 1.04 | 0.96 | 0.98 | 0.93 | 1.02 |
| | (-44.73, -24.57) | (-33,-17) | **1.16E+08** | 0.92 | 1.03 | 1.03 | 1.00 | 1.09 | 0.83 | 1.01 | 0.94 | 0.80 | 1.05 | 0.95 | 0.96 | 0.93 | 1.01 |
| | (-42.21, -28.35) | (-31,-20) | **9.53E+07** | 0.95 | 1.03 | 1.02 | 1.01 | 1.11 | 0.90 | 1.00 | 0.93 | 0.78 | 1.05 | 0.97 | 0.95 | 0.91 | 1.00 |
| | (-38.43, -33.39) | (-28,-24) | **7.15E+07** | 0.96 | 1.03 | 1.00 | 1.01 | 1.13 | 1.01 | 1.00 | 0.93 | 0.75 | 1.06 | 0.99 | 0.97 | 0.93 | 1.00 |
| | (-35.91, -35.91) | (-26,-26) | **6.87E+07** | 0.96 | 1.02 | 1.04 | 1.02 | 1.14 | 1.06 | 1.01 | 0.93 | 0.74 | 1.04 | 0.99 | 0.99 | 0.95 | 0.96 |
| Neutron Pad | (-58.54, -22.47) | 21 degree | **1.36E+07** | 1.03 | 1.12 | 1.13 | 1.09 | 1.26 | 1.25 | 1.10 | 0.95 | 0.69 | 1.16 | 1.03 | 1.08 | 0.99 | 0.99 |
| | (-46.60, -41.95) | 42 degree | **9.27E+06** | 1.06 | 1.10 | 1.13 | 1.12 | 1.34 | 1.50 | 1.13 | 1.01 | 0.69 | 1.13 | 1.01 | 1.14 | 0.89 | 0.81 |
| Number of positions within +-5% = | | | | 7 | 17 | 17 | 16 | 2 | 1 | 17 | 4 | 4 | 13 | 18 | 13 | 5 | 18 |
| Number of positions within +-10% = | | | | 13 | 17 | 17 | 18 | 14 | 2 | 17 | 14 | 8 | 17 | 19 | 16 | 15 | 18 |
| Number of positions within +-20% = | | | | 19 | 19 | 19 | 19 | 17 | 5 | 19 | 19 | 9 | 19 | 19 | 19 | 19 | 19 |

# Table 4.16(b). Fast neutron fluxes E > 0.1 MeV: Comparison relative to KI MCU calculations in water zones

Calculated results

| Flux E>0.1MeV | Position in cm | Grid Position | KI-MCU Russia | HYU-TORT Korea | HYU-MCNP Korea | HYU-MCNPX Korea | Transpire Inc.-ATTILA USA | KOPEC-DORT Korea | VTI/SUT-HELIOS Slovak | WTI-MCNP Germany | VTT-TORT Finland | VTT-MT Finland | KI-LUCKY Russia | KAERI-DANTSYS Korea | VTT-MCNP-K Finland | VTT-MCNP-F Finland | SCK-MCNPX Belgium |
|---|---|---|---|---|---|---|---|---|---|---|---|---|---|---|---|---|---|
| Central Hole | ( 0.0, 0.0) | (+2.5,+2.5) | **1.93E+09** | 1.97E+09 | 4.89E+08 | 4.89E+08 | 1.94E+09 | 2.14E+09 | 1.34E+09 | 1.97E+09 | 2.02E+09 | 1.68E+09 | 0.203E+10 | 1.85E+09 | 1.94E+09 | 2.13E+09 | 4.73E+08 |
| Water Gap | (-54.36, -9.59) | 10.75 degree | **4.09E+07** | 3.77E+07 | 4.22E+07 | 4.17E+07 | 4.14E+07 | 4.48E+07 | 3.32E+07 | 4.13E+07 | 3.78E+07 | 3.56E+07 | 0.397E+08 | 3.67E+07 | 4.23E+07 | 3.64E+07 | 4.24E+07 |
| | (-52.89, -15.80) | 16.63 degree | **4.21E+07** | 4.05E+07 | 4.32E+07 | 4.31E+07 | 4.30E+07 | 4.61E+07 | 3.64E+07 | 4.31E+07 | 3.97E+07 | 3.60E+07 | 0.407E+08 | 5.02E+07 | 4.15E+07 | 3.92E+07 | 4.30E+07 |
| | (-51.53, -19.78) | 21.14 degree | **4.21E+07** | 3.98E+07 | 4.28E+07 | 4.39E+07 | 4.25E+07 | 4.59E+07 | 3.53E+07 | 4.27E+07 | 3.97E+07 | 3.71E+07 | 0.398E+08 | 4.89E+07 | 4.37E+07 | 3.96E+07 | 4.20E+07 |
| | (-50.03, -23.33) | 25.62 degree | **4.03E+07** | 3.87E+07 | 4.10E+07 | 4.05E+07 | 4.17E+07 | 4.32E+07 | 3.35E+07 | 4.08E+07 | 3.80E+07 | 3.28E+07 | 0.384E+08 | 4.11E+07 | 3.88E+07 | 3.74E+07 | 3.89E+07 |
| | (-48.74, -25.91) | 28.78 degree | **3.75E+07** | 3.48E+07 | 3.78E+07 | 3.81E+07 | 3.80E+07 | 4.00E+07 | 3.35E+07 | 3.80E+07 | 3.57E+07 | 3.40E+07 | 0.362E+08 | 3.88E+07 | 3.75E+07 | 3.54E+07 | 3.91E+07 |
| | (-46.29, -30.06) | 33.89 degree | **3.18E+07** | 3.09E+07 | 3.20E+07 | 3.32E+07 | 3.30E+07 | 3.42E+07 | 3.02E+07 | 3.21E+07 | 2.98E+07 | 3.06E+07 | 0.299E+08 | 3.54E+07 | 3.21E+07 | 3.01E+07 | 3.20E+07 |
| | (-44.08, -33.22) | 37.44 degree | **2.75E+07** | 2.68E+07 | 2.72E+07 | 2.86E+07 | 2.74E+07 | 3.06E+07 | 2.77E+07 | 2.79E+07 | 2.69E+07 | 2.40E+07 | 0.273E+08 | 2.95E+07 | 2.68E+07 | 2.71E+07 | 2.58E+07 |
| | (-42.29, -35.48) | 40.99 degree | **2.54E+07** | 2.33E+07 | 2.58E+07 | 2.60E+07 | 2.61E+07 | 2.81E+07 | 2.72E+07 | 2.55E+07 | 2.44E+07 | 2.21E+07 | 0.250E+08 | 2.33E+07 | 2.51E+07 | 2.37E+07 | 2.45E+07 |
| | (-39.03, -39.03) | 45 degree | **2.38E+07** | 2.23E+07 | 2.33E+07 | 2.40E+07 | 2.43E+07 | 2.72E+07 | 2.65E+07 | 2.39E+07 | 2.32E+07 | 1.96E+07 | 0.233E+08 | 2.87E+07 | 2.24E+07 | 2.20E+07 | 2.18E+07 |
| Reflector | (-23.31, -23.31) | (-16,-16) | **1.24E+09** | 1.23E+09 | 1.26E+09 | 1.24E+09 | 1.32E+09 | 1.34E+09 | 8.02E+08 | 1.25E+09 | 1.29E+09 | 1.39E+09 | 0.121E+10 | 1.20E+09 | 1.20E+09 | 1.26E+09 | 1.25E+09 |
| | (-25.83, -25.83) | (-18,-18) | **5.64E+08** | 5.54E+08 | 5.73E+08 | 5.71E+08 | 5.76E+08 | 6.15E+08 | 3.89E+08 | 5.67E+08 | 5.64E+08 | 6.71E+08 | 0.554E+09 | 5.54E+08 | 5.58E+08 | 5.56E+08 | 5.64E+08 |
| | (-28.35, -28.35) | (-20,-20) | **2.73E+08** | 2.64E+08 | 2.77E+08 | 2.72E+08 | 2.76E+08 | 2.99E+08 | 2.08E+08 | 2.74E+08 | 2.71E+08 | 3.03E+08 | 0.269E+09 | 2.68E+08 | 2.69E+08 | 2.69E+08 | 2.74E+08 |
| | (-30.87, -30.87) | (-22,-22) | **1.38E+08** | 1.31E+08 | 1.40E+08 | 1.40E+08 | 1.40E+08 | 1.55E+08 | 1.19E+08 | 1.39E+08 | 1.25E+08 | 1.25E+08 | 0.138E+09 | 1.38E+08 | 1.35E+08 | 1.37E+08 | 1.40E+08 |
| | (-33.39, -33.39) | (-24,-24) | **8.37E+07** | 7.87E+07 | 8.50E+07 | 8.48E+07 | 8.51E+07 | 9.52E+07 | 8.14E+07 | 8.39E+07 | 7.67E+07 | 6.28E+07 | 0.840E+08 | 8.33E+07 | 8.39E+07 | 8.00E+07 | 8.45E+07 |

Comparison relative to KI MCU calculation

| Flux E>0.1MeV | Position in cm | Grid Position | KI-MCU Russia | HYU-TORT Korea | HYU-MCNP Korea | HYU-MCNPX Korea | Transpire Inc.-ATTILA USA | KOPEC-DORT Korea | VTI/SUT-HELIOS Slovak | WTI-MCNP Germany | VTT-TORT Finland | VTT-MT Finland | KI-LUCKY Russia | KAERI-DANTSYS Korea | VTT-MCNP-K Finland | VTT-MCNP-F Finland | SCK-MCNPX Belgium |
|---|---|---|---|---|---|---|---|---|---|---|---|---|---|---|---|---|---|
| Central Hole | ( 0.0, 0.0) | (+2.5,+2.5) | **1.93E+09** | 1.02 | 0.25 | 0.25 | 1.00 | 1.11 | 0.69 | 1.02 | 1.05 | 0.87 | 1.05 | 0.96 | 1.00 | 1.10 | 0.24 |
| Water Gap | (-54.36, -9.59) | 10.75 degree | **4.09E+07** | 0.92 | 1.03 | 1.02 | 1.01 | 1.09 | 0.81 | 1.01 | 0.92 | 0.87 | 0.97 | 0.90 | 1.03 | 0.89 | 1.04 |
| | (-52.89, -15.80) | 16.63 degree | **4.21E+07** | 0.96 | 1.03 | 1.02 | 1.02 | 1.10 | 0.86 | 1.02 | 0.94 | 0.86 | 0.97 | 1.19 | 0.99 | 0.93 | 1.02 |
| | (-51.53, -19.78) | 21.14 degree | **4.21E+07** | 0.95 | 1.02 | 1.04 | 1.01 | 1.09 | 0.84 | 1.02 | 0.94 | 0.88 | 0.95 | 1.16 | 1.04 | 0.94 | 1.00 |
| | (-50.03, -23.33) | 25.62 degree | **4.03E+07** | 0.96 | 1.02 | 1.00 | 1.04 | 1.07 | 0.83 | 1.01 | 0.94 | 0.81 | 0.95 | 1.02 | 0.96 | 0.93 | 0.96 |
| | (-48.74, -25.91) | 28.78 degree | **3.75E+07** | 0.93 | 1.01 | 1.02 | 1.01 | 1.07 | 0.89 | 1.01 | 0.95 | 0.91 | 0.97 | 1.04 | 1.00 | 0.95 | 1.04 |
| | (-46.29, -30.06) | 33.89 degree | **3.18E+07** | 0.97 | 1.01 | 1.04 | 1.04 | 1.07 | 0.95 | 1.01 | 0.94 | 0.96 | 0.94 | 1.11 | 1.01 | 0.95 | 1.01 |
| | (-44.08, -33.22) | 37.44 degree | **2.75E+07** | 0.98 | 0.99 | 1.04 | 1.00 | 1.11 | 1.01 | 1.02 | 0.98 | 0.88 | 0.99 | 1.07 | 0.98 | 0.99 | 0.94 |
| | (-42.29, -35.48) | 40.99 degree | **2.54E+07** | 0.92 | 1.01 | 1.02 | 1.03 | 1.11 | 1.07 | 1.00 | 0.96 | 0.87 | 0.98 | 0.92 | 0.99 | 0.93 | 0.96 |
| | (-39.03, -39.03) | 45 degree | **2.38E+07** | 0.93 | 0.98 | 1.00 | 1.02 | 1.14 | 1.11 | 1.00 | 0.97 | 0.82 | 0.98 | 1.21 | 0.94 | 0.92 | 0.91 |
| Reflector | (-23.31, -23.31) | (-16,-16) | **1.24E+09** | 0.99 | 1.02 | 1.01 | 1.07 | 1.08 | 0.65 | 1.01 | 1.04 | 1.13 | 0.98 | 0.97 | 0.97 | 1.02 | 1.01 |
| | (-25.83, -25.83) | (-18,-18) | **5.64E+08** | 0.98 | 1.02 | 1.01 | 1.02 | 1.09 | 0.69 | 1.00 | 1.00 | 1.19 | 0.98 | 0.98 | 0.99 | 0.99 | 1.00 |
| | (-28.35, -28.35) | (-20,-20) | **2.73E+08** | 0.97 | 1.01 | 1.00 | 1.01 | 1.10 | 0.76 | 1.00 | 0.99 | 1.11 | 0.99 | 0.98 | 0.99 | 0.98 | 1.00 |
| | (-30.87, -30.87) | (-22,-22) | **1.38E+08** | 0.95 | 1.02 | 1.01 | 1.02 | 1.12 | 0.86 | 1.01 | 0.91 | 0.90 | 1.00 | 1.00 | 0.98 | 0.99 | 1.01 |
| | (-33.39, -33.39) | (-24,-24) | **8.37E+07** | 0.94 | 1.02 | 1.01 | 1.02 | 1.14 | 0.97 | 1.00 | 0.92 | 0.75 | 1.00 | 1.00 | 1.00 | 0.96 | 1.01 |
| | Number of positions within +-5% = | | | 8 | 14 | 14 | 14 | 0 | 2 | 15 | 8 | 1 | 12 | 8 | 14 | 6 | 12 |
| | Number of positions within +-10% = | | | 15 | 14 | 14 | 15 | 9 | 4 | 15 | 15 | 3 | 15 | 10 | 15 | 14 | 14 |
| | Number of positions within +-20% = | | | 15 | 14 | 14 | 15 | 15 | 11 | 15 | 15 | 14 | 15 | 14 | 15 | 15 | 14 |

# Table 4.17(a). Fast neutron fluxes E > 1.0 MeV: Comparison relative to KI MCU calculations in stainless steel zones

Calculated results

| Flux E>1.0 MeV | Position in cm | Grid Position | KI-MCU Russia | HYU-TORT Korea | HYU-MCNP Korea | HYU-MCNPX Korea | Transpire Inc.-ATTILA USA | KOPEC-DORT Korea | VTI/SUT-HELIOS Slovak | WTI-MCNP Germany | VTT-TORT Finland | VTT-MT Finland | KI-LUCKY Russia | KAERI-DANTSYS Korea | VTT-MCNP-K Finland | VTT-MCNP-F Finland | SCK-MCNPX Belgium |
|---|---|---|---|---|---|---|---|---|---|---|---|---|---|---|---|---|---|
| Inner Baffle | ( -4.41, -0.63) | (-1,+2) | **1.39E+09** | 1.36E+09 | 1.38E+09 | 1.37E+09 | 1.49E+09 | 1.47E+09 | 9.03E+08 | 1.40E+09 | 1.49E+09 | 1.37E+09 | 0.141E+10 | 1.33E+09 | 1.21E+09 | 1.31E+09 | 1.38E+09 |
| | ( -4.41, -4.41) | (-1,-1) | **1.66E+09** | 1.62E+09 | 1.66E+09 | 1.66E+09 | 1.76E+09 | 1.76E+09 | 1.06E+09 | 1.68E+09 | 1.71E+09 | 1.76E+09 | 0.166E+10 | 1.58E+09 | 1.56E+09 | 1.74E+09 | 1.65E+09 |
| Outer Baffle | (-39.69, -0.63) | (-29,+2) | **5.20E+08** | 4.36E+08 | 5.32E+08 | 5.19E+08 | 5.23E+08 | 5.41E+08 | 3.43E+08 | 5.27E+08 | 4.75E+08 | 4.69E+08 | 0.471E+09 | 5.12E+08 | 4.85E+08 | 4.37E+08 | 5.15E+08 |
| | (-39.69, -5.67) | (-29,-2) | **4.95E+08** | 4.15E+08 | 5.05E+08 | 5.16E+08 | 5.00E+08 | 5.15E+08 | 3.27E+08 | 4.98E+08 | 4.43E+08 | 4.52E+08 | 0.448E+09 | 4.87E+08 | 4.82E+08 | 4.47E+08 | 4.98E+08 |
| | (-39.69, -11.97) | (-29,-7) | **3.98E+08** | 3.41E+08 | 4.04E+08 | 4.08E+08 | 4.07E+08 | 4.20E+08 | 2.66E+08 | 4.10E+08 | 3.54E+08 | 3.70E+08 | 0.366E+09 | 3.98E+08 | 3.95E+08 | 3.67E+08 | 4.01E+08 |
| | (-39.69, -18.27) | (-29,-12) | **2.38E+08** | 2.09E+08 | 2.45E+08 | 2.45E+08 | 2.45E+08 | 2.57E+08 | 1.69E+08 | 2.48E+08 | 2.04E+08 | 2.22E+08 | 0.221E+09 | 2.39E+08 | 2.44E+08 | 2.21E+08 | 2.41E+08 |
| | (-37.17, -20.79) | (-27,-14) | **2.51E+08** | 2.29E+08 | 2.61E+08 | 2.54E+08 | 2.57E+08 | 2.68E+08 | 1.77E+08 | 2.56E+08 | 2.27E+08 | 2.34E+08 | 0.226E+09 | 2.48E+08 | 2.49E+08 | 2.32E+08 | 2.50E+08 |
| | (-30.87, -20.79) | (-22,-14) | **4.95E+08** | 4.59E+08 | 5.03E+08 | 4.94E+08 | 5.11E+08 | 5.21E+08 | 3.17E+08 | 4.99E+08 | 5.02E+08 | 4.81E+08 | 0.452E+09 | 4.83E+08 | 4.84E+08 | 4.56E+08 | 4.93E+08 |
| | (-24.57, -20.79) | (-17,-14) | **8.05E+08** | 7.85E+08 | 8.16E+08 | 8.14E+08 | 8.48E+08 | 8.68E+08 | 5.10E+08 | 8.14E+08 | 7.72E+08 | 8.48E+08 | 0.783E+09 | 7.84E+08 | 7.75E+08 | 8.12E+08 | 7.92E+08 |
| Barrel | (-49.77, -0.63) | (-37,+2) | **6.52E+07** | 5.54E+07 | 6.65E+07 | 6.59E+07 | 6.55E+07 | 6.92E+07 | 5.20E+07 | 6.55E+07 | 5.60E+07 | 4.85E+07 | 0.615E+08 | 6.72E+07 | 5.75E+07 | 5.57E+07 | 6.39E+07 |
| | (-49.77, -9.45) | (-37,-5) | **5.84E+07** | 4.93E+07 | 5.86E+07 | 5.93E+07 | 5.86E+07 | 6.18E+07 | 4.93E+07 | 5.84E+07 | 4.86E+07 | 4.38E+07 | 0.544E+08 | 5.90E+07 | 5.67E+07 | 5.36E+07 | 5.65E+07 |
| | (-47.25, -18.27) | (-35,-12) | **5.85E+07** | 4.96E+07 | 5.80E+07 | 5.85E+07 | 5.91E+07 | 6.15E+07 | 4.72E+07 | 5.81E+07 | 4.97E+07 | 4.60E+07 | 0.532E+08 | 5.71E+07 | 5.73E+07 | 5.25E+07 | 5.90E+07 |
| | (-45.99, -22.05) | (-34,-15) | **5.05E+07** | 4.48E+07 | 5.10E+07 | 5.03E+07 | 5.20E+07 | 5.34E+07 | 4.17E+07 | 5.06E+07 | 4.66E+07 | 4.07E+07 | 0.474E+08 | 4.86E+07 | 4.82E+07 | 4.65E+07 | 5.18E+07 |
| | (-44.73, -24.57) | (-33,-17) | **4.55E+07** | 3.98E+07 | 4.57E+07 | 4.68E+07 | 4.62E+07 | 4.86E+07 | 4.13E+07 | 4.60E+07 | 4.22E+07 | 3.76E+07 | 0.431E+08 | 4.27E+07 | 4.42E+07 | 4.21E+07 | 4.64E+07 |
| | (-42.21, -28.35) | (-31,-20) | **3.97E+07** | 3.57E+07 | 3.97E+07 | 4.02E+07 | 4.09E+07 | 4.28E+07 | 3.86E+07 | 3.96E+07 | 3.60E+07 | 3.17E+07 | 0.380E+08 | 3.77E+07 | 3.66E+07 | 3.58E+07 | 3.81E+07 |
| | (-38.43, -33.39) | (-28,-24) | **3.19E+07** | 2.95E+07 | 3.27E+07 | 3.13E+07 | 3.24E+07 | 3.53E+07 | 3.50E+07 | 3.17E+07 | 2.95E+07 | 2.44E+07 | 0.310E+08 | 3.11E+07 | 3.07E+07 | 2.88E+07 | 3.01E+07 |
| | (-35.91, -35.91) | (-26,-26) | **3.14E+07** | 2.88E+07 | 3.16E+07 | 3.22E+07 | 3.20E+07 | 3.48E+07 | 3.58E+07 | 3.13E+07 | 2.87E+07 | 2.38E+07 | 0.298E+08 | 3.05E+07 | 3.09E+07 | 2.93E+07 | 2.98E+07 |
| Neutron Pad | (-58.54, -22.47) | 21 degree | **5.63E+06** | 5.28E+06 | 5.89E+06 | 6.12E+06 | 6.02E+06 | 6.38E+06 | 6.53E+06 | 5.84E+06 | 4.98E+06 | 4.04E+06 | 0.556E+07 | 5.67E+06 | 5.78E+06 | 4.98E+06 | 4.94E+06 |
| | (-46.60, -41.95) | 42 degree | **3.99E+06** | 3.73E+06 | 3.99E+06 | 4.13E+06 | 4.24E+06 | 4.72E+06 | 5.44E+06 | 4.17E+06 | 3.70E+06 | 2.79E+06 | 0.389E+07 | 3.86E+06 | 4.11E+06 | 3.30E+06 | 3.05E+06 |

Comparison relative to KI MCU calculation

| Flux E>1.0 MeV | Position in cm | Grid Position | KI-MCU Russia | HYU-TORT Korea | HYU-MCNP Korea | HYU-MCNPX Korea | Transpire Inc.-ATTILA USA | KOPEC-DORT Korea | VTI/SUT-HELIOS Slovak | WTI-MCNP Germany | VTT-TORT Finland | VTT-MT Finland | KI-LUCKY Russia | KAERI-DANTSYS Korea | VTT-MCNP-K Finland | VTT-MCNP-F Finland | SCK-MCNPX Belgium |
|---|---|---|---|---|---|---|---|---|---|---|---|---|---|---|---|---|---|
| Inner Baffle | ( -4.41, -0.63) | (-1,+2) | **1.39E+09** | 0.98 | 0.99 | 0.99 | 1.07 | 1.06 | 0.65 | 1.01 | 1.08 | 0.99 | 1.02 | 0.96 | 0.87 | 0.94 | 1.00 |
| | ( -4.41, -4.41) | (-1,-1) | **1.66E+09** | 0.98 | 1.00 | 1.00 | 1.06 | 1.06 | 0.64 | 1.01 | 1.03 | 1.06 | 1.00 | 0.95 | 0.94 | 1.05 | 0.99 |
| Outer Baffle | (-39.69, -0.63) | (-29,+2) | **5.20E+08** | 0.84 | 1.02 | 1.00 | 1.00 | 1.04 | 0.66 | 1.01 | 0.91 | 0.90 | 0.91 | 0.98 | 0.93 | 0.84 | 0.99 |
| | (-39.69, -5.67) | (-29,-2) | **4.95E+08** | 0.84 | 1.02 | 1.04 | 1.01 | 1.04 | 0.66 | 1.01 | 0.89 | 0.91 | 0.90 | 0.98 | 0.97 | 0.90 | 1.00 |
| | (-39.69, -11.97) | (-29,-7) | **3.98E+08** | 0.86 | 1.02 | 1.02 | 1.02 | 1.05 | 0.67 | 1.03 | 0.89 | 0.93 | 0.92 | 1.00 | 0.99 | 0.92 | 1.01 |
| | (-39.69, -18.27) | (-29,-12) | **2.38E+08** | 0.88 | 1.03 | 1.03 | 1.03 | 1.08 | 0.71 | 1.04 | 0.86 | 0.93 | 0.93 | 1.00 | 1.03 | 0.93 | 1.01 |
| | (-37.17, -20.79) | (-27,-14) | **2.51E+08** | 0.91 | 1.04 | 1.01 | 1.02 | 1.07 | 0.70 | 1.02 | 0.90 | 0.93 | 0.90 | 0.99 | 0.99 | 0.92 | 1.00 |
| | (-30.87, -20.79) | (-22,-14) | **4.95E+08** | 0.93 | 1.02 | 1.00 | 1.03 | 1.05 | 0.64 | 1.01 | 1.01 | 0.97 | 0.91 | 0.98 | 0.98 | 0.92 | 1.00 |
| | (-24.57, -20.79) | (-17,-14) | **8.05E+08** | 0.98 | 1.01 | 1.01 | 1.05 | 1.08 | 0.63 | 1.01 | 0.96 | 1.05 | 0.97 | 0.97 | 0.96 | 1.01 | 0.98 |
| Barrel | (-49.77, -0.63) | (-37,+2) | **6.52E+07** | 0.85 | 1.02 | 1.01 | 1.01 | 1.06 | 0.80 | 1.01 | 0.86 | 0.74 | 0.94 | 1.03 | 0.88 | 0.85 | 0.98 |
| | (-49.77, -9.45) | (-37,-5) | **5.84E+07** | 0.84 | 1.00 | 1.01 | 1.00 | 1.06 | 0.84 | 1.00 | 0.83 | 0.75 | 0.93 | 1.01 | 0.97 | 0.92 | 0.97 |
| | (-47.25, -18.27) | (-35,-12) | **5.85E+07** | 0.85 | 0.99 | 1.00 | 1.01 | 1.05 | 0.81 | 0.99 | 0.85 | 0.79 | 0.91 | 0.98 | 0.98 | 0.90 | 1.01 |
| | (-45.99, -22.05) | (-34,-15) | **5.05E+07** | 0.89 | 1.01 | 1.00 | 1.03 | 1.06 | 0.82 | 1.00 | 0.92 | 0.81 | 0.94 | 0.96 | 0.95 | 0.92 | 1.02 |
| | (-44.73, -24.57) | (-33,-17) | **4.55E+07** | 0.87 | 1.01 | 1.03 | 1.02 | 1.07 | 0.91 | 1.01 | 0.93 | 0.83 | 0.95 | 0.94 | 0.97 | 0.93 | 1.02 |
| | (-42.21, -28.35) | (-31,-20) | **3.97E+07** | 0.90 | 1.00 | 1.01 | 1.03 | 1.08 | 0.97 | 1.00 | 0.91 | 0.80 | 0.96 | 0.95 | 0.92 | 0.90 | 0.96 |
| | (-38.43, -33.39) | (-28,-24) | **3.19E+07** | 0.92 | 1.02 | 0.98 | 1.02 | 1.10 | 1.09 | 0.99 | 0.92 | 0.77 | 0.97 | 0.97 | 0.96 | 0.90 | 0.94 |
| | (-35.91, -35.91) | (-26,-26) | **3.14E+07** | 0.92 | 1.01 | 1.03 | 1.02 | 1.11 | 1.14 | 1.00 | 0.92 | 0.76 | 0.95 | 0.97 | 0.98 | 0.94 | 0.95 |
| Neutron Pad | (-58.54, -22.47) | 21 degree | **5.63E+06** | 0.94 | 1.05 | 1.09 | 1.07 | 1.13 | 1.16 | 1.04 | 0.88 | 0.72 | 0.99 | 1.01 | 1.03 | 0.88 | 0.88 |
| | (-46.60, -41.95) | 42 degree | **3.99E+06** | 0.93 | 1.00 | 1.03 | 1.06 | 1.18 | 1.36 | 1.04 | 0.93 | 0.70 | 0.97 | 0.97 | 1.03 | 0.83 | 0.76 |
| Number of positions within +-5% = | | | | 3 | 19 | 18 | 14 | 2 | 1 | 19 | 3 | 2 | 8 | 18 | 14 | 2 | 15 |
| Number of positions within +-10% = | | | | 10 | 19 | 19 | 19 | 15 | 3 | 19 | 12 | 9 | 18 | 19 | 17 | 14 | 17 |
| Number of positions within +-20% = | | | | 19 | 19 | 19 | 19 | 19 | 8 | 19 | 19 | 11 | 19 | 19 | 19 | 19 | 18 |

# Table 4.17(b). Fast neutron fluxes E > 1.0 MeV: Comparison relative to KI MCU calculations in water zones

Calculated results

| Flux E>1.0 MeV | Position in cm | Grid Position | KI-MCU Russia | HYU-TORT Korea | HYU-MCNP Korea | HYU-MCNPX Korea | Transpire Inc.-ATTILA USA | KOPEC-DORT Korea | VTI/SUT-HELIOS Slovak | WTI-MCNP Germany | VTT-TORT Finland | VTT-MT Finland | KI-LUCKY Russia | KAERI-DANTSYS Korea | VTT-MCNP-K Finland | VTT-MCNP-F Finland | SCK-MCNPX Belgium |
|---|---|---|---|---|---|---|---|---|---|---|---|---|---|---|---|---|---|
| Central Hole | ( 0.0, 0.0) | (+2.5,+2.5) | **8.68E+08** | 8.73E+08 | 2.18E+08 | 2.23E+08 | 9.08E+08 | 9.49E+08 | 6.18E+08 | 8.87E+08 | 9.06E+08 | 8.03E+08 | 0.912E+09 | 8.44E+08 | 8.69E+08 | 9.48E+08 | 2.10E+08 |
| Water Gap | (-54.36, -9.59) | 10.75 degree | **1.83E+07** | 1.62E+07 | 1.83E+07 | 1.82E+07 | 1.88E+07 | 1.95E+07 | 1.61E+07 | 1.81E+07 | 1.65E+07 | 1.59E+07 | 0.174E+08 | 1.67E+07 | 1.81E+07 | 1.65E+07 | 1.81E+07 |
| | (-52.89, -15.80) | 16.63 degree | **1.83E+07** | 1.68E+07 | 1.82E+07 | 1.86E+07 | 1.89E+07 | 1.96E+07 | 1.65E+07 | 1.85E+07 | 1.68E+07 | 1.57E+07 | 0.173E+08 | 2.14E+07 | 1.84E+07 | 1.74E+07 | 1.88E+07 |
| | (-51.53, -19.78) | 21.14 degree | **1.79E+07** | 1.63E+07 | 1.79E+07 | 1.89E+07 | 1.85E+07 | 1.91E+07 | 1.56E+07 | 1.79E+07 | 1.65E+07 | 1.58E+07 | 0.167E+08 | 2.03E+07 | 1.86E+07 | 1.64E+07 | 1.76E+07 |
| | (-50.03, -23.33) | 25.62 degree | **1.68E+07** | 1.55E+07 | 1.72E+07 | 1.68E+07 | 1.76E+07 | 1.75E+07 | 1.47E+07 | 1.67E+07 | 1.53E+07 | 1.43E+07 | 0.157E+08 | 1.69E+07 | 1.60E+07 | 1.53E+07 | 1.61E+07 |
| | (-48.74, -25.91) | 28.78 degree | **1.56E+07** | 1.40E+07 | 1.50E+07 | 1.56E+07 | 1.61E+07 | 1.63E+07 | 1.50E+07 | 1.55E+07 | 1.45E+07 | 1.43E+07 | 0.147E+08 | 1.58E+07 | 1.54E+07 | 1.46E+07 | 1.64E+07 |
| | (-46.29, -30.06) | 33.89 degree | **1.36E+07** | 1.26E+07 | 1.41E+07 | 1.38E+07 | 1.44E+07 | 1.44E+07 | 1.39E+07 | 1.35E+07 | 1.25E+07 | 1.31E+07 | 0.127E+08 | 1.48E+07 | 1.33E+07 | 1.29E+07 | 1.34E+07 |
| | (-44.08, -33.22) | 37.44 degree | **1.22E+07** | 1.14E+07 | 1.22E+07 | 1.28E+07 | 1.24E+07 | 1.33E+07 | 1.31E+07 | 1.22E+07 | 1.16E+07 | 1.08E+07 | 0.119E+08 | 1.27E+07 | 1.12E+07 | 1.18E+07 | 1.21E+07 |
| | (-42.29, -35.48) | 40.99 degree | **1.16E+07** | 1.03E+07 | 1.17E+07 | 1.20E+07 | 1.20E+07 | 1.26E+07 | 1.31E+07 | 1.13E+07 | 1.09E+07 | 1.01E+07 | 0.112E+08 | 1.06E+07 | 1.16E+07 | 1.00E+07 | 1.06E+07 |
| | (-39.03, -39.03) | 45 degree | **1.11E+07** | 1.01E+07 | 1.07E+07 | 1.10E+07 | 1.14E+07 | 1.23E+07 | 1.30E+07 | 1.08E+07 | 1.06E+07 | 9.27E+06 | 0.107E+08 | 1.29E+07 | 1.00E+07 | 9.84E+06 | 9.74E+06 |
| Reflector | (-23.31, -23.31) | (-16,-16) | **5.35E+08** | 5.22E+08 | 5.41E+08 | 5.30E+08 | 5.76E+08 | 5.76E+08 | 3.56E+08 | 5.39E+08 | 5.51E+08 | 6.04E+08 | 0.521E+09 | 5.21E+08 | 5.14E+08 | 5.30E+08 | 5.37E+08 |
| | (-25.83, -25.83) | (-18,-18) | **2.64E+08** | 2.55E+08 | 2.67E+08 | 2.65E+08 | 2.77E+08 | 2.88E+08 | 1.87E+08 | 2.65E+08 | 2.63E+08 | 3.06E+08 | 0.261E+09 | 2.63E+08 | 2.60E+08 | 2.64E+08 | 2.64E+08 |
| | (-28.35, -28.35) | (-20,-20) | **1.38E+08** | 1.30E+08 | 1.39E+08 | 1.35E+08 | 1.43E+08 | 1.52E+08 | 1.09E+08 | 1.38E+08 | 1.36E+08 | 1.50E+08 | 0.136E+09 | 1.37E+08 | 1.32E+08 | 1.37E+08 | 1.36E+08 |
| | (-30.87, -30.87) | (-22,-22) | **7.33E+07** | 6.81E+07 | 7.41E+07 | 7.46E+07 | 7.66E+07 | 8.26E+07 | 6.55E+07 | 7.32E+07 | 6.65E+07 | 6.86E+07 | 0.737E+08 | 7.42E+07 | 6.90E+07 | 7.25E+07 | 7.92E+07 |
| | (-33.39, -33.39) | (-24,-24) | **4.37E+07** | 4.03E+07 | 4.45E+07 | 4.40E+07 | 4.55E+07 | 4.97E+07 | 4.44E+07 | 4.36E+07 | 3.96E+07 | 3.48E+07 | 0.436E+08 | 4.40E+07 | 4.37E+07 | 4.25E+07 | 4.21E+07 |

Comparison relative to KI MCU calculation

| Flux E>1.0 MeV | Position in cm | Grid Position | KI-MCU Russia | HYU-TORT Korea | HYU-MCNP Korea | HYU-MCNPX Korea | Transpire Inc.-ATTILA USA | KOPEC-DORT Korea | VTI/SUT-HELIOS Slovak | WTI-MCNP Germany | VTT-TORT Finland | VTT-MT Finland | KI-LUCKY Russia | KAERI-DANTSYS Korea | VTT-MCNP-K Finland | VTT-MCNP-F Finland | SCK-MCNPX Belgium |
|---|---|---|---|---|---|---|---|---|---|---|---|---|---|---|---|---|---|
| Central Hole | ( 0.0, 0.0) | (+2.5,+2.5) | **8.68E+08** | 1.01 | 0.25 | 0.26 | 1.05 | 1.09 | 0.71 | 1.02 | 1.04 | 0.92 | 1.05 | 0.97 | 1.00 | 1.09 | 0.24 |
| Water Gap | (-54.36, -9.59) | 10.75 degree | **1.83E+07** | 0.89 | 1.00 | 0.99 | 1.03 | 1.07 | 0.88 | 0.99 | 0.90 | 0.87 | 0.95 | 0.91 | 0.99 | 0.90 | 0.99 |
| | (-52.89, -15.80) | 16.63 degree | **1.83E+07** | 0.92 | 1.00 | 1.02 | 1.04 | 1.07 | 0.90 | 1.01 | 0.92 | 0.86 | 0.95 | 1.17 | 1.00 | 0.95 | 1.03 |
| | (-51.53, -19.78) | 21.14 degree | **1.79E+07** | 0.91 | 1.00 | 1.06 | 1.03 | 1.07 | 0.87 | 1.00 | 0.92 | 0.88 | 0.93 | 1.13 | 1.04 | 0.92 | 0.98 |
| | (-50.03, -23.33) | 25.62 degree | **1.68E+07** | 0.92 | 1.02 | 1.00 | 1.05 | 1.04 | 0.88 | 0.99 | 0.91 | 0.85 | 0.93 | 1.01 | 0.95 | 0.91 | 0.96 |
| | (-48.74, -25.91) | 28.78 degree | **1.56E+07** | 0.90 | 0.96 | 1.00 | 1.04 | 1.05 | 0.96 | 1.00 | 0.93 | 0.92 | 0.95 | 1.01 | 0.99 | 0.94 | 1.05 |
| | (-46.29, -30.06) | 33.89 degree | **1.36E+07** | 0.93 | 1.04 | 1.02 | 1.06 | 1.07 | 1.02 | 1.00 | 0.93 | 0.96 | 0.94 | 1.09 | 0.98 | 0.95 | 0.99 |
| | (-44.08, -33.22) | 37.44 degree | **1.22E+07** | 0.93 | 1.00 | 1.05 | 1.02 | 1.09 | 1.07 | 1.00 | 0.95 | 0.88 | 0.97 | 1.04 | 0.92 | 0.97 | 0.99 |
| | (-42.29, -35.48) | 40.99 degree | **1.16E+07** | 0.89 | 1.01 | 1.04 | 1.04 | 1.09 | 1.13 | 0.98 | 0.94 | 0.87 | 0.97 | 0.91 | 1.00 | 0.87 | 0.92 |
| | (-39.03, -39.03) | 45 degree | **1.11E+07** | 0.91 | 0.97 | 0.99 | 1.03 | 1.11 | 1.17 | 0.98 | 0.95 | 0.83 | 0.96 | 1.16 | 0.90 | 0.89 | 0.88 |
| Reflector | (-23.31, -23.31) | (-16,-16) | **5.35E+08** | 0.98 | 1.01 | 0.99 | 1.08 | 1.08 | 0.67 | 1.01 | 1.03 | 1.13 | 0.97 | 0.97 | 0.96 | 0.99 | 1.00 |
| | (-25.83, -25.83) | (-18,-18) | **2.64E+08** | 0.96 | 1.01 | 1.00 | 1.05 | 1.09 | 0.71 | 1.00 | 0.99 | 1.16 | 0.99 | 0.99 | 0.98 | 1.00 | 1.00 |
| | (-28.35, -28.35) | (-20,-20) | **1.38E+08** | 0.94 | 1.01 | 0.97 | 1.04 | 1.10 | 0.79 | 1.00 | 0.98 | 1.08 | 0.98 | 0.99 | 0.95 | 0.99 | 0.98 |
| | (-30.87, -30.87) | (-22,-22) | **7.33E+07** | 0.93 | 1.01 | 1.02 | 1.05 | 1.13 | 0.89 | 1.00 | 0.91 | 0.94 | 1.01 | 1.01 | 0.94 | 0.99 | 1.08 |
| | (-33.39, -33.39) | (-24,-24) | **4.37E+07** | 0.92 | 1.02 | 1.01 | 1.04 | 1.14 | 1.02 | 1.00 | 0.91 | 0.80 | 1.00 | 1.01 | 1.00 | 0.97 | 0.96 |
| | Number of positions within +-5% = | | | 3 | 14 | 13 | 13 | 1 | 3 | 15 | 6 | 1 | 9 | 9 | 12 | 8 | 10 |
| | Number of positions within +-10% = | | | 12 | 14 | 14 | 15 | 12 | 5 | 15 | 14 | 5 | 15 | 12 | 15 | 12 | 13 |
| | Number of positions within +-20% = | | | 15 | 14 | 14 | 15 | 15 | 11 | 15 | 15 | 14 | 15 | 15 | 15 | 15 | 14 |

## Table 4.18(a). DPA rates: Comparison relative to KI MCU calculations in stainless steel zones

Calculated results

| DPA | Position in cm | Grid Position | KI-MCU Russia | HYU-TORT Korea | HYU-MCNP Korea | HYU-MCNPX Korea | KOPEC-DORT Korea |
|---|---|---|---|---|---|---|---|
| Inner Baffle | ( -4.41, -0.63) | (-1,+2) | **2.04E-12** | 2.5938E-12 | 2.35E-12 | 2.33E-12 | 2.18E-12 |
| | ( -4.41, -4.41) | (-1,-1) | **2.42E-12** | 3.0637E-12 | 2.79E-12 | 2.79E-12 | 2.58E-12 |
| Outer Baffle | (-39.69, -0.63) | (-29,+2) | **7.58E-13** | 8.2254E-13 | 8.90E-13 | 8.80E-13 | 7.92E-13 |
| | (-39.69, -5.67) | (-29,-2) | **7.20E-13** | 7.8272E-13 | 8.61E-13 | 8.64E-13 | 7.54E-13 |
| | (-39.69, -11.97) | (-29,-7) | **5.83E-13** | 6.4328E-13 | 6.86E-13 | 6.88E-13 | 6.15E-13 |
| | (-39.69, -18.27) | (-29,-12) | **3.55E-13** | 3.9864E-13 | 4.10E-13 | 4.15E-13 | 3.80E-13 |
| | (-37.17, -20.79) | (-27,-14) | **3.69E-13** | 4.3727E-13 | 4.40E-13 | 4.31E-13 | 3.97E-13 |
| | (-30.87, -20.79) | (-22,-14) | **7.19E-13** | 8.7005E-13 | 8.50E-13 | 8.42E-13 | 7.68E-13 |
| | (-24.57, -20.79) | (-17,-14) | **1.18E-12** | 1.4919E-12 | 1.38E-12 | 1.39E-12 | 1.28E-12 |
| Barrel | (-49.77, -0.63) | (-37,+2) | **9.23E-14** | 1.0478E-13 | 1.13E-13 | 1.11E-13 | 1.01E-13 |
| | (-49.77, -9.45) | (-37,-5) | **8.27E-14** | 9.4396E-14 | 9.78E-14 | 9.89E-14 | 9.11E-14 |
| | (-47.25, -18.27) | (-35,-12) | **8.57E-14** | 9.6978E-14 | 9.85E-14 | 1.01E-13 | 9.22E-14 |
| | (-45.99, -22.05) | (-34,-15) | **7.59E-14** | 8.8474E-14 | 8.83E-14 | 8.59E-14 | 8.11E-14 |
| | (-44.73, -24.57) | (-33,-17) | **6.84E-14** | 7.8873E-14 | 7.89E-14 | 7.97E-14 | 7.38E-14 |
| | (-42.21, -28.35) | (-31,-20) | **5.78E-14** | 6.9447E-14 | 6.77E-14 | 6.87E-14 | 6.39E-14 |
| | (-38.43, -33.39) | (-28,-24) | **4.62E-14** | 5.6043E-14 | 5.39E-14 | 5.27E-14 | 5.16E-14 |
| | (-35.91, -35.91) | (-26,-26) | **4.52E-14** | 5.4505E-14 | 5.26E-14 | 5.37E-14 | 5.08E-14 |
| Neutron Pad | (-58.54, -22.47) | 21 degree | **8.12E-15** | 1.0484E-14 | 9.99E-15 | 1.01E-14 | 9.77E-15 |
| | (-46.60, -41.95) | 42 degree | **5.77E-15** | 7.4099E-15 | 6.74E-15 | 7.16E-15 | 7.20E-15 |

Comparison relative to KI MCU calculation

| DPA | Position in cm | Grid Position | KI-MCU Russia | HYU-TORT Korea | HYU-MCNP Korea | HYU-MCNPX Korea | KOPEC-DORT Korea |
|---|---|---|---|---|---|---|---|
| Inner Baffle | ( -4.41, -0.63) | (-1,+2) | **2.04E-12** | 1.27 | 1.15 | 1.14 | 1.07 |
| | ( -4.41, -4.41) | (-1,-1) | **2.42E-12** | 1.27 | 1.15 | 1.15 | 1.07 |
| Outer Baffle | (-39.69, -0.63) | (-29,+2) | **7.58E-13** | 1.08 | 1.17 | 1.16 | 1.04 |
| | (-39.69, -5.67) | (-29,-2) | **7.20E-13** | 1.09 | 1.20 | 1.20 | 1.05 |
| | (-39.69, -11.97) | (-29,-7) | **5.83E-13** | 1.10 | 1.18 | 1.18 | 1.05 |
| | (-39.69, -18.27) | (-29,-12) | **3.55E-13** | 1.12 | 1.15 | 1.17 | 1.07 |
| | (-37.17, -20.79) | (-27,-14) | **3.69E-13** | 1.19 | 1.19 | 1.17 | 1.08 |
| | (-30.87, -20.79) | (-22,-14) | **7.19E-13** | 1.21 | 1.18 | 1.17 | 1.07 |
| | (-24.57, -20.79) | (-17,-14) | **1.18E-12** | 1.26 | 1.17 | 1.18 | 1.09 |
| Barrel | (-49.77, -0.63) | (-37,+2) | **9.23E-14** | 1.13 | 1.22 | 1.20 | 1.10 |
| | (-49.77, -9.45) | (-37,-5) | **8.27E-14** | 1.14 | 1.18 | 1.20 | 1.10 |
| | (-47.25, -18.27) | (-35,-12) | **8.57E-14** | 1.13 | 1.15 | 1.17 | 1.08 |
| | (-45.99, -22.05) | (-34,-15) | **7.59E-14** | 1.17 | 1.16 | 1.13 | 1.07 |
| | (-44.73, -24.57) | (-33,-17) | **6.84E-14** | 1.15 | 1.15 | 1.17 | 1.08 |
| | (-42.21, -28.35) | (-31,-20) | **5.78E-14** | 1.20 | 1.17 | 1.19 | 1.11 |
| | (-38.43, -33.39) | (-28,-24) | **4.62E-14** | 1.21 | 1.17 | 1.14 | 1.12 |
| | (-35.91, -35.91) | (-26,-26) | **4.52E-14** | 1.21 | 1.16 | 1.19 | 1.12 |
| Neutron Pad | (-58.54, -22.47) | 21 degree | **8.12E-15** | 1.29 | 1.23 | 1.25 | 1.20 |
| | (-46.60, -41.95) | 42 degree | **5.77E-15** | 1.28 | 1.17 | 1.24 | 1.25 |
| Number of positions within +-5% = | | | | 0 | 0 | 0 | 2 |
| Number of positions within +-10% = | | | | 2 | 0 | 0 | 13 |
| Number of positions within +-20% = | | | | 10 | 17 | 15 | 17 |
| Number of positions within +-30% = | | | | 19 | 19 | 19 | 19 |

## Table 4.18(b). DPA rates: Comparison relative to KI MCU calculations in water zones

Calculated results

| DPA | Position in cm | Grid Position | KI-MCU Russia | HYU-TORT Korea | HYU-MCNP Korea | HYU-MCNPX Korea | KOPEC-DORT Korea |
|---|---|---|---|---|---|---|---|
| Central Hole | ( 0.0, 0.0) | (+2.5,+2.5) | **3.31E-13** | 1.67E-12 | 4.13E-13 | 4.18E-13 | 1.45E-12 |
| Water Gap | (-54.36, -9.59) | 10.75 degree | **2.79E-14** | 3.15E-14 | 3.44E-14 | 3.47E-14 | 3.04E-14 |
| | (-52.89, -15.80) | 16.63 degree | **2.82E-14** | 3.29E-14 | 3.42E-14 | 3.48E-14 | 3.07E-14 |
| | (-51.53, -19.78) | 21.14 degree | **2.77E-14** | 3.22E-14 | 3.41E-14 | 3.51E-14 | 3.02E-14 |
| | (-50.03, -23.33) | 25.62 degree | **2.61E-14** | 3.08E-14 | 3.23E-14 | 3.21E-14 | 2.79E-14 |
| | (-48.74, -25.91) | 28.78 degree | **2.44E-14** | 2.78E-14 | 2.91E-14 | 2.97E-14 | 2.60E-14 |
| | (-46.29, -30.06) | 33.89 degree | **2.10E-14** | 2.50E-14 | 2.63E-14 | 2.63E-14 | 2.27E-14 |
| | (-44.08, -33.22) | 37.44 degree | **1.90E-14** | 2.23E-14 | 2.24E-14 | 2.43E-14 | 2.08E-14 |
| | (-42.29, -35.48) | 40.99 degree | **1.75E-14** | 2.00E-14 | 2.18E-14 | 2.21E-14 | 1.95E-14 |
| | (-39.03, -39.03) | 45 degree | **1.69E-14** | 1.94E-14 | 1.98E-14 | 2.02E-14 | 1.90E-14 |
| Reflector | (-23.31, -23.31) | (-16,-16) | **8.06E-13** | 1.00E-12 | 9.85E-13 | 9.72E-13 | 8.77E-13 |
| | (-25.83, -25.83) | (-18,-18) | **4.06E-13** | 4.83E-13 | 5.08E-13 | 5.07E-13 | 4.49E-13 |
| | (-28.35, -28.35) | (-20,-20) | **2.11E-13** | 2.44E-13 | 2.66E-13 | 2.61E-13 | 2.38E-13 |
| | (-30.87, -30.87) | (-22,-22) | **1.13E-13** | 1.26E-13 | 1.43E-13 | 1.43E-13 | 1.30E-13 |
| | (-33.39, -33.39) | (-24,-24) | **6.51E-14** | 7.47E-14 | 8.27E-14 | 8.10E-14 | 7.52E-14 |

Comparison relative to KI MCU calculation

| DPA | Position in cm | Grid Position | KI-MCU Russia | HYU-TORT Korea | HYU-MCNP Korea | HYU-MCNPX Korea | KOPEC-DORT Korea |
|---|---|---|---|---|---|---|---|
| Central Hole | ( 0.0, 0.0) | (+2.5,+2.5) | **3.31E-13** | 5.05 | 1.25 | 1.26 | 4.38 |
| Water Gap | (-54.36, -9.59) | 10.75 degree | **2.79E-14** | 1.13 | 1.23 | 1.24 | 1.09 |
| | (-52.89, -15.80) | 16.63 degree | **2.82E-14** | 1.17 | 1.21 | 1.24 | 1.09 |
| | (-51.53, -19.78) | 21.14 degree | **2.77E-14** | 1.16 | 1.23 | 1.27 | 1.09 |
| | (-50.03, -23.33) | 25.62 degree | **2.61E-14** | 1.18 | 1.24 | 1.23 | 1.07 |
| | (-48.74, -25.91) | 28.78 degree | **2.44E-14** | 1.14 | 1.20 | 1.22 | 1.07 |
| | (-46.29, -30.06) | 33.89 degree | **2.10E-14** | 1.19 | 1.25 | 1.25 | 1.08 |
| | (-44.08, -33.22) | 37.44 degree | **1.90E-14** | 1.17 | 1.18 | 1.28 | 1.10 |
| | (-42.29, -35.48) | 40.99 degree | **1.75E-14** | 1.14 | 1.25 | 1.26 | 1.12 |
| | (-39.03, -39.03) | 45 degree | **1.69E-14** | 1.15 | 1.17 | 1.20 | 1.13 |
| Reflector | (-23.31, -23.31) | (-16,-16) | **8.06E-13** | 1.24 | 1.22 | 1.21 | 1.09 |
| | (-25.83, -25.83) | (-18,-18) | **4.06E-13** | 1.19 | 1.25 | 1.25 | 1.10 |
| | (-28.35, -28.35) | (-20,-20) | **2.11E-13** | 1.15 | 1.26 | 1.24 | 1.13 |
| | (-30.87, -30.87) | (-22,-22) | **1.13E-13** | 1.11 | 1.26 | 1.26 | 1.14 |
| | (-33.39, -33.39) | (-24,-24) | **6.51E-14** | 1.15 | 1.27 | 1.24 | 1.16 |
| Number of positions within +-5% = | | | | 0 | 0 | 0 | 0 |
| Number of positions within +-10% = | | | | 0 | 0 | 0 | 8 |
| Number of positions within +-20% = | | | | 13 | 3 | 1 | 14 |
| Number of positions within +-30% = | | | | 14 | 15 | 15 | 14 |

# FIGURES

**Figure 2.1. VENUS-2 core geometry**

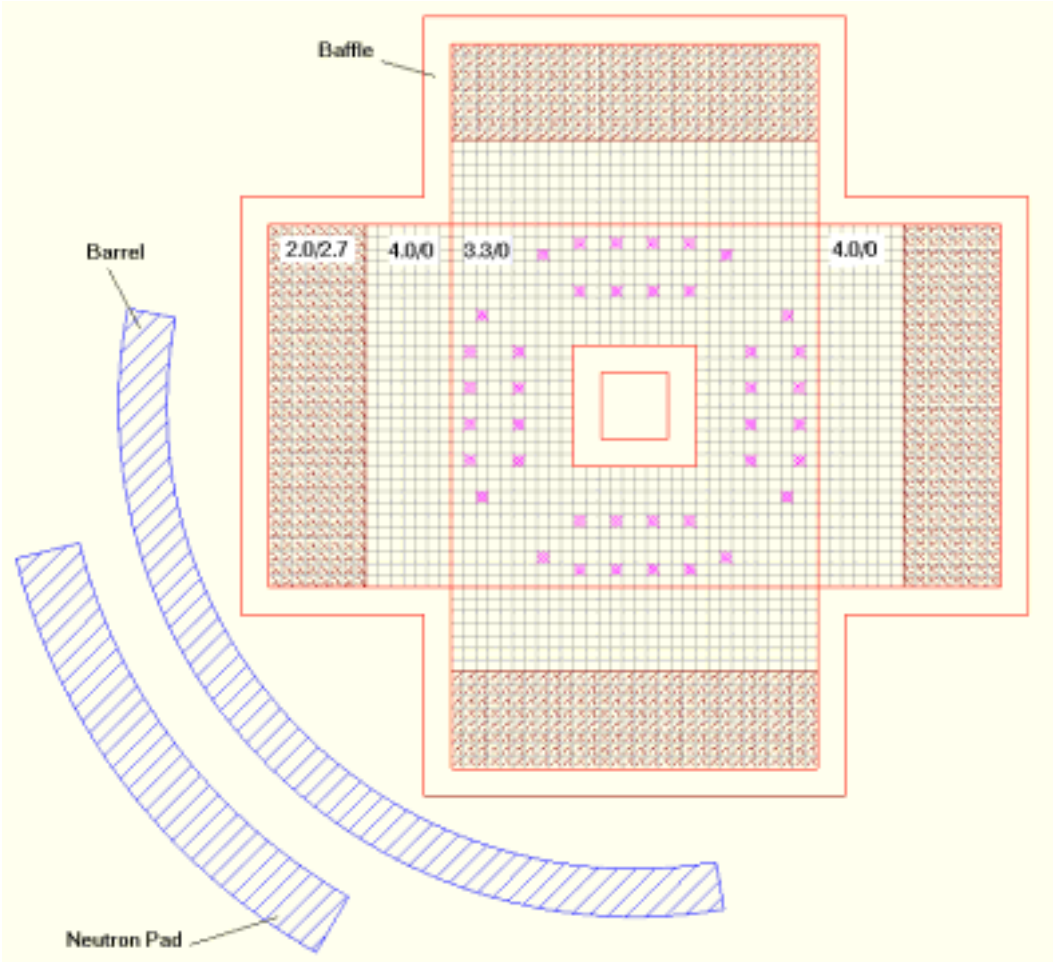

**Figure 2.2. Measurement positions in VENUS-2**

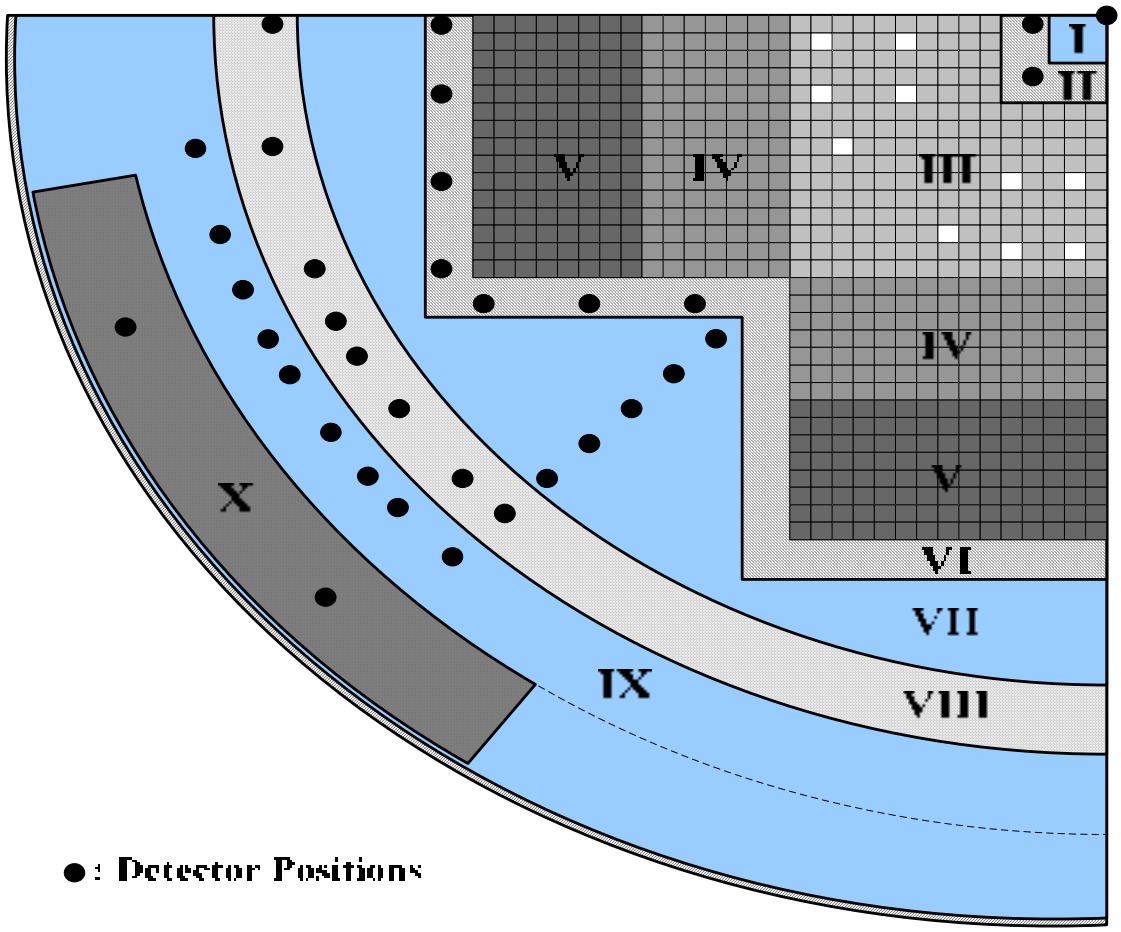


| | | | |
|---|---|---|---|
| I | Central Hole | VI | Outer Baffle |
| II | Inner Baffle | VII | Reflector |
| III | 3.3/0 Fuel Region (White Color: Pyrex) | VIII | Barrel |
| | | IX | Water Gap |
| IV | 4.0/0 Fuel Region | X | Neutron Pad |
| V | 2.0/2.7 Fuel Region | | |

**Figure 2.3. Horizontal reactor description**

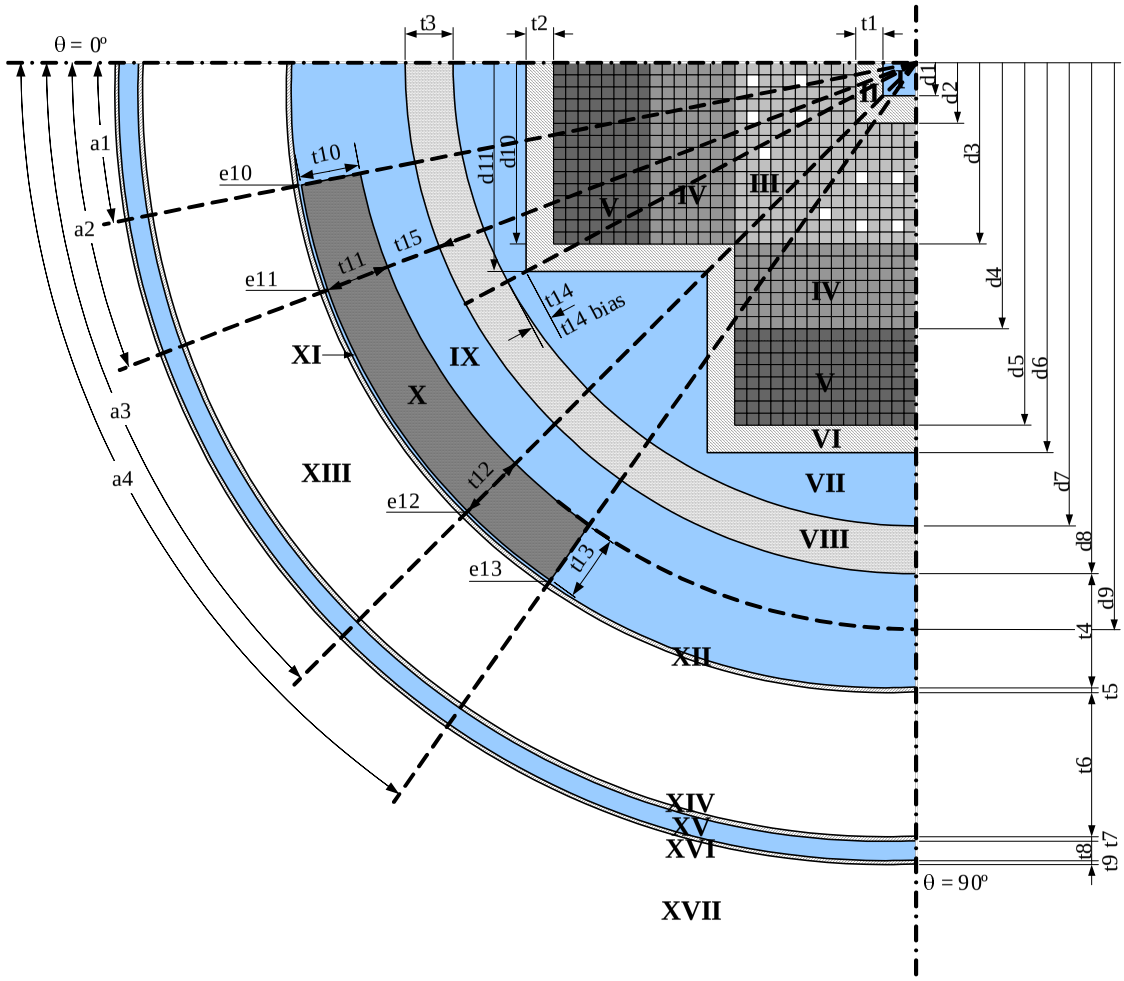


| | | | |
|---|---|---|---|
| **I** | **Central Hole** | **IX** | **Water Gap** |
| **II** | **Inner Baffle** | **X** | **Neutron Pad** |
| **III** | **3.3/0 Fuel Region (White Color: Pyrex)** | **XI** | **Space between Neutron Pad and Jacket** |
| | | **XII** | **Jacket Inner Wall** |
| **IV** | **4.0/0 Fuel Region** | **XIII** | **Jacket Volume** |
| **V** | **2.0/2.7 Fuel Region** | **XIV** | **Jacket Outer Wall** |
| **VI** | **Outer Baffle** | **XV** | **Space between Jacket and Reactor Vessel** |
| **VII** | **Reflector** | **XVI** | **Reactor Vessel Wall** |
| **VIII** | **Barrel** | **XVII** | **Reactor Room** |

**Figure 2.4. Vertical reactor description**

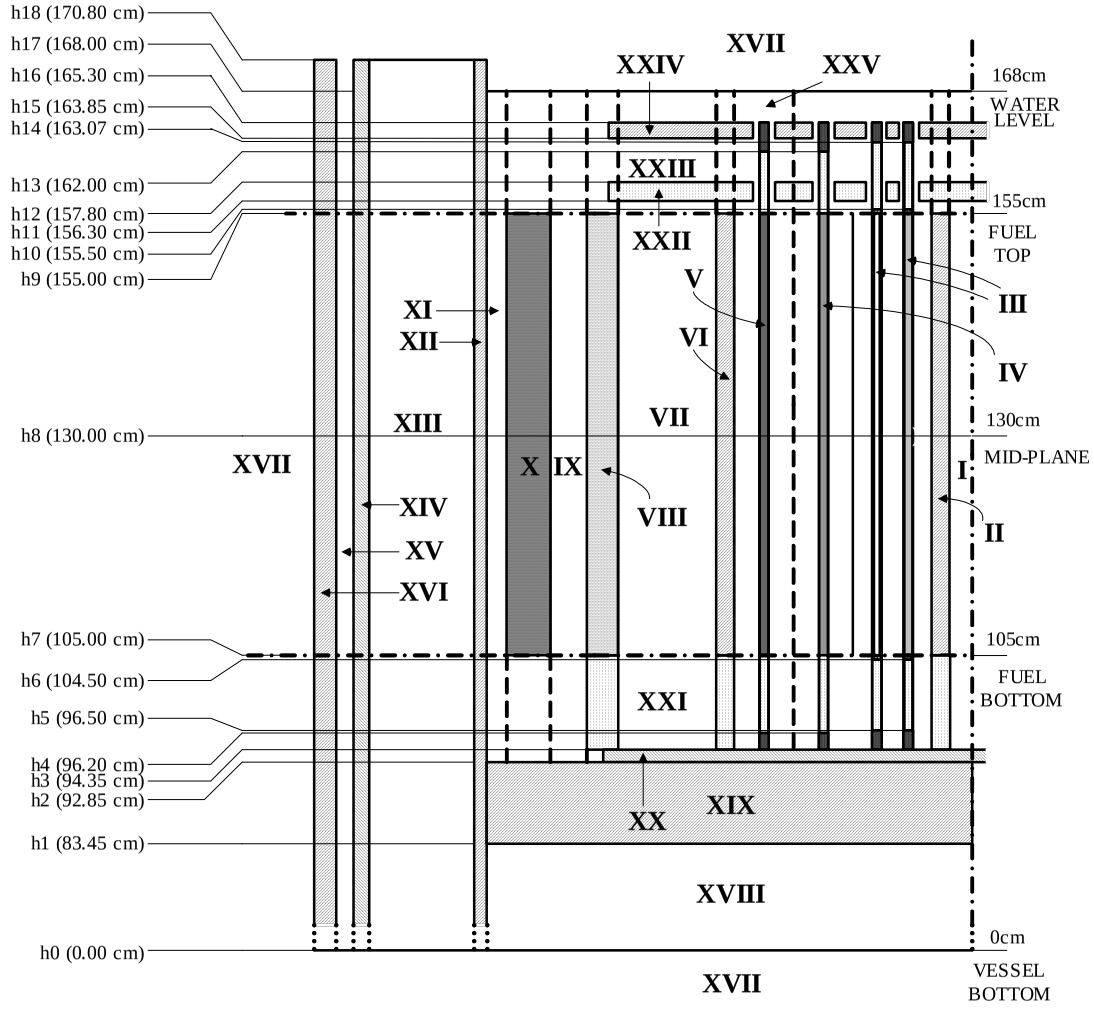


**I** Central Hole
**II** Inner Baffle
**III** 3.3/0 Fuel Region
**IV** 4.0/0 Fuel Region
**V** 2.0/2.7 Fuel Region
**VI** Outer Baffle
**VII** Reflector
**VIII** Barrel
**IX** Water Gap
**X** Neutron Pad
**XI** Space between Neutron Pad and Jacket
**XII** Jacket Inner Wall
**XIII** Jacket Volume
**XIV** Jacket Outer Wall
**XV** Space between Jacket and Reactor Vessel
**XVI** Reactor Vessel Wall
**XVII** Reactor Room
**XVIII** Lower Filling
**XIX** Reactor Support
**XX** Bottom Grid
**XXI** Lower Reflector
**XXII** Intermediate Grid
**XXIII** Upper Reflector
**XXIV** Upper Reactor Grid
**XXV** Upper Filling

**Figure 4.1. C/E comparison of equivalent fission fluxes at $^{58}$Ni(n,p) detector positions in stainless steel zones**

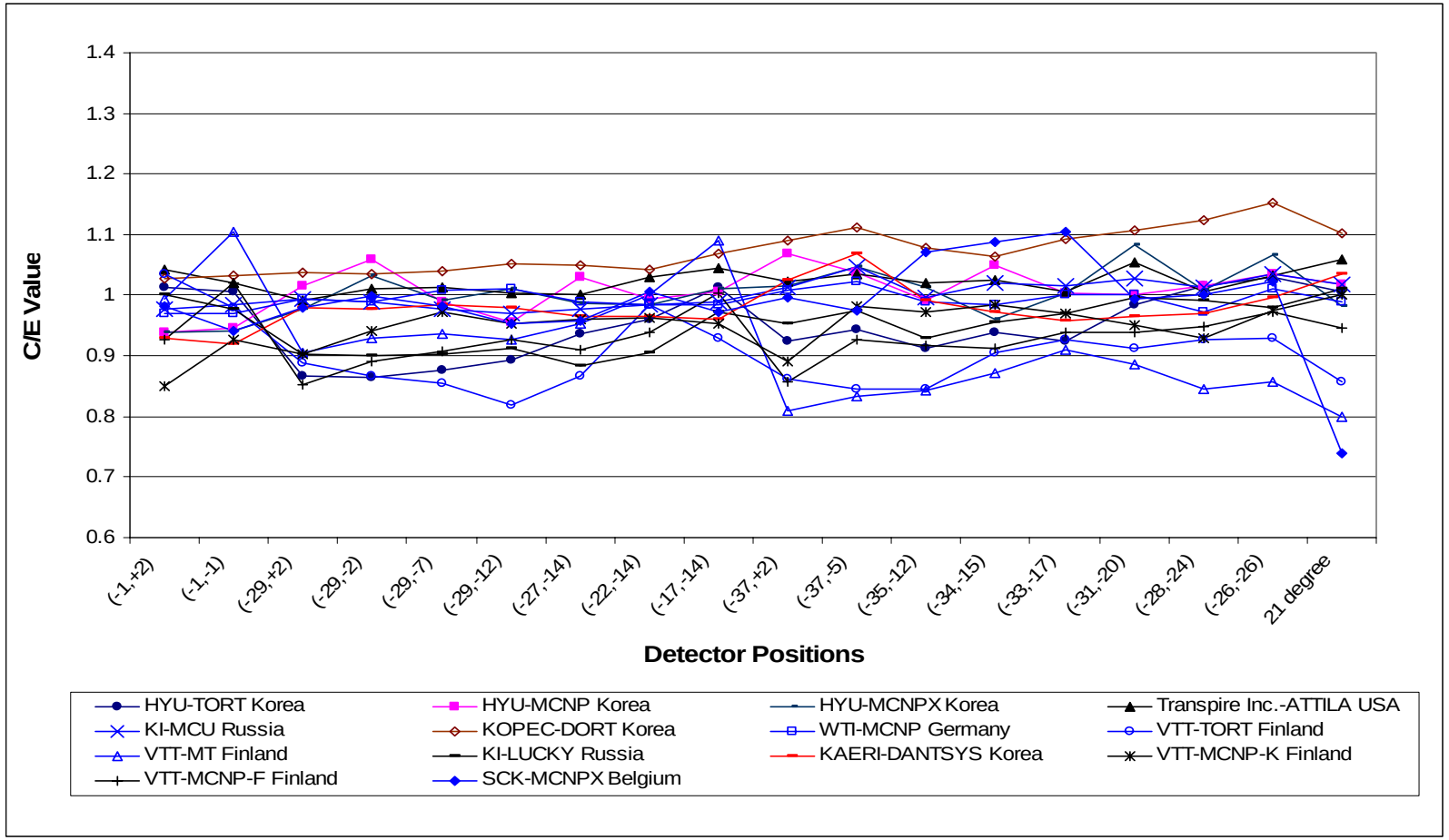

**Figure 4.1(a). C/E comparison of equivalent fission fluxes at $^{58}$Ni(n,p) detector positions in stainless steel zones: Deterministic calculation results**

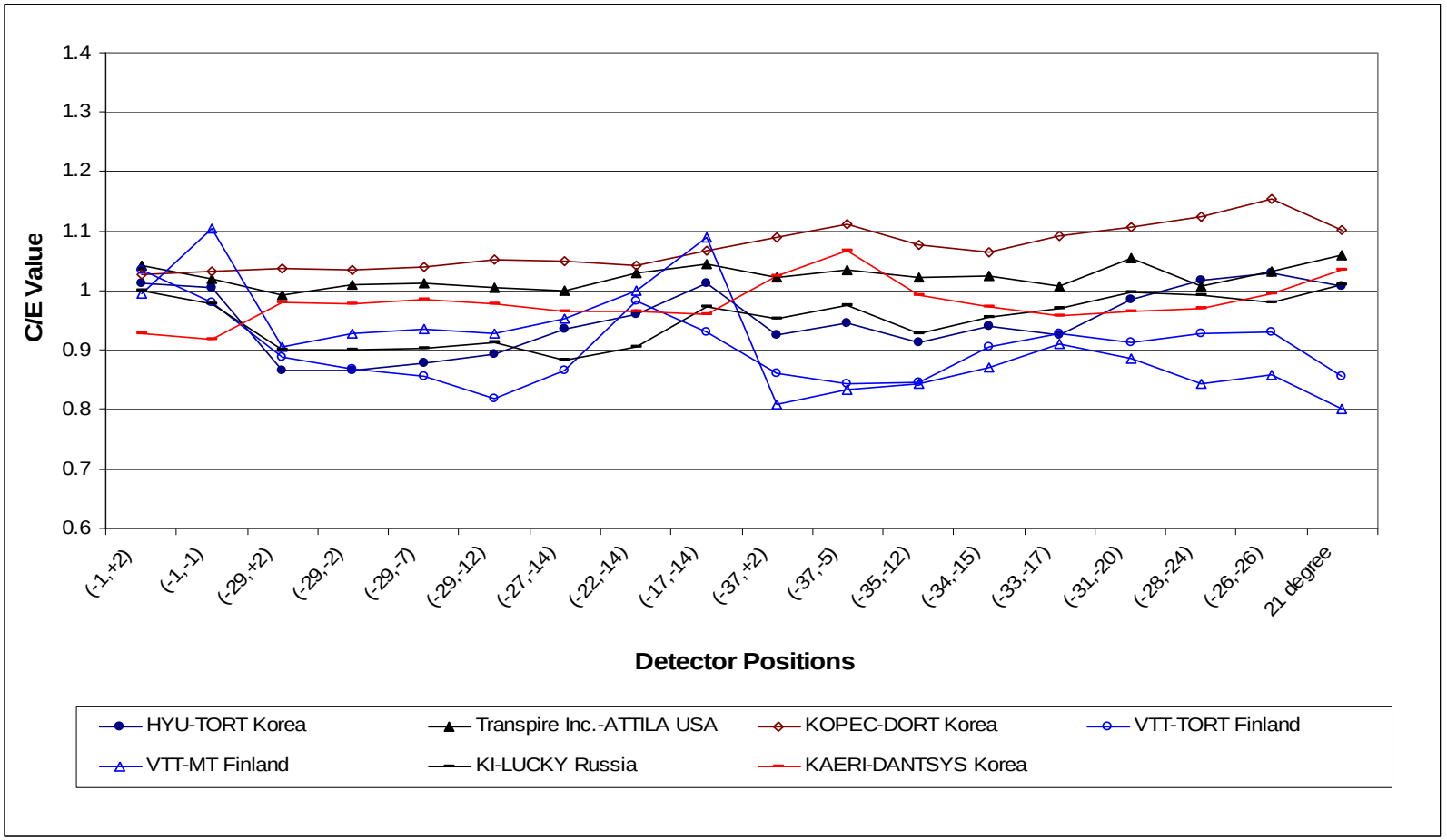

**Figure 4.1(b). C/E comparison of equivalent fission fluxes at $^{58}$Ni(n,p) detector positions in stainless steel zones: Monte Carlo calculation results**

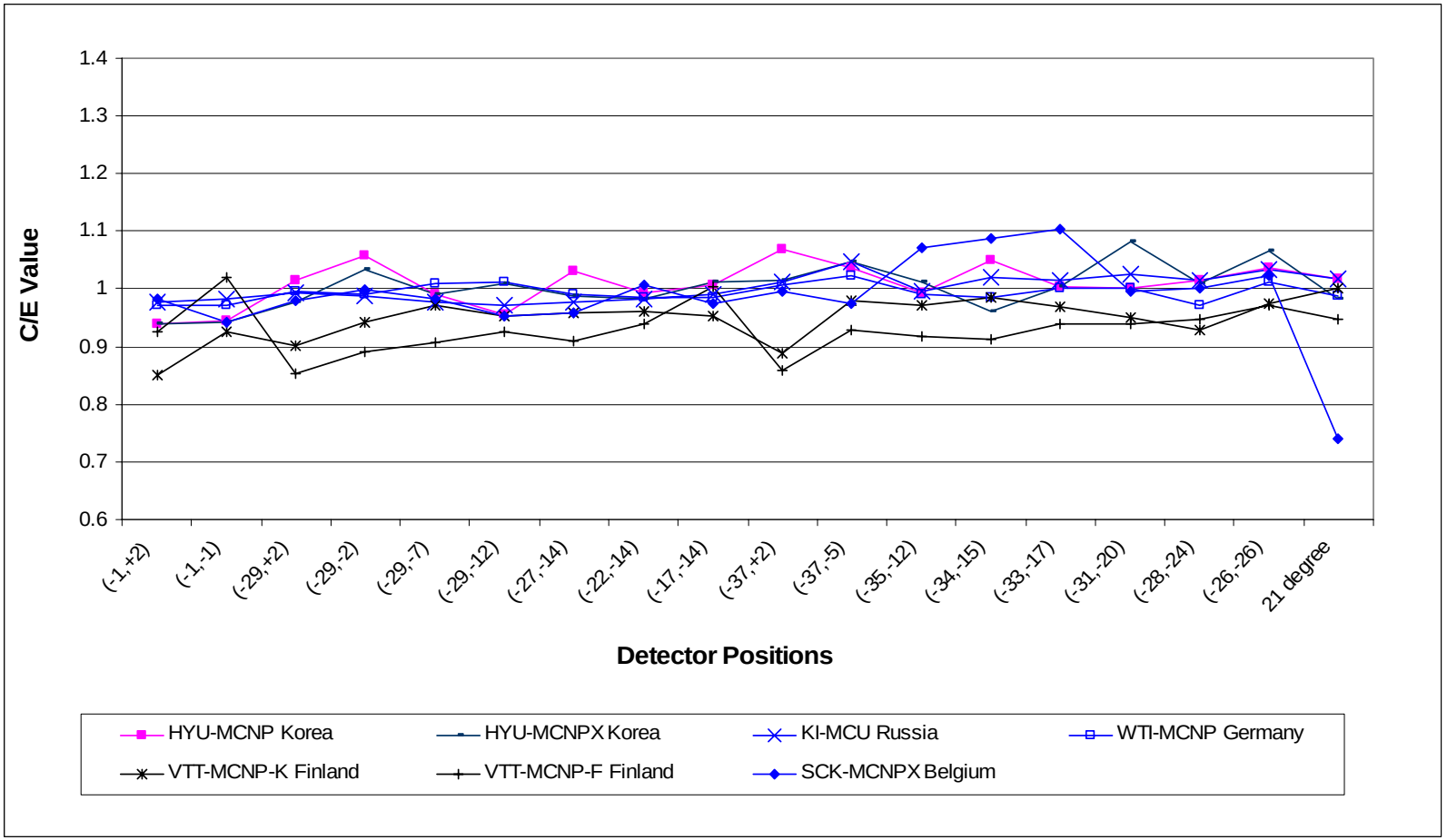

**Figure 4.2. C/E comparison of equivalent fission fluxes at $^{58}$Ni(n,p) detector positions in water zones**

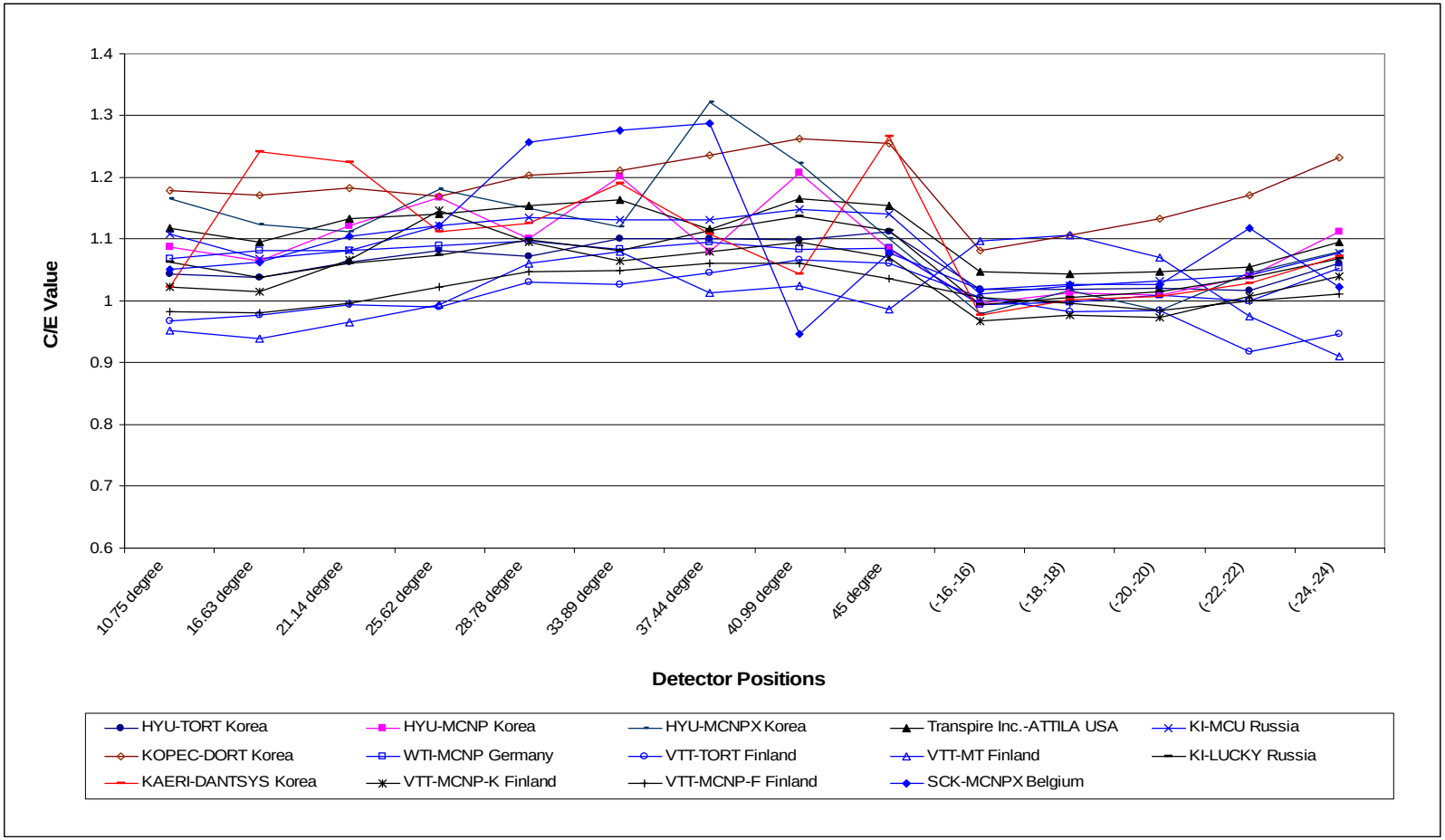

**Figure 4.2(a). C/E comparison of equivalent fission fluxes at $^{58}$Ni(n,p) detector positions in water zones: Deterministic calculation results**

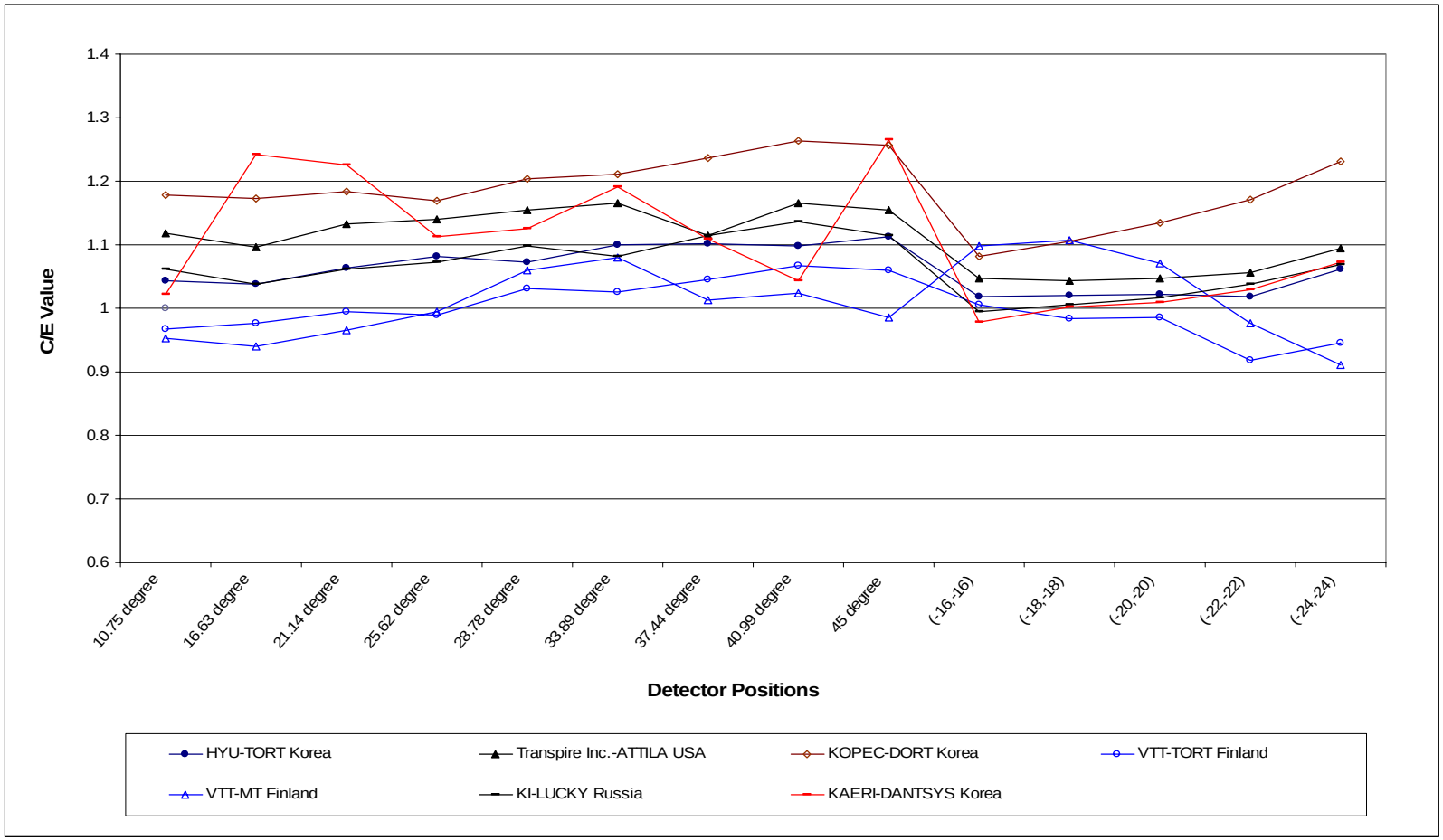

**Figure 4.2(b). C/E comparison of equivalent fission fluxes at $^{58}$Ni(n,p) detector positions in water zones: Monte Carlo calculation results**

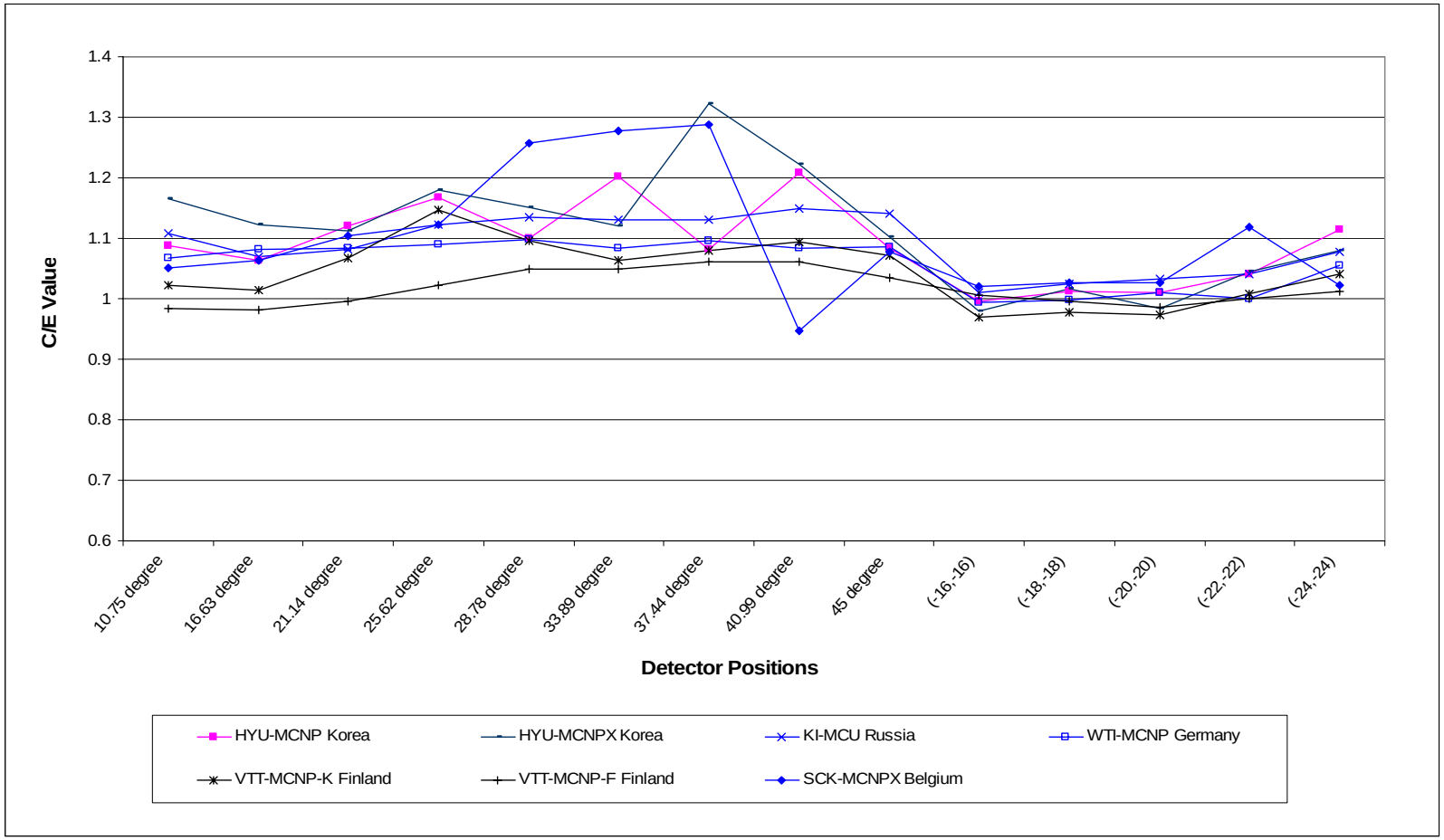

**Figure 4.3. C/E comparison of equivalent fission fluxes at $^{115}$In(n,n′) detector positions in stainless steel zones**

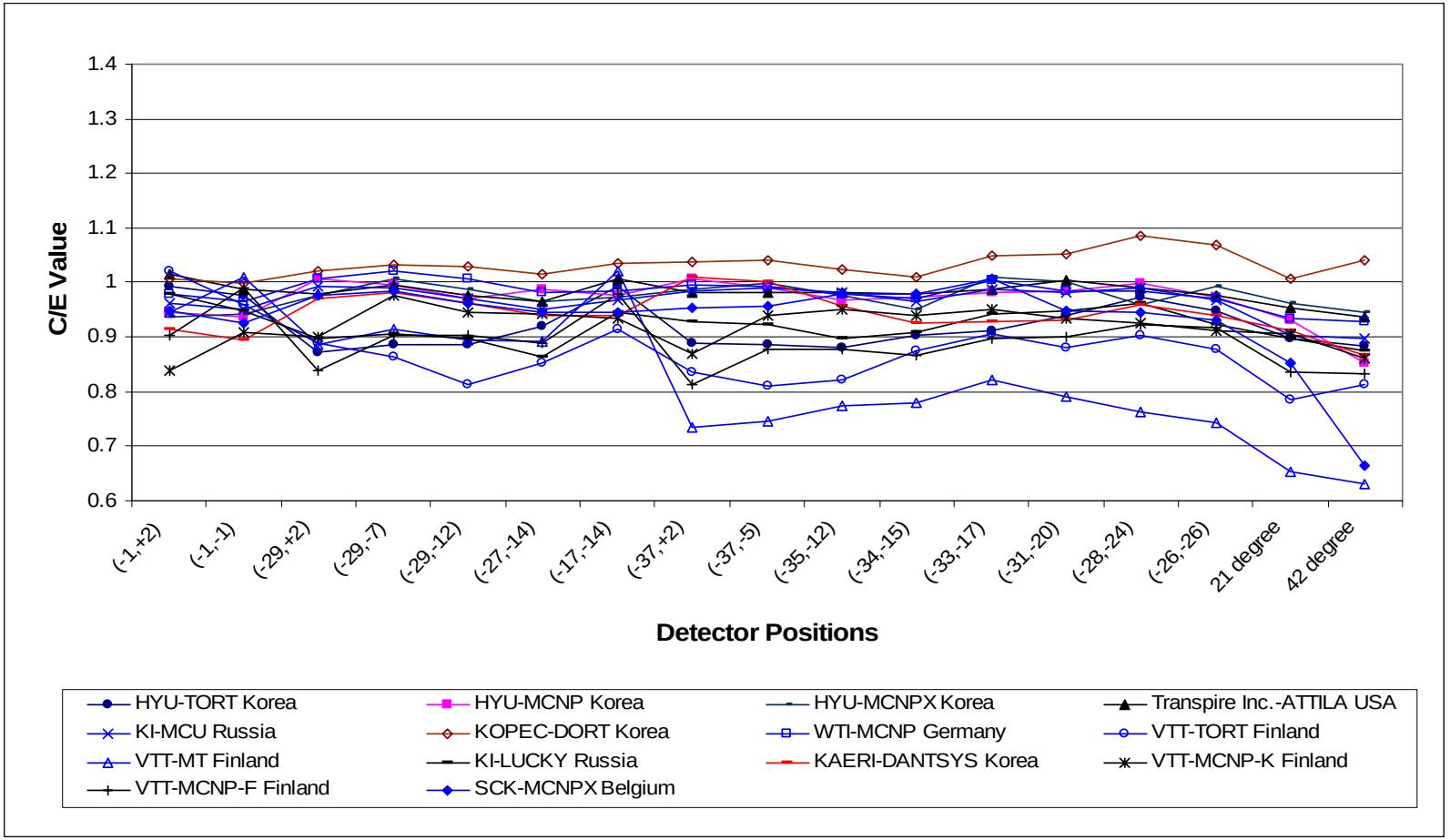

**Figure 4.3(a). C/E comparison of equivalent fission fluxes at $^{115}$In(n,n′) detector positions in stainless steel zones: Deterministic calculation results**

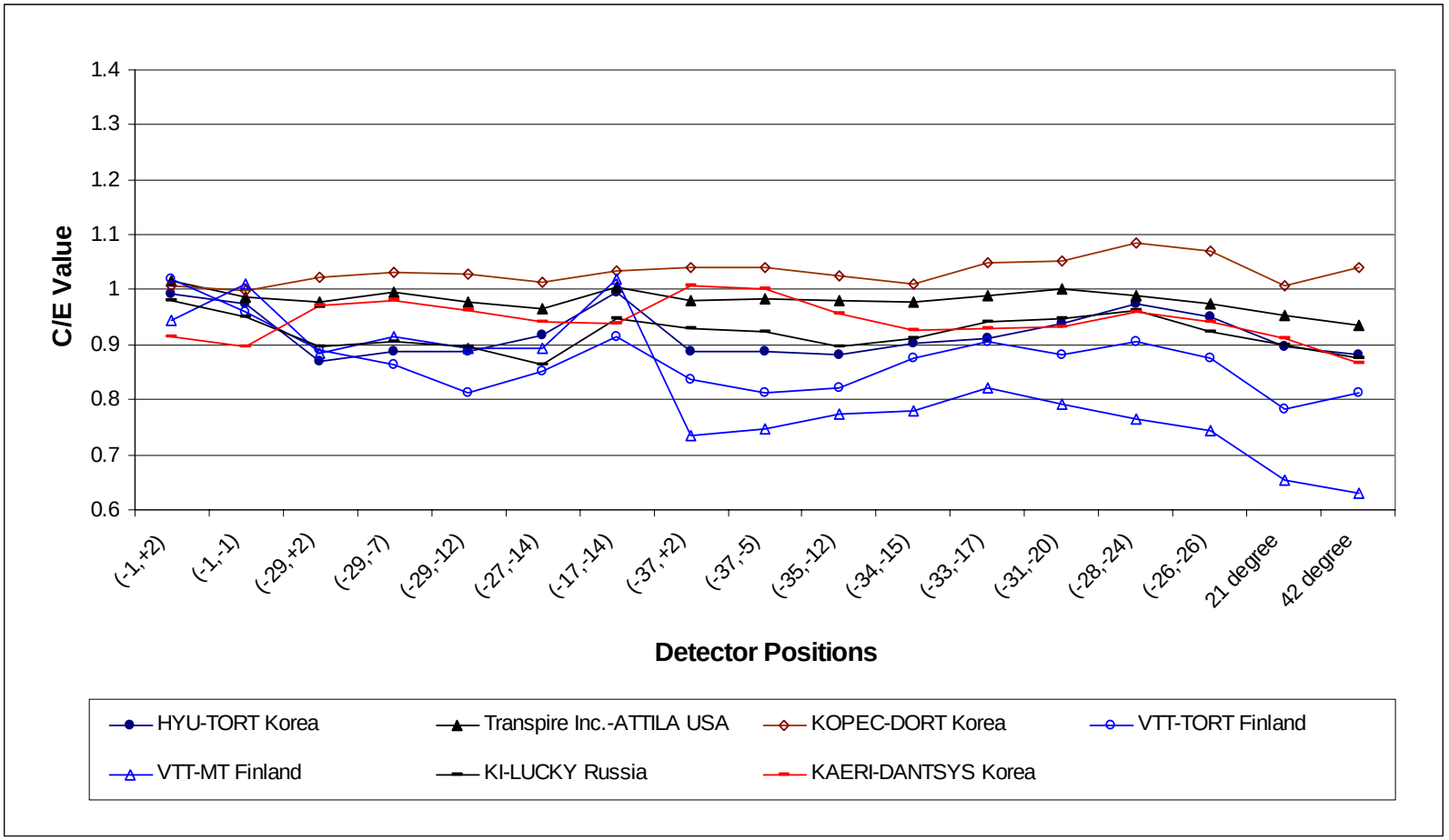

**Figure 4.3(b). C/E comparison of equivalent fission fluxes at $^{115}In(n,n')$ detector positions in stainless steel zones: Monte Carlo calculation results**

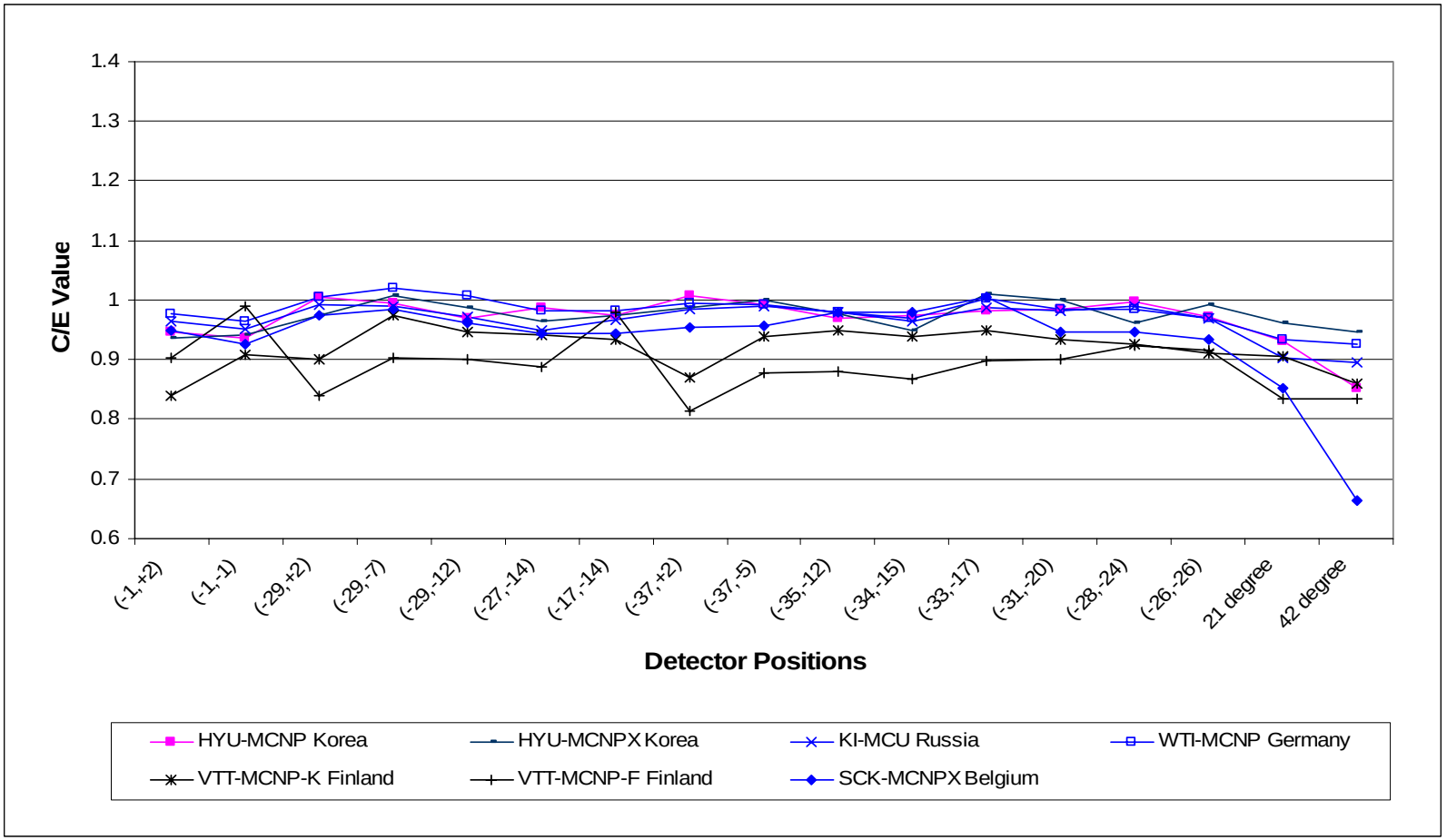

**Figure 4.4. C/E comparison of equivalent fission fluxes at $^{115}$In(n,n′) detector positions in water zones**

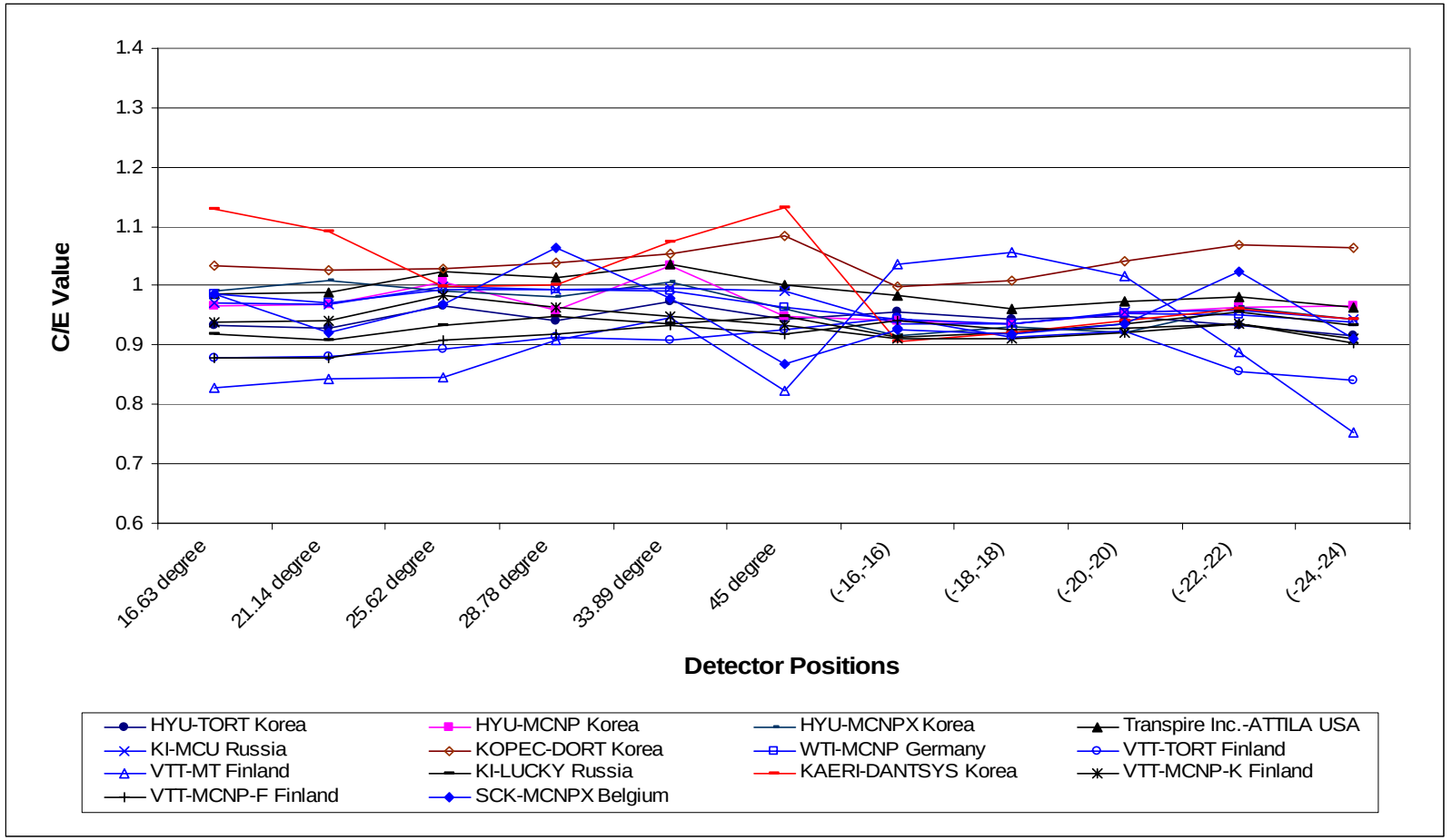

**Figure 4.4(a). C/E comparison of equivalent fission fluxes at $^{115}In(n,n')$ detector positions in water zones: Deterministic calculation results**

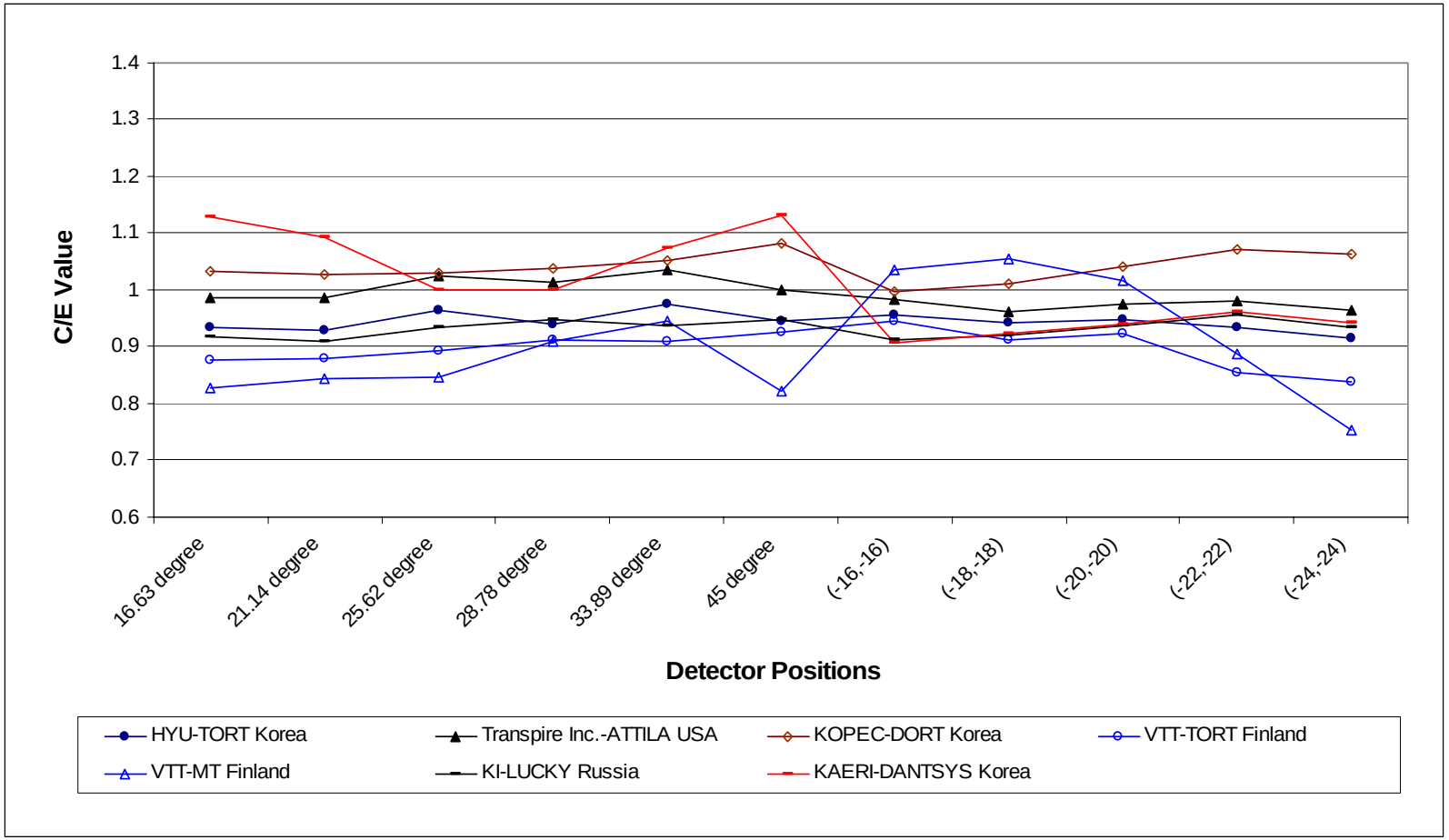

**Figure 4.4(b). C/E comparison of equivalent fission fluxes at $^{115}In(n,n')$ detector positions in water zones: Monte Carlo calculation results**

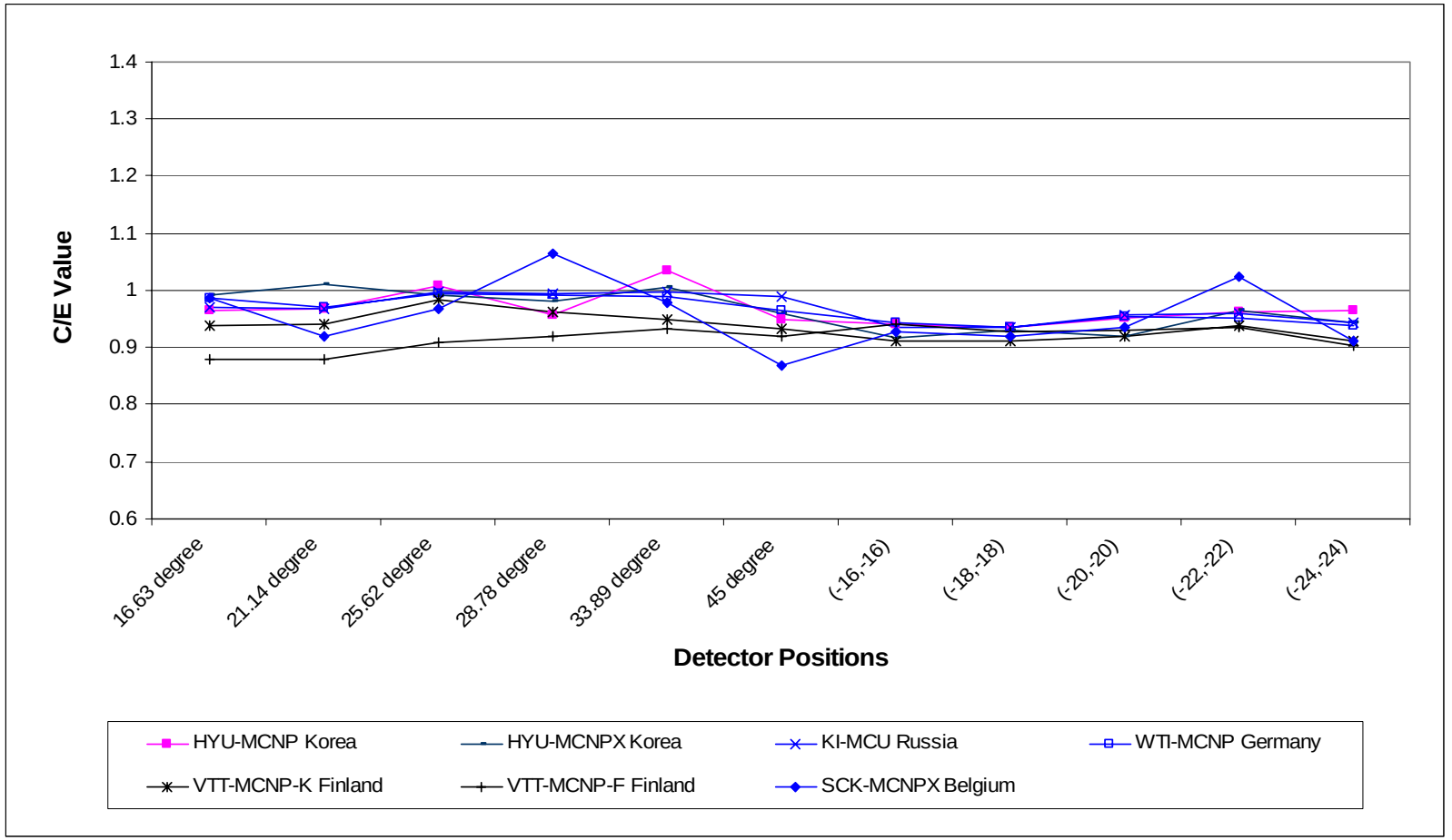

**Figure 4.5. C/E comparison of equivalent fission fluxes at $^{103}$Rh(n,n′) detector positions in stainless steel zones**

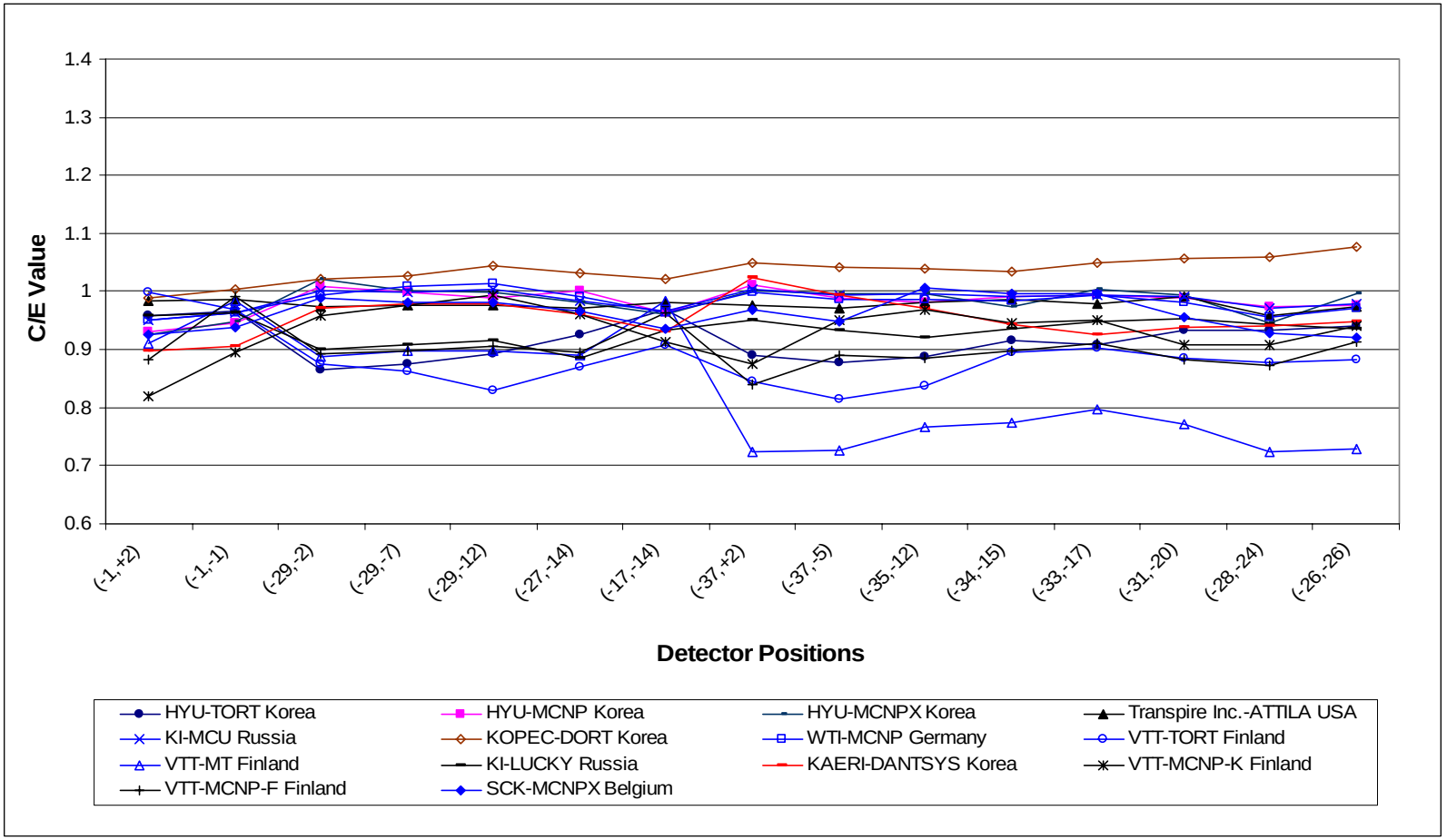

**Figure 4.5(a). C/E comparison of equivalent fission fluxes at $^{103}$Rh(n,n′) detector positions in stainless steel zones: Deterministic calculation results**

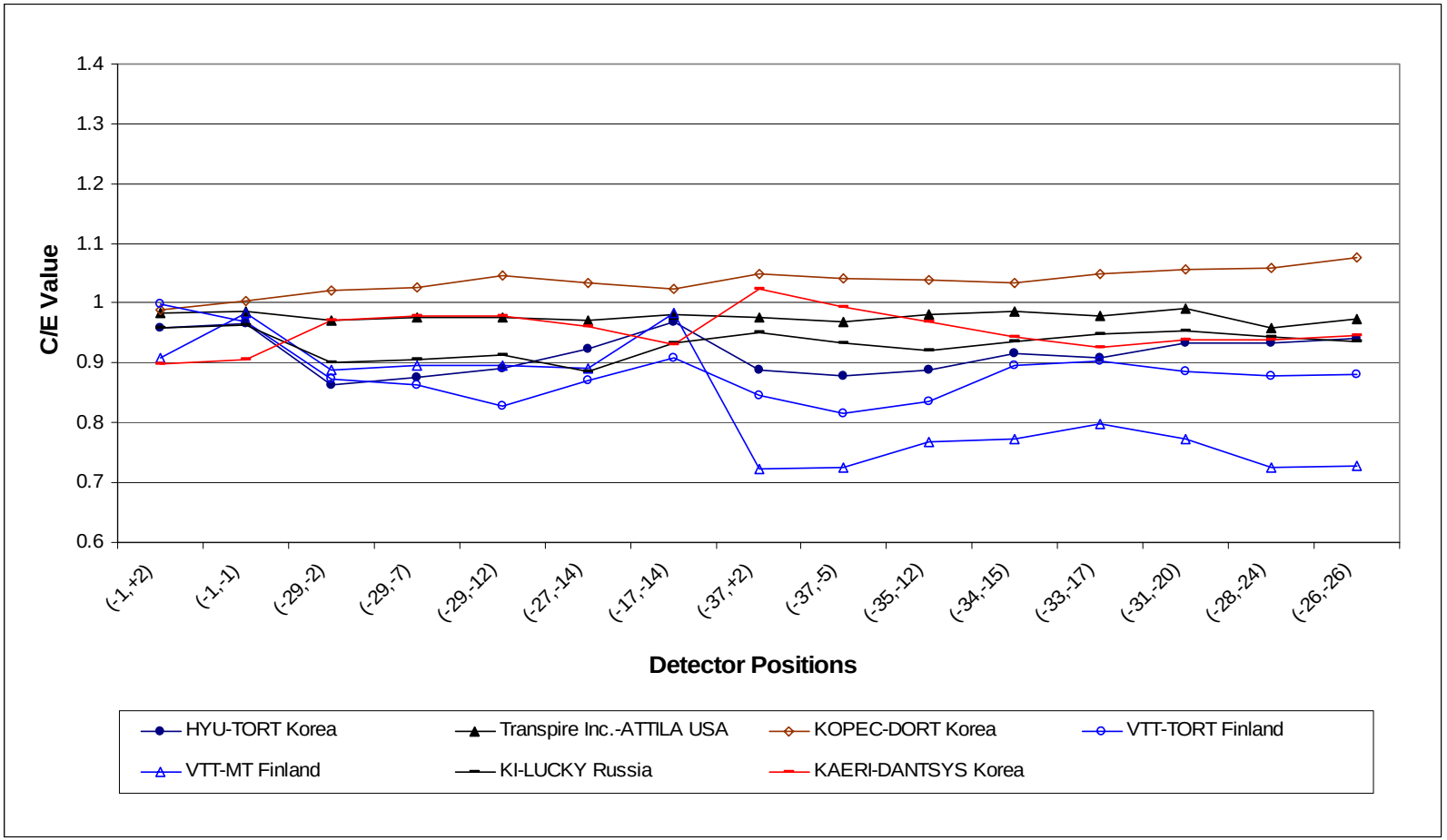

**Figure 4.5(b). C/E comparison of equivalent fission fluxes at $^{103}$Rh(n,n′) detector positions in stainless steel zones: Monte Carlo calculation results**

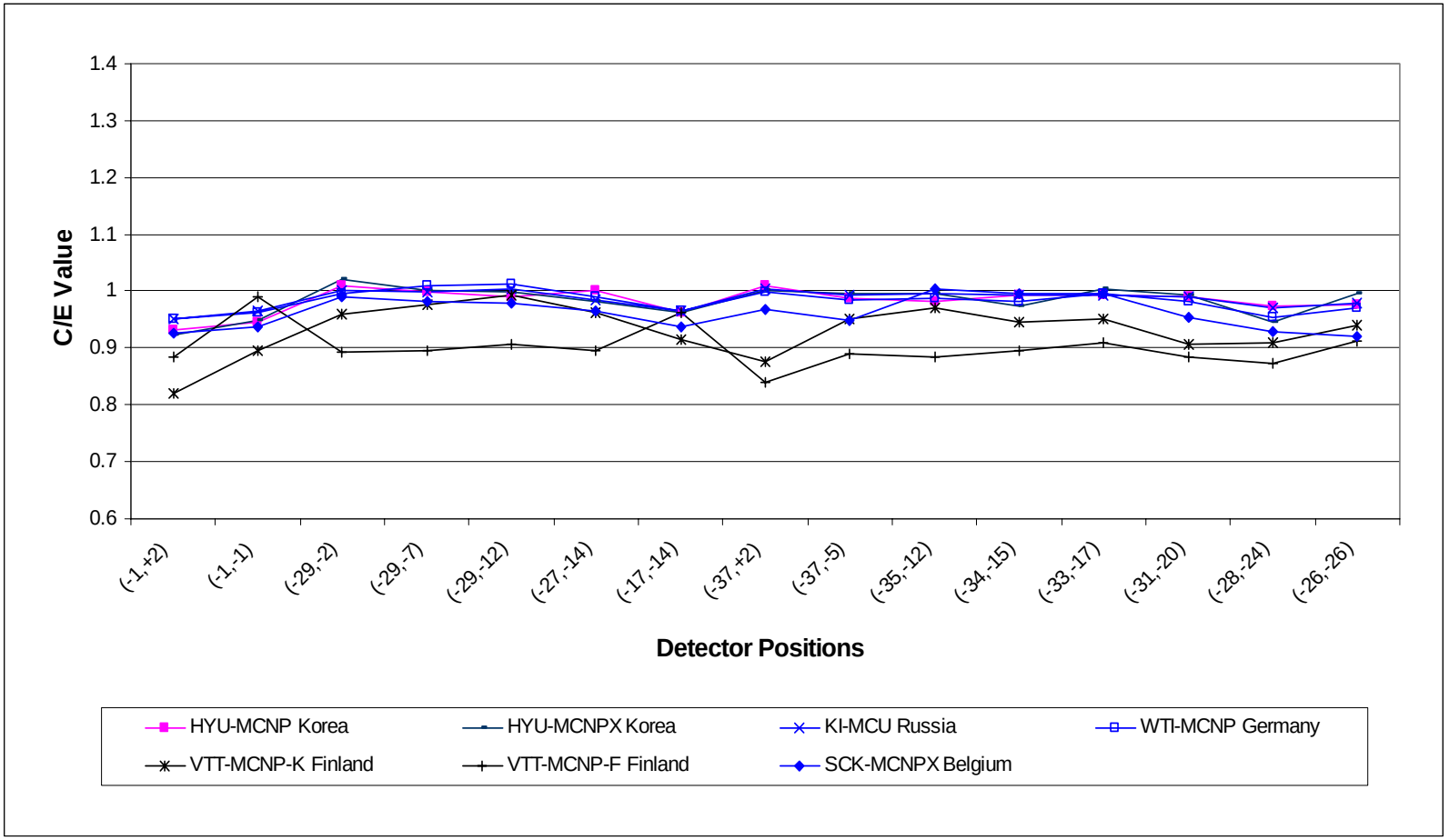

**Figure 4.6. C/E comparison of equivalent fission fluxes at $^{103}$Rh(n,n′) detector positions in water zones**

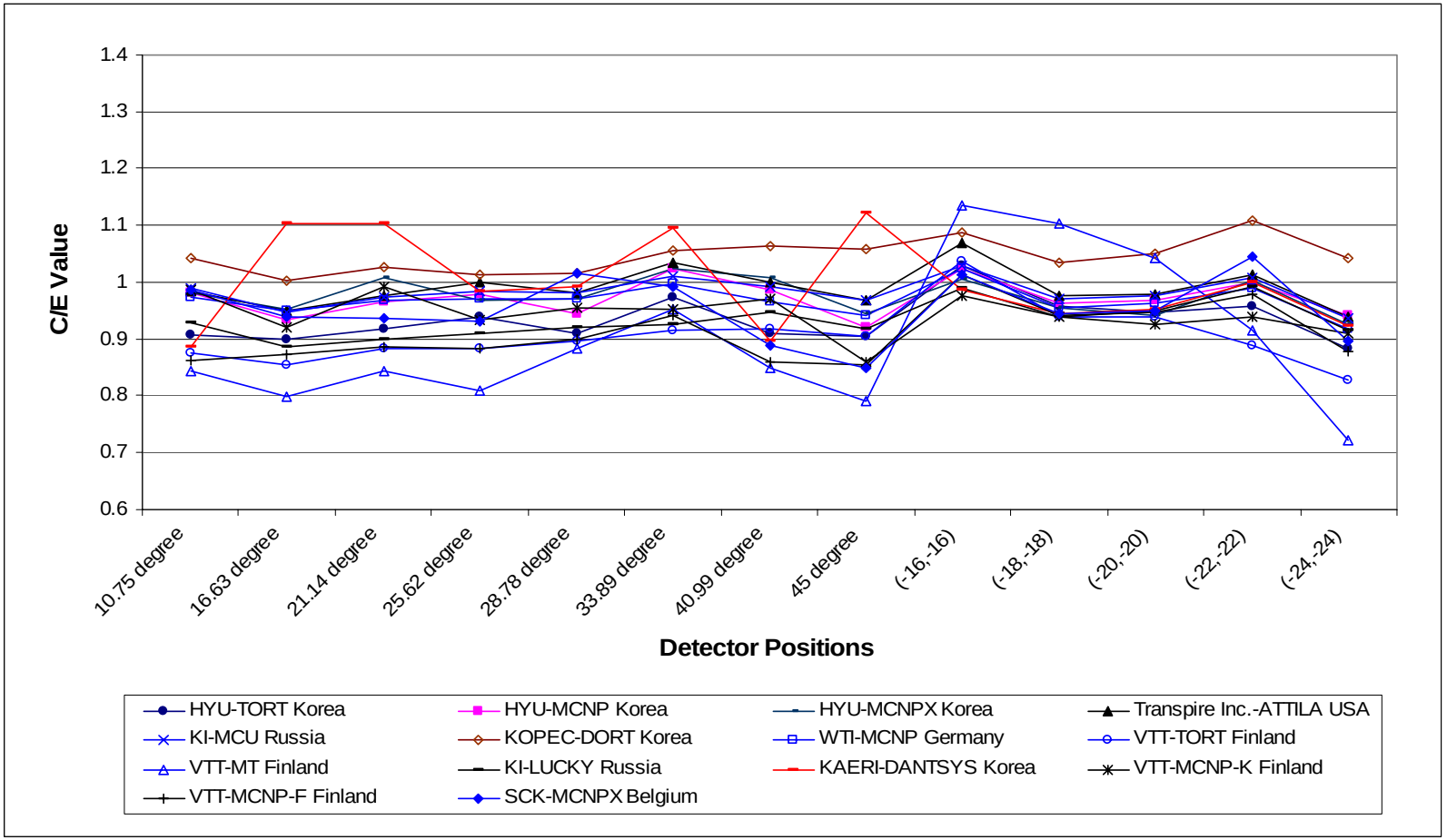

**Figure 4.6(a). C/E comparison of equivalent fission fluxes at $^{103}$Rh(n,n′) detector positions in water zones: Deterministic calculation results**

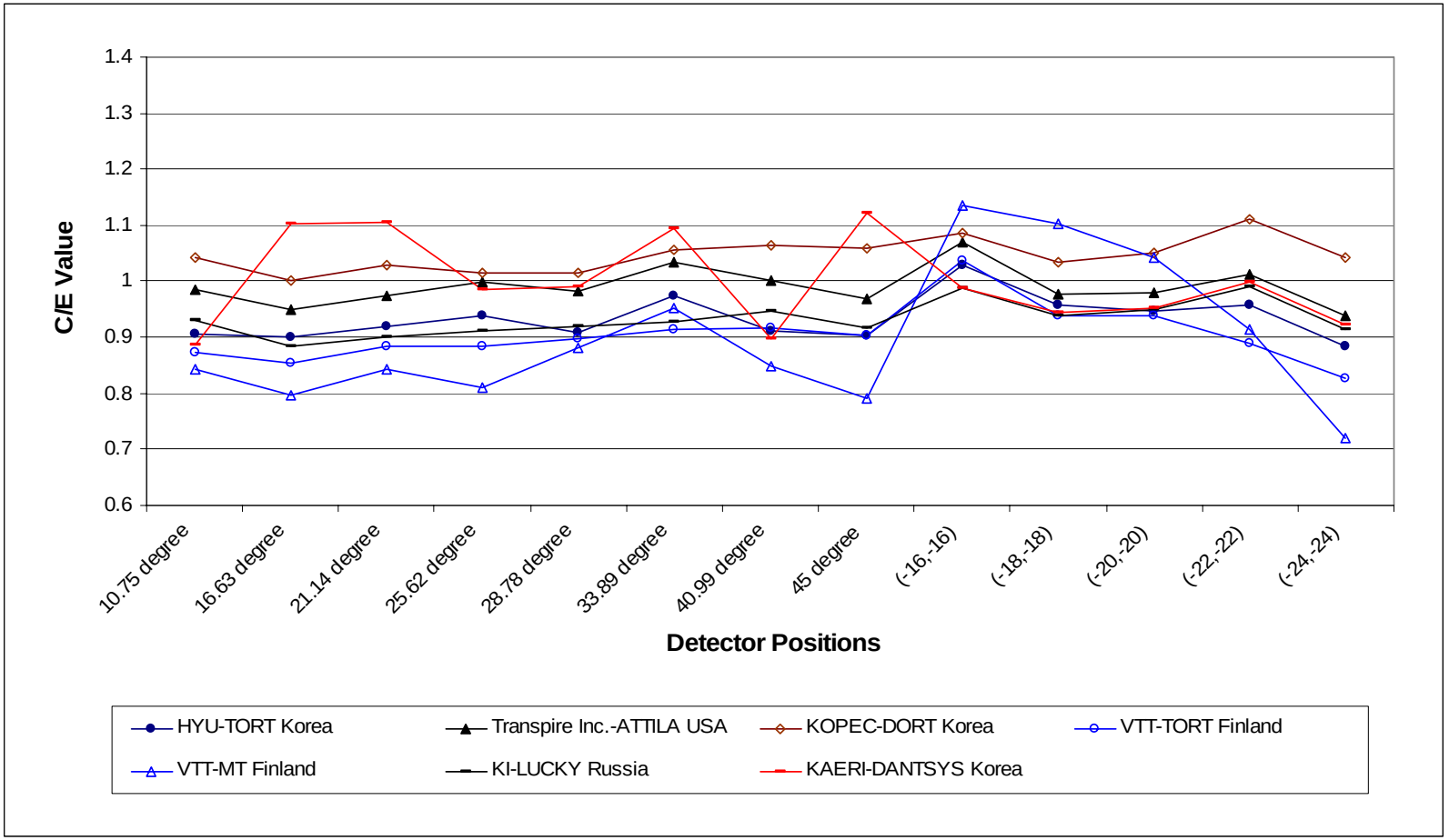

**Figure 4.6(b). C/E comparison of equivalent fission fluxes at $^{103}$Rh(n,n′) detector positions in water zones: Monte Carlo calculation results**

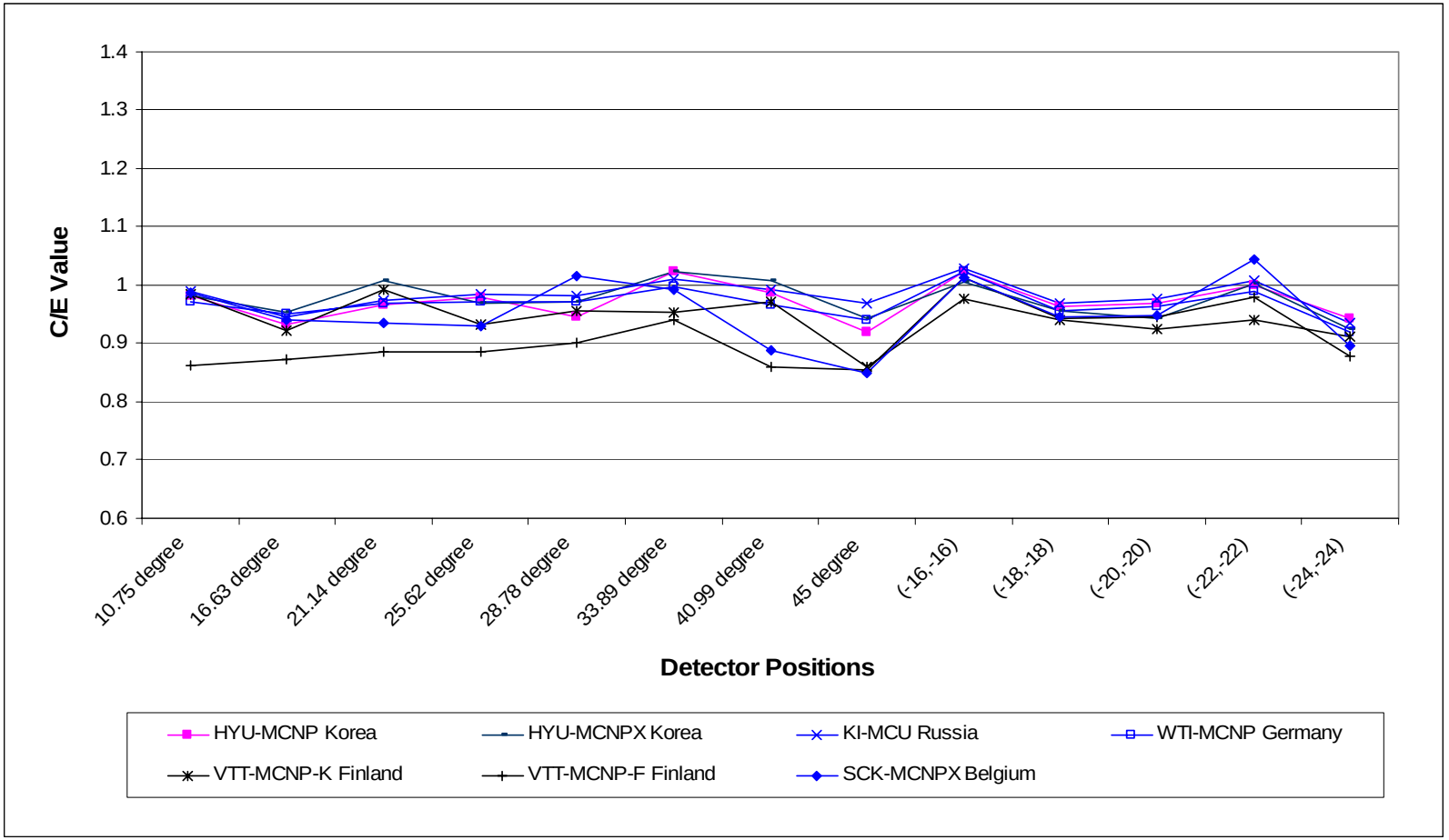

**Figure 4.7. C/E comparison of equivalent fission fluxes at $^{64}Zn(n,p)$ detector positions in stainless steel zones**

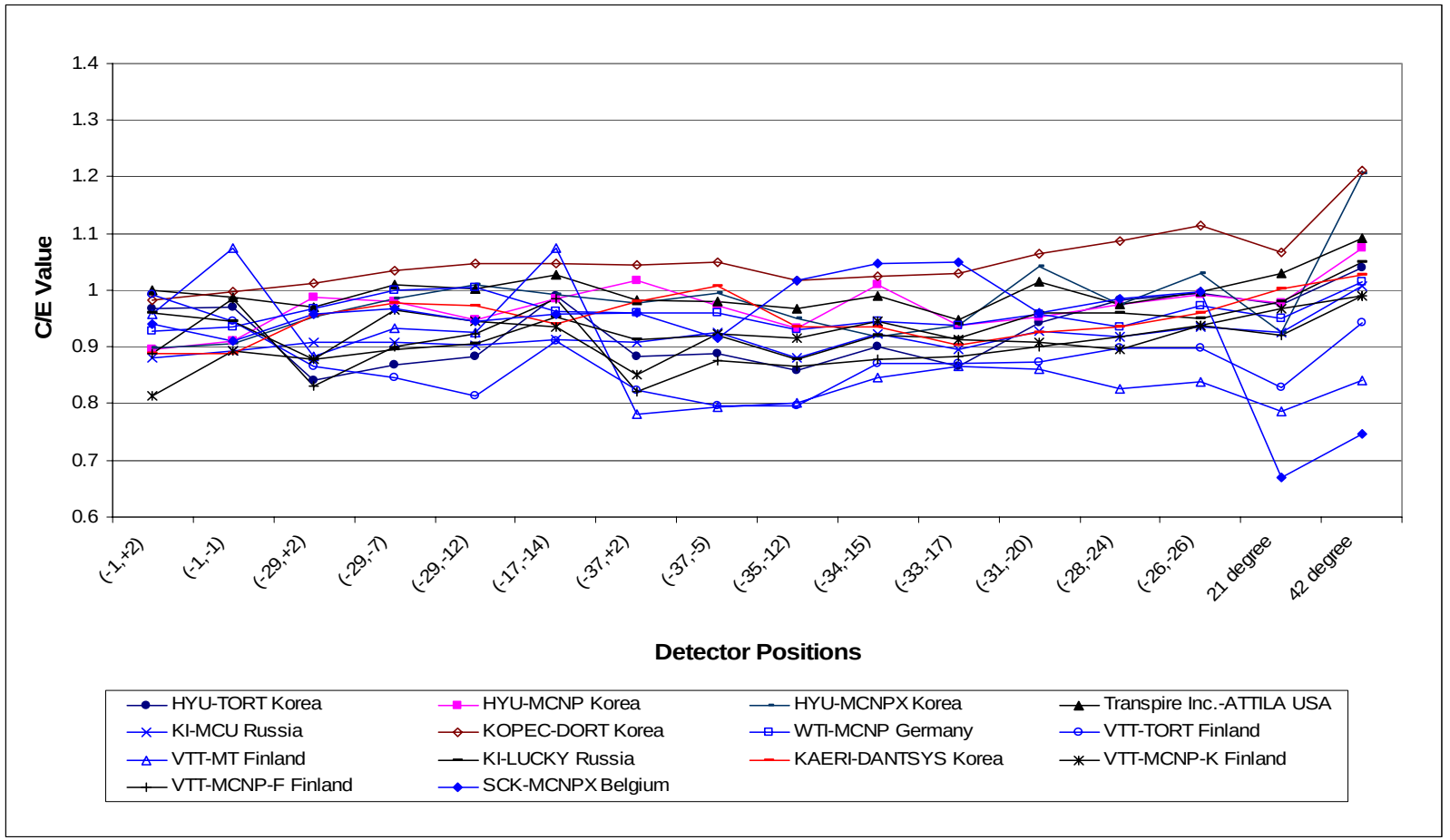

**Figure 4.7(a). C/E comparison of equivalent fission fluxes at $^{64}$Zn(n,p) detector positions in stainless steel zones: Deterministic calculation results**

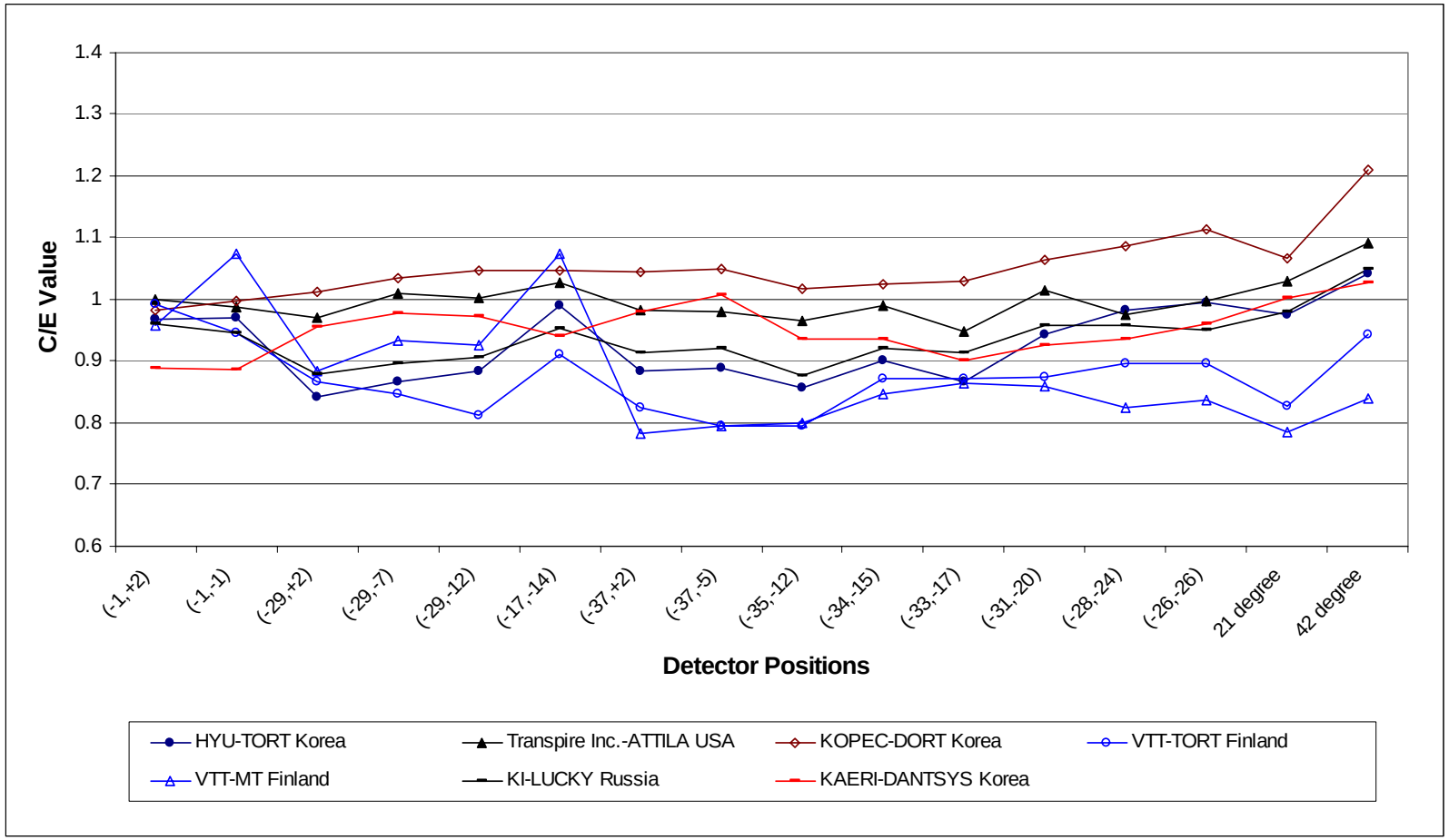

**Figure 4.7(b). C/E comparison of equivalent fission fluxes at $^{64}$Zn(n,p) detector positions in stainless steel zones: Monte Carlo calculation results**

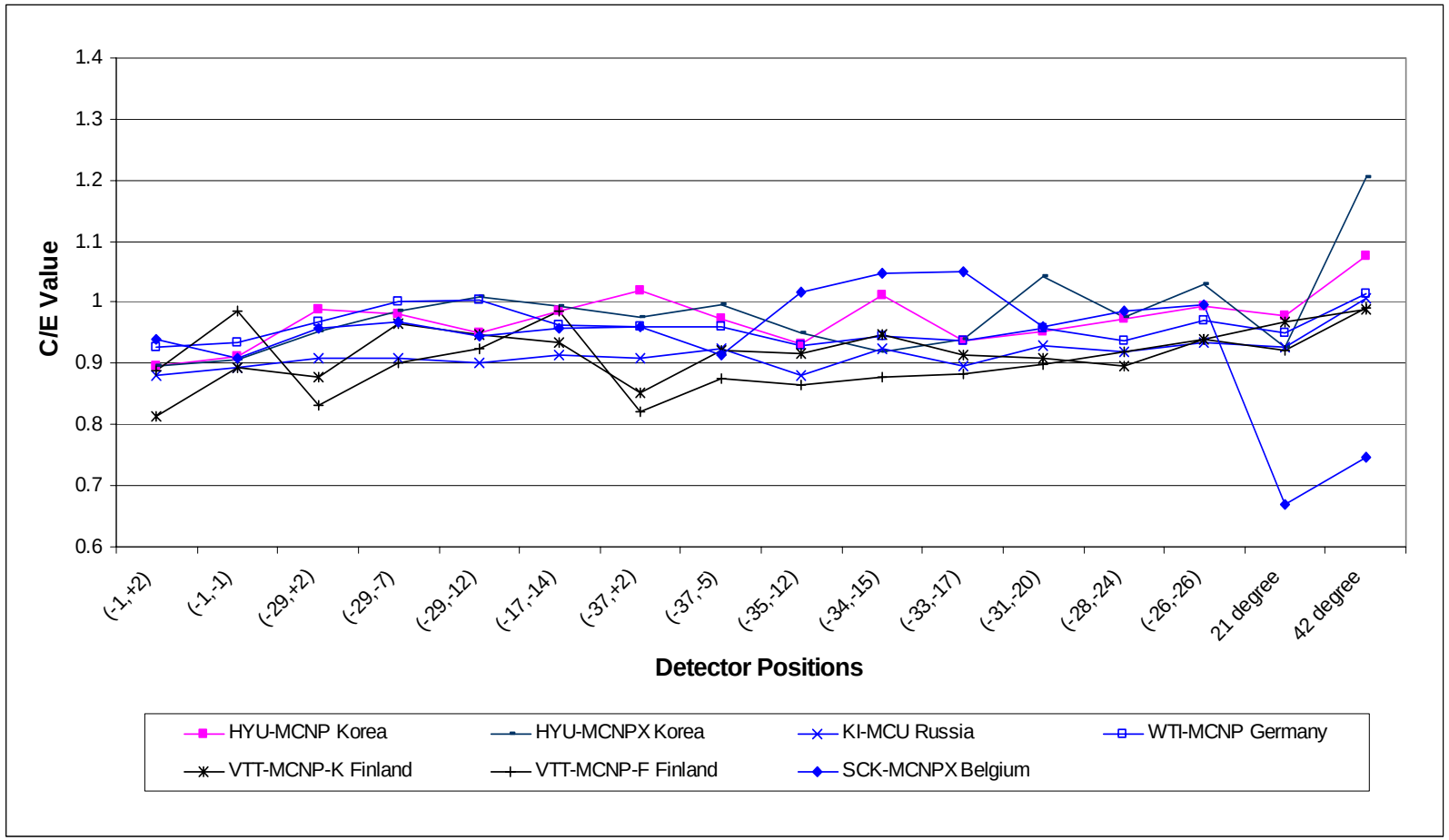

**Figure 4.8. C/E comparison of equivalent fission fluxes at $^{64}$Zn(n,p) detector positions in water zones**

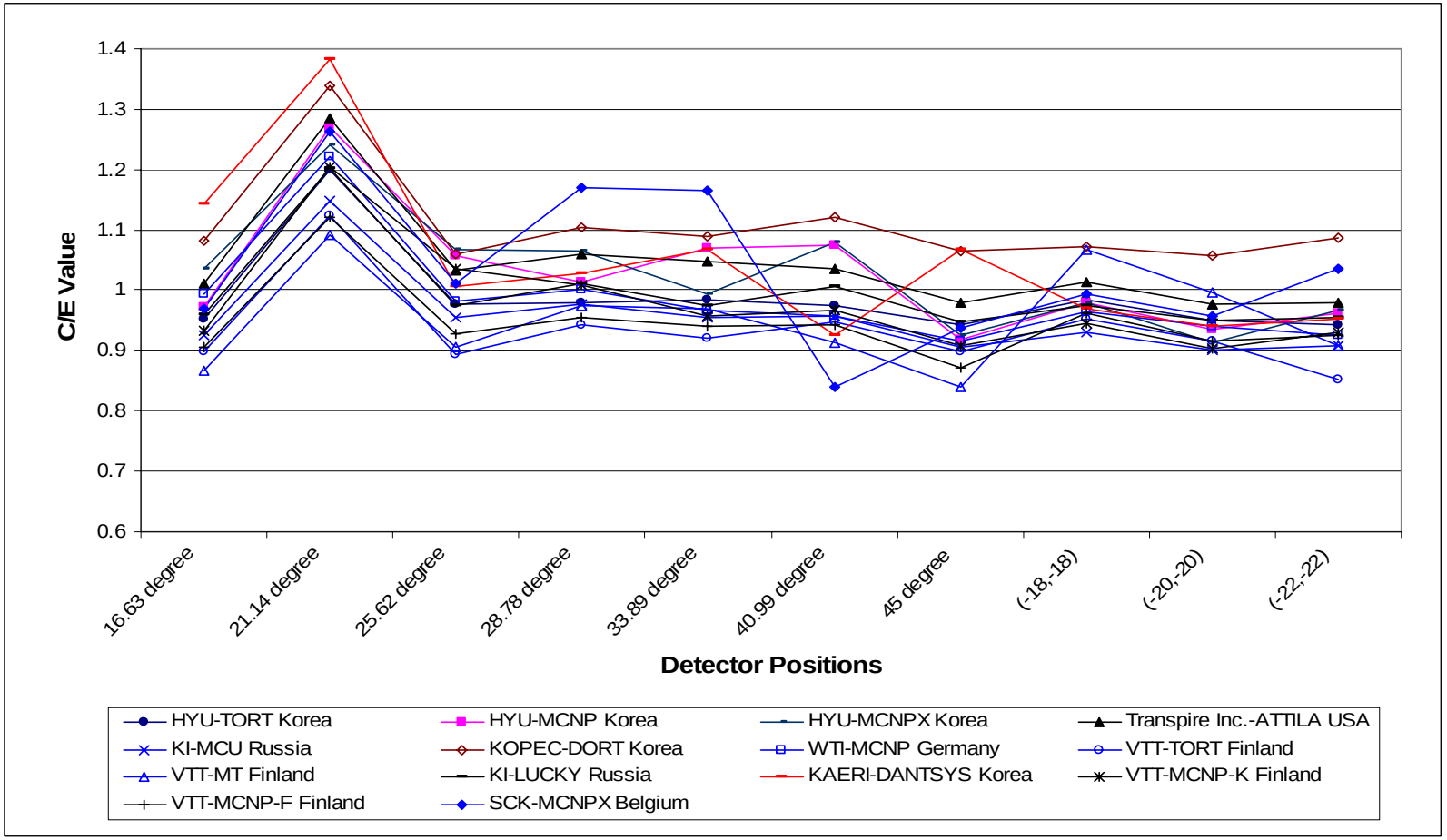

**Figure 4.8(a). C/E comparison of equivalent fission fluxes at $^{64}Zn(n,p)$ detector positions in water zones: Deterministic calculation results**

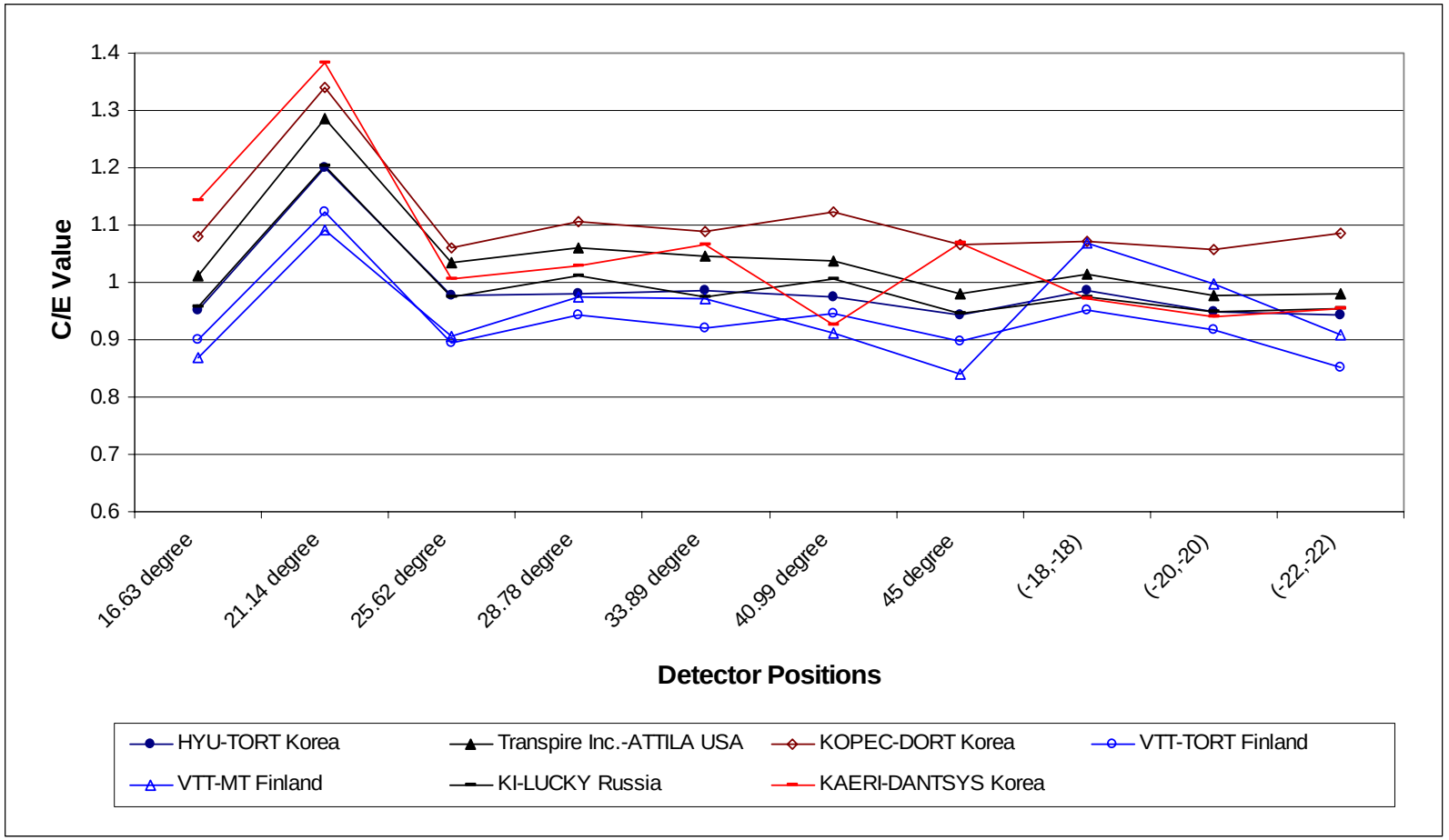

**Figure 4.8(b). C/E comparison of equivalent fission fluxes at $^{64}Zn(n,p)$ detector positions in water zones: Monte Carlo calculation results**

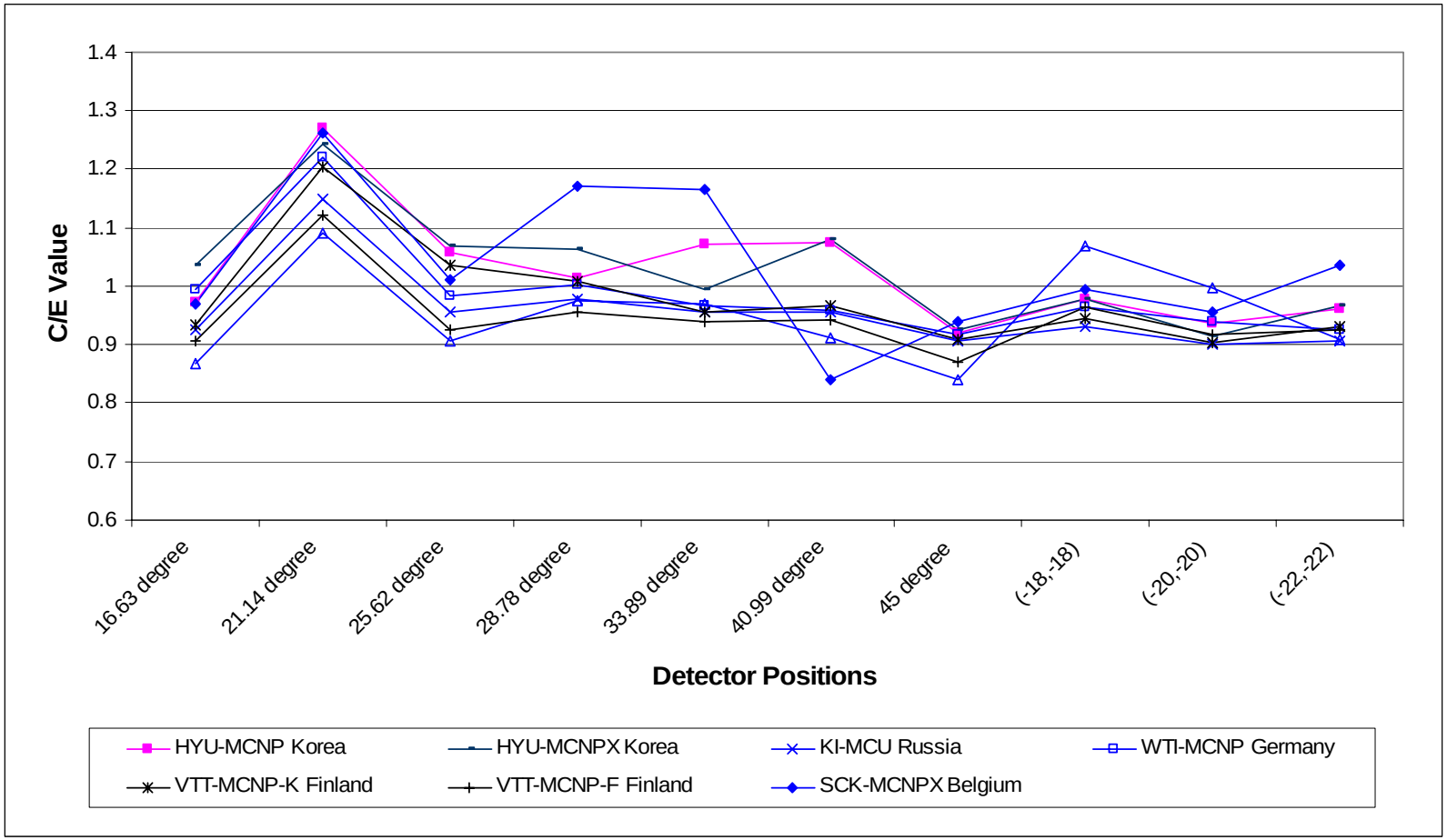

**Figure 4.9. C/E comparison of equivalent fission fluxes at $^{237}$Np(n,f) detector positions in stainless steel zones**

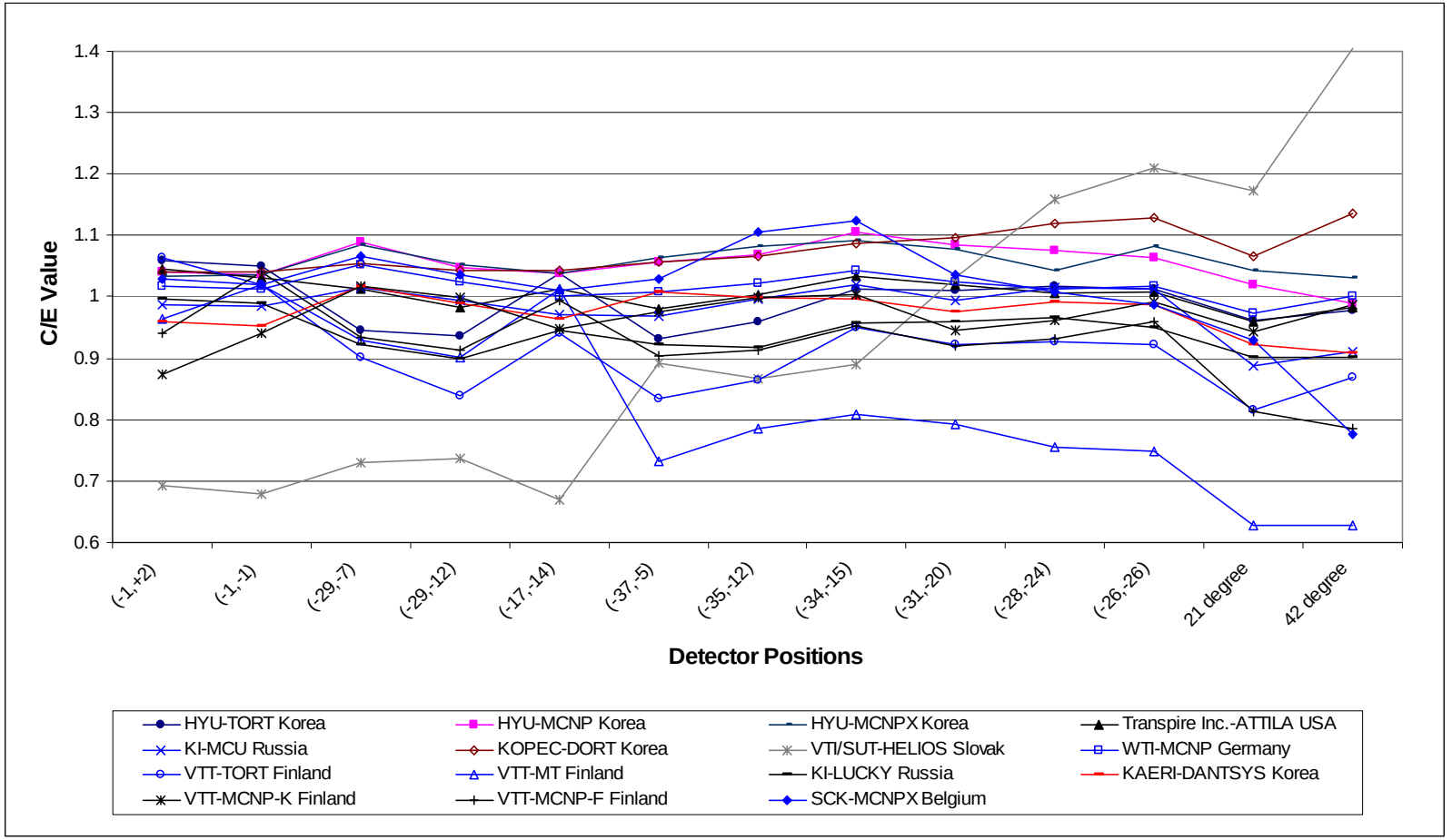

**Figure 4.9(a). C/E comparison of equivalent fission fluxes at $^{237}$Np(n,f) detector positions in stainless steel zones: Deterministic calculation results**

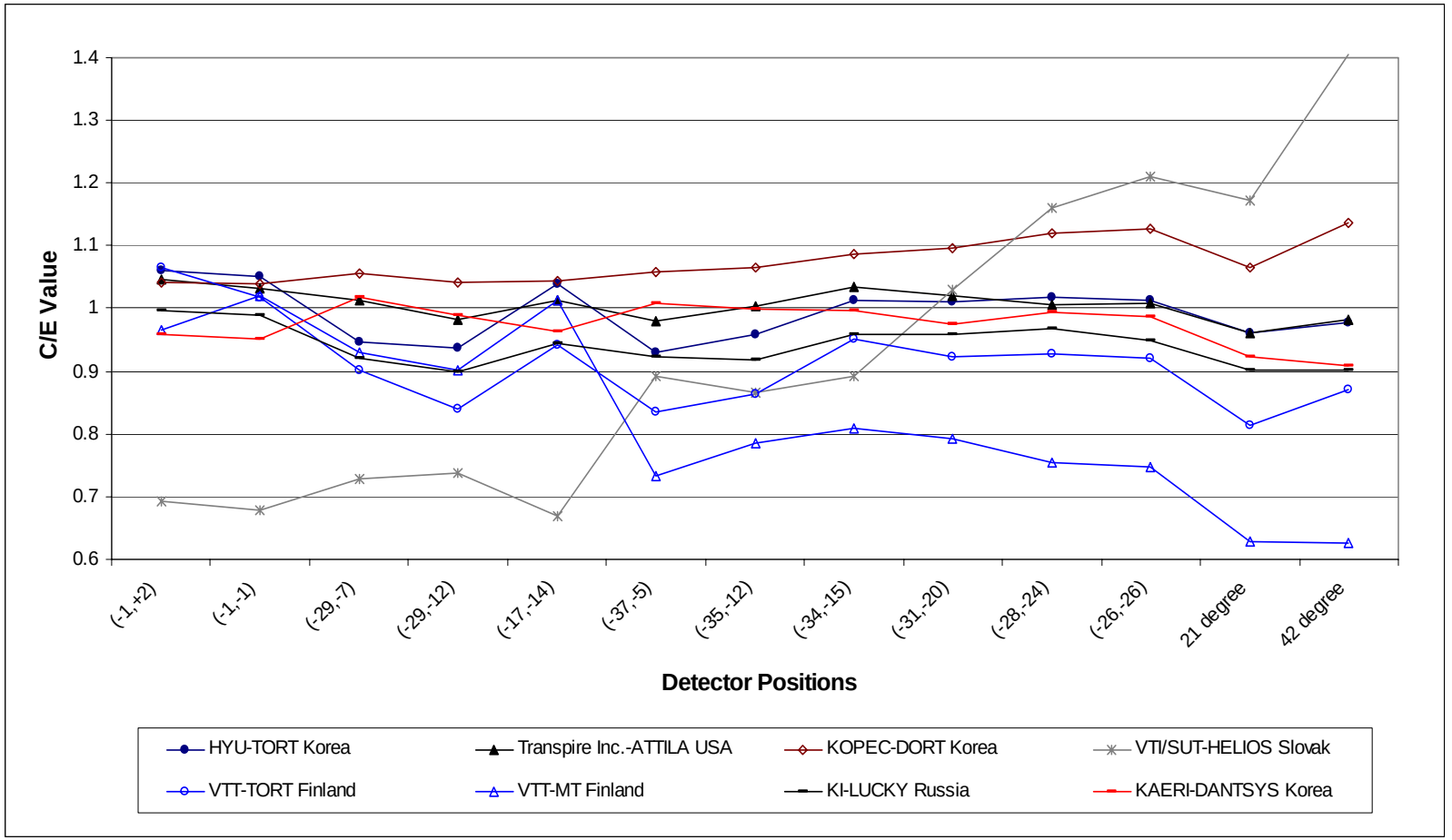

**Figure 4.9(b). C/E comparison of equivalent fission fluxes at $^{237}$Np(n,f) detector positions in stainless steel zones: Monte Carlo calculation results**

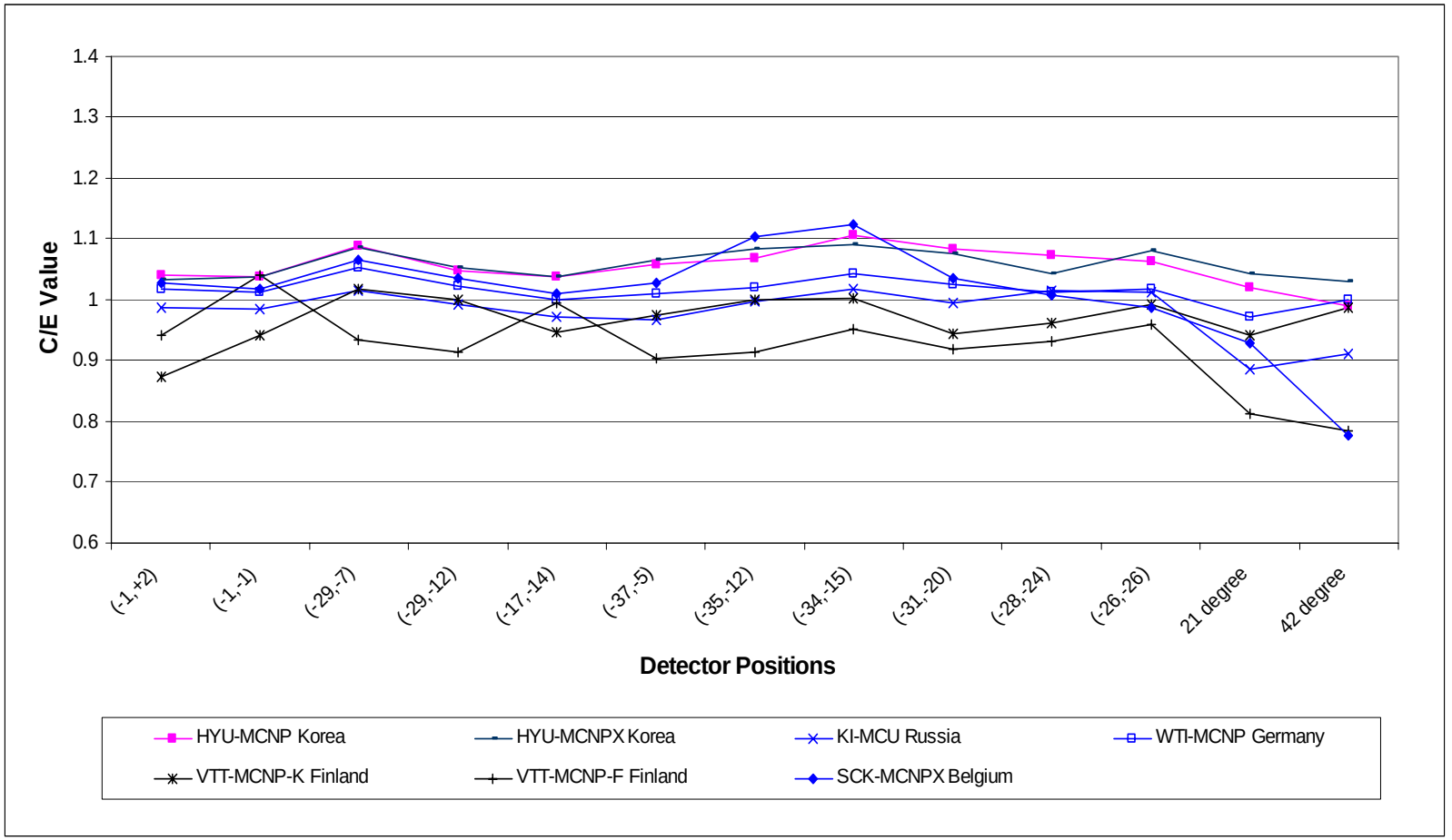

**Figure 4.10. C/E comparison of equivalent fission fluxes at $^{237}$Np(n,f) detector positions in water zones**

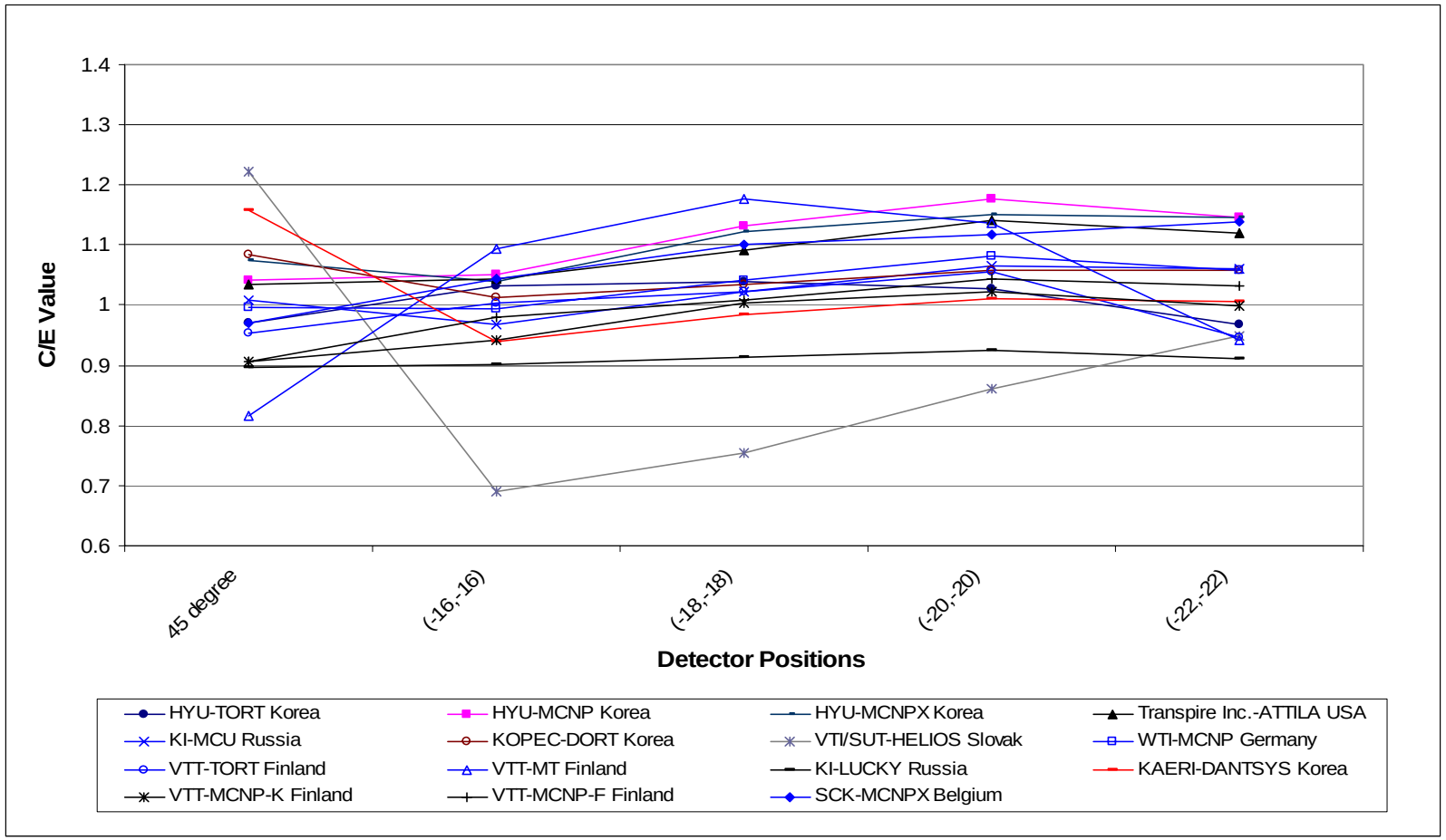

**Figure 4.10(a). C/E comparison of equivalent fission fluxes at $^{237}$Np(n,f) detector positions in water zones: Deterministic calculation results**

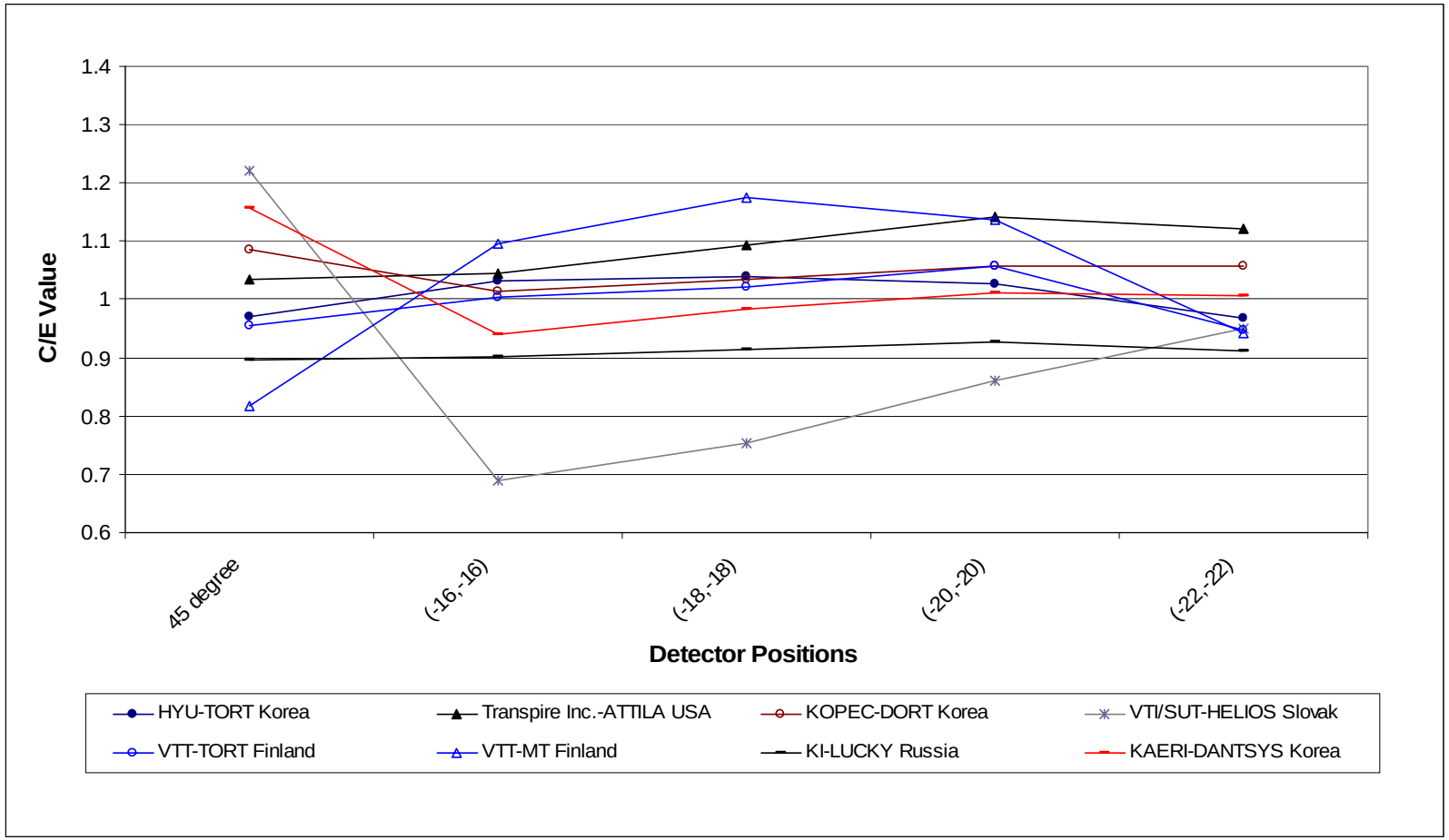

**Figure 4.10(b). C/E comparison of equivalent fission fluxes at $^{237}$Np(n,f) detector positions in water zones: Monte Carlo calculation results**

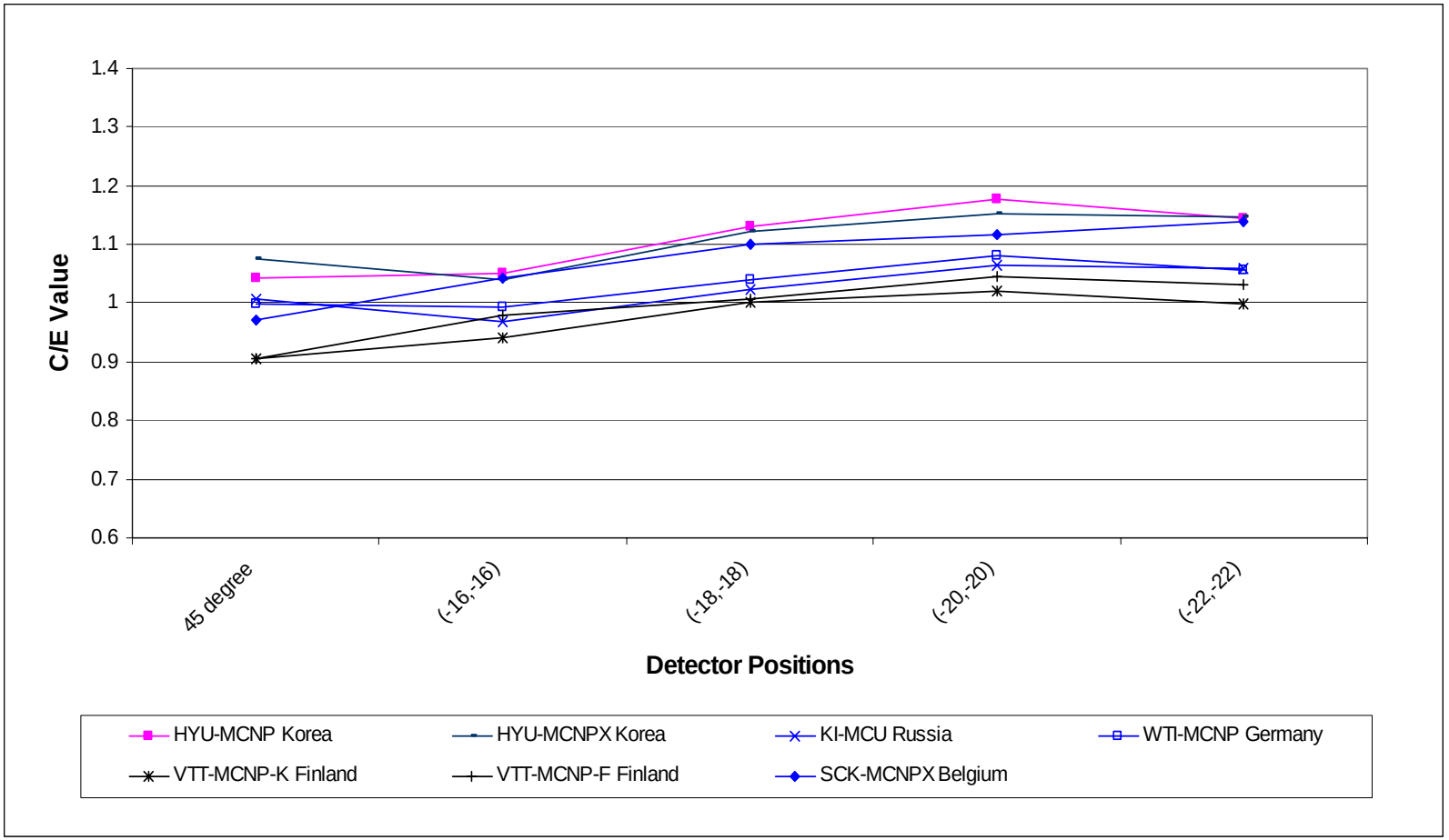

**Figure 4.11. C/E comparison of equivalent fission fluxes at $^{27}Al(n,\alpha)$ detector positions in stainless steel zones**

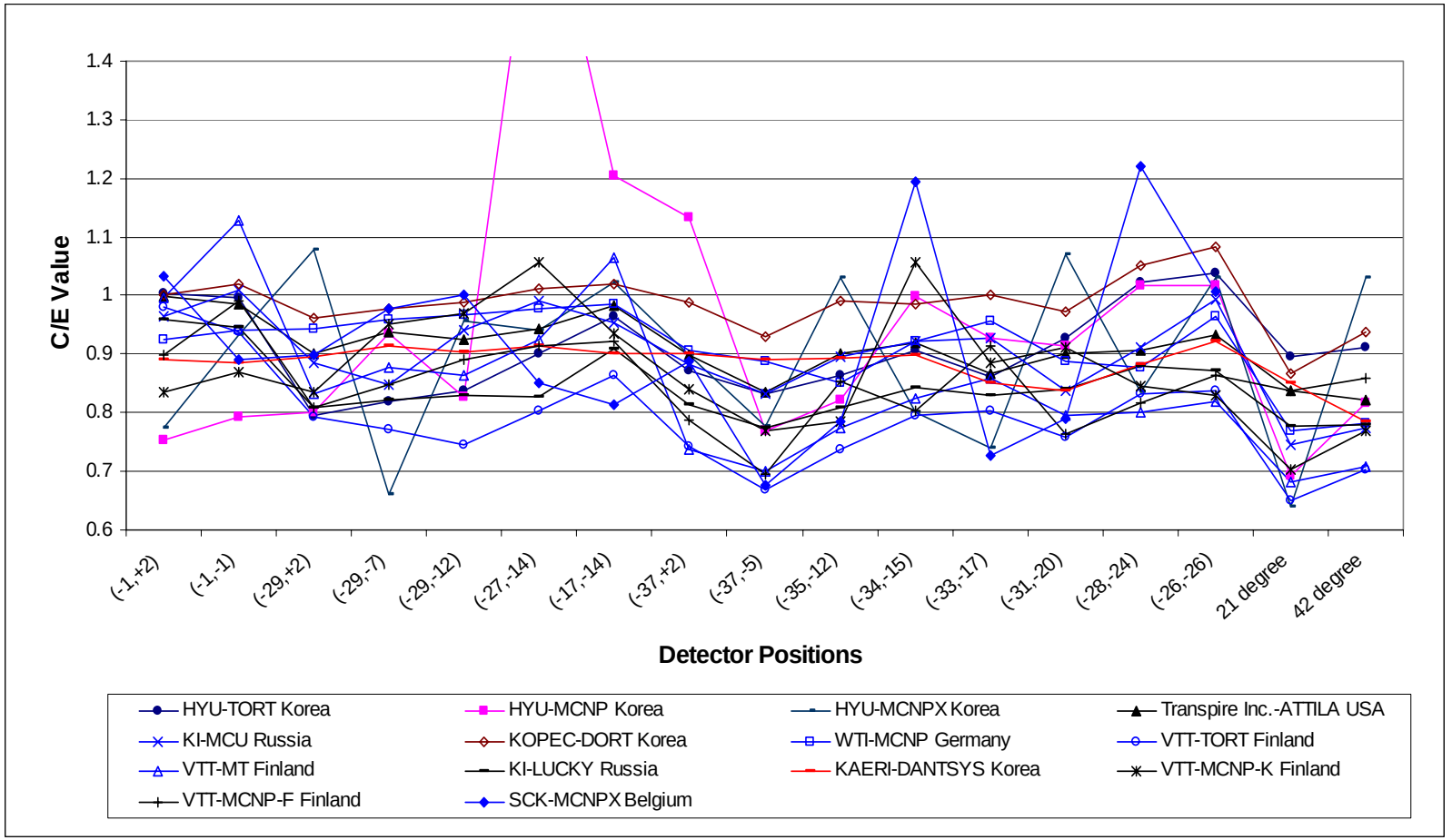

**Figure 4.11(a). C/E comparison of equivalent fission fluxes at $^{27}Al(n,\alpha)$ detector positions in stainless steel zones: Deterministic calculation results**

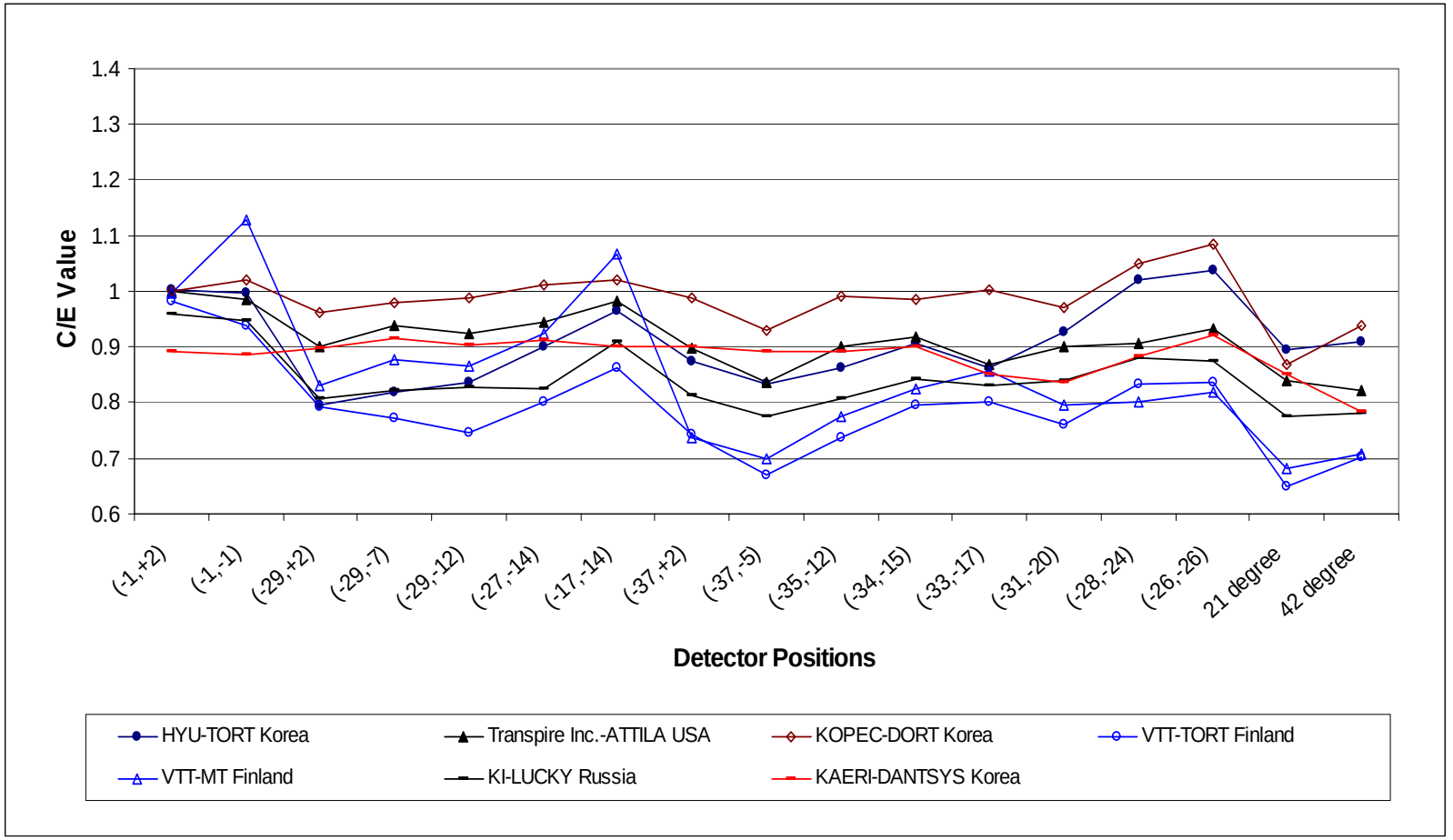

**Figure 4.11(b). C/E comparison of equivalent fission fluxes at $^{27}Al(n,\alpha)$ detector positions in stainless steel zones: Monte Carlo calculation results**

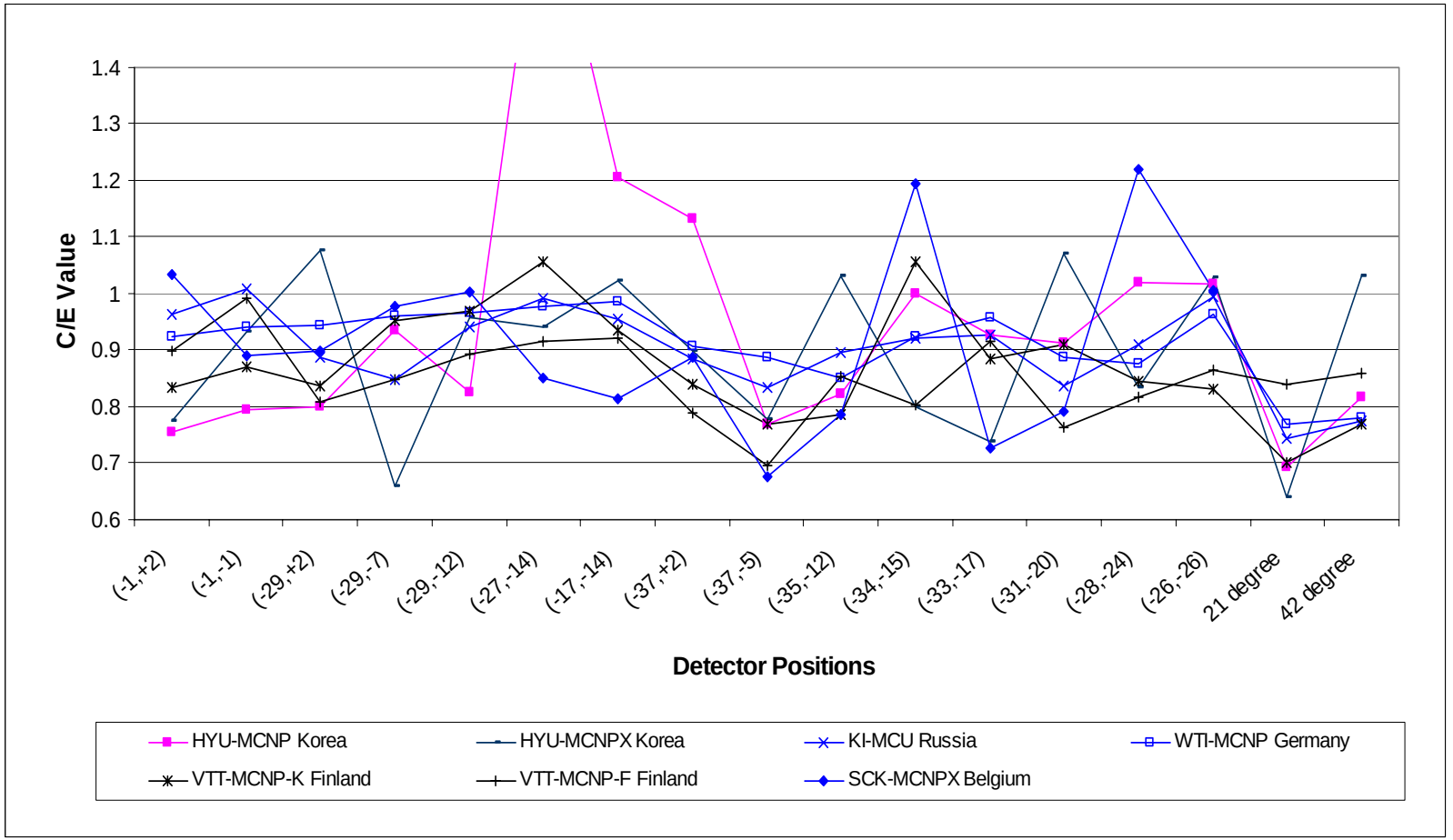

**Figure 4.12. C/E comparison of equivalent fission fluxes at $^{27}Al(n,\alpha)$ detector positions in water zones**

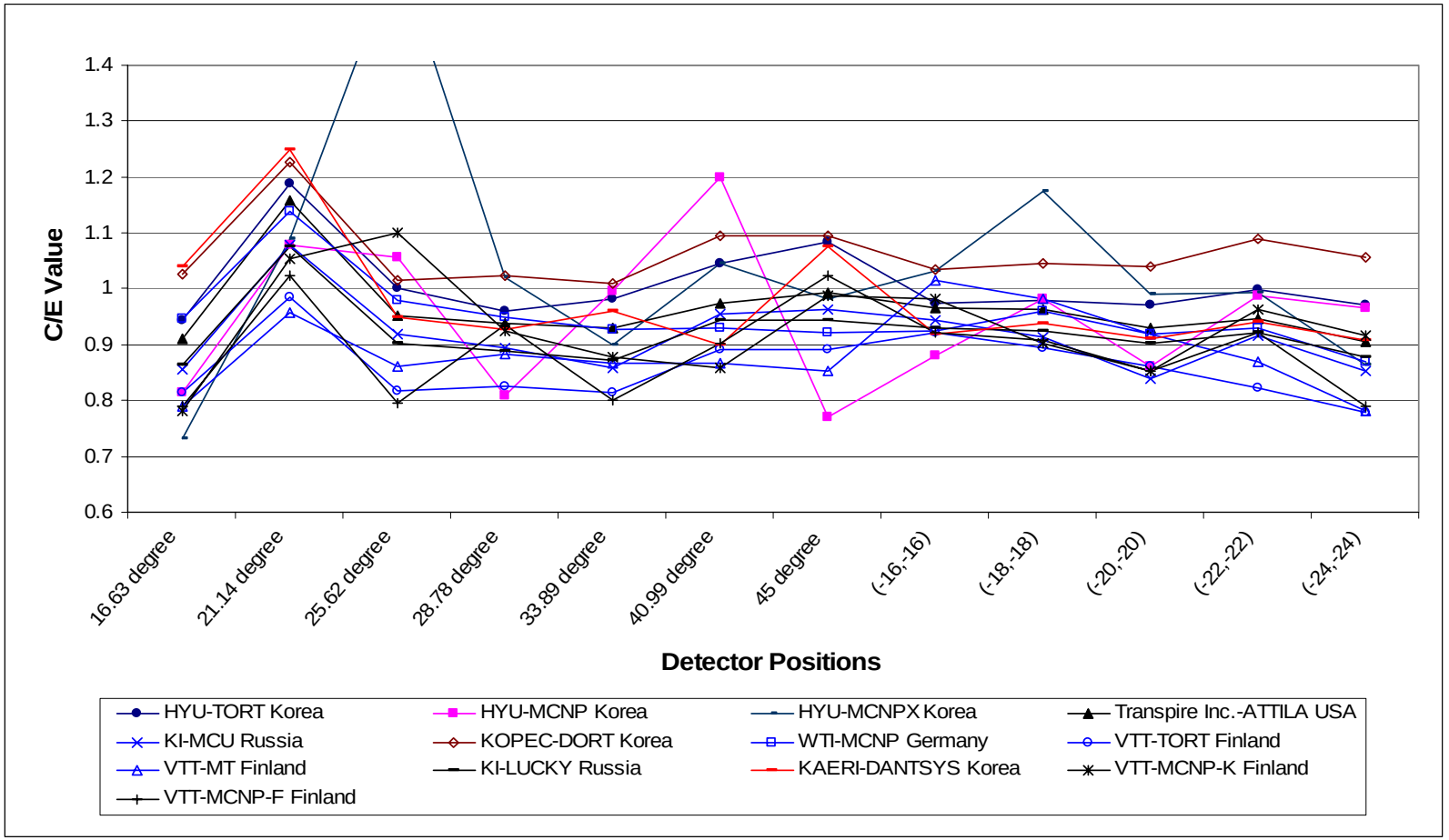

**Figure 4.12(a). C/E comparison of equivalent fission fluxes at $^{27}Al(n,\alpha)$ detector positions in water zones: Deterministic calculation results**

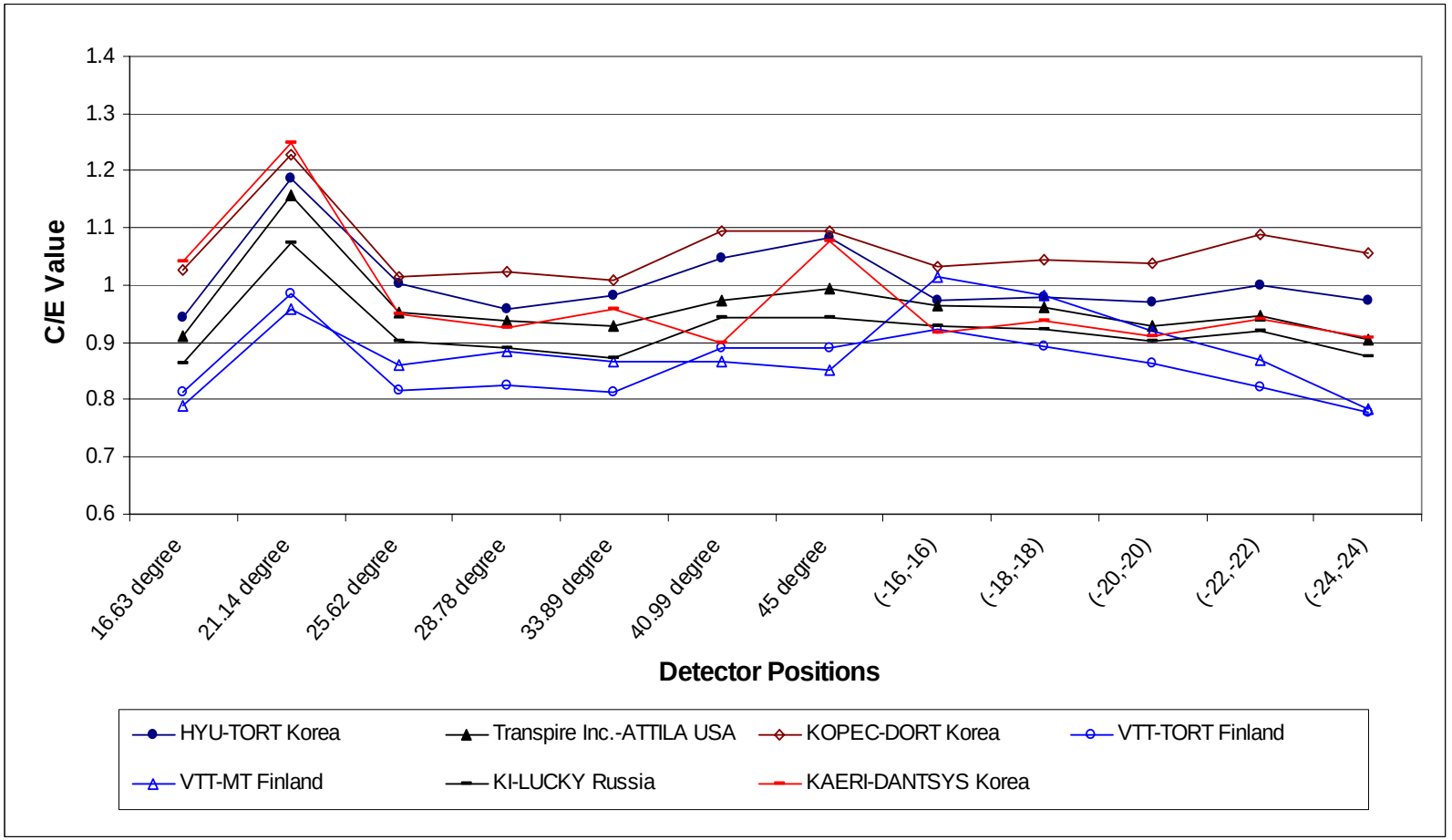

**Figure 4.12(b). C/E comparison of equivalent fission fluxes at $^{27}Al(n,\alpha)$ detector positions in water zones: Monte Carlo calculation results**

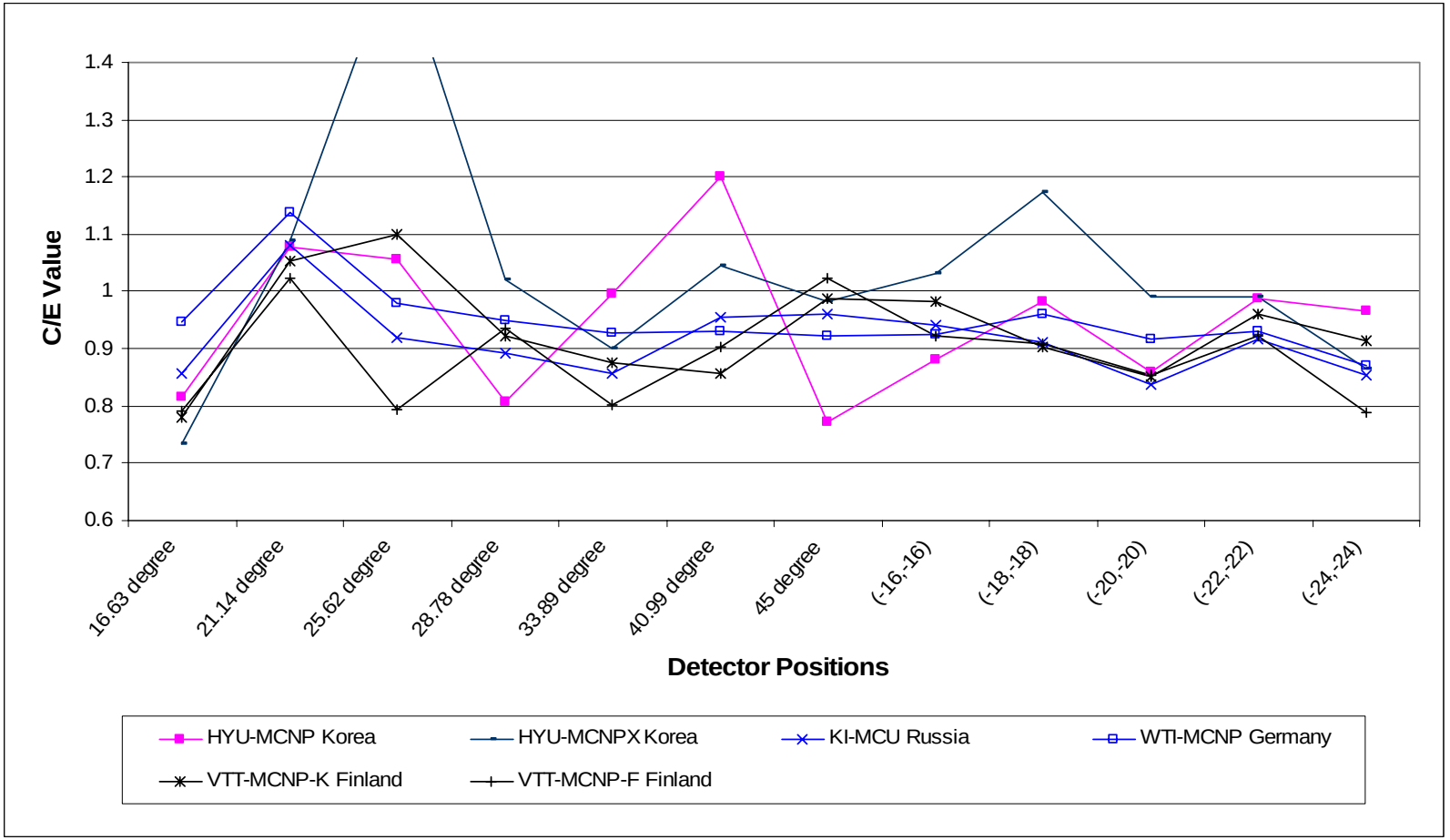

**Figure 4.13. C/E comparison of reaction rates at $^{58}$Ni(n,p) detector positions in stainless steel zones**

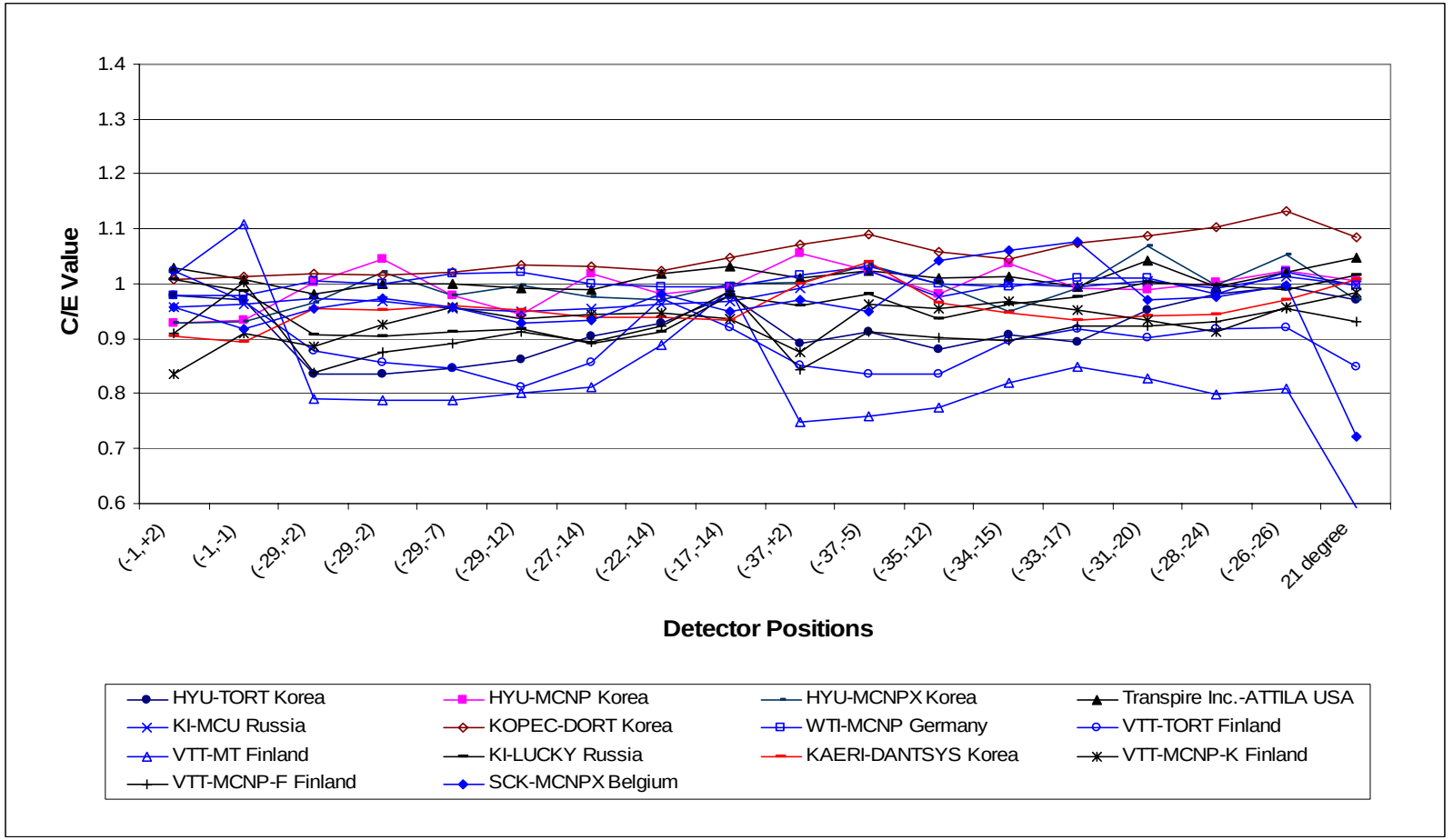

**Figure 4.13(a). C/E comparison of reaction rates at $^{58}$Ni(n,p) detector positions in stainless steel zones: Deterministic calculation results**

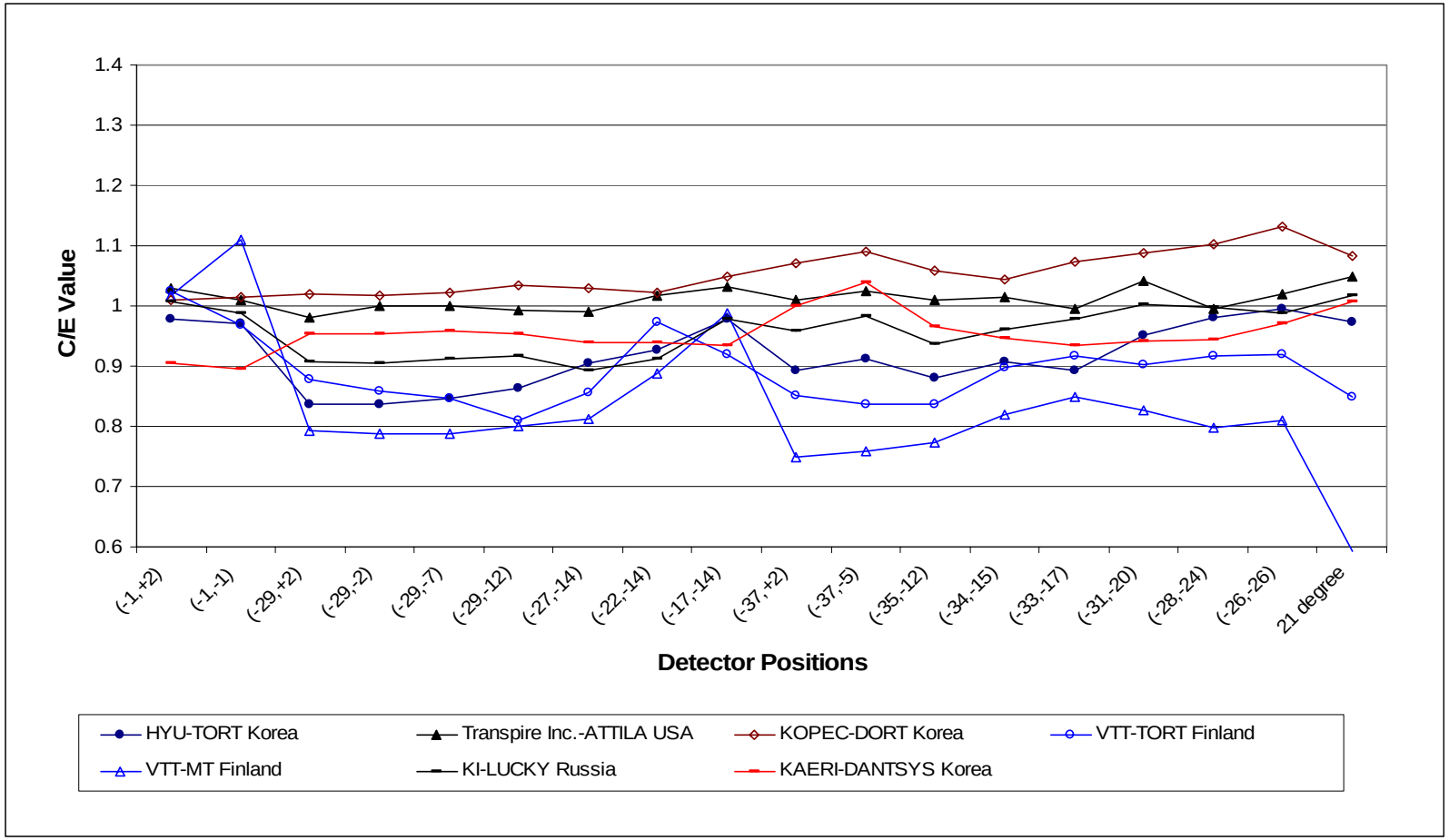

**Figure 4.13(b). C/E comparison of reaction rates at $^{58}$Ni(n,p) detector positions in stainless steel zones: Monte Carlo calculation results**

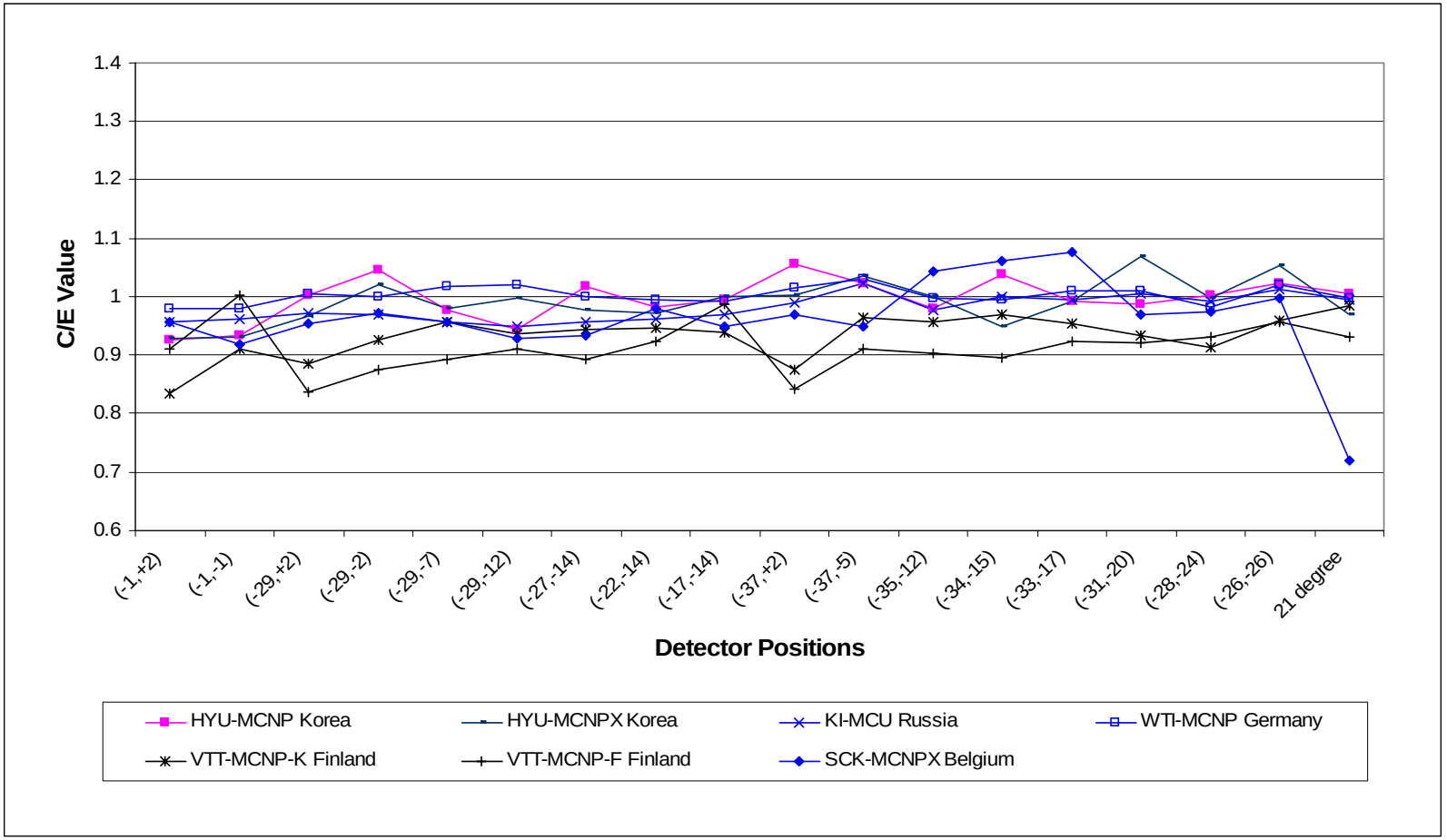

**Figure 4.14. C/E comparison of reaction rates at $^{58}$Ni(n,p) detector positions in water zones**

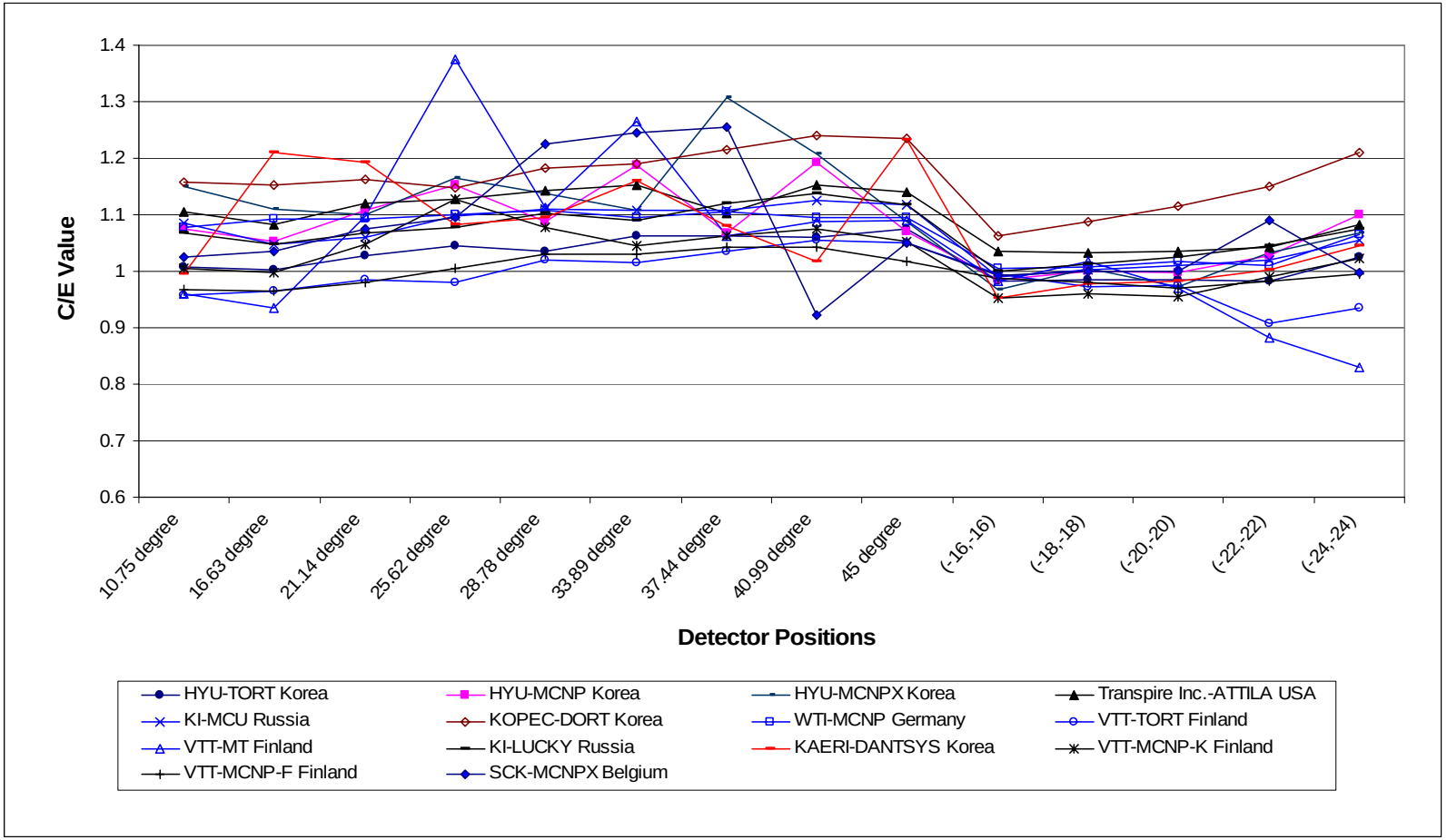

**Figure 4.14(a). C/E comparison of reaction rates at $^{58}$Ni(n,p) detector positions in water zones: Deterministic calculation results**

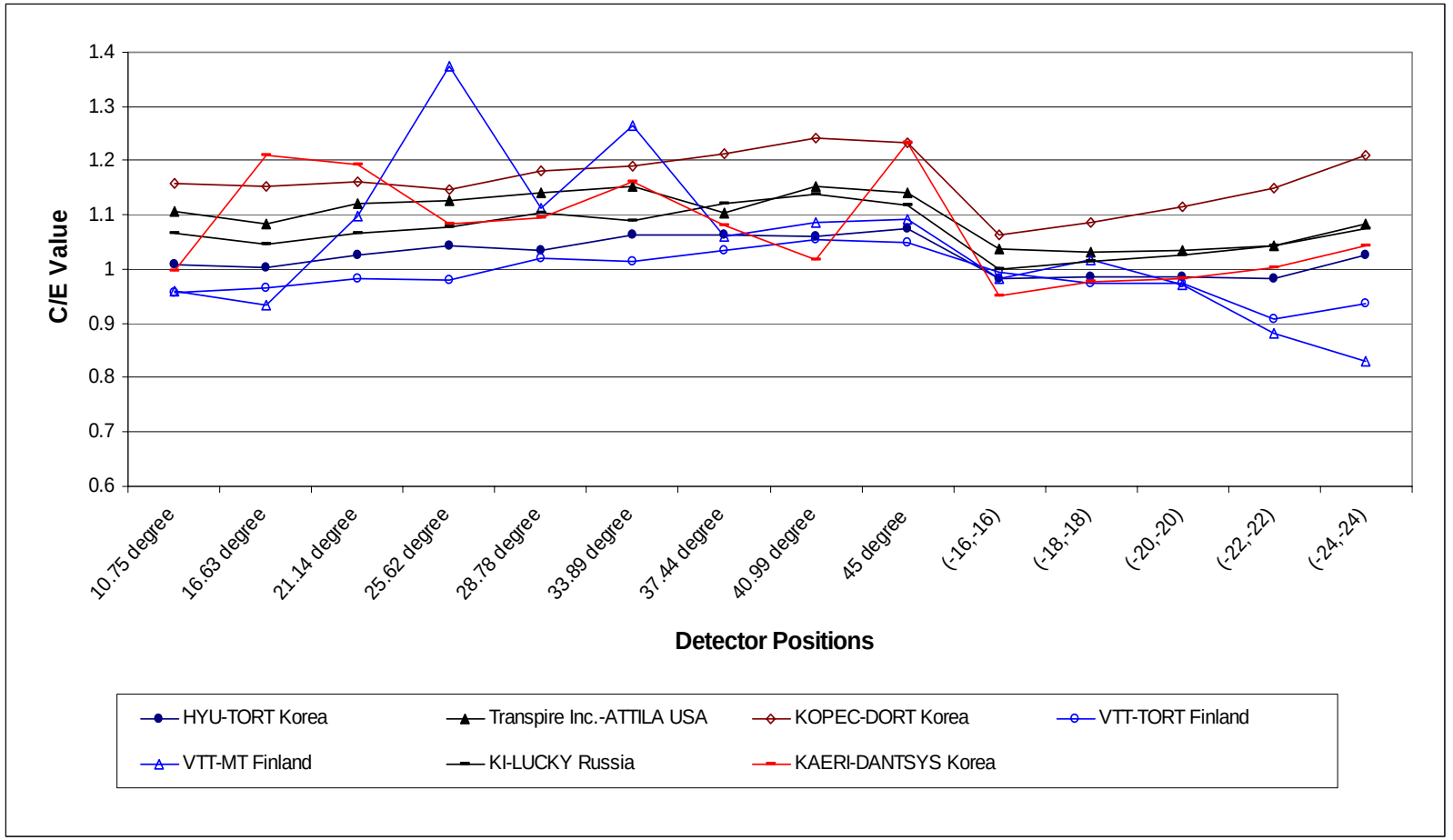

**Figure 4.14(b). C/E comparison of reaction rates at $^{58}$Ni(n,p) detector positions in water zones: Monte Carlo calculation results**

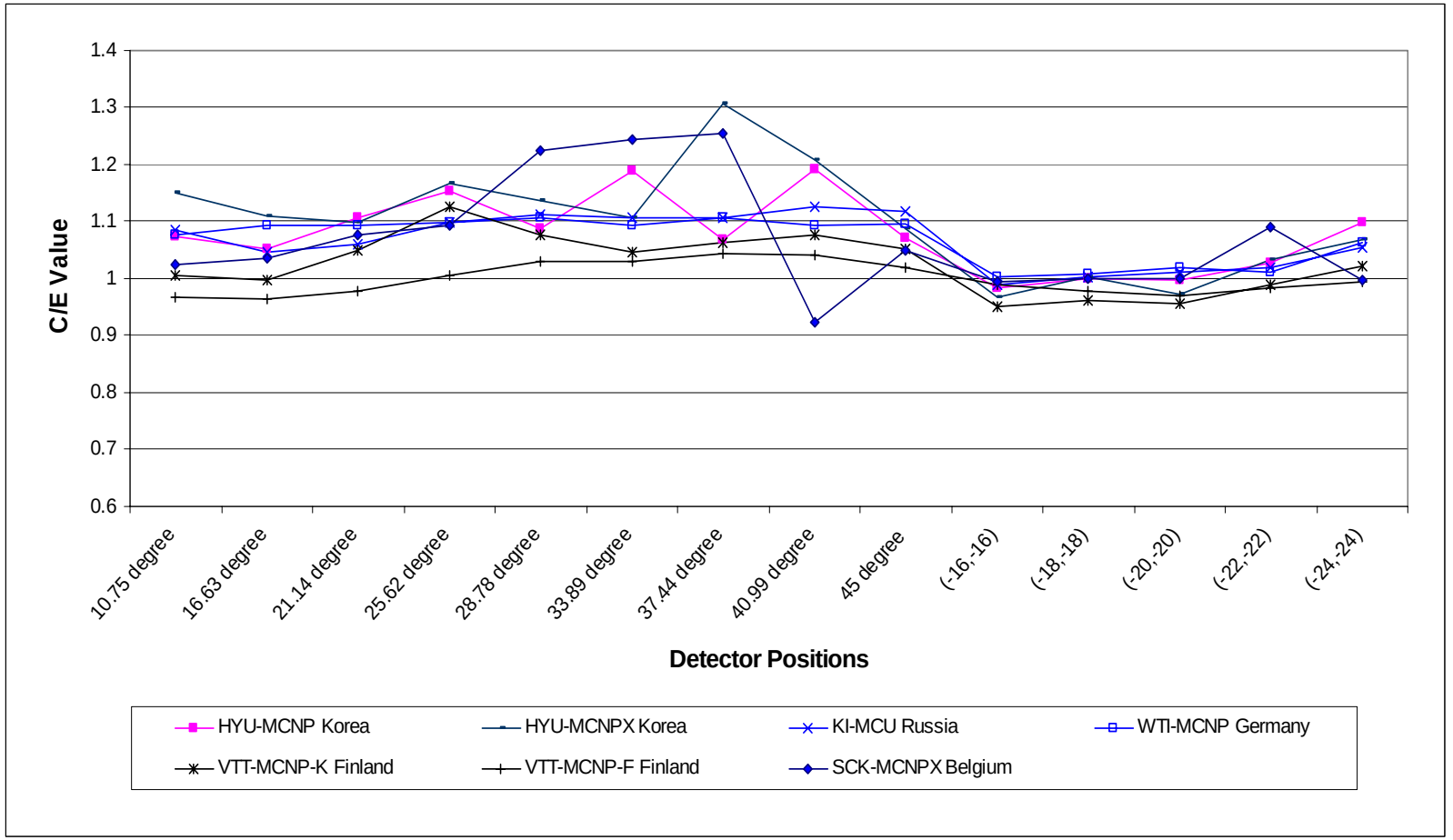

**Figure 4.15. C/E comparison of reaction rates at $^{115}$In(n,n′) detector positions in stainless steel zones**

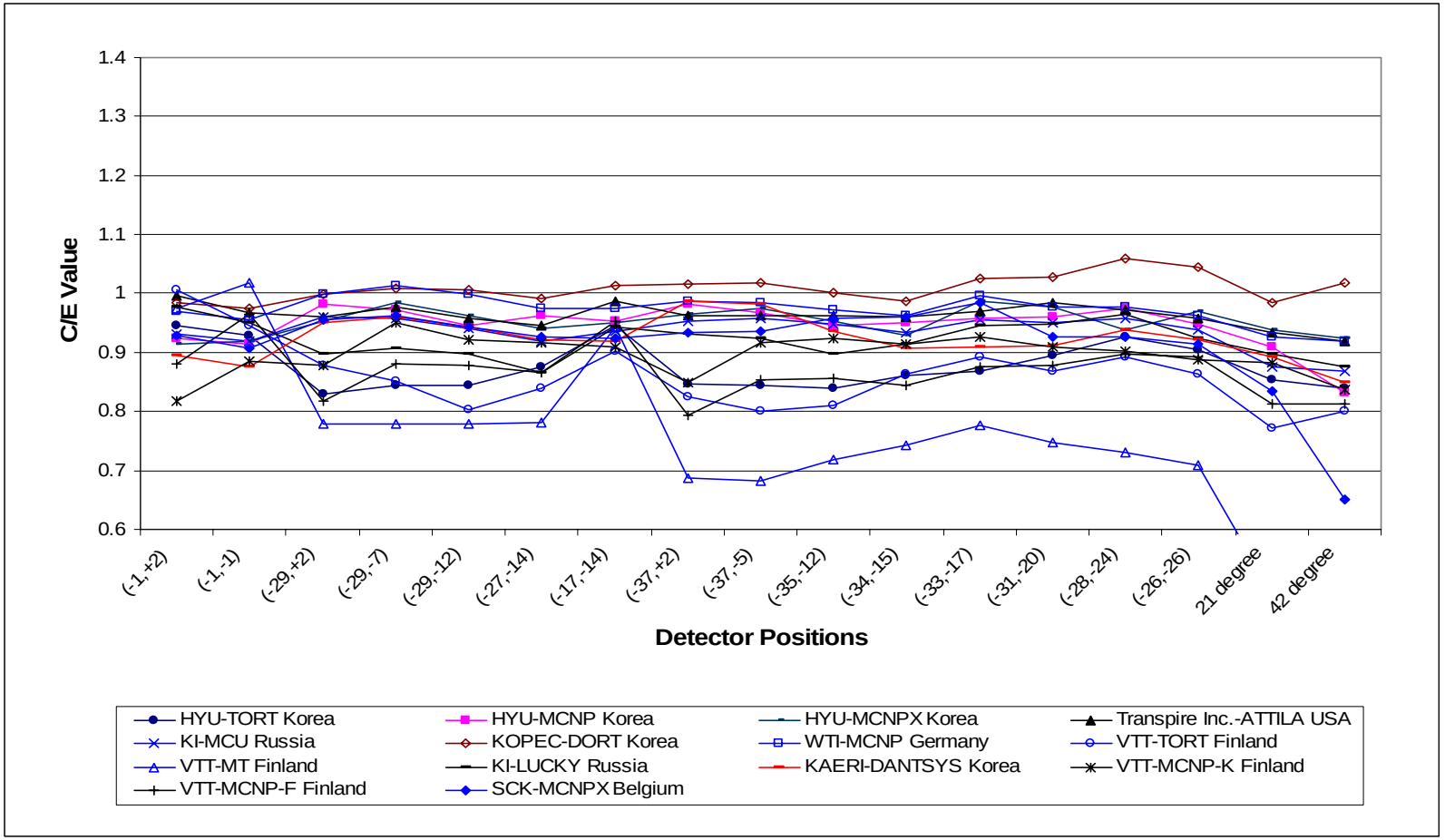

**Figure 4.15(a). C/E comparison of reaction rates at $^{115}$In(n,n′) detector positions in stainless steel zones: Deterministic calculation results**

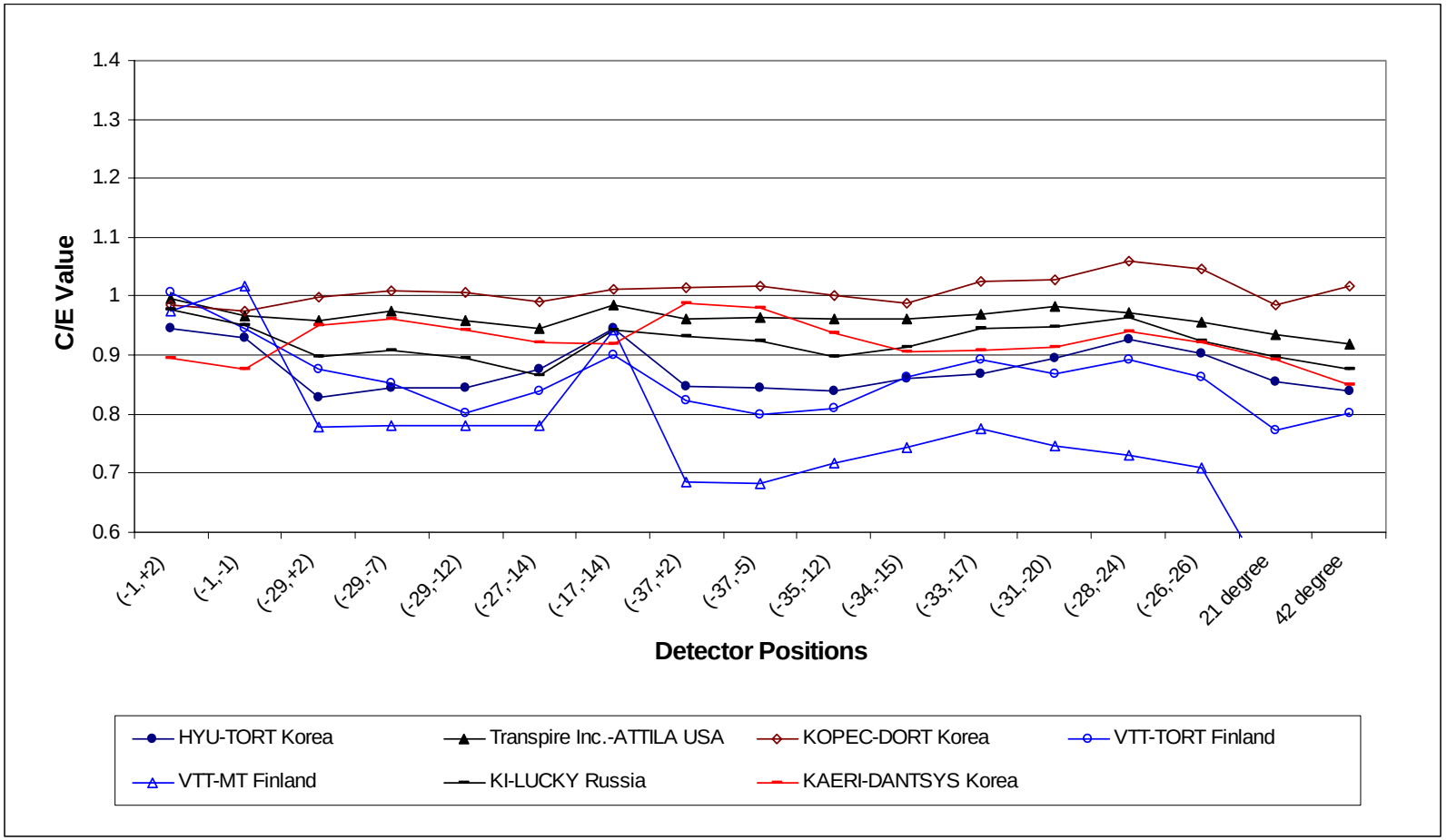

**Figure 4.15(b). C/E comparison of reaction rates at $^{115}In(n,n')$ detector positions in stainless steel zones: Monte Carlo calculation results**

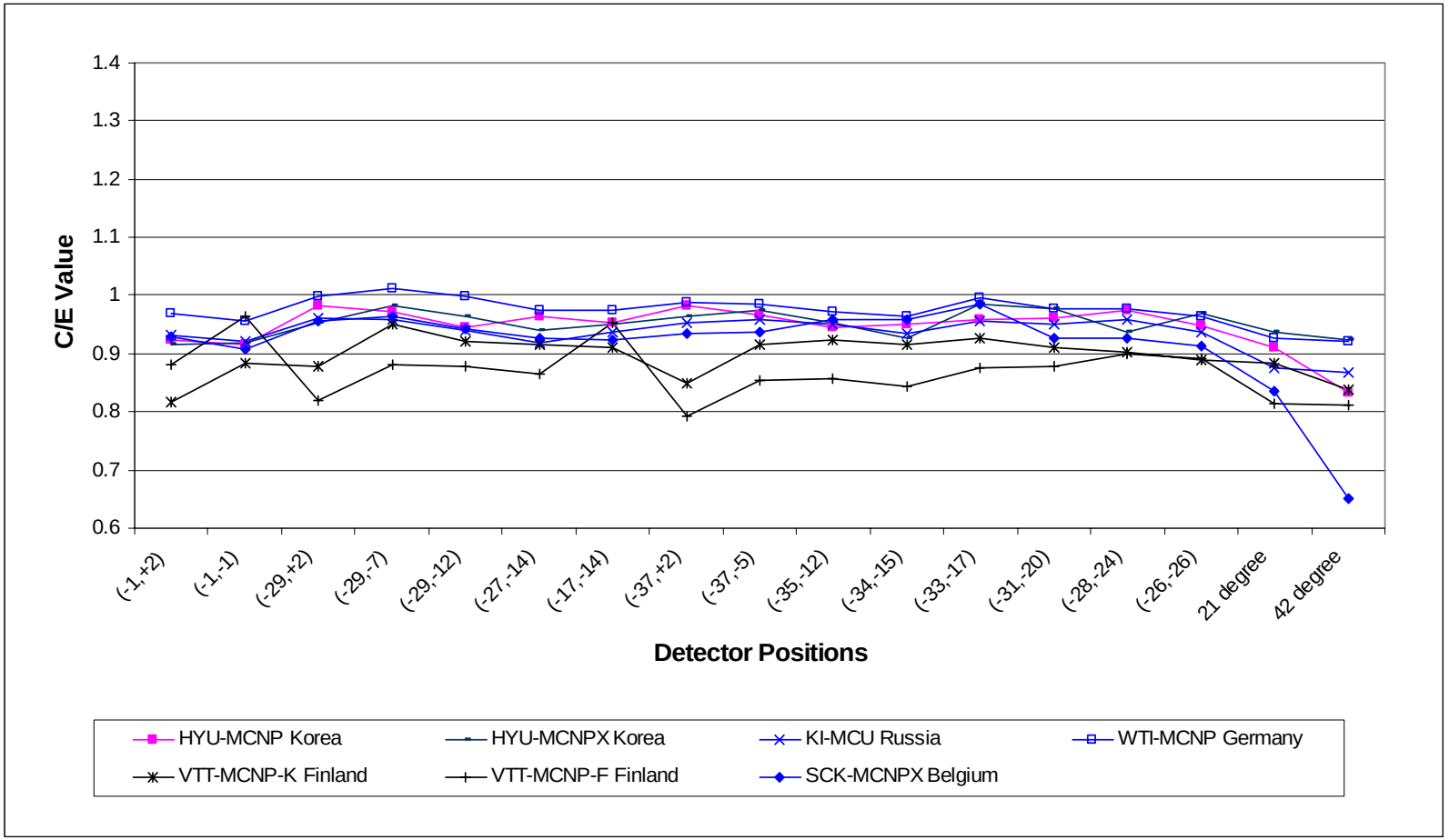

**Figure 4.16. C/E comparison of reaction rates at $^{115}$In(n,n′) detector positions in water zones**

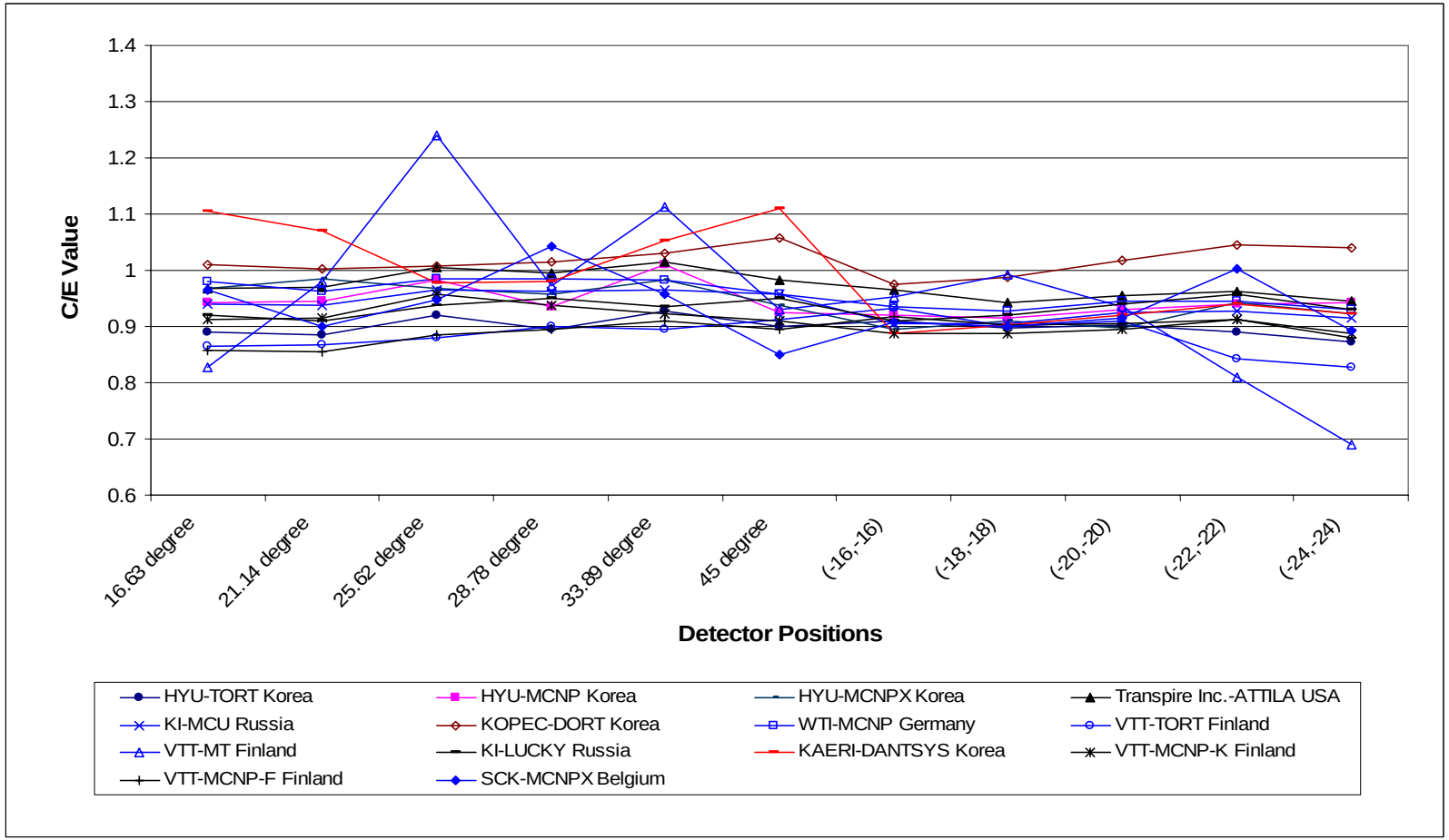

**Figure 4.16(a). C/E comparison of reaction rates at $^{115}In(n,n')$ detector positions in water zones: Deterministic calculation results**

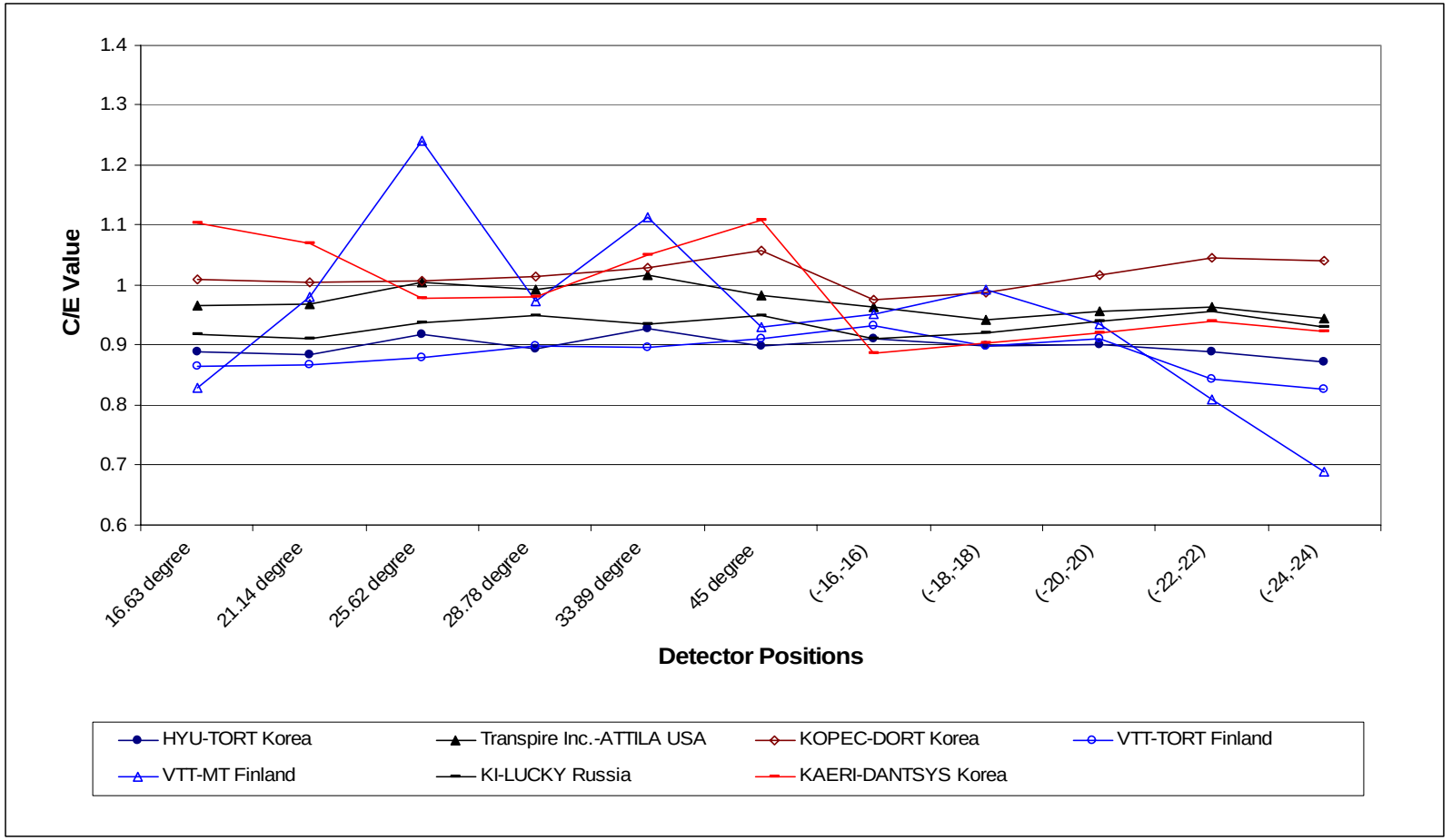

**Figure 4.16(b). C/E comparison of reaction rates at $^{115}$In(n,n′) detector positions in water zones: Monte Carlo calculation results**

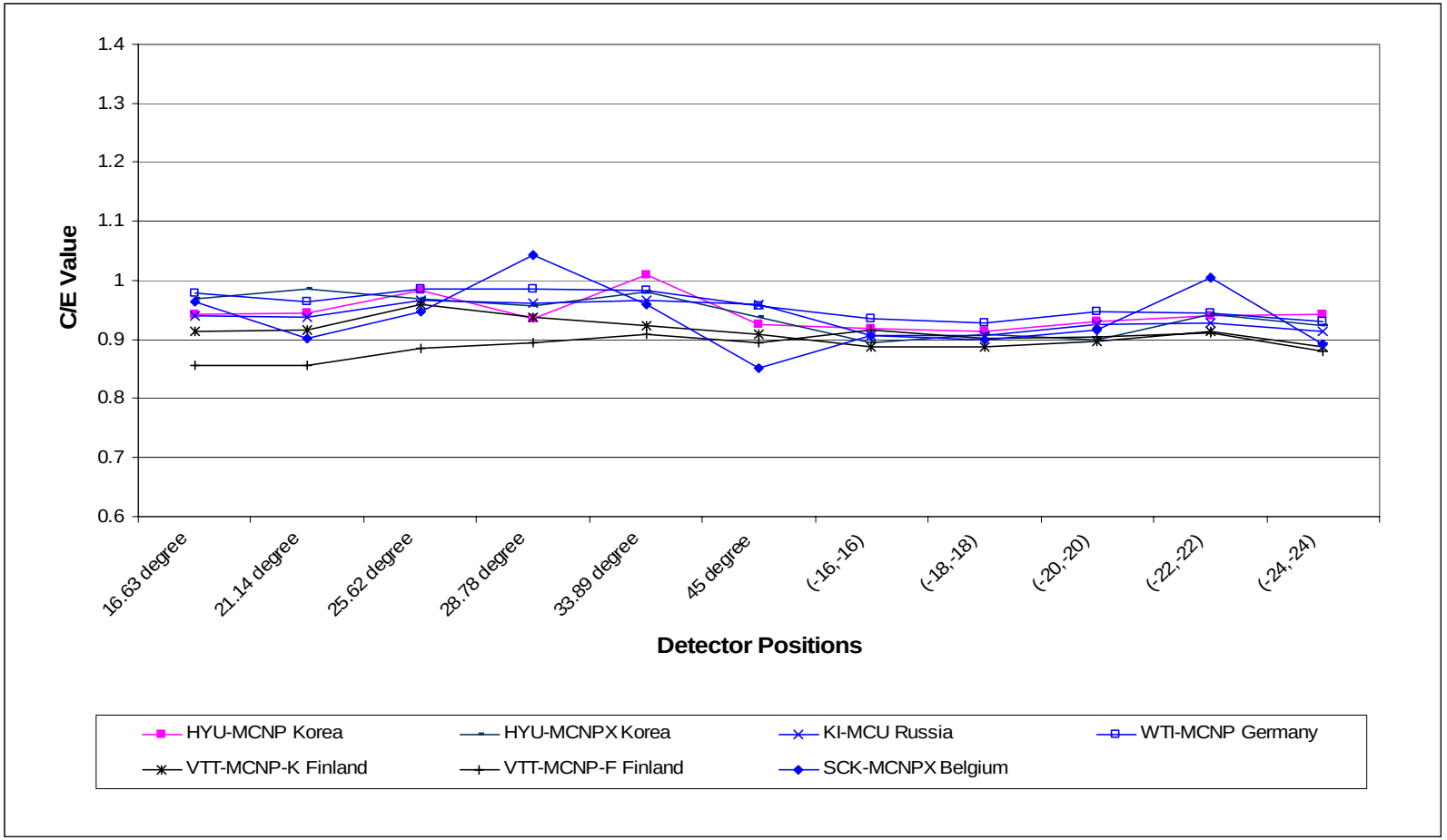

**Figure 4.17. C/E comparison of reaction rates at $^{27}Al(n,\alpha)$ detector positions in stainless steel zones**

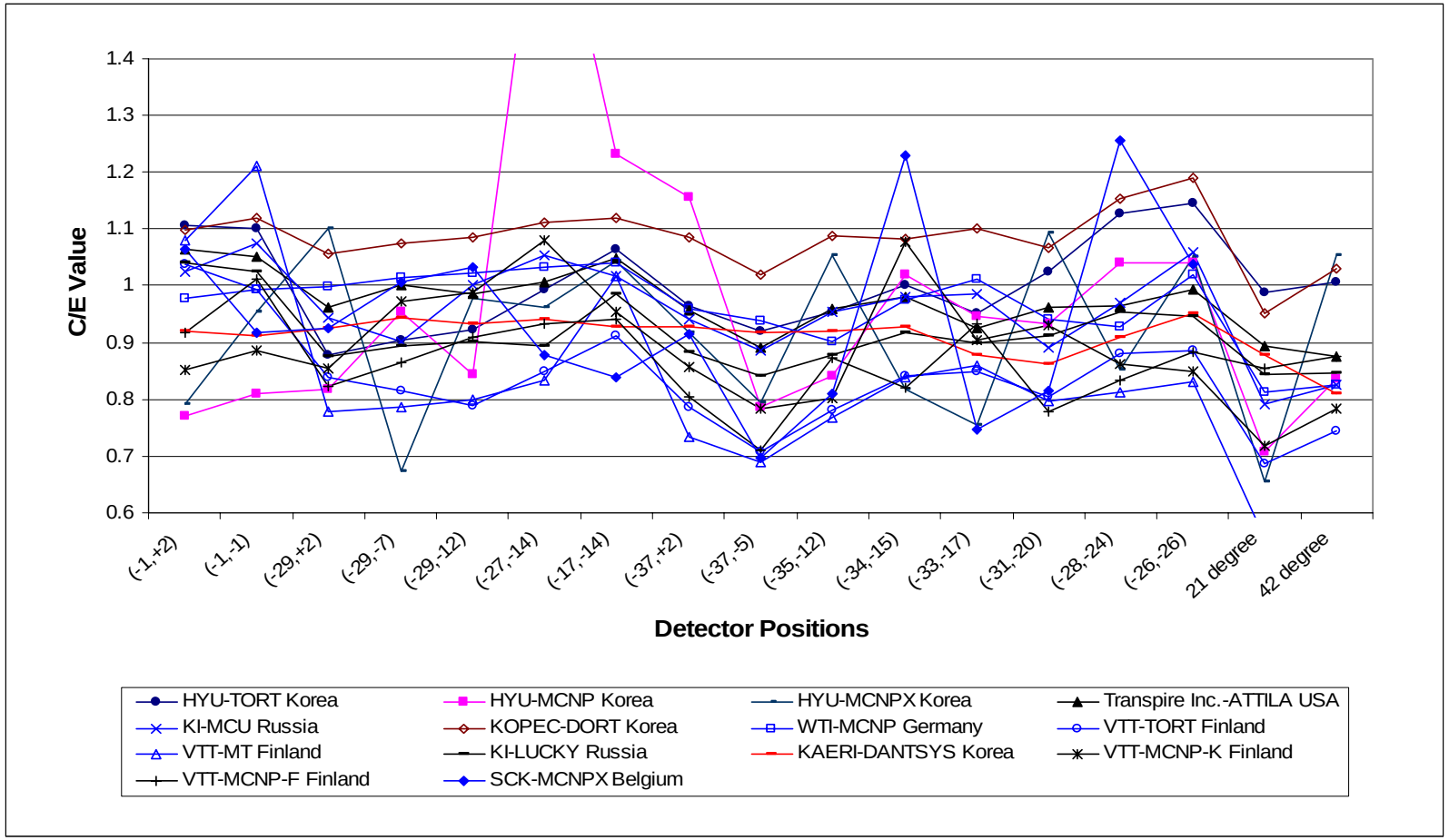

**Figure 4.17(a). C/E comparison of reaction rates at $^{27}Al(n,\alpha)$ detector positions in stainless steel zones: Deterministic calculation results**

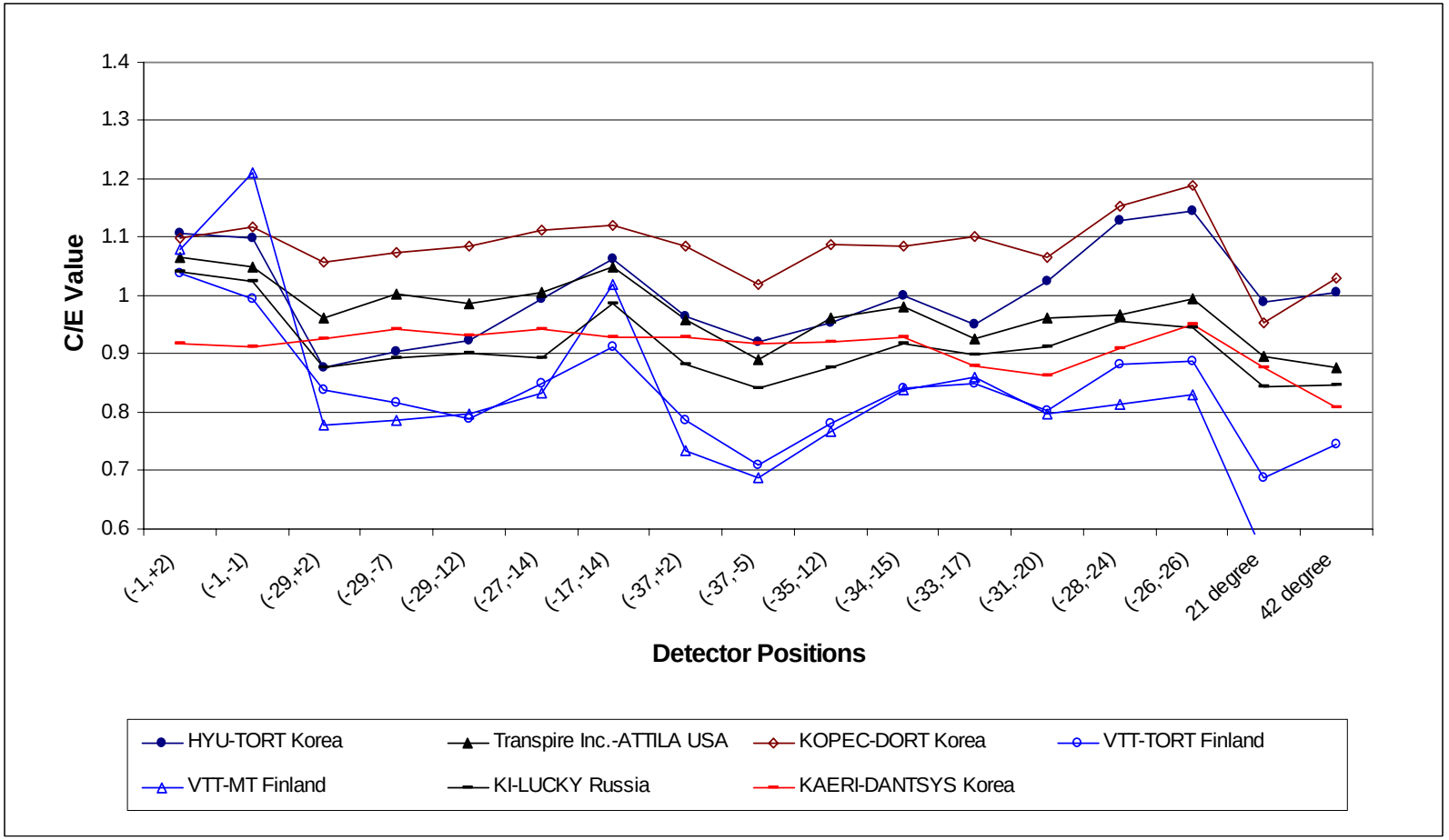

**Figure 4.17(b). C/E comparison of reaction rates at $^{27}Al(n,\alpha)$ detector positions in stainless steel zones: Monte Carlo calculation results**

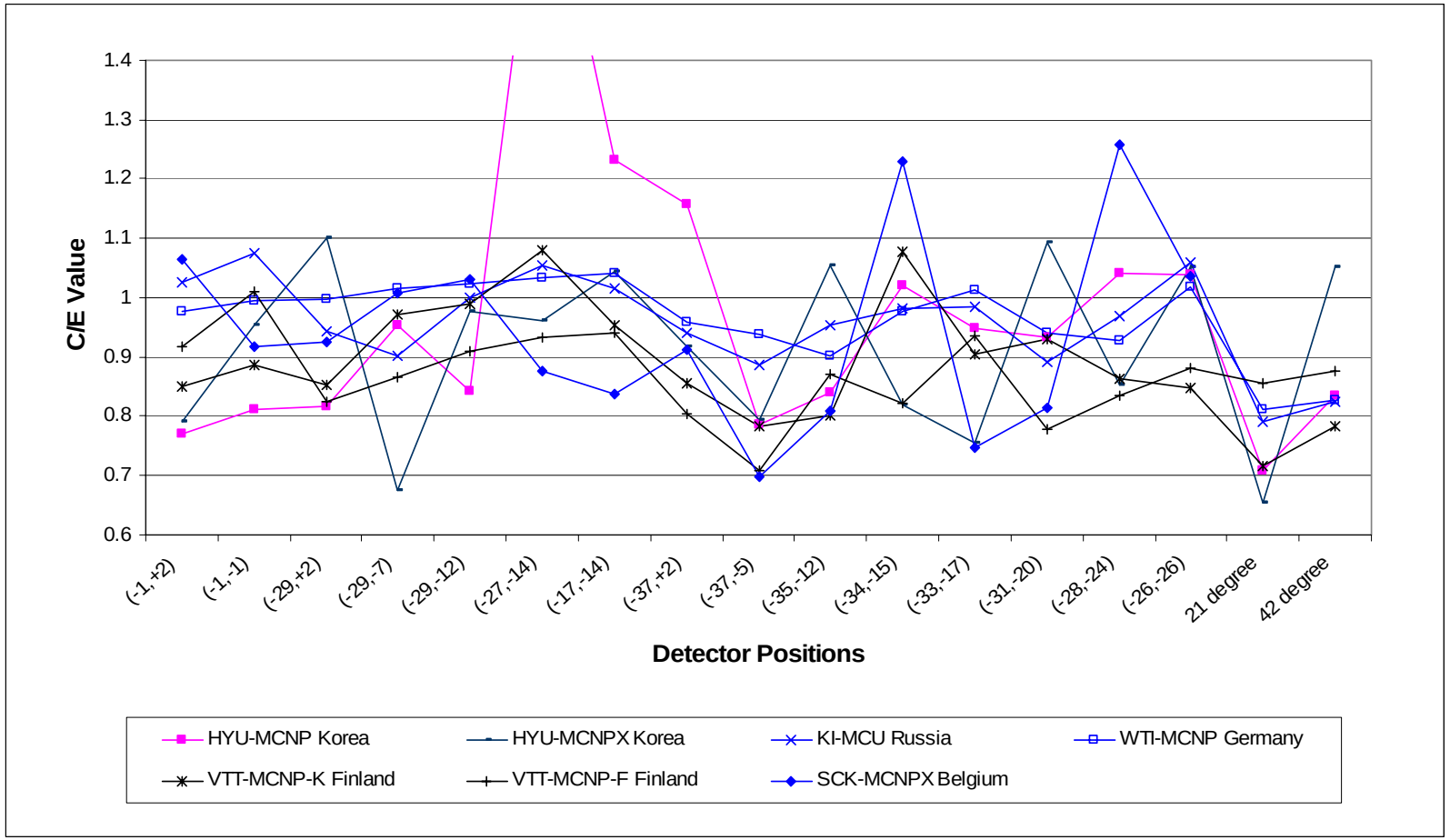

**Figure 4.18. C/E comparison of reaction rates at $^{27}Al(n,\alpha)$ detector positions in water zones**

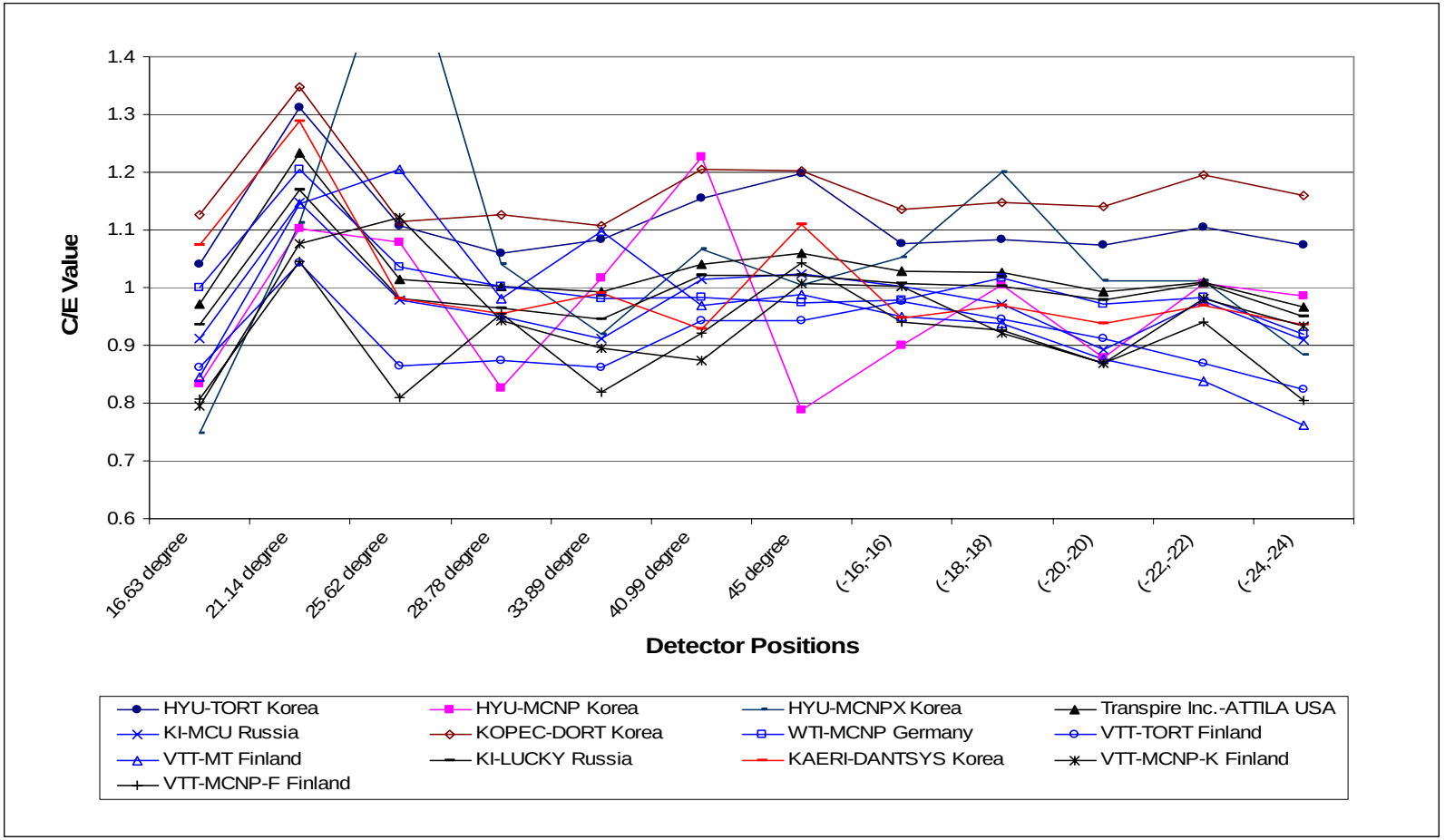

**Figure 4.18(a). C/E comparison of reaction rates at $^{27}Al(n,\alpha)$ detector positions in water zones: Deterministic calculation results**

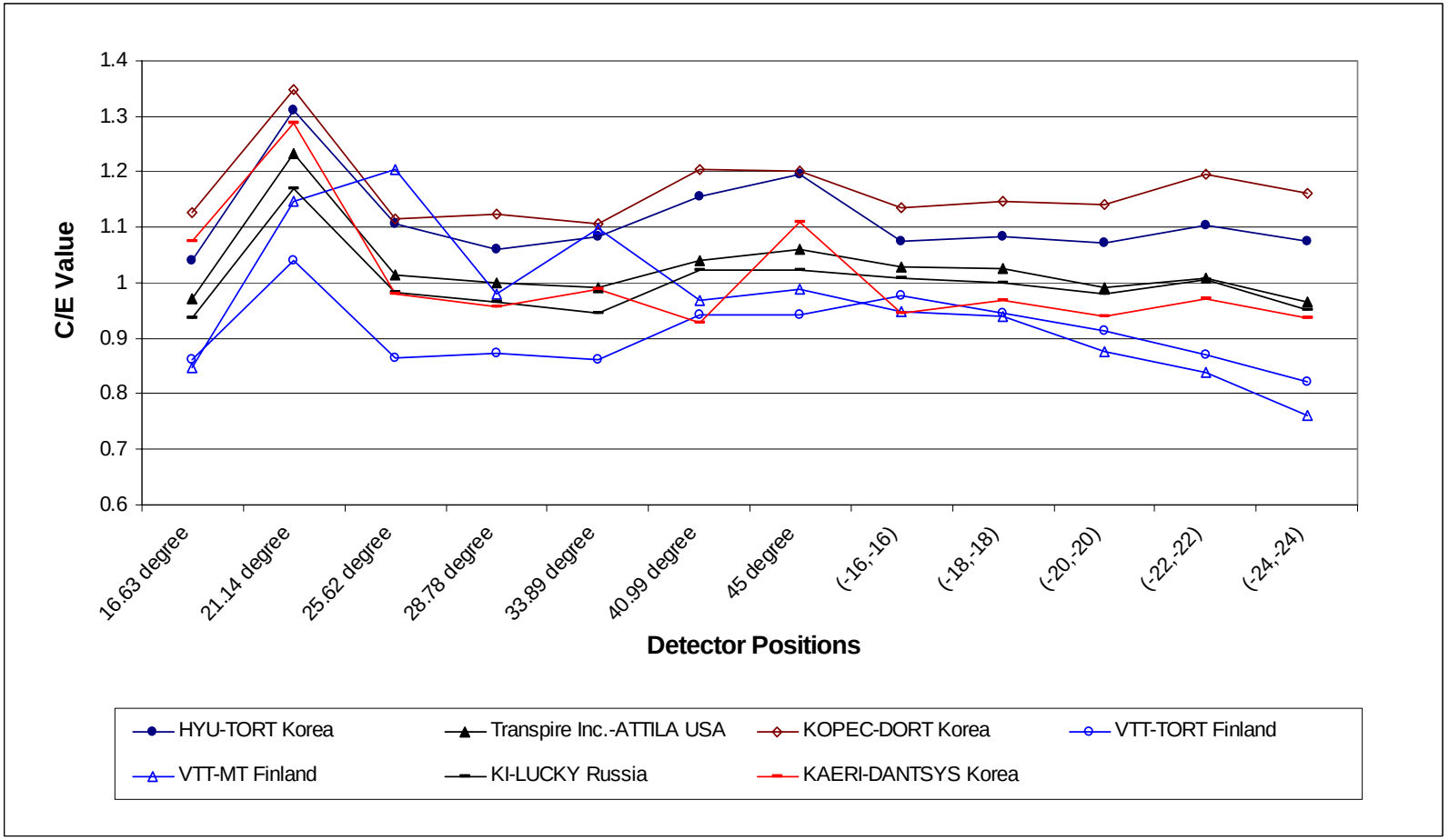

**Figure 4.18(b). C/E comparison of reaction rates at $^{27}Al(n,\alpha)$ detector positions in water zones: Monte Carlo calculation results**

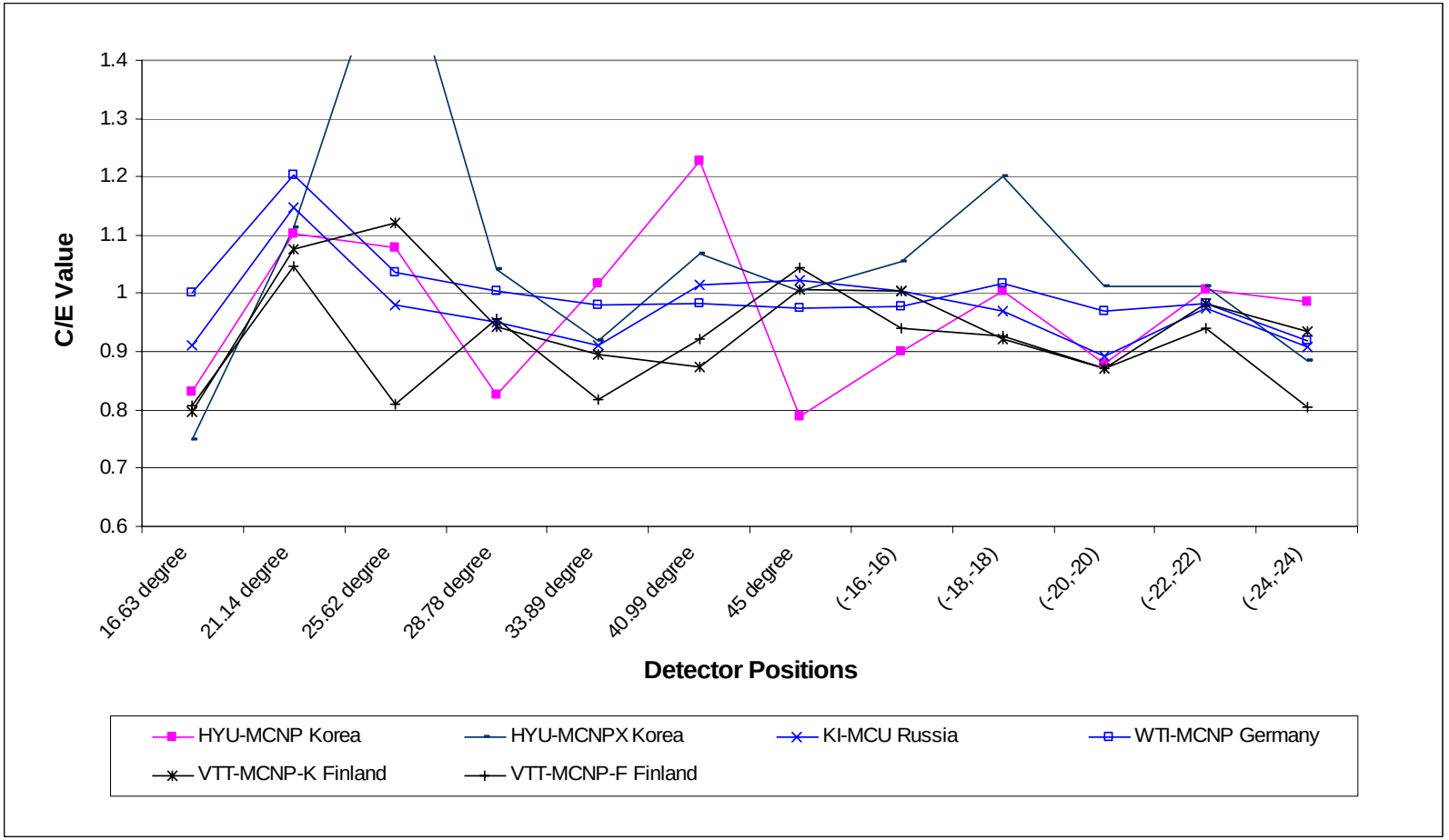

**Figure 4.19. Intercomparison of calculated fluxes E > 0.1 MeV relative to MCU calculations in stainless steel zones**

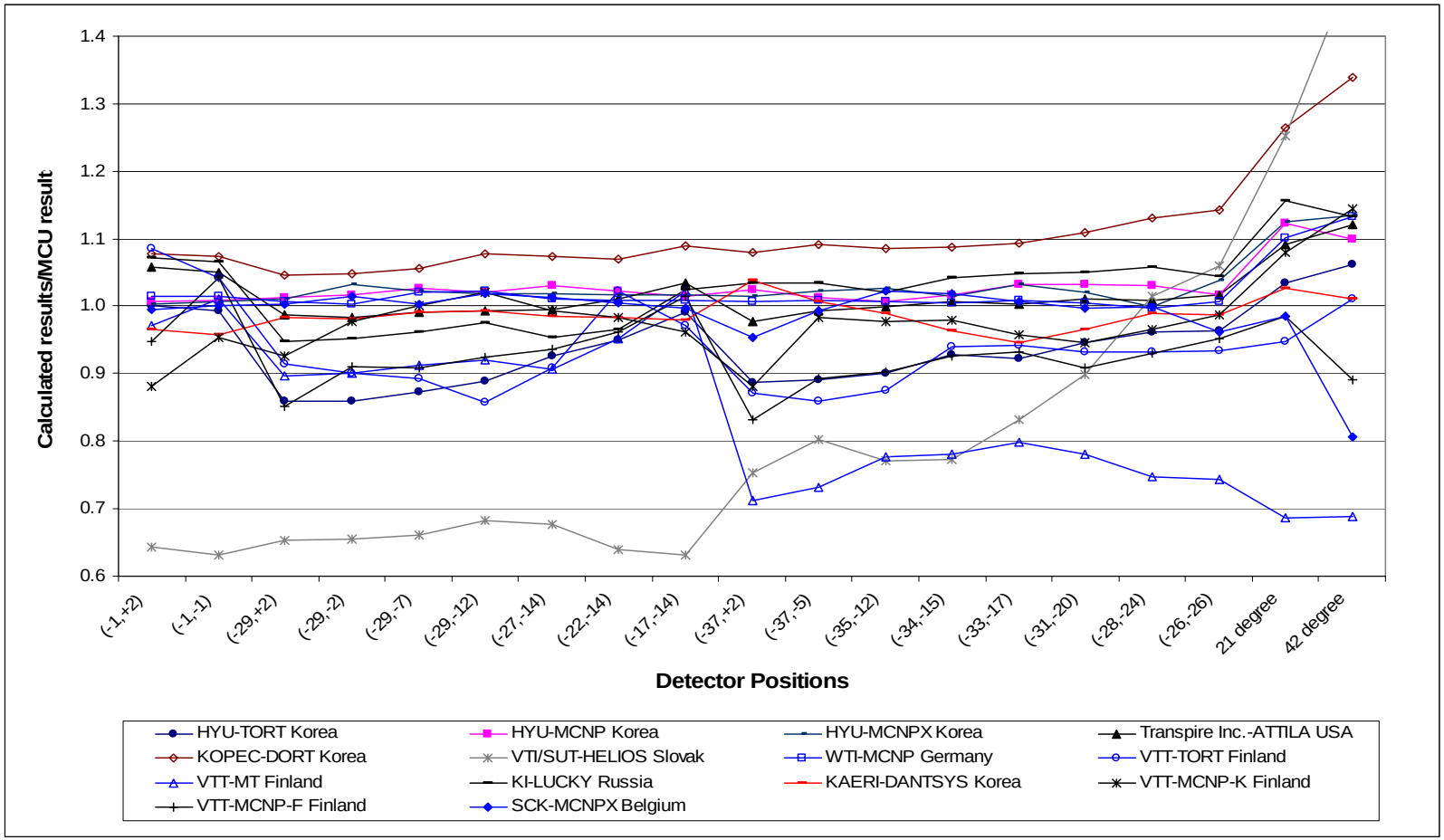

**Figure 4.19(a). Intercomparison of calculated fluxes E > 0.1 MeV relative to MCU calculations in stainless steel zones: Deterministic calculation results**

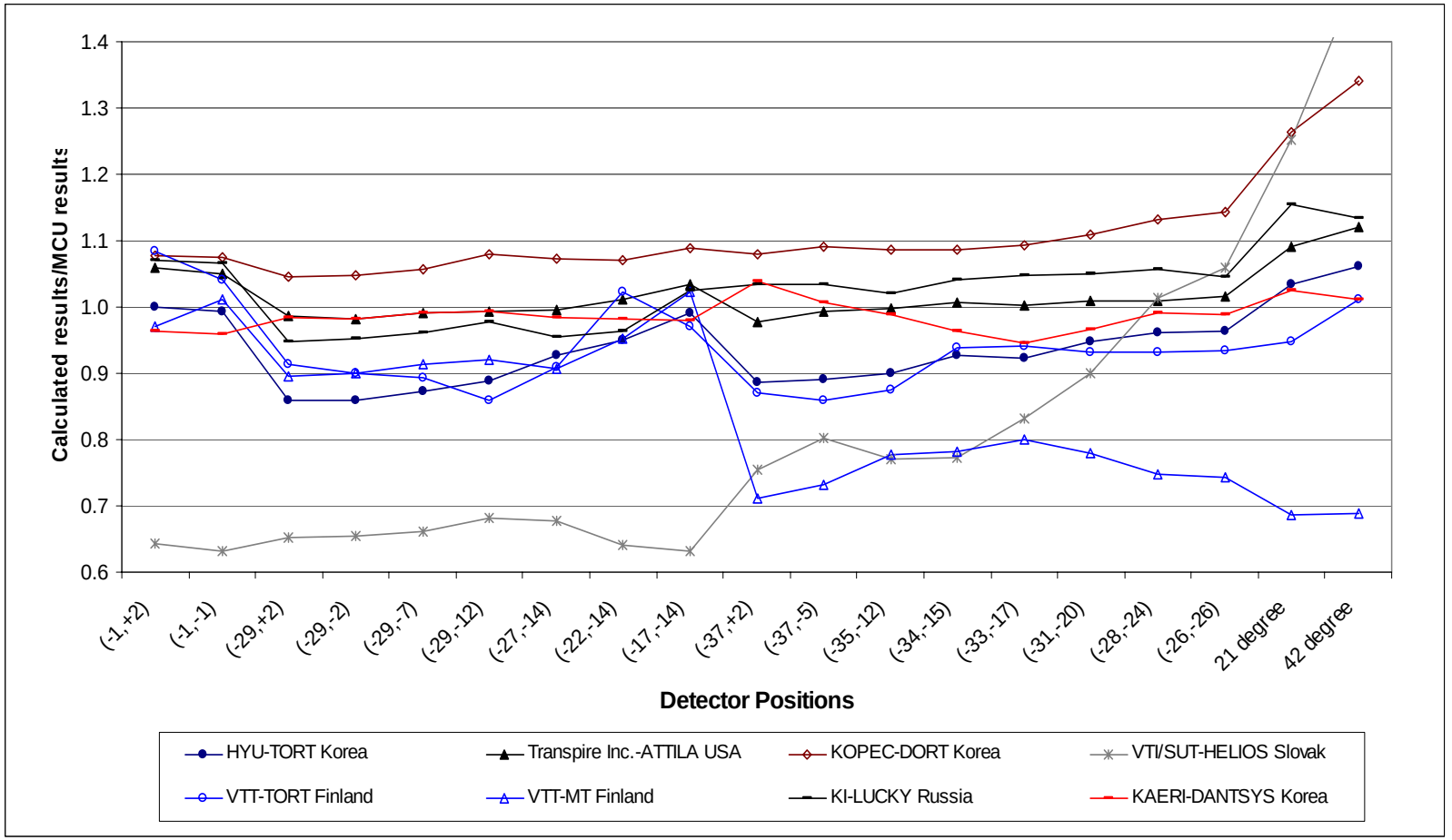

**Figure 4.19(b). Intercomparison of calculated fluxes E > 0.1 MeV relative to MCU calculations in stainless steel zones: Monte Carlo calculation results**

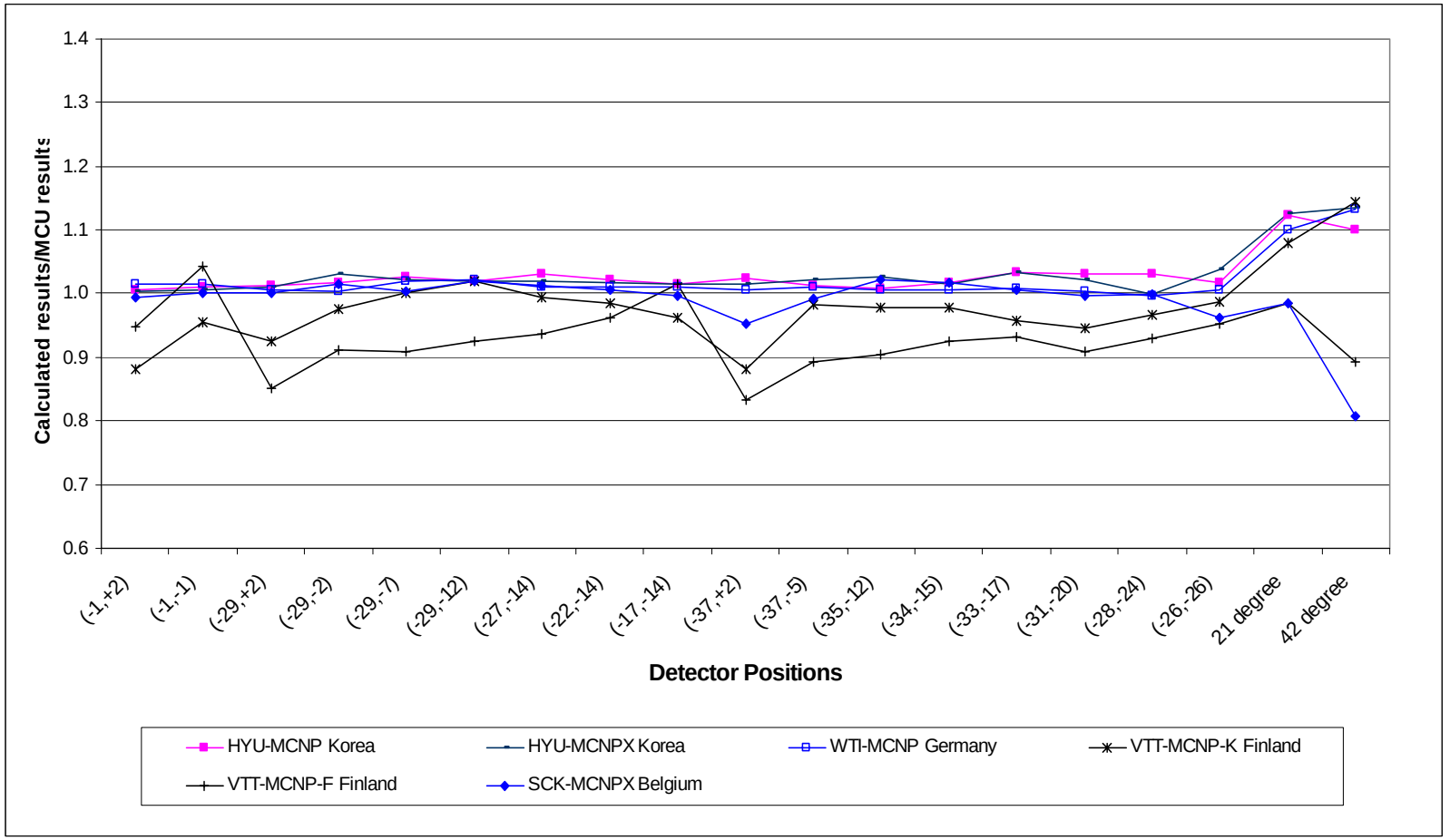

**Figure 4.20. Intercomparison of calculated fluxes E > 0.1 MeV relative to MCU calculations in water zones**

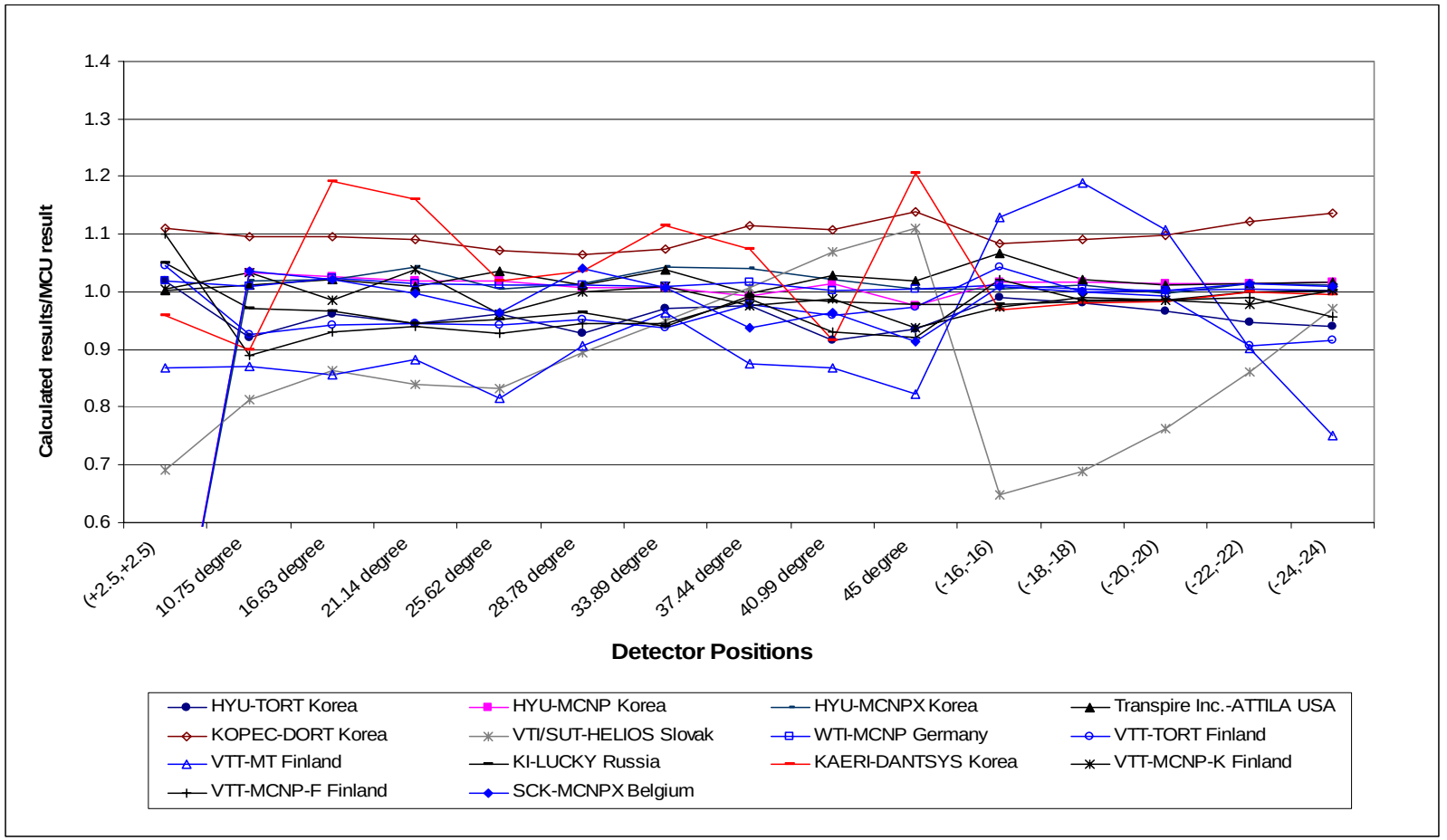

**Figure 4.20(a). Intercomparison of calculated fluxes E > 0.1 MeV relative to MCU calculations in water zones: Deterministic calculation results**

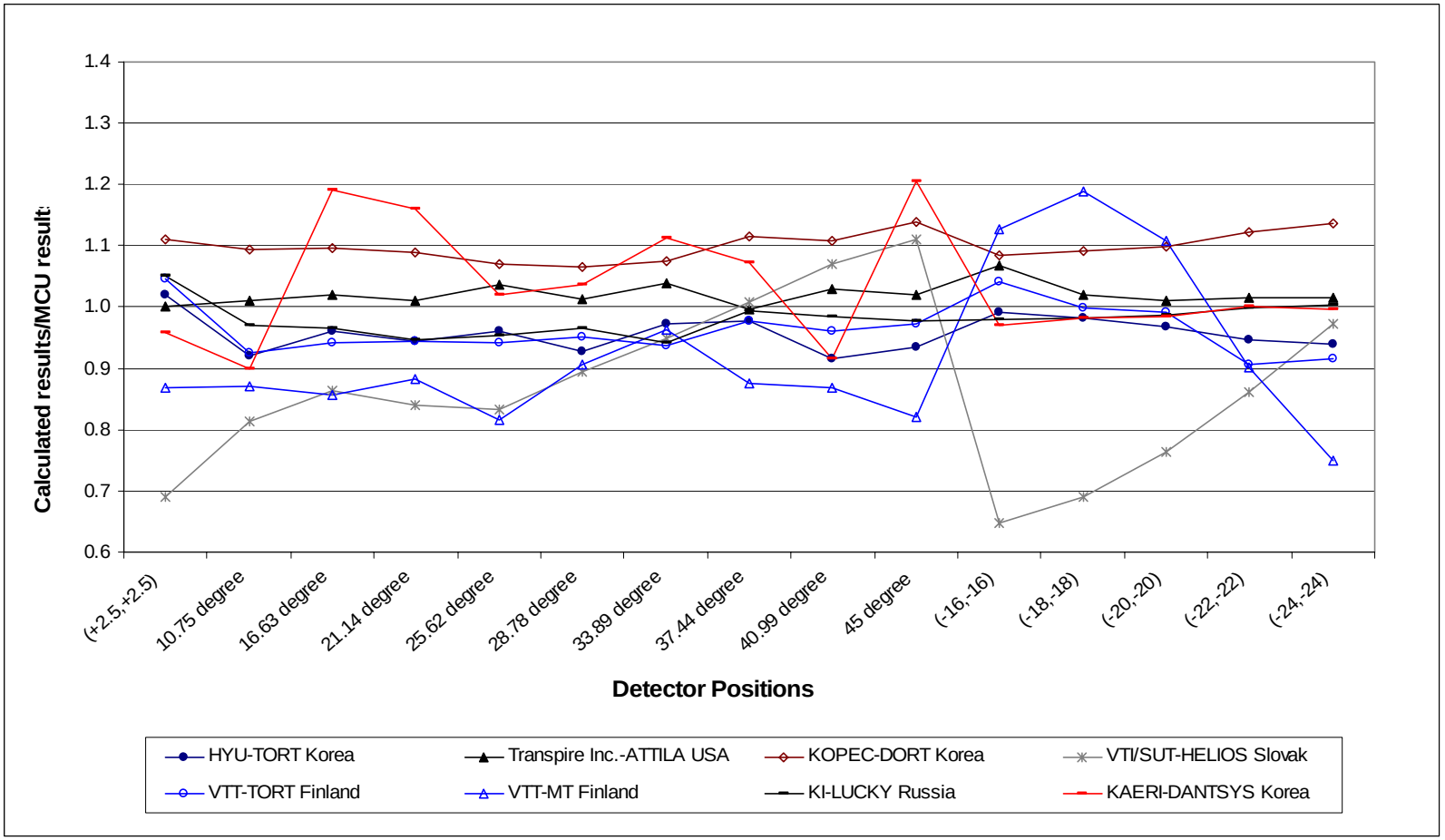

**Figure 4.20(b). Intercomparison of calculated fluxes E > 0.1 MeV relative to MCU calculations in water zones: Monte Carlo calculation results**

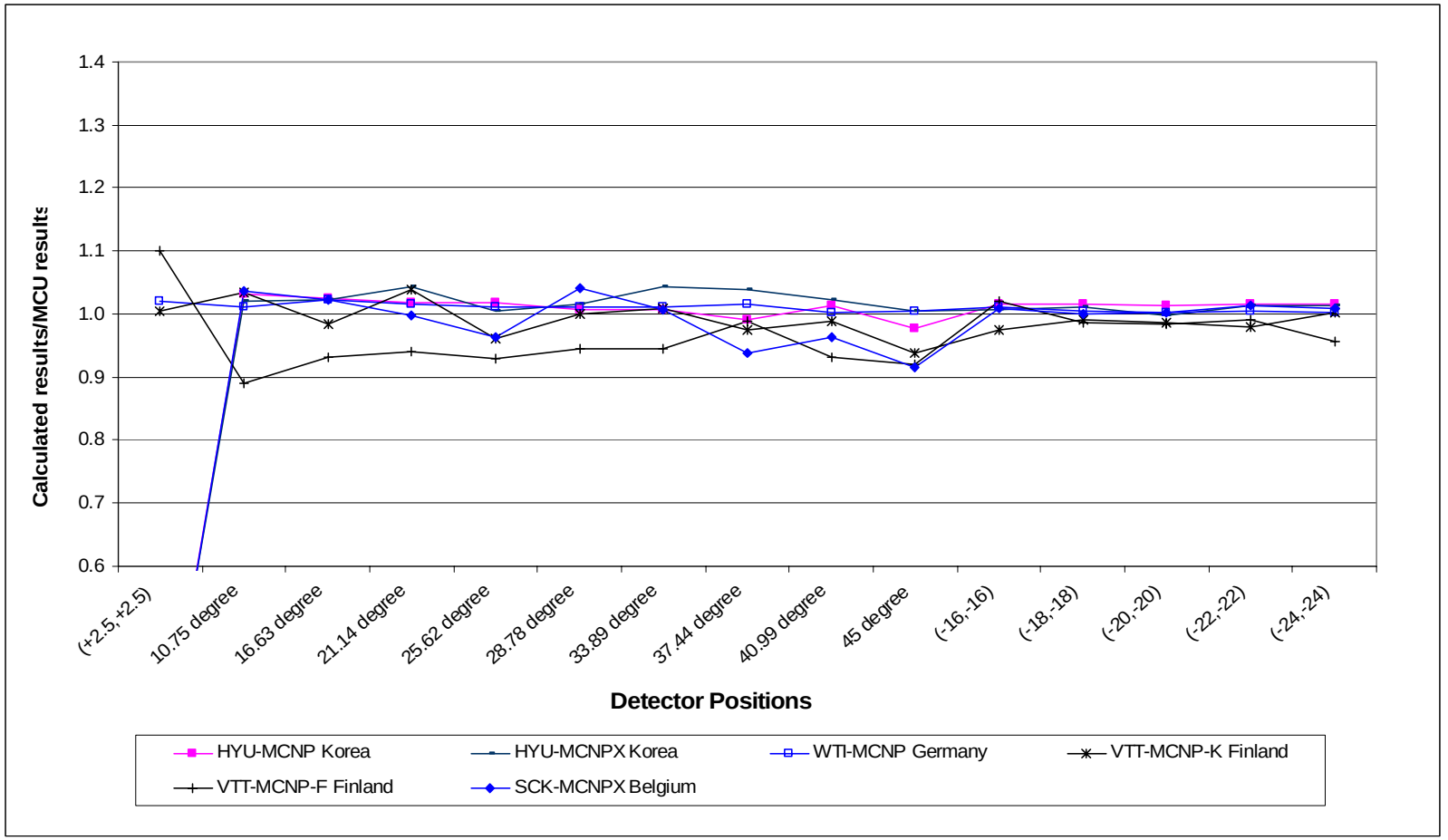

**Figure 4.21. Intercomparison of calculated fluxes E > 1.0 MeV relative to MCU calculations in stainless steel zones**

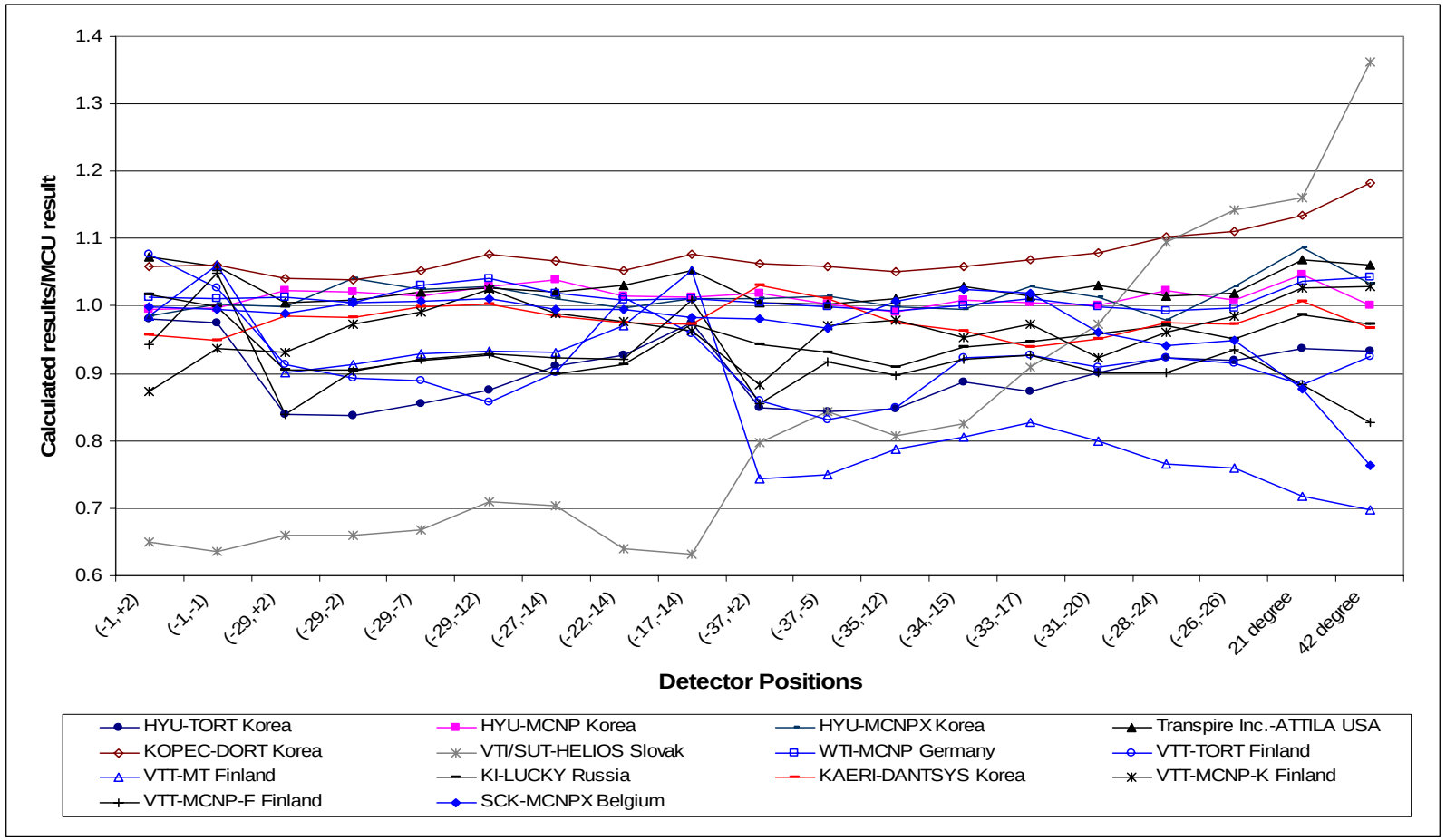

**Figure 4.21(a). Intercomparison of calculated fluxes E > 1.0 MeV relative to MCU calculations in stainless steel zones: Deterministic calculation results**

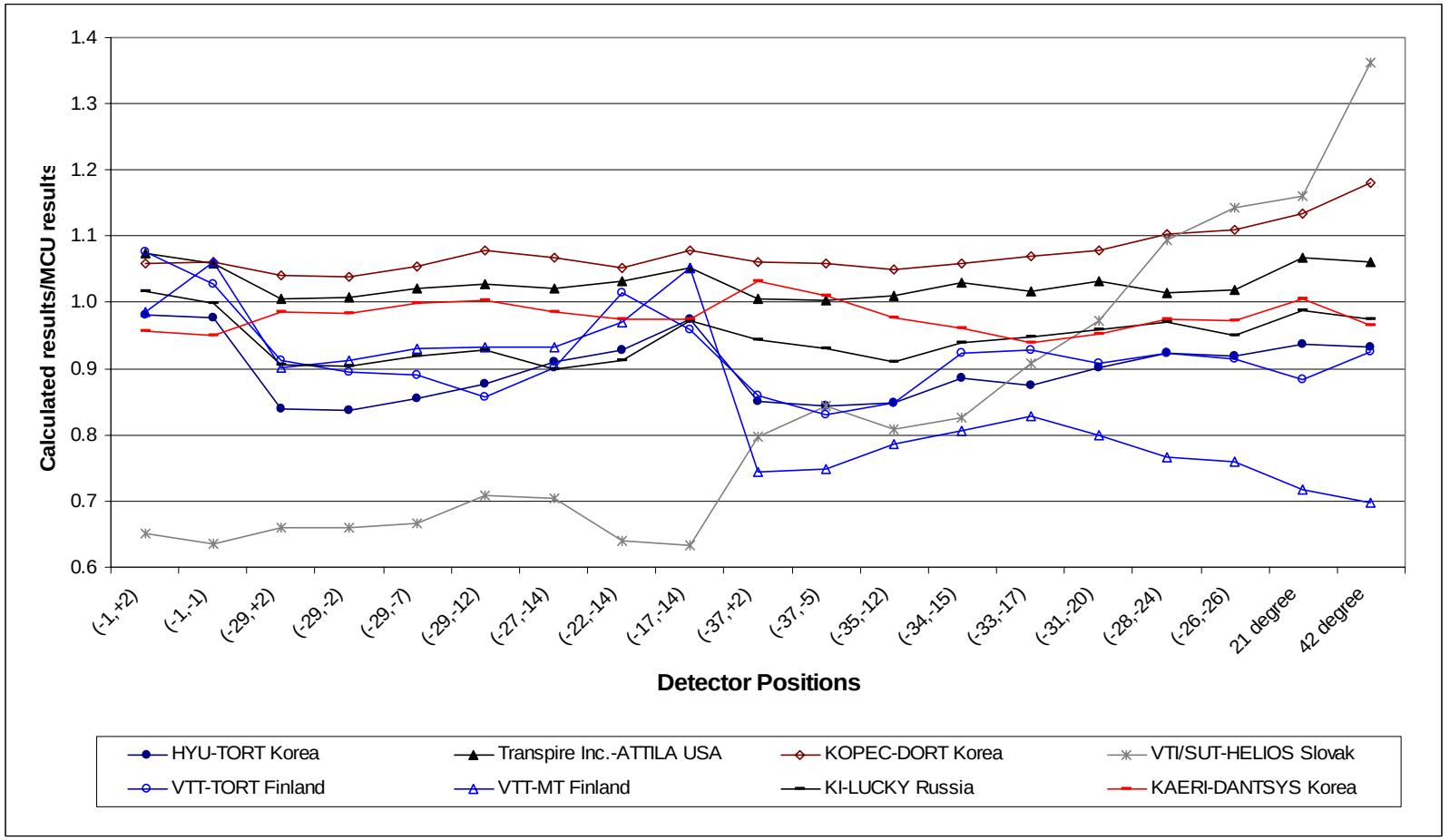

**Figure 4.21(b). Intercomparison of calculated fluxes E > 1.0 MeV relative to MCU calculations in stainless steel zones: Monte Carlo calculation results**

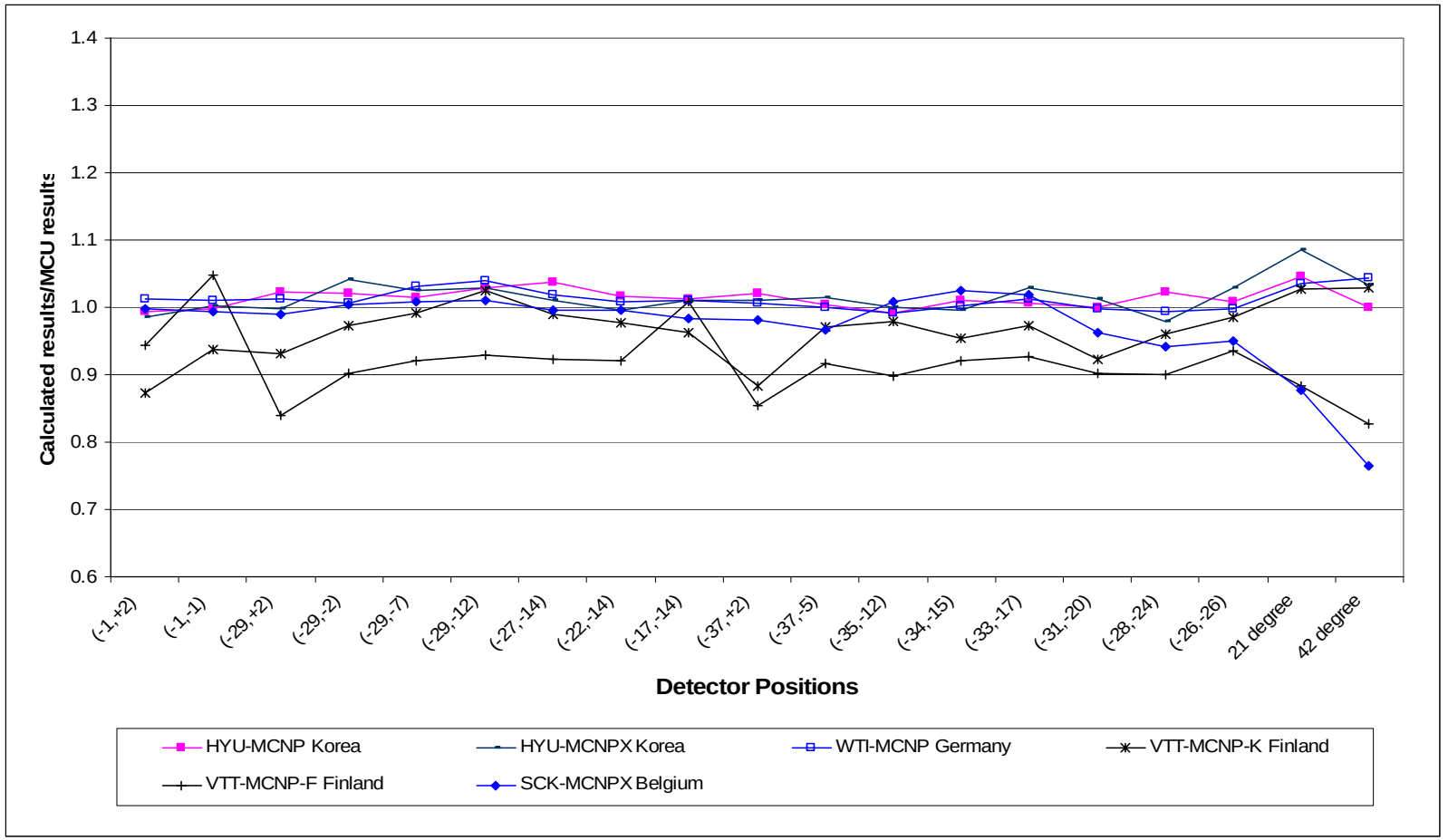

**Figure 4.22. Intercomparison of calculated fluxes E > 1.0 MeV relative to MCU calculations in water zones**

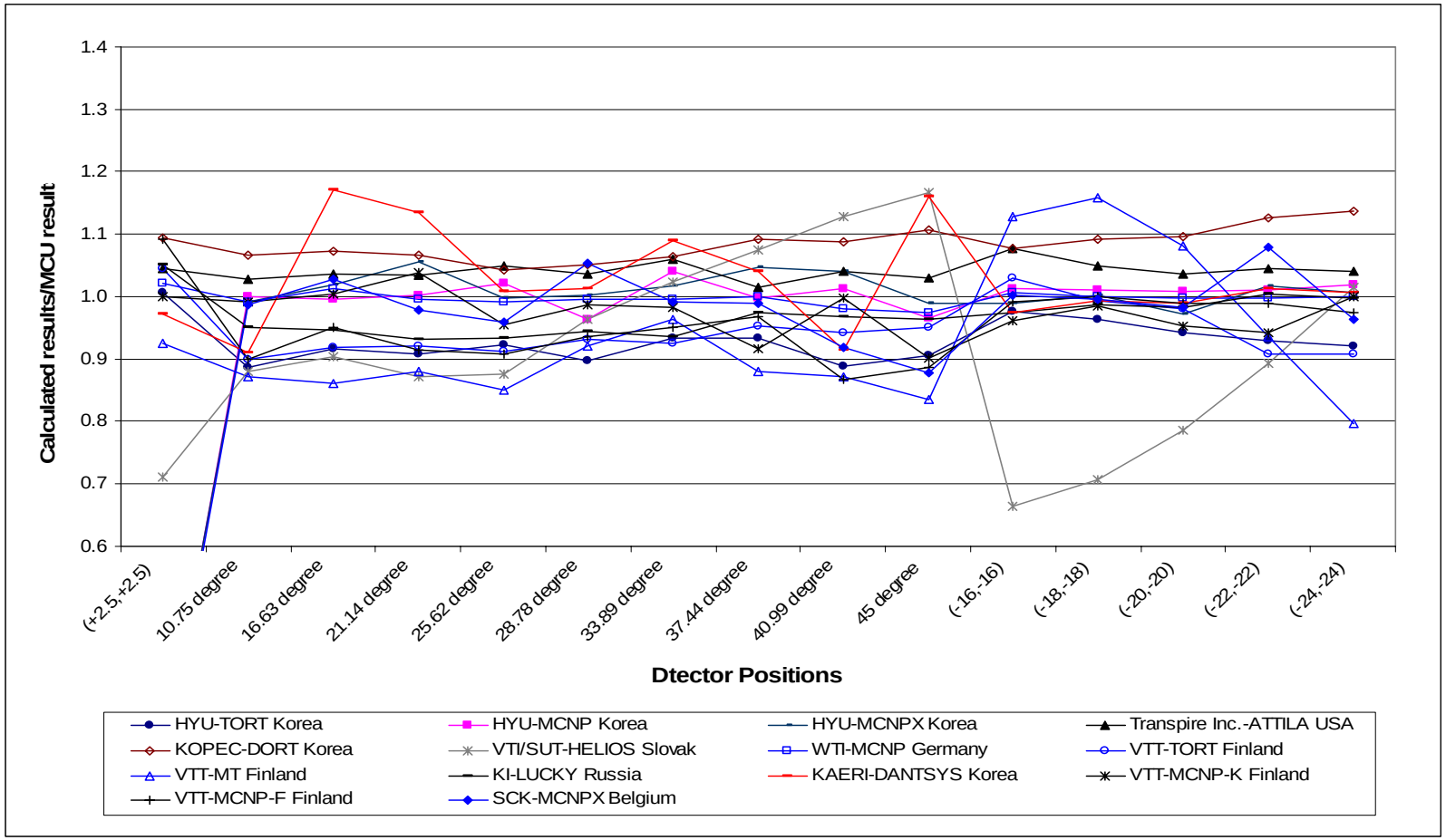

**Figure 4.22(a). Intercomparison of calculated fluxes E > 1.0 MeV relative to MCU calculations in water zones: Deterministic calculation results**

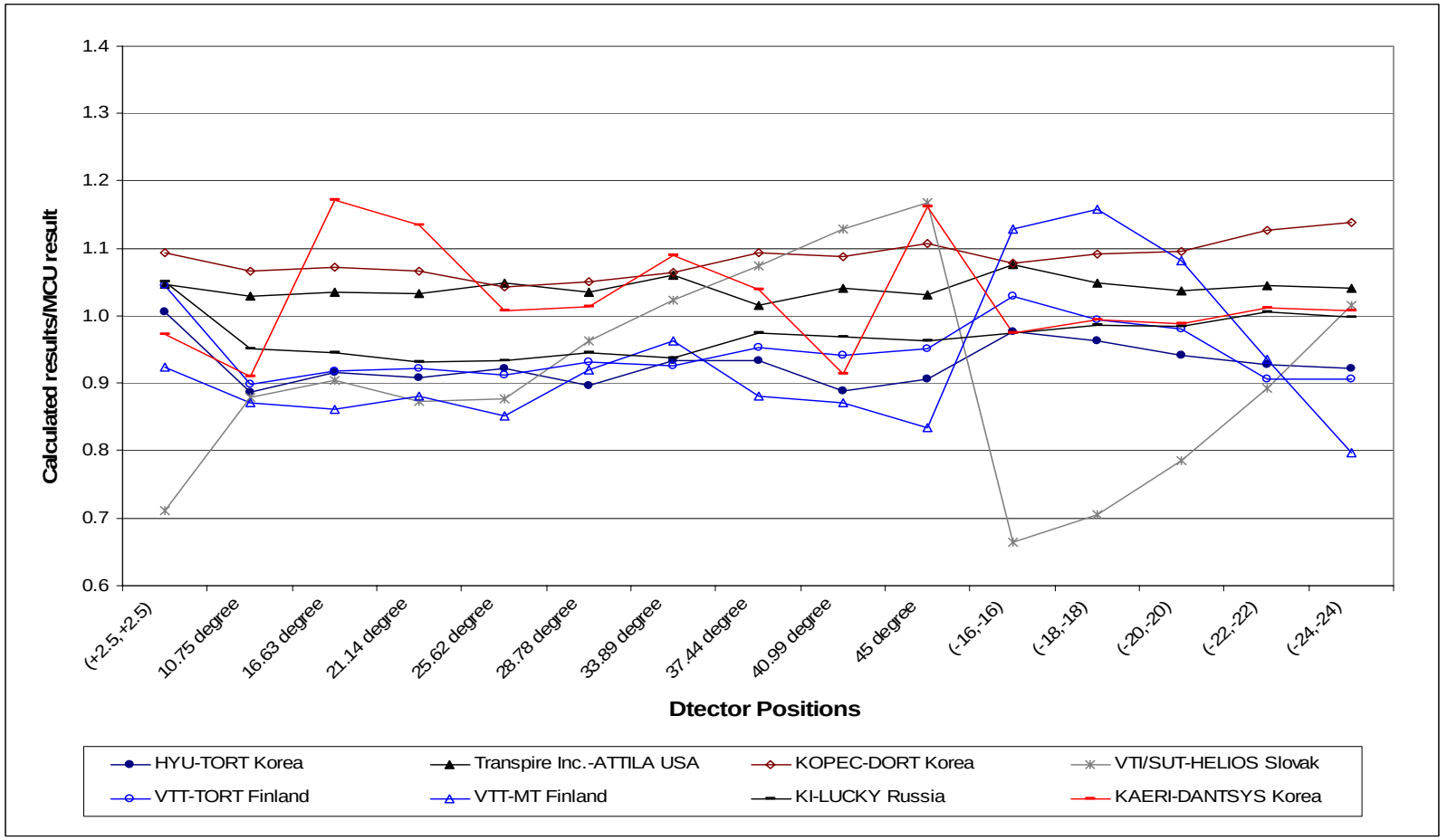

**Figure 4.22(b). Intercomparison of calculated fluxes E > 1.0 MeV relative to MCU calculations in water zones: Monte Carlo calculation results**

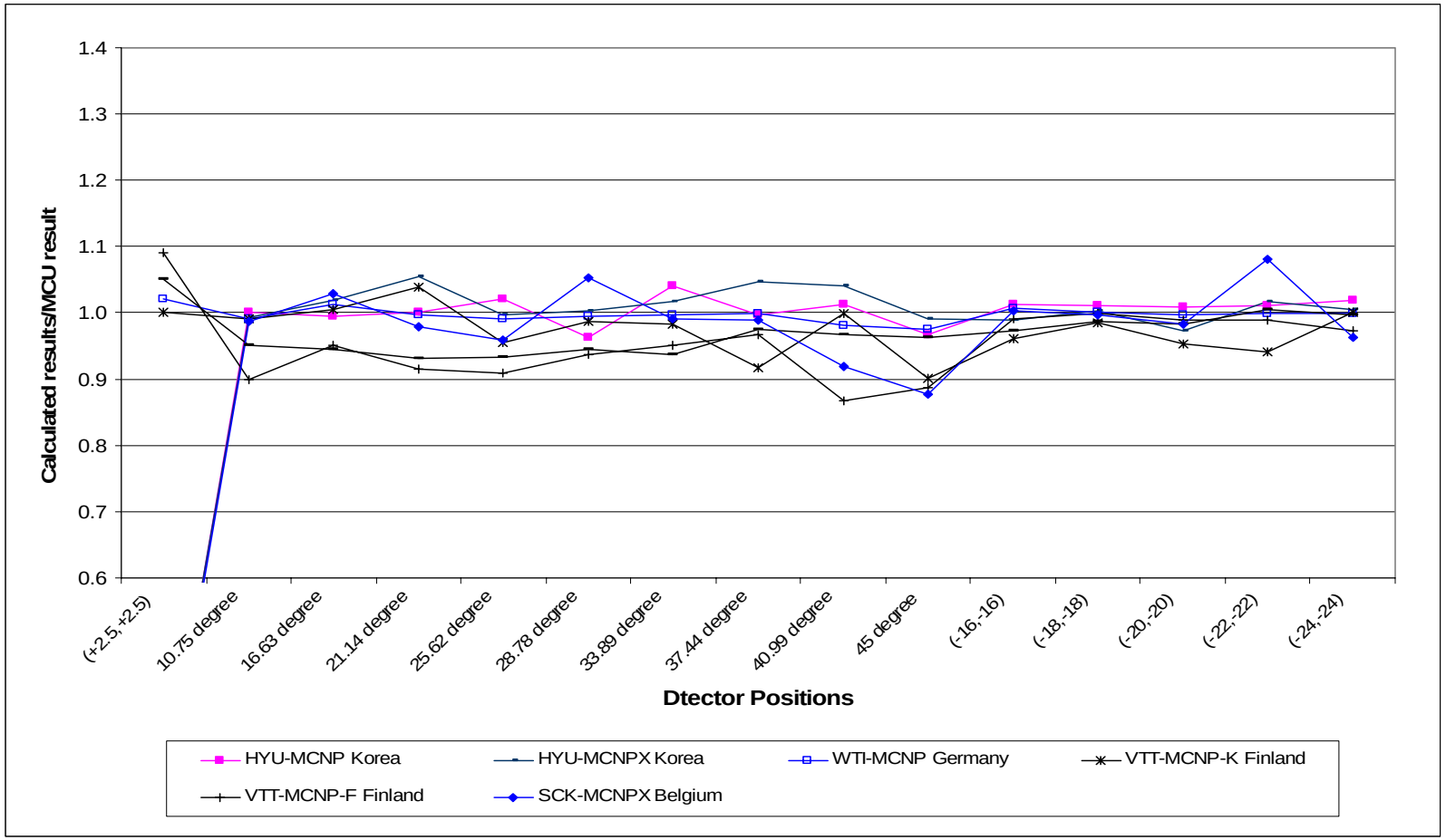

**Figure 4.23. Intercomparison of calculated DPA rates relative to MCU calculations in stainless steel zones**

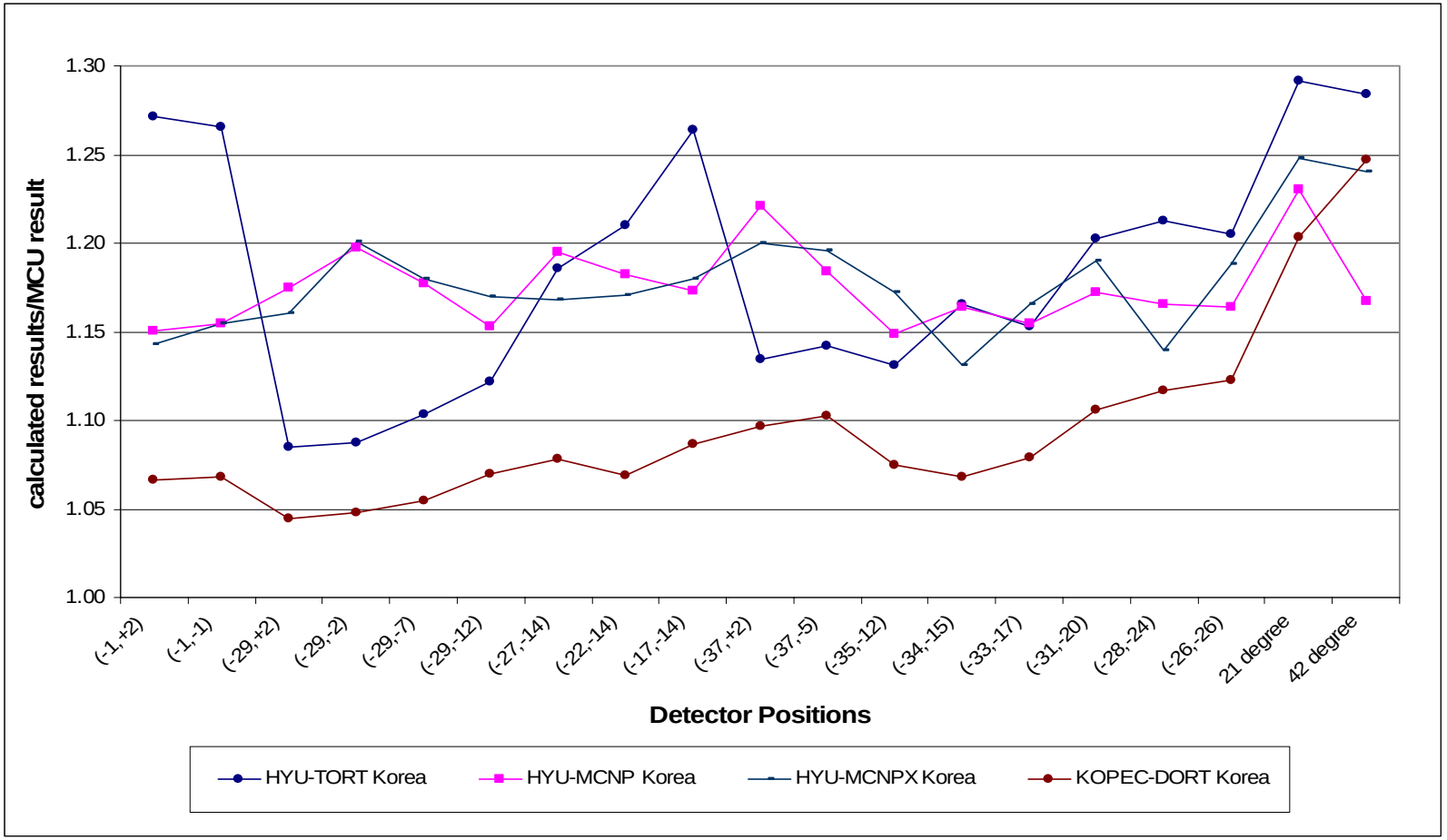

**Figure 4.24. Intercomparison of calculated DPA rates relative to MCU calculations in water zones**

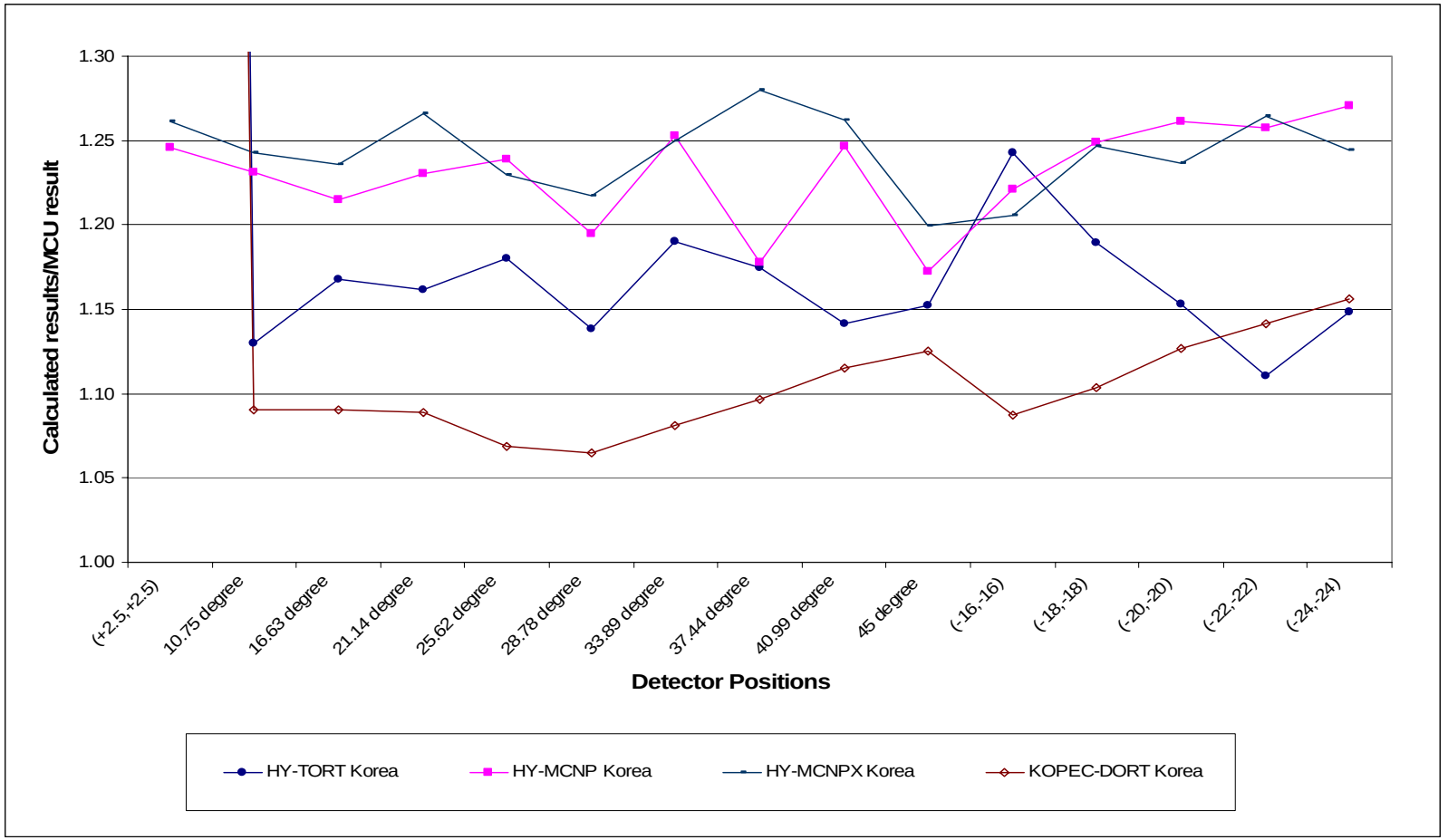

*Appendix A*

# BENCHMARK SPECIFICATION

# VENUS-2 MOX-FUELLED REACTOR DOSIMETRY CALCULATIONS

***Benchmark Specification***

*Chi Young Han, Chang-ho Shin, Hong-Chul Kim and Jong Kyung Kim*
Hanyang University, Republic of Korea

*Nadia Messaoudi*
SCK•CEN, Belgium

*Byung-Chan Na*
OECD/NEA

## I. General comments

In this benchmark exercise, the goal is to test the current state-of-the-art computation methods of calculating neutron flux to reactor components against the measured data of the VENUS-2 MOX-fuelled critical experiments. The measured data to be used for this benchmark are the equivalent fission fluxes measured using $^{58}$Ni(n,p), $^{115}$In(n,n′), $^{103}$Rh(n,n′), $^{64}$Zn(n,p), $^{237}$Np(n,f) and $^{27}$Al(n,α) detectors at several important positions on the core mid-plane of the reactor [1]. The present benchmark is therefore defined to calculate reaction rates and corresponding equivalent fission fluxes measured on the core mid-plane at specific positions outside the core of the VENUS-2 MOX-fuelled reactor. This is a follow-up exercise to the previously completed $UO_2$-fuelled VENUS-1 two-dimensional and VENUS-3 three-dimensional exercises [2]. The use of MOX fuel in LWRs presents different neutron characteristics, this being the main interest of the current benchmark as compared to the previous ones. For the current benchmark, a full set of the source term is not provided and the participants are invited to calculate their own source term for the subsequent calculations. However, the fission rate distribution of 121 fuel pins measured on the core mid-plane and the axial fission rate distribution of six fuel pins are given for the participants to be able to obtain as exact a source term as possible. The reference core average fission rate and corresponding power should be used by the participants to define the fission source for neutron transport calculations.

As with the VENUS-1 and VENUS-3 benchmarks, this is a “blind” test, hence the measured values of the reaction rates and corresponding equivalent fission flux at specified VENUS-2 locations are not revealed to the participants *a priori* but will be provided when benchmark results are analysed.

A complete specification of the VENUS-2 problem is given in *Appendix A.1: VENUS-2 Core Description and Qualification* [1]. The information given fully specifies all geometry and material data required in developing the detailed 3-D computational model of the 1/4 fraction of the VENUS-2 reactor. As the previous VENUS-3 benchmark demonstrated the precision of results obtained using three-dimensional calculations, the participants are invited to apply 3-D transport methods for the present benchmark. Though full 3-D calculations are recommended for obtaining the requested results, this document also provides values of experimentally measured vertical bucklings in the VENUS-2 configuration of the VENUS reactor. These vertical bucklings should be used as input data only if 2-D neutron transport calculations are applied.

## II. Co-ordinate systems

The co-ordinates of the measurement positions are given in three different co-ordinate systems (see Figure 2 in Appendix A.1):

- (x,y) co-ordinates with respect to the reactor grid (used in the experiments);
- (x,y) co-ordinates with respect to the core centre (for use in calculation model);
- (r,θ) co-ordinates with respect to the core centre (for use in calculation model).

The origin of the (x,y) co-ordinates with respect to the reactor grid is located in the inner baffle at a point 2.5 pitches (1 pitch = 1.26 cm) to the left and 2.5 pitches below the geometric centre of the core. Therefore, the origin of the (x,y) co-ordinates with respect to the reactor grid are at $X' = -3.15$ cm and $Y' = -3.15$ cm from the geometric centre of the core. The south-west quadrant of the core to be considered in the calculations is thus defined by the ranges $-27 < x < +2$ and $-27 < y < +2$, where the limits represent cell centre-to-centre distances in units of pitches. Positions exterior to the core may also be located by extending the grid to include the outer baffle, barrel and water.

## III. Preparation of source term

The 1/8 of the core comprises 325 fuel rods in which the fission rates of 121 fuel rods (41 3/0 $UO_2$, 35 4/0 $UO_2$ and 45 2/2.7 MOX pins) were directly measured after an irradiation of 13.5 h at 90% of the VENUS maximum power. The experimental data were taken from the gamma activity of the $^{140}La$ (fission yields ~6.3% for $^{235}U$ and ~5.5% for $^{239}Pu$, energy ~1.6 MeV, effective half-life ~12.8 d). The fission rates of 204 fuel rods were interpolated from the measured values. The corresponding measured and interpolated fuel pin positions can be found in Figure 1. Seven additional fuel pins measured were located in symmetric positions out of 1/8 of the core. The measured fission rate values were arbitrarily normalised to a core averaged fission rate = 1 fission/sec/fuel cell (or to a total core fission rate of 2 560 fissions/sec). The fission rate distribution in 1/8 of the VENUS-2 core is given in Table 1 [3]. The reported uncertainty of the measured data (1σ) is ±1.0% in $UO_2$ and ±1.5% in MOX pins and that of the interpolated data (1σ) is ±2%.

In addition, the fission rate distributions of six fuel pins (two 3/0 $UO_2$, two 4/0 $UO_2$ and two 2/2.7 MOX pins) were measured *axially* by γ-scanning after an irradiation of 8 h at 90% of the VENUS maximum power. According to the (x,y) co-ordinates with respect to the reactor grid, the axially measured pin positions are (-27,-12), (-22,-2), (-15,+2), (-13,-12), (-11,+2) and (-6,-6). If the (x,y) co-ordinates with respect to the core centre are used, they are in positions (-37.17,+18.27), (-30.87,+5.67), (-22.05,+0.63), (-19.53,+18.27), (-17.01,+0.63) and (-10.71,+10.71) in cm. The axial measurements were carried out at 21 different vertical planes along 50 cm of the fuel pin length (from 105 cm to 155 cm): starting from 110 cm, and at every 2 cm upwards to 150 cm. Originally, this measurement was employed in order to obtain vertical buckling representative of the core. The axially measured fission rate values of the six fuel pins are arbitrarily normalised to one (1) and given in Table 2. The measured fission rate value at 132 cm of the MOX pin (-27,-12) and those at 114 and 148 cm of the MOX pin (-22,-2) were not available, and the values given in the table for these three positions are interpolated values [4,5]. The reported uncertainties of the axially measured data (1σ) of pin power distributions of the six fuel pins are ±2.2% in $UO_2$ and ±3.4% in MOX pins.

The average fission rate in the core corresponding to absolute reference irradiation is 1.87E+08 fissions/cm/sec at the mid-plane. From this, we can deduce a value of 4.596E+12* fissions/sec/core quadrant as corresponding to 100% power and 7.181E+09** as a multiplication factor for converting the arbitrary source employed in the calculations to the source at 100% power. These average fission rates correspond to a power of 595 Watts.

## IV. Results to be provided and their format

As mentioned, the equivalent fission fluxes at several important positions on the core mid-plane of the reactor were measured using $^{58}$Ni(n,p), $^{115}$In(n,n′), $^{103}$Rh(n,n′), $^{64}$Zn(n,p), $^{237}$Np(n,f), and $^{27}$Al(n,α) detectors. $^{64}$Zn(n,p) detectors – which have the same activation threshold as $^{58}$Ni(n,p) 2.8 MeV – have been used for measurement at energies beyond the barrel. $^{27}$Al(n,α) detectors, which have a threshold of 7.6 MeV, have been used to observe the performance of calculation tools at that high energy level.

The measurement positions in VENUS-2, which were identical to those in VENUS-1, are defined in Table 3. The detectors were placed along the core mid-plane at 34 locations in the outer core region, the core baffle, the water reflector, the core barrel and the neutron pad.

For the measurement points in Table 3, the reaction rates and corresponding equivalent fission fluxes, and neutron fluxes at threshold energies $E_{th}$ > 1.0 MeV and $E_{th}$ > 0.1 MeV should be calculated and reported in Tables 4 to 7.

In the calculations, the participants are kindly requested to use **IRDF-90 *Version* 2** dosimeter cross-section data in order to ensure the comparability of results. If this data is not used, it should be reported.

The equivalent fission fluxes are the reaction rates divided by the $^{235}$U fission spectrum averaged cross-sections of the corresponding dosimeter. That is, the equivalent fission flux can be calculated as follows:

$$\phi_{eq.fiss.} = \frac{\int_0^\infty \sigma_i(E)\phi(E)dE}{<\sigma_i>_{fiss.}}$$

where $\sigma_i(E)$ is the energy-dependent cross-section of reaction i, $\phi(E)$ is the energy-dependent calculated flux at the measured position and $<\sigma_i>_{fiss.}$ is the $^{235}$U fission spectrum averaged cross-section of reaction i.

The $^{235}$U fission spectrum averaged cross-section of reaction i is defined as follows:

$$<\sigma_i>_{fiss.} = \frac{\int_0^\infty \chi_5(E)\sigma_i(E)dE}{\int_0^\infty \chi_5(E)dE}$$

where $\chi_5(E)$ is the $^{235}$U fission spectrum.

---

* 1.87E+08 × 0.768 (axial form factor) × 50 (active length) × 640 (number of pins in the ¼ core) = 4.596E+12.
** 4.596E+12 divided by 640 fissions/sec.

All calculated reaction rates and corresponding equivalent fission fluxes and neutron fluxes are to be normalised to 100% VENUS-2 power by using the given fission rates in the core corresponding to absolute reference irradiation (1.87E+08 fissions/cm/sec at the core mid-plane and 4.596E+12 fissions/sec/core quadrant).

Finally, the calculated $^{235}U$ fission spectrum averaged dosimeter cross-sections used for converting calculated reaction rates into equivalent fission fluxes are to be reported in Table 8.

Together with the results of the benchmark, detailed information on calculations is required for the analysis of results. A list of requested information can be found in Appendix A.2. The participants are kindly invited to provide all information requested in the list, to be submitted along with the benchmark results.

## V. Optional calculations

**Two** additional but **optional** calculations are suggested:

1) The participants who wish to do so are kindly invited to calculate the DPA using pre-calculated neutron spectra. The DPAs should be reported in columns marked **"Optional DPA"** in Tables 5 and 7.

2) The participants who wish to perform the uncertainty analysis of their benchmark calculations are encouraged to do so as an additional option.

*Acknowledgements*

The OECD/NEA Secretariat expresses its special thanks to SCK•CEN (Mol) Belgium for the release of valuable experimental results for this benchmark exercise.

## REFERENCES


[1] *LWR-PV Surveillance Dosimetry Improvement Program: VENUS-2 PWR Core Source and Azimuthal Lead Factor Experiments and Calculational Tests*, SCK•CEN Report (1983).

[2] Hehn, G. and B-C. Na, *Prediction of Neutron Embrittlement in the Reactor Pressure Vessel: VENUS-1 and VENUS-3 Benchmarks*, OECD/NEA Report, NEA/NSC/DOC (2000)5, ISBN 92-64-17637-3 (2000).

[3] Na, B-C., *Benchmark on the VENUS-2 MOX Core Measurements*, OECD/NEA Report, NEA/NSC/DOC(2000)7, ISBN 92-64-18276-4 (2000).

[4] Messaoudi, N. and B-C. Na, *Benchmark on the Three-dimensional VENUS-2 MOX Core Measurements*, OECD/NEA Report, NEA/NSC/DOC(2003)5, ISBN 92-64-02160-4, January 2004.

[5] van der Meer, K., P. D'hondt and H. Aït Abederrahim, *Additional Data for the 3-D VENUS-2 Benchmark*, SCK•CEN Report, TN-0008, September 2000.

**Figure 1. Numbering of the fuel pin positions measured in VENUS-2**

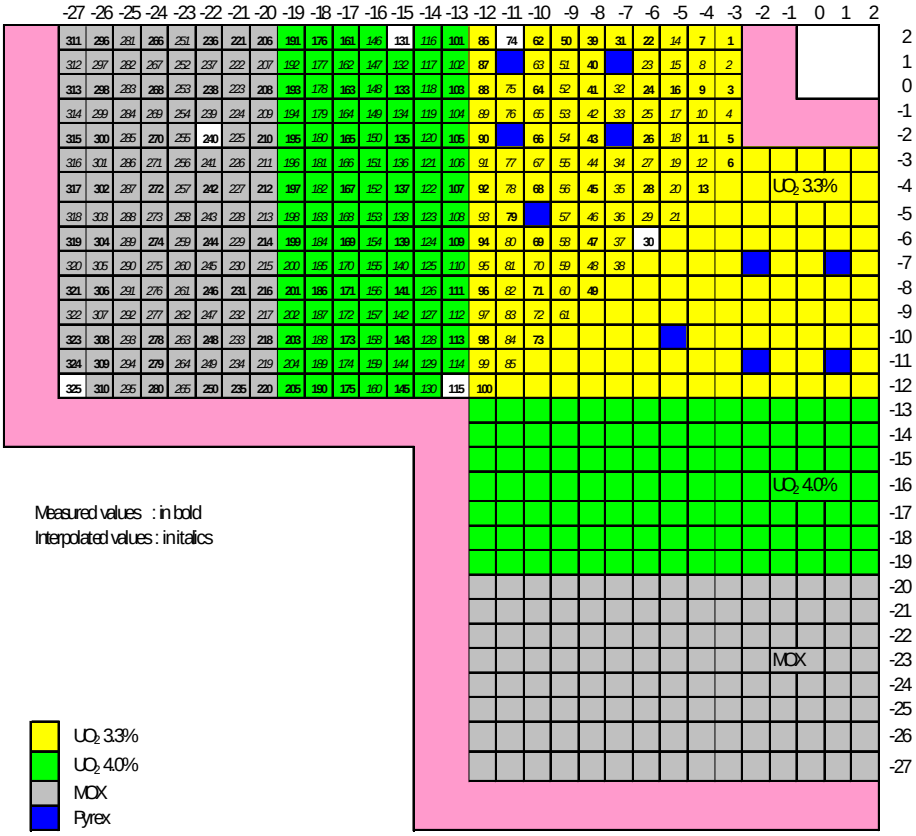

## Table 1. Radial experimental fission rate distribution (normalised to 1 fission/sec/cell) on the core mid-plane

| X→ | | -37.17 | -35.91 | -34.65 | -33.39 | -32.13 | -30.87 | -29.61 | -28.35 | -27.09 | -25.83 | -24.57 | -23.31 | -22.05 | -20.79 | -19.53 | -18.27 | -17.01 | -15.75 | -14.49 | -13.23 | -11.97 | -10.71 | -9.45 | -8.19 | -6.93 |
|---|---|---|---|---|---|---|---|---|---|---|---|---|---|---|---|---|---|---|---|---|---|---|---|---|---|---|
| Y↓ | | -27 | -26 | -25 | -24 | -23 | -22 | -21 | -20 | -19 | -18 | -17 | -16 | -15 | -14 | -13 | -12 | -11 | -10 | -9 | -8 | -7 | -6 | -5 | -4 | -3 |
| 0.63 | +2 | **0.433** | **0.517** | *0.577* | **0.641** | *0.713* | **0.804** | **0.902** | **1.059** | **1.035** | **1.177** | **1.279** | *1.34* | **1.393** | *1.469* | **1.561** | **1.236** | **1.223** | **1.349** | **1.397** | **1.397** | **1.293** | **1.334** | *1.329* | **1.248** | **1.08** |
| 1.89 | +1 | *0.438* | *0.514* | *0.577* | *0.643* | *0.717* | *0.797* | *0.907* | *1.065* | *1.033* | *1.17* | *1.27* | *1.336* | *1.391* | *1.464* | *1.556* | **1.183** | **Pyrex** | *1.283* | *1.399* | **1.321** | **Pyrex** | *1.283* | *1.345* | *1.25* | *1.053* |
| 3.15 | 0 | **0.442** | **0.506** | *0.571* | **0.643** | *0.717* | **0.797** | *0.909* | **1.061** | **1.027** | *1.16* | **1.262** | *1.323* | **1.38** | *1.454* | **1.557** | **1.246** | *1.233* | **1.358** | *1.395* | **1.388** | *1.324* | **1.364** | **1.329** | **1.26** | **1.026** |
| 4.41 | -1 | *0.428* | *0.5* | *0.563* | *0.631* | *0.705* | *0.79* | *0.895* | *1.049* | *1.022* | *1.141* | *1.25* | *1.312* | *1.374* | *1.452* | *1.544* | *1.25* | *1.237* | *1.366* | *1.387* | *1.374* | *1.308* | *1.382* | *1.387* | *1.27* | *1.076* |
| 5.67 | -2 | **0.422** | **0.497** | *0.547* | **0.614** | *0.692* | **0.781** | *0.882* | **1.031** | **1.016** | *1.126* | **1.241** | *1.304* | **1.36** | *1.446* | **1.536** | **1.187** | **Pyrex** | **1.313** | *1.362* | **1.331** | **Pyrex** | **1.336** | *1.374* | **1.298** | **1.131** |
| 6.93 | -3 | *0.41* | *0.477* | *0.531* | *0.599* | *0.673* | *0.756* | *0.859* | *1.013* | *1.001* | *1.05* | *1.213* | *1.282* | *1.357* | *1.437* | *1.536* | *1.237* | *1.26* | *1.345* | *1.378* | *1.399* | *1.374* | *1.449* | *1.428* | *1.378* | **1.303** |
| 8.19 | -4 | **0.39** | **0.451** | *0.513* | **0.579** | *0.65* | **0.736** | *0.842* | **0.978** | **0.971** | *1.081* | **1.174** | *1.264* | **1.348** | *1.425* | **1.526** | **1.265** | *1.279* | **1.286** | *1.399* | **1.454** | *1.488* | **1.507** | *1.482* | **1.46** | |
| 9.45 | -5 | *0.382* | *0.447* | *0.494* | *0.559* | *0.628* | *0.715* | *0.811* | *0.952* | *0.943* | *1.056* | *1.146* | *1.236* | *1.323* | *1.418* | *1.518* | *1.275* | **1.271** | **Pyrex** | *1.382* | *1.477* | *1.515* | *1.515* | *1.509* | | |
| 10.71 | -6 | **0.366** | **0.422** | *0.474* | **0.535** | *0.602* | **0.689** | *0.79* | **0.927** | **0.91** | *1.024* | **1.114** | *1.2* | **1.287** | *1.387* | **1.506** | **1.278** | *1.304* | **1.339** | *1.436* | **1.492** | *1.519* | **1.522** | | | |
| 11.97 | -7 | *0.343* | *0.402* | *0.449* | *0.506* | *0.578* | *0.655* | *0.742* | *0.884* | *0.87* | *0.992* | *1.075* | *1.166* | *1.256* | *1.362* | *1.479* | *1.267* | *1.329* | *1.39* | *1.465* | *1.506* | *1.523* | | | | |
| 13.23 | -8 | **0.317** | **0.375** | *0.429* | *0.477* | *0.539* | **0.62** | **0.689** | **0.826** | **0.823** | **0.953** | **1.032** | *1.12* | **1.219** | *1.327* | **1.446** | **1.244** | *1.362* | **1.411** | *1.461* | **1.501** | | | | | |
| 14.49 | -9 | *0.3* | *0.354* | *0.394* | *0.447* | *0.508* | *0.582* | *0.65* | *0.774* | *0.776* | *0.883* | *0.975* | *1.069* | *1.164* | *1.27* | *1.398* | *1.209* | *1.349* | *1.387* | *1.449* | | | | | | |
| 15.75 | -10 | **0.278** | **0.331** | *0.366* | **0.414** | *0.473* | **0.541** | *0.607* | **0.721** | **0.716** | *0.808* | **0.907** | *0.988* | **1.08** | *1.198* | **1.327** | **1.149** | *1.262* | **1.353** | | | | | | | |
| 17.01 | -11 | **0.251** | **0.296** | *0.337* | **0.38** | *0.427* | *0.482* | *0.54* | *0.643* | *0.64* | *0.719* | *0.81* | *0.882* | *0.95* | *1.06* | *1.209* | *1.068* | *1.24* | | | | | | | | |
| 18.27 | -12 | **0.224** | **0.267** | *0.302* | **0.338** | *0.376* | **0.423** | **0.465** | **0.561** | **0.536** | **0.608** | **0.673** | *0.727* | **0.787** | *0.88* | **1.019** | **0.926** | | | | | | | | | |

**Bold**: Measured values.
*Italics*: Interpolated values.

**Table 2. Axial experimental fission rate values of the six fuel pins measured (normalised to 1)**

| Pin type | MOX | | 4/0 $UO_2$ | | 3/0 $UO_2$ | |
|---|---|---|---|---|---|---|
| Pin position | (-27,-12) | (-22,-2) | (-15,+2) | (-13,-12) | (-11,+2) | (-6,-6) |
| Pin number | 325 | 240 | 131 | 115 | 74 | 30 |
| Axial position (cm) | Measured fission rates (normalised to 1) | | | | | |
| 110 | 0.0333 | 0.0322 | 0.0321 | 0.0323 | 0.0322 | 0.0324 |
| 112 | 0.0356 | 0.0366 | 0.0363 | 0.0358 | 0.0366 | 0.0364 |
| 114 | 0.0399 | 0.0395* | 0.0404 | 0.0402 | 0.0399 | 0.0405 |
| 116 | 0.0438 | 0.0424 | 0.0441 | 0.0444 | 0.0441 | 0.0440 |
| 118 | 0.0466 | 0.0478 | 0.0477 | 0.0472 | 0.0481 | 0.0477 |
| 120 | 0.0500 | 0.0507 | 0.0504 | 0.0503 | 0.0500 | 0.0505 |
| 122 | 0.0527 | 0.0516 | 0.0531 | 0.0527 | 0.0528 | 0.0524 |
| 124 | 0.0548 | 0.0545 | 0.0542 | 0.0544 | 0.0550 | 0.0546 |
| 126 | 0.0558 | 0.0559 | 0.0564 | 0.0557 | 0.0563 | 0.0554 |
| 128 | 0.0557 | 0.0558 | 0.0572 | 0.0564 | 0.0563 | 0.0567 |
| 130 | 0.0574 | 0.0567 | 0.0568 | 0.0564 | 0.0571 | 0.0562 |
| 132 | 0.0567* | 0.0578 | 0.0565 | 0.0572 | 0.0565 | 0.0569 |
| 134 | 0.0559 | 0.0564 | 0.0562 | 0.0561 | 0.0560 | 0.0559 |
| 136 | 0.0548 | 0.0560 | 0.0548 | 0.0555 | 0.0546 | 0.0545 |
| 138 | 0.0529 | 0.0533 | 0.0530 | 0.0524 | 0.0526 | 0.0524 |
| 140 | 0.0506 | 0.0508 | 0.0504 | 0.0506 | 0.0503 | 0.0504 |
| 142 | 0.0481 | 0.0477 | 0.0477 | 0.0476 | 0.0476 | 0.0474 |
| 144 | 0.0438 | 0.0445 | 0.0439 | 0.0446 | 0.0442 | 0.0446 |
| 146 | 0.0411 | 0.0412 | 0.0403 | 0.0413 | 0.0409 | 0.0407 |
| 148 | 0.0375 | 0.0366* | 0.0365 | 0.0366 | 0.0366 | 0.0369 |
| 150 | 0.0331 | 0.0320 | 0.0321 | 0.0321 | 0.0325 | 0.0337 |
| **Total** | **1.0** | **1.0** | **1.0** | **1.0** | **1.0** | **1.0** |

* Interpolated values.

**Table 3. Co-ordinates of VENUS-2 measurement positions**

| No. | Measurement point zone | (x,y) co-ordinates with respect to reactor grid | (r,θ) in [cm,°] co-ordinates with respect to core centre | (x,y) in [cm,cm] co-ordinates with respect to core centre |
|---|---|---|---|---|
| | Central hole | | | |
| 1 | | (+2.5,+2.5) | | (0.00,0.00) |
| | Inner baffle | | | |
| 2 | | (-1,+2) | (–,8.1°) | (-4.41,-0.63) |
| 3 | | (-1,-1) | (–,45.0°) | (-4.41,-4.41) |
| | Outer baffle | | | |
| 4 | | (-29,+2) | (–,0.9°) | (-39.69,-0.69) |
| 5 | | (-29,-2) | (–,8.1°) | (-39.69,-5.67) |
| 6 | | (-29,-7) | (–,16.8°) | (-39.69,-11.97) |
| 7 | | (-29,-12) | (–,24.7°) | (-39.69,-18.27) |
| 8 | | (-27,-14) | (–,29.2°) | (-37.17,-20.79) |
| 9 | | (-22,-14) | (–,34.0°) | (-30.87,-20.79) |
| 10 | | (-17,-14) | (–,40.2°) | (-24.57,-20.79) |
| | Barrel | | | |
| 11 | | (-37,+2) | (–,0.7°) | (-49.77,-0.63) |
| 12 | | (-37,-5) | (–,10.8°) | (-49.77,-9.45) |
| 13 | | (-35,-12) | (–,21.1°) | (-47.25,-18.27) |
| 14 | | (-34,-15) | (–,25.6°) | (-45.99,-22.05) |
| 15 | | (-33,-17) | (–,28.8°) | (-44.73,-24.57) |
| 16 | | (-31,-20) | (–,33.9°) | (-42.21,-28.35) |
| 17 | | (-28,-24) | (–,41.0°) | (-38.43,-33.39) |
| 18 | | (-26,-26) | (–,45.0°) | (-35.91,-35.91) |
| | Water gap | | | |
| 19 | | (–,–) | (55.2,10.8°) | (-54.36,-9.59) |
| 20 | | (–,–) | (55.2,16.6°) | (-52.89,-15.80) |
| 21 | | (–,–) | (55.2,21.1°) | (-51.53,-19.78) |
| 22 | | (–,–) | (55.2,25.6°) | (-50.03,-23.33) |
| 23 | | (–,–) | (55.2,28.8°) | (-48.74,-25.91) |
| 24 | | (–,–) | (55.2,33.9°) | (-46.29,-30.06) |
| 25 | | (–,–) | (55.2,37.4°) | (-44.08,-33.22) |
| 26 | | (–,–) | (55.2,41.0°) | (-42.29,-35.48) |
| 27 | | (–,–) | (55.2,45.0°) | (-39.03,-39.03) |
| | Neutron pad | | | |
| 28 | | (–,–) | (62.7,21.1°) | (-58.54,-22.47) |
| 29 | | (–,–) | (62.7,42.0°) | (-46.60,-41.95) |
| | Reflector | | | |
| 30 | | (-16,-16) | (–,45°) | (-23.31,-23.31) |
| 31 | | (-18,-18) | (–,45°) | (-25.83,-25.83) |
| 32 | | (-20,-20) | (–,45°) | (-28.35,-28.35) |
| 33 | | (-22,-22) | (–,45°) | (-30.87,-30.87) |
| 34 | | (-24,-24) | (–,45°) | (-33.39,-33.39) |

**Table 4. Reaction rates at 100% power in stainless steel zones**

*[Unit: reactions/sec·nucleus]*

| Measurement position[1] | $^{58}$Ni (n,p) | $^{115}$In (n,n′) | $^{103}$Rh (n,n′) | $^{64}$Zn (n,p) | $^{237}$Np (n,f) | $^{27}$Al (n,α) |
|---|---|---|---|---|---|---|
| Inner baffle | | | | | | |
| (-4.41,-0.63) | | | | | | |
| (-4.41,-4.41) | | | | | | |
| Outer baffle | | | | | | |
| (-39.69,-0.69) | | | | | | |
| (-39.69,-5.67) | | | | | | |
| (-39.69,-11.97) | | | | | | |
| (-39.69,-18.27) | | | | | | |
| (-37.17,-20.79) | | | | | | |
| (-30.87,-20.79) | | | | | | |
| (-24.57,-20.79) | | | | | | |
| Barrel | | | | | | |
| (-49.77,-0.63) | | | | | | |
| (-49.77,-9.45) | | | | | | |
| (-47.25,-18.27) | | | | | | |
| (-45.99,-22.05) | | | | | | |
| (-44.73,-24.57) | | | | | | |
| (-42.21,-28.35) | | | | | | |
| (-38.43,-33.39) | | | | | | |
| (-35.91,-35.91) | | | | | | |
| Neutron pad | | | | | | |
| (-58.54,-22.47) | | | | | | |
| (-46.60,-41.95) | | | | | | |

[1] (x,y) in [cm,cm] co-ordinates with respect to core centre.

**Table 5. Equivalent fission fluxes at 100% power in stainless steel zones**

*[Unit: n/cm$^2$/sec]*

| **Measurement position**[1] | **$^{58}$Ni (n,p)** | **$^{115}$In (n,n′)** | **$^{103}$Rh (n,n′)** | **$^{64}$Zn (n,p)** | **$^{237}$Np (n,f)** | **$^{27}$Al (n,α)** | **Flux at E > 0.1 MeV** | **Flux at E > 1.0 MeV** | **Optional DPA**[2] |
|---|---|---|---|---|---|---|---|---|---|
| Inner baffle | | | | | | | | | |
| (-4.41,-0.63) | | | | | | | | | |
| (-4.41,-4.41) | | | | | | | | | |
| Outer baffle | | | | | | | | | |
| (-39.69,-0.69) | | | | | | | | | |
| (-39.69,-5.67) | | | | | | | | | |
| (-39.69,-11.97) | | | | | | | | | |
| (-39.69,-18.27) | | | | | | | | | |
| (-37.17,-20.79) | | | | | | | | | |
| (-30.87,-20.79) | | | | | | | | | |
| (-24.57,-20.79) | | | | | | | | | |
| Barrel | | | | | | | | | |
| (-49.77,-0.63) | | | | | | | | | |
| (-49.77,-9.45) | | | | | | | | | |
| (-47.25,-18.27) | | | | | | | | | |
| (-45.99,-22.05) | | | | | | | | | |
| (-44.73,-24.57) | | | | | | | | | |
| (-42.21,-28.35) | | | | | | | | | |
| (-38.43,-33.39) | | | | | | | | | |
| (-35.91,-35.91) | | | | | | | | | |
| Neutron pad | | | | | | | | | |
| (-58.54,-22.47) | | | | | | | | | |
| (-46.60,-41.95) | | | | | | | | | |

[1] (x,y) in [cm,cm] co-ordinates with respect to core centre.
[2] Unit : DPAs/sec.

**Table 6. Reaction rates at 100% power in water zones**

*[Unit: reactions/sec·nucleus]*

| Measurement position[1] | $^{58}$Ni (n,p) | $^{115}$In (n,n′) | $^{103}$Rh (n,n′) | $^{64}$Zn (n,p) | $^{237}$Np (n,f) | $^{27}$Al (n,α) |
|---|---|---|---|---|---|---|
| Central hole (0.00,0.00) | | | | | | |
| Water gap (-54.36,-9.59) (-52.89,-15.80) (-51.53,-19.78) (-50.03,-23.33) (-48.74,-25.91) (-46.29,-30.06) (-44.08,-33.22) (-42.29,-35.48) (-39.03,-39.03) | | | | | | |
| Reflector (-23.31,-23.31) (-25.83,-25.83) (-28.35,-28.35) (-30.87,-30.87) (-33.39,-33.39) | | | | | | |

[1] (x,y) in [cm,cm] co-ordinates with respect to core centre.

**Table 7. Equivalent fission fluxes at 100% power in water zones**

*[Unit: n/cm$^2$/sec]*

| Measurement position[1] | $^{58}$Ni (n,p) | $^{115}$In (n,n′) | $^{103}$Rh (n,n′) | $^{64}$Zn (n,p) | $^{237}$Np (n,f) | $^{27}$Al (n,α) | Flux at E > 0.1 MeV | Flux at E > 1.0 MeV | Optional DPA[2] |
|---|---|---|---|---|---|---|---|---|---|
| Central hole (0.00,0.00) | | | | | | | | | |
| Water gap (-54.36,-9.59) | | | | | | | | | |
| (-52.89,-15.80) | | | | | | | | | |
| (-51.53,-19.78) | | | | | | | | | |
| (-50.03,-23.33) | | | | | | | | | |
| (-48.74,-25.91) | | | | | | | | | |
| (-46.29,-30.06) | | | | | | | | | |
| (-44.08,-33.22) | | | | | | | | | |
| (-42.29,-35.48) | | | | | | | | | |
| (-39.03,-39.03) | | | | | | | | | |
| Reflector (-23.31,-23.31) | | | | | | | | | |
| (-25.83,-25.83) | | | | | | | | | |
| (-28.35,-28.35) | | | | | | | | | |
| (-30.87,-30.87) | | | | | | | | | |
| (-33.39,-33.39) | | | | | | | | | |

[1] (x,y) in [cm,cm] co-ordinates with respect to core centre.
[2] Unit : DPAs/sec.

**Table 8. Dosimeter cross-section averaged over the $^{235}$U fission spectrum**

*[Unit: mbarn]*

| Reaction | $^{58}$Ni (n,p) | $^{115}$In (n,n′) | $^{103}$Rh (n,n′) | $^{64}$Zn (n,p) | $^{237}$Np (n,f) | $^{27}$Al (n,α) |
|---|---|---|---|---|---|---|
| Cross-section | | | | | | |

*Appendix A.1*

## VENUS-2 CORE DESCRIPTION AND QUALIFICATION

**Outline**

I. General

II. Description of the facility

III. Core description

IV. Qualified data on the core geometry

V. Qualified data on the core materials

VI. Absolute core power

VII. Vertical bucklings in the core and outside

VIII. References

*Annex to Appendix A.1: VENUS-2 PWR core source and azimuthal lead factor experiments – description of the composition of different materials*

## I. General

The VENUS critical facility is a zero power reactor located at SCK•CEN in Belgium. This facility was built in 1963-1964, as a nuclear mock-up of a projected marine reactor called VULCAIN; hence the name VENUS which means "***V***ULCAIN ***E***XPERIMENTAL ***NU***CLEAR ***S***TUDY".

In 1967, this facility was adapted and improved in order to study LWR core designs and to provide experimental data for nuclear code validation. Great flexibility was looked for, as well as easy handling of the fuel pins, handled one by one, and a great precision of results had to be achieved.

In 1980, additional material was purchased with a view to studying typical $17 \times 17$ PWR fuel assemblies. Such an adaptation is easy; only new reactor grids and small devices adapted to the new fuel geometry are necessary. In 1982, special stainless steel pieces were manufactured in order to build a mock-up of the pressure vessel internals representative of a three-loop Westinghouse power plant. These stainless steel pieces were delivered at the beginning of December 1982. Since this date, the facility has been used for three LWR-PVS benchmark experiments as follows:

- *VENUS-1*: This mock-up was aimed to check the calculation procedure for a standard LWR core, i.e. with fresh $UO_2$ fuel assemblies at the periphery. The VENUS-1 core was made critical for the first time on 20 Dec. 1982. The experimental programme was carried out from 26 Jan. 1983 until 6 June 1986.

- *VENUS-2*: Between the possible solutions to reduce the lead factor at the pressure vessel (PV), it was proposed to replace some fresh $UO_2$ fuel assemblies by burnt fuel assemblies at the most critical corners of the core periphery. For benchmark purposes, the VENUS-2 core was obtained by replacing the peripheral $UO_2$ fuel by a MOX fuel, actually simulating a two-cycle burnt $UO_2$ fuel (except for FP poisoning). The VENUS-2 core was made critical for the first time on 16 Sept. 1986. The corresponding experimental programme was carried out from 6 Oct. 1986 until 16 Dec. 1987.

- *VENUS-3*: For some early-built reactors, it is proposed to reduce the lead factor at the level of the PV horizontal welding by loading partial length shielded assemblies at the most critical corners of the core periphery (the shielded part is obtained by replacing part of the fuel length by a stainless steel rod). For benchmarking this improvement, the VENUS-3 core was built with 3.3/0 SS rods at the periphery (the 3.3/0 SS rods are made of half a length of stainless steel and half a length of 3.3 w/o $^{235}U$ enriched $UO_2$ fuel). The VENUS-3 core was made critical for the first time on 16 March 1988. The experimental programme was started on 29 March 1988 and went on until the end of Dec. 1988.

## II. Description of the facility

The VENUS facility comprises a reactor shielded room and several associated facilities: the control room, the fuel storage area, the gamma scanning device, the counting room and the plutonium laboratory.

The shielded room is partly illustrated in Figure 1. Under the floor, it contains (1) the reactor vessel (~2.6 $m^3$), (2) the reactor grids (1 m diameter), (3) the safety neutron detectors, (4) the safety system (moderator fast dump) and (5) the water and compressed air circuitries (not shown in the figure). The working room (6) above the floor gives a direct access to the reactor core for loading and unloading fuel pins or experimental thimbles. This room contains the start-up neutron source, the reactor and health physics controls, the regulating rod or fission chamber mechanisms, and the handling tools.

Due to the direct access to the fuel, the reactor is shut down when the shielded room is open. The neutron flux level in operation is limited to $10^9$ neutrons/cm$^2$/sec, with a view to limiting the irradiation level of the core and the radioactivity of unloaded fuel pins.

## III. Core description

The VENUS-2 core configuration is shown in Figure 2. The 1/4 of the core comprises 640 fuel rods (190 with 3.3 w/o $UO_2$, 210 with 4.0 w/o $UO_2$, and 240 with 2.0/2.7 w/o MOX). For experimental and analytical purposes, it should be regarded as a perfect symmetrical core reproducing four times the quadrant between 0° and 90°. The other quadrants are loaded with fuel pins "quasi" identical to the fuel pins of the first quadrant (due to fuel inventory limitations) and with some absorbing rods for criticality balance adjustment. Starting from the centre, the core may be divided in 17 regions as follows:

- the central hole (water);
- the inner baffle (stainless steel: 2.858 cm thick);
- the 3.3/0 fuel region, containing zircaloy-clad $UO_2$ rods, with 3.3 w/o enriched uranium, in a "17 × 17" type lattice; 10 Pyrex rods, typical of PWR poison clusters are loaded per quadrant (in VENUS language: 3.3/0 means 3.3 w/o $^{235}U$ and 0 w/o $PuO_2$);
- the 4.0/0 fuel and 2.0/2.7 fuel regions, containing stainless-steel clad $UO_2$ rods, with 4.0 w/o enriched uranium; the rods are typical of a "15 × 15" lattice (first generation of Westinghouse plants), and are loaded with the same pin-to-pin pitch typical of the "17 × 17" type lattice; eight rows of the most external fuel pins have been replaced by mixed oxide fuel pins ($UO_2$-$PuO_2$) enriched 2.0 w/o in $^{235}U$ and 2.7 w/o in Pu;
- the outer baffle (stainless steel: 2.858 cm thick);
- the reflector (minimum thickness: 2.169 cm);
- the barrel (stainless steel: 4.99 cm thick);
- the water gap (water: 5.80 cm thick);
- the neutron pad (stainless steel, average thickness: 6.72 cm);
- the space between neutron pad and jacket (water);
- the jacket inner wall (stainless steel: 0.5 cm thick);
- the jacket volume (air filled, 15.0 cm thick);
- the jacket outer wall (stainless steel: 0.5 cm thick);
- the space between jacket and reactor vessel (water: 2.0 cm thick);
- the reactor vessel wall (stainless steel: 0.4 cm thick);
- the reactor room (infinite medium filled by air).

**Figure 1. Vertical cross-section of the facility**

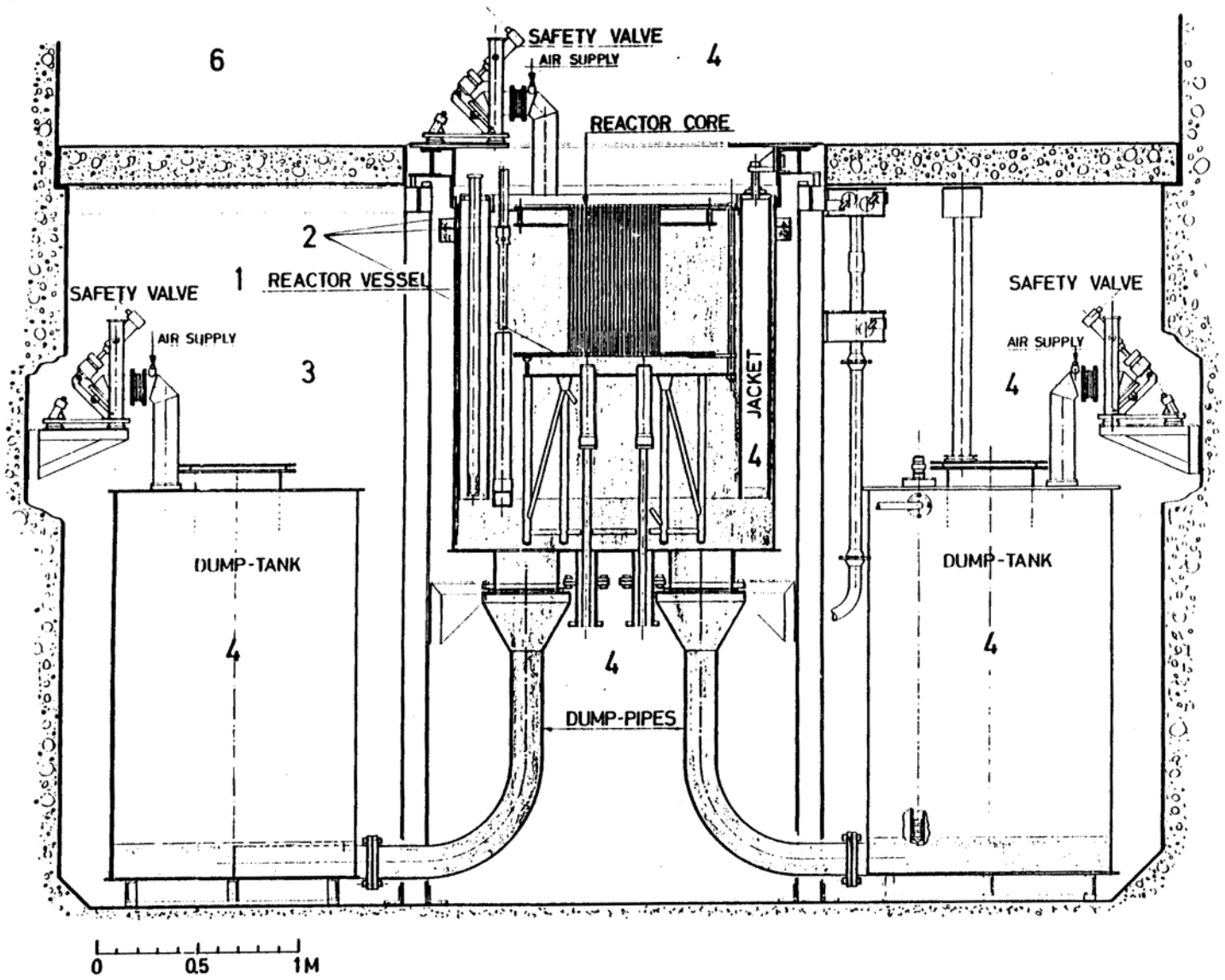

## Figure 2. Horizontal cross-section of the core

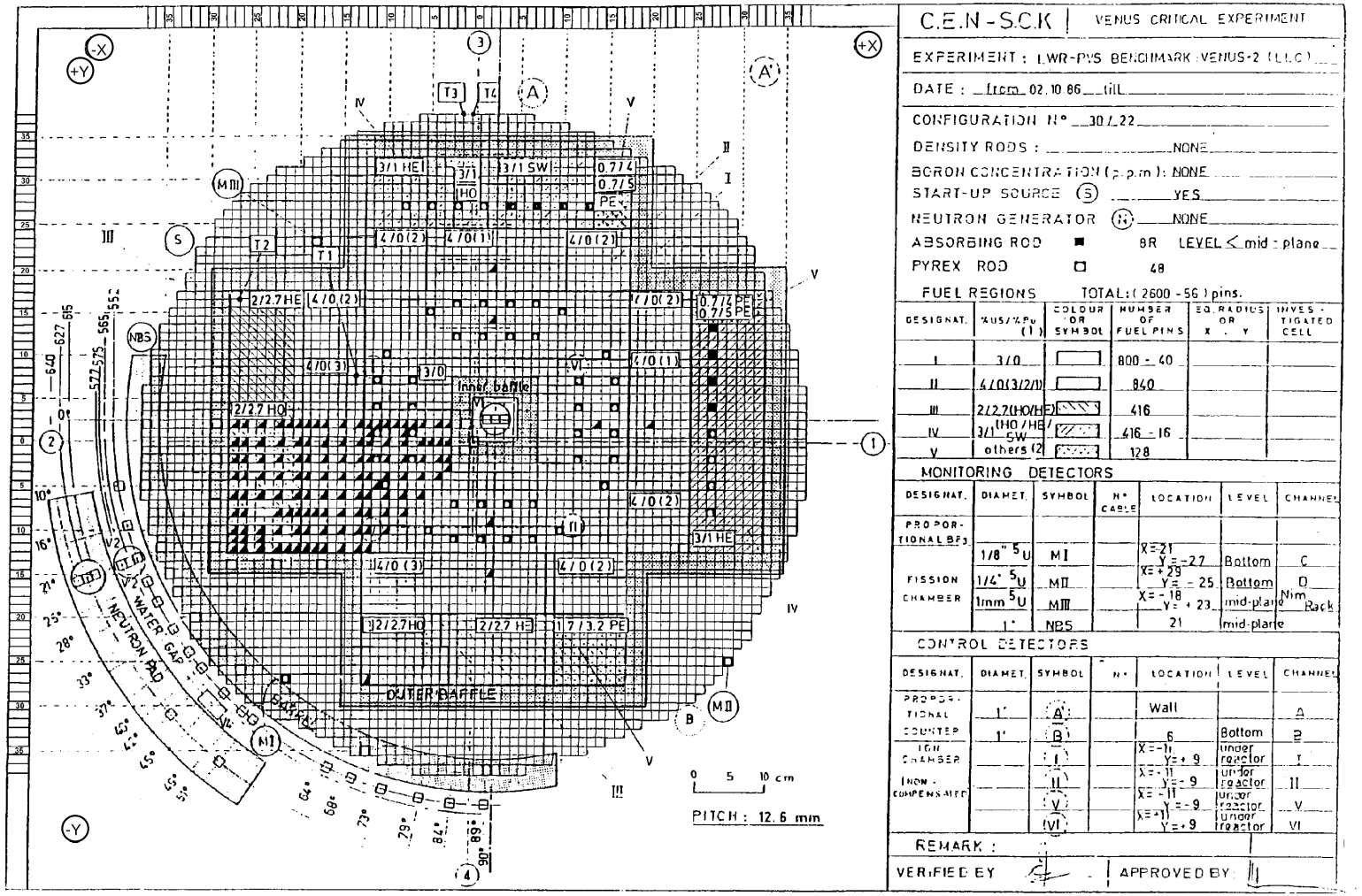


REMARKS: (1) between brackets: – or supply order
– or fabrication mode: HO = Homogeneous vibrated
HE = Heterogeneous vibrated
SW = Heterogeneous swaged
PE = Pelletised

(2) Other means: – or 1.7/3.2 PE
– or a mixture of 0.7/5 PE + some 0.7/4 PE & 2/2.7 PE

86/66053 A – Issued 18/09/86
– Updated 15/10/86

Figure 3 shows a vertical cross-section of the core with corresponding axial co-ordinates. Vertically the core may be divided, from bottom to top, as follows:

- the VENUS room environment (air);
- the lower filling (water);
- the reactor support (water and stainless steel, not shown in the figure);
- the bottom grid (32.8 vol.% water and 67.2 vol.% stainless steel*);
- the lower reflector (mainly water and Plexiglas); the reflector composition changes a little from one fuel region to another, depending on the structure of the corresponding fuel pins;
- the active height (fuel and stainless steel);
- the upper reflector (mainly water and Plexiglas), including the intermediate grid (63.4 vol.% water and 36.6 vol.% Plexiglas*); the reflector composition changes a little from one fuel region to another, depending on the structure of the corresponding fuel pins;
- the upper grid (63.4 vol.% water and 36.6 vol.% stainless steel*);
- the upper filling (water).

## IV. Qualified data on the core geometry

The components of the mock-up were qualified in sizes during fabrication and before loading in the core, special attention was paid to the stainless steel thicknesses. The detailed qualification is given in a work document [1].

Some data, particularly sensitive for the fast neutron depletion, were checked in the core as built. For instance, the minimum outer baffle-barrel distance, the water gap thickness and the azimuthal location of the neutron pad. All the recorded data were combined to describe the mock-up as given in Figures 4 and 5. Where no qualification was possible, the data were deduced from the fabrication specifications.

During the mounting, it was stated that the neutron pad did not take its designed azimuthal location, probably due to some machining mistake; it has been decided, on site, to adjust the V3 hole (foreseen at the highest azimuthal fast neutron flux and accommodated for spectrometry) at the angle 21.1°. Up to the inner diameter of the neutron pad, all the components are concentric with respect to the core centre, they are defined by distances or radii d1 to d9; the VENUS internals (jacket and reactor vessel) are concentric with respect to a point located at X′ = -3.15 cm, Y′ = -3.15 cm in the core model, as a consequence their locations are no longer given by radii but by thicknesses t4 to t9 and the neutron pad has a variable thickness. The core configuration is described in Table 1 with the following data: LL = lower level, UL = upper level, H = height, R = radius, and T = thickness (see Figure 4). The descriptions of fuel and Pyrex cells are given in Table 2.

* The given composition values assume that no pin is loaded.

**Figure 3. Vertical cross-section of the core**

SCK/CEN-Mol
VENUS critical facility, LWR-PVS benchmark

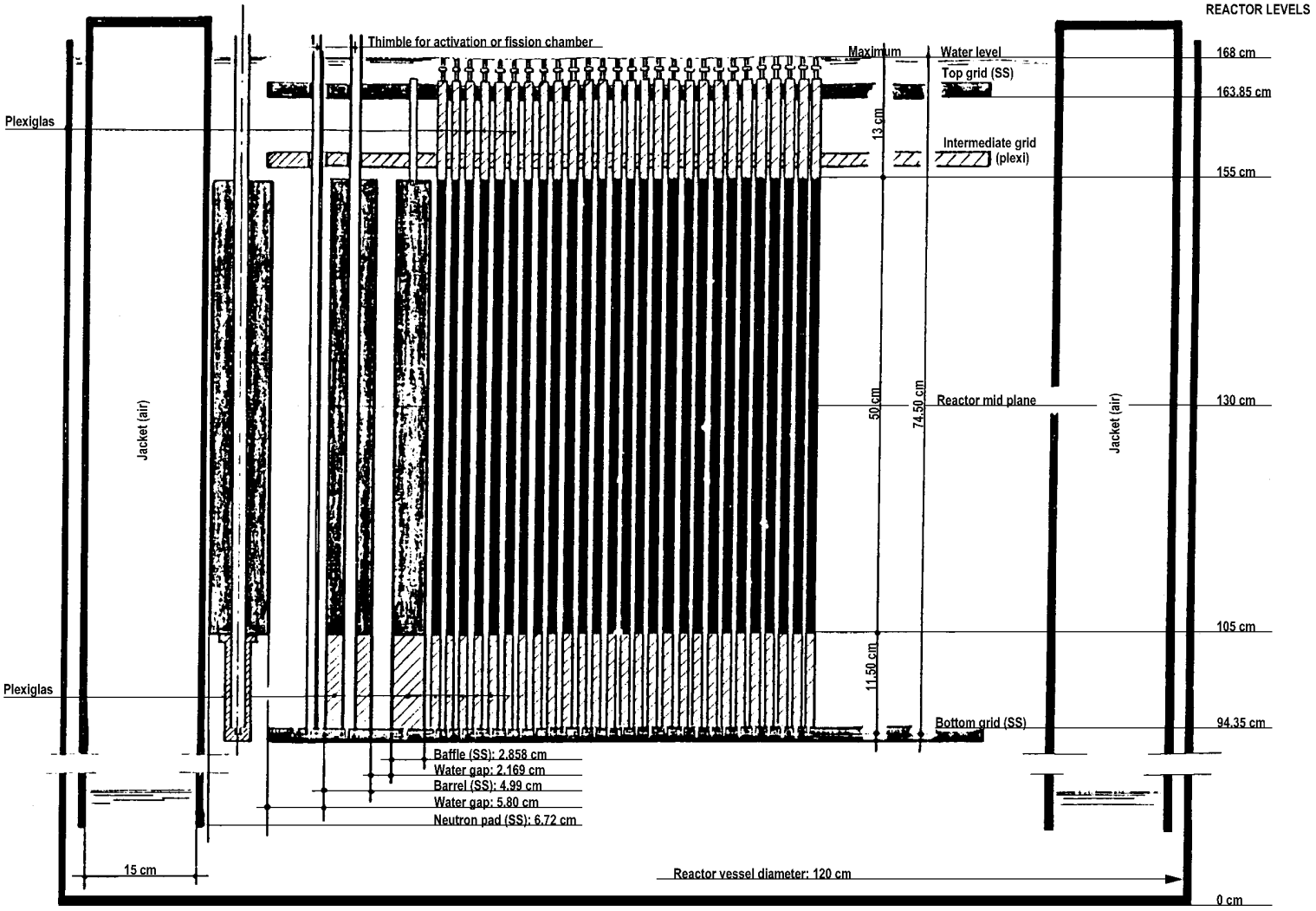

**Figure 4. Horizontal core description**

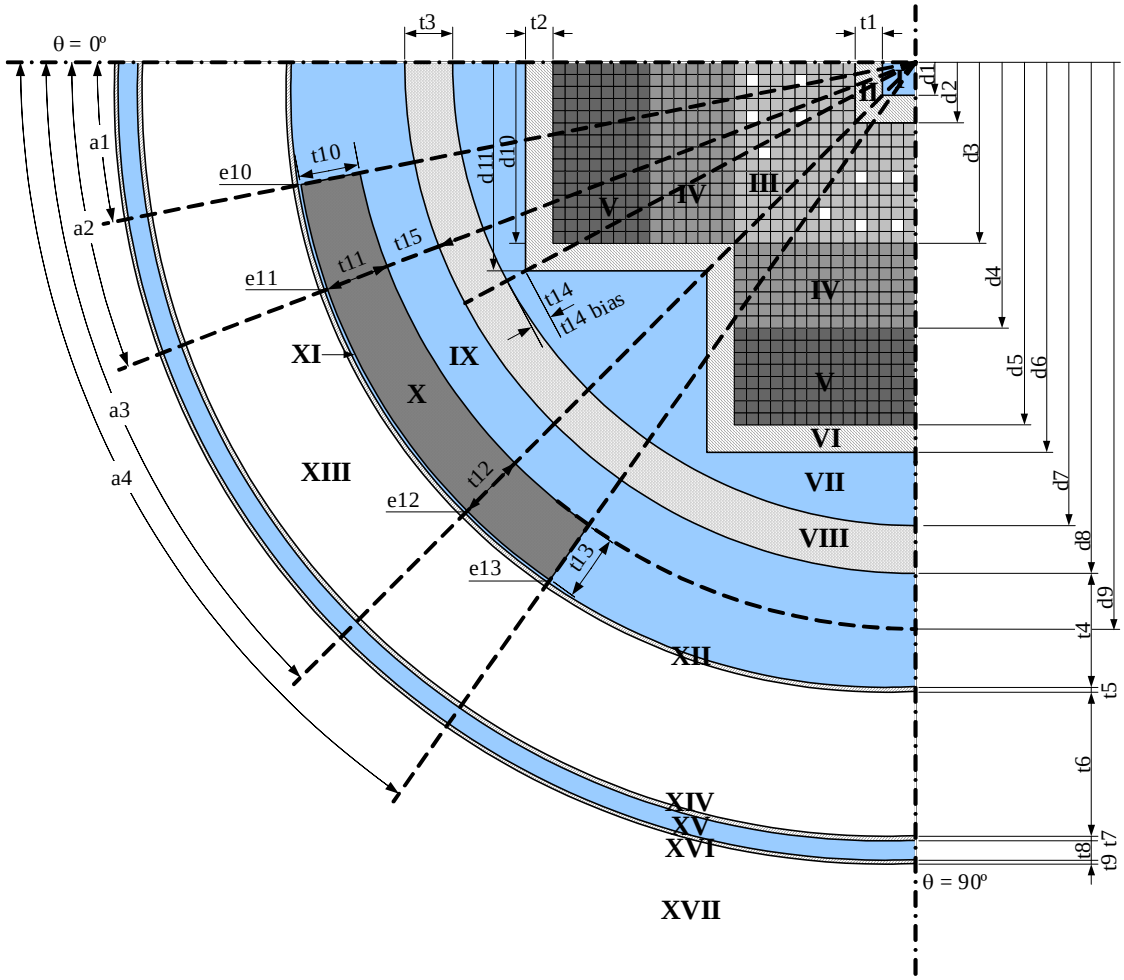


| | | | |
|---|---|---|---|
| **I** | **Central Hole** | **IX** | **Water Gap** |
| **II** | **Inner Baffle** | **X** | **Neutron Pad** |
| **III** | **3.3/0 Fuel Region (White Color: Pyrex)** | **XI** | **Space between Neutron Pad and Jacket** |
| | | **XII** | **Jacket Inner Wall** |
| **IV** | **4.0/0 Fuel Region** | **XIII** | **Jacket Volume** |
| **V** | **2.0/2.7 Fuel Region** | **XIV** | **Jacket Outer Wall** |
| **VI** | **Outer Baffle** | **XV** | **Space between Jacket and Reactor Vessel** |
| **VII** | **Reflector** | **XVI** | **Reactor Vessel Wall** |
| **VIII** | **Barrel** | **XVII** | **Reactor Room** |

**Figure 5. Vertical core description**

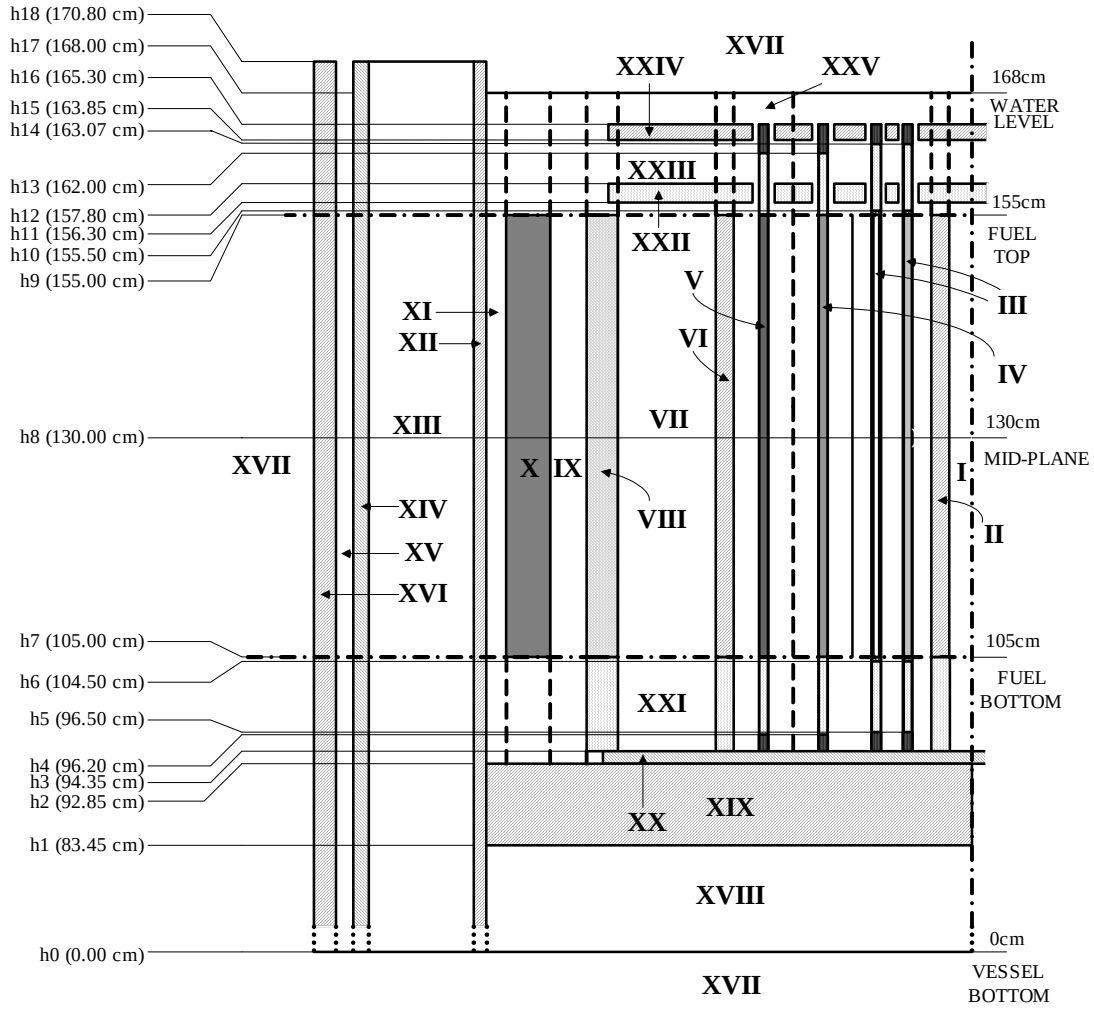


**I** Central Hole
**II** Inner Baffle
**III** 3.3/0 Fuel Region
**IV** 4.0/0 Fuel Region
**V** 2.0/2.7 Fuel Region
**VI** Outer Baffle
**VII** Reflector
**VIII** Barrel
**IX** Water Gap
**X** Neutron Pad
**XI** Space between Neutron Pad and Jacket
**XII** Jacket Inner Wall
**XIII** Jacket Volume
**XIV** Jacket Outer Wall
**XV** Space between Jacket and Reactor Vessel
**XVI** Reactor Vessel Wall
**XVII** Reactor Room
**XVIII** Lower Filling
**XIX** Reactor Support
**XX** Bottom Grid
**XXI** Lower Reflector
**XXII** Intermediate Grid
**XXIII** Upper Reflector
**XXIV** Upper Reactor Grid
**XXV** Upper Filling

**Table 1. Core configuration**

| Region | Notation | Dimensions |
|---|---|---|
| Central hole (I) | d1 | (3.442 ± .021) cm |
| Inner baffle (II) | d2 | (6.300 ± .013) cm |
| | t1 | (2.858 ± .003) cm |
| | LL II* | (104.849 ± .032) cm |
| | UL II* | (154.856 ± .036) cm |
| | H II* | (50.006 ± .004) cm |
| 3.3/0 fuel region (III) | d3 | (18.900 ± .005) cm |
| | LL III* | (105.00 ± .05) cm |
| | UL III* | (155.00 ± .15) cm |
| | H III* | (50.0 ± .1) cm |
| 4.0/0 fuel region (IV) | d4 | 27.72 cm ( = d3 × 22/15) |
| | d10 | (18.900 ± .013) cm |
| | LL IV* | (105.00 ± .05) cm |
| | UL IV* | (155.00 ± .55) cm |
| | H IV* | (50.0 ± .05) cm |
| 2.0/2.7 fuel region (V) | d5 | (37.800 ± .013) cm |
| | d10 | (18.900 ± .013) cm |
| | LL V* | (105.00 ± .05) cm |
| | UL V* | (155.00 ± .55) cm |
| | H V* | (50.0 ± .05) cm |
| Outer baffle (VI) | d6 | (40.658 ± .021) cm |
| | d11 | (21.758 ± .021) cm |
| | t2 | (2.858 ± .003) cm |
| | LL VI* | (104.850 ± .033) cm |
| | UL VI* | (154.850 ± .039) cm |
| | H VI* | (50.000 ± .006) cm |
| Reflector (VII) | t14[1] | (2.169 ± .080) cm |
| | t14 bis[2] | (2.251 ± .080) cm |
| | d7[3] | (48.283 ± .050) cm |
| Barrel (VIII) | d7 | (48.283 ± .050) cm |
| | d8 | (53.273 ± .060) cm |
| | t3 | (4.99 ± .01) cm |
| | LL VIII* | (105.00 ± .06) cm |
| | UL VIII* | (155.00 ± .16) cm |
| | H VIII* | (50.0 ± .1) cm |
| Water gap (IX) | t15 | (5.800 ± .060) cm |

[1] Distance between baffle corner and barrel.
[2] Idem, but taking account of broken corners.
[3] Barrel inner radius.
* Active height only.

**Table 1. Core configuration (*continued*)**

| Region | Notation | Dimensions |
|---|---|---|
| Neutron pad (X) | d9 | (59.073 ± .120) cm |
| | t10 | (6.300 ± .030) cm |
| | t11 | (6.690 ± .030) cm |
| | t12 | (7.050 ± .030) cm |
| | t13 | (6.900 ± .030) cm |
| | a1 | (11.25 ± .25)° |
| | a2 | (21.10 ± .10)° |
| | a3 | 45° |
| | a4 | (54.75 ± .25)° |
| | LL X* | (105.00 ± .26) cm |
| | UL X* | (155.00 ± .16) cm |
| | H X* | (50.0 ± .1) cm |
| Space between neutron pad and jacket (XI) | e10 | (.3 ± .3) cm at 11.25° |
| | e11 | (.3 ± .3) cm at 21.10° |
| | e12 | (.332 ± .310) cm at 45° |
| | e13 | (.3 ± .3) cm at 54.75° |
| Jacket inner wall (XII) | t4 | (11.80 ± .21) cm |
| | t5 | 0.5 cm |
| Jacket volume (XIII) | t6 | (15.0 ± .3) cm |
| Jacket outer wall (XIV)[4)] | t7 | 0.5 cm |
| Space between jacket and reactor vessel (XV) | t8 | (2.0 ± .3) cm |
| Reactor vessel wall (XVI) | t9 | 0.4 cm |
| Reactor room (XVII) | | Infinite medium filled by air |
| Lower filling (XVIII) | h0 | 0 cm |
| | h1 | 83.45 cm |
| | R XVIII | Defined by jacket inner wall |
| Reactor support (XIX) | h2 | 92.85 cm |
| | T XIX | (9.40 ± .05) cm |
| Bottom grid (XX) [5] | h3 | 94.35 cm |
| | T XX | (1.50 ± .01) cm |
| | R XX | (50.00 ± .01) cm |

[4] The inner radius of the jacket inner wall is (62.0 ± .15) cm with respect to a centre being at (X′ = -3.15 cm, Y′ = -3.15 cm) from the core centre, all the next internals are concentric with this jacket inner wall.

[5] The grid centre is at (X′ = -3.15 cm, Y′ = -3.15 cm) from the core centre.

* Active height only.

**Table 1. Core configuration (*continued*)**

| Region | Notation | Dimensions |
|---|---|---|
| Lower reflector (XXI) | h4 | 96.20 cm (upper end of bottom stop of the 4.0/0 and 2.0/2.7 fuel pins) |
| | h5 | 96.50 cm (upper end of bottom stop of the 3.3/0 fuel and Pyrex pins) |
| | h6 | 104.50 cm (lower end of blanket of the 3.3/0 fuel and Pyrex pins) |
| | h7 | 105.00 cm (bottom active height) |
| | R XXI | defined by jacket inner wall |
| Intermediate grid (XXII)[6] | h11 | 156.30 cm |
| | h12 | 157.80 cm |
| | T XXII | 1.5 cm |
| | R XXII | (50.00 ± .01) cm |
| Upper reflector (XXIII) | h9 | 155.00 cm (top active height) |
| | h10 | 155.50 cm (upper end of blanket of the 3.3/0 fuel and Pyrex pins) |
| | h13 | 162.00 cm (upper end of reflector of the 4.0/0 and 2.0/2.7 fuel pins) |
| | h14 | 163.07 cm (upper end of reflector of the 3.3/0 fuel and Pyrex pins) |
| | R XXIII | Defined by jacket inner wall |
| Upper reactor grid (XXIV) [6)] | h15 | 163.85 cm |
| | h16 | 165.30 cm |
| | T XXIV | (1.45 ± .01) cm |
| | R XXIV | (50.00 ± .01) cm |
| Upper filling (XXV) | h17 | 168.0 cm (water level) |

[6] The grid centre is at (X′ = -3.15 cm, Y′ = -3.15 cm) from the core centre.

*Note: h18 is the top of both the jacket and the reactor vessel, h18 = 170.8 cm*
*h8 is the mid-plane of the reactor active height, h8 = 130.0 cm*

**Table 2. Descriptions of fuel and Pyrex cells**

| *(1) 3.3/0 fuel cell* | |
|---|---|
| Fuel type | $UO_2$ |
| Fuel diameter [cm] | 0.819 ± .002 |
| Fuel pellet length [cm] | 0.992 ± .040 |
| Fuel length [cm] | 50.0 ± .1 |
| Cladding material | Zircaloy 4 |
| Cladding outer diameter [cm] | 0.950 ± .001 |
| Cladding inner diameter [cm] | 0.836 ± .001 |
| Fuel cell pitch [cm] | 1.260 ± .001 |
| Top/bottom blanket material | AISI 304 stainless steel |
| Top/bottom blanket diameter [cm] | 0.820 ± .005 |
| Top/bottom blanket length [cm] | 0.50 ± .01 |
| Bottom reflector material | Plexiglas |
| Bottom reflector diameter [cm] | 0.820 ± .005 |
| Bottom reflector length [cm] | 8.0 ± .01 |
| Top reflector material | Plexiglas |
| Top reflector diameter [cm] | 0.820 ± .005 |
| Top reflector length [1] [cm] | 7.57 ± .01 |
| Bottom stop material | Upper part: Zircaloy 4<br>Lower part: AISI 304 |
| Bottom stop diameter [cm] | 0.950 |
| Bottom stop length [cm] | Upper part: 1.25<br>Lower part: 0.90 |
| Top stop material | AISI 304 stainless steel |
| Top stop diameter [cm] | 0.950 |
| Top stop length [2] [cm] | 2.23 |

[1] The top reflector is filling the intermediate reactor gird over 1.5 cm of its length.
[2] The top stop is assumed to end with the upper face of the upper reactor grid, the highest 1.45 cm of this stop is filling the hole of the upper reactor grid.

*Note: The gap between fuel and cladding is void.*

**Table 2. Descriptions of fuel and Pyrex cells (*continued*)**

| *(2) 4.0/0 fuel cell* | |
|---|---|
| Fuel type | $UO_2$ |
| Fuel diameter [cm] | 0.8926 ± .0005 |
| Fuel pellet length [cm] | 1.114 ± .115 |
| Fuel length [cm] | 50.0 ± .5 |
| Cladding material | AISI 304 stainless steel |
| Cladding outer diameter [cm] | 0.978 ± .002 |
| Cladding inner diameter [cm] | 0.902 ± .004 |
| Fuel cell pitch [cm] | 1.260 ± .001 |
| Bottom reflector material | Plexiglas |
| Bottom reflector diameter [cm] | 0.89 ± .03 |
| Bottom reflector length [cm] | 8.80 ± .02 |
| Top reflector material | Plexiglas |
| Top reflector diameter [cm] | 0.89 ± .03 |
| Top reflector length [3] [cm] | 7.00 ± .02 |
| Bottom stop material | AISI 304 L stainless steel |
| Bottom stop diameter [cm] | 0.978 |
| Bottom stop length [cm] | 1.85 |
| Top stop material | AISI 304 L stainless steel |
| Top stop diameter [cm] | 0.978 |
| Top stop length [4] [cm] | 3.3 |
| Fuel type | $UO_2$ |
| Fuel diameter [cm] | 0.8926 ± .0005 |
| Fuel pellet length [cm] | 1.114 ± .115 |

[3] The top reflector is filling the intermediate reactor gird over 1.5 cm of its length.
[4] The top stop is assumed to end with the upper face of the upper reactor grid, the highest 1.45 cm of this stop is filling the hole of the upper reactor grid.

*Note: The gap between fuel and cladding is void.*

**Table 2. Descriptions of fuel and Pyrex cells (*continued*)**

| *(3) 2.0/2.7 fuel cell (MOX)* | |
|---|---|
| Fuel type | $UO_2$+$PuO_2$ |
| Fuel diameter [cm] | 0.9020 |
| Cladding material | Stainless steel |
| Cladding outer diameter [cm] | 0.9780 |
| Cladding inner diameter [cm] | 0.9020 |
| Fuel cell pitch [cm] | 1.260 ± .001 |
| Bottom reflector material | For the reflector and stop of the 2.0/2.7 fuel cell, no qualification was made so the description of 4.0/0 fuel cell was given. (*See "(2) 4.0/0 fuel cell"*) |
| Bottom reflector diameter [cm] | |
| Bottom reflector length [cm] | |
| Top reflector material | |
| Top reflector diameter [cm] | |
| Top reflector length [cm] | |
| Bottom stop material | |
| Bottom stop diameter [cm] | |
| Bottom stop length [cm] | |
| Top stop material | |
| Top stop diameter [cm] | |
| Top stop length [cm] | |

**Table 2. Descriptions of fuel and Pyrex cells (*continued*)**

| *(4) Pyrex cell* | |
|---|---|
| Pyrex material | Corning glass code 7740 |
| Pyrex outer diameter [cm] | 0.9048 ± .0043 |
| Pyrex inner diameter [cm] | 0.6058 ± .0031 |
| Cladding material | AISI 304 stainless steel |
| Cladding outer diameter [cm] | 0.978 ± .005 |
| Cladding inner diameter [cm] | 0.940 ± .003 |
| Pyrex cell pitch [cm] | 1.260 ± .001 |
| Top/bottom blanket material | Aluminium (purity: 99.5%) |
| Top/bottom blanket diameter [cm] | 0.930 ± .005 |
| Top/bottom blanket length [cm] | 0.50 ± .01 |
| Bottom reflector material | Plexiglas |
| Bottom reflector diameter [cm] | 0.930 ± .005 |
| Bottom reflector length [cm] | 8.00 ± .01 |
| Top reflector material | Plexiglas |
| Top reflector diameter [cm] | 0.930 ± .005 |
| Top reflector length [5] [cm] | 7.57 ± .01 |
| Bottom stop material | AISI 304 stainless steel |
| Bottom stop diameter [cm] | 0.978 |
| Bottom stop length [cm] | 2.15 |
| Top stop material | AISI 304 stainless steel |
| Top stop diameter [cm] | 0.978 |
| Top stop length [6] [cm] | 2.23 |

[5] The top reflector is filling the intermediate reactor gird over 1.5 cm of its length.
[6] The top stop is assumed to end with the upper face of the upper reactor grid, the highest 1.45 cm of this stop is filling the hole of the upper reactor grid.

*Note: The inner hole of the Pyrex cell and the gap between Pyrex cell and cladding are void.*

## V. Qualified data on the core materials

The core materials were qualified in several ways. For the stainless steels, for instance, the qualification was based on a comparison between the corresponding standard, the certificate delivered by the supplier and at least one analysis carried out by SCK•CEN. The adopted value was generally the average of the consistent data (if necessary a weighted average is made) and the given error was the range defined by the extreme values ($\varepsilon = \pm$ (max.-min.)/2). For most materials, there was at least one more sample for documentation or later cross-check. For the fuel cladding and the Pyrex tubes, the linear specific weight was determined instead of the volume specific weight as the accuracy of checking the tube thickness is too small. The impurities of water were checked in the worst conditions, i.e. when the water resistivity reached its lowest value (250 kΩcm); the water temperature was the median value for the experimental period (from 24.01.83 to 23.06.83) and the range was defined by the extreme recorded values. For the VENUS internals outside the LWR-PVS benchmark mock-up, no qualification was made so that average stainless steel characteristics were given. The detailed qualification was given in a work document [2].

The atomic number densities of each medium in the core were obtained from the compositions of all constituents [3,4] and are given in Table 3 (Avogadro's number used is $0.60221367 \times 10^{24}$ nuclei/mol and the atomic weights of isotopes are taken from the *CRC Handbook of Chemistry and Physics* [5]). The participants are encouraged to use these values for their calculations. Nevertheless, the detailed compositions of the materials are given in the Annex. The theoretical composition of Plexiglas is $[C_5H_8O_2]_n$ and the density used is 1.19 g/cm$^3$.

## VI. Absolute core power

The average fission rate in the core which corresponds to the absolute reference irradiation is 1.87E+08 fission/cm/sec from fuel at the mid-plane. This average fission rate corresponds to a power ($P_{v2}$) of 595 Watt. $P_{v2}$ can be calculated as follows:

$$P_{V2} = T_{avg} \times F_{ax} \times L \times 8 \times \left( E_u \sum_i t_{ri} + E_{MOX} \sum_j t_{rj} \right)$$

where $T_{avg}$ is the average fission rate in the core (1.87E+08), $F_{ax}$ is the axial form factor (0.768), $L$ is the active length (50 cm), $E_u$ is the average energy released by a fission in the zone $U$ (201.9 MeV), $E_{MOX}$ is the average energy released by a fission in the zone MOX (207.15 MeV), $\sum_i t_{ri}$ is the sum of relative fission rate in the zones $UO_2$ (3.3 and 4.0 w/o) in 1/8 of the core and $\sum_j t_{rj}$ is the sum of relative fission rate in the zones MOX in 1/8 of the core. The values of $\sum_i t_{ri}$ and $\sum_j t_{rj}$ are 247.69 and 71.08, respectively.

## VII. Vertical bucklings in the core and outside

Vertical bucklings in the core have been proven to be independent on the energy by scanning $^{235}U$ and $^{237}Np$ fission chambers.

**Table 3. Isotopic concentrations of each medium**

*[Unit: $\times 10^{24}$ atoms/cm$^3$]*

| Isotope | *(1) Fuel* | | | |
|---|---|---|---|---|
| | **Fuel 3.3 (III)** | **Fuel 4.0 (IV)** | **Fuel 2.0/2.7 (V)** | **Pyrex (III)** |
| $^{234}$U | 6.74355E-06 | 7.18011E-06 | 3.30640E-06 | |
| $^{235}$U | 7.65484E-04 | 9.27587E-04 | 4.11948E-04 | |
| $^{236}$U | 3.68898E-06 | 5.28194E-06 | 2.66363E-06 | |
| $^{238}$U | 2.20958E-02 | 2.18433E-02 | 1.99057E-02 | |
| $^{239}$Pu | | | 4.45532E-04 | |
| $^{240}$Pu | | | 9.58115E-05 | |
| $^{241}$Pu | | | 1.69784E-05 | |
| $^{242}$Pu | | | 2.43920E-06 | |
| $^{241}$Am | | | 4.17501E-07 | |
| O | 4.56748E-02 | 4.55668E-02 | 4.27315E-02 | 4.52349E-02 |
| Si | | | | 1.74982E-02 |
| $^{10}$B | 3.61831E-09 | | | 1.11422E-03 |
| $^{11}$B | 1.46791E-08 | | | 4.52026E-03 |
| Al | | | | 5.80360E-04 |
| Fe | | | | 8.38333E-06 |
| Na | | | | 1.48604E-03 |
| K | | | | 3.21181E-04 |
| **Isotope** | *(2) Cladding* | | | |
| | **Fuel 3.3 (III)** | **Fuel 4.0 (IV)** | **Fuel 2.0/2.7 (V)** | **Pyrex (III)** |
| C | | 1.58259E-04 | 1.58259E-04 | 1.18831E-04 |
| Mn | | 1.11582E-03 | 1.11582E-03 | 7.53397E-04 |
| P | | 3.06841E-05 | 3.06841E-05 | |
| S | | 2.22292E-05 | 2.22292E-05 | |
| Si | | 2.28418E-04 | 2.28418E-04 | 4.91242E-04 |
| Cr | 7.69687E-05 | 1.67247E-02 | 1.67247E-02 | 1.68354E-02 |
| Ni | | 8.12063E-03 | 8.12063E-03 | 7.70038E-03 |
| Mo | | 6.53870E-05 | 6.53870E-05 | 3.47149E-05 |
| Fe | 1.43328E-04 | 5.95972E-02 | 5.95972E-02 | 6.03491E-02 |
| Sn | 4.75353E-04 | | | |
| O | 3.00251E-04 | | | |
| Zr | 4.30682E-02 | | | |

**Table 3. Isotopic concentrations of each medium (*continued*)**

*[Unit: $\times 10^{24}$ atoms/cm$^3$]*

| Isotope | *(3) Top stop* | | | |
|---|---|---|---|---|
| | **Fuel 3.3 (III)** | **Fuel 4.0 (IV)** | **Fuel 2.0/2.7 (V)** | **Pyrex (III)** |
| C | 1.67561E-04 | 1.78287E-05 | 1.78287E-05 | 1.67354E-04 |
| Mn | 1.37809E-03 | 1.46630E-04 | 1.46630E-04 | 1.37639E-03 |
| P | 3.86757E-05 | 4.11515E-06 | 4.11515E-06 | 3.86281E-05 |
| S | 4.18413E-05 | 4.45197E-06 | 4.45197E-06 | 4.17897E-05 |
| Si | 7.84820E-04 | 8.35060E-05 | 8.35060E-05 | 7.83853E-04 |
| Cr | 1.67723E-02 | 1.78460E-03 | 1.78460E-03 | 1.67517E-02 |
| Ni | 7.02105E-03 | 7.47050E-04 | 7.47050E-04 | 7.01240E-03 |
| Co | 9.75694E-05 | 1.03815E-05 | 1.03815E-05 | 9.74493E-05 |
| Fe | 6.08736E-02 | 6.47704E-03 | 6.47704E-03 | 6.07986E-02 |
| **Isotope** | *(4) Top and bottom reflectors* | | | |
| | **Fuel 3.3 (III)** | **Fuel 4.0 (IV)** | **Fuel 2.0/2.7 (V)** | **Pyrex (III)** |
| Top reflector | | | | |
| H | 5.34934E-02 | 5.70908E-02 | 5.70908E-02 | 5.44817E-02 |
| O | 1.33734E-02 | 1.42727E-02 | 1.42727E-02 | 1.36204E-02 |
| C | 3.34334E-02 | 3.56818E-02 | 3.56818E-02 | 3.40511E-02 |
| Bottom reflector | | | | |
| H | 5.71386E-02 | 5.70908E-02 | 5.70908E-02 | 5.71030E-02 |
| O | 1.42847E-02 | 1.42727E-02 | 1.42727E-02 | 1.42758E-02 |
| C | 3.57117E-02 | 3.56818E-02 | 3.56818E-02 | 3.56894E-02 |
| **Isotope** | *(5) Top and bottom blankets* | | | |
| | **Fuel 3.3 (III)** | **Fuel 4.0 (IV)** | **Fuel 2.0/2.7 (V)** | **Pyrex (III)** |
| C | 1.65087E-04 | | | |
| Mn | 1.35774E-03 | | | |
| P | 3.81048E-05 | | | |
| S | 4.12236E-05 | | | |
| Si | 7.73234E-04 | | | |
| Cr | 1.65247E-02 | | | |
| Ni | 6.91740E-03 | | | |
| Co | 9.61290E-05 | | | |
| Fe | 5.99749E-02 | | | |
| Al | | | | 6.01283E-02 |

**Table 3. Isotopic concentrations of each medium (*continued*)**

*[Unit: $\times 10^{24}$ atoms/cm$^3$]*

| Isotope | *(6) Bottom stop* | | | |
|---|---|---|---|---|
| | **Fuel 3.3 (III)** | **Fuel 4.0 (IV)** | **Fuel 2.0/2.7 (V)** | **Pyrex (III)** |
| | <Upper part> | | | |
| Sn | 3.77162E-04 | | | |
| Fe | 1.16809E-04 | | | |
| Cr | 6.84304E-05 | | | |
| O | 2.40991E-04 | | | |
| Zr | 3.18600E-02 | | | |
| | <Lower part> | | | |
| C | 1.65778E-04 | 1.66233E-05 | 1.66233E-05 | 1.41004E-04 |
| Mn | 1.36343E-03 | 1.36717E-04 | 1.36717E-04 | 1.15967E-03 |
| P | 3.82643E-05 | 3.83693E-06 | 3.83693E-06 | 3.25460E-05 |
| S | 4.13961E-05 | 4.15097E-06 | 4.15097E-06 | 3.52098E-05 |
| Si | 7.76471E-04 | 7.78601E-05 | 7.78601E-05 | 6.60433E-04 |
| Cr | 1.65939E-02 | 1.66394E-03 | 1.66394E-03 | 1.41140E-02 |
| Ni | 6.94636E-03 | 6.96542E-04 | 6.96542E-04 | 5.90827E-03 |
| Co | 9.65315E-05 | 9.67963E-06 | 9.67963E-06 | 8.21055E-05 |
| Fe | 6.02260E-02 | 6.03913E-03 | 6.03913E-03 | 5.12256E-02 |

**Table 3. Isotopic concentrations of each medium (*continued*)**

*[Unit: $\times 10^{24}$ atoms/cm$^3$]*

| Isotope | *(7) Some regions (II, VIII, X, XII, and XIX), water and Plexiglas* | | | |
|---|---|---|---|---|
| | **Inner baffle (II)** | **Barrel (VIII)** | **Neutron pad (X)** | **Jacket inner wall (XII)** |
| C | 2.33758E-04 | 5.94172E-05 | 6.33765E-05 | 9.50647E-05 |
| Mn | 1.43007E-03 | 1.12840E-03 | 7.18758E-04 | 1.01146E-03 |
| P | 4.60904E-05 | 4.30086E-05 | 3.99353E-05 | 3.83993E-05 |
| S | 1.92922E-05 | 7.41848E-06 | 5.93460E-06 | 1.18692E-05 |
| Si | 4.82890E-04 | 8.69016E-04 | 6.69105E-04 | 6.33533E-04 |
| Cr | 1.49817E-02 | 1.68945E-02 | 1.64896E-02 | 1.61208E-02 |
| Ni | 7.06986E-03 | 8.26722E-03 | 8.58228E-03 | 7.97273E-03 |
| Mo | 2.25205E-04 | 2.35076E-04 | 2.10769E-04 | 2.24159E-04 |
| Co | 1.11430E-04 | 7.83073E-05 | 1.58225E-04 | 9.12213E-05 |
| Fe | 6.15917E-02 | 5.86292E-02 | 5.92058E-02 | 5.99351E-02 |
| N | | 2.71734E-04 | | 9.17074E-05 |
| **Isotope** | **Reactor support (XIX)** | **Water** | **Plexiglas** | |
| C | 6.31230E-06 | | 3.57937E-02 | |
| Mn | 6.71607E-05 | | | |
| P | 2.54972E-06 | | | |
| S | 7.88115E-07 | | | |
| Si | 4.20666E-05 | | | |
| Cr | 1.07042E-03 | | | |
| Ni | 5.29390E-04 | | | |
| Mo | 1.48841E-05 | | | |
| Co | 6.05709E-06 | | | |
| Fe | 3.97969E-03 | | | |
| N | 6.08937E-06 | | | |
| H | 6.24330E-02 | 6.68734E-02 | 5.72700E-02 | |
| O | 3.12165E-02 | 3.34367E-02 | 1.43175E-02 | |

**Table 3. Isotopic concentrations of each medium (*continued*)**

| *(8) The others* | |
|---|---|
| **Region** | **Material** |
| Central hole (I) | Water: See “Water” |
| Outer baffle (VI) | Stainless steel: See “Inner baffle” |
| Reflector (VII) | Water: See “Water” |
| Water gap (IX) | Water: See “Water” |
| Space between neutron pad and jacket (XI) | Water: See “Water” |
| Jacket (XIII) | Air with 100% relative humidity |
| Jacket outer wall (XIV) | Stainless steel: See “Jacket inner wall” |
| Space between jacket and reactor vessel (XV) | Water: See “Water” |
| Reactor vessel wall (XVI) | Stainless steel: See “Jacket inner wall” |
| Lower filling (XVIII) | Water: See “Water” |
| Bottom grid (XX)[1] | – Water (32.8 vol.%): See “Water”<br>– Plexiglas (67.2 vol.%): See “Plexiglas” |
| Lower reflector (XXI) | Water: See “Water” |
| Intermediate grid (XXII)[2] | – Water (63.4 vol.%): See “Water”<br>– Plexiglas (36.6 vol.%): See “Plexiglas” |
| Upper reflector (XXIII) | Water: See “Water” |
| Upper grid (XXIV)[3] | – Water (63.4 vol.%): See “Water”<br>– Stainless steel (36.6 vol.%): See “Jacket inner wall” |
| Upper filling (XXV) | Water: See “Water” |
| Below inner baffle | Plexiglas: See “Plexiglas” |
| Below outer baffle | Plexiglas: See “Plexiglas” |
| Below barrel | Plexiglas: See “Plexiglas” |

[1] The bottom pin of the fuel pin is included in the bottom stop, which is assumed to be cylindrical and to be supported by the upper face of the bottom grid.

[2] The intermediate reactor grid is partially filled by the pins, such that water is partially replaced by Plexiglas and cladding tube.

[3] This is the composition where no pin is loaded, in the loaded part the water is partially replaced by stainless steel due to the top stop of the pins (Regions III, IV and V).

In order to obtain vertical bucklings representative of the core, six fuel pins (three 4.0/0 and three 3.3/0 ones) were measured axially by γ-scanning after an irradiation of eight hours at 90% of the VENUS maximum power. The data correspond to the gamma activity of the $^{140}$La (fission yield ~6%, energy ~1.6 MeV, effective half-life ~12.8 d). The measured gamma activities were improved for decay and analysed by a least square cosine fitting, which defines the extrapolated height of the reactor and the corresponding buckling.

As no significant geometrical dependence appears, it is proposed to adopt a unique vertical buckling for the fuel region of the VENUS mock-up.

$$B_{v,\,core} = (4.90 \pm 0.01)\ 10^{-2}\ cm^{-1} \quad \textit{or} \quad B^2_{\,v,\,core} = (2400 \pm 12)\ 10^{-6}\ cm^{-2}$$

Vertical bucklings were measured by scanning in 17 locations from the central hole to neutron pad.

In VENUS, the azimuthal buckling variation is "felt" as an effect of the distance to the core; as the variation is not very high it is recommended to adopt an average buckling per region as a function of the distance to the core:

| | | | |
|---|---|---|---|
| Water reflector | : from 0 to ~ 16.7 cm | $B_{v,\,reflector}$ | $= (4.84 \pm 0.06)\ 10^{-2}\ cm^{-1}$ |
| Barrel | : from 10 to ~ 19.3 cm | $B_{v,\,barrel}$ | $= (4.79 \pm 0.03)\ 10^{-2}\ cm^{-1}$ |
| Water gap | : from 15.7 to ~ 24.8 cm | $B_{v,\,water\ gap}$ | $= (4.75 \pm 0.03)\ 10^{-2}\ cm^{-1}$ |
| Neutron pad | : from 22.1 to ~ 31.3 cm | $B_{v,\,neutron\ pad}$ | $= (4.71 \pm 0.03)\ 10^{-2}\ cm^{-1}$ |

## VIII. References


[1] Leenders, L., "VENUS LWR-PVS-Benchmark: Definition and Qualifications of the Geometry", Letters to Dr. Kam and Dr. Williams (ORNL), Dated 7 July 1983.

[2] Leenders, L. "VENUS-Core: Definition and Qualifications of the Materials, and Up-dating" Letters to Dr. Kam and Dr. Williams (ORNL), Dated 22 June 1983 and 7 September 1983.

[3] Na, B-C. and N. Messaoudi, *Blind Benchmark on the 3-D VENUS-2 MOX Core Measurements*, OECD/NEA Document, Final Specification, NEA/SEN/NSC/WPPR(2001)1 (2001); Appendix A: VENUS-2 PWR Core Source and Azimuthal Lead Factor Experiments.

[4] Hehn, G. and B-C. Na, *Prediction of Neutron Embrittlement in the Reactor Pressure Vessel: VENUS-1 and VENUS-3 Benchmarks*, OECD/NEA Report, NEA/NSC/DOC(2000)5, ISBN 92-64-17637-3 (2000).

[5] C*RC Handbook of Chemistry and Physics, 2002-2003*, 83rd Edition, David R. Lide, Ed.

*Annex to Appendix A.1*

## VENUS-2 PWR CORE SOURCE AND AZIMUTHAL LEAD FACTOR EXPERIMENTS – DESCRIPTION OF THE COMPOSITION OF DIFFERENT MATERIALS

The compositions of all the materials in the VENUS-2 core are given in Tables A.1-A.11. All the data are extracted from the SCK•CEN report *VENUS-2 PWR Core Source and Azimuthal Lead Factor Experiments and Calculational Tests*.

**Table A.1. Compositions of the 3.0/0 fuel cell**

| | |
|---|---|
| **Fuel composition** | $UO_2$ |
| **Fuel stoichiometry [O/U]** | 1.997 ± .005 |
| **Fuel linear specific weight [g/cm]** | (5.40 ± .05) |
| **Fuel isotopic composition of U [w/o]** | $^{234}U$ (.029 ± .001)<br>$^{235}U$ (3.306 ± .010)<br>$^{236}U$ (.016 ± .001)<br>$^{238}U$ (96.649 ± .012) |
| **Total impurities** | .8 ppm B equivalent in U |
| **Cladding composition** | Zircaloy 4 |
| **Cladding linear specific weight [g/cm]** | (1.0627 ± .0004) |
| **Cladding isotopic composition [w/o]** | Sn (1.41 ± .06)<br>Fe (.20 ± .01)<br>Cr (.10 ± .01)<br>O (.12 ± .01)<br>Zr (98.17 ± .06) |
| **Detected impurities in the cladding** | – < 1 ppm: B, Cd, U<br>– < 10 ppm: C1, Co, Cu, H, Mg, Mn, Ti, Zn<br>– < 50 ppm: Al, Hf, N, Nb, Ni, V, W, Au, Ir, Mo, Pb<br>– < 100 ppm: Ta, Si, Sm, Eu, Dy, Gd, Lu<br>– 146 ppm: C |
| **Moderator** | Water |

**Table A.2. Compositions of the 4.0/0 fuel cell**

| | |
|---|---|
| **Fuel composition** | $UO_2$ |
| **Fuel stoichiometry [O/U]** | 2.00 ± .01 |
| **Fuel linear specific weight [g/cm]** | (6.39 ± .70) |
| **Fuel isotopic composition of U [w/o]** | $^{234}U$ (.031 ± .009)<br>$^{235}U$ (4.022 ± .008)<br>$^{236}U$ (.023 ± .006)<br>$^{238}U$ (95.924 ± .010) |
| **Total impurities** | Not available |
| **Cladding composition** | AISI 304 stainless steel |
| **Cladding linear specific weight [g/cm]** | (.8855 ± .0007) |
| **Cladding isotopic composition [w/o]** | C (.040 ± .040)<br>Mn (1.290 ± .030)<br>P (.020 ± .020)<br>S (.015 ± .015)<br>Si (.135 ± .003)<br>Cr (18.300 ± .400)<br>Ni (10.030 ± .200)<br>Mo (.132 ± .003)<br>Fe (70.038 ± .711) |
| **Detected impurities** | – < 10 ppm: Cd, Ta, Au, B, Co<br>– < 100 ppm: Sm, Eu, Dy, Ir, Gd |
| **Moderator** | Water |

**Table A.3. Compositions of the 2.0/2.7 MOX fuel cell**

| | |
|---|---|
| **Stoichiometry [O/(U+Pu)]** | 2.046 |
| **Linear density [g/cm]** | 6.000 |
| **Chemical composition [w/o]**<br>**$UO_2/[UO_2+PuO_2)]$**<br>**$PuO_2/[UO_2+PuO_2)]$** | <br>97.3<br>2.70 |
| **Fuel isotopic composition [w/o]** | $^{233}U/U$ 0.0000<br>$^{234}U/U$ 0.0160<br>$^{235}U/U$ 2.0020<br>$^{236}U/U$ 0.0130<br>$^{238}U/U$ 97.976<br>$^{238}Pu/Pu$ 0.0000<br>$^{239}Pu/Pu$ 79.370<br>$^{240}Pu/Pu$ 17.140<br>$^{241}Pu/Pu$ 3.0500<br>$^{242}Pu/Pu$ 0.4400<br>$^{241}Am/Pu$ 0.0750 |
| **Specific weight of components [g/cm$^3$]** | Mixture ($UO_2+PuO_2$) 9.389633<br>$UO_2$ in mixture 9.136113<br>$PuO_2$ in mixture 0.253520<br>U metal 8.031689<br>Pu metal 0.2229926<br>$^{16}O$ total 1.134957 |
| **Cladding** | Stainless Steel |
| **Cladding linear specific weight [g/cm]** | 0.8855 |
| **Cladding isotopic composition [w/o]** | C 0.0400<br>Mn 1.2900<br>P 0.0200<br>S 0.0150<br>Si 0.1350<br>Cr 18.300<br>Ni 10.030<br>Mo 0.1320<br>Fe 70.038 |
| **Moderator** | Water |

**Table A.4. Compositions of the Pyrex cell**

| | |
|---|---|
| **Pyrex material** | Corning glass code 7740 |
| **Pyrex linear specific weight [g/cm]** | (.7886 ± .0052) |
| **Pyrex isotopic composition [w/o]** | $SiO_2$ 78.53<br>$B_2O_3$ (14.65 ± .15)<br>$Al_2O_3$ 2.21<br>$Fe_2O_3$ .05<br>$Na_2O$ 3.44<br>$K_2O$ 1.13 |
| **Isotopic composition of B [a/o]** | $^{10}B$: (19.775 ± .005)<br>$^{11}B$: (80.225 ± .005) |
| **Cladding material** | AISI 304 stainless steel |
| **Cladding specific weight [g/cm$^3$]** | (7.9 ± .1) |
| **Cladding isotopic composition [w/o]** | C (.03 ± .03)<br>Mn (.87 ± .42)<br>Si (.29 ± .16)<br>Cr (18.40 ± .10)<br>Ni (9.50 ± .50)<br>Mo (.07 ± .07)<br>Fe (70.84 ± 1.28) |
| **Moderator** | Water |

**Table A.5. Compositions of the central hole/reflector/water gap/space between neutron pad and jacket/space between jacket and reactor vessel**

| | |
|---|---|
| **Chemical composition** | Water ($H_2O$) |
| **Diluted oxygen** | O 8.6 ppm (saturation for air-water contact) |
| **Detected impurities** | B 12 ppb (1.E-9 g/l) ~ ppm (weight)<br>Si 46<br>Mn 2.5<br>Fe 0.7<br>Mg 5<br>Cu 5<br>Ca 75<br>Al 8<br>Sr .5<br>Zn 25<br>V 5<br>Ag 2<br>Ba 15 |
| **Non-detected impurities** | Li, Zr, Ti, Be, Nb, Ga, Hf, Co, In, Bi, Ni, Pb, Cd, Te, P, Ge, W, Sb, Cr, Mo, Hg, As, Tl, Sn |
| **Temperature [°C]** | (23.0 ± 1.5) |

**Table A.6. Compositions of the inner and outer baffles**

| | |
|---|---|
| **Chemical composition** | AISI 304 stainless steel |
| **Isotopic composition [w/o]** | C (.059 ± .020)<br>Mn (1.651 ± .053)<br>P (.030 ± .015)<br>S (.013 ± .013)<br>Si (.285 ± .129)<br>Cr (16.370 ± .327)<br>Ni (8.720 ± .185)<br>Mo (.454 ± .075)<br>Co (.138 ± .070)<br>Fe (72.281 ± .231) |
| **Detected impurities** | – < 10 ppm: Cd, Ta, Au, B<br>– < 100 ppm: Sm, Eu, Dy, Ir, Gd |
| **Non-detected impurity** | Cu |
| **Specific weight [g/cm$^3$]** | (7.902 ± .002) |

**Table A.7. Compositions of the barrel**

| **Chemical composition** | AISI 304 stainless steel |
|---|---|
| **Isotopic composition [w/o]** | C .015<br>Mn (1.303 ± .430)<br>P .028<br>S .005<br>Si .513<br>Cr (18.464 ± .200)<br>Ni (10.199 ± .380)<br>Mo .474<br>Co .097<br>Fe (68.819 ± 1.010)<br>N .080 |
| **Non-detected impurity** | Cd, Sm, Eu, Dy, Ir, Gd, Ta, Cu, Au, B |
| **Specific weight [g/cm$^3$]** | (7.9 ± .1) |

**Table A.8. Compositions of the neutron pad**

| **Chemical composition** | AISI 304 stainless steel |
|---|---|
| **Isotopic composition [w/o]** | C .016<br>Mn (.830 ± .280)<br>P .026<br>S .004<br>Si .395<br>Cr (18.022 ± .030)<br>Ni (10.588 ± .360)<br>Mo .425<br>Co .196<br>Fe (69.498 ± .670) |
| **Non-detected impurity** | Cd, Sm, Eu, Dy, Ir, Gd, Ta, Cu, Au, B |
| **Specific weight [g/cm$^3$]** | (7.9 ± .1) |

**Table A.10. Compositions of the jacket inner wall/jacket outer wall/reactor vessel wall**

| **Chemical composition** | AISI 304 stainless steel |
|---|---|
| **Isotopic composition [w/o]** | C (.024 ± .012)<br>Mn (1.168 ± .270)<br>P (.025 ± .003)<br>S (.008 ± .005)<br>Si (.374 ± .150)<br>Cr (17.619 ± 1.047)<br>Ni (9.836 ± .934)<br>Mo (.452 ± .024)<br>Co (.113 ± .074)<br>Fe (70.354 ± 1.963)<br>N (.027 ± .040) |
| **Specific weight [g/cm$^3$]** | (7.9 ± .1) |

**Table A.11. Compositions of the jacket volume and around the reactor vessel**

| **Jacket volume** | Air with 100% relative humidity |
|---|---|
| **Around the reactor vessel** | Dry air |

*Appendix A.2*

## CALCULATION DETAILS

Please provide as detailed a description as possible of your treatment of this problem. You are requested to include the following:

**1**. **Authors.**

**2**. **Transport method and modelling assumptions, including:**

- description of the calculations procedure (all important information about modelling assumptions and codes/methods used); if $S_N$ method is used then the quadrature set order should be reported (a symmetric or not quadrature is used?), etc.;

- grid/mesh structure of the model ***(including a picture of the geometrical model used).***

**3. Transport cross-sections, including:**

- the name and version of the point library neutron transport cross-section data and the energy group structure;

- method/model used in cross-section collapsing.

**4. Neutron source.**

**5. Axial leakage treatment (for two-dimensional calculation only).**

**6. Response functions and fission averaged data, including:**

- the name and version of the dosimeter cross-sections data.

**7. Comments/special references:**

- any other information not listed above but judged by the participant as important in interpreting the benchmark results should be included.

*Appendix B*

# CALCULATION DETAILS PROVIDED BY THE PARTICIPANTS

## 1. Hanyang University, Korea

### 1. Authors

Chang-ho Shin and Jong Kyung Kim
Dept. of Nuclear Engineering
Hanyang University
Seoul, Korea

### 2. Transport method and modelling assumptions

For the VENUS-2 core dosimetry benchmark, the 3-D discrete ordinate method was used with the TORT code. The VENUS-2 core was modelled with a $119 \times 126 \times 111$ mesh in a Cartesian co-ordinate. A $S_8$ order symmetric quadrature set was used. Using the BOT3P code, a 3-D discrete model was developed. In this VENUS-2 core modelling, the outside of the reactor core was modelled as air and the vacuum boundary condition was employed.

### 3. Transport cross-sections

A 35-group, $P_3$ Legendre polynomial, cross-section was generated for 20 material mixtures using the NJOY and TRANSX codes with the ENDF-B/VI Release 8 library. The neutron energy group structure in the cross-section was shown in Table 1.

### 4. Neutron source

The relative power distribution in the VENUS-2 core was generated for the subsequent dosimetry calculation as the neutron source using TORT. A multiplication factor of $1.13736 \times 10^{13}$ sources/sec was calculated in order to consider the total fission source and then all the TORT results were multiplied by the value.

### 5. Axial leakage treatment (for 2-D calculation only)

N/A

### 6. Response functions and fission averaged data

The IRDF-90 Version 2 cross-section library was used for the dosimetry calculation.

### 7. Comments/special references

The DPA cross-section of $^{56}Fe$ within ENDF/B-VI Release 8 was used to calculate the DPAs.

### References

[1] Chi Young Han, *et al*., *VENUS-2 MOX-fuelled Reactor Dosimetry Calculations – Benchmark Specification*, NEA/NSC/DOC(2004)6, Nuclear Energy Agency (2004).

[2] "Code System for Producing Pointwise and Multigroup Neutron and Photon Cross-sections from ENDF/B Data, NJOY99.0", RSICC Code Package PSR-480, Oak Ridge National Laboratory (2000).

[3] MacFarlane, R.E., *TRANSX 2: A Code for Interfacing MATXS Cross-section Libraries to Nuclear Transport Codes*, LA-12312-MS, Los Alamos National Laboratory (1992).

[4] Rose, P.F., "ENDF/B-VI Summary Documentation (ENDF-201)", BNL-NCS-17541, 4th edition, Brookhaven National Laboratory (1991).

[5] Kocherov, McLaughlin, *The International Reactor Dosimetry File (IRDF-90)*, IAEA-NDS-141, Rev. 2, International Atomic Energy Agency (1993).

[6] "One-, Two- and Three-dimensional Discrete Ordinates Neutron/Photon Transport Code System, DOORS, Version 3.2", RSICC Code Package CCC-650, Oak Ridge National Laboratory (1998).

[7] *The ENEA Bologna Pre-processors of the DORT, TORT, TWODANT, THREEDANT and MCNP Transport Codes and Post-processors of DORT and TORT, BOT3P, Version 3.0*, FIS-P129-001, ENEA (2002).

**Table 1. Neutron energy group structure**

*[Unit: MeV]*

| Group | Upper bound | Lower bound | Group | Upper bound | Lower bound |
|---|---|---|---|---|---|
| 1 | 2.0000E+01 | 8.8250E+00 | 19 | 4.0868E-02 | 2.8088E-02 |
| 2 | 8.8250E+00 | 6.0653E+00 | 20 | 2.8088E-02 | 1.5034E-02 |
| 3 | 6.0653E+00 | 4.7237E+00 | 21 | 1.5034E-02 | 1.1709E-02 |
| 4 | 4.7237E+00 | 4.0657E+00 | 22 | 1.1709E-02 | 7.1017E-03 |
| 5 | 4.0657E+00 | 3.1664E+00 | 23 | 7.1017E-03 | 1.7956E-03 |
| 6 | 3.1664E+00 | 2.8650E+00 | 24 | 1.7956E-03 | 8.4818E-04 |
| 7 | 2.8650E+00 | 2.7253E+00 | 25 | 8.4818E-04 | 5.1445E-04 |
| 8 | 2.7253E+00 | 2.3650E+00 | 26 | 5.1445E-04 | 3.1203E-04 |
| 9 | 2.3650E+00 | 2.0189E+00 | 27 | 3.1203E-04 | 1.8926E-04 |
| 10 | 2.0189E+00 | 1.3534E+00 | 28 | 1.8926E-04 | 1.2099E-05 |
| 11 | 1.3534E+00 | 6.3928E-01 | 29 | 1.2099E-05 | 3.0590E-06 |
| 12 | 6.3928E-01 | 4.2852E-01 | 30 | 3.0590E-06 | 1.1254E-06 |
| 13 | 4.2852E-01 | 3.0197E-01 | 31 | 1.1254E-06 | 1.0137E-06 |
| 14 | 3.0197E-01 | 2.3518E-01 | 32 | 1.0137E-06 | 7.3000E-07 |
| 15 | 2.3518E-01 | 1.8316E-01 | 33 | 7.3000E-07 | 3.5767E-07 |
| 16 | 1.8316E-01 | 1.1109E-01 | 34 | 3.5767E-07 | 6.7000E-08 |
| 17 | 1.1109E-01 | 6.7379E-02 | 35 | 6.7000E-08 | 1.0000E-10 |
| 18 | 6.7379E-02 | 4.0868E-02 | | | |

## 2. Hanyang University, Korea

***MCNP-4C***

### 1. Authors

Chi Young Han and Jong Kyung Kim
Dept. of Nuclear Engineering
Hanyang University
Seoul, Korea

### 2. Transport method and modelling assumptions

The Monte Carlo method was used with the MCNP-4C code and the VENUS-2 core was modelled explicitly with no assumption.

### 3. Transport cross-sections

The ENDF/B-6.8 cross-section library was used for transport calculation.

### 4. Neutron source

The SSW card of the MCNP code was used to generate a KCODE (criticality calculation) fission volume source file for use in a subsequent dosimeter calculation using the SSR card.

For the total fission source employed in the MCNP calculation, a multiplication factor of 1.15909E+13 sources/sec was calculated and MCNP results were multiplied by this value.

### 5. Axial leakage treatment (for two-dimensional calculation only)

### 6. Response functions and fission averaged data

The IRDF-90 Version 2 cross-section library was used for dosimeter calculation.

### 7. Comments/special references

The DPA cross-section of $^{56}Fe$ within ENDF/B-6.8 was used to calculate the DPAs.

***MCNPX***

### 1. Authors

Hong-Chul Kim, Chang-ho Shin, Chi Young Han, and Jong Kyung Kim
Dept. of Nuclear Engineering
Hanyang University
Seoul, Korea

### 2. Transport method and modelling assumptions

The Monte Carlo method was used with the MCNPX (Version 2.5.d) code and the VENUS-2 core was modelled explicitly with no assumption.

**3. Transport cross-sections**

The ENDF/B-6.8 cross-section library was used for transport calculation.

**4. Neutron source**

The SSW card of the MCNP code was used to generate a KCODE (criticality calculation) fission volume source file for use in a subsequent dosimeter calculation using the SSR card.

For the total fission source employed in the MCNP calculation, a multiplication factor of 1.15976E+13 sources/sec was calculated and MCNP results were multiplied by this value.

**5. Axial leakage treatment (for two-dimensional calculation only)**

**6. Response functions and fission averaged data**

The IRDF-90 Version 2 cross-section library was used for dosimeter calculation.

**7. Comments/special references**

The DPA cross-section of $^{56}$Fe within ENDF/B-6.8 was used to calculate the DPAs.

## 3. Transpire Inc., USA

### 1. Authors

Todd Wareing, Allen Barnett, John McGhee and Greg Failla
Transpire, Inc.
6659 Kimball Drive Suite D-404
Gig Harbor, WA 98335

### 2. Transport method and modelling assumptions

The performance of the Attila™ radiation transport code, provided by Transpire, Inc., was evaluated for reactor dosimetry calculations. Attila is a complete transport system which combines a 3-D unstructured grid discrete ordinates solver with an intuitive graphical user interface (GUI) for pre-processing (mesh generation), analysis set-up and post-processing (visualisation). Attila uses an accurate linear discontinuous finite-element spatial differencing scheme in conjunction with an efficient diffusion synthetic acceleration algorithm [1,2]. Through direct integration with CAD and the use of variably-sized, body-fitted tetrahedral elements, Attila can model any level of geometric complexity.

The quarter-core VENUS-2 model was generated using Solidworks®, a widely-used solid modelling CAD system, and was imported directly into Attila. With the exception of the homogenised fuel elements, the complete geometry was modelled, which is shown in Figure 1 (some components hidden for clarity). Figure 2 shows the corresponding computational mesh generated by Attila, which includes 117 752 tetrahedral elements. The Attila calculations were performed using $S_8$ level symmetric quadrature and $P_3$ scattering.

### 3. Transport cross-sections

The Radion-5 multi-group cross-section library was used. This is a new library generated by Transpire, Inc. for use in shielding calculations. It was created through NJOY using ENDF/B-VI data, and consists of 30 neutron groups and 25 gamma groups. The neutron group structure is provided in Table 1. No additional cross-section collapsing was performed.

### 4. Neutron source

To generate the 3-D neutron source, the normalised axial fission source data provided in the benchmark specification was averaged to obtain a single axial fission source profile. This was then combined with the normalised radial fission source profile to create the 3-D fission source profile. To translate the fission source to the corresponding neutron source, the fission source was multiplied by the average number of neutrons per fission, $\upsilon$. For the MOX pins, an average value for $\upsilon$ was obtained by multiplying the fraction of the $^{235}U$ atoms by 2.43 (average $\upsilon$ for $^{235}U$) plus the fraction of $^{239}Pu$ atoms times 2.91 (average $\upsilon$ for $^{239}Pu$), yielding a value of $\upsilon = 2.68$. For the $UO_2$ pins, $\upsilon = 2.43$ was used. Thus, the pin fission source in the MOX regions were multiplied by 2.68 and the pin fission source in the $UO_2$ regions were multiplied by 2.43. The resulting 3-D relative neutron source distribution was then mapped onto the unstructured tetrahedral mesh using built-in routines in Attila. The energy spectrum of the neutron source consisted of using the fission spectra, $\chi$, of $^{235}U$ in the $UO_2$ regions. That for the MOX regions consisted of taking the fraction of $^{235}U$ atoms times the fission spectra for $^{235}U$ plus the fraction of $^{239}Pu$ atoms times the fission spectra for $^{239}Pu$. The total source in the problem was normalised to $4.596 \times 10^{12}$ fissions/sec/quadrant $\times$ $(240/640 \times 2.68 + 400/640 \times 2.43)$ neutrons/fission or $1.160 \times 10^{13}$ neutrons/sec/quadrant.

## 5. Axial leakage treatment (for two-dimensional calculation only)

## 6. Response functions and fission averaged data

All reaction cross-sections were obtained from the 620 group IRDF-90 Version 2 [3]. These data were collapsed to the 30 group structure of the Radion-5 cross-sections using a flat flux weighting. The average reaction cross-sections are given in Table 2.

## 7. Comments

The calculation was performed using a single 2.4 GHz Pentium IV processor, with a total CPU time of approximately 100 minutes. The Attila geometry (Figure 1) includes components that do not substantially influence the solution field in the regions of interest, such as structures above and below the reactor core and beyond the neutron pad. Eliminating or simplifying these structures could substantially reduce the total element count and the associated CPU time. However, since the CPU time was relatively small for this benchmark, no effort was made to optimise the model for computational speed.

The results for the scalar flux below 1 MeV and 0.1 MeV may have slight errors, since the Radion-5 cross-section library used for this benchmark does not contain groups with these lower bounds. The Attila results were obtained by taking only the portion of the flux in last group based upon the required energy bounds. That is, the flux was reduced by [(required lowest energy –lower energy of last group)/(upper energy of last group – lower energy of last group)] × (scalar flux of last group).

## References


[1] Wareing, T.A., J.M. McGhee and J.E. Morel, "ATTILA: A Three-dimensional, Unstructured Tetrahedral Mesh Discrete Ordinates Transport Code", *Trans. Am. Nucl. Soc*., Washington, DC, Volume 75, page 146, November 1996.

[2] Wareing, T.A., *et al*., "Discontinuous Finite Element Sn Methods on 3-D Unstructured Grids", *Nucl. Sci. Engr*., Volume 138, Number 2, July 2001.

[3] Kocherov, McLaughlin, "The International Reactor Dosimetry File (IRDF-90)**"**, IAEA-NDS-141, Rev. 2, October 1993.

**Table 1. Energy group structure of Radion-5 cross-sections**

| Group number | Upper energy | Lower energy |
|---|---|---|
| 1 | 2.00000E+01 | 1.70000E+01 |
| 2 | 1.70000E+01 | 1.60000E+01 |
| 3 | 1.60000E+01 | 1.50000E+01 |
| 4 | 1.50000E+01 | 1.39400E+01 |
| 5 | 1.39400E+01 | 1.30000E+01 |
| 6 | 1.30000E+01 | 1.20000E+01 |
| 7 | 1.20000E+01 | 1.10000E+01 |
| 8 | 1.10000E+01 | 1.00000E+01 |
| 9 | 1.00000E+01 | 8.82497E+00 |
| 10 | 8.82497E+00 | 7.78801E+00 |
| 11 | 7.78801E+00 | 6.87289E+00 |
| 12 | 6.87289E+00 | 6.06531E+00 |
| 13 | 6.06531E+00 | 5.35261E+00 |
| 14 | 5.35261E+00 | 4.72367E+00 |
| 15 | 4.72367E+00 | 3.67879E+00 |
| 16 | 3.67879E+00 | 2.86505E+00 |
| 17 | 2.86505E+00 | 2.23130E+00 |
| 18 | 2.23130E+00 | 1.73774E+00 |
| 19 | 1.73774E+00 | 1.19433E+00 |
| 20 | 1.19433E+00 | 8.20850E-01 |
| 21 | 8.20850E-01 | 2.35178E-01 |
| 22 | 2.35178E-01 | 6.73795e-02 |
| 23 | 6.73795e-02 | 1.93045e-02 |
| 24 | 1.93045e-02 | 5.53084e-03 |
| 25 | 5.53084e-03 | 3.53575e-04 |
| 26 | 3.53575e-04 | 2.26033e-05 |
| 27 | 2.26033e-05 | 3.46633e-06 |
| 28 | 3.46633e-06 | 6.25060e-07 |
| 29 | 6.25060e-07 | 1.23960e-08 |
| 30 | 1.23960e-08 | 1.00000e-11 |

**Table 2. Fission averaged reaction cross-sections**

| **Reaction** | $^{58}$Ni(n,p) | $^{115}$In(n,n′) | $^{103}$Rh(n,n′) | $^{64}$Zn(n,p) | $^{237}$Np(n,f) | $^{27}$Al(n,α) |
|---|---|---|---|---|---|---|
| **Cross-section (mbarn)** | 107.252 | 186.690 | 705.660 | 39.015 | 1349.940 | 0.753 |

**Figure 1. CAD geometry used for the Attila calculations**

*Some components hidden for clarity*

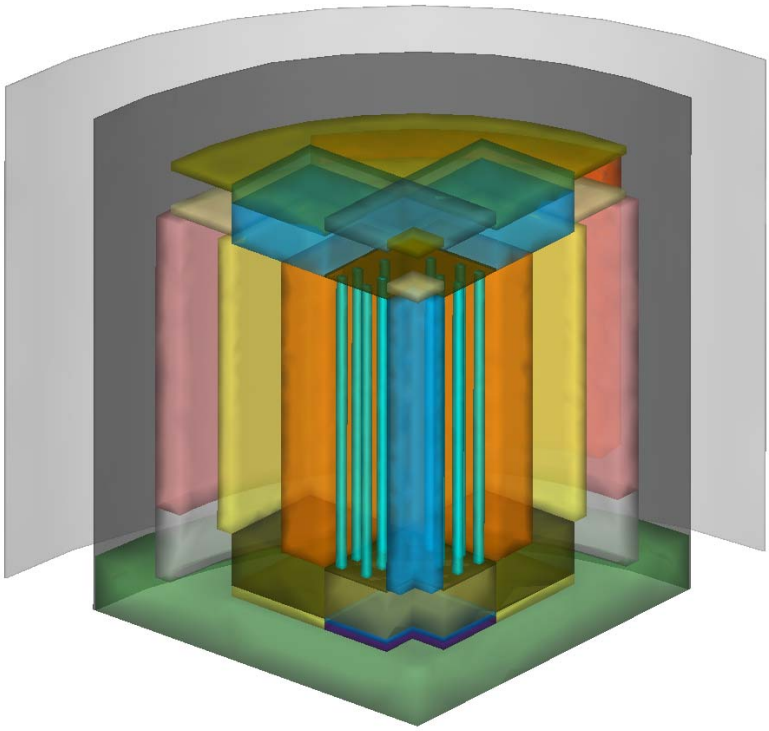

**Figure 2. Computational domain used by Attila**

*Some components hidden for clarity*

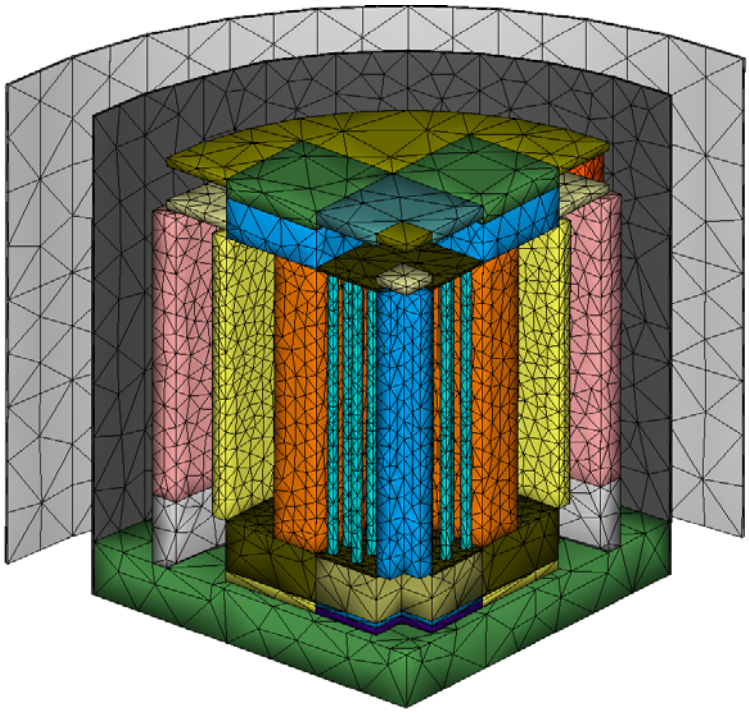

**Figure 3. Total scalar flux calculated by Attila**

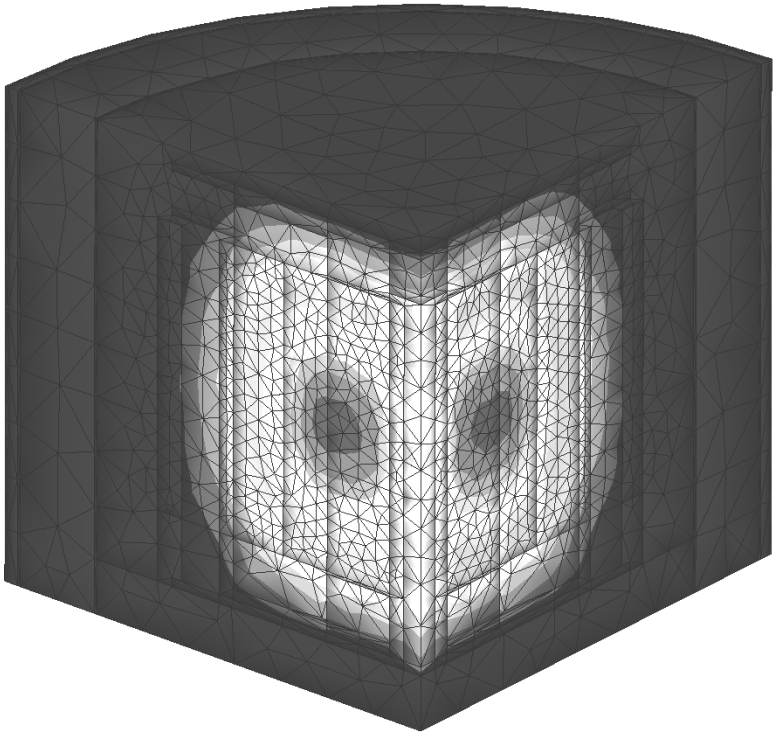

## 4. Kurchatov Institute, Russia

### 1. Author

Mikhail A. Kalugin

### 2. Transport method and modelling assumptions

#### *2.1 Description of the calculations procedure (all important information about modelling assumptions and codes/methods used)*

For calculations of this benchmark the MCU Monte Carlo code was used. The bibliographic references for the code are as follows:


[1] Abagjan, L.P., N.I. Alexeyev, V.I. Bryzgalov, "The Use of the Codes from MCU Family for Calculations of VVER Type Reactors", *Proceedings of the 10th AER International Topical Meeting*, Moscow, Russia, 18-22 September 2000.

[2] "The MCU/REA Code with Data Library DLC/MCUDAT-2.2", *Voprosy atomnoy nauki and Techniki*, Ser. FYaR. Issue, 3, pp. 55-62 (2001) (in Russian).

[3] Kalugin, M.A. and L.V. Maiorov, "Application of the Monte Carlo Method for Analyzing the IGR Reactor Experiments", *Proc. of the 1996 Topical Meeting Radiation Protection and Shielding*, No. Falmouth, Massachusetts, USA, 21-25 April 1996.


#### *2.2 Grid/mesh structure of the model (including a picture of the geometrical model used)*

The 3-D model is based on the benchmark specification provided in the document entitled: *VENUS-2 MOX-fuelled Reactor Dosimetry Calculations: Benchmark Specification* [OECD/NEA, NEA/NSC/DOC(2004)6] without any approximation except on the neutron pad. Neutron pad outer radius was taken as 65.073 cm instead of the one found in the benchmark specification. This approximation does not influence the results. XOY and XOZ cross-sections of the calculational models are shown in Figures 1 and 2.

### 3. Transport cross-sections

#### *3.1 The name and version of the point library neutron transport cross-section data and the energy group structure*

MCU data library is DLC/MCUDAT-2.1 based on:

- ENDF/B-VI, JENDL-3.2, BROND.
- MCU group own evaluations and compilations:
  - LIPAR – parameters of the fully resolved resonances.
  - BFS – phonon spectra library including the ENDF data.
  - KORT – cross-sections for E = 0.0253 eV, resonance integrals etc.

### *3.2 Method/model used in cross-section collapsing*

Monte Carlo method.

**4. Neutron source**

Neutron source was calculated directly during Monte Carlo modelling of the criticality problem.

**5. Axial leakage treatment (for two-dimensional calculation only).**

None.

**6. Response functions and fission averaged data, including the name and version of the dosimeter cross-sections data.**

The dosimeter cross-section libraries used for the calculations of all the desired reactions are mentioned below:

| | |
|---|---|
| $^{58}$Ni(n,p) | IRDF-90 Version 2 |
| $^{115}$In(n,n′) | IRDF-90 Version 2 |
| $^{103}$Rh(n,n′) | IRDF-90 Version 2 |
| $^{64}$Zn(n,p) | IRDF-90 Version 2 |
| $^{237}$Np(n,f) | ENDF/B-VI.5 |
| $^{27}$Al(n,$\alpha$) | IRDF-90 Version 2 |
| DPA | Damage Cross-section in Steel (EUR Standart) |

**7. Comments/special references: any other information not listed above but judged by the participant as important in interpreting the benchmark results**

Taking into account the peculiarities of the problem considered it is easy to see that the analogous simulation of the reactor is ineffective.

The special ALIGR [4] technique that is realised in the MCU code was used to overcome the difficulties. The ALIGR as a variance reduction tool is a combination of the following methods: geometry truncation, energy cut-off and splitting.

The ALIGR technique is based on solving the problem in several steps. This algorithm permits one to divide the criticality problem solution (first step) from the detectors reactions rate tally problem for detectors that placed far enough from the reactor core. It gives the possibility to calculate selected detectors (with different activation threshold) without repeated reactor calculation. The three-step ALIGR technique was used.

On the first step the homogeneous problem (the criticality problem) was solved and a neutron flux at the inner surface of the outer baffle is tallied. Additionally the dosimeter reaction rates and fluxes in the detectors placed in the inner baffle and central hole were obtained. $90 * 10^6$ neutron histories were modelled.

On the second step the non-homogeneous problem (problem with given neutron source S-1 – see Figure 1 that was calculated during the first step) was solved and neutron flux at the inner surface of the barrel is tallied. Additionally the dosimeter reaction rates and fluxes in the detectors placed in the outer baffle and reflector were obtained.

The second step game is played as follows. All the neutrons being tallied during the first step are considered as the surface source neutrons. Every such neutron is split into N neutrons with the weights changed accordingly. Then their histories are simulated. Every trajectory is terminated if the neutron is absorbed inside the region surrounded by the inner surface of the outer baffle and the inner surface of the barrel or leaves this region.

On the third step the non-homogeneous problem (problem with given neutron source S-2 – see Figure 2 that was calculated on the second step) was solved and the dosimeter reaction rates and fluxes in the detectors placed in the barrel, water gap and neutron pad were obtained. The third step game is played analogically to the second step.

The use of the ALIGR technique allowed to determine the activation detector reaction rates and the neutron fluxes in the detector's positions with acceptable statistical uncertainty. The MCU results with statistical uncertainties are presented in Tables 1, 2 and 3. For the reactions $^{58}$Ni(n,p); $^{115}$In(n,n′); $^{103}$Rh(n,n′); $^{64}$Zn(n,p); $^{237}$Np(n,f) and Fe DPA the statistical uncertainty does not exceed 1-2%, for $^{27}$Al (n,$\alpha$) – 3-5%.

**Table 1. Dosimetry reaction rates in stainless steel zones obtained by MCU code, reactions/sec-nucleus**

| | Detector position | $^{58}$Ni (n,p) | δ,% | $^{115}$In (n,n') | δ,% | $^{103}$Rh (n,n') | δ,% | $^{64}$Zn (n,p) | δ,% | $^{237}$Np (n,f) | δ,% | $^{27}$Al (n,a) | δ,% |
|---|---|---|---|---|---|---|---|---|---|---|---|---|---|
| **Inner baffle** | ( -4.41, -0.63) | 1.568E-16 | 0.7 | 3.442E-16 | 0.5 | 1.576E-15 | 0.4 | 5.507E-17 | 0.8 | 3.227E-15 | 0.4 | 1.036E-18 | 3.7 |
| | ( -4.41, -4.41) | 1.912E-16 | 0.6 | 4.133E-16 | 0.4 | 1.878E-15 | 0.3 | 6.731E-17 | 0.7 | 3.819E-15 | 0.3 | 1.289E-18 | 3.3 |
| **Outer baffle** | (-39.69, -0.69) | 6.120E-17 | 1.1 | 1.305E-16 | 0.7 | 5.864E-16 | 0.6 | 2.150E-17 | 1.2 | 1.190E-15 | 0.6 | 3.942E-19 | 4.4 |
| | (-39.69, -5.67) | 5.799E-17 | 1.1 | 1.235E-16 | 0.7 | 5.572E-16 | 0.6 | 2.048E-17 | 1.2 | 1.132E-15 | 0.5 | 3.825E-19 | 4.3 |
| | (-39.69, -11.97) | 4.636E-17 | 1.2 | 9.992E-17 | 0.8 | 4.516E-16 | 0.6 | 1.629E-17 | 1.3 | 9.180E-16 | 0.6 | 2.878E-19 | 4.7 |
| | (-39.69, -18.27) | 2.700E-17 | 1.6 | 5.960E-17 | 1.0 | 2.755E-16 | 0.8 | 9.424E-18 | 1.7 | 5.660E-16 | 0.8 | 1.900E-19 | 5.6 |
| | (-37.17, -20.79) | 2.853E-17 | 1.5 | 6.177E-17 | 1.0 | 2.854E-16 | 0.8 | 9.999E-18 | 1.6 | 5.847E-16 | 0.7 | 2.055E-19 | 5.6 |
| | (-30.87, -20.79) | 5.680E-17 | 1.1 | 1.221E-16 | 0.7 | 5.568E-16 | 0.6 | 1.996E-17 | 1.2 | 1.135E-15 | 0.5 | 3.640E-19 | 4.2 |
| | (-24.57, -20.79) | 9.131E-17 | 0.9 | 1.996E-16 | 0.5 | 9.129E-16 | 0.4 | 3.209E-17 | 0.9 | 1.863E-15 | 0.4 | 5.954E-19 | 3.3 |
| **Barrel** | (-49.77, -0.63) | 7.913E-18 | 1.4 | 1.628E-17 | 0.8 | 7.218E-17 | 0.6 | 2.770E-18 | 1.4 | 1.447E-16 | 1.1 | 6.383E-20 | 4.4 |
| | (-49.77, -9.45) | 6.811E-18 | 1.2 | 1.441E-17 | 0.6 | 6.510E-17 | 0.5 | 2.373E-18 | 1.2 | 1.309E-16 | 0.9 | 5.318E-20 | 4.4 |
| | (-47.25, -18.27) | 6.376E-18 | 1.3 | 1.429E-17 | 0.7 | 6.608E-17 | 0.6 | 2.211E-18 | 1.4 | 1.361E-16 | 1.0 | 4.932E-20 | 4.7 |
| | (-45.99, -22.05) | 5.488E-18 | 1.4 | 1.226E-17 | 0.7 | 5.822E-17 | 0.6 | 1.900E-18 | 1.5 | 1.209E-16 | 0.9 | 4.164E-20 | 5.5 |
| | (-44.73, -24.57) | 4.852E-18 | 1.3 | 1.101E-17 | 0.7 | 5.239E-17 | 0.6 | 1.675E-18 | 1.4 | 1.096E-16 | 0.9 | 3.813E-20 | 4.4 |
| | (-42.21, -28.35) | 4.535E-18 | 1.3 | 9.705E-18 | 0.7 | 4.483E-17 | 0.5 | 1.585E-18 | 1.4 | 9.172E-17 | 0.9 | 3.590E-20 | 4.1 |
| | (-38.43, -33.39) | 3.954E-18 | 1.2 | 7.943E-18 | 0.6 | 3.550E-17 | 0.5 | 1.383E-18 | 1.2 | 7.314E-17 | 0.8 | 3.550E-20 | 4.0 |
| | (-35.91, -35.91) | 3.943E-18 | 1.2 | 7.817E-18 | 0.6 | 3.456E-17 | 0.5 | 1.380E-18 | 1.3 | 7.108E-17 | 0.9 | 3.825E-20 | 4.3 |
| **Neutron pad** | (-58.54, -22.47) | 6.365E-19 | 1.2 | 1.363E-18 | 0.6 | 6.377E-18 | 0.5 | 2.200E-19 | 1.2 | 1.304E-17 | 0.9 | 5.870E-21 | 3.3 |
| | (-46.60, -41.95) | 4.757E-19 | 1.1 | 9.745E-19 | 0.6 | 4.488E-18 | 0.5 | 1.653E-19 | 1.1 | 9.212E-18 | 0.9 | 4.883E-21 | 3.3 |
| **Central hole** | ( 00.00, 00.00) | 7.161E-18 | 1.5 | 1.395E-17 | 0.9 | 6.029E-17 | 0.8 | 2.551E-18 | 1.5 | 1.272E-16 | 0.7 | 5.482E-20 | 5.9 |
| **Water gap** | (-54.36, -9.59) | 2.459E-18 | 1.1 | 4.679E-18 | 0.6 | 2.036E-17 | 0.5 | 8.685E-19 | 1.1 | 4.295E-17 | 0.8 | 2.163E-20 | 3.2 |
| | (-52.89, -15.80) | 2.339E-18 | 1.0 | 4.628E-18 | 0.6 | 2.045E-17 | 0.5 | 8.253E-19 | 1.1 | 4.369E-17 | 0.8 | 2.026E-20 | 3.2 |
| | (-51.53, -19.78) | 2.253E-18 | 1.1 | 4.516E-18 | 0.6 | 2.012E-17 | 0.5 | 7.935E-19 | 1.2 | 4.292E-17 | 0.8 | 2.043E-20 | 3.5 |
| | (-50.03, -23.33) | 2.110E-18 | 1.2 | 4.229E-18 | 0.6 | 1.903E-17 | 0.5 | 7.422E-19 | 1.2 | 4.054E-17 | 0.9 | 1.845E-20 | 4.6 |
| | (-48.74, -25.91) | 1.953E-18 | 1.1 | 3.900E-18 | 0.6 | 1.761E-17 | 0.5 | 6.870E-19 | 1.2 | 3.792E-17 | 0.9 | 1.705E-20 | 3.7 |
| | (-46.29, -30.06) | 1.777E-18 | 1.1 | 3.436E-18 | 0.6 | 1.527E-17 | 0.5 | 6.284E-19 | 1.1 | 3.255E-17 | 0.8 | 1.610E-20 | 3.8 |
| | (-44.08, -33.22) | 1.669E-18 | 1.1 | 3.113E-18 | 0.6 | 1.359E-17 | 0.5 | 5.907E-19 | 1.2 | 2.919E-17 | 0.8 | 1.641E-20 | 3.6 |
| | (-42.29, -35.48) | 1.611E-18 | 1.0 | 2.962E-18 | 0.6 | 1.281E-17 | 0.5 | 5.707E-19 | 1.1 | 2.666E-17 | 0.8 | 1.648E-20 | 3.2 |
| | (-39.03, -39.03) | 1.588E-18 | 1.0 | 2.863E-18 | 0.6 | 1.224E-17 | 0.5 | 5.633E-19 | 1.0 | 2.580E-17 | 0.8 | 1.662E-20 | 3.2 |
| **Reflector** | (-23.31, -23.31) | 6.786E-17 | 0.9 | 1.363E-16 | 0.5 | 6.015E-16 | 0.4 | 2.404E-17 | 0.9 | 1.242E-15 | 0.5 | 4.716E-19 | 2.9 |
| | (-25.83, -25.83) | 3.708E-17 | 0.9 | 6.894E-17 | 0.6 | 2.913E-16 | 0.5 | 1.324E-17 | 1.0 | 6.207E-16 | 0.6 | 2.782E-19 | 2.9 |
| | (-28.35, -28.35) | 2.061E-17 | 1.1 | 3.646E-17 | 0.6 | 1.491E-16 | 0.5 | 7.383E-18 | 1.1 | 3.233E-16 | 0.8 | 1.594E-19 | 3.3 |
| | (-30.87, -30.87) | 1.161E-17 | 1.2 | 1.960E-17 | 0.7 | 7.857E-17 | 0.6 | 4.178E-18 | 1.2 | 1.725E-16 | 1.0 | 1.047E-19 | 3.8 |
| | (-33.39, -33.39) | 6.765E-18 | 1.4 | 1.159E-17 | 0.9 | 4.695E-17 | 0.7 | 2.422E-18 | 1.4 | 9.838E-17 | 1.2 | 6.228E-20 | 4.0 |

**Table 2. DPA reaction rates obtained by MCU code, reactions/sec-nucleus**

| | Detector position | Fe DPA ASTM standard | δ,% | Fe DPA EUR standard | δ,% |
|---|---|---|---|---|---|
| **Inner baffle** | (-4.41, -0.63) | 2.070E-12 | 0.4 | 2.040E-12 | 0.4 |
| | (-4.41, -4.41) | 2.456E-12 | 0.3 | 2.421E-12 | 0.3 |
| **Outer baffle** | (-39.69, -0.69) | 7.703E-13 | 0.6 | 7.582E-13 | 0.6 |
| | (-39.69, -5.67) | 7.302E-13 | 0.5 | 7.195E-13 | 0.5 |
| | (-39.69, -11.97) | 5.916E-13 | 0.6 | 5.830E-13 | 0.6 |
| | (-39.69, -18.27) | 3.604E-13 | 0.8 | 3.553E-13 | 0.7 |
| | (-37.17, -20.79) | 3.738E-13 | 0.7 | 3.687E-13 | 0.7 |
| | (-30.87, -20.79) | 7.292E-13 | 0.5 | 7.189E-13 | 0.5 |
| | (-24.57, -20.79) | 1.197E-12 | 0.4 | 1.180E-12 | 0.4 |
| **Barrel** | (-49.77, -0.63) | 9.410E-14 | 1.2 | 9.233E-14 | 1.1 |
| | (-49.77, -9.45) | 8.406E-14 | 1.0 | 8.265E-14 | 0.9 |
| | (-47.25, -18.27) | 8.702E-14 | 1.0 | 8.574E-14 | 1.0 |
| | (-45.99, -22.05) | 7.687E-14 | 1.0 | 7.590E-14 | 1.0 |
| | (-44.73, -24.57) | 6.928E-14 | 1.0 | 6.839E-14 | 1.0 |
| | (-42.21, -28.35) | 5.867E-14 | 1.0 | 5.776E-14 | 1.0 |
| | (-38.43, -33.39) | 4.713E-14 | 0.9 | 4.622E-14 | 0.9 |
| | (-35.91, -35.91) | 4.615E-14 | 1.0 | 4.523E-14 | 0.9 |
| **Neutron pad** | (-58.54, -22.47) | 8.250E-15 | 0.9 | 8.119E-15 | 0.9 |
| | (-46.60, -41.95) | 5.884E-15 | 1.0 | 5.771E-15 | 1.0 |
| **Central hole** | (00.00, 00.00) | 3.387E-13 | 0.7 | 3.313E-13 | 0.7 |
| **Water gap** | (-54.36, -9.59) | 2.856E-14 | 0.9 | 2.791E-14 | 0.9 |
| | (-52.89, -15.80) | 2.878E-14 | 0.9 | 2.819E-14 | 0.9 |
| | (-51.53, -19.78) | 2.831E-14 | 0.9 | 2.771E-14 | 0.9 |
| | (-50.03, -23.33) | 2.662E-14 | 0.9 | 2.610E-14 | 0.9 |
| | (-48.74, -25.91) | 2.487E-14 | 0.9 | 2.438E-14 | 0.9 |
| | (-46.29, -30.06) | 2.147E-14 | 0.9 | 2.103E-14 | 0.9 |
| | (-44.08, -33.22) | 1.947E-14 | 1.0 | 1.898E-14 | 0.9 |
| | (-42.29, -35.48) | 1.792E-14 | 0.9 | 1.747E-14 | 0.9 |
| | (-39.03, -39.03) | 1.730E-14 | 0.9 | 1.685E-14 | 0.8 |
| **Reflector** | (-23.31, -23.31) | 8.212E-13 | 0.5 | 8.062E-13 | 0.5 |
| | (-25.83, -25.83) | 4.174E-13 | 0.6 | 4.065E-13 | 0.6 |
| | (-28.35, -28.35) | 2.185E-13 | 0.9 | 2.113E-13 | 0.9 |
| | (-30.87, -30.87) | 1.175E-13 | 1.1 | 1.135E-13 | 1.1 |
| | (-33.39, -33.39) | 6.716E-14 | 1.3 | 6.507E-14 | 1.3 |

**Table 3. Neutron fluxes obtained by MCU code, neutrons/cm$^2$/sec**

| | Detector position | E > 0.1 MeV | δ,% | E > 1.0 MeV | δ,% |
|---|---|---|---|---|---|
| **Inner baffle** | (-4.41, -0.63) | 3.315E+09 | 0.6 | 1.387E+09 | 0.5 |
| | (-4.41, -4.41) | 3.903E+09 | 0.5 | 1.660E+09 | 0.4 |
| **Outer baffle** | (-39.69, -0.69) | 1.203E+09 | 1.0 | 5.201E+08 | 0.8 |
| | (-39.69, -5.67) | 1.145E+09 | 1.0 | 4.954E+08 | 0.8 |
| | (-39.69, -11.97) | 9.270E+08 | 1.0 | 3.983E+08 | 0.8 |
| | (-39.69, -18.27) | 5.757E+08 | 1.2 | 2.382E+08 | 1.0 |
| | (-37.17, -20.79) | 6.056E+08 | 1.2 | 2.514E+08 | 1.0 |
| | (-30.87, -20.79) | 1.161E+09 | 0.9 | 4.952E+08 | 0.7 |
| | (-24.57, -20.79) | 1.923E+09 | 0.7 | 8.054E+08 | 0.6 |
| **Barrel** | (-49.77, -0.63) | 1.450E+08 | 0.8 | 6.516E+07 | 0.7 |
| | (-49.77, -9.45) | 1.345E+08 | 0.7 | 5.842E+07 | 0.6 |
| | (-47.25, -18.27) | 1.419E+08 | 0.7 | 5.850E+07 | 0.6 |
| | (-45.99, -22.05) | 1.287E+08 | 0.8 | 5.051E+07 | 0.7 |
| | (-44.73, -24.57) | 1.163E+08 | 0.8 | 4.548E+07 | 0.7 |
| | (-42.21, -28.35) | 9.529E+07 | 0.7 | 3.965E+07 | 0.6 |
| | (-38.43, -33.39) | 7.151E+07 | 0.7 | 3.194E+07 | 0.6 |
| | (-35.91, -35.91) | 6.871E+07 | 0.7 | 3.135E+07 | 0.6 |
| **Neutron pad** | (-58.54, -22.47) | 1.359E+07 | 0.8 | 5.631E+06 | 0.6 |
| | (-46.60, -41.95) | 9.265E+06 | 0.8 | 3.995E+06 | 0.6 |
| **Central hole** | (00.00, 00.00) | 1.933E+09 | 1.2 | 8.682E+08 | 0.9 |
| **Water gap** | (-54.36, -9.59) | 4.090E+07 | 0.6 | 1.830E+07 | 0.5 |
| | (-52.89, -15.80) | 4.211E+07 | 0.7 | 1.829E+07 | 0.6 |
| | (-51.53, -19.78) | 4.208E+07 | 0.7 | 1.792E+07 | 0.6 |
| | (-50.03, -23.33) | 4.029E+07 | 0.7 | 1.681E+07 | 0.6 |
| | (-48.74, -25.91) | 3.751E+07 | 0.7 | 1.555E+07 | 0.6 |
| | (-46.29, -30.06) | 3.179E+07 | 0.7 | 1.356E+07 | 0.6 |
| | (-44.08, -33.22) | 2.747E+07 | 0.7 | 1.221E+07 | 0.6 |
| | (-42.29, -35.48) | 2.540E+07 | 0.6 | 1.157E+07 | 0.5 |
| | (-39.03, -39.03) | 2.384E+07 | 0.6 | 1.111E+07 | 0.5 |
| **Reflector** | (-23.31, -23.31) | 1.236E+09 | 0.6 | 5.349E+08 | 0.5 |
| | (-25.83, -25.83) | 5.640E+08 | 0.6 | 2.644E+08 | 0.5 |
| | (-28.35, -28.35) | 2.729E+08 | 0.7 | 1.383E+08 | 0.6 |
| | (-30.87, -30.87) | 1.381E+08 | 0.9 | 7.333E+07 | 0.7 |
| | (-33.39, -33.39) | 8.370E+07 | 1.1 | 4.369E+07 | 0.8 |

**Figure 1. Azimutal cross-section of the VENUS-2 calculational model. S-1 and S-2 – surface sources**

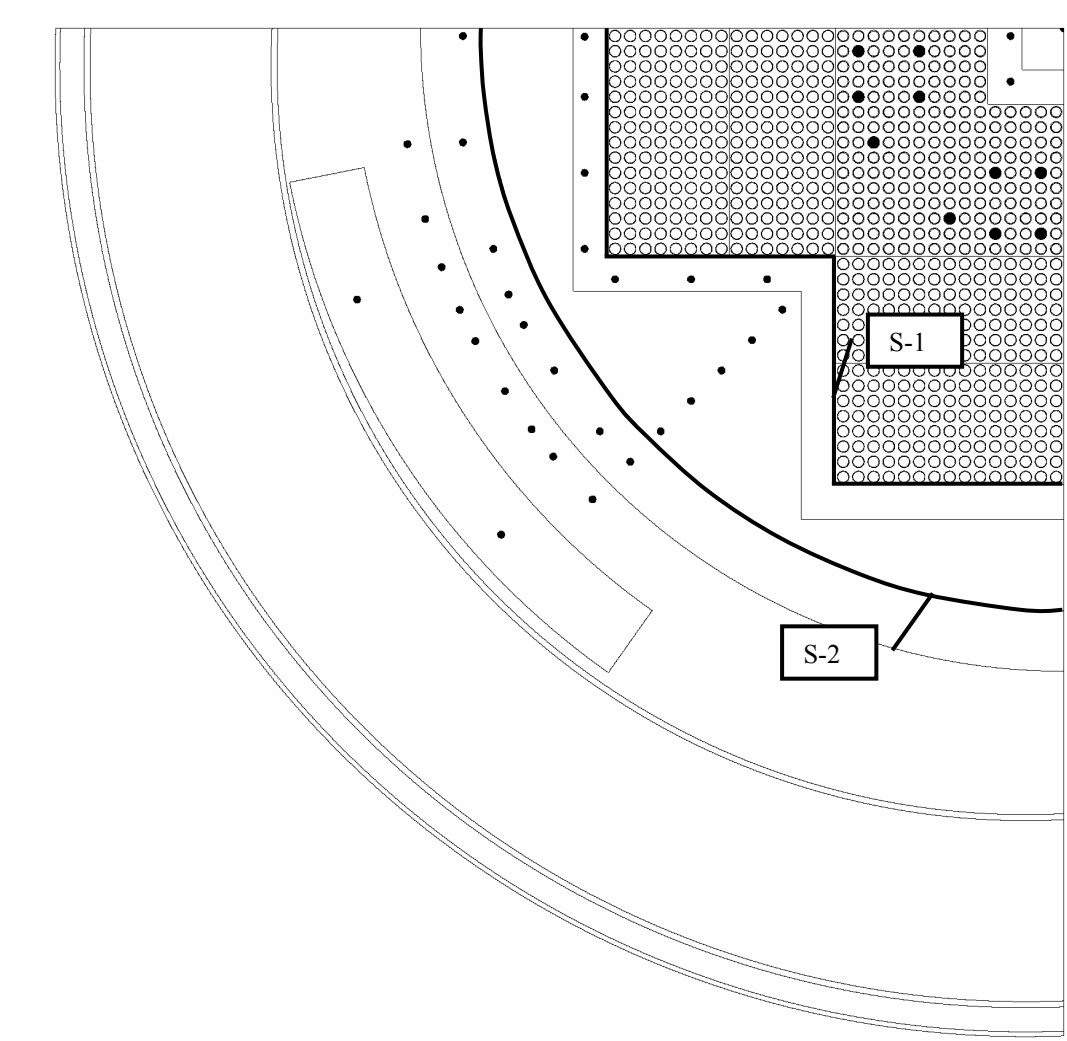

**Figure 2. Axial cross-section of the VENUS-2 calculational model**

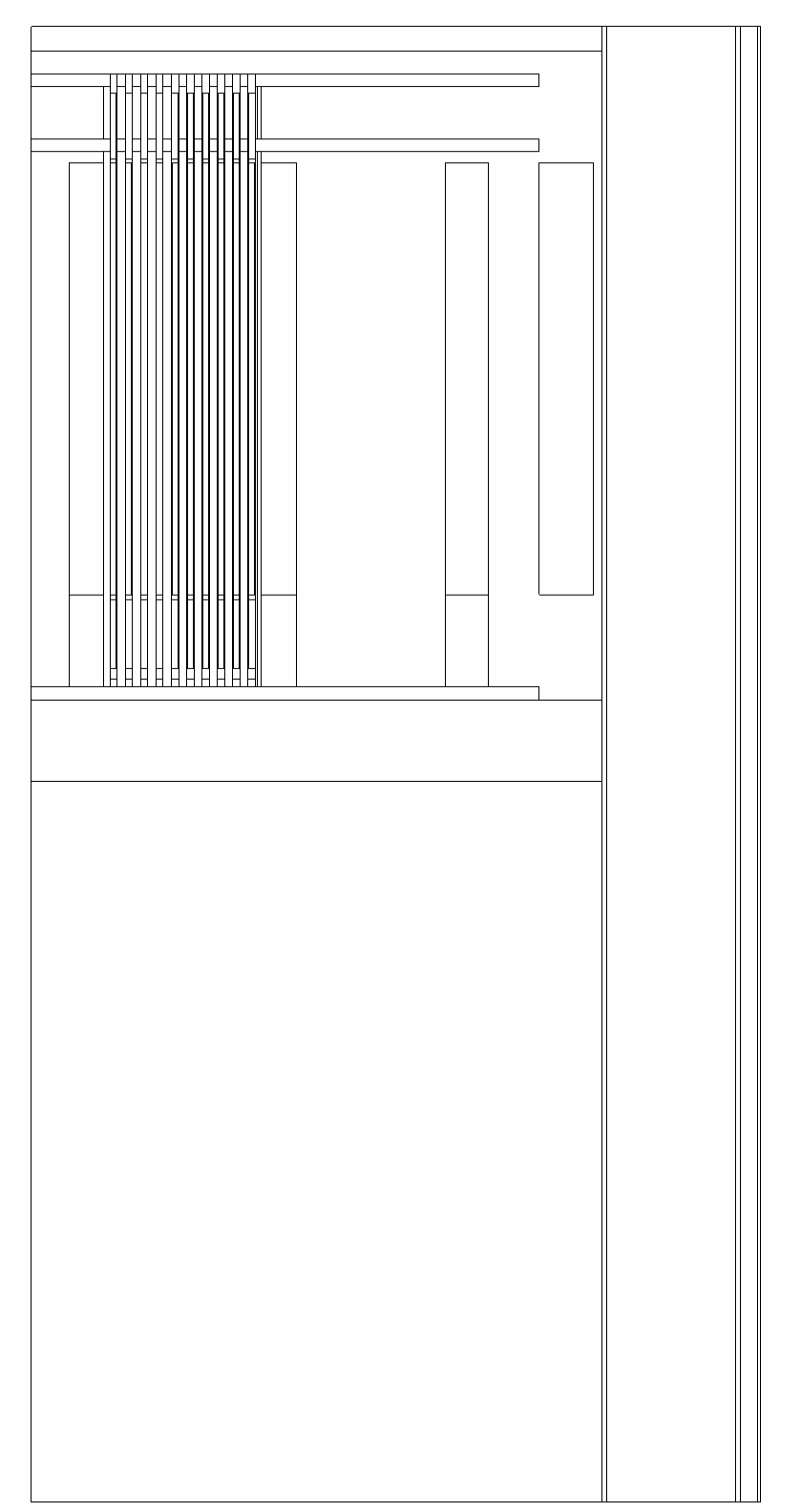

## 5. Kurchatov Institute, Russia

### 1. Author

Alexey V. Moriakov

### 2. Transport method and modelling assumptions

#### *2.1 Description of the calculations procedure (all important information about modelling assumptions and codes/methods used)*

For calculations of this benchmark the LUCKY code was used. The bibliographic references for the code used are as follows:

[1] Moriakov A., V. Vasyukhno, M. Netecha, G. Khacheresov, "Programs LUCKY & LUCKY_C – 3-D Parallel Transport Codes for the Multi-group Transport Equation Solution for XYZ Geometry by PmSn Method", *The International Conference on Supercomputing in Nuclear Applications (SNA-2003)*, Paris, 22-24 September 2003.

#### *2.2 Grid/mesh structure of the model (including a picture of the geometrical model used)*

The 3-D model is based on the benchmark specification provided in the document entitled: *VENUS-2 MOX-fuelled Reactor Dosimetry Calculations: Benchmark Specification* [OECD/NEA, NEA/NSC/DOC(2004)6]. Only XYZ geometry is supported by the LUCKY code. Thus the uniform little space mesh was used to approximate the geometry of this task. The homogeneous procedure was carried out to get nuclear concentrations for fuel and Pyrex cells only. Other details for the VENUS composition were taken as is. A simplified X0Y cross-section for the model is shown in Figure 1 (see No. 4). Results were obtained with inner iteration precision 0.001.

### 3. Transport cross-sections

#### *3.1 The name and version of the point library neutron transport cross-section data and the energy group structure*

Calculations based on BUGLE96 cross-section library.

#### *3.2 Method/model used in cross-section collapsing*

BUGLE96 cross-section library was used as the original one.

### 4. Neutron source

The neutron source was taken from *VENUS-2 MOX-fuelled Reactor Dosimetry Calculations: Benchmark Specification* [OECD/NEA, NEA/NSC/DOC(2004)6] document as multiplication axial and plane distributions of the one.

### 5. Axial leakage treatment (for two-dimensional calculation only)

None.

**6. Response functions and fission averaged data, including the name and version of the dosimeter cross-sections data**

The dosimeter cross-section libraries used for the calculations of the all the desired reactions are mentioned below:

| | |
|---|---|
| $^{58}$Ni (n,p) | IRDF-90 Version 2 |
| $^{115}$In (n,n′) | IRDF-90 Version 2 |
| $^{103}$Rh (n,n′) | IRDF-90 Version 2 |
| $^{64}$Zn (n,p) | IRDF-90 Version 2 |
| $^{237}$Np (n,f) | IRDF-90 Version 2 |
| $^{27}$Al (n,a) | IRDF-90 Version 2 |

**7. Comments/special references: any other information not listed above but judged by the participant as important in interpreting the benchmark results**

Some references for MBC-1000 supercomputer: www.jscc.ru.

## 6. Korea Power Engineering Co. (KOPEC), Korea

### 1. Authors

Bok Ja Moon and Joon Ghi Ahn
Korea Power Engineering Co. (KOPEC)
Yuseong-gu, Daejeon-si, Korea

### 2. Transport method and modelling assumptions

For this calculation, the $S_N$ code DORT (Version 2.8.14) was used. The reactor was assumed to have quadrant symmetry and the quadrant reactor was modelled using RΘ co-ordinates. The central water hole, inner and outer baffle, core, barrel, neutron pad, air jacket and vessel were modelled. The 141 × 122 meshes were used for the DORT RΘ model. Finer meshes were given to the regions around the inner and outer baffle. All dosimeters were assumed to be point detectors without surrounding structures and the reaction rates were calculated using the fluxes at the corresponding detector position.

### 3. Transport cross-sections

The macroscopic cross-sections for the DORT calculation were obtained using the BUGLE96 library and GIP code. The nuclide number densities of each structure were taken from the report NEA/NSC/DOC(2004)6.

### 4. Neutron source

The pin power distribution was used as the spatial source distribution. The average fission rate in the core was given as $1.87 \times 10^8$ [fissions/cm/sec/pin] at the mid-plane level and the axial form factor was given as 0.768. The neutron source spectrum was obtained from $^{235}$U and $^{239}$Pu fission spectrums in the BUGLE96 library. For the 3/0 and 4/0 fuel regions, the $^{235}$U fission spectrum was used. For the MOX fuel region, the combined spectrum of $^{235}$U and $^{239}$Pu fission spectrums was calculated considering their fission rates.

### 5. Axial leakage treatment

Since all the neutron responses were measured at the mid-plane, the fluxes calculated using RΘ co-ordinates were corrected to reflect the axial flux distribution. The synthesis method was used for this calculation. In the synthesis method, a three-dimensional flux representation is constructed by synthesising calculations of lower dimensions. For the calculation of mid-plane fluxes, the two-dimensional RΘ calculation with core average power is performed and then the axial factor at the mid-plane is multiplied using the expression:

$$\Phi_g^{mid}(r,\theta) = \Phi_g(r,\theta,z=130\,\text{cm}) = \Phi_g(r,\theta) \times \frac{\Phi_g(r,z=130\,\text{cm})}{\Phi_g(r)}$$

where $z$ = 130 cm is the height of the mid-plane.

Axial flux distribution was calculated using two-dimensional RZ flux normalised to one-dimensional radial flux. The 97 × 67 meshes were applied to the two-dimensional RZ model. As the axial power shapes measured at six pins are very similar, the average of those shapes was used as the axial

source distribution for DORT RZ calculation. The one-dimensional radial flux was calculated using one-dimensional ANISN calculation. The radial mesh intervals were the same as those of the RZ calculation.

The axial factors for each region were averaged and the region-wise axial factors were applied to the reaction rates obtained from DORT RΘ calculations.

## 6. Response functions and fission averaged data

The dosimeter cross-sections were taken from IRDF-90 Version 2 and generated using NJOY-97 code system except $^{237}$Np dosimeter. The dosimeter cross-section of $^{237}$Np was taken from the BUGLE96 library. Most results were almost the same with the calculation using the dosimeter cross-sections taken from the BUGLE96 library except for the Rh reaction.

The equivalent fission flux for dosimeter *d* is defined as a ratio of calculated reaction rate and the average dosimeter cross-section. Thus, it can be calculated as follows:

$$\Phi_{eq}^{d} = \sum_{g} \sigma_{r}^{d}\left(E_{g}\right)\phi\left(E_{g}\right) \Big/ \sum_{g} \sigma_{r}^{d}\left(E_{g}\right)\chi\left(E_{g}\right)$$

where: $\sigma_{r}^{d}\left(E_{g}\right) \equiv$ reaction cross-section of $g^{th}$ energy group for dosimeter *d*

$\phi \equiv$ neutron flux from DORT output

$\chi \equiv$ $^{235}$U fission spectrum

The average dosimeter cross-sections were calculated using reaction cross-section and $^{235}$U fission spectrum in the BUGLE96 library.

## 7. Comments/special references

The photo-fission effect was included and the reaction rate was integrated from 1 to 45 groups in the BUGLE96 library because of Cd cut-off energy for $^{237}$Np dosimeters.

## 7. Vuje Trnava Inc. (VTI)/Slovak University of Technology (SUT), Slovak

### 1. Authors

Vladimir Sebian, Petr Darilek, Vladimir Necas

### 2. Transport method and modelling assumptions

- Current-coupling collision-probability method (CCCP), first-flight probabilities evaluation, criticality spectrum evaluation by $B_1$ method.
- The model was created by AURORA 1.7 input pre-processor (Figure 1). Geometry of the central hole, the inner baffle, the fuel regions and the outer baffle was made by utilisation of the fuel cell pitch grid. There was a larger step used in the reflector with respect to the other grid of the outer reactor parts. The outer reactor parts: the barrel, the water gap, etc., are subdivided in the radial direction in agreement with the notation of Table 1 (in the specification document) and in the azimuthal orientation by the step of 5°. The same step was used for approximation of the reactor circles by the polygon. The measurement positions in the reactor were simulated by small circles filled with material identical with the vicinity. The radius of circles was 0.1 cm.

### 3. Transport cross-sections

- 190 neutron/48 gamma groups, based on ENDF/B-VI.
- Cross-section collapsing method is used by HEBE code.

### 4. Neutron source

Volume-integrated neutron source depending on a region and a neutron group.

### 5. Axial leakage treatment (for two-dimensional calculation only)

Covered by the vertical buckling parameter $B_{v,core}$ = 4.90E-02 $cm^{-1}$ in the HELIOS code.

### 6. Response functions and fission averaged data

190 neutron/48 gamma groups, based on ENDF/B-VI.

### 7. Comments/special references

- In the conditions of the HELIOS 1.7 code only the $^{237}$Np(n,f) reaction, of all those requested, is available.
- The nearest value of 1.87E+08 fission/cm/sec for the HELIOS calculation was determined as 1.8623E+08 fission/cm/sec because of the small value of the fission rate.
- The $^{235}$U fission spectrum and $^{237}$Np fission cross-sections were obtained from the fuel area.
- The neutron fluxes at threshold energies E > 0.1 MeV and E > 1.0 MeV were obtained from the nearest neutron energy group ranges. They are: 2.0000E+07 eV – 1.1109E+05 eV and 2.0000E+07 eV – 1.0026E+06 eV.
- All the calculations were performed at a burn-up 0 MWd/tHM.

**Figure 1. The geometric model of the VENUS-2 MOX-fuelled benchmark**

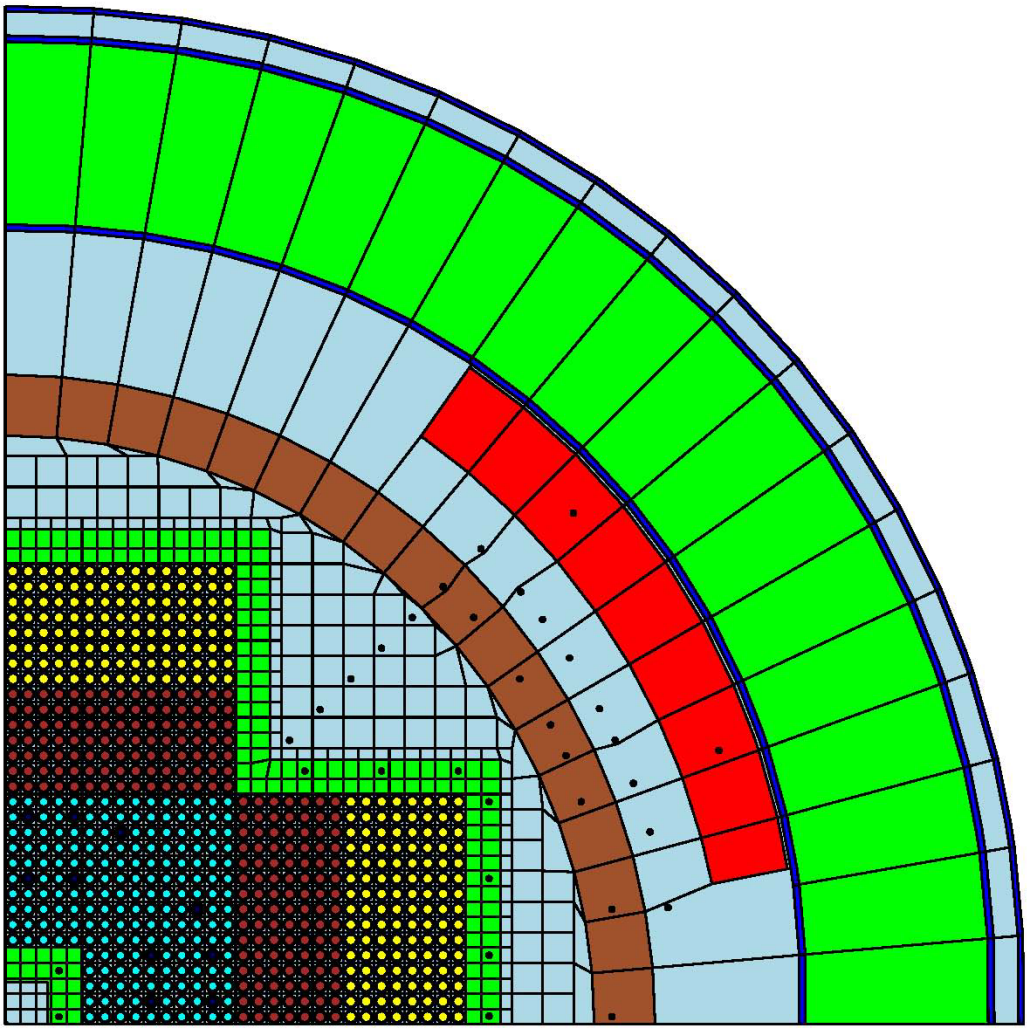

## 8. WTI GmbH, Germany

### 1. Author

Maik Hennebach
WTI Jülich

### 2. Transport method and modelling assumptions

***Transport method***

Monte Carlo calculation with MCNP-4C2.

***Geometry and other modelling assumptions***

One quadrant of the VENUS core was explicitly modelled according to the benchmark specification. The space between neutron pad and jacket (XI) was neglected, as were the unspecified radial gaps between fuel rod cladding and the upper and intermediate reactor grid.

Figure 1 shows the horizontal geometry at z = 130.00 cm and Figure 2 shows the axial geometry at y = -0.63 cm. The cylindrical detector cells are marked in green colour in these plots. They consist of the same material as their direct environment and have different radii and a uniform height of 4 cm. This height was selected as a compromise between rate optimisation and good representation of neutron fluxes at the core mid-plane.

For polyethylene, S($\alpha$,$\beta$) scattering data for Plexiglas was used.

The only variance reduction used in the model is geometry splitting/Russian Roulette. In brief, cell importances are increased vertically towards the reactor mid-plane and horizontally towards the detector locations.

***Statistics and normalisation***

The reaction rates given result from a weighted average of two calculations; one (150 000 generations with 1 000 neutrons each) was performed on a Windows PC, the other (4 000 generations with 100 000 neutrons each) on a Linux cluster with eight PCs.

To normalise the calculation results to 100% VENUS-2 power ($4.596 \cdot 10^{12}$ fissions/sec/core quadrant), fission rates in all three fuel regions were tallied during the calculation.

### 3. Transport cross-sections

Default MCNP-4C2 cross-section libraries, which means ENDF/B-VI for most isotopes with a few from ENDL-92 (Sn), ENDF/B-V (Cr, Ni) and LANL T-2 (Fe).

### 4. Neutron source

Since the modelling approach was essentially a criticality calculation with added flux detectors, the neutron source was not explicitly modelled. Comparison of fission rates from this calculation with the experimental values provided in the benchmark specification showed good agreement for axial fission rate distributions and reasonable agreement for the radial fission rate distribution at core mid-plane.

The $k_{eff}$ value for the calculation is 0.9961 with a statistical error of less than 0.0001.

## 5. Axial leakage treatment

## 6. Response functions and fission averaged data

The six required dosimetry cross-sections are all based on IRDF-90 Version 2 dosimetry data. They were derived from the file IRDF90-data_NEA available at NEA and converted from ENDF format into MCNP type 1 format.

The $^{235}$U fission spectrum to determine equivalent fission fluxes is approximated by a Watt Fission spectrum:

$$f(E) = e^{(-E/0.988)} \cdot sinh(2.249 \cdot E)^{1/2}$$

## 7. Comments/special references

Relative statistical errors σ of the reaction rates are given in the EXCEL file VENUS2sigma.xls. Since the error from the $^{235}$U fission spectrum approximation should be comparably small, these also apply for the equivalent fission fluxes.

**Figure 1. Horizontal cross-section of the model**

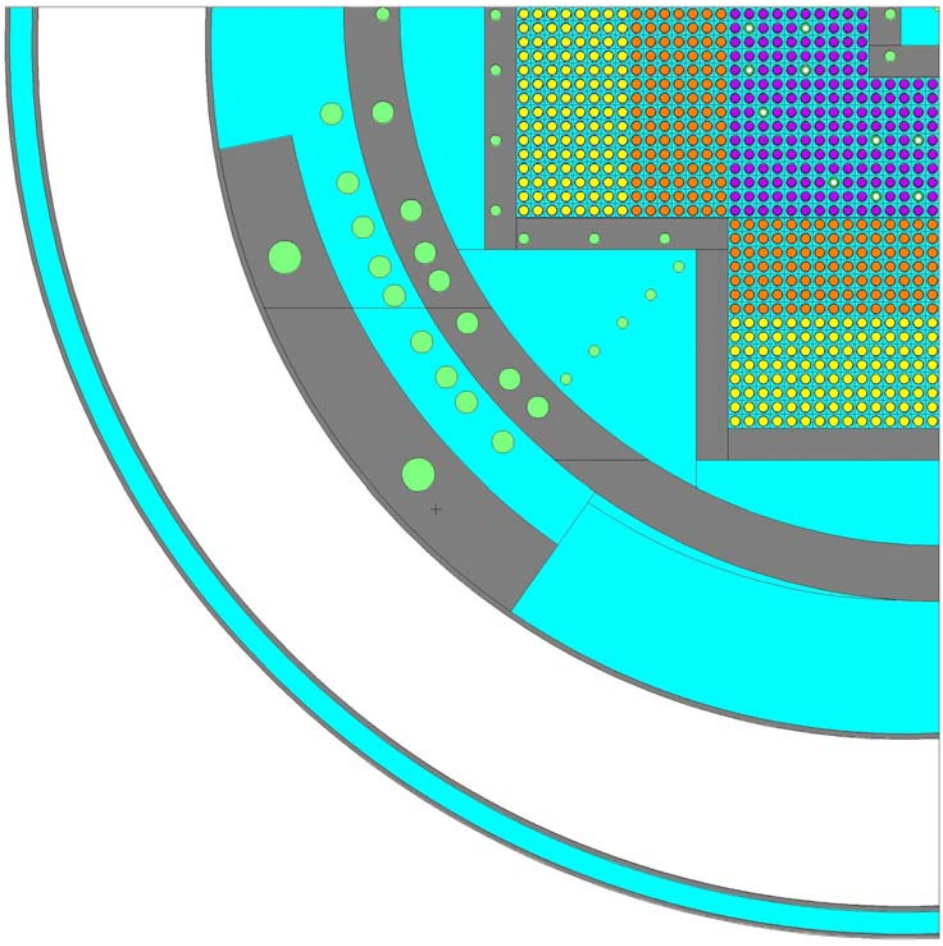

**Figure 2. Vertical cross-section of the model**

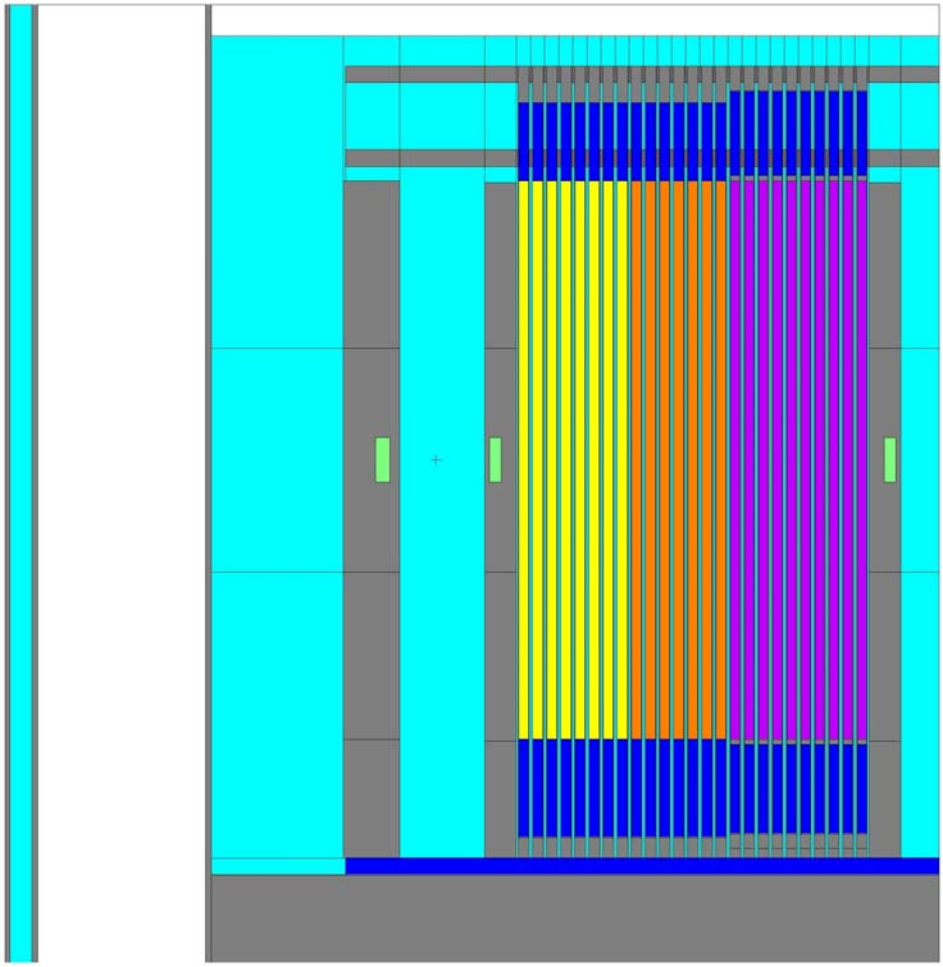

## 9. VTT, Finland

### 1. Author

P. Kotiluoto
VTT Technical Research Centre of Finland
P.O. Box 1608
FI-02044 VTT, Finland

### 2. Transport method and modelling assumptions

Two different three-dimensional deterministic radiation transport codes were used for the benchmark problem: a well known TORT code, and a new MultiTrans code that is under development [1,2].

With the TORT code, full symmetrical $S_8$ quadrature set was used with Legendre order $P_3$ representation for the angular flux.

With the MultiTrans code, a simplified spherical harmonics approximation ($SP_3$) is used as a radiation transport approximation. A special tree multi-grid technique is used for solving the multi-group $SP_3$ approximation [1,2].

All material regions were modelled in detail, except that fuel pin, fuel cladding and water regions were homogenised over each fuel zone. The external regions outside the jacket inner wall (air, jacket outer wall, reactor vessel, water, and reactor room) were left away from the model, as they can be assumed to have no significant effect on the responses at the measurement points.

The geometry input for the TORT code was prepared using BOT3P: a 147R × 98Θ × 45Z TORT mesh was created. For the MultiTrans code, the geometry was constructed using commercial Pro/ENGINEER® CAD software, and the tree multi-grid (octree grid) was generated from the exported stereolitography (STL) files, resulting in 2 530 817 octree cells (2 204 715 leaf cells, i.e. cells that are not divided further). Horizontal cross-sections of the generated TORT and MultiTrans meshes at core height are shown in Figures 1 and 2.

**Figure 1. RΘ mesh of the core**

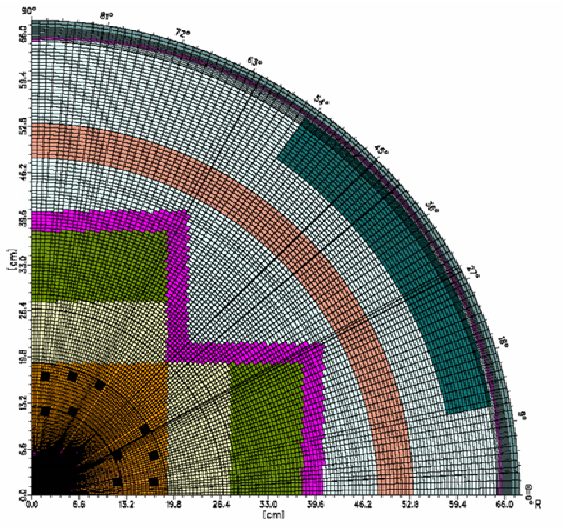

**Figure 2. Octree cross-section of the core**

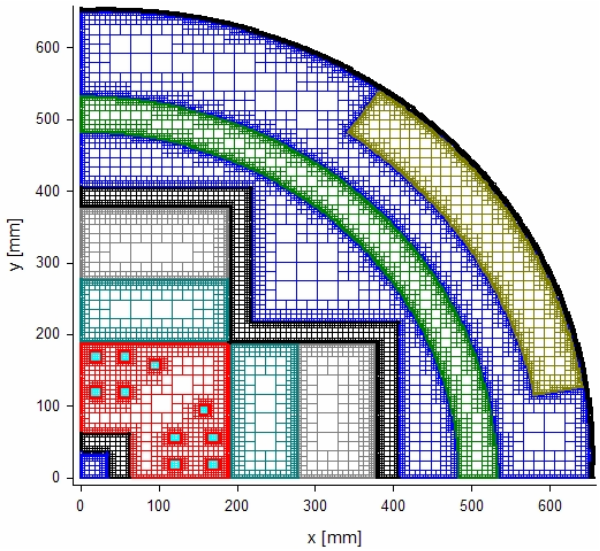


## 3. Transport cross-sections

BUGLE96 transport cross-sections with 47 neutron groups (with 26 groups above 0.1 MeV) were used for both codes with Legendre order 3 and without upscattering. For the TORT code, the macroscopic cross-sections for compound materials were mixed by using TOPICS-B cross-section preparation program. For MultiTrans, the elemental atomic densities were input for each material, and the mixing of BUGLE cross-sections was performed by MultiTrans.

## 4. Neutron source

Fixed neutron source was *not* separately generated: a direct k-effective search (with the BUGLE library and homogenised core as explained above) was performed by both codes instead. $^{235}$U and $^{239}$Pu fission spectra from the BUGLE library were used, weighted by the relative portions of the main fissile isotopes in the VENUS-2 core: $\chi = 0.7930 \times \chi(^{235}\text{U}) + 0.2070 \times \chi(^{239}\text{Pu})$. The reference fission rate was given as 4.596E+12 fissions/sec/core quadrant; by using values of $\nu(^{235}\text{U}) = 2.432$ and $\nu(^{239}\text{Pu}) = 2.8815$ neutrons released per fission event, a normalisation factor (the XNF entry for TORT) of $4.596\text{E+12} \times (0.7930 \times 2.432 + 0.2070 \times 2.8815) = 1.161\text{E+13}$ fission neutrons/sec/core quadrant at 100% VENUS-2 power was derived.

## 5. Axial leakage treatment (for two-dimensional calculation only)

## 6. Response functions and fission averaged data

The IRDF-90 Version 2 dosimetry cross-sections for reactions $^{58}$Ni(n,p), $^{115}$In(n,n′), $^{103}$Rh(n,n′), $^{64}$Zn(n,p), $^{237}$Np(n,f), and $^{27}$Al(n,α) were condensed into the BUGLE energy group structure from the SAND II energy group structure (640 groups) using the X333 utility program from the neutron metrology file NMF-90. Combined Maxwell, 1/E and fission weighting spectrum was used. The fission spectrum averaged dosimetry cross-sections are given in Table A. The fission spectrum averaging of the cross-sections in BUGLE multi-group structure were performed with a formula:

$$< \sigma_i >_{fiss.} = \frac{\sum_{g=1}^{47} \chi_5^g \sigma_i^g}{\sum_{g=1}^{47} \chi_5^g}$$

where $\chi_5^g$ is the fission spectrum in neutron groups $g \in [1,47]$ and $\sigma_i^g$ is the corresponding cross-section of the reaction *i* condensed into the same energy group structure.

**Table A. Fission spectrum averaged dosimetry cross-sections**

| Reaction | $^{58}$Ni(n,p) | $^{115}$In(n,n′) | $^{103}$Rh(n,n′) | $^{64}$Zn(n,p) | $^{237}$Np(n,f) | $^{27}$Al(n,α) |
|---|---|---|---|---|---|---|
| Cross-section [mbarn] | 107.339 | 187.544 | 708.720 | 39.024 | 1 357.720 | 0.747 |

## 7. Comments/special references

There seems to be over 20% discrepancies in calculated reaction rates and fluxes between MultiTrans and TORT at some detector positions, especially in the E > 0.1 MeV flux inside the neutron pad (maximum 28% and 32% discrepancy) and in one position inside the barrel (20% discrepancy). Also, the calculated $^{27}$Al(n,α) fission flux differs more than 20% in one detector position inside the inner baffle, and in one detector position inside the outer baffle. These discrepancies are probably due to different radiation transport methods ($S_8$ and $SP_3$), especially in the barrel and the neutron pad positions. It is known that $SP_3$ approximation is not capable of producing accurate results when the solution starts to behave more transport-like. Therefore, $SP_3$ approximation is not applicable for deep penetration problems. The TORT results should be more reliable in these detector areas.

## References


[1] Kotiluoto, P., "Fast Tree Multigrid Transport Application for the Simplified $P_3$ Approximation", *Nucl. Sci. Eng.*, 138, pp. 269-278 (2001).

[2] Kotiluoto, P., "Application of the New MultiTrans $SP_3$ Radiation Transport Code in Criticality Problems and Potential Use in Dosimetry," in *Reactor Dosimetry in the 21st Century*, World Scientific, pp. 580-587 (2002).

## 10. Korea Atomic Energy Research Institute (KAERI), Korea

### 1. Authors

Do Heon Kim, Choong-Sup Gil, Jonghwa Chang, and Jung-Do Kim
Nuclear Data Evaluation Laboratory
Korea Atomic Energy Research Institute
P.O. Box 105, Yuseong, Daejeon, 305-600, Korea
Tel: +82-42-868-8651
Eml: kimdh@kaeri.re.kr

### 2. Transport method and modelling assumptions

Computer codes used: TRANSX/DANTSYS 3.0.

Method used:

- Discrete ordinates ($S_N$) method.
- $S_{16}$-$P_3$ for cell calculations and $S_8$-$P_3$ for core calculations.
- The mesh sizes are less than ~0.03 cm for 1-D cell calculations. For 3-D core calculations, the mesh sizes are ~0.63 cm (a half pitch) up to the outer baffle region and 1.26 cm outside of the region.

### 3. Transport cross-sections

- The latest version of ENDF/B-VI (ENDF/B-VI Release 8) for all isotopes except natural tin (from ENDL-84 library) is used.
- The MATXS-formatted master library with the 199-group structure of VITAMIN-B6 is generated by the NJOY99.90 code.
- The ISOTXS-formatted library with the 47-group structure of BUGLE96 is generated by collapsing the master library with the weighting fluxes resulting from the 1-D cell calculations. For other regions besides the fuel and Pyrex cells, the group collapse is carried out with the built-in $P_0$ flux.

### 4. Neutron source

The flux-, mixture- and region-dependent fission spectra are used.

### 5. Axial leakage treatment (for two-dimensional calculation only)

N/A

### 6. Response functions and fission averaged data

The IRDF-90 Version 2 dosimeter cross-section data are taken to estimate the dosimetry reaction rates. These data are condensed into a 47-group library with a smoothly varying combination of a Maxwellian thermal spectrum, a 1/E slowing down spectrum and a fission spectrum (IWT=4 in GROUPR module of NJOY).

## 7. Comments/special references

- The VENUS-2 core was modelled explicitly from bottom to top with the proper use of homogenisation for the grid regions.

- The VENUS-2 core was modelled up to the neutron pad in the x- and y-direction. It is assumed that the regions beyond the neutron pad were filled with water.

- The energy bounds used are 1.0026 MeV (groups 1 to 18) and 0.11109 MeV (groups 1 to 26) for fluxes at E > 1.0 MeV and E > 0.1 MeV, respectively.

## 11. VTT, Finland

### 1. Author

Frej Wasastjerna
PL 1608
FIN-02044 VTT
Finland
Eml: frej.wasastjerna@vtt.fi

### Introduction

The VENUS-2 dosimetry benchmark [1] was calculated by two different groups at VTT, the Technical Research Centre of Finland. The calculations done by group Pro11 have been submitted separately. This report describes only the work done by Pro14.

It should be noted that little time and funding were available for this work. This means that the work could not aim at any high accuracy. It also means that there was a significant risk of serious input errors. Fortunately the work of Pro11 provided a badly needed sanity check, see below.

### Method, cross-section data, material compositions

The calculations were performed using MCNP-4C [2], making them complementary to the deterministic calculations of Kotiluoto in Pro11. Cross-sections from the endf60 library (.60c), released together with MCNP-4C and based on ENDF/B-VI, were used for the transport calculations.

The isotopic compositions of actinides were taken from the benchmark specifications. Otherwise natural element cross-sections were used where available in endf60. Where they were not available, the full isotopic compositions given in the nuclide chart published by the Japanese Nuclear Data Committee in 1992 were used for Cr and heavier elements, but for H, N and O minor isotopes were ignored on the basis that they were present only in negligible amounts, except for $^{18}O$, which is not included in endf60 anyway.

### Geometry

The geometry was modelled according to the specifications, see Figures 1-3.

The geometry plotter of MCNP did not work perfectly in producing the pictures; many cell boundaries were not drawn. However, they are often visible as boundaries between different colours.

### Source

Two different sources were used: a KCODE source calculated by MCNP-4C itself and the fixed source given in the benchmark specifications.

In the KCODE calculations, a constant starting source, equal everywhere in the core, was used. This was obtained by using a constant source in a box circumscribing the core and then using cell selection to discard neutrons not starting in the core (between the baffles). Two hundred inactive cycles were run, followed by 2 000 active cycles, each of 5 000 starters. The $k_{eff}$ was calculated to be 0.99857 with an estimated standard deviation of 0.00026. There was no indication that the number of inactive cycles was insufficient, and for such a small core and a flat starting source there was also no reason to suppose that more would have been needed.

**Figure 1. Plan overview**

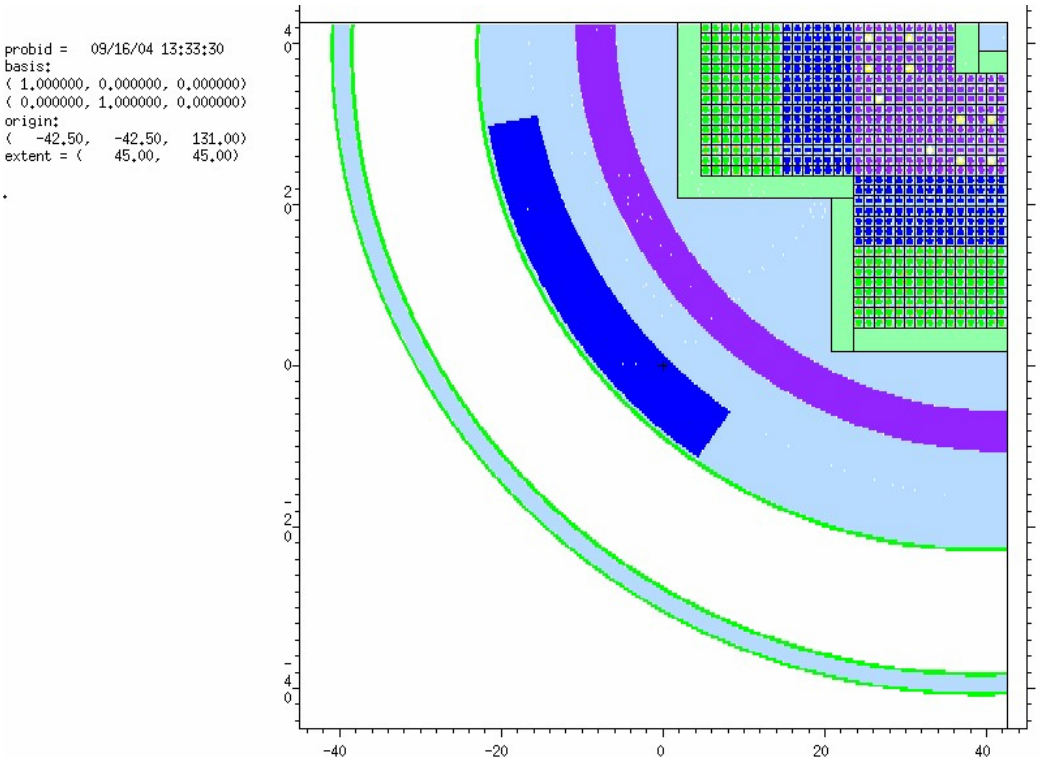


**Figure 2. Elevation overview**

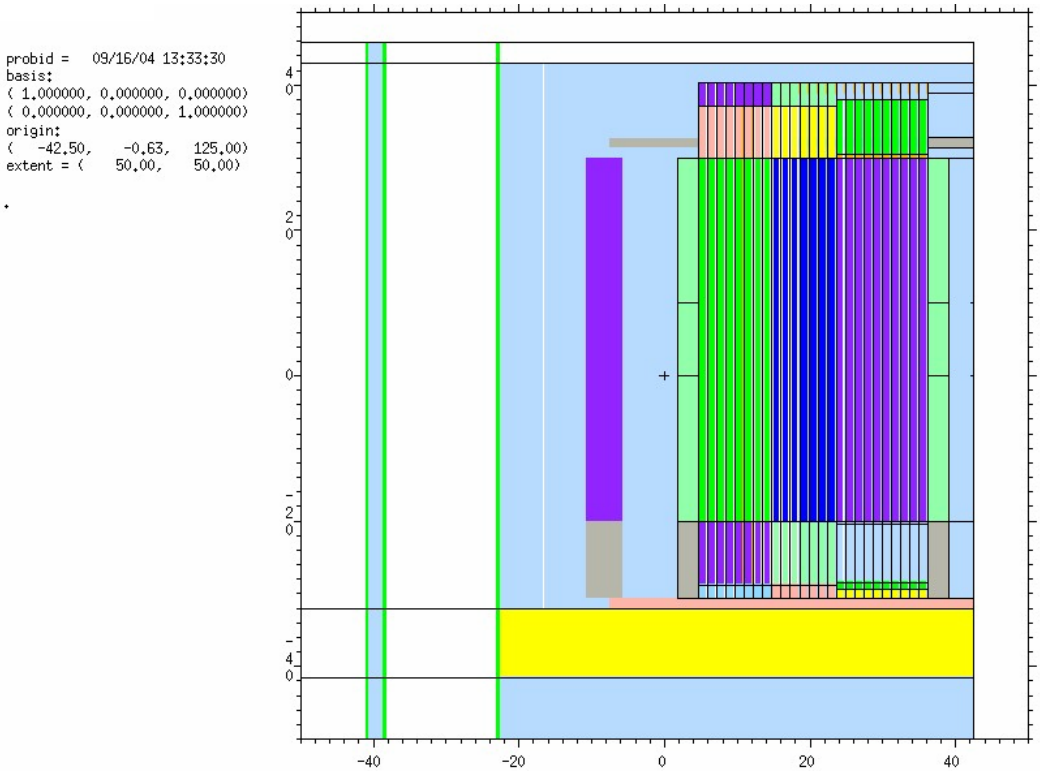

**Figure 3. Plan view, detail of fuel pin**

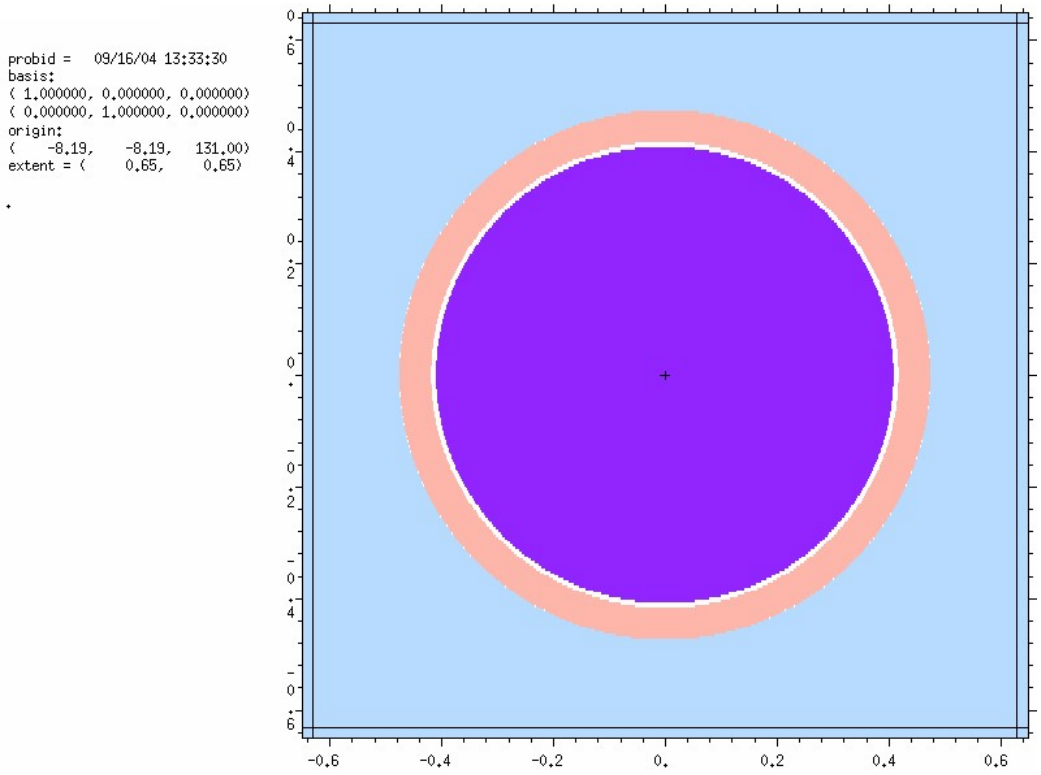


In the fixed source calculations, the **source distribution** was set equal to the **fission rate distribution** given in the specifications. This was not correct, since υ is higher for MOX fuel than for $^{235}$U, but the extra work it would have taken to adjust the distribution to account for this was considered impracticable.

However, in calculating the normalisation factor for source strength the correct υ value for **thermal fission** was determined. For $^{235}$U we used the thermal υ value given by Mughabghab, *et al.* [3] i.e. 2.425. In the MOX fuel, the υ values (2.877 for $^{239}$Pu and 2.937 for $^{241}$Pu) were weighted with the number densities and thermal fission cross-sections of each isotope, giving an average υ of 2.695. The respective υ values for pure $UO_2$ fuel and MOX fuel were then weighted with the fission rates in the respective parts of the core, giving an overall average of 2.485. This was then used to multiply the total fission rate, giving a total source in one quadrant of 1.142E13 $s^{-1}$. Taking υ values for fast fission into account would have required a full spectrum calculation, which was deemed impracticable.

At least the different fission spectra for different nuclides were taken into account.

Another problem was that the given axial distributions did not extend over the full length of the fuel pins. This was solved using module "four" of the source preparation program PVIS-4 [4] to make a Fourier transform of the given distribution and extend this to the full pin length. This transform was:

$$0.001277 + 0.055683 \cos(\pi z/64) + 0.000333 \sin(\pi z/64)$$

where the 64 in the denominator comes from adding reflector savings of 7 cm at the top and bottom. The fit is excellent, as shown in Figure 4, where Series 1 is the Fourier fit and Series 2 is the average of the six given axial distributions. The maximum deviation at any point is 0.0005, less than 1% of 0.0569, the maximum value of the average of the given distributions, and the rms error is 0.0002.

**Figure 4. Comparison of the Fourier fit (Series 1) with the average (Series 2) of all axial fission rate distributions in the benchmark specifications**

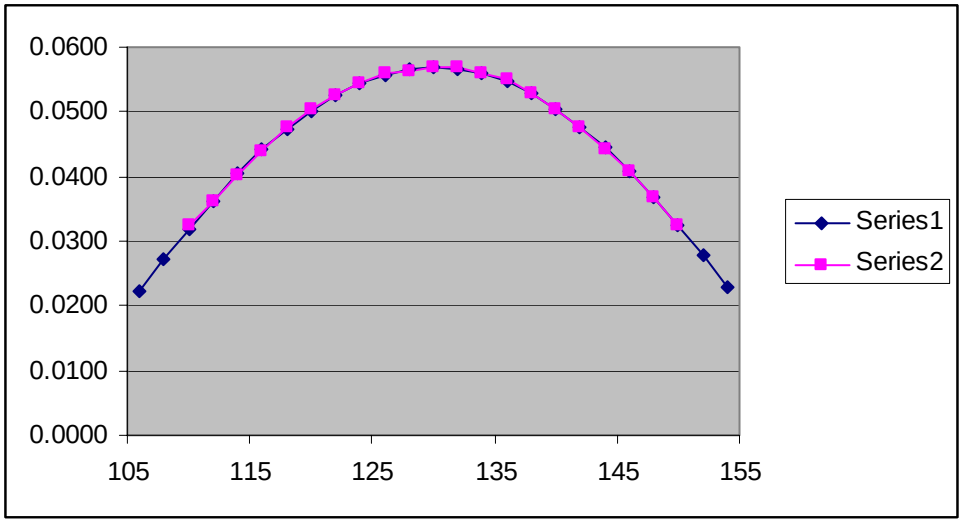


## Tallies and variance reduction

First, the induced fission rate distribution was tallied, using an F4 tally multiplied by the fission cross-section. For the KCODE calculation, this should be identical with the fission rate giving the source, since the source has presumably converged to a constant distribution. For the fixed source calculation, it is the "next generation" fission rate that would be induced by the fixed source if there were no NONU card.

The distributions for the two cases were significantly different. In the KCODE calculation, the fission rate was higher in the MOX fuel, by 10% or sometimes more near the outer edge, and lower in the $UO_2$ fuel. This is in fact reasonable, considering the neglect of the difference in $\upsilon$ for different fuels in the fixed source distribution, mentioned in the preceding section. Taking this into account would have shifted the source – and thus also the flux distribution – outward. It therefore seems likely that the KCODE results may be more accurate.

The reaction rates requested in the benchmark specification were tallied next. Since the detector locations were specified only as points, it would have seemed natural to use point detectors in MCNP-4C, but there were three reasons not to do so:

1. Point detectors are incompatible with reflecting boundaries. In principle it would have been possible to avoid this problem by modelling the whole system instead of one quadrant, but this would have required more work and was therefore dismissed as impracticable.

2. Tracing paths to a large number of point detectors requires inordinate amounts of computing time.

3. No more than 20 point detectors are allowed in one run, so many runs would have been required.

Therefore we decided to use F4 tallies, inserting small cylindrical cells containing the ambient material at each detector location. The radius of these cells was set to 0.9 cm, the largest value that could be used without crossing any material boundaries. (The detector at the core centre was an exception. For this a radius of 1.8 cm was used, giving the same volume since only a quarter of this detector is in the modelled quadrant.) The height was set to 10 cm. These cells should be small enough that the difference between the average flux and the flux at the centre should be small. The disadvantage of using such small cells is obviously the difficulty of obtaining adequate statistics, but it was thought that using 10 000 000 histories might be enough.

To reduce the variance, a mild importance biasing was used. Importances were set to 0.5 or less above and below the core and to 2 in the outer baffle and reflector in the range 105 cm < z < 155 cm, to 4 in the water gap and neutron pad, then decreasing back to 2 in the jacket inner wall and to 1 beyond that.

The dosimetry cross-sections were taken from IRDF-90 V2. We did not have continuous energy IRDF-90 V2 cross-sections available but had to use cross-sections given in the 640-group SAND-II scheme. This group structure is sufficiently fine that one would expect the reaction rates to be effectively equivalent to what continuous energy data would give, unless some resonances in the dosimeters and the ambient materials nearly coincide.

The input files included DPA tallies. However, there turned out to be an input error which made the DPA results invalid, and it was not considered worthwhile to rerun the calculations to get DPA data.

**Statistical quality of the results**

The statistics were pretty good for $^{103}$Rh(n,n′), $^{115}$In(n,n′), $^{237}$Np(n,f) and the group fluxes, with fractional standard deviations below 0.1 even in the neutron pad, below 0.05 in the water gap and mostly below 0.03 elsewhere. The results also passed most of the statistical tests (applied to the tally cell at x = -46.6 cm, y = -41.95 cm, i.e. in the neutron pad). The only exception was $^{115}$In(n,n′), for which the error message “there is not enough information in the largest history scores (usually less than 500 scores) for a reliable estimate of the slope” was obtained.

For $^{27}$Al(n,α), on the other hand, the statistics were quite bad, with some fractional standard deviations exceeding 0.3. The results for $^{58}$Ni(n,p) and $^{64}$Zn(n,p) were intermediate. Obviously there were not enough high-energy neutrons to permit adequate sampling of these reactions. Therefore the calculations were rerun for $^{27}$Al(n,α), $^{58}$Ni(n,p), $^{64}$Zn(n,p) and $^{115}$In(n,n′) with an energy cut-off at 0.3 MeV and the number of histories increased to 100 000 000. In the KCODE case, an SSW source recorded in the previous run was used.

The resulting statistics for $^{58}$Ni(n,p), $^{64}$Zn(n,p) and $^{115}$In(n,n′) were even better than those previously obtained for $^{103}$Rh(n,n′), $^{237}$Np(n,f) and the group fluxes. For $^{27}$Al(n,α) the results were still not really good, but the fsd was below 0.1 everywhere except in the neutron pad, where fsd’s of 0.1326 and 0.1566 were registered. It was decided that this had to suffice.

**Sanity check**

Since insufficient time and funding were available to permit proper checking of the input, a sanity check was essential. Fortunately the results calculated by Kotiluoto could serve this purpose.

In fact, a comparison of our original results with those of Kotiluoto showed our results to be higher by a factor of 4. This was quickly traced to an error in the calculation of the volumes of our tally

cells (the SD card). When our results were divided by 4 to account for this error, the agreement with Kotiluoto's results was good, with the maximum difference amounting to about 15%. This does not guarantee that there may not be other input errors, but they are likely to be minor ones.

## Results

Since the final results were to be presented as equivalent fission fluxes, the dosimetry cross-sections had to be averaged over the $^{235}$U fission spectrum. This was done by performing an MCNP-4C calculation with a single void cell with a $^{235}$U fission source.

The results are presented in two separate Excel files. VTTpro14results-k1.xls gives our KCODE results. As pointed out above, these should be considered our official results. For comparison, the fixed source results are given in VTTpro14results-f1.xls.

## References


[1] Han, Chi Young, Chang-ho Shin, Hong-Chul Kim, Jong Kyung Kim, Nadia Messaoudi and Byung-Chan Na, *VENUS-2 MOX-fuelled Reactor Dosimetry Calculations*, OECD/NEA, NEA/NSC/DOC(2004)6.

[2] Briesmeister, J.F., Ed., *MCNP™ – A General Monte Carlo N-particle Transport Code, Version 4C*, Los Alamos National Laboratory, LA-13709-M (2000).

[3] Mughabghab, S.F., "Neutron Cross Sections", Volume 1, *Neutron Resonance Parameters and Thermal Cross Section,* Part B: Z = 61-100, Academic Press (1984).

[4] Wasastjerna, F., *PVIS-4 – A Program Intended to Prepare a Fixed Fission Source for Pressure Vessel Irradiation Calculations with ANISN, DORT or TORT in Hexagonal or Square Geometry*, VTT Energy Technical Report RFD-2/99 (1999).

## 12. SCK•CEN, Belgium

### 1. Authors

Nadia Messaoudi and Wim Haeck
SCK•CEN
Boeretang 200
B-2400 Mol, Belgium

### 2. Transport method and modelling assumptions

The Monte Carlo code MCNPX (version 2.5.e) was used for both K calculation and fixed source calculation.

The VENUS-2 core was modelled explicitly with no assumption. All details were taken into account axially and radially: grid, stops, reflectors.

### 3. Transport cross-sections

For both K and fixed source calculations, a cross-section library based on ENDF/B-6.8 evaluation was generated with the NJOY99.90 code.

### 4. Neutron source

A fission volume source file was generated by an SSW card with MCNPX in K mode. This neutron source inside fuel pin volumes was used later for dosimetry calculation (in fixed source mode) by using the SSR card.

The normalisation factor 1.16222E+13 $s^{-1}$ was derived from the ratio of the experimental fission rate value to the calculated one from MCNPX output.

### 5. Axial leakage treatment (for two-dimensional calculation only)

### 6. Response functions and fission averaged data

The IRDF-90 Version 2 cross-section library was used for dosimetry calculation.

### 7. Comments/special references

For K calculation and to derive the neutron source, a large number of particles per cycle were used: 300 000 with a total number of cycles of 300 (50 are inactive).

## LIST OF CONTRIBUTORS

### *Authors*

Nadia Messaoudi (SCK•CEN, Belgium) and Byung-Chan Na (OECD/NEA)

### *Problem specification*

Chi Young Han (Hanyang University, Korea)
Chang-ho Shin (Hanyang University, Korea),
Hong-Chul Kim (Hanyang University, Korea)
Jong Kyung Kim (Hanyang University, Korea)
Nadia Messaoudi (SCK•CEN, Belgium)
Byung-Chan Na (OECD/NEA)

### *Benchmark participants*

Chang-Ho Shin (Hanyang University, Korea)
Jong Kyung Kim (Hanyang University, Korea)
Hong-Chul Kim (Hanyang University, Korea)
Chi Young Han (Hanyang University, Korea)
Todd Wareing (Transpire, Inc., USA)
Allen Barnett (Transpire, Inc., USA)
John McGhee (Transpire, Inc., USA)
Greg Failla (Transpire, Inc., USA)
Mikhail A. Kalugin (KI, Russia)
Alexey V. Moriakov (KI, Russia)
Sergei M. Zaritsky (KI, Russia)
Bok Ja Moon (KOPEC, Korea)
Joon Ghi Ahn (KOPEC, Korea)
Petr Darilek (VTI/SUT, Slovak)
Vladimir Sebian (VTI/SUT, Slovak)
Vladimir Necas (VTI/SUT, Slovak)
Maik Hennebach (WTI GmbH, Germany)
Helmut Kühl (WTI GmbH, Germany)
Petri Kotiluoto (VTT, Finland)
Do-Heon Kim (KAERI, Korea)
Choong-Sub Gil (KAERI, Korea)
Jonghwa Chang (KAERI, Korea)
Jung-Do Kim (KAERI, Korea)
Frej Wasastjerna (VTT, Finland)
Nadia Messaoudi (SCK•CEN, Belgium)
Wim Haeck (SCK•CEN, Belgium)